

University of South Wales



2064795

THE GRILLAGE ANALYSIS OF MULTI-CELL STEEL STRUCTURES

by

DAVID KENNETH PUGH B.Sc., C.Eng., M.I.C.E.

A thesis submitted for the
degree of Master of Philosophy

CNAALondon

January 1986

SPONSORING ESTABLISHMENT:

The Department of Civil Engineering and Building.

The Polytechnic of Wales.


COLLABORATING ESTABLISHMENT:

The Department of Civil and Structural Engineering.

University College, Cardiff.

DECLARATION.

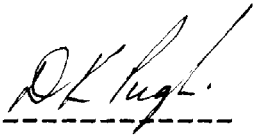
This is to certify that neither this thesis, nor any part of it, has been presented, or is being concurrently submitted in candidature for any degree at any other academic or professional institution.



Candidate

CERTIFICATION OF RESEARCH.

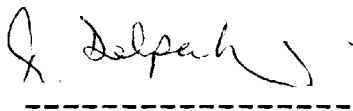
This is to certify that, except when specific reference to other investigations is made, the work described in this thesis is the result of the investigations of the candidate.



Candidate



Director of Studies



Supervisor

CONTENTS

	Page
Acknowledgements	i
Synopsis	ii
List of Symbols	iii
Chapter 1. INTRODUCTION	
1.1. Multi-cell Structures	1
1.2. Computer Applications	2
1.3. Aim of the Investigation	3
1.4. Scope of the Investigation	4
Chapter 2. REVIEW OF THE METHODS AVAILABLE FOR THE ANALYSIS OF MULTI-CELL STRUCTURES	
2.1. Introduction	8
2.2. Finite Element Method	9
2.3. Folded Plate Method	13
2.4. Finite Strip Method	16
2.5. Nodal Section Method	17
2.6. Orthotropic Plate Theory	19
2.7. Space Frame Analysis	20
2.8. McHenry Lattice Space Truss	21
2.9. Grillage Analysis	22
2.10. Skew multi-cell structures	24
2.11. Conclusions	25

	Page
Chapter 3. DEVELOPMENT OF THE GRILLAGE IDEALIZATION FOR THE ANALYSIS OF MULTI-CELL STRUCTURES	
3.1. Introduction	32
3.2. Development of grillage element stiffness matrix	34
3.3. Idealization of multi-cell structures	37
3.4. Longitudinal Bending	40
3.5. Transverse Bending	63
3.6. Distortion	65
3.7. Summary	77
Chapter 4. IDEALIZATION FOR TORSION IN MULTI-CELL STRUCTURES	
4.1. Introduction	102
4.2. Grillage representation	110
4.3. 3-cell structure under torsional loading	114
4.4. Distribution of torsional inertia between longitudinal and transverse grillage beams	121
4.5. Conclusions	126
Chapter 5. GRILLAGE ANALYSIS OF STRAIGHT MULTI-CELL STRUCTURES	
5.1. Introduction	149
5.2. Effect of number of transverse grillage beams on accuracy of analysis	150
5.3. Analysis of straight multi-cell structures	157
5.4. Conclusions	175

	Page
Chapter 6. FINITE ELEMENT ANALYSIS OF SKEW SINGLE-CELL STRUCTURES	
6.1. Introduction	203
6.2. Asymmetrically loaded straight single cell structure	204
6.3. Symmetrically loaded skew single cell structure	208
6.4. Influence of span/breadth ratio	216
6.5. Influence of intermediate diaphragms	221
6.6. Conclusions	234
Chapter 7. GRILLAGE ANALYSIS OF SKEW MULTI-CELL STRUCTURES	
7.1. Introduction	280
7.2. Finite element analysis of three-cell structure	283
7.3. Grillage analysis of three-cell structure	285
7.4. Analysis of four-cell structure	303
7.5. Effect of skew angle on accuracy of analysis	306
7.6. Conclusions	311
Chapter 8. CONCLUSIONS AND RECOMMENDATIONS FOR FURTHER WORK	
8.1. Conclusions	348
8.2. Recommendations for further work	353
REFERENCES	355

	Page
App A. DEVELOPMENT OF SHEAR-DEFORMABLE GRILLAGE ELEMENT STIFFNESS MATRIX	A1
App B. DERIVATION OF DEFLECTION FORMULAE FOR SHEAR -DEFORMABLE SIMPLY SUPPORTED BEAM	A7
App C. CONVERGENCE STUDY OF THE FINITE ELEMENT PROGRAM - QUEST	A12
App D. DEVELOPMENT OF EQUIVALENT FRAME ELEMENT STIFFNESS MATRIX	A21
App E. DERIVATION OF STRAIN ENERGY FORMULAE FOR GRILLAGE BEAM	A26
App F. ANALYSIS OF SHEAR-DEFORMABLE FIXED-ENDED BEAMS	A30

ACKNOWLEDGEMENTS

I would like to express my sincere thanks to Professor H. R. Evans who has acted as Director of Studies throughout the research period. I am grateful for his valued guidance, support and constant encouragement.

I am also grateful for the contribution made by my ex-colleague, Dr. N. E. Shanmugam, who was responsible for the establishment of the research project and acted as Supervisor in the early stages of the work before his departure to the National University of Singapore.

I also wish to thank Dr. Ray Delpak, who has acted as Supervisor since the departure of Dr. Shanmugam, for his encouragement and support in the latter stages of the studies.

I am also grateful to the Department of Civil Engineering and Building, The Polytechnic of Wales for allowing me to pursue the research program and for all financial support given.

The role played by The Department of Civil and Structural Engineering, University College, Cardiff as the collaborating establishment is appreciated.

Finally, the support and understanding of my wife, Linda, and daughters, Melanie and Katherine, is truly appreciated.

SYNOPSIS.

THE GRILLAGE ANALYSIS OF MULTI-CELL STEEL STRUCTURES.

D.K. PUGH.

The presented work is concerned with the development of a grillage method for predicting the behaviour of steel multi-cell structures. Simply supported, straight and skew structures will be considered subjected to a variety of loading conditions. The proposed analysis can be achieved using a low cost micro-computer, and it is considered that the method will assist in the initial stages of design, where a number of alternative solutions may require investigation.

In the development of a two-dimensional grillage method for the analysis of a three-dimensional structure, the actual structural response under load must be modelled by the assemblage of rigidly-jointed beams that constitute the grillage structure. Multi-cell structures resist applied load by a combination of longitudinal bending, transverse bending, torsion and distortion. The development of the appropriate stiffness parameters for each grillage beam constitutes the major part of the investigation.

In a finite element study of skew single cell structures, recommendations for the determination of the effective breadth ratio for flange plates in skew structures are presented.

Numerous examples are presented for both single cell and multi-cell structures with straight and skew supports. The grillage results are compared with results from a finite element study. In the case of straight structures the grillage results for maximum web deflection agreed to within -5% and +6% of the finite element values. The results for maximum longitudinal flange stress are less accurate, the grillage method tending to overestimate the stress intensity, with a maximum overestimation of 16% of the finite element value.

The skew structure results using an orthogonal mesh idealization are less accurate. The degree of accuracy decreases with increasing angle of skew and also when the loading produces transverse hogging effects.

It is considered that the grillage method is capable of producing results to an acceptable degree of accuracy for initial design purposes.

LIST OF SYMBOLS.

A	total area of cross-section
A _f	area of flange
A _i	enclosed area of cell i
A _s	effective shear area of beam cross-section
A _w	area of web
B	overall width of structure
b _f	flange width
2b	width of flange plates between webs
2b _e	effective width of flange plates between webs
D	overall depth of structure
{d}	vector of nodal displacements
d _z	vertical deflection of grillage beam
E	Modulus of Elasticity
{F}	vector of applied nodal forces
G	Modulus of Rigidity
I	second moment of area of member
I _f	second moment of area of flange
I _w	second moment of area of web
I _Y	second moment of area of grillage beam
J	polar second moment of area of member
J _l	torsional inertia of longitudinal section
J _t	torsional inertia of transverse cross-section
[K]	element stiffness matrix
L	length of member or span of structure
M _y	bending moment in grillage beam
M _x	torsion moment in grillage beam
P _z	shear force in grillage beam
q _i	shear flow in cell i

T	torsion moment
td	thickness of diaphragm
tf	thickness of flange
tw	thickness of web
β	form factor
ψ	effective breadth ratio
v	poisson's ratio
θ	angle of skew
θ_x	rotation about x-axis
θ_y	rotation about y-axis
σ	longitudinal flange stress

These symbols may be used with alternative definitions when reference is made to the work of other authors. In which case their definitions will be given where they occur.

CHAPTER ONE

INTRODUCTION

1.1. MULTI-CELL STRUCTURES.

Many modern civil engineering structures take the form of thin-walled cellular boxes which incorporate the advantages of low weight with high strength. Examples of such structures are box-girder bridges, storage tanks for offshore structures, box gates for dry docks and double bottoms used in ship construction.

Thin-walled cellular structures used in bridge construction consist of top and bottom flange plates separated by a combination of longitudinal web plates, transverse end or support diaphragms and possibly transverse intermediate diaphragms as shown in figure 1.1. The top and bottom flange plates may be longitudinally stiffened.

In addition to the high longitudinal bending strength and the inherent torsional strength, the ease, speed and economics of construction has resulted in the steel cellular structure becoming a popular form of construction for medium to long span bridges.

Cellular or box structures are also increasingly used in concrete bridge construction in preference to beam and slab decks for medium span structures because of the benefits of reduced weight and high strength properties.

For in-situ type construction the cells may be formed using void formers which can be circular or rectangular in cross-section. It is normally considered that structures where the void area exceeds 60% of the cross-sectional area should be treated as cellular structures. The use of deeper concrete box-girders with one or more cells has also evolved over the last 25 to 30 years.

1.2. COMPUTER APPLICATIONS.

The methods available for the analysis of multi-cell and box girder structures are generally dependent on the solution of a large number of simultaneous equations using a digital computer. The developments in computer hardware over the years has resulted in machines with ever increasing storage capacity and greater speed of execution. This has permitted the development of sophisticated analysis methods such as the finite element method.

However, over the past five years, one has seen the introduction of micro-computer systems. These systems, which are inexpensive and are becoming more and more powerful, have made computer applications more readily available, especially at the important initial stage of design. At this stage many repeated calculations may be necessary in order that the designer can establish all critical structural details such as plate thicknesses, web spacing, longitudinal stiffener arrangement, critical

loading positions and the effect of intermediate diaphragms, etc..

The availability of a micro-computer at his disposal, which can be used repeatedly at minimal cost, will considerably assist the designer in the development of an economic solution for a particular problem. Once the proportions of the structure are established, the structure can then be analysed in detail by more accurate techniques such as the finite element method and all the necessary design checks carried out.

1.3. AIM OF THE INVESTIGATION.

The aim of the investigation is to establish a method of analysis which will assist the designer in establishing relevant proportions of multi-cell structures at the initial stages of design.

It is considered that such a method must satisfy the following criteria

- (i). It must be easy to use, inexpensive and provide an 'immediate' solution.
- (ii). It should utilize a method of analysis which is familiar to the designer and which he can use with confidence.
- (iii). The solutions provided need not be exact, but the relative accuracy of the solution must be quantifiable.

It is considered that the grillage method of analysis satisfies these criteria and hence the object of the work presented in this thesis is to develop a simple grillage method of analysis which can operate on a low-cost micro-computer system. The application to the analysis of simply supported, straight and skewed, steel multi-cell structures under a variety of loading conditions will be presented.

1.4. SCOPE OF THE INVESTIGATION.

In chapter 2 a review of the existing methods for the analysis of multi-cell structures is presented. These methods range from the sophistication of the finite element method, where the full three dimensional behaviour of the structure is modelled, to simpler methods based on two-dimensional idealization.

The development of the element stiffness matrix used in the computer program SHEARGRID2 for the analysis of shear-deformable grillages is described in chapter 3. The geometrical and sectional idealization of multi-cell structures is also considered. In the idealization of section properties one has to consider longitudinal and transverse bending, distortion and torsion effects.

In the longitudinal direction the shear lag effect in the flange plates can be considered using the effective breadth concept. The accuracy of the grillage method is confirmed for single and multi-cell structures

subjected to longitudinal bending action, where the effective breadth ratios specified in Part 3 of BS 5400 are used in the determination of the second moment of area of the longitudinal grillage beams. The validity of using the cross-sectional area of the web plates for the effective shear area of the longitudinal grillage beams is also confirmed.

Chapter 3 is concluded with a consideration of the methods available to cater for cell distortion in the grillage idealization. The usual method adopted is to consider the cross-section as a Vierendeel frame and calculate either the second moment of area or effective shear area of the equivalent beam that produces comparable deflections. The use of an equivalent frame element is presented as an alternative to the equivalent beam approach.

In chapter 4 the torsional idealization of multi-cell structures is considered. Proposals are presented for apportioning the torsional inertia of the cross-section of the structure to the longitudinal and transverse grillage beams. The proposals are developed from a consideration of the strain energy contributions due to bending moment, torsional moment and shear force for both the longitudinal and transverse grillage beams.

The recommendations of chapters 3 and 4 are used in chapter 5 for the grillage analysis of a number of straight multi-cell structures under a variety of loading conditions. Three, four and five cell structures subjected

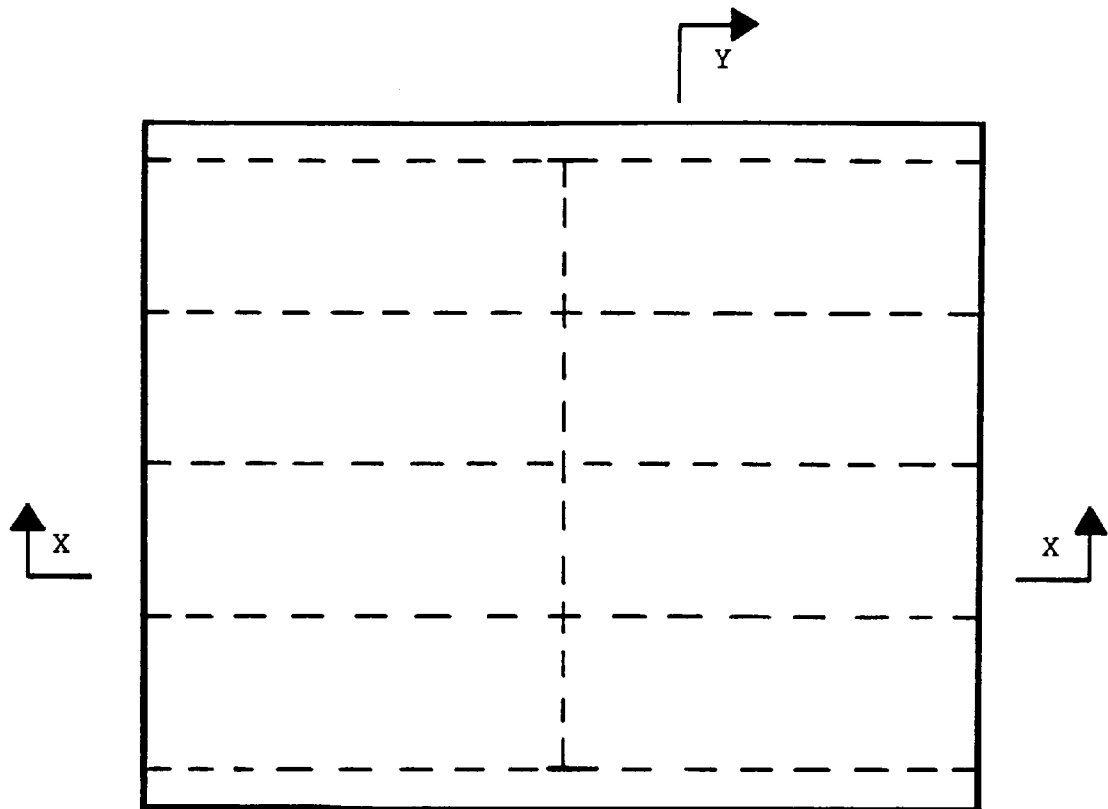
to both midspan point and uniform line loading are analysed. The results are compared to those obtained from a finite element analysis.

In chapter 6 a finite element study of skew single cell structures is reported. In this study the effective breadth ratio for a variety of skew angles and breadth/span ratios are calculated. This is achieved by separating the torsional and bending flange stress distributions. Recommendations are presented for the determination of the effective breadth ratios from Part 3 of BS 5400 based on the breadth/span ratio and the degree of skew of the structure.

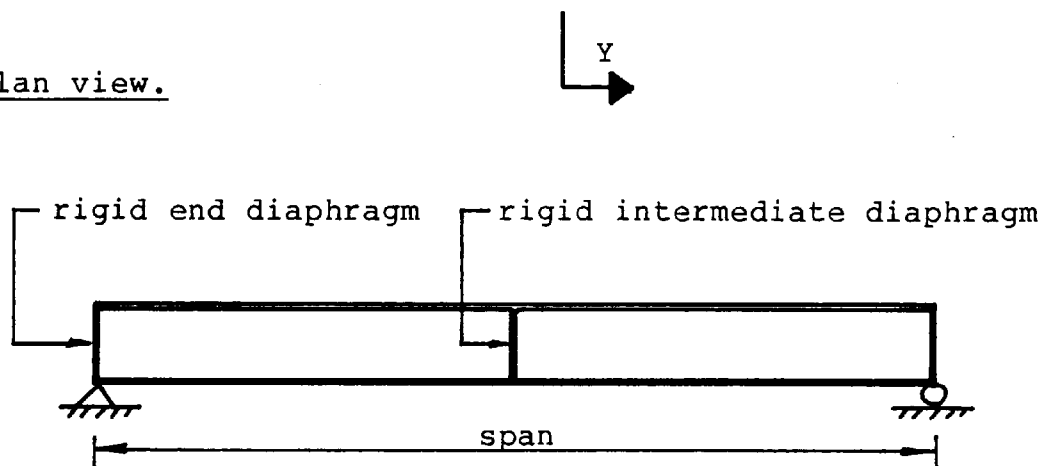
The influence of intermediate diaphragms on the distribution of the longitudinal flange stress and web deflection is also considered with the use of both midspan and quarterspan diaphragms.

The grillage analysis of skew multi-cell structures is considered in chapter 7. The use of both an orthogonal and skew mesh idealization is presented. Angles of skew up to 45 degrees are considered and the relationship between degree of skew and accuracy of analysis is established. The grillage results are again compared to those from a finite element study.

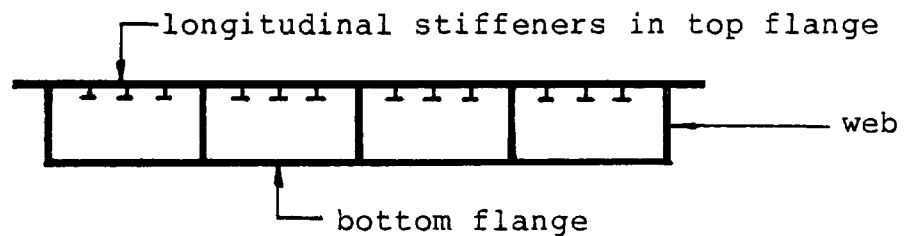
Finally, in chapter 8, the conclusions drawn from the work described in the thesis are presented and recommendations for further studies are made.



(a) Plan view.



(b) Longitudinal section X-X.



(c) Cross-section Y-Y.

FIGURE 1.1. - TYPICAL MULTI-CELL STRUCTURE.

CHAPTER TWO

REVIEW OF THE METHODS AVAILABLE FOR THE ANALYSIS OF MULTI-CELL STRUCTURES

2.1. INTRODUCTION.

Various methods have been developed in the last twenty years for the analysis of multi-cell structures. Most require the solution of a series of simultaneous equations which can easily be performed with the use of digital computers. Some of these methods have limitations regarding the geometry of the structure. For example, the folded plate and the finite strip methods require simply supported end conditions (unless special steps are taken) and can only analyse structures of uniform cross-section.

The finite element method is more comprehensive and can deal with varying cross-sections and arbitrary boundary conditions, but requires extensive labour and computer time which tends to make the method prohibitively expensive. Other methods, such as the grillage and orthotropic plate methods, resort to modelling the three-dimensional structure using two-dimensional idealization procedures, thus substantially reducing the labour and computer time for solution. The development of these methods is described in the following sections.

2.2. FINITE ELEMENT METHOD.

The finite element method is a technique for analysing complicated structures by notionally cutting the continuum of the prototype into a number of finite elements which are connected at discrete joints called nodes. For each element, approximate stiffness equations are derived relating the displacements of the nodes to the nodal forces between elements and a computer is used to solve the very large number of simultaneous equations that relate nodal forces and displacements.

Since the basic principle of subdivision of the structure into simple elements can be applied to structures of all forms and complexity, there is no logical limit to the type of structure that can be analysed if the computer program is written in the appropriate form. Consequently, the finite element method provides the most versatile method of analysis available at present, and for some structures the only practical method.

The technique was pioneered for two-dimensional elastic structures by TURNER et al (1956) and CLOUGH (1960) during the 1950's. Since then very considerable developments have been made by many people. Much more detailed and comprehensive descriptions of the method are given by ZIENKIEWICZ (1977), with useful demonstrations of bridge analyses by ROCKEY, BANNISTER and EVANS (1971).

A wide range of computer programs based on the finite element method are now available and experimental

evidence indicates that such programs may be confidently used for the analysis of multi-cell structures. The accuracy of solution achieved is directly related to the fineness of the mesh used to model the structure, and consequently, the excessive demands upon computer time and storage space makes the finite element method very expensive.

The finite element method was used by MOFFATT and DOWLING (1972) in their extensive parametric study of the shear lag phenomenon in steel box girder bridges. To predict accurately the longitudinal flange stress distribution in the flange plate of a cantilevered box girder, 11 elements were used in the span direction, 8 across the half width of the flange plates and one element represented the web plates.

The finite element program QUEST, used as the basis for comparison in this thesis, is a program designed for the linear elastic analysis of box girder bridges of arbitrary shape having arbitrary supports and arbitrarily applied loads. The theory for the program and the basic analysis and solution routines were developed at the Centre for Numerical Methods in Engineering, University College of Swansea.

The structure is represented in three dimensions by quadrilateral thin shell elements which are capable of resisting both plate bending effects and in-plane forces. The elements are connected at their corner nodes where six degrees of freedom (three displacements and three

rotations) are considered as shown in figure 2.1. The results obtained from the analysis of each load case are the displacements at each node, the reactions at the supported nodes, the flexural and membrane forces at each corner of the element, and optionally, the extreme fibre stresses on each surface of the element.

The stiffness matrix for the quadrilateral shell element used is formed by combining the stiffnesses of a quadrilateral plane stress element with those of a quadrilateral plate bending element. The result is an element capable of resisting both in-plane forces and out-of-plane shear force and bending moments, as shown in figure 2.2(a). Because six degrees of freedom are considered at every node, the in-plane rotation at each corner node is given an arbitrary small value to avoid the possibility of zero stiffness in this direction where elements meet in the same plane.

For each aspect of the element stiffness, a displacement function is assumed which has the same number of unknown coefficients as the number of degrees of freedom associated with the relevant mode of action, i.e 8 for plane stress and 12 for plate bending. These displacement functions are integrated with the isotropic elastic properties to obtain the stiffnesses. Because the in-plane behaviour of the element is capable of representing linearly varying direct stress, a reasonable approximation to the web stiffness may be obtained with a single element in the depth of the web and a better representation of

longitudinal flange stresses, including shear lag effects, is available than with a constant stress element, as shown in figure 2.2(b).

A number of researchers have developed modified finite element solution procedures for multi-cell structures in an attempt to reduce the computational requirements of a full three-dimensional analysis whilst still providing a workable and accurate analytical approach.

SAWKO and COPE (1969) considered that examination of the structural behaviour of cellular bridges indicated that the primary stress conditions were those of direct stresses in the top and bottom flanges and flexural stresses in the transverse medium. The proposed method assumed that a cellular deck can be represented as an assemblage of plane stress elements only.

Because of the importance of transverse flexural behaviour it was necessary to simulate its action if the analysis were to succeed. This was achieved with the use of equivalent diaphragms which simulated the distortional stiffness of cells. These diaphragms have no physical significance when simulating the stiffness of the transverse medium, but they can incorporate actual properties of diaphragms if they are present in the bridge.

With this approach the number of degrees of freedom at each node was reduced to three and the size of the stiffness matrix reduced to one quarter of that in an

equivalent three-dimensional analysis. It was found that this reduction in computational effort enabled practical bridge systems to be conveniently analysed using this technique.

This method was compared to the experimental results of a single box by RICHMOND (1966) and also a six-cell perspex model. The results indicated that little is gained by using a full three-dimensional analysis for a single cell, and it would seem that the approximate method provides a sufficient degree of accuracy for design purposes.

CRISFIELD (1971) presented two element models, chosen such that economy of computer storage be achieved. Wall bending was directly included in one of the methods; whilst in the other, its effects were simulated by an approximate approach. Both elements required symmetry about the mid-depth of the webs limiting the analysis to cellular structures with top and bottom flange plates of equal thicknesses. Both elements were successfully verified with comparison to a number of experimental models and analytical solutions obtained from other sources.

2.3. FOLDED PLATE METHOD.

The folded plate method for the analysis of multi-cell structures is based on the elasticity analysis of GOLDBERG and LEVE (1957) and developed by DE FRIES-SKENE and SCORDELIS (1964) and SCORDELIS (1966). The method was initially developed for the analysis of right, simply

supported decks of constant depth and comprising plate elements of uniform thickness. Internal diaphragms may be present, but like the support diaphragms, must be considered infinitely stiff in their own plane and perfectly flexible normal to their own plane. The analysis automatically takes into account effects such as shear lag and transverse distribution of loading between boxes.

The analysis is performed using a harmonic analysis technique. The applied loads are resolved into a number of Fourier Series components. The solution is carried out for all the loading components and is repetitive for each harmonic. For each harmonic, loads will produce displacements of the same longitudinal variation and vice versa. Therefore, a single characteristic value may be used to describe any force or displacement pattern. For example, the displacement pattern along the bridge, $r(x)$ may be described by the single value r_0 where

$$r(x) = r_0 \frac{\sin n \pi x}{L} \quad \text{----- eqn 2.1}$$

Consequently, the entire length of joint (L) can be treated as a single node point and it is only necessary to perform a stiffness analysis on a typical cross-section.

The structure to be analysed must first be split up into one or more elements, each element being a rectangular plate of constant thickness and extending over the full length of the structure. At each element boundary, or where two or more elements have a common boundary, there is a joint. As with the elements, every joint runs along

the whole length of the structure. Joints need not occur only at the junctions of webs and flange plates, but can occur anywhere along these plates between junctions. Figure 2.3(a) shows a box section bridge divided into elements.

In the analysis, the actual loading of the bridge is represented by means of a Fourier Series. For a bridge deck without internal diaphragms, 10 non-zero terms of the Fourier Series will be sufficient to analyse the uniform load response. However, if reactions at exterior supports are to be calculated or if design analysis is to be carried out in the region of a concentrated load, then up to 100 harmonics may be necessary, as shown in figure 2.3(b).

The method was used by SCORDELIS (1966) to analyse four actual bridge superstructures. Three were concrete multi-cell structures, whilst the fourth was a two cell structure consisting of a top slab of concrete integrally cast with a steel system consisting of top flange plates, stiffened web plates, and a stiffened bottom plate used to form the box girder system.

He also reported on a parametric study conducted on multi-cell concrete structures. The case studies included two spans of 60 and 80 ft; four cross-sections containing 3, 4, 6 and 8 cells; and four transverse load positions of a single concentrated load at midspan.

The computer program, MUPDI, uses the folded plate method which has been developed to incorporate the analysis of continuous structures and can also consider the

effects of elastic external supports. The results of the program were compared to a number of experimental results, firstly with a folded plate model and also both concrete and steel multi-cell structures. The folded plate method revealed close agreement in all three cases.

The restriction that end diaphragms must be considered as infinitely rigid in their own plane prevents any distortion of end cross-sections, and represents a severe limitation and is a disadvantage of the folded plate theory. KRISTEK (1983) presented a solution for the analysis of prismatic folded plates with arbitrary boundary conditions at the ends. The proposed method employs the series-type solution of folded plates in combination with classic thin-walled beam theory.

2.4. FINITE STRIP METHOD.

This method is basically a transition between the folded plate and the finite element methods; it combines some of their advantages and presents an efficient method for the solution of many forms of structures, including multi-cell structures. It was first proposed by CHEUNG (1968) for rectangular slabs. The method was rapidly developed by a number of research teams as reported by CUSENS and PAMA (1975).

The structure is assumed to be made up of finite elements called 'strips' which extend from one end of the deck to the other. The strips are connected by nodes which also run from one end to the other. Like the folded plate

method, the displacement functions for the in-plane and out-of-plane deformation of the strips are of the form

$$w, \theta, u \text{ or } v = \sum f(y) \sin (n \pi x/L) \text{ --- eqn 2.2}$$

where x is the direction along the structure and y is the direction across the strip. The analytical procedure is also the same in that the stiffness equations are obtained and solved for each harmonic component of the load in turn, and the results summed to give the total stress distribution.

The method has been applied to the analysis of curved bridge decks where the Fourier Series for displacement is written in polar co-ordinates as follows

$$u = \sum u(n) \cos (n \pi \theta/\theta_0) \text{ ---- eqn 2.3}$$

2.5. NODAL SECTION METHOD.

The Nodal Section method was developed by ROCKEY and EVANS (1972) to provide a relatively simple method of analysis for both single span and continuous box girders. This method allows for geometrical variation of the cross-section along the length of the girder.

The Nodal Section theory is based on the Ordinary Folded Plate theory in which the only assumptions additional to those employed in a conventional elastic analysis are the following.

1. The bending action of an individual plate normal to its plane may be represented by considering a transverse

one-way slab strip.

2. The in-plane longitudinal loading action of an individual plate is similar to that of a beam spanning between the end diaphragms.

On the basis of these assumptions, the behaviour of a box girder may be considered to consist of the action of a series of transverse one-way frames elastically supported by a system of interconnected plate beams spanning longitudinally between the supporting diaphragms.

Although the method assumes a simplified structural behaviour in order to reduce the amount of computation required, it provides results of a high degree of accuracy. The authors considered the method would prove to be useful during the design of box girders, when several analyses may be necessary in order to investigate the effect of changing dimensions. In such a situation, the use of the finite element method would prove to be prohibitively expensive.

ROCKEY and EVANS (1975) showed that for double cell and discrete-cell structures the method compared favourably with the folded plate method. Solution times for the nodal section method were also shown to be 20 times faster than the finite element method for a single cell structure.

The Nodal Section method can also consider the effects of shear lag by the use of the appropriate effective breadth ratios. The program BOXGDR issued by the

Highway Engineering Computer Branch of the Department of the Environment utilised the Nodal Section method for the analysis of box girder bridges.

2.6. ORTHOTROPIC PLATE THEORY.

The concept of considering an actual bridge deck as an equivalent plate for the purposes of determining the distribution of stresses is well established. The load distribution charts developed by MORICE and LITTLE (1956) have been extensively used for the analysis of slab and pseudo-slab decks by designers. There are two series of charts which give the load distribution of slabs having no torsional stiffness and for slabs having the full torsional stiffness of isotropic slabs. For most bridge decks, interpolation between the sets of charts is necessary and a tabulated procedure can be accomplished relatively easily.

The HECB (1973) presented an enhancement to this method due to CUSENS, which not only produced solutions of greater accuracy for the range of decks covered by the Morice and Little charts, but also extended the analysis to decks which may be considered as torsionally stiff or flexurally soft.

Simply supported right bridge decks may be considered as orthotropic plates where the relationship between displacement and load takes the form of a fourth order differential equation. The precise solution of this equation depends upon the relative stiffness parameters, there being three distinct cases where in each case, the

deflection may be expressed in the form

$$w = \sum_{n=1}^{\infty} \frac{H_n \sin(\alpha_n x)}{\alpha_n^4 D_x 2b} K_1 \text{ ----- eqn 2.4}$$

The coefficient K_1 is referred to as a distribution coefficient. The longitudinal and transverse bending moments are functions of the mean beam moments multiplied by the appropriate distribution coefficients.

Multi-cell structures fall within the category defined as torsionally stiff and Cusens and Pama considered that the method should be applied to structures containing at least four longitudinal cells. The effects of cell distortion can be incorporated in the distribution method by inclusion of the shear stiffness of the deck in the flexural parameter, θ . The appropriate shear stiffness may be determined by treating the cross-section as a Vierendeel frame.

2.7. SPACE FRAME ANALYSIS.

Multi-cell structures can be modelled in three dimensions using a space frame analysis. In this approach the flanges and webs of the structure are sub-divided into rectangular elements, and each of these is represented in the equivalent space frame by a cruciform of beam elements as shown in figure 2.4.

These beam elements are assigned axial, bending and torsional stiffnesses to approximate the two-way plate behaviour and are considered rigidly connected at the

joints. The effect of shear lag can be included with the use of the appropriate effective breadth of flange when determining the bending stiffness of the flange plates.

A standard space frame program can be used to determine the internal member forces in each element which in turn are interpreted and converted into the appropriate force effect in each member.

SMYTH and SRINIVASAN (1973) used the space frame method to analyse a continuous multi-cellular prestressed concrete box structure. The space frame analysis was used to check, calibrate and modify the results from a grillage analysis, which was the method used for the majority of the design calculations. The space frame analysis was verified by tests carried out on models, one of perspex and the other of plaster. The results from both model tests showed acceptable agreement with the numerical analysis.

2.8. McHENRY LATTICE SPACE TRUSS.

McHENRY (1943) showed that the in-plane deformation of a plate could be investigated using an equivalent square lattice, consisting of pin-jointed, axially loaded members as shown in figure 2.5(a). Each element of the flange and web plates in the structure is represented by a framework of pin-jointed lattices. Thus a multi-cell structure can be represented as a three-dimensional space truss as shown in figure 2.5(b). One disadvantage of this method is that the Poisson's Ratio of the plate must be taken as $1/3$.

AL-NAJJAR (1984) showed that a rectangular lattice can be developed to model plates of any aspect ratio, but again the Poisson's Ratio is limited to the value of 1/3. He considered the use of square lattices for the analysis of a simply supported three-cell steel structure. He concluded that the results for web deflection and longitudinal flange stress provided by this method were comparable in accuracy to a grillage analysis.

This solution was achieved using the same number of lattices as rectangular elements in a finite element study of the structure. Because only three degrees of freedom are considered in the plane truss solution, against six in the finite element analysis, the number of degrees of freedom in the structure was halved. This resulted in lower execution times for the lattice analysis. However, unless the equivalent lattice structure can be automatically generated at the input stage and the stresses automatically calculated from the displacements at the output stage, this method requires a substantial amount of time and effort to be spent in the preparation of data and the interpretation of results.

2.9. GRILLAGE ANALYSIS.

Grillage Analysis is probably the most popular computer method for the analysis of bridge decks. This is because it is easy to comprehend and use, relatively inexpensive, and has been proved to be reliably accurate for a wide variety of bridge types.

In this method, the bridge deck is idealized as a plane grillage of discrete rigidly connected beams which resist the action of applied loads by the development of bending moments, torsion moments and shear forces in the grillage beams. By an appropriate consideration of these effects the actual force effects in the actual structure can be determined.

WEST (1973) developed recommendations on the use of the grillage method for the analysis of slab and pseudo-slab structures. The analysis of multi-cell structures can be accomplished using a grillage element which considers shear deformation of the element, thus allowing cell distortion to be modelled by assigning an appropriate shear area value to the transverse grillage beams.

SMYTH and SRINIVASAN (1973) used the grillage method for the analysis of a multi-cellular prestressed concrete viaduct with complex ramps. The method was considered appropriate because the transverse bending action of the structure was more significant than the warping action, and thus the results would be reasonable if correctly interpreted. As reported in Section 2.7 the grillage results were verified against a space frame analysis.

MAISEL, ROWE and SWANN (1973) considered that the grillage method was appropriate for the analysis of concrete box-girder bridges consisting of more than four cells, although this statement was subsequently challenged

by HAMBLY in the written discussion on the paper (1974). He cited his experience with the use of a shear-flexible grillage program for the analysis of a 21 degree skew, three span, twin-cell box girder deck. The analytical accuracy of the grillage method was checked against a finite strip analysis of the deck, both analyses revealed close agreement.

SHANMUGAM (1978) used the grillage method for the analysis of double bottom ship structures. He showed that the grillage method can deal with web openings by using design curves developed for the determination of effective shear area and torsional inertia of the grillage beams representing the webs. These design curves were developed from theoretical and experimental parametric studies of single cell beams with web openings. An incremental grillage method for predicting the failure load of double bottom structures was also proposed.

2.10. SKEW MULTI-CELL STRUCTURES.

Most researchers once they have established the validity of a particular method of analysis for structures with right supports turn to the problem of skew. These investigations have revealed that some of the methods cannot be used for the analysis of skew structures, whilst others have had limited success.

The one method that has proved to be successful for the accurate analysis of skew multi-cell structures is the finite element method. COMARTIN and SCORDELIS (1972)

used the finite element method to analyse a number of four-cell structures of various angles of skew ranging from 0 to 45 degrees. They also considered the significance of an internal diaphragm at the midspan cross-section on the distribution of stress within the skew structure.

The results from the analyses were compared with those from an experimental investigation of aluminium models. The study confirmed the accuracy of the finite element method, and some tentative design recommendations were presented for comparable structures.

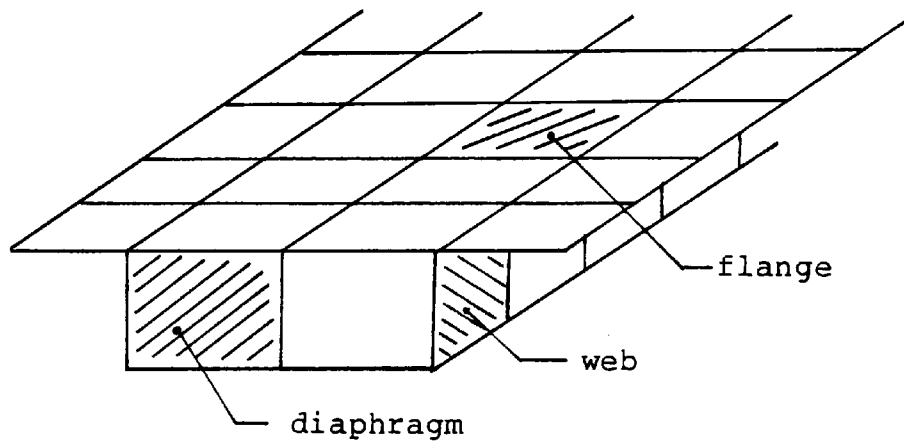
KRISTEK (1979) presented a solution procedure for the analysis of skew multi-cell structures using the folded plate method. The solution is based on a direct stiffness harmonic analysis of individual girders and on a force method where the interaction forces acting between the girders at discrete positions are taken as the redundants. The interaction forces and moments are determined by satisfying the required compatibility conditions at these discrete positions.

2.11. CONCLUSIONS.

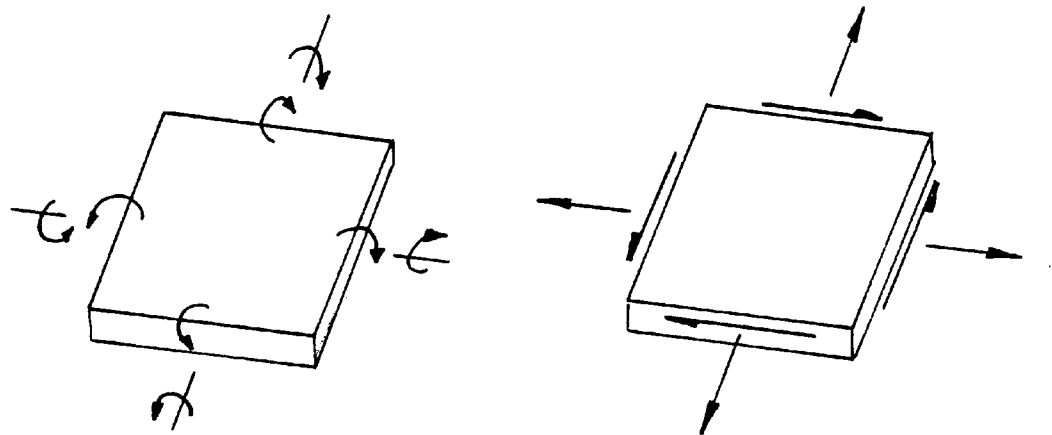
All the solution methods discussed in this chapter may be used for the analysis of multi-cell and box girder structures. The level of accuracy and the restrictions placed on geometry of the structure, loading, support conditions, etc., vary from method to method. The designer must decide from all the possible methods, the one that is best suited to his particular problem.

It has not been the intention in this chapter to make any recommendations to designers as to the most appropriate method of analysis for a particular situation. However, the following two conclusions have been formulated as a result of firstly, the author's experience and secondly, the review of the methods available for analysis.

1. Although the finite element method is accepted as the most accurate for a wide variety of structures, many designers are reluctant to use it, preferring other less accurate methods if they are considered appropriate for the problem in hand.
2. The grillage method stands out amongst all others, as a simple, straightforward approach which has become a popular design method in most design offices. Because of the simplified techniques for the idealization of multi-cell structures, its degree of accuracy is questionable, especially in the case of thin-walled steel structures. However, it is considered that this method, from all the methods discussed, is the most appropriate to satisfy the stated aim of this project.



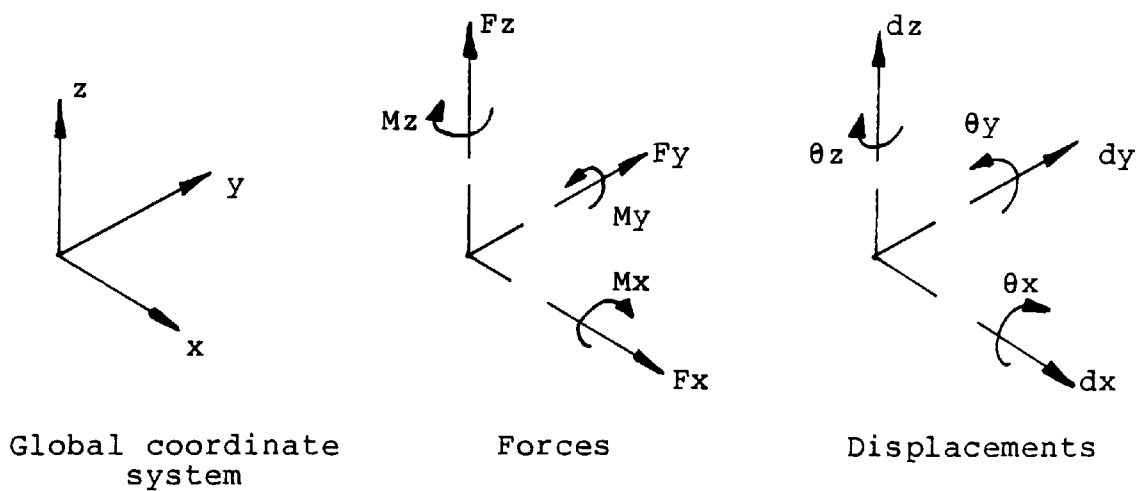
(a) Structure represented by quadrilateral elements.



Flexural resistance
bending and twisting moments

In-plane resistance
direct forces and shear

(b) Element resistance.



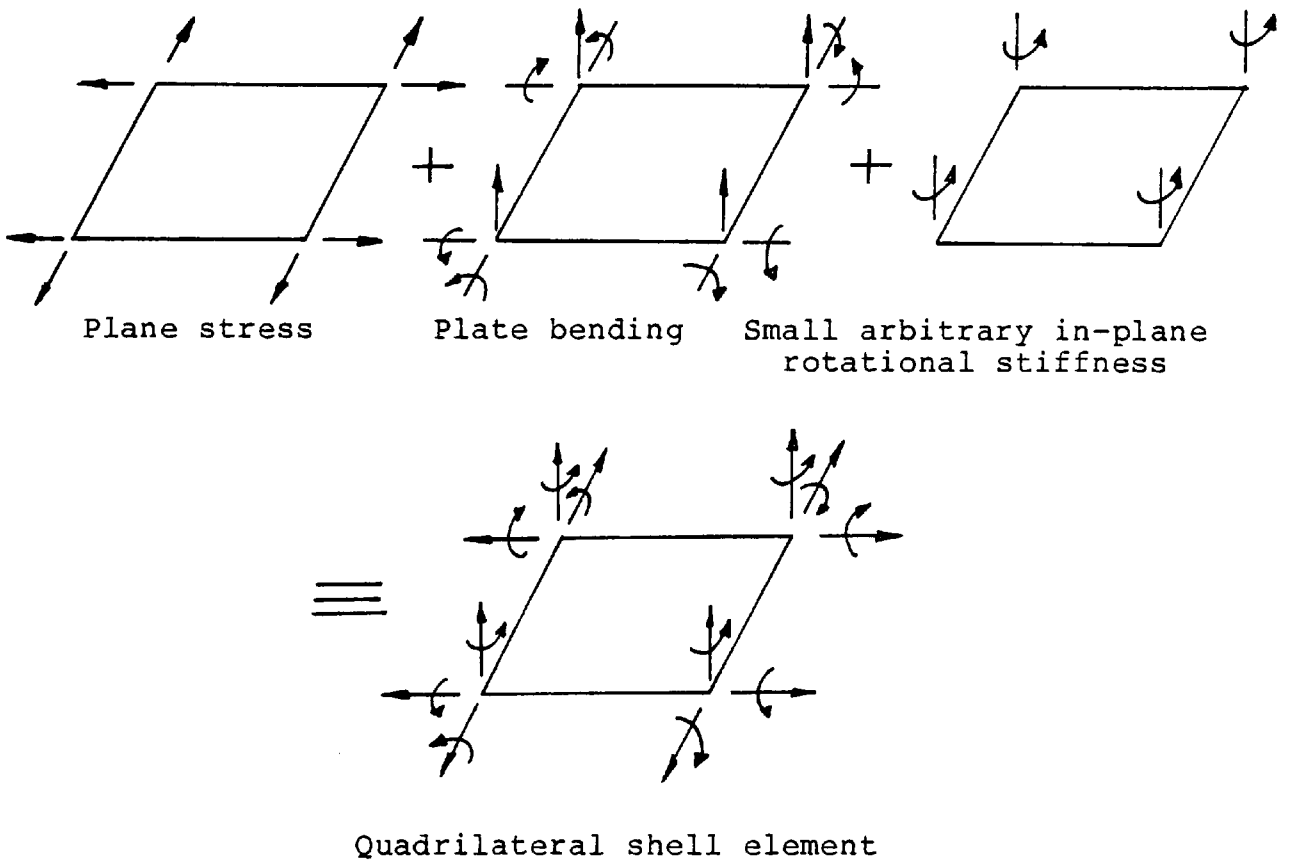
Global coordinate
system

Forces

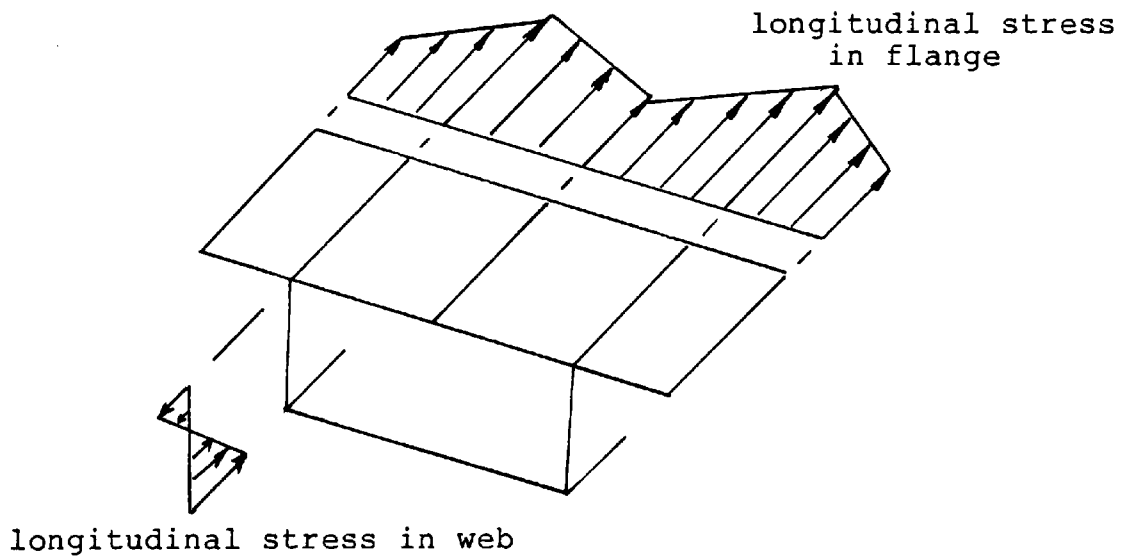
Displacements

(c) Axes and degrees of freedom.

FIGURE 2.1. - FINITE ELEMENT IDEALIZATION OF STRUCTURE.

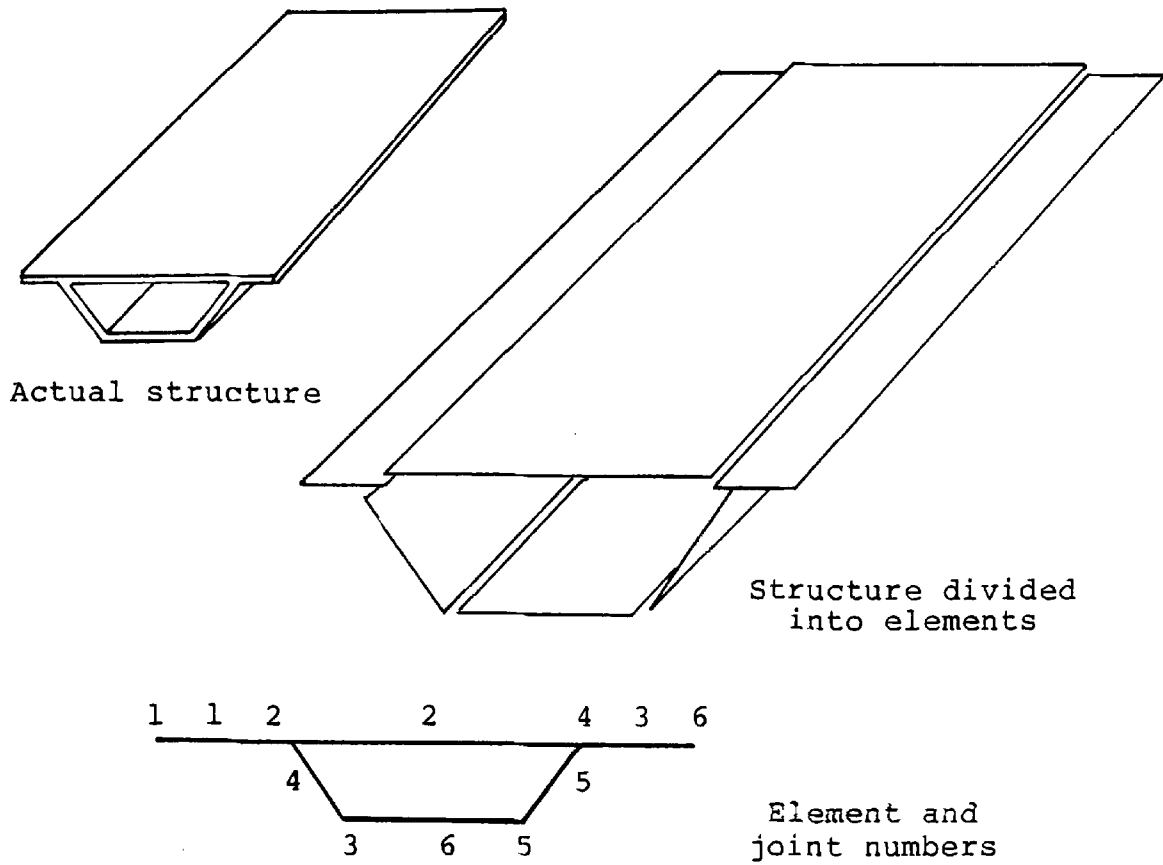


(a) Formulation of element stiffness matrix.

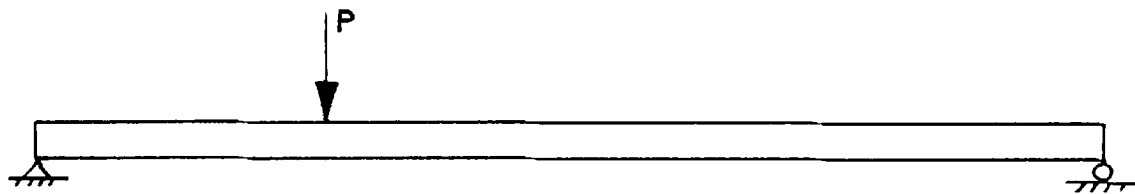


(b) Linear stress variation in elements.

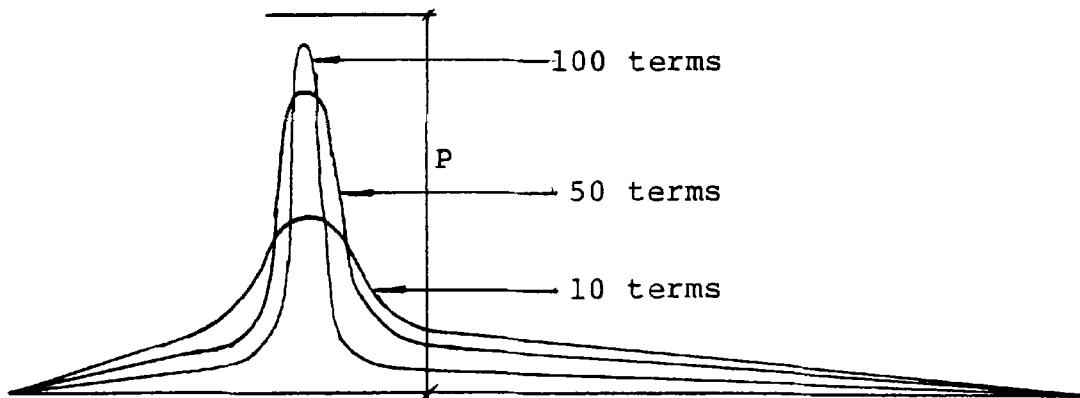
FIGURE 2.2. - FINITE ELEMENT IDEALIZATION OF STRUCTURE.



(a) A typical Box Section bridge.



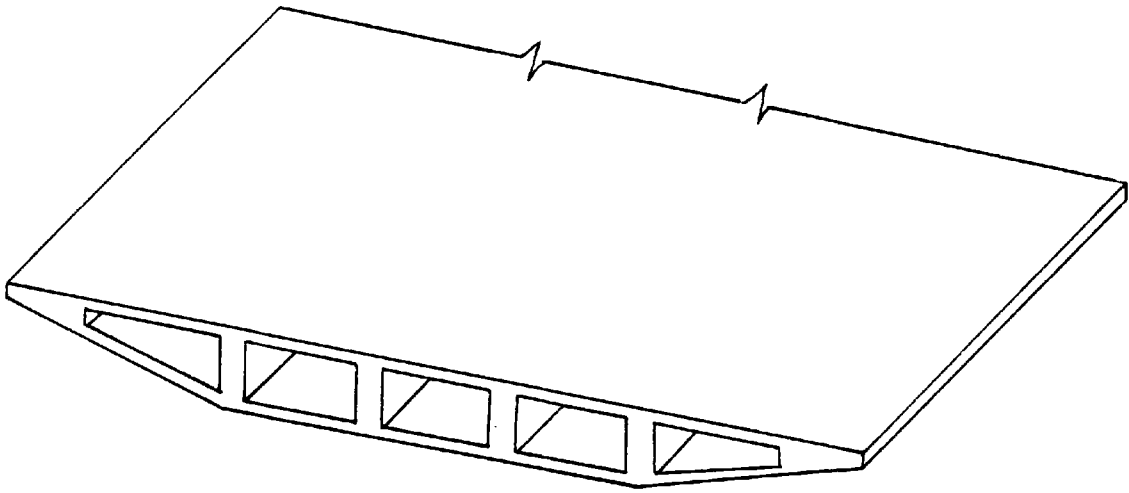
(i) transverse line load on bridge.



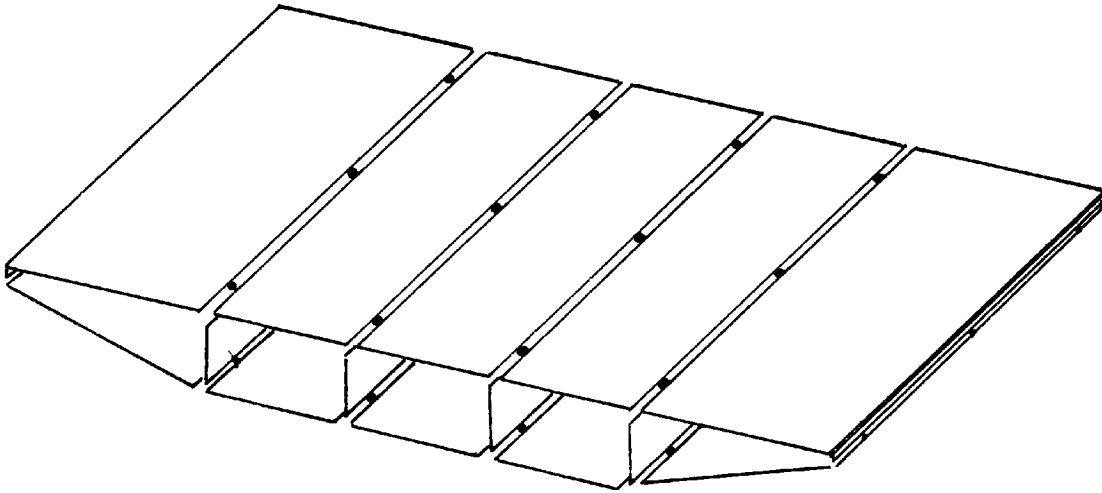
(ii) fourier representation.

(b) Harmonic Analysis - representation of a line load.

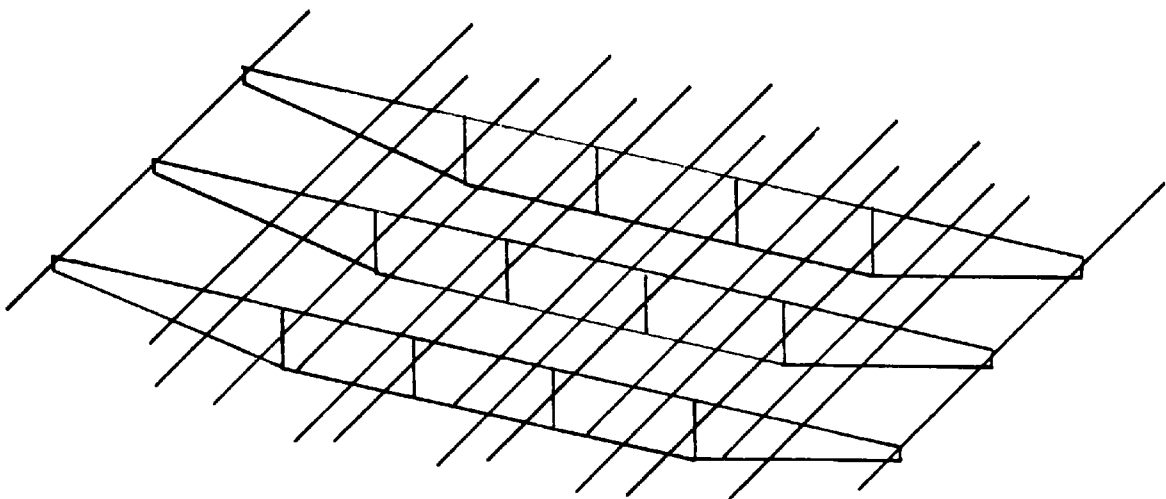
FIGURE 2.3. - FOLDED PLATE METHOD.



(a) Actual Structure.

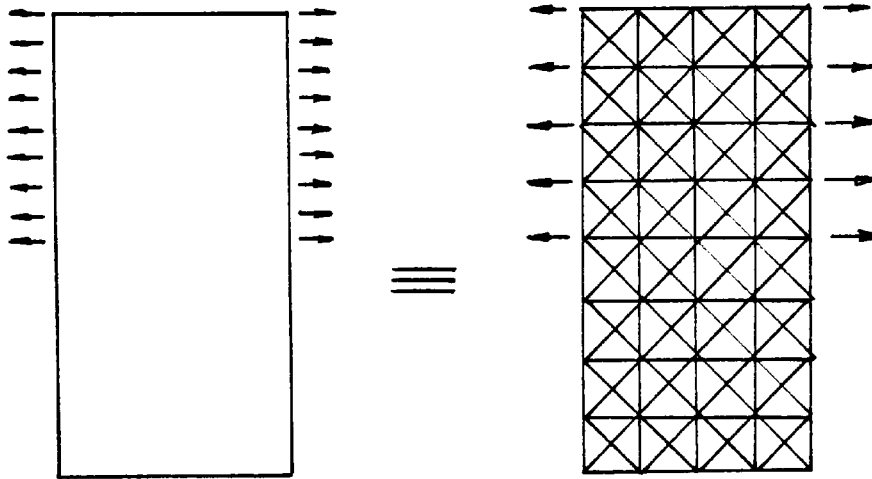


(b) Plates connected at discrete points.

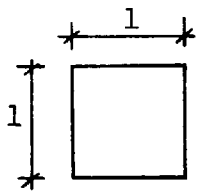


(c) Equivalent space frame.

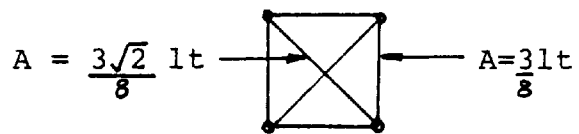
FIGURE 2.4. - SPACE FRAME IDEALIZATION
OF MULTI-CELL STRUCTURE.



(i) plate (thickness t) (ii) equivalent lattice frame

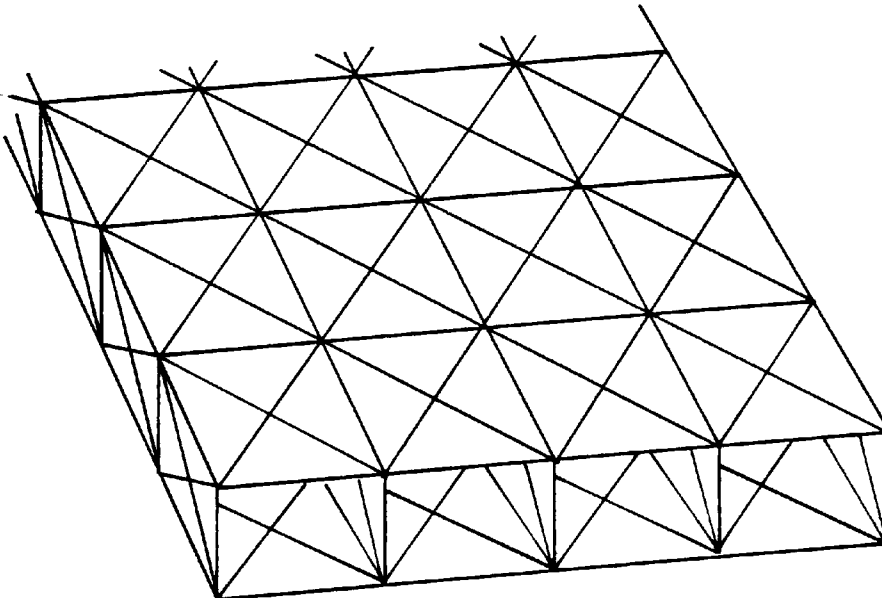


(iii) plate element



(iv) pin-jointed lattice

(a) McHenry Lattice.



(b) McHenry Lattice space truss model.

FIGURE 2.5. - MCHENRY LATTICE IDEALIZATION OF MULTI-CELL STRUCTURE.

CHAPTER THREE

DEVELOPMENT OF GRILLAGE IDEALISATION FOR THE ANALYSIS OF MULTI-CELL STRUCTURES

3.1. INTRODUCTION.

A structure that consists of a number of intersecting beam members is termed a "Grillage". The members are connected at their ends via rigid joints, which allow the members to rotate about orthogonal axes and deflect normal to the plane of the structure. Because the in-plane effects are considered negligible, and hence may be ignored, the structure resists the applied loading by the development of shear forces, twisting moments and bending moments in the beam members.

The analysis of structures of this form requires the solution of the equilibrium equations that are established at the joints between the external applied loads and the internal member forces. The member forces are related through the stiffness characteristics of the member to the joint displacements. In the analysis the joint displacements are the unknown quantities which can be calculated for any loading and support conditions. This method of analysis is termed the "stiffness" or the "displacement" method.

Bridge decks that consist of a system of longitudinal and transverse beams may be considered as grillages, and hence can be analysed as such. However the

recent trend in bridge construction has been towards the use of slab or pseudo-slab superstructures. This requires the idealization of the slab deck using intersecting beam members forming an equivalent grid or grillage.

In the classical plate analysis the bending and twisting stiffnesses of a plate have been defined by two orthogonal rigidities. This suggests that an analogy exists between a plate and an orthogonal grid, with the possibility of analysing plates as equivalent grillages. WEST (1973) has made a valuable contribution to the idealization of slab and pseudo-slab decks using equivalent grillages. This development has resulted in the grillage method being used extensively for the analysis of bridge decks of various form and geometry.

The use of the grillage method for the analysis of concrete cellular decks has also been investigated by SAWKO (1968) and HAMBLY (1976). The application of the method for the analysis of ship double-bottom structures was investigated by SHANMUGAM (1978). This work showed how the method could be used for the solution of three-dimensional cellular steel structures where the effects of in-plane shear effects in both the flange plates and webs was significant. These structures tend to be two-way spanning and contain diaphragms or webs in both directions, hence distortion of the cross-section does not present a problem in the grillage idealization.

This and the following chapter will consider the suitability of the grillage method for the analysis of

steel cellular bridge decks, where the absence of in-span diaphragms results in considerable cross-sectional distortion under load. Various methods of idealization will be presented, their validity investigated and recommendations made with respect to the most suitable method of structural idealization.

3.2. DEVELOPMENT OF GRILLAGE ELEMENT STIFFNESS MATRIX.

The stiffness method of analysis is well established and the basic theory has been documented in many texts and will not be repeated here. The formulation of the shear deformable grillage element stiffness matrix will be described with reference to the global axes system used.

A grillage beam element has nodes at both ends, each node possesses three degrees of freedom, one displacement and two rotations about mutually perpendicular axes. These displacements are associated with transverse shear force, torsion moment and bending moment as shown in figure 3.1.

The relationship between applied member force F and the nodal displacement d may be expressed as follows

$$\{F\} = [K]\{d\} \quad \text{---- eqn 3.1}$$

where $[K]$ is the element stiffness matrix which when expanded to include all three member end forces and displacements, becomes

$$\begin{Bmatrix} Pz1 \\ Mx1 \\ My1 \\ Pz2 \\ Mx2 \\ My2 \end{Bmatrix} = [K] \begin{Bmatrix} dz1 \\ \theta x1 \\ \theta y1 \\ dz2 \\ \theta x2 \\ \theta y2 \end{Bmatrix} \quad \text{----- eqn 3.2}$$

where Pz = member shear force
 Mx = member torsion moment
 My = member bending moment

and $[K]$ = member stiffness matrix which may be written in full as follows

$$[K] = \begin{bmatrix} \frac{12EI}{L^3} & 0 & \frac{6EI}{L^2} & -\frac{12EI}{L^3} & 0 & \frac{6EI}{L^2} \\ 0 & \frac{GJ}{L} & 0 & 0 & -\frac{GJ}{L} & 0 \\ \frac{6EI}{L^2} & 0 & \frac{4EI}{L} & -\frac{6EI}{L^2} & 0 & \frac{2EI}{L} \\ -\frac{12EI}{L^3} & 0 & -\frac{6EI}{L^2} & \frac{12EI}{L^3} & 0 & -\frac{6EI}{L^2} \\ 0 & -\frac{GJ}{L} & 0 & 0 & \frac{GJ}{L} & 0 \\ \frac{6EI}{L^2} & 0 & \frac{2EI}{L} & -\frac{6EI}{L^2} & 0 & \frac{4EI}{L} \end{bmatrix} \quad \text{-- 3.3}$$

where E = Modulus of Elasticity
 G = Modulus of Rigidity
 L = length of member
 I = second moment of area of member
 J = polar second moment of area of member

When the grillage element is used in the idealization of structures where shear deflection may be significant, the element stiffness matrix must be modified to include the effects due to shear deflection. The derivation of the revised element stiffness matrix is presented in Appendix A using the principle of virtual work. Equation 3.3 can also be confirmed if the shear force contribution is ignored.

The revised element stiffness matrix may be written as follows

$$[K] = \begin{bmatrix} \frac{12EI(N1)}{L^3} & 0 & \frac{6EI(N1)}{L^2} & \frac{-12EI(N1)}{L^3} & 0 & \frac{6EI(N1)}{L^2} \\ 0 & \frac{GJ}{L} & 0 & 0 & \frac{-GJ}{L} & 0 \\ \frac{6EI(N1)}{L^2} & 0 & \frac{4EI(N2)}{L} & \frac{-6EI(N1)}{L^2} & 0 & \frac{2EI(N3)}{L} \\ \frac{-12EI(N1)}{L^3} & 0 & \frac{-6EI(N1)}{L^2} & \frac{12EI(N1)}{L^3} & 0 & \frac{-6EI(N1)}{L^2} \\ 0 & \frac{-GJ}{L} & 0 & 0 & \frac{GJ}{L} & 0 \\ \frac{6EI(N1)}{L^2} & 0 & \frac{2EI(N3)}{L} & \frac{-6EI(N1)}{L^2} & 0 & \frac{4EI(N2)}{L} \end{bmatrix} \quad \text{-- 3.4}$$

$$\text{where } N1 = 1/(1+2N)$$

$$N2 = (1+0.5N)/(1+2N)$$

$$N3 = (1-N)/(1+2N)$$

$$N = 6EI / GAsL^2$$

and As = effective shear area of cross-section

This element stiffness matrix was incorporated in the grillage program, SHEARGRID2, developed to run on a 32K Commodore micro-computer which was used to analyse the

multi-cell structures described later in this chapter. The accuracy of this program was verified using the grillage element of the established mainframe program STRESS.

3.3. IDEALIZATION OF MULTI-CELL STRUCTURES.

3.3.1. INTRODUCTION.

The accuracy of the analysis of any structure using the grillage method is dependent on the geometrical and sectional idealization. The geometrical idealization involves the establishment of an equivalent grillage layout from the actual structure geometry, whilst the sectional idealization requires correct apportioning of the stiffnesses to the equivalent grillage members. Recommendations have been made by WEST (1973) and HECB (1981) for the idealization of slab and pseudo-slab bridge decks.

3.3.2. GEOMETRICAL IDEALIZATION.

The geometrical idealization of a multi-cell structure will be described with reference to the three cell structure shown in figure 3.2. The structure spans 16 metres simply supported, has an overall width of 9 metres and an overall depth of 1.5 metres. There are diaphragms at each support only. The flange, web and diaphragm plates are 1.2cm in thickness.

The equivalent grillage consists of a number of orthogonal longitudinal and transverse beam elements as

shown in figure 3.3(a). One grillage beam is used to represent each longitudinal web, hence the longitudinal representation requires a total of four grillage beams. The longitudinal grillage beams also represent the top and bottom flange plates and it is assumed that the plates are divided at the mid-web position and shared appropriately to the adjacent webs as shown in figure 3.3(b).

In the transverse direction the idealization is not so apparent. A grillage beam will be used to represent each support diaphragm and the provision of additional grillage beams will be dependent on a number of factors. When the structure contains one or more in-span diaphragms, grillage beams will be provided at least at each diaphragm location.

When no diaphragms are present then a grillage beam is provided at midspan in order that displacement and member force effects can be calculated at this critical section. Additional beams are included to provide satisfactory distribution of loading amongst the longitudinal members. These additional transverse grillage beams represent the top and bottom flange plates over a width equal to the spacing of the chosen grillage beams, as shown in figure 3.3(c). It is considered that the minimum number of transverse beams should be five. The relationship between the number of transverse grillage beams and the accuracy of the grillage analysis will be discussed in chapter five.

The grillage idealization using four longitudinal and five transverse grillage beams, shown in figure 3.3(a), comprises 20 joints and 31 elements. This produces a 60 degree of freedom problem with a narrow band width which allows solution to be achieved using a low cost micro-computer.

3.3.3. SECTIONAL IDEALIZATION.

Sectional idealization is concerned with the determination of appropriate stiffness parameters for the equivalent grillage layout in order that it will accurately model the actual structure. It was shown in section 3.2 that the element stiffness matrix is defined in terms of a number of parameters. The material parameters of moduli of elasticity and rigidity, E and G , are known. The length of the element has been defined by the geometrical idealization. The stiffness parameters that have to be determined for both the longitudinal and transverse grillage beams are second moment of area (or bending inertia), polar second moment of area (or torsional inertia) and effective shear area.

Multi-cell structures resist applied loads by a combination of longitudinal bending, transverse bending, torsion and distortion. Figure 3.4 shows the displacement and deformation of the cross-section of a three cell structure split up into these four principal modes. It is the consideration of these four modes that determines the appropriate stiffness parameters for the equivalent grillage layout.

Consideration of longitudinal bending will determine the second moment of area and the effective shear area of the longitudinal beams. Correspondingly transverse bending will determine the second moment of area, and if diaphragms are present the effective shear area of the transverse grillage beams. The torsional twisting of the cross-section will be shared between the longitudinal and transverse beams and will determine the torsional inertia of the longitudinal and transverse beams. Finally, distortion of the cross-section can be modelled by using either an equivalent beam or equivalent frame representation for the transverse grillage beams.

Each of these four principal modes of structural behaviour will be investigated in this and the following chapter, and recommendations given as to the most suitable method of sectional idealization for steel multi-cell structures.

3.4. LONGITUDINAL BENDING.

3.4.1. SECOND MOMENT OF AREA.

When single or multi-cell structures are subjected to longitudinal bending moments each flange plate is subjected to longitudinal in-plane shear forces developed by virtue of the interaction between the flange and web plates. These forces are illustrated in figure 3.5 for a single cell structure subjected to a symmetrical loading arrangement, in which case the edge forces are of equal magnitude.

If the flange plates had an infinite shear stiffness, then the longitudinal stress set up within the flange plate would be uniform across the full width, the magnitude of this uniform stress being determined using the theory of simple bending. When the structure comprises wide, thin flange plates a non-uniform distribution of longitudinal stress will be developed across the full width of the flange plates, as shown in figure 3.5. This phenomenon, known as "shear lag", is produced because of the shear deformations set up within the flange plates.

The longitudinal stresses will be a maximum at the flange/web intersection and a minimum midway between the webs. Neglect of the shear lag effect will lead to an underestimation of the stresses developed in the flange plates of cellular structures. The practice of representing the effect of shear lag by adopting the concept of effective breadth, in which the actual flange plate width is replaced by a reduced width over which the longitudinal stress may be considered to be uniformly distributed, has been adopted by design engineers. This uniform stress is assumed equal to the maximum stress at the flange/web intersection, and is shown in figure 3.6.

A comprehensive parametric study of the shear lag phenomenon in box girders was described by MOFFATT and DOWLING (1972) using the finite element method. The results obtained from the study were used as the basis for the formulation of the INTERIM DESIGN RULES (1973) and more recently in the Steel Bridge Code BS 5400 (1982). These

rules provide effective breadth ratios which enable the effective flange width to be determined at all positions on the span of a box girder of any plan dimensions and cross-sectional proportions subjected to distributed or concentrated loading.

To allow deflections of box girders to be determined the study proposed the use of the effective breadth ratio for the quarter span position under uniformly distributed loading for the calculation of the appropriate second moment of area of the box girder. This effective breadth ratio is used to determine the effective width of flange plates for the calculation of the second moment of area of the longitudinal grillage beams.

The second moment of areas of the longitudinal grillage beams shown in figure 3.3 were evaluated in accordance with Part 3 of BS 5400 as follows

$$\begin{aligned}
 2b &= \text{width of flange plates between webs} = 300\text{cm.} \\
 L &= \text{span of beams} = 1600\text{cm.} \\
 b/L &= 0.1875 \\
 \psi &= \text{effective breadth ratio for deflection calculations} \\
 &\quad (\text{Table 4, Part 3, BS 5400}) = 0.936 \\
 &\quad \text{web and flange thickness} = 1.2\text{cm.}
 \end{aligned}$$

External grillage beam.

$$\begin{aligned}
 \text{effective flange width} &= 0.936 * 150 = 140.4\text{cm.} \\
 \text{second moment of area, } IY &= \frac{1.2 * 150^3}{12} + 2 * 140.4 * 1.2 * 75^2 \\
 &= \underline{2\,232\,900\text{ cm}^4}
 \end{aligned}$$

Internal grillage beam.

$$\begin{aligned}\text{effective flange width} &= 0.936 * 300 = 280.8\text{cm.} \\ \text{second moment of area, } IY &= \frac{1.2 * 150^3}{12} + 2 * 280.8 * 1.2 * 75^2 \\ &= \underline{4\ 128\ 300\ \text{cm}^4}\end{aligned}$$

3.4.2. EFFECTIVE SHEAR AREA.

The effect of shear deformation must be considered in the analysis of thin walled cellular structures when the span/depth ratio of the web is low. For the structure defined in figure 3.2, where the span/depth ratio is 10.7, the contribution of shear deflection to the overall deflection of the inner web under symmetrical point loading at midspan was found to be 20%. These effects can be considered by including the effective shear area of the web in the grillage analysis.

The effective shear area of the equivalent grillage beams was taken as equal to the cross sectional area of the web by SHANMUGAM (1978). This approach is consistent with that of JUST (1978) and GERE and WEAVER (1965) who introduced the parameter, β , the form factor for the section where

$$\beta = \frac{\text{total area of cross-section}}{\text{effective shear area of cross-section}} \quad \text{--- 3.5}$$

and the effective shear area of the cross-section is defined as the depth of the section multiplied by the web thickness i.e. the area of the web.

MEGSON (1980) showed that the form factor, β , can be determined for any shape of cross section using the equation

$$\beta = \frac{A}{IY^2} \int_A \frac{(A' \bar{y})^2}{b_o} dy \quad \text{----} \quad 3.6$$

where A = total area of cross section

IY = second moment of area of cross section

y = distance from neutral axis to section X-X

A' = area of cross section above X-X

\bar{y} = distance from neutral axis to centroid of A'

b_o = width of cross section at section X-X

It was considered that the significance of shear deflection merited an investigation of the value of the form factor, β , for the cross-sections used in the longitudinal idealization of multi-cell structures. Equation 3.6 was used to determine the effective shear area, A_s , for the typical cross-section shown in figure 3.7(a) where

flange width = bf cm.

flange thickness = 1.2cm.

web thickness = 1.2cm.

distance between centroid of flanges = 150cm.

giving

$$A = 2(1.2 * bf + 74.4 * 1.2) = 2.4(bf + 74.4) \text{ cm}^2$$

$$\text{and } IY = \frac{bf * 151.2^3}{12} - \frac{(bf - 1.2) * 148.8^3}{12}$$

$$= (0.0135bf + 0.329465) * 10^6 \text{ cm}^4$$

hence
$$\beta = \frac{2A}{IY^2} \left[\int_0^{74.4} \frac{(A'\bar{y})^2 dy}{bw} + \int_{74.4}^{75.6} \frac{(A'\bar{y})^2 dy}{bf} \right]$$

Calculation showed that the contribution of the second term was insignificant and when ignored

$$\beta = \frac{2A}{bw IY^2} \int_0^{74.4} \left[90bf + 1.2(74.4 - y) \frac{(74.4 + y)}{2} \right]^2 dy \quad \text{---- 3.7}$$

and taking effective shear area , $As = A / \beta$ ---- 3.8

then equation 3.7 and 3.8 reduces to

$$As = \frac{181.45bf^2 + 8856.586bf + 108071.67}{bf^2 + 49.203bf + 726.286} \quad \text{---- 3.9}$$

This equation is plotted in figure 3.8(a) and shows that the effective shear area, As , quickly converges to a value approximately equal to the depth of the section multiplied by the thickness of the web, i.e. $151.2 * 1.2 = 181.44 \text{ cm}^2$, the cross-sectional area of the web. When the value of bf is taken as zero, that is the section is rectangular in form, the form factor is equal to the correct value of 1.2.

The effect of the variation in the flange thickness was also considered in the analysis of the section detailed in figure 3.7(b) where the flange thickness was increased to 3.6cm. all other parameters remaining constant. A similar analysis produced the following expression for effective shear area

$$A_s = \frac{184.50bf^2 + 2858.279bf + 11070.29}{bf^2 + 15.876bf + 75.617} \quad \text{---- 3.10}$$

which is shown plotted in figure 3.8(b). Again the effective shear area, A_s , quickly converges to a value approximately equal to the area of the web, i.e. 184.32 cm².

These investigations show that when the ratio of depth of section to effective breadth of flange is not less than 2, the effective shear area may be taken as the depth of the section multiplied by the web thickness, and this value has been used in all subsequent analyses.

3.4.3. SINGLE CELL STUDY.

The use of simple beam theory for the analysis of single cell structures, can be considered as the simplest application of the grillage method for the analysis of cellular structures. In this section it is proposed that the accuracy of the simple beam theory can be compared to finite element solutions. These comparisons will indicate what level of accuracy can be expected when the grillage method is applied to multi-cell structure analysis.

The single cell box considered is shown in figure 3.9(a), where

$$\begin{aligned} \text{flange breadth, } 2b &= 300 \text{ cm.} \\ \text{web depth, } D &= 150 \text{ cm.} \\ \text{flange, web and diaphragm thickness} &= 1.2 \text{ cm.} \end{aligned}$$

Three different simply supported span values of 9, 16 and 24 metres were considered. The boxes were subjected to midspan point loads and uniformly distributed loads over each web. The load intensities are indicated in figure 3.9(b).

The effect of varying the flange thickness was considered with the 16 metre span box analysed with a flange thickness of both 1.2 cm. and 3.6 cm.

The simple beam theory method will be illustrated with respect to the 16m. span box with the flange thickness of 1.2cm. Tables 4 and 13, Part 3, BS 5400 give the following effective breadth ratios for stress calculations.

point load	(midspan)	$\Psi = 0.686$
point load	(quarterspan)	$\Psi = 1.000$
line load	(midspan)	$\Psi = 0.954$
line load	(quarterspan)	$\Psi = 0.936$

and for deflection calculations

point and line load	$\Psi = 0.936$
---------------------	----------------

producing the following values of second moment of area, IY , for

- (i) deflection and line load stress calculations at quarterspan = 4 465 800 cm⁴
- (ii) line load stress calculations at midspan = 4 538 700 cm⁴
- (iii) midspan point load stress calculations at midspan = 3 453 300 cm⁴
- (iv) midspan point load stress calculations at quarterspan = 4 725 000 cm⁴

and the effective shear area, $A_s = 360 \text{ cm}^2$

Midspan Point Load.

$$\begin{aligned} \text{midspan bending moment} &= 240\,000 \text{ kNcm.} \\ \text{midspan bending stress} &= \frac{240\,000 * 75 * 10}{3\,453\,300} \\ &= 52.12 \text{ N/mm}^2 \\ \text{quarterspan bending moment} &= 120\,000 \text{ kNcm.} \\ \text{quarterspan bending stress} &= \frac{120\,000 * 75 * 10}{4\,725\,000} \\ &= 19.05 \text{ N/mm}^2 \end{aligned}$$

The relevant deflection formulae at midspan and quarterspan for both midspan point load and line load cases are derived in Appendix B and have the following values

$$\begin{aligned} \text{midspan deflection} &= \frac{WL^3}{48EIY} + \frac{WL}{4GAs} \\ &= 0.546 + 0.083 \\ &= 0.629 \text{ cm.} \\ \text{quarterspan deflection} &= \frac{11WL^3}{768EIY} + \frac{WL}{8GAs} \\ &= 0.375 + 0.041 \\ &= 0.416 \text{ cm.} \end{aligned}$$

Uniform Line Load.

$$\begin{aligned} \text{midspan bending moment} &= 360\,000 \text{ kNcm.} \\ \text{midspan bending stress} &= \frac{360\,000 * 75 * 10}{4\,538\,700} \\ &= 59.49 \text{ N/mm}^2 \\ \text{quarterspan bending moment} &= 270\,000 \text{ kNcm.} \\ \text{quarterspan bending stress} &= \frac{270\,000 * 75 * 10}{4\,465\,800} \\ &= 45.34 \text{ N/mm}^2 \end{aligned}$$

$$\begin{aligned}
\text{midspan deflection} &= \frac{5WL^3}{384EIY} + \frac{WL}{8GAs} \\
&= 1.024 + 0.124 \\
&= 1.148 \text{ cm.}
\end{aligned}$$

$$\begin{aligned}
\text{quarterspan deflection} &= \frac{19WL^3}{2048EIY} + \frac{3WL}{32GAs} \\
&= 0.729 + 0.093 \\
&= 0.822 \text{ cm.}
\end{aligned}$$

This single cell box was also analysed using the grillage program SHEARGRID2 based on the idealization shown in figure 3.9(c). Two longitudinal beams were used to model each web and five transverse beams allowed deflection and bending moment values to be obtained at quarterspan and midspan positions. The results thus obtained agreed exactly with the simple beam theory values presented above.

To determine the accuracy of the simple beam method the structures were also analysed using the finite element solution package QUEST (1974), which has been used for many years for the solution of box girder bridge decks. Earlier work by TAHERIAN and EVANS (1977) and EVANS and SHANMUGAM (1979) indicated that the finite element mesh shown in figure 3.10(a) would produce results of acceptable accuracy.

The mesh comprised 8 elements across each flange plate, 1 element in the depth of each web and end diaphragm and 20 elements along the span with a graded region at midspan. Other mesh configurations were considered as part of a convergence study on the accuracy of the results, and are discussed in Appendix C.

The contribution of web shear effects to the overall behaviour of the structure brought into question the validity of modelling the webs using only one element. Consequently a further convergence study was undertaken where the webs were modelled using up to 8 elements in their depth. These results are also presented in Appendix C.

The three single cell structures were also analysed using the fine mesh shown in figure 3.10(b) where one quarter of the structure was modelled using 6 elements across each half flange, 8 elements in each web plate and 12 elements representing half the span.

The results from both finite element analyses are presented together with the grillage (or simple beam theory) results in Tables 3.1, 3.2, 3.3 and 3.4. Consideration of the results for the 16m. span box with a flange thickness of 1.2cm., presented in Table 3.2, produced the following conclusions.

Uniform Line Load.

1. Both finite element idealizations produced results of comparable accuracy. The maximum flange edge stress, web deflection and effective breadth ratio agreeing closely with a maximum difference of 2%.
2. The effective breadth ratio calculated from the finite element analyses agreed with the value specified in BS 5400 for both the midspan and quarterspan positions with a maximum discrepancy of 0.5%.

3. The web deflection at both midspan and quarterspan calculated by the grillage method using the effective breadth ratio agreed with the finite element solutions with a maximum discrepancy of 3%.
4. The maximum flange edge stress showed a maximum difference of only 1.3% at the quarterspan position.

Midspan Point Load.

5. The finite element results agreed closely for flange edge stress and effective breadth ratio at the quarterspan position. At midspan the maximum flange edge stress varies from 48.20 N/mm² to 52.10 N/mm² and the effective breadth ratio varied from 0.741 to 0.693, the BS 5400 value being 0.686. There was an 8.1% overestimation of the stress using the grillage method when compared with the coarse mesh finite element analysis. These results show that the accuracy of the stress under the point load, predicted by the finite element analysis, must be questionable. The level of stress obtained is directly related to the fineness of the mesh used in the idealization of the structure. (The convergence study in Appendix C confirms this conclusion).
6. The web deflections at both midspan and quarterspan calculated by the grillage method agreed with the finite element solutions with a maximum discrepancy of 1.7%. The closer agreement was obtained using the coarse mesh finite element idealization.

The analysis of the 24m span box girder, presented in Table 3.4, produced similar results. The uniform line load case showed close agreement between both finite element analyses and the grillage analysis for maximum flange edge stress, web deflection and effective breadth ratio. The quarter span flange edge stress produced the largest difference of only 1.7%.

The results at quarterspan for the midspan point load case showed an accuracy of 99%. It should be noted that the effective breadth ratio at this position was unity and the contribution of shear effects to the total deflection was only 5%. At the midspan position the maximum flange edge stress varied from 44.27 N/mm² to 46.47 N/mm². The effective breadth ratio varied from 0.824 to 0.790, the BS5400 value being 0.768. This variation between the finite element analyses was similar to that for the 16m. span case.

The results for the 9.6m. span box, presented in Table 3.1, show a significant reduction in accuracy when compared to the 16m. and 24. span values. At this breadth/span ratio and depth/span ratio the effects of shear lag in the flange and shear deformation in the web are considerable. The following conclusions were drawn from a study of the results.

Uniform Line Load.

1. The midspan values of flange edge stress and effective breadth ratio were in close agreement with a maximum difference of 1.4%.
2. The quarterspan effective breadth ratio differed from the BS 5400 value of 0.840 by 7.3% and 9.6% for the coarse and fine mesh finite element analyses. This discrepancy resulted in the grillage method underestimating the web deflection at midspan by 7.2% and quarterspan by 10.6%. The quarterspan flange edge stress was also underestimated by 7.1%.

Midspan Point Load.

3. The midspan and quarterspan web deflections were also underestimated using the grillage method by 6.0% and 7.3% respectively, because of the discrepancy of the line load effective breadth ratio at quarterspan.
4. The effective breadth ratio at the midspan and quarterspan positions calculated from the finite element analyses showed discrepancies of +7.0% and -5.1% for the coarse mesh, and -4.0% and -8.2% for the fine mesh, when compared to the BS 5400 values of 0.569 and 0.989 respectively.
5. The maximum flange edge stress varied from 56.14 N/mm² to 63.67 N/mm² at midspan again showing the difficulty in determining the stress under concentrated point loads. The grillage value of 60.41 N/mm² showed a

variation of +7.6% to -5.1% from the finite element analyses.

6. The maximum flange edge stress at quarterspan also varied from 20.09 N/mm² to 20.71 N/mm² indicating an underestimation of the stress by the grillage method.

The results for the 16m. span box with the thickened flange plates, where $t_f = 3.6\text{cm.}$, are presented in Table 3.3. These results follow a similar pattern to those for the same box with $t_f = 1.2\text{cm.}$, Table 3.2. The web deflection values are less accurate with a maximum underestimation of 6.2% ($t_f = 3.6\text{cm.}$) and 3.0% ($t_f = 1.2\text{cm.}$) at quarterspan under uniform line load. The web shear deflection contribution where $t_f = 3.6\text{cm.}$ is double that of the box where $t_f = 1.2\text{cm.}$

The web shear deflection is 25% of the total deflection for both the 9.6m. span box and the 16m. span box with the thickened flange plates. These two structures show the greatest underestimation of deflection.

The following overall conclusions were reached from the single cell study.

1. The effective breadth ratio for stress calculations at midspan under midspan point loading was overestimated by the coarse mesh finite element analysis; this resulted in the similar overestimation of the maximum flange edge stress by the grillage method. This overestimation varied between 4.2% and 8.1%, and

suggests that a difference of up to 10% between the grillage and finite element methods can be expected when using the effective breadth ratios specified in Tables 4 and 13, Part 3, BS 5400.

2. The maximum flange edge stress at quarter span under midspan point load varied from an underestimation of 4.3% to an overestimation of 0.4%. When the flange breadth to span ratio is less than 0.2 (i.e. $b/L = 0.1$) the stress calculated by the grillage method should agree very closely to the finite element method.
3. The effective breadth ratio for stress calculations under uniform line load calculated by the coarse finite element mesh agrees very closely with the specified BS 5400 values. The one exception was the 9.6m. span box structure where the underestimation of the ratio by the finite element method was 7.3%. When the b/L ratio is less than 0.1 the effective breadth ratio agrees very closely and consequently the maximum flange edge stress calculated by the grillage method can be expected to agree to within 2% with the finite element method.
4. The web deflection at quarterspan and midspan calculated by the grillage method varied from an underestimation of 7.7% to an overestimation of 0.3% when compared to the coarse mesh finite element analysis. The underestimation of deflection occurred when the b/L ratio is 0.16 and the shear deflection contribution is 25% of the total deflection. When the b/L ratio is less than 0.1 and the shear deflection

contribution less than 13%, the deflection can be expected to agree to within 2% with the finite element result.

3.4.4. MULTI-CELL STUDY.

The preceding section investigated the analysis of single cell structures using the simple beam theory, which can be considered as an exact grillage analysis. In this section the grillage method will be used to analyse various multi-cell structures subjected to loading that produces a constant midspan deflection at all web positions under uniform line loading and midspan point loading. It was considered that this loading condition eliminated the distortional, torsional and transverse bending behaviour of the structures, and thus their longitudinal bending behaviour only could be investigated in isolation.

Three structures were analysed consisting of two, three and four cells. The cells were kept to constant proportions where

flange breadth, $2b$	= 300cm.
web depth, D	= 150cm.
flange thickness, t_f	= 1.2cm.
web thickness, t_w	= 1.2cm.
end diaphragm thickness, t_d	= 1.2cm.
simply supported span, L	= 16m.

Details of the structure, the loading intensities used to develop constant deflection across the cross-section and the finite element meshes used for the

analysis are shown in figures 3.11, 3.12 and 3.13 for the two, three and four cell structures respectively.

The grillage idealization consisted of a longitudinal beam representing each web plate and five transverse beams allowing deflections and stresses to be determined at the midspan and quarterspan positions. The three cell structure was idealized using a 4 * 5 grillage consisting of 20 nodes and 31 members. The structural idealization was carried out as described in section 3.3, and figure 3.3 shows the grillage layout for the three cell structure.

The grillage analysis was initially carried out with the transverse members being assigned stiffness properties that allowed for distortion of the cross-section, although it was considered that under this distribution of loading no distortion of the cross-section would occur. The results from this grillage analysis did not produce constant web deflections across the cross-section, consequently a second set of analyses was undertaken where no distortion of the cross-section was allowed for in the transverse member stiffness properties. The results from the finite element and both grillage analyses are presented in Tables 3.5 to 3.7 and analysis of these results produced the following conclusions.

1. The grillage method predicted the web deflections at the midspan and quarterspan positions under both loading_Λ for all three structures to within 97% of the finite element analyses.

The no-distortion grillage idealization produced the more accurate results revealing a maximum difference of only 1.7% for the four cell structure. The accuracy of the grillage method was independent of the number of cells in the structure and there was a variation of 2.0% and 3.2% in the results for the no-distortion and distortion idealizations respectively.

The levels of accuracy achieved by the grillage analyses was attributable to the accuracy of the effective breadth ratio used for deflection calculations. The BS 5400 value of 0.936 agreed very closely with the value calculated from the finite element study, which produced values of 0.92 and 0.93 for the three and four cell structures respectively. MOFFATT and DOWLING (1975) obtained values for deflection using the effective breadth ratios which differed by less than 5% when compared with finite element values.

2. The accuracy of the effective breadth ratio at quarterspan under uniform line load, used for deflection calculations, was also attributable to the accuracy of the quarterspan flange edge stresses under uniform line load. The grillage stresses varied from an underestimation of 3.4% for the two cell structure to an overestimation of 2.7% for the four cell structure, when compared with the finite element results. The results from the no-distortion grillage idealization

were marginally more accurate than the idealization which allowed for distortion of the cross-section.

3. At the midspan position under uniform line loading the effective breadth ratios calculated from the finite element analysis were 0.93, 0.94 and 0.95 for the two, three and four cell structures respectively. These values agree closely with the value of 0.954 specified in BS 5400. The midspan flange edge stresses from the grillage analysis are less accurate than the quarterspan stresses showing a variation of between -3.9% and +5.9% for the four cell structure with cross-section distortion.

The grillage method tends to overestimate the stress at the outer web/flange intersection and underestimate the stress at the innermost web/flange intersection. This variation increases with the number of cells and also when cross-section distortion is allowed for in the grillage idealization.

4. At the quarterspan position under midspan point loading the effective breadth ratios from the finite element analysis agreed very closely with the value of 1.00 specified in BS 5400. The flange edge stress at quarterspan shows a variation of between -2.7% and +6.6% for the four cell structure with cross-section distortion. The variation where no-distortion was allowed was less at -1.3% and +3.8%. The variation is directly proportional to the number of cells in the cross-section, being least for the two cell structure.

The stresses calculated by the grillage method were again overestimated for the outer web and underestimated for the innermost web position. The idealization for no-distortion of the cross-section produced more accurate results for all three structures.

5. The effective breadth ratio at midspan for midspan point loading specified in Table 13, Part 3, BS 5400 is 0.686. The finite element analyses of the two, three and four cell structures produced effective breadth ratios of 0.736, 0.749 and 0.735 respectively. The flange edge stress at midspan was consistently overestimated when compared with the finite element results, this overestimation varying from 6.8% to 11.7%.

There was a slight reduction in accuracy when the number of cells in the cross-section increased, from 9.0% to 10.6% and from 9.8% to 11.7% for the no-distortion and distortion idealizations respectively for the three structures analysed. The greatest overestimation was apparent at the outer web position, consistent with the results for the uniform line load case.

The deviation of the finite element values for effective breadth ratio from the BS 5400 value which was of the order of 7.3%, resulted in an underestimation of the second moment of area of 5.9% and 6.5% for the external and internal longitudinal

grillage beams respectively. This second moment of area was used in the determination of the stress in the grillage analysis, and was the major contribution to the overestimation of the flange edge stress.

3.4.5. CONCLUSIONS.

In the preceding sections the ability of the grillage method to analyse single and multi-cell structures subjected to longitudinal bending action was considered. The following conclusions were established from a consideration of the results.

1. The deflection at midspan and quarterspan sections at all web positions across the section should be predicted with 95% accuracy for b/L ratios not greater than 0.1 and when the contribution to overall deflection from web shear effects is not greater than 12%. When the b/L ratio increases to 0.15 and the shear deflection to 25% of the overall deflection then the calculated deflection may differ by up to 10% from the finite element value.
2. The flange edge stresses developed by uniform line loading over the webs should be predicted to within an accuracy of 5% to 8%.
3. The flange edge stresses developed by midspan point loads over the webs should be predicted to within an accuracy of 10% to 12% when using the effective breadth ratios specified in Table 13, Part 3, BS 5400.

Clause 6.3.2(b)(i) of the Interim Design Rules states that the effective breadth ratio from Table 6.1, which specifies the same ratios as Table 13, shall be multiplied by the factor

$$\alpha_p = 1.08 - 0.04 \frac{A_f}{A_w}$$

where A_f = total area of cross-section of entire flange under consideration

A_w = total area of cross-section of all web plates at the same section

This will produce α_p factors and effective breadth ratios for the structures with constant section thicknesses of 1.2cm. as follows.

No. of cells	α_p	ψ
1	1.040	0.713
2	1.027	0.704
3	1.020	0.700
4	1.016	0.697

The use of this factor although improving the accuracy of the stresses in the single cell structure by 4% only improves the accuracy of the four cell structure by 1.5%. For this reason and because the stresses are consistently overestimated using the BS 5400 ratios, and hence will tend to be on the safe side, the ratios specified in Table 13, Part 3, BS 5400 will be used.

4. In multi-cell structures the greatest overestimation of stress will occur at the outermost web position and reduce towards the centre of the cross-section. It is possible that there will be a slight underestimation of

the stress at the inner web positions especially under line loading.

3.5. TRANSVERSE BENDING.

The transverse bending action of the multi-cell structure has to be represented by the transverse beams used in the grillage idealization. This representation was shown in figure 3.3 for the three cell structure defined in figure 3.2. Each transverse internal grillage beam must represent the bending action of the top and bottom flange plates as shown. The second moment of area apportioned to the grillage beam is given by the full bending stiffness of the flange plates

$$IY = 2 * Af \left\{ \frac{D}{2} \right\}^2 \quad \text{---- 3.11}$$

where Af = area of portion of flange plate represented by grillage beam.

D = depth of structure

In the case of the external grillage beams, i.e. at the ends of the span, the effect of the end diaphragms must be included in the second moment of area calculations. In-span diaphragms are considered in the same manner, a transverse grillage beam being located at the diaphragm position.

For the structure defined in figure 3.2 where

span, L	= 16m.
depth, D	= 1.5m.
flange thickness, tf	= 1.2cm.
end diaphragm thickness, td	= 1.2cm.

and five transverse grillage beams are used in the idealization, the appropriate second moment of areas may be calculated as follows

Internal grillage beam.

$$\begin{aligned} IY &= 2 * 400 * 1.2 * 75^2 \\ &= \underline{5\,400\,000 \text{ cm}^4} \end{aligned}$$

External grillage beam.

$$\begin{aligned} IY &= 2 * 200 * 1.2 * 75^2 + \frac{1.2 * 150^3}{12} \\ &= \underline{3\,037\,500 \text{ cm}^4} \end{aligned}$$

The effects of shear deformation of diaphragms must also be considered in the transverse bending behaviour. The effective shear area of the diaphragm, i.e. the product of diaphragm thickness and depth of section, must be included in the idealization of the appropriate grillage beams.

For the particular structure considered the effective shear area of $1.2 * 150 = 180\text{cm}^2$. is assigned to the external transverse grillage beams.

3.6. DISTORTION.

3.6.1. INTRODUCTION.

In box girders and other cellular and voided structures without intermediate transverse diaphragms, cell distortion may occur due to the secondary bending of the flanges and webs. This effect would be pronounced in steel box sections consisting of thin flange and web plates, producing highly localized effects in the vicinity of the load. WEST (1973) suggested that cell distortion should be taken into account when the void area in cellular sections exceeds 60% of the total cross-section.

In thin-walled cellular sections, cell distortion results in substantial variation in web deflection, and hence longitudinal bending moment, across the width of the section. Although this behaviour cannot be reproduced precisely in an equivalent grillage, an approximation to this behaviour can be introduced by the use of appropriate bending or shear stiffness properties for the transverse grillage beams.

Both CUSENS (1974) and HAMBLY (1976) compared the behaviour of the cross-section to the deformation of a Vierendeel frame of elevation similar to the cross-section of the deck. Cusens proposed that the transverse flexural rigidity to be used in the load distribution analysis of cellular concrete decks could be determined by comparing deflections, or slopes at supports, of an equivalent beam to the vierendeel frame. Using this proposal the flexural

rigidity of the transverse grillage beams would be adjusted to allow the grillage to model cell distortion.

Hambly proposed that the vierendeel frame behaviour can be introduced by giving the transverse grillage beams a low shear stiffness. The stiffness is chosen so that when the grillage beam and vierendeel frame are subjected to the same loading they experience similar distortions.

Both proposals were presented with reference to concrete decks, hence it is intended in this section to investigate whether these proposals can be used to model the distortional behaviour of steel cellular structures to an acceptable degree of accuracy. A third method of idealization based on the use of an "equivalent frame" element, developed by the author, will also be presented.

The three possible methods of idealization will be investigated through the analysis of the three cell structure shown in figure 3.14(a). The structure was used in the earlier section when longitudinal bending behaviour was considered. The structure was now subjected to midspan point loads of 600kN acting over each inner web, and analysed using the finite element program, QUEST, using the mesh shown in figure 3.12.

The structure was initially analysed using the grillage method without any modification for distortion of the cross-section. The grillage layout consisted of four longitudinal beams and five transverse beams. The results

from this analysis are presented in Table 3.8 together with the finite element results and the subsequent modified grillage method.

The results show the inability of the standard grillage idealization to model distortion of the cross-section. The variation in midspan deflection from 0.237cm. to 0.641cm. for the loaded and unloaded webs predicted by the finite element analysis is not produced by the grillage method. The comparable grillage results were 0.454cm. and 0.482cm. respectively. This results in a 91% overestimation and a 25% underestimation of the midspan deflection of the unloaded and loaded webs respectively.

The maximum flange edge stresses calculated by the grillage method also reveal substantial discrepancies when compared with the finite element results. At the midspan position the stresses at the unloaded web position are 27.33 N/mm² and 13.90 N/mm², an overestimation of 96%, whilst at the loaded web position the stresses are 37.12 N/mm² and 44.12 N/mm², an underestimation of 16%. The high transverse bending stiffness of the standard grillage idealization allows load to be transferred away from the loaded regions to the unloaded regions of the cross-section, resulting in poor modelling of the transverse behaviour.

These results confirm that distortion of the cross-section must be allowed for in the grillage idealization, if results of acceptable accuracy are to be achieved.

The equivalent vierendeel frame used to model the cross-section is shown in figure 3.14(b), each member has been allocated stiffness properties equivalent to a one metre length of the box structure, giving

$$\text{second moment of area, } IY = 14.4 \text{ cm}^4.$$

$$\text{cross-sectional area, } Ax = 120 \text{ cm}^2.$$

Analysis of this frame using a standard plane frame program gave a deflection at joint D of 5.4467cm. under the action of two 1kN point loads applied at the inner joint positions.

3.6.2 MODIFIED TRANSVERSE FLEXURAL STIFFNESS.

In this section the method proposed by Cusens will be investigated in detail. Figure 3.15 shows the proposed equivalent beam spanning L metres and subjected to third span point loading of W kN. The deflection at the third span position due to bending alone can be determined using the principle of virtual work to be equal to

$$\delta_d = \frac{5WL^3}{162EIY} \quad \text{----- 3.12}$$

The beam is given a modified second moment of area, IY, such that the deflection is compatible with the deflection of the vierendeel frame shown in figure 3.14.

When

$$L = 900 \text{ cm.}$$

$$W = 1 \text{ kN.}$$

$$\delta_d = 5.4467 \text{ cm.}$$

$$\begin{aligned} \text{then } IY &= \frac{5 * 1 * 900 * 900 * 900}{162 * 21000 * 5.4467} \\ &= \underline{\underline{196 \text{ cm}^4 / \text{metre of flange.}}} \end{aligned}$$

The full transverse second moment of area using equation 3.11 is 1 350 000cm⁴. per metre of flange. Comparison of the two values indicates the significance of cross-section distortion in structures of this type.

Cusens also proposed the use of the following equation for the determination of the effective transverse flexural rigidity

$$\frac{1}{D_{ye}} = \frac{1}{D_y} + \frac{18}{GA' (2b)^2} \quad \text{----} \quad 3.13$$

$$\text{where } GA' = \frac{2 E t^3 (tx)^3 d}{bx h (h t^3 + bx tx^3)} \quad \text{----} \quad 3.14$$

- and D_{ye} = effective transverse flexural rigidity
 D_y = full transverse flexural rigidity
 $2b$ = overall width of structure
 E = modulus of elasticity
 t = top and bottom flange thicknesses
 tx = web thickness
 d = overall depth of section
 bx = width of single cell
 h = internal dimensions between top and bottom flange plates = $d - 2t \approx d$

When these equations are applied to the cross-section shown in figure 3.14 where

- h = 150cm.
 d = 150cm.
 bx = 300cm.
 $2b$ = 900cm.

$$\begin{aligned}
 t &= 1.2\text{cm.} \\
 t_x &= 1.2\text{cm.} \\
 I_Y &= 13\,500\text{cm}^4/\text{cm of flange.} \\
 \text{giving } I_{Ye} &= 1.1519\text{cm}^4/\text{cm of flange} \\
 &= 115.2\text{ cm}^4 / \text{metre of flange}
 \end{aligned}$$

The structure was analysed using a 4 by 5 grillage mesh where the transverse second moment of area assigned to each internal transverse grillage beam was changed from 5 400 000cm⁴ to 784cm⁴ and 461cm⁴. The results from both analyses are presented in Table 3.8 and indicated that the values of deflection and flange edge stress are virtually the same for both analyses. When these results were compared to the finite element values they reveal a significant improvement over the no-distortion grillage analysis.

The loaded web midspan deflection calculated by the grillage analysis was 0.604cm. compared to 0.641cm. from the finite element analysis, an underestimation of 5.8%. The unloaded web values were 0.280cm. and 0.237cm. from the two analyses, an overestimation of 18% by the grillage method. The quarterspan deflection values produced comparable results to the midspan position.

The flange edge stress values at the loaded web at midspan were 46.45N/mm² and 44.12N/mm², and at the unloaded web were 14.92N/mm² and 13.90N/mm² for the grillage and finite element analyses respectively. The overestimation of stress using the grillage method was 5.3% and 7.4%. The stress at the unloaded web position was

determined using the full width of the flange plate without any reduction for shear lag. At the quarterspan position the grillage stresses were 11.02N/mm² and 14.58N/mm² compared to the finite element values of 10.51N/mm² and 14.69N/mm². An overestimation of 5.3% at the unloaded web and a slight underestimation of 0.7% at the loaded web position.

The accuracy of these results is consistent with the degree of accuracy achieved from the longitudinal bending study in section 3.4.4, the predicted values of stress and deflection at the critical loaded web position agreeing to within an accuracy of 6%.

3.6.3. EQUIVALENT SHEAR AREA.

In this section the method proposed by Hambly will be investigated. The deflection behaviour of the equivalent vierendeel frame in figure 3.14 will be modelled using an equivalent beam with a second moment of area, IY , equal to the full transverse bending stiffness of the three cell structure shown in figure 3.14 and a low effective shear area, A_s . The beam is shown in figure 3.15 and from the corresponding bending moment and shear force diagrams the following equation for deflection at the third span position may be determined.

$$\delta_d = \frac{5WL^3}{162EIY} + \frac{WL}{3GAs} \quad \text{-----} \quad 3.15$$

Substitution of the following values

$$W = 1 \text{ kN.}$$

$$L = 900 \text{ cm.}$$

$$E = 21\,000 \text{ kN/cm}^2.$$

$$IY = 1\,350\,000 \text{ cm}^4.$$

$$G = E/2(1+\nu) = E/2.6$$

into equation 3.15 gives

$$A_s = 0.00682 \text{ cm}^2 / \text{metre of flange.}$$

Another method proposed by Hambly for the determination of the equivalent shear area of the transverse grillage beam requires the determination of the complex relationship between vertical shear across a cell and the effective shear displacement of the cell. An approximation can be obtained by assuming that the shear force is shared between top and bottom flange plates in proportion to their individual flexural stiffnesses and that there are points of contraflexure midway between webs. This approximation leads to the following expression for effective shear area

$$A_s = \frac{(t_1^3 + t_2^3)}{b^2} \left[\frac{t_w^3 b}{t_w^3 b + (t_1^3 + t_2^3) d} \right] \frac{E}{G} \quad \text{--- 3.16}$$

where t_1 = top flange thickness

t_2 = bottom flange thickness

b = width of cell

t_w = web thickness

d = depth of cell

when this equation is applied to the cross-section shown in figure 3.14 where

$$t_1 = t_2 = t_w = 1.2 \text{ cm.}$$

$$b = 300 \text{ cm.}$$

$$d = 150 \text{ cm.}$$

the effective shear area of the transverse grillage beam is

$$\begin{aligned} A_s &= 0.00005 \text{ cm}^2/\text{cm}. \\ &= 0.005 \text{ cm}^2 / \text{metre of flange}. \end{aligned}$$

The three cell structure was again analysed using a 4 by 5 grillage layout where the internal transverse grillage beams were assigned an equivalent shear area of 0.027cm². and 0.020cm². The analyses showed that both shear areas produce exactly the same results for midspan and quarterspan stress and deflection values. The results, presented in Table 3.8, are also virtually the same as those using the modified flexural stiffness method.

3.6.4. EQUIVALENT FRAME ELEMENT.

In the previous sections the proposals of Cusens and Hambly were studied. Although the grillage method produced values of web deflection and flange stress to an acceptable accuracy, the overall distortional behaviour of the structure was not accurately modelled. One error in the equivalent shear area analogy is that for the grillage beam the shear force is solely proportional to the shear displacement, while in the cell the shear force is to some extent dependent on the continuity of moments from flexure of the flanges in the adjacent cells.

This point is confirmed when the torsional rotations of the webs predicted by the finite element and grillage method are compared. The values being $0.3 * 10E-3$ radians and $0.3 * 10E-6$ radians for the finite element and grillage methods respectively, showing that distortion of

the cross-section is achieved by shear deformation of the transverse grillage beams with very little contribution from transverse bending action.

In an attempt to improve the distortional modelling of the grillage method an "equivalent frame" element was developed. This element has the same three degrees of freedom at each end as the standard grillage beam element and hence will be compatible with it. One element can be used to model each cell of the structure cross-section. The development of the element stiffness matrix is presented in Appendix D. It was derived from the analysis of a single cell unit subjected to end shear forces and moments, to which was added the standard torsional characteristics of the grillage beam.

The relationship between applied member force and nodal displacement is comparable to that for the standard grillage beam element, as defined in equation 3.2, Section 3.2, and the element stiffness matrix [K] takes the following form

$$\left[\begin{array}{cccccc}
 \frac{24EIf}{b^3} & 0 & \frac{12EIf}{b^2} & -\frac{24EIf}{b^3} & 0 & \frac{12EIf}{b^2} \\
 & \frac{GJ}{b} & 0 & 0 & -\frac{GJ}{b} & 0 \\
 & & \frac{8EIf+12EIw}{b} & -\frac{12EIf}{b^2} & 0 & \frac{4EIf}{b} \\
 & & & \frac{24EIf}{b^3} & 0 & -\frac{12EIf}{b^2} \\
 \text{symmetrical} & & & & \frac{GJ}{b} & 0 \\
 & & & & & \frac{8EIf+12EIw}{b} & \frac{12EIf}{b^2}
 \end{array} \right] \quad \text{--- 3.17}$$

where I_f = second moment of area of flange
 I_w = second moment of area of web
 b = breadth of cell
 d = depth of cell
 J = polar second moment of area

This "equivalent frame" element was used to analyse the three vierendeel frames shown in figure 3.16, which consisted of two, three and four cells. The proportions of each cell were

$b = 300\text{cm.}$
 $d = 150\text{cm.}$
 $t_w = 1.2\text{cm.}$
 $t_f = 1.2\text{cm.}$

The frames were also analysed using a standard rigid frame program, and as an equivalent beam with both modified flexural stiffness and equivalent shear area using equations 3.13 and 3.16. The results for rotation and deflection at each web position for all four analyses are presented in figure 3.16. Consideration of these results show that the "equivalent frame" element produced the most accurate results for rotation and deflection when compared to the rigid frame analysis.

The equivalent frame element was incorporated into the grillage analysis program, SHEARGRID2, and the three cell structure shown in figure 3.14 was re-analysed. The results are presented in Table 3.8 and reveal agreement with both the previous set of results using the modified flexural stiffness and equivalent shear area methods. The

torsional rotations were also in close agreement with values of the order of $2 * 10E-6$ radians.

3.6.5. CONCLUSIONS.

1. The three methods proposed for the modifications to the grillage method to cater for cell distortion all produced the same results. These results were considered to be of acceptable accuracy.
2. The flange edge stresses showed a variation from an overestimation of 8% to an underestimation of only 1%. The grillage method predicted the stress at the critical loaded web more accurately than at the unloaded web.
3. The prediction of web deflections was less accurate with an underestimation of 6% at the loaded web and an overestimation of 18% at the unloaded web.

The criteria for development of the transverse stiffness parameters in all three proposed methods was that compatibility of slope and/or deflection be achieved with the equivalent vierendeel frame. The K_{11} portion of the element stiffness matrices were calculated for each method and were shown to be

MODIFIED FLEXURAL STIFFNESS.

$$\begin{bmatrix} 4.303 & 645.4 & 0 \\ 645.4 & 129080 & 0 \\ 0 & 0 & 1.12*10E8 \end{bmatrix} \begin{Bmatrix} dz \\ \theta x \\ \theta y \end{Bmatrix}$$

EQUIVALENT SHEAR AREA.

$$\begin{bmatrix} 0.5384 & 80.76 & 0 \\ 80.76 & 3.78*10E8 & 0 \\ 0 & 0 & 1.12*10E8 \end{bmatrix} \begin{Bmatrix} dz \\ \theta_x \\ \theta_y \end{Bmatrix}$$

EQUIVALENT FRAME ELEMENT.

$$\begin{bmatrix} 1.0752 & 161.28 & 0 \\ 161.28 & 129024 & 0 \\ 0 & 0 & 1.12*10E8 \end{bmatrix} \begin{Bmatrix} dz \\ \theta_x \\ \theta_y \end{Bmatrix}$$

The K11 element stiffness matrix for the longitudinal grillage beam was

$$\begin{bmatrix} 2980 & 0 & 595977 \\ 0 & 1.05*10E8 & 0 \\ 595 977 & 0 & 3.4*10E8 \end{bmatrix} \begin{Bmatrix} dz \\ \theta_x \\ \theta_y \end{Bmatrix}$$

The three transverse grillage element sub-matrices show close numerical agreement. The direct stiffness term associated with vertical deflection, dz, is dominated by the value of 2980 in the longitudinal grillage element and confirms why all three proposals gave similar results.

3.7. SUMMARY.

In this chapter the methods available for the development of the sectional properties of the grillage beams to cater for longitudinal bending, transverse bending and cell distortion have been studied. Conclusions have been established at the end of each stage of the investigation. In the next chapter the methods available for torsional idealization will be considered.

Load Case	Span posn		Simple Beam	F.E. Mesh 1	%	F.E. Mesh 2	%
M I D S P A N P O I N T	1/2	Stress	60.41	56.14	+7.6	63.67	-5.1
		Defl	0.298	0.308	-3.2	0.317	-6.0
		Ψ	0.569	0.609	+7.0	0.546	-4.0
	1/4	Stress	19.23	20.09	-4.3	20.71	-7.1
		Defl	0.189	0.197	-4.1	0.204	-7.3
		Ψ	0.989	0.939	-5.1	0.908	-8.2
U N I F O R M L I N E	1/2	Stress	64.25	63.34	+1.4	63.62	+1.0
		Defl	0.528	0.555	-4.9	0.569	-7.2
		Ψ	0.871	0.873	+0.2	0.877	+0.7
	1/4	Stress	49.67	51.46	-3.5	53.49	-7.1
		Defl	0.381	0.413	-7.7	0.426	-10.6
		Ψ	0.840	0.779	-7.3	0.759	-9.6

Stress - Longitudinal flange stress (N/mm²)

Defl - Web deflection (cm)

Ψ - effective breadth ratio

TABLE 3.1. - Comparison of longitudinal flange stress (N/mm²) web deflection (cm) and effective breadth ratio for Grillage and Finite Element analyses. Single cell structure. L = 9.6m., tf = 1.2cm.

Load Case	Span posn		Simple Beam	F.E. Mesh 1	%	F.E. Mesh 2	%
M I D S P A N	1/2	Stress	52.12	48.20	+8.1	52.10	0.0
		Defl	0.629	0.632	-0.5	0.639	-1.6
		Ψ	0.686	0.741	+8.0	0.693	+1.0
P O I N T	1/4	Stress	19.05	19.00	+0.3	19.05	+0.3
		Defl	0.416	0.417	-0.2	0.423	-1.7
		Ψ	1.000	1.002	+0.2	0.999	-0.1
U N I F O R M	1/2	Stress	59.49	59.36	+0.2	59.48	0.0
		Defl	1.148	1.152	-0.3	1.166	-1.5
		Ψ	0.954	0.951	-0.3	0.952	-0.2
L I N E	1/4	Stress	45.34	44.77	+1.3	45.11	+0.5
		Defl	0.822	0.832	-1.1	0.847	-3.0
		Ψ	0.936	0.931	-0.5	0.931	-0.5

Stress - Longitudinal flange stress (N/mm²)

Defl - Web deflection (cm)

Ψ - effective breadth ratio

TABLE 3.2. - Comparison of longitudinal flange stress (N/mm²) web deflection (cm) and effective breadth ratio for Grillage and Finite Element analyses. Single cell structure. L = 16.0m., tf = 1.2cm.

Load Case	Span posn		Simple Beam	F.E. Mesh 1	%	F.E. Mesh 2	%
M I D S P A N	1/2	Stress	19.98	19.17	+4.2	20.59	-3.0
		Defl	0.285	0.289	-1.4	0.294	-3.1
		Ψ	0.686	0.700	+2.0	0.658	-4.1
P O I N T	1/4	Stress	7.02	6.99	+0.4	6.99	+0.4
		Defl	0.180	0.183	-1.7	0.187	-3.7
		Ψ	1.000	1.003	+0.3	1.003	+0.3
U N I F O R M	1/2	Stress	22.01	21.94	+0.3	21.99	+0.1
		Defl	0.503	0.513	-1.9	0.524	-4.0
		Ψ	0.954	0.951	-0.3	0.953	-0.1
L I N E	1/4	Stress	16.81	16.54	+1.6	16.63	+1.1
		Defl	0.363	0.375	-3.1	0.387	-6.2
		Ψ	0.936	0.932	-0.4	0.935	-0.1

Stress - Longitudinal flange stress (N/mm²)

Defl - Web deflection (cm)

Ψ - effective breadth ratio

TABLE 3.3. - Comparison of longitudinal flange stress (N/mm²) web deflection (cm) and effective breadth ratio for Grillage and Finite Element analyses. Single cell structure. L = 16.0m., tf = 3.6cm.

Load Case	Span posn		Simple Beam	F.E. Mesh 1	%	F.E. Mesh 2	%	
M I D S P A N	1/2	Stress	47.55	44.27	+7.4	46.47	+2.3	
		Defl	1.277	1.275	+0.2	1.278	-0.1	
		Ψ	0.768	0.824	+7.3	0.790	+2.9	
	P O I N T	1/4	Stress	19.05	19.03	+0.1	18.99	+0.3
			Defl	0.862	0.859	+0.3	0.861	+0.1
			Ψ	1.000	1.001	+0.1	1.002	+0.2
U N I F O R M	1/2	Stress	58.55	58.11	+0.8	58.15	+0.7	
		Defl	2.362	2.354	+0.3	2.358	+0.2	
		Ψ	0.972	0.978	+0.6	0.978	+0.6	
	L I N E	1/4	Stress	44.07	43.33	+1.7	43.45	+1.4
			Defl	1.688	1.688	0.0	1.693	-0.3
			Ψ	0.968	0.971	+0.3	0.974	+0.6

Stress - Longitudinal flange stress (N/mm²)

Defl - Web deflection (cm)

Ψ - effective breadth ratio

TABLE 3.4. - Comparison of longitudinal flange stress (N/mm²) web deflection (cm) and effective breadth ratio for Grillage and Finite Element analyses. Single cell structure. L = 24.0m., tf = 1.2cm.

Load Case		Span posn	Web No.	F.E.	Gr.1	%	Gr.2	%	
M I D S P A N	S t r e s s	1/2	1	52.84	57.57	+9.0	58.00	+9.8	
			2	47.99	51.73	+7.8	51.26	+6.8	
		1/4	1	19.82	19.96	+0.7	20.40	+2.9	
			2	19.59	19.53	-0.3	19.05	-2.8	
	P O I N T	D e f l n	1/2	1	0.683	0.684	+0.1	0.692	+1.3
				2	0.683	0.683	0.0	0.672	-1.6
1/4			1	0.448	0.449	+0.2	0.456	+1.8	
			2	0.443	0.448	+1.1	0.439	-0.9	
U N I F O R M	S t r e s s	1/2	1	41.39	42.49	+2.7	43.04	+4.0	
			2	40.82	39.78	-2.5	39.19	-4.0	
		1/4	1	33.68	32.55	-3.4	32.72	-2.8	
			2	30.12	30.20	+0.2	30.01	-0.4	
	L I N E	D e f l n	1/2	1	0.824	0.826	+0.2	0.834	+1.2
				2	0.824	0.826	+0.2	0.815	-1.1
1/4			1	0.598	0.593	-0.8	0.598	0.0	
			2	0.594	0.593	-0.2	0.586	-1.3	

Gr.1 - Grillage (without distortion)

Gr.2 - Grillage (with distortion)

TABLE 3.5. - Comparison of longitudinal flange stress (N/mm²) and web deflection (cm) for Grillage and Finite Element analyses. Two-cell structure.

Load Case		Span posn	Web No.	F.E.	Gr.1	%	Gr.2	%	
M I D S P A N	S t r e s s	1/2	1	53.90	59.75	+10.8	60.24	+11.8	
			2	48.62	53.55	+10.1	53.27	+9.6	
		1/4	1	20.02	20.30	+1.4	20.85	+4.1	
			2	19.92	19.84	-0.4	19.54	-1.9	
	P O I N T	D e f l n	1/2	1	0.702	0.705	+0.4	0.716	+2.0
				2	0.702	0.705	+0.4	0.698	-0.6
1/4			1	0.459	0.462	+0.6	0.470	+2.4	
			2	0.454	0.460	+1.3	0.454	0.0	
U N I F O R M L I N E	S t r e s s	1/2	1	42.07	43.59	+3.6	44.27	+5.2	
			2	41.52	40.72	-1.9	40.35	-2.7	
		1/4	1	33.05	33.42	+1.1	33.63	+1.7	
			2	31.03	30.98	-0.2	30.86	-0.5	
	D e f l n	1/2	1	0.844	0.850	+0.7	0.860	+1.9	
			2	0.844	0.849	+0.6	0.842	-0.2	
1/4		1	0.614	0.610	-0.7	0.616	+0.3		
		2	0.610	0.610	0.0	0.606	-0.6		

Gr.1 - Grillage (without distortion)

Gr.2 - Grillage (with distortion)

TABLE 3.6. - Comparison of longitudinal flange stress (N/mm²) and web deflection (cm) for Grillage and Finite Element analyses. Three-cell structure.

Load Case		Span posn	Web No.	F.E.	Gr.1	⊘	Gr.2	⊘
M I D S P A N	S t r e s s	1/2	1	55.07	60.94	+10.6	61.52	+11.7
			2	49.52	54.57	+10.2	54.41	+9.9
			3	49.70	54.40	+9.5	54.07	+8.8
	1/4	1	19.75	20.51	+3.8	21.05	+6.6	
		2	20.17	20.04	-0.7	19.89	-1.4	
		3	20.15	19.89	-1.3	19.61	-2.7	
P O I N T	D e f l n	1/2	1	0.710	0.718	+1.1	0.729	+2.7
			2	0.710	0.717	+1.0	0.712	+0.3
			3	0.710	0.716	+0.8	0.708	-0.3
	1/4	1	0.463	0.469	+1.3	0.477	+3.0	
		2	0.459	0.467	+1.7	0.463	+0.9	
		3	0.458	0.466	+1.7	0.460	+0.4	
U N I F O R M	S t r e s s	1/2	1	42.44	44.19	+4.1	44.94	+5.9
			2	42.37	41.30	-2.5	41.10	-3.0
			3	42.29	41.04	-3.0	40.63	-3.9
	1/4	1	33.22	33.87	+1.9	34.13	+2.7	
		2	31.66	31.44	-0.7	31.40	-0.8	
		3	31.77	31.29	-1.5	31.09	-2.1	
L I N E	D e f l n	1/2	1	0.850	0.864	+1.6	0.875	+2.9
			2	0.850	0.862	+1.4	0.857	+0.8
			3	0.850	0.860	+1.2	0.852	+0.2
	1/4	1	0.618	0.620	+0.3	0.627	+1.5	
		2	0.613	0.619	+1.0	0.617	+0.6	
		3	0.614	0.618	+0.6	0.613	-0.2	

Gr.1 - Grillage (without distortion)

Gr.2 - Grillage (with distortion)

TABLE 3.7. - Comparison of longitudinal flange stress (N/mm²) and web deflection (cm) for Grillage and Finite Element analyses. Four-cell structure.

	Analysis	MIDSPAN		QUARTERSPAN	
		Web 1	Web 2	Web 1	Web 2
W E B D E F L E C T I O N	F.E.	0.237	0.641	0.168	0.403
	Grill no dist %	0.454 +91	0.482 -25	0.303 +80	0.310 -23
	Grill IY=461cm ⁴ %	0.279 +18	0.605 -6	0.199 +18	0.381 -5.5
	Grill IY=784cm ⁴ %	0.280 +18	0.604 -5.8	0.200 +19	0.380 -5.7
	Grill Eff As %	0.277 +17	0.606 -5.5	0.198 +18	0.382 -5.2
	Grill Eq. Frame %	0.278 +17	0.605 -5.6	0.198 +18	0.382 -5.2
L O N G I T U D I N A L S T R E S S	F.E.	13.90	44.12	10.51	14.69
	Grill no dist %	27.23 +96	37.12 -16	14.03 +33	12.96 -12
	Grill IY=461cm ⁴ %	14.92 +7.4	46.45 +5.3	11.02 +4.8	14.58 -0.7
	Grill IY=784cm ⁴ %	14.99 +7.9	46.40 +5.2	11.06 +5.2	14.56 -0.9
	Grill Eff As %	14.84 +6.7	46.52 +5.4	10.97 +4.4	14.61 -0.6
	Grill Eq. Frame %	14.85 +6.8	46.51 +5.4	10.98 +4.4	14.60 -0.6

Eff As = 0.02cm² and 0.027cm²

TABLE 3.8. - Comparison of web deflection (cm) and Longitudinal flange stress (N/mm²) for Finite Element and Grillage analyses. Distortion Idealization of Three-cell Structure.

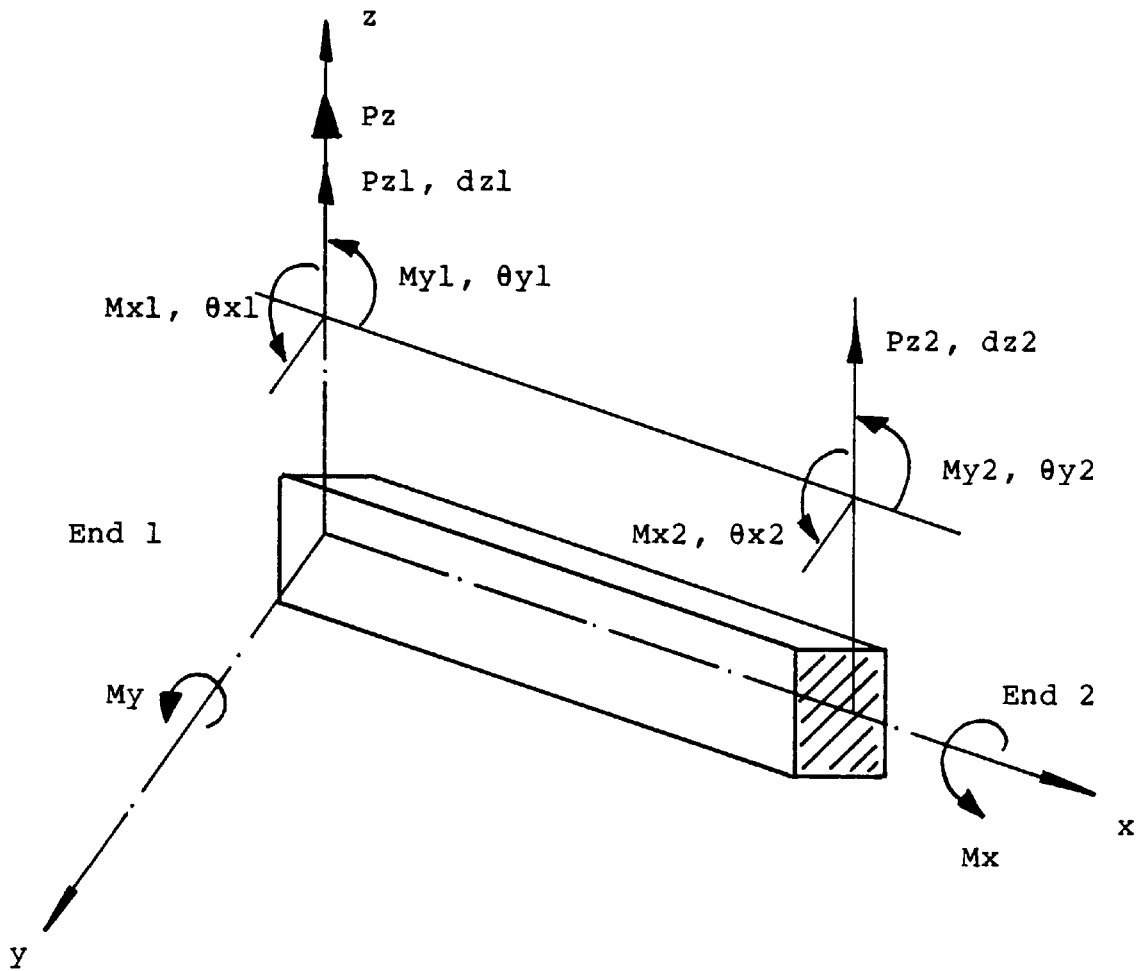
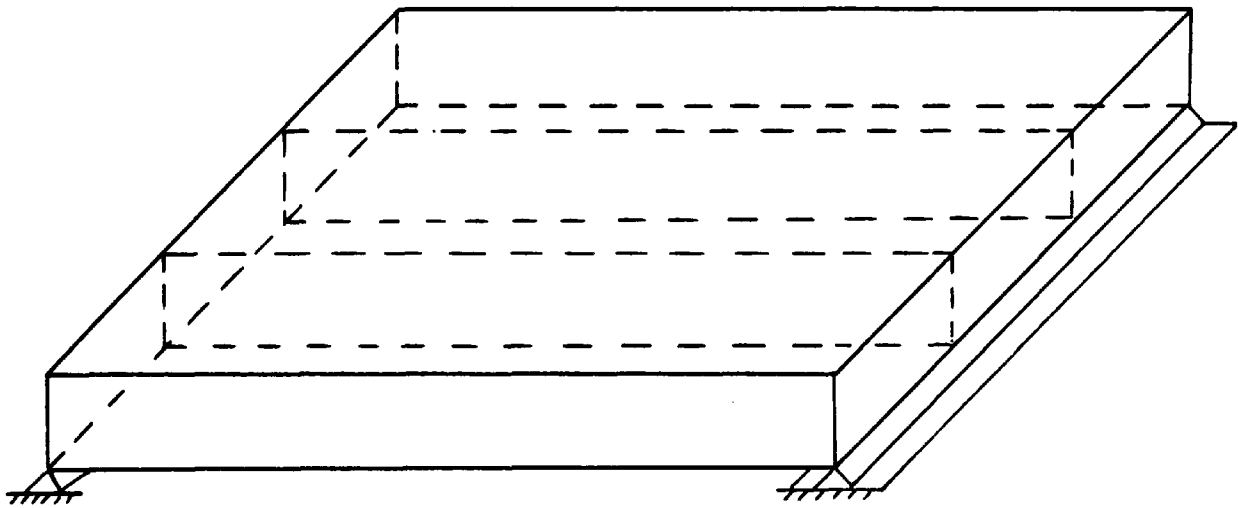
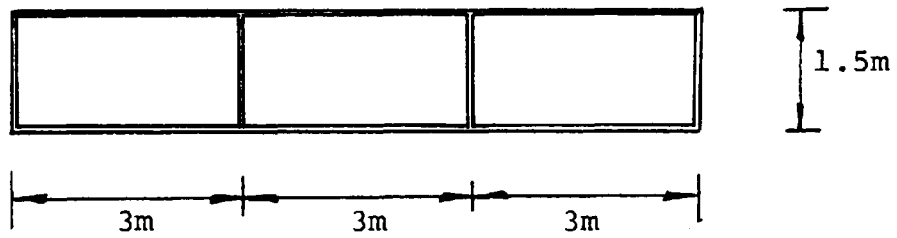


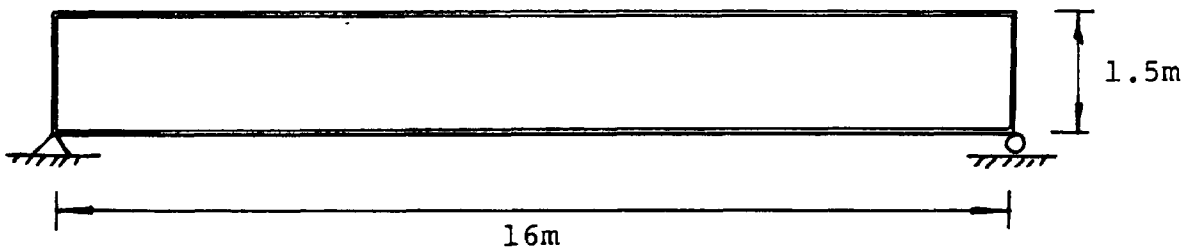
FIGURE 3.1 - DETAILS OF GRILLAGE BEAM ELEMENT.



(a) Isometric view.

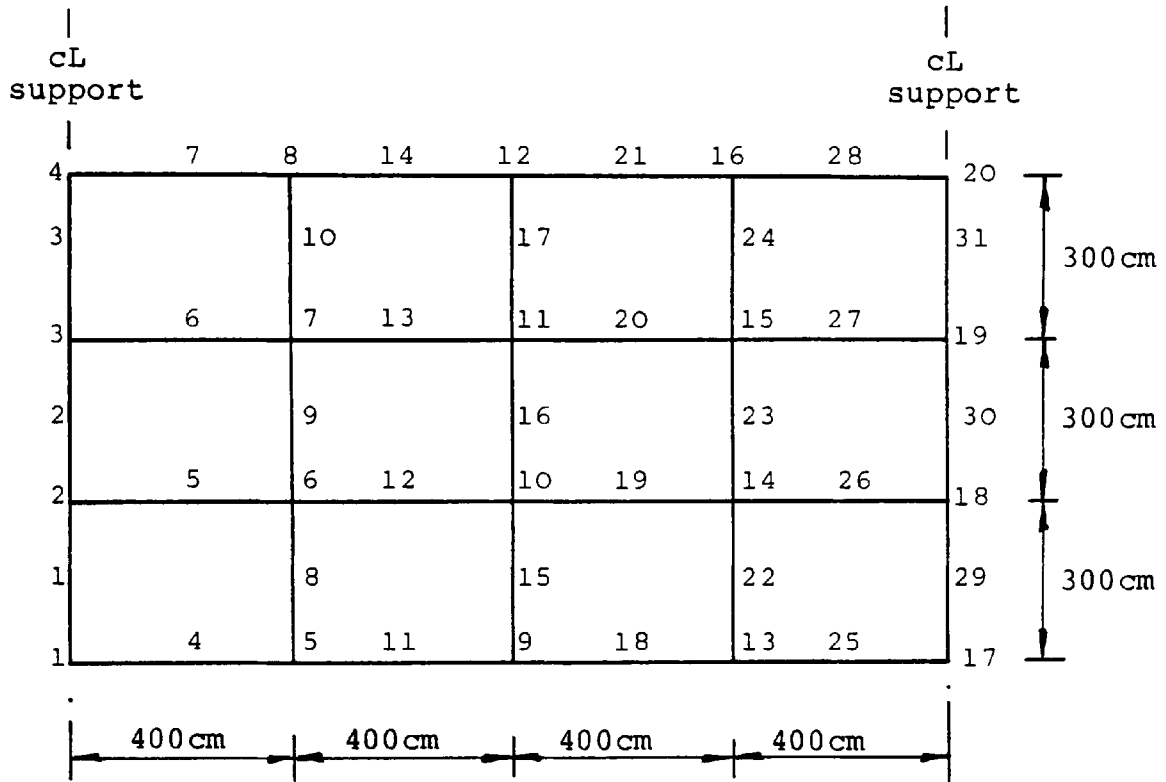


(b) Cross-section detail.

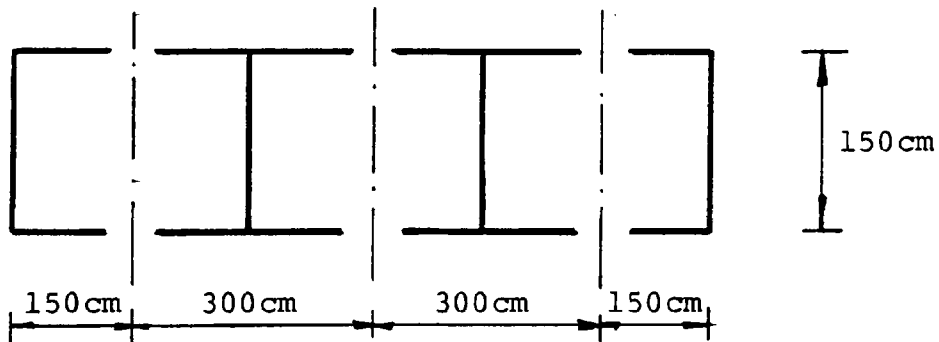


Longitudinal section detail.

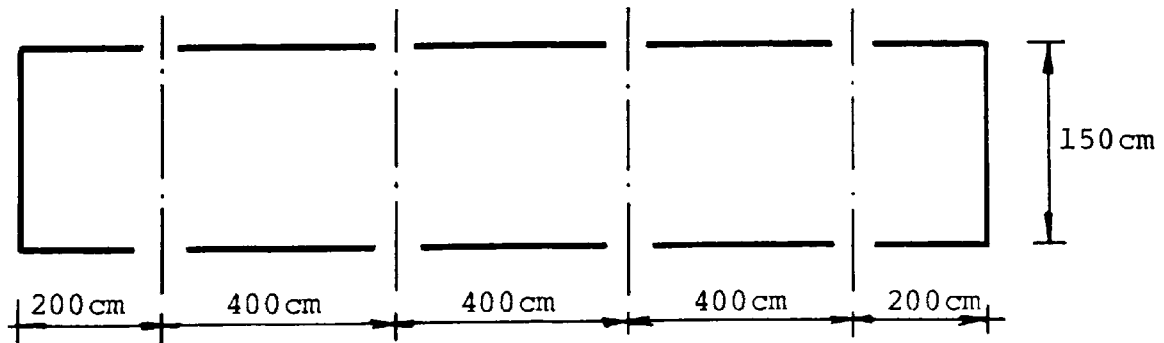
FIGURE 3.2 - TYPICAL THREE-CELL STRUCTURE.



(a) Grillage mesh layout.

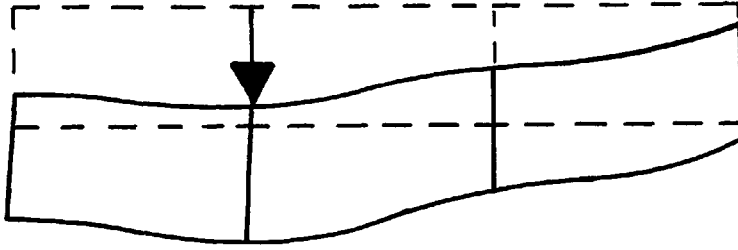


(b) Longitudinal grillage beam representation.

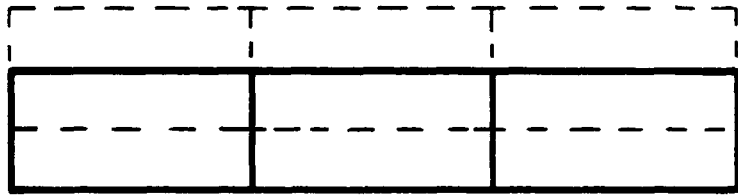


(c) Transverse grillage beam representation.

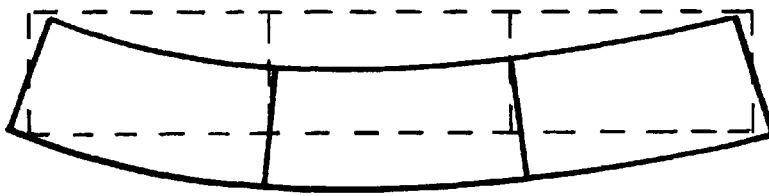
FIGURE 3.3 - GRILLAGE IDEALIZATION OF THREE-CELL STRUCTURE.



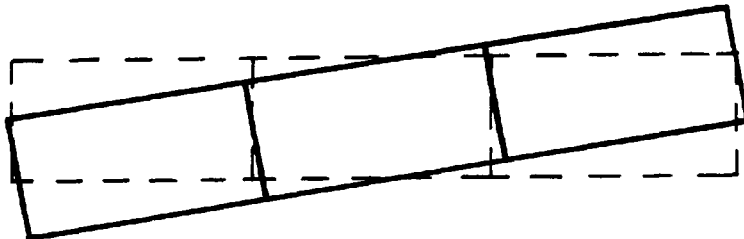
(a) Combined.



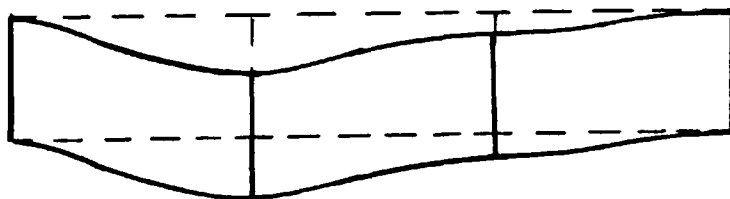
(b) Longitudinal bending.



(c) Transverse bending.



(d) Torsion.



(e) Distortion.

FIGURE 3.4 - TYPICAL CROSS-SECTION
DISPLACEMENT AND DEFORMATION.

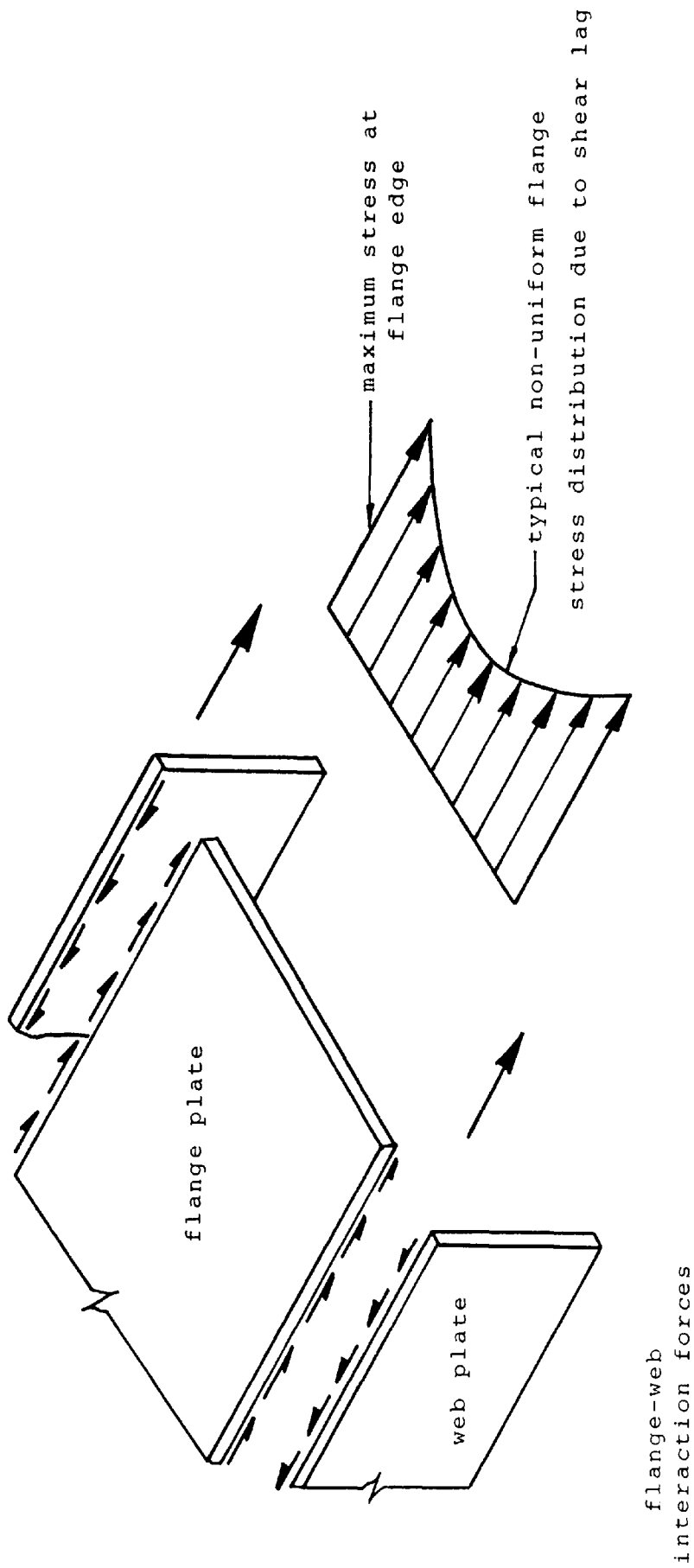


FIGURE 3.5 - SHEAR LAG EFFECT IN SINGLE CELL STRUCTURE.

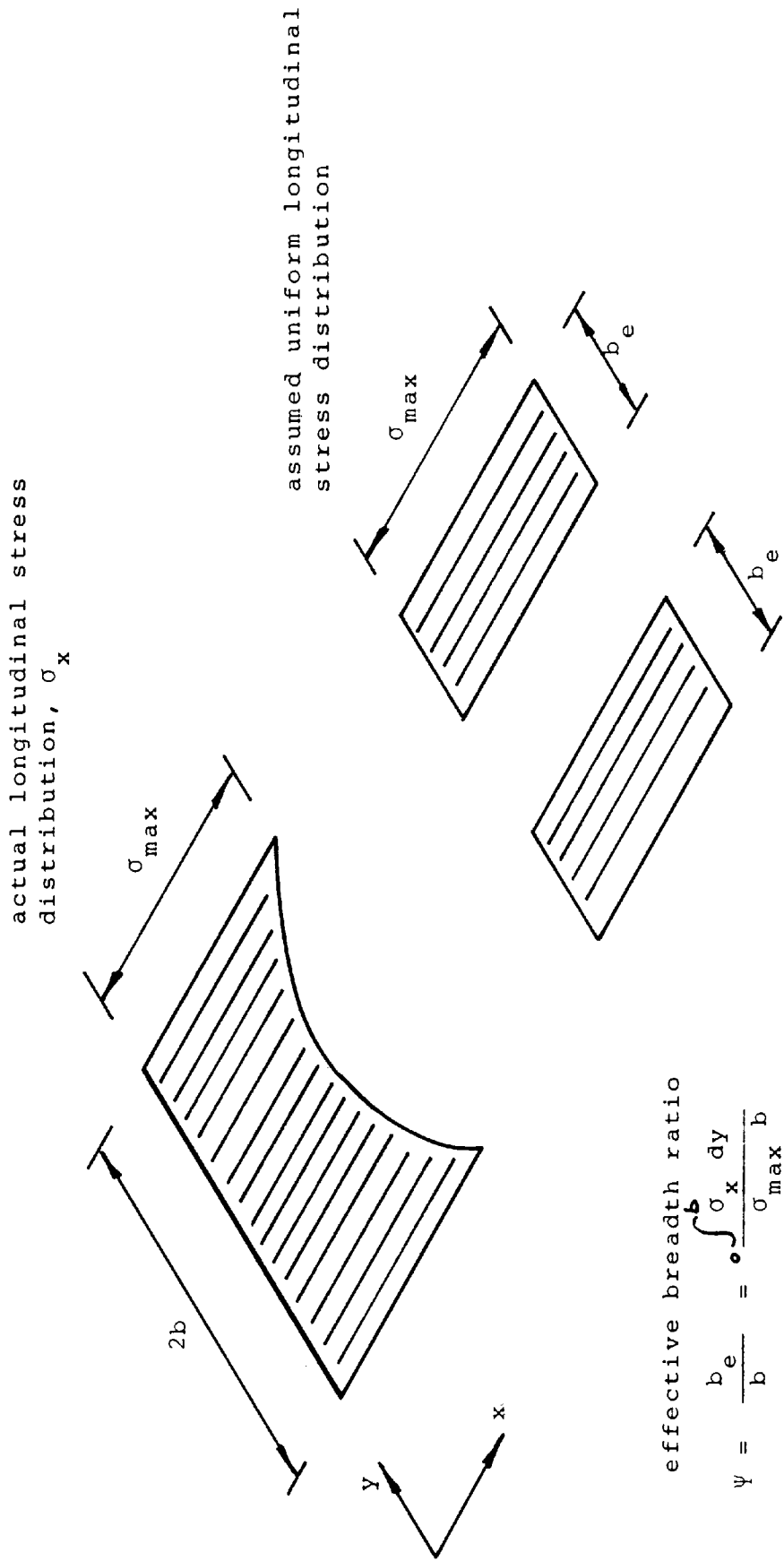
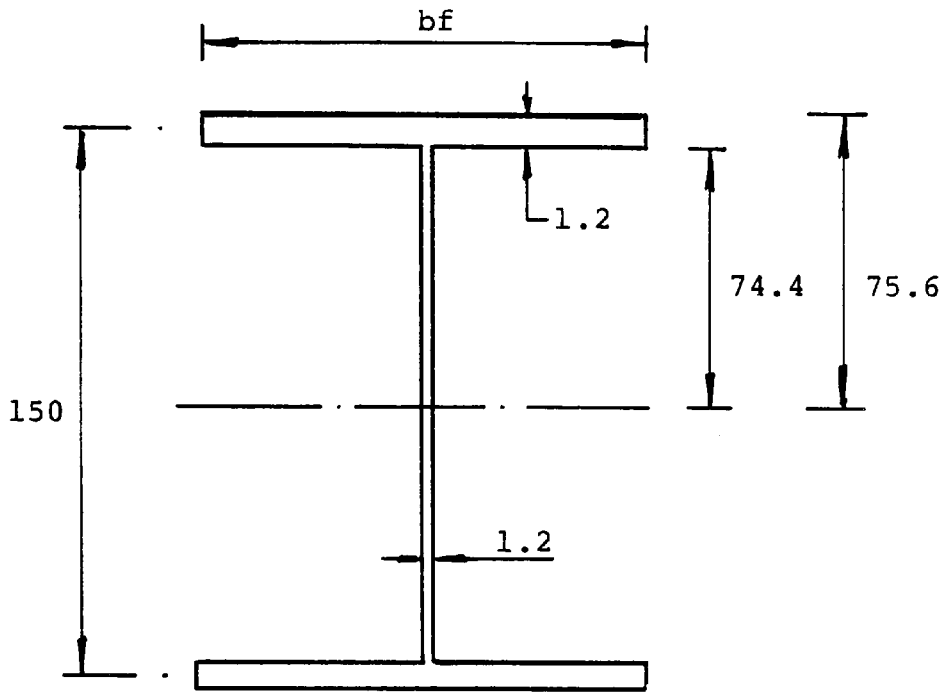
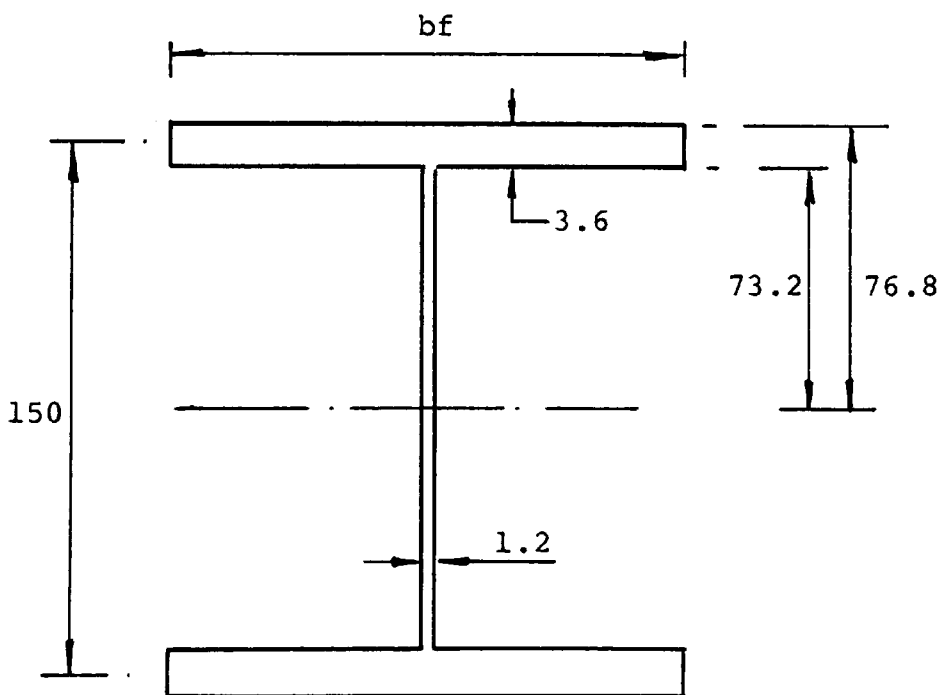


FIGURE 3.6 - EFFECTIVE BREADTH RATIO FOR FLANGE PLATE STRESS.

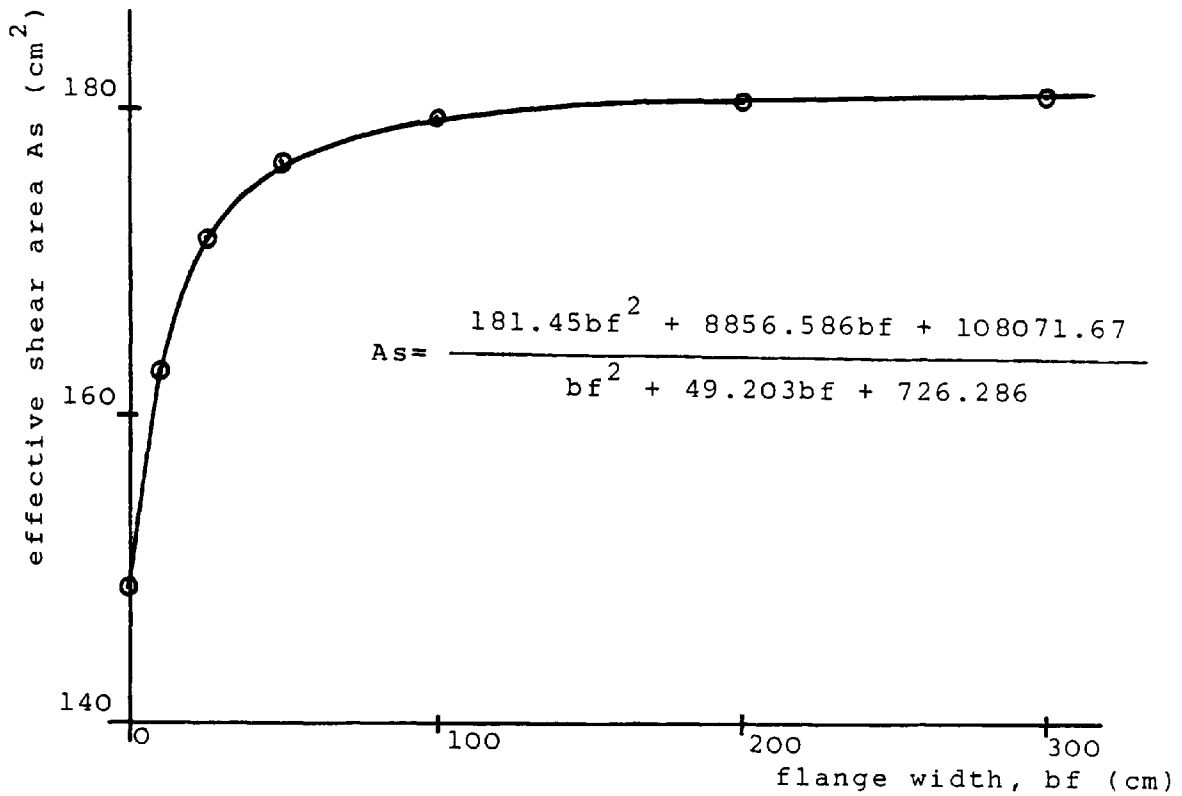


(a) flange thickness, $t_f = 1.2$ cm.

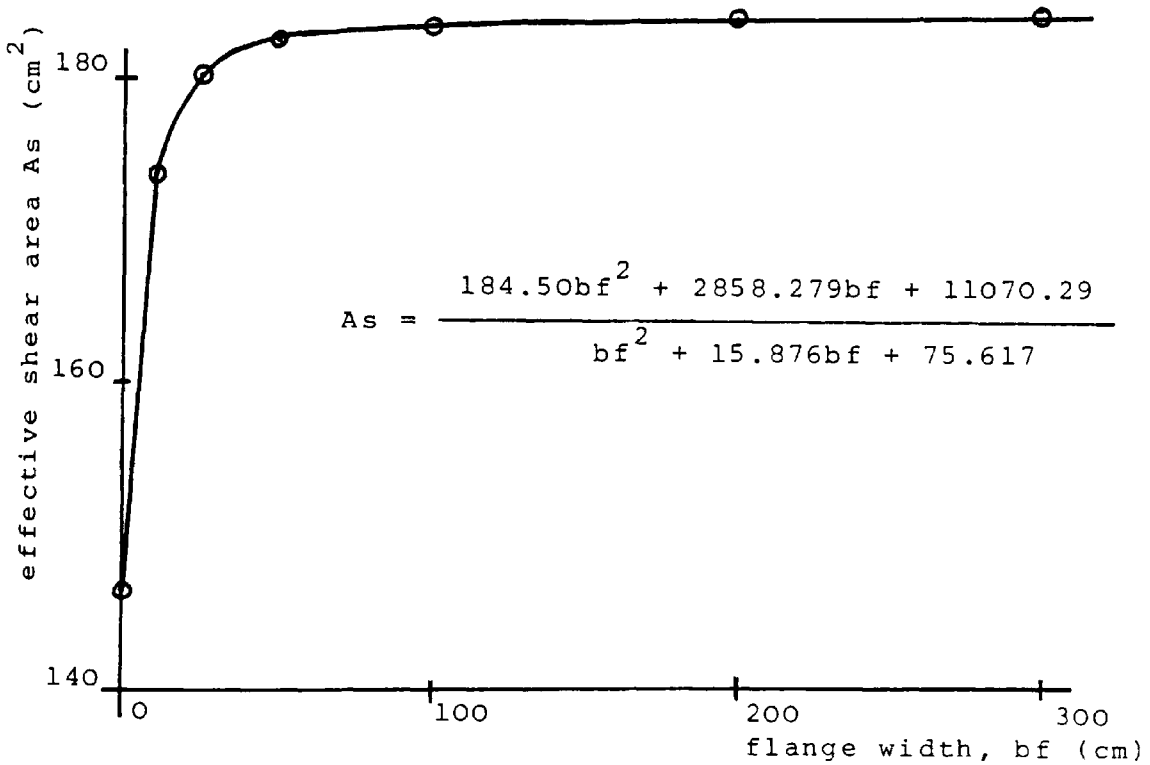


(b) flange thickness, $t_f = 3.6$ cm.

FIGURE 3.7 - DETAILS OF CROSS-SECTIONS USED TO DETERMINE EFFECTIVE SHEAR AREA.

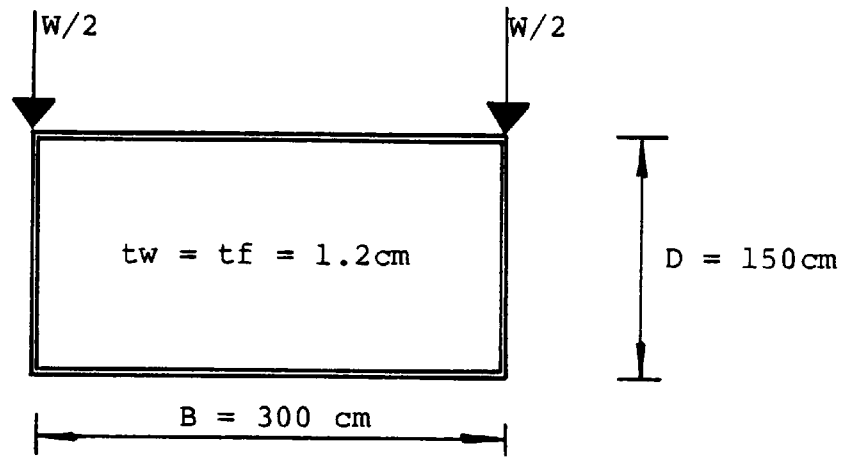


(a) flange thickness, $t_f = 1.2$ cm.

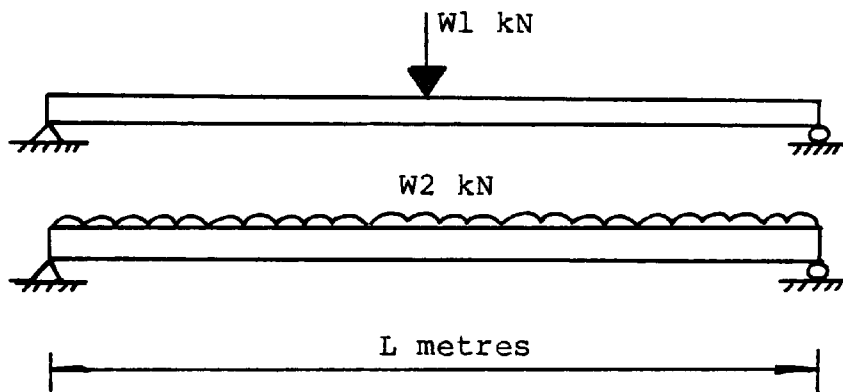


(b) flange thickness, $t_f = 3.6$ cm.

FIGURE 3.8 - VARIATION OF EFFECTIVE SHEAR AREA, A_s WITH FLANGE WIDTH, b_f .

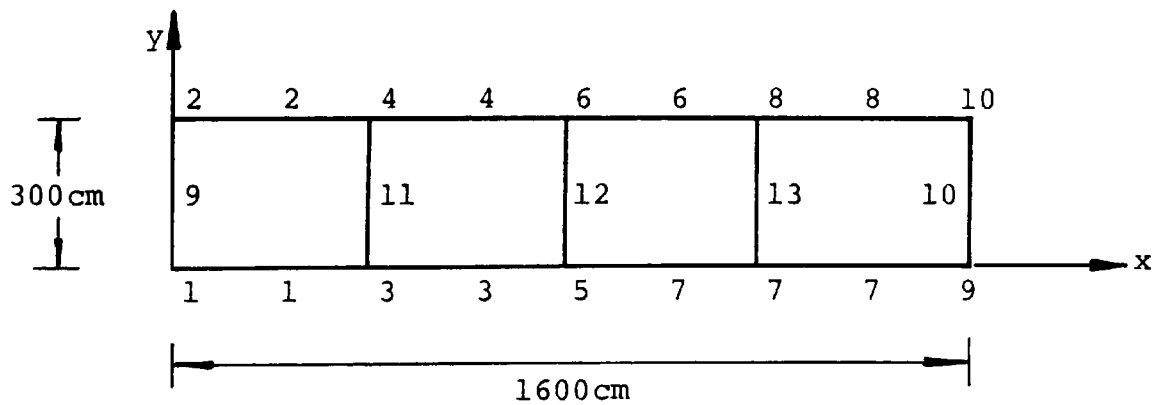


(a) Cross-section.



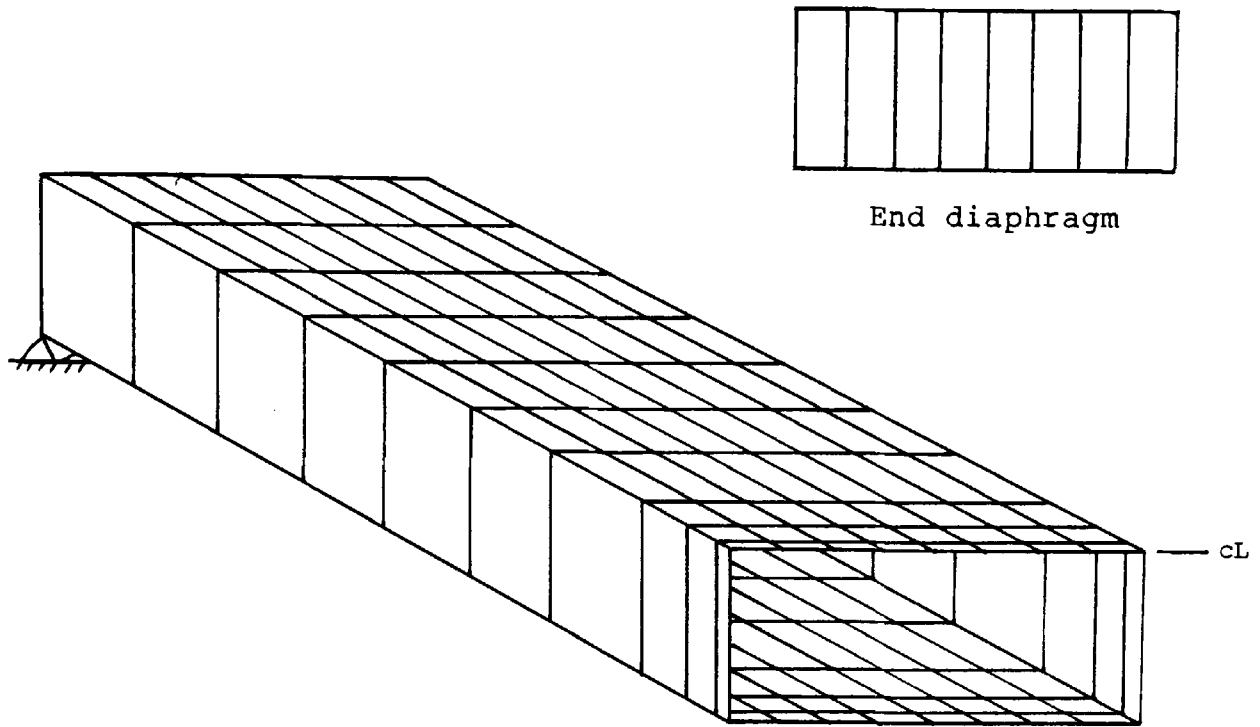
L (m)	W1 (kN)	W2 (kN)
9.6	1000	3000
16.0	600	1800
24.0	400	1200

(b) Load and span details.

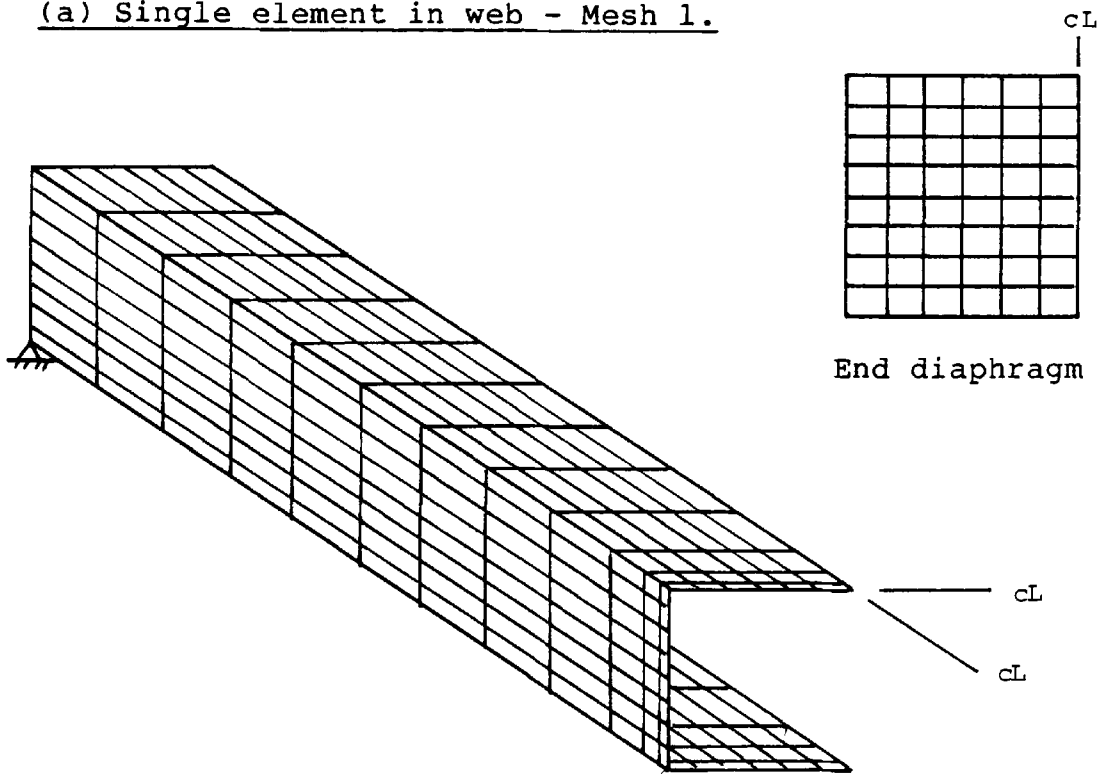


(c) Grillage idealization.

FIGURE 3.9 - DETAILS OF LOADING AND GRILLAGE IDEALIZATION OF SINGLE CELL STRUCTURE.

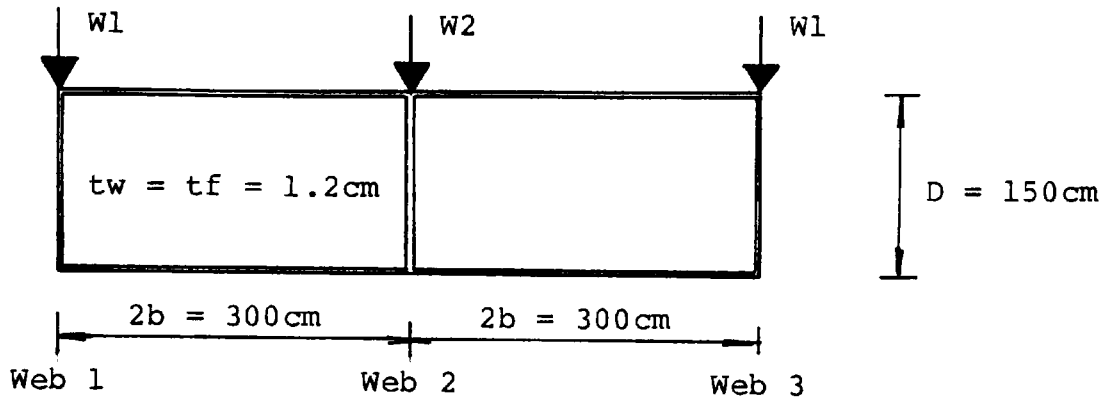


(a) Single element in web - Mesh 1.

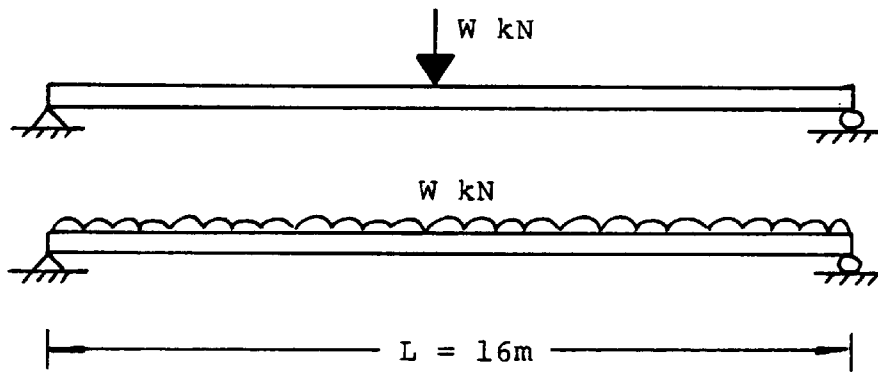


(b) 8 elements in web - Mesh 2.

FIGURE 3.10 - FINITE ELEMENT IDEALIZATION OF SINGLE CELL STRUCTURE.

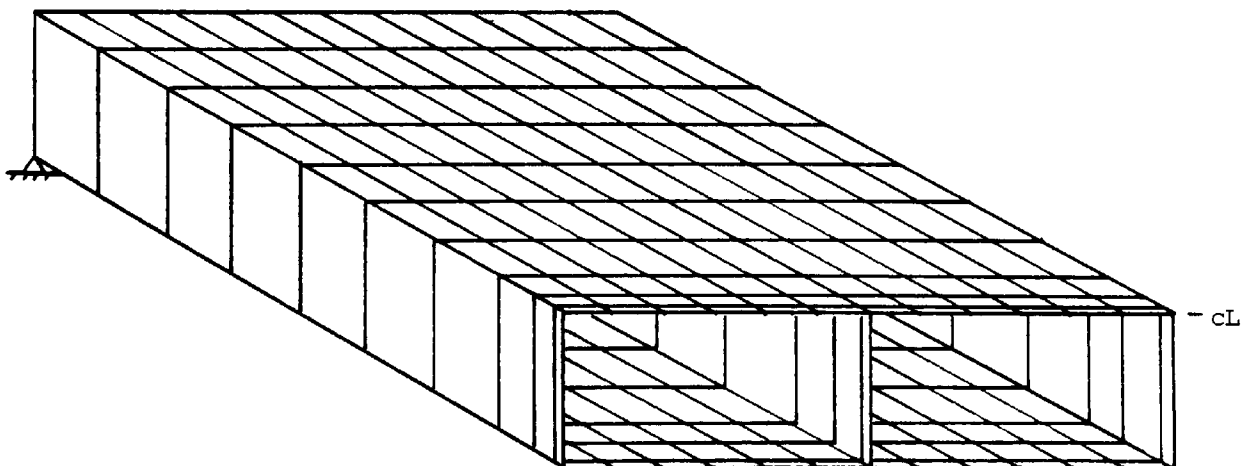


(a) Cross-section.



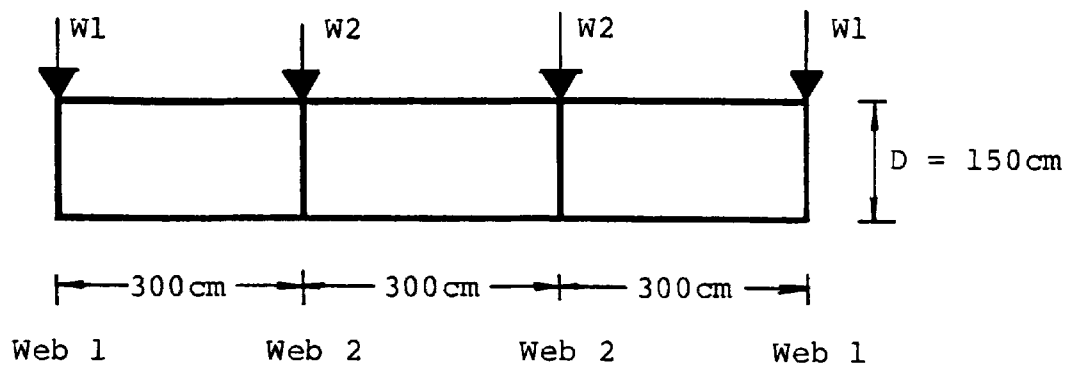
LOAD	W1 (kN)	W2 (kN)
Point	359.4	481.2
Line	709.5	981.0

(b) Span and load details.

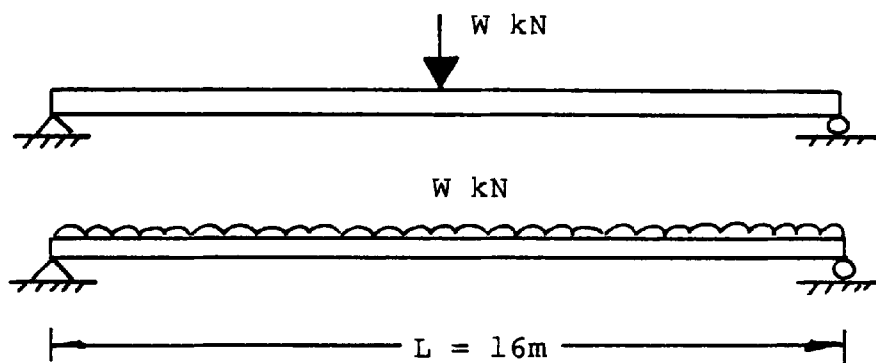


(c) Finite element idealization.

FIGURE 3.11 - DETAILS OF TWO-CELL STRUCTURE.

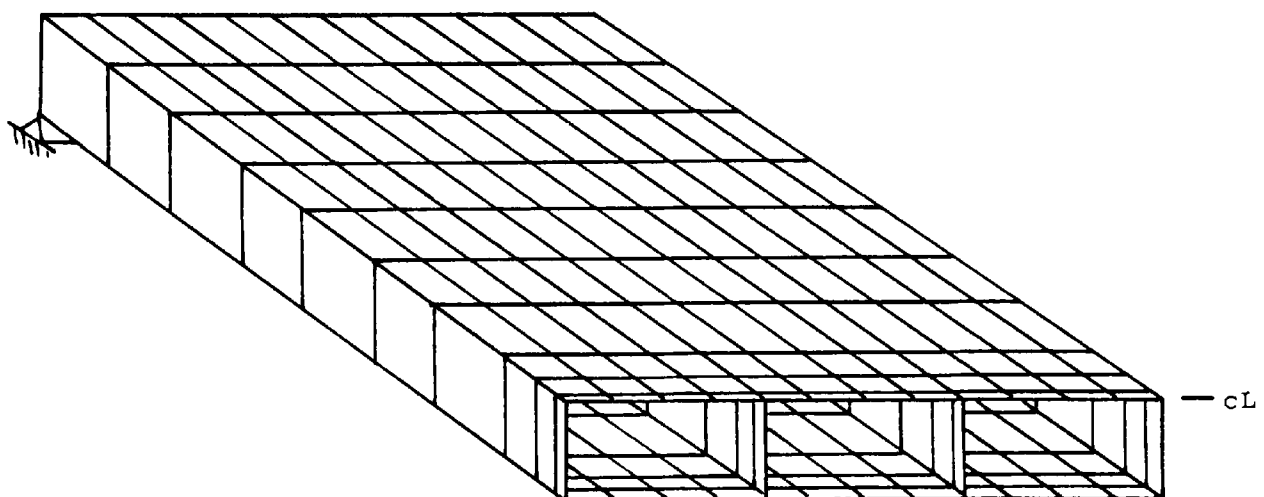


(a) Cross-section.



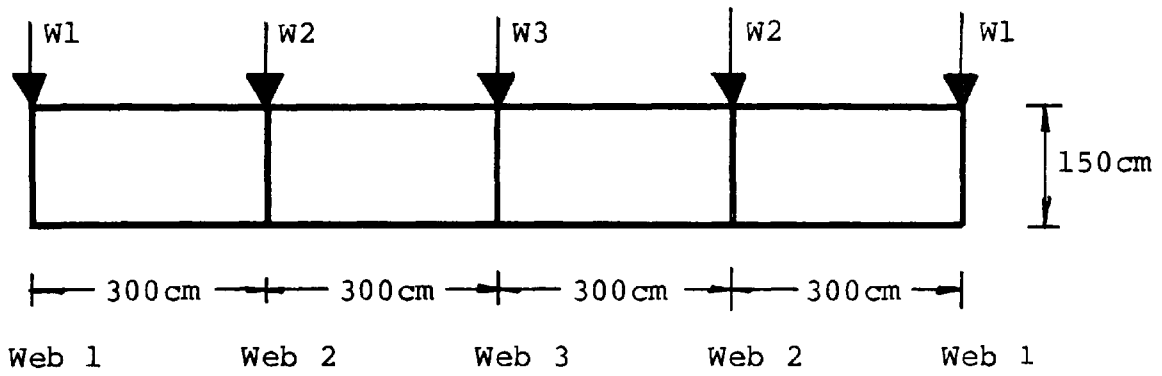
LOAD	W1 (kN)	W2 (kN)
Point	385	515
Line	758	1042

(b) Span and load details.

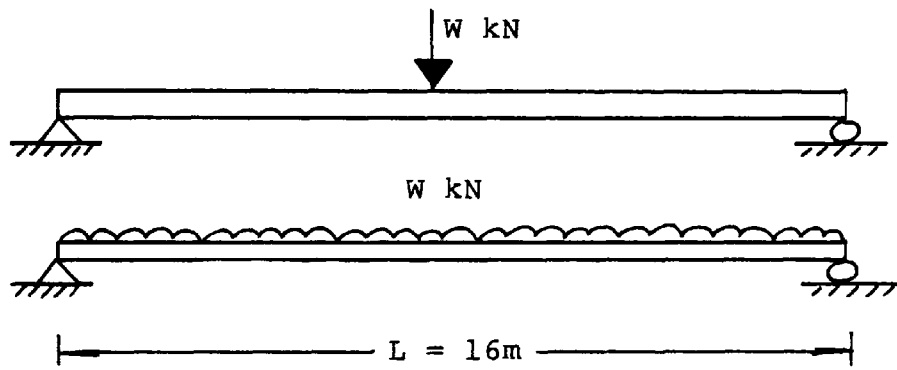


(c) Finite element idealization.

FIGURE 3.12 - DETAILS OF THREE-CELL STRUCTURE.

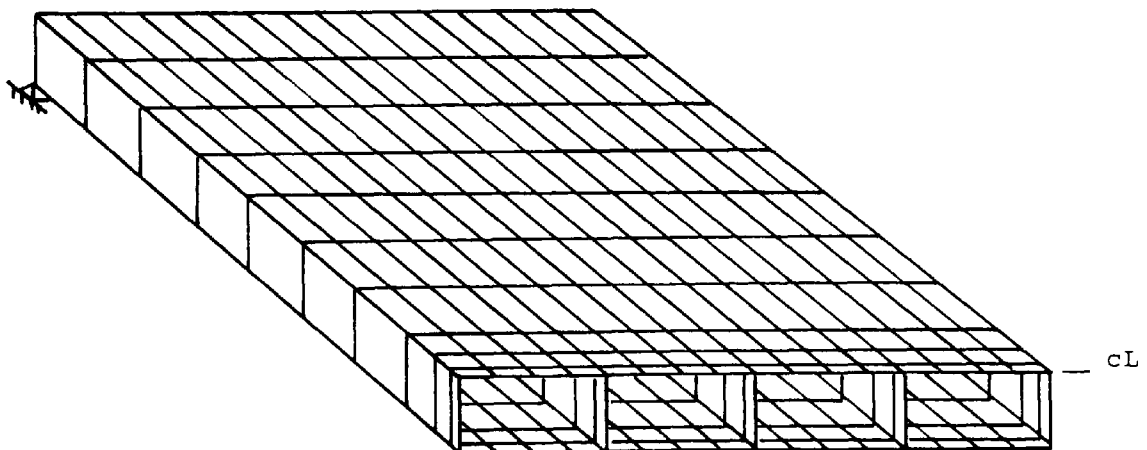


(a) Cross-section.



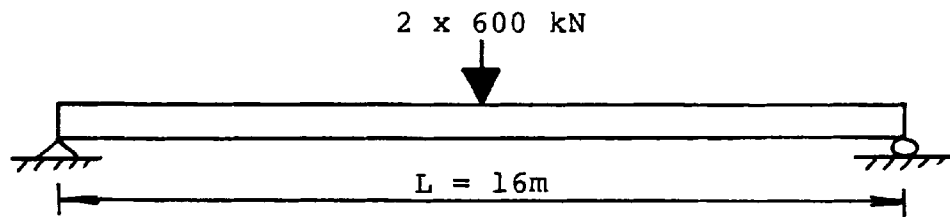
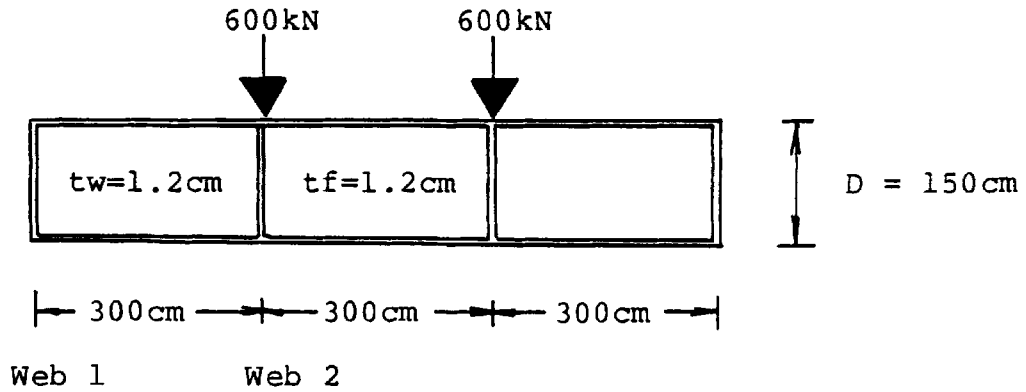
LOAD	W1 (kN)	W2 (kN)	W3 (kN)
Point	402.4	527.6	540.0
Line	793.2	1063.7	1086.2

(b) Span and load details.

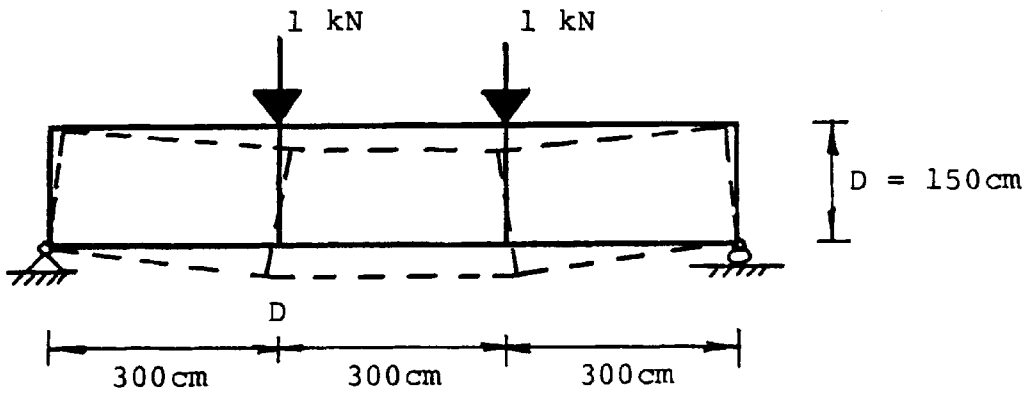


(c) Finite element idealization.

FIGURE 3.13 - DETAILS OF FOUR-CELL STRUCTURE.



(a) Loading and cross-section details.



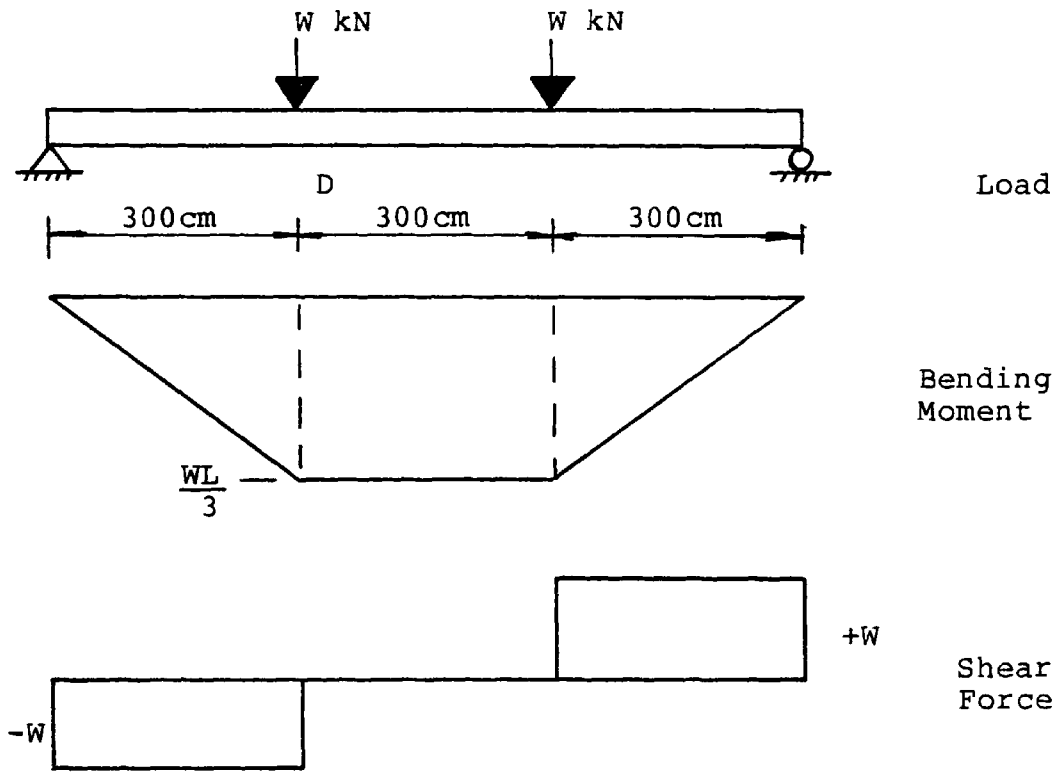
Second moment of area of members, $IY = 14.4 \text{ cm}^4$

Cross-sectional area of members, $Ax = 120 \text{ cm}^2$

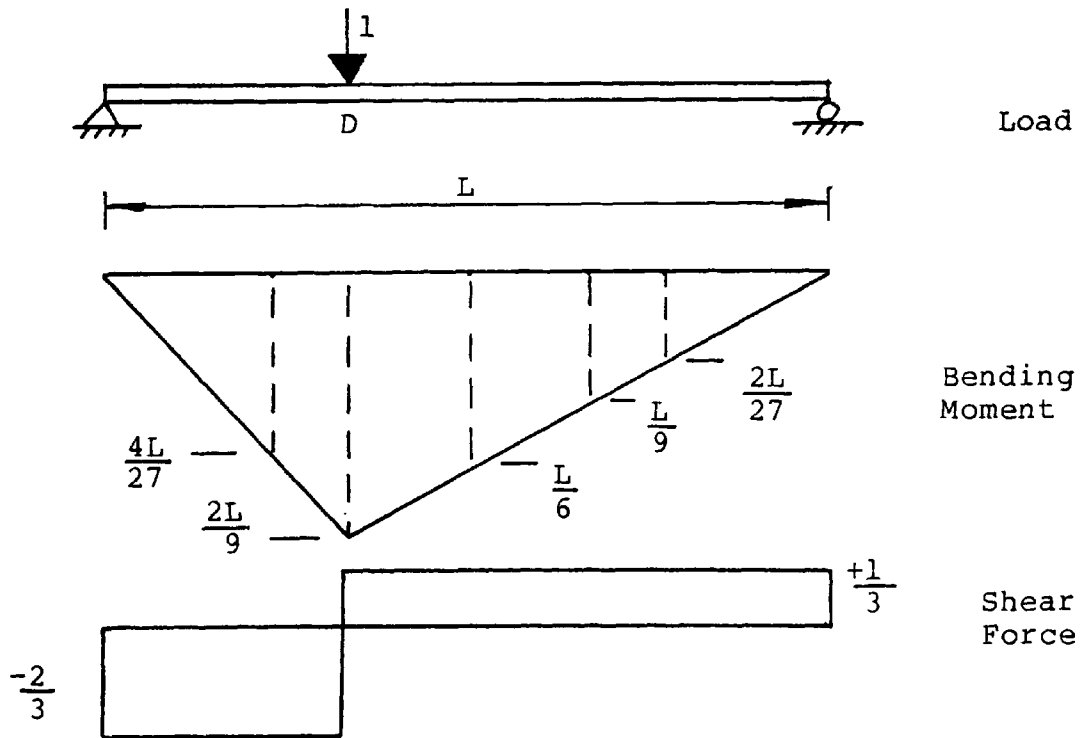
vertical deflection of joint D = 5.4467 cm

(b) Equivalent Vierendeel frame details.

FIGURE 3.14 - DETAILS OF THREE-CELL STRUCTURE USED IN DISTORTION STUDY.

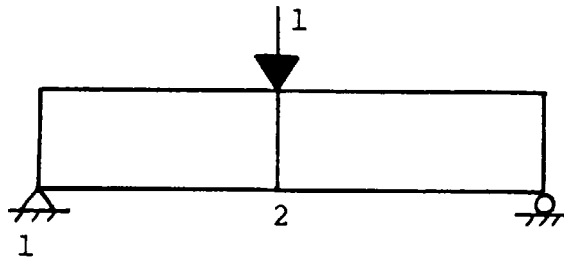


(a) Real system - loading, B.M. and S.F. diagrams.



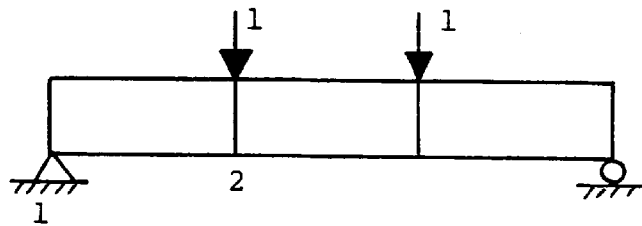
(b) Virtual system - loading, B.M. and S.F. diagrams.

FIGURE 3.15 - EQUIVALENT BEAM DETAILS
REAL AND VIRTUAL SYSTEMS.



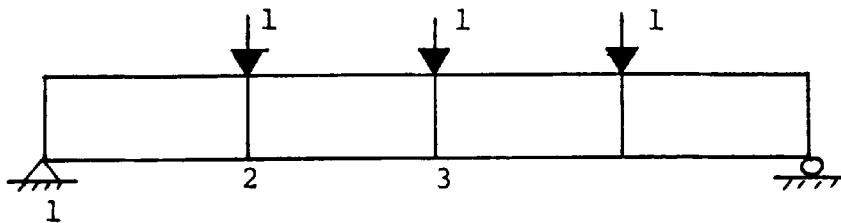
	Plane frame	Eq. frame	Eq. As	Eq. IY
θ_1	-0.00286	-0.00286	0	-0.0186
d_2	-2.289	-2.289	-3.714	-4.186

(a) Two-Cell.



	Plane frame	Eq. frame	Eq. As	Eq. IY
θ_1	-0.00614	-0.00595	0	-0.0373
d_2	-5.446	-5.059	-7.429	-9.317
θ_2	-0.00537	-0.00298	0	-0.0186

(b) Three-Cell.



	Plane frame	Eq. frame	Eq. As	Eq. IY
θ_1	-0.00946	-0.00905	0	-0.0522
d_2	-8.696	-7.849	-11.145	-14.111
θ_2	-0.0113	-0.0061	0	-0.0366
d_3	-12.252	-10.620	-14.860	-19.861

(c) Four-Cell.

FIGURE 3.16 - COMPARISON OF SLOPES AND DEFLECTIONS FOR VIERENDEEL FRAME, EQUIVALENT FRAME AND EQUIVALENT BEAM.

CHAPTER FOUR

IDEALIZATION FOR TORSION IN MULTI-CELL STRUCTURES

4.1. INTRODUCTION.

In this chapter the grillage idealization of multi-cell structures will be concluded with a consideration of the methods available for torsional idealization. The application of torsional loading to multi-cell structures causes stresses and deformations to be set up as a result of twisting and warping of the cross-section. Torsional effects on multi-cell structures are developed by shear loads whose lines of action do not coincide with the shear centre of the cross-section. This torsional loading can be divided into a pure torsional component and a distortional component, the latter has been considered in the previous chapter.

The pure torsional component produces rigid body rotation of the cross-section which develops shear stresses, or flows, predominantly around the perimeter flanges and webs, with some flow passing through the intermediate webs of the cross-section. In addition to this rigid body rotation the cross-section warps out of plane. If the cross-section is prevented from warping then considerable longitudinal stresses are developed as a consequence of the torsional loading.

Thin walled steel multi-cell structures possess high torsional inertia, hence it becomes necessary to adequately represent this torsional inertia in the grillage representation of structures of this form. The exact value of torsional inertia, J , may be evaluated by considering the shear flow around the section as described by KOLLBRUNNER and BASLER (1969).

Consider the multi-cell cross-section shown in figure 4.1(a) which has N cells and is subjected to a torsion moment, T . The torsion moment, T is related to the torsional inertia, J and the rate of twist, $d\theta/dx$ by the equation

$$T = G J \frac{d\theta}{dx} \quad \text{-----} \quad 4.1$$

The torsion moment is shared by the N cells each of which develops a constant shear flow $q_1, q_2 \dots q_i \dots q_n$, given by the Bredt-Batho formula

$$T = 2 \cdot A_i \cdot q_i$$

The total torsion moment is equal to the sum of individual torques for each cell, thus

$$T = \sum_{i=1}^N 2 \cdot A_i \cdot q_i \quad \text{-----} \quad 4.2$$

where A_i = enclosed area of cell i

q_i = shear flow in cell i

Considering the equilibrium of each cell of the cross-section the following system of linear equations can be developed

$$\begin{aligned}
q_1 \oint_1 \frac{ds}{t} - q_2 \oint_{1,2} \frac{ds}{t} &= \frac{2T}{J} A_1 \\
-q_{i-1} \oint_{i-1,i} \frac{ds}{t} + q_i \oint_i \frac{ds}{t} - q_{i+1} \oint_{i,i+1} \frac{ds}{t} &= \frac{2T}{J} A_i \\
- q_{n-1} \oint_{n-1,n} \frac{ds}{t} + q_n \oint_n \frac{ds}{t} &= \frac{2T}{J} A_n
\end{aligned}$$

where $\oint_i \frac{ds}{t}$ = summation of ratio of length/thickness around perimeter of cell i

$\oint_{i-1,i} \frac{ds}{t}$ = ratio of length/thickness of web between cell $i-1$ and cell i

The right hand side of the system of equations shows the torsion inertia, J , which is not yet determined. J is part of the factor $2T/J$ which is constant for every equation, because the rate of twist $d\theta/dx$ is assumed to be constant, and which may therefore temporarily be put equal to 1.

If the solution of the system with A_i on the right hand side only is denoted by q_i' then the solution of the actual system is given by

$$q_i = q_i' (2T/J) \quad \text{---- 4.3}$$

substitution of equation 4.3 into equation 4.2 and rearranging gives

$$J = 4 \sum_{i=1}^n A_i q_i' \quad \text{---- 4.4}$$

The use of the method will be demonstrated for the five cell structure defined in figure 4.1(b), where

from symmetry shear flows q_1 , q_2 and q_3 have to be evaluated such that J may be calculated.

Cell 1

$$\frac{6a}{t} q_1 - \frac{a}{t} q_2 = \frac{2T}{J} 2a^2$$

Cell 2

$$-\frac{a}{t} q_1 + \frac{6a}{t} q_2 - \frac{a}{t} q_3 = \frac{2T}{J} 2a^2$$

Cell 3

$$-\frac{a}{t} q_2 + \frac{6a}{t} q_3 - \frac{a}{t} q_2 = \frac{2T}{J} 2a^2$$

$$\text{or } \begin{bmatrix} 6 & -1 & 0 \\ -1 & 6 & -1 \\ 0 & -2 & 6 \end{bmatrix} \begin{Bmatrix} q_1 \\ q_2 \\ q_3 \end{Bmatrix} = \frac{2T}{J} \begin{Bmatrix} 2at \\ 2at \\ 2at \end{Bmatrix}$$

solution of this set of simultaneous equations gave the following values for shear flow

$$q_1 = \frac{41at}{99} \left(\frac{2T}{J} \right)$$

$$q_2 = \frac{48at}{99} \left(\frac{2T}{J} \right)$$

$$q_3 = \frac{49at}{99} \left(\frac{2T}{J} \right)$$

$$\begin{aligned} \text{and } J &= 4 \sum_{i=1}^5 A_i q_i' \\ &= 4 \left[\frac{41}{99} + \frac{48}{99} + \frac{49}{99} + \frac{48}{99} + \frac{41}{99} \right] 2a^3t \\ &= 18.35 a^3t \end{aligned}$$

These values together with those for the other multi-cell structures shown in figure 4.1(b) are presented in Table 4.1.

Alternatively the following equation, proposed by WITTRICK (1963), may be used for the evaluation of the torsional inertia for a structure consisting of several cells where the thicknesses of the flanges and webs are small compared with the overall dimensions of the section.

$$J = \frac{A^2 t}{b} \left[1 - \frac{2 \rho \alpha (\alpha^n - 1)}{n(\alpha - 1)(\alpha - 1)(\alpha^n - 1) + (\alpha^n + \alpha)} \right] \text{---- 4.5}$$

where $2b$ = overall width of section

d_1 = depth of section

A = area of section = $d_1 * 2b$

n = number of cells

t_3 = thickness of end webs

t = thickness of flanges

t_x = thickness of internal webs

$$r = \frac{2b * t_x}{n * d_1 * t_3}$$

$$\alpha = 1 + r + \sqrt{(2r + r^2)}$$

$$\rho = t_x / t_3$$

This equation was used to calculate the torsional inertia of the multi-cell structures shown in figure 4.1(b) and are presented in Table 4.1. These values show that when there are at least three cells in the cross-section equation 4.5 produces results to an accuracy of at least 97% of the exact values using equation 4.4.

CUSENS and PAMA (1975) proposed that for concrete box sections consisting of five or more cells, the torsional inertia of the section may be approximated by

considering the enclosed section as a single box and the total torsional inertia may be obtained using Bredt's formula for a single closed section

$$J = \frac{4 * A^2}{\oint \frac{ds}{t}} \quad \text{-----} \quad 4.6$$

which may be expressed as

$$J = \frac{2 * B^2 * D^2}{\left[\frac{B}{t_f} + \frac{D}{t_w} \right]} \quad \text{-----} \quad 4.7$$

where B = overall width of section

D = overall depth of section

t_f = flange thickness

t_w = web thickness

Cusens and Pama justified the approximation with the fact that for a multi-cell structure the net shear flow through an interior web is negligible and only the shear flow around the outer web and top and bottom flange plates is of prime significance.

The torsional inertias for the five single and multi-cell cross-sections shown in figure 4.1(b) were calculated using equation 4.7 and are presented in Table 4.1. These results show very close agreement with the exact values for all five cross-sections considered. The single and two cell structures produce exact values, in the case of the two cell structure the shear flow through the central web is zero because of the symmetry of the cross-section.

The three, four and five cell structures produced values to an accuracy of 99% of the exact values. The shear flow in the sections for the exact solution and the approximate solution based on shear flow around the outside perimeter is also shown in Table 4.1 and confirms that the predominant shear flow is around the perimeter of the cross-section.

SHANMUGAM (1978) proposed that double bottom ship structures act as a series of inter-connected closed cell tubes running in both the transverse and longitudinal directions. Consequently the torsional stiffness of each cell can be calculated using equation 4.6 for each cell. Thus the total stiffness of the cross-section is given by the summation of the individual cell stiffnesses as follows

$$J = \frac{2 * n * (2b)^2 * D^2}{\left[\frac{2b + D}{t_f} + \frac{D}{t_w} \right]} \quad \text{----- 4.8}$$

where $2b$ = width of each cell

n = number of cells

hence B = overall width of structure = $n * 2b$

This equation was used to evaluate the torsional inertia for the five cross-sections shown in figure 4.1(b) and the results are given in Table 4.1. These results show an underestimation of the torsional inertia using this method; the underestimation being 27% for the five cell structure.

The single cell and four cell structures subjected to torsional loading as shown in figure 4.2 were analysed using the finite element program QUEST. No diaphragms were present within the structure to restrict any distortional behaviour of the cross-section.

For the single cell structure the shear flow around the cross-section calculated by the finite element analysis was 1.1999 kN/cm. The theoretical value of shear flow, q , calculated using equation 4.2 was 1.2 kN/cm, indicating exact agreement between the theoretical and finite element calculations.

In the case of the four cell structure the finite element analysis produced a shear flow of 0.667 kN/cm around the outside webs and flanges, with negligible shear flow through the interior webs. This value agreed with the theoretical value obtained using equation 4.7 for the determination of torsional inertia based on the enclosed section being treated as a single cell.

The finite element results for both structures indicated that the cross-sectional deformation was due to a combination of distortional and torsional behaviour, resulting in the shear flow around the perimeter section.

It was thus concluded that for the purpose of the grillage idealization of multi-cell structures the torsional inertia will be calculated from the enclosed section using equation 4.7.

4.2. GRILLAGE REPRESENTATION.

It was shown in the previous section how torsional loading of a multi-cell structure produces shear flows around the flanges and through the webs of the cross-section. These shear flows will develop complementary shear flows in the longitudinal direction. The pattern of shear flow is shown in figure 4.3. When the multi-cell structure is analysed using the grillage method the torsional inertia of the multi-cell cross-section must be represented by the apportioning of appropriate values of torsional inertia to the longitudinal and transverse grillage beams. The torsion moments developed in the grillage beams are equivalent to the shear flows in the multi-cell structure; these torsion moments are shown in figure 4.3.

CUSENS and PAMA (1975) proposed that for a concrete multi-cell structure treated as an orthotropic plate, its torsional rigidities will come from the twist in two orthogonal directions. Because the top and bottom flange plate contributions are considered in both directions, the overall torsional stiffness of the structure will tend to be overestimated. Consequently, it was proposed that each of the equivalent torsional plate rigidities may be taken as one half of the total torsional rigidity of the multi-cell section. For the transverse cross-section the torsional inertia, J_t , is calculated based on equation 4.7 for a single cell representing the perimeter wall of the section.

The torsional inertia of each longitudinal grillage beam is thus

$$J(\text{long}) = \frac{Jt}{2 * n1} \quad \text{----} \quad 4.9$$

where n1 = number of longitudinal grillage beams

For a multi-cell structure with end diaphragms only, the longitudinal section is also a single cell box and the longitudinal torsional inertia, J1, may be expressed as

$$J1 = \frac{2 * L^2 * D^2}{\left[\frac{L}{t_f} + \frac{D}{t_d} \right]} \quad \text{----} \quad 4.10$$

where L = span of structure

t_d = thickness of end diaphragm

The torsional inertia of each transverse grillage beam is thus

$$J(\text{tran}) = \frac{J1}{2 * n_t} \quad \text{----} \quad 4.11$$

where n_t = number of transverse grillage beams

For the three cell structure shown in figure 4.4
where

$$B = 900 \text{ cm.}$$

$$D = 150 \text{ cm.}$$

$$L = 1600 \text{ cm.}$$

$$t_w = t_f = t_d = 1.2 \text{ cm.}$$

$$n1 = 4$$

$$n_t = 5$$

then equations 4.9 and 4.11 give longitudinal and transverse grillage beam torsional inertias of 5,207,000cm⁴ and 7,900,000cm⁴ respectively.

WEST (1973) considered that for concrete pseudo-slab and voided slab structures the transverse torsional inertia presented a good estimate of the overall twisting inertia of the structure. He proposed that the transverse torsional inertia, J_t , be shared between the transverse and longitudinal grillage beams as follows

$$\sum J(\text{long}) = \frac{J_t}{1 + Q}$$

$$\sum J(\text{tran}) = \frac{Q * J_t}{1 + Q}$$

$$\text{i.e. } J_t = \sum J(\text{long}) + \sum J(\text{tran})$$

where $Q = \text{ratio of } \frac{\text{longitudinal torsional inertia}}{\text{transverse torsional inertia}}$

Both torsional inertia values being expressed per unit length or width. For thin walled structures it can be shown that Q is approximately 1, hence the following equations may be used for the torsional inertia of the longitudinal and transverse grillage beams.

$$J(\text{long}) = \frac{J_t}{2 * n_t} \quad \text{----} \quad 4.12$$

$$J(\text{tran}) = \frac{J_t}{2 * n_l} \quad \text{----} \quad 4.13$$

For the three cell structure shown in figure 4.4 then equations 4.12 and 4.13 give longitudinal and

transverse grillage beam torsional inertias of 5,207,000cm⁴ and 4,166,000cm⁴ respectively. This method of idealization was used in all previous grillage analyses reported in Chapter Three. Preliminary investigations had suggested it to be the most appropriate method for torsional idealization.

SHANMUGAM (1978) proposed that for a multi-cell structure the torsional inertia be evaluated for each single cell in isolation and that this inertia be shared equally to the adjacent grillage beams. This results in the external longitudinal grillage beams being assigned a torsional inertia of one half the torsional inertia of a single cell and the internal longitudinal grillage beams the full torsional inertia of a single cell.

Using this approach the following values of torsional inertia were evaluated for the three cell structure defined in figure 4.4.

Torsional inertia of single cell = 10,800,000cm⁴

hence longitudinal grillage beam torsional inertias are 5,400,000cm⁴ and 10,800,000cm⁴ for the external and internal grillage beams respectively.

Treating the longitudinal section as a single cell the torsional inertia may be evaluated using equation 4.10 and sharing this equally between all transverse grillage beams gives a torsional inertia of 15,800,000cm⁴ per beam.

4.3. THREE CELL STRUCTURE UNDER TORSIONAL LOADING.

The three cell structure shown in figure 4.4 subjected to a midspan point load of 300 kN over one outer web represents the most severe condition of torsional loading that such structures would be expected to carry. The structure was analysed using the finite element program QUEST using the mesh shown in figure 3.12. The results, presented in Table 4.2, show that considerable rotation of the cross-section occurs resulting in an upward deflection of the unloaded outer web of 0.128cm. This upward deflection represents approximately 25% of the downward deflection of the loaded web. The nodal rotations and deflections also indicate that considerable distortion of the cross-section takes place.

The same structure was analysed using the grillage method, where the torsional idealizations of Cusens and Pama, West and Shanmugam were each used in turn in the determination of the torsional inertia of the longitudinal and transverse grillage beams. The results from all three analyses are also presented in Table 4.2. All three methods of idealization underestimated the deflection of the loaded web, the value of 0.340cm using West's proposals being the closest, representing an underestimation of the finite element value of 0.517cm by 34%. Another significant discrepancy was the inability of the grillage method, using each of the three idealizations, to predict the upward deflection of the unloaded outer web.

Comparison of the flange edge stress values revealed similar discrepancies. The values for stress at the loaded web calculated using the finite element and the grillage method using West's idealization were 40.96 N/mm² and 31.09 N/mm² respectively, representing an underestimation of 24%. At the unloaded outer web the finite element analysis predicted a tensile stress of 8.25 N/mm² in the top flange, whilst the grillage method predicted a compressive stress of 2.27 N/mm².

These results indicated that all three methods of idealization proposed were unsatisfactory when applied to the analysis of thin-walled steel multi-cell structures subjected to torsional loading. To develop an understanding of the structural behaviour of the grillage method a routine was incorporated into the grillage program SHEARGRID2 which calculated the strain energy developed in the grillage structure.

The strain energy due to bending moment, torsion moment and shear force was calculated for both the longitudinal and transverse grillage beams. The total strain energy in the structure was shown to equal the work done by the external loading on the structure. Details of the strain energy calculations are presented in Appendix E.

The torsional strain energy in the longitudinal and transverse grillage beams are presented in Table 4.2. These results reveal that the torsional strain energy of the longitudinal grillage beams was insignificant. The

transverse grillage beam torsional strain energy varied from 6.22kNm to 12.18kNm for the grillage analyses based on the idealizations of Shanmugam and West respectively.

The near zero value of torsional strain energy in the longitudinal grillage beams is attributable to the method used to allow distortion of the cross-section. The apportioning of a low shear area to the internal transverse grillage beams allows the cross-section to deform under load without the need for torsional rotation of the longitudinal grillage beams. Torsional rotations of the order of $1 * 10E-6$ radians are calculated for the longitudinal grillage beams, which bear no relationship to the values predicted by the finite element method. The idealizations of West and Shanmugam using longitudinal grillage beam torsional inertias of 5,400,000cm⁴ and 10,800,000cm⁴ respectively showed no significant change in torsional strain energy for the longitudinal grillage beams, the values being $8.9 * 10E-6$ and $2.1 * 10E-6$ respectively.

The value of torsional inertia apportioned to the transverse grillage beams did have an effect on the torsional strain energy of the transverse beams. When the torsional inertia was reduced from 15,800,000cm⁴ per beam (Shanmugam) to 4,166,000cm⁴ per beam (West) the torsional strain energy increased from 6.22kNm to 12.18kNm. This variation suggested that a reduction in the transverse grillage beam torsional inertia could lead to an improvement in the accuracy of analysis with respect to both deflection and stress.

To assess the significance of the apportioning of torsional inertia in both the longitudinal and transverse directions the following investigation was undertaken. The idealization proposed by West allocated 50% of the torsional inertia of the cross-section to both directions. The effect of varying this percentage allocation between the longitudinal and transverse grillage beams was considered using ratios of 60/40, 70/30, 80/20 and 90/10. The results of this investigation are presented in Table 4.2 and reveal that a significant improvement in accuracy can be achieved for both deflection and stress at the loaded web with an increase in the percentage allocation of torsional inertia to the longitudinal grillage beams.

The variation of deflection and flange edge stress at the loaded web against percentage allocation of torsional inertia is plotted in figure 4.5. The variation in torsional strain energy for the transverse grillage beams is also shown in figure 4.5. This showed the torsional strain energy reaching a maximum when 80% of the torsional inertia of the cross-section is apportioned to the longitudinal grillage beams. When the percentage allocation is 90% the grillage method predicted a web deflection of 0.485cm, an underestimation of 6%, and a flange edge stress of 41.83N/mm², an overestimation of 2%.

The grillage method was still unable to predict the upward deflection of the unloaded outer web. This was expected because the distortional modelling of the

cross-section prevents the grillage method from modelling the pure torsional behaviour of the structure.

If one considers the three cell structure as a cantilever whose length is equal to half the simply supported span, then the 300kN load at the outer web develops a torsional moment of 135,000kNcm on the cross-section of the structure. The torsional inertia of the cross-section is 41,657,000cm⁴ and the rate of twist of the cross-section may be calculated using equation 4.1 giving

$$\frac{d\theta}{dx} = \frac{T}{GJ} = 4.01 * 10E-7$$

The rotation at the end of the cantilever will be

$$4.01 * 10E-7 * 800 = 3.21 * 10E-4 \text{ radians}$$

producing a vertical deflection at the outer webs of the cross-section of

$$3.21 * 10E-4 * 450 = 0.144\text{cm}$$

and a vertical deflection at the inner webs of

$$3.21 * 10E-4 * 150 = 0.048\text{cm}$$

If one considers that comparable deflections are developed in the simply supported structure at the midspan section, then if these values are subtracted from the finite element results the effect of torsional rotation is omitted from the deflected shape of the cross-section.

web1	web2	web3	web4
0.517	0.125	-0.007	-0.128
<u>-0.144</u>	<u>-0.048</u>	<u>+0.048</u>	<u>+0.144</u>
0.373cm	0.073cm	0.041cm	0.016cm

These values of deflection agree with the grillage method where approximately 65% of the torsional inertia is allocated to the longitudinal grillage beams.

The cross-section of the structure also warps out of plane under the action of the torsional loading. MEGSON (1974) showed that the warping displacement at the corners of a rectangular thin-walled cross-section can be expressed as

$$w_o = + \frac{T}{8*b*d*G} \left[\frac{d}{t_w} - \frac{b}{t_f} \right] \text{ ---- 4.14}$$

where w_o = warping displacement

T = torsion moment = 135,000kNcm

b = width of cross-section = 900cm

d = depth of cross-section = 150cm

t_w = web thickness = 1.2cm

t_f = flange thickness = 1.2cm

G = modulus of rigidity = 8077kN/cm²

In the case of the cross-section considered, equation 4.14 gives a warping displacement at the corners of +/- 0.00967cm.

In a cross-section where this warping displacement is prevented because of axial restraint a direct stress is developed in the structure. This direct stress may be determined using the following equation

$$\sigma = \mu * E * w_o \frac{\sinh \mu (L-z)}{\cosh \mu L} \text{ ---- 4.15}$$

$$\text{where } \mu^2 = \frac{8 \cdot G \cdot t_w \cdot t_f}{A_b \cdot E \cdot (d \cdot t_f + b \cdot t_w)}$$

L = length of structure

z = distance from section where axial restraint is applied

and A_b = area of longitudinal boom located at corner of section, replacing direct stress carrying capacity of webs and flanges

$$= \frac{1}{6} [d \cdot t_w + b \cdot t_f]$$

$$= \frac{[150 \cdot 1.2 + 900 \cdot 1.2]}{6}$$

$$= \underline{210 \text{ cm}^2}$$

A condition of axial restraint exists at the midspan cross-section as a result of the symmetrical loading at this position. Hence, the direct stress developed at this section may be calculated using equation 4.15 where $z = 0$ and $L = \text{half span of structure} = 900 \text{ cm}$. Substitution of the relevant values into equation 4.15 gave a direct stress of $\pm 8.29 \text{ N/mm}^2$ at the corners of the cross-section, and a direct stress of $\pm 2.76 \text{ N/mm}^2$ at the inner web positions.

When these direct stress values are subtracted from the finite element results the flange stress values are

web1	web2	web3	web4
40.96	8.51	-0.14	-8.25
<u>-8.29</u>	<u>-2.76</u>	<u>+2.76</u>	<u>+8.29</u>
32.67N/mm2	5.75N/mm2	2.62N/mm2	0.04N/mm2

These values of flange stress agree with the grillage method where 60% of the torsional inertia is

allocated to the longitudinal grillage beams.

This study revealed the limitations of the grillage method when the loading developed high torsional effects on the structure. The grillage idealization is unable to model the torsional rotation of the cross-section and predict the direct flange stresses developed from warping of the cross-section. The displacements and stresses predicted by the grillage method were 20 - 25% lower than the finite element results.

4.4. DISTRIBUTION OF TORSIONAL INERTIA BETWEEN LONGITUDINAL AND TRANSVERSE GRILLAGE BEAMS.

The distribution of torsional inertia between the longitudinal and transverse grillage beams was shown to have an effect on the values of web deflection and flange edge stress predicted by the grillage method. In this section a method of distributing the torsional inertia of the cross-section will be developed for multi-cell structures in accordance with the breadth/span ratio of the structure.

The three multi-cell structures shown in figure 4.6 were considered, and comprised two, three and four cell structures with each cell of constant proportions where

cell breadth	=	300cm
cell depth	=	150cm
span	=	1600cm
flange, web and end diaphragm thickness	=	1.2cm

Each structure was subjected to four symmetrical loading patterns which did not produce torsional loading of the cross-section. These four loading patterns were

- (i) midspan point load over outer webs
- (ii) midspan point load over inner web(s)
- (iii) uniform line load over outer webs
- (iv) uniform line load over inner web(s)

These loading patterns and their intensities are shown in figure 4.6

The structures were analysed using the finite element method to produce values of web deflection and flange edge stress at midspan for comparison purposes. In the grillage idealization nine transverse grillage beams were used, and one longitudinal grillage beam represented each longitudinal web. The appropriate stiffness parameters of the grillage beams are presented in Table 4.3 for all three structures. This table also shows the distribution of torsional inertia considered for each structure.

The finite element and grillage method results for midspan web deflection and flange edge stress for all four loading cases are presented in Tables 4.4, 4.5 and 4.6 for the two, three and four cell structures respectively. These results are also presented in graphical form in figures 4.7 to 4.12 and show the variation of web deflection and flange edge stress against the distribution of torsional inertia between the longitudinal and transverse grillage beams.

Detailed investigation of these results, with particular reference to the accuracy of the deflection and stress values at the loaded webs, resulted in the following recommendation.

The ratio of overall breadth/span of structure should be used to apportion the torsional inertia of the cross-section to the longitudinal grillage beams, as follows.

The breadth/span ratios of each of the three structures considered are.

<u>No. of cells</u>	<u>breadth</u>	<u>span</u>	<u>ratio br/span</u>
2	600	1600	0.375
3	900	1600	0.5625
4	1200	1600	0.75

Using this recommendation for the four cell structure, 75% of the torsional inertia would be allocated to the longitudinal grillage beams and 25% to the transverse grillage beams.

The results from the finite element method and the grillage method using this recommendation are presented in Tables 4.7 and 4.8 for the two, three and four cell structures. The following conclusions were reached from a consideration of the results.

Midspan Point Load.

1. The midspan web deflection of the loaded web was consistently underestimated by the grillage method. The

greatest underestimation was -5.4% for the inner web loading condition on the three cell structure.

2. The midspan web deflection of the unloaded webs was consistently overestimated by the grillage method. This overestimation varied from 3% for the two cell structure to 52% for the four cell structure. It should be noted that for the four cell structure the unloaded web deflections were extremely small, the lowest value being 0.064cm, which represented only 17% of the loaded web deflection.
3. The midspan flange edge stress at the loaded web position was accurately predicted, revealing discrepancies within the range of -1.3% to +4.0% when compared with the finite element results.
4. The midspan flange edge stress at the unloaded web position was consistently overestimated, revealing discrepancies within the range 16.2% to 122.9%. The latter figure refers to the condition where the flange stress was extremely low, being predicted as 2.18N/mm² and 4.86N/mm² by the finite element and grillage methods respectively.

Uniform Line Load.

5. The midspan web deflection of the loaded web was consistently underestimated by the grillage method revealing discrepancies within the range -0.2% to -5.3%.

6. The midspan web deflection of the unloaded web was consistently overestimated, apart from one case which showed an underestimation of 11% for web 2 of the four cell structure. The overestimation varied from 3.5% for the two cell structure to 50.9% for the four cell structure. In the latter case the actual deflection values were 0.054cm and 0.081cm for the finite element and grillage methods respectively.
7. The midspan flange stress at the loaded web was consistently overestimated by the grillage method, revealing discrepancies within the range +0.7% to +8.5% when compared with the finite element results.
8. The midspan flange stress at the unloaded web position varied from an underestimation of -8.4% to an overestimation of +42.2%. The maximum underestimation occurred in the two cell structure when the outer webs were loaded; the stresses being 17.24N/mm² and 15.79N/mm² from the finite element and grillage methods respectively. The maximum overestimation occurred in the four cell structure when the central web was loaded; the actual stress values being low at 3.36N/mm² and 4.78N/mm² from the finite element and grillage methods respectively.

4.5. CONCLUSIONS.

The following conclusions can be drawn from the investigations reported in this chapter.

1. The overall torsional behaviour of a multi-cell structure may be represented in the grillage model by the torsional inertia of the transverse cross-section. The torsional inertia is calculated on the basis of the equivalent single cell represented by the flanges and outer webs only. The shear flow through the interior webs is considered to be negligible and hence can be ignored; this was confirmed by the finite element study on the four cell structure in Section 4.1.
2. The grillage idealization for cell distortion, where a low shear area is assigned to the transverse grillage beams, renders the behaviour of the grillage model insensitive to the value of torsional inertia assigned to the longitudinal grillage beams. The low shear area of the transverse grillage beams allows the cross-section to deform under load without the need for torsional rotation of the longitudinal grillage beams.
3. The values of deflection and flange stress predicted by the grillage method were dependent on the torsional inertia of the transverse grillage beams. The investigations in Section 4.4 revealed the importance of the correct allocation of torsional inertia of the cross-section to the longitudinal and transverse grillage beams. The recommendation, that the ratio of

overall breadth to span of structure be used to determine the percentage allocation of torsional inertia to the longitudinal direction, was shown to produce results of acceptable accuracy for symmetrical distortional loading.

4. Symmetrical distortional loading of the cross-section can be accurately analysed using the grillage method. The values of web deflection and flange stress at the critical loaded webs were accurately predicted to within an accuracy of 10% of the finite element values. The stresses were consistently overestimated, yielding an upper bound solution, whilst the deflections were consistently underestimated. The unloaded web values of stress and deflection were not so accurately predicted, but the grillage method did model the distribution of stress and the deflected profile across the cross-section.
5. The grillage method was unable to model the behaviour of the structure when subjected to asymmetrical loading conditions which developed torsional loading on the cross-section of the structure. The grillage beam cannot accurately model the torsional rotation of the cross-section and hence underestimates the web deflection values across the section. The grillage method cannot predict the upward deflections that can occur in unloaded webs as a result of this torsional rotation of the cross-section. Underestimations of the order of 35% were observed in web deflection values and

studies show that the accuracy reduces as the eccentricity of torsional loading increases.

6. The grillage method was also unable to predict the longitudinal stresses developed due to restraint of the in-plane warping deflection of the cross-section when torsional loading conditions are present. This results in an underestimation of flange stresses of the order of 36% when compared to the finite element values. The accuracy of the predicted flange stresses also reduces with increasing torsional loading.

The accuracy of the grillage results for the asymmetrical loading condition considered was disappointing. However, this loading condition represents a very severe test on the validity of the proposed method of analysis. In practice the uniformly distributed dead load component will tend to diminish the torsional effect of asymmetrical loading. Under these conditions the grillage method will be more able to predict the behaviour of the structure to an acceptable degree of accuracy.

The encouraging results from chapter three and for symmetrical distortional loading in this chapter confirms that the grillage method can predict the behaviour of multi-cell structures under a variety of loading conditions. Consequently, in the next chapter the conclusions reached from this and the previous chapter will be applied to the analysis of a number of straight, simply supported multi-cell structures under various conditions of point and uniform line loading.

		No. of cells				
		1	2	3	4	5
T O R S I O N A L I N E R T I A	Exact Eqn 4.4	2.67	6.40	10.36	14.35	18.35
	Enclosed Area Eqn 4.7 %	2.67	6.40	10.28	14.24	18.19
		0.0	0.0	-0.8	-0.8	-0.9
	Wittrick Eqn 4.5 %	2.19	6.05	10.03	14.02	18.02
-18.0		-5.5	-3.2	-2.3	-1.8	
Single Cell Eqn 4.8 %	2.67	5.33	8.00	10.67	13.33	
	0.0	-16.7	-22.8	-25.6	-27.4	
S H E A R F L O W	q1	0.667	0.800	0.824	0.828	0.828
	q2	-	0.000	0.941	0.966	0.970
	q3	-	-	-	-	0.990
	qe	0.667	0.800	0.857	0.889	0.909

Torsional Inertia, J (* a³ t)

Shear Flow, q (* $\frac{T}{J}$ a t)

q1 , q2 and q3 are defined in figure 4.1.

qe - shear flow around median line only.

TABLE 4.1. - Torsional Inertia and Shear flow
in multi-cell structure.

		Web number				Torsional Strain Energy	
		1	2	3	4	Long. *10E-6	Trans.
W E B D E F L E C T I O N	Finite Element	0.517	0.125	-0.007	-0.128		
	Cusens	0.294	0.095	0.059	0.049	5.5	9.36
	/Pama	0.258	0.095	0.071	0.064	2.1	6.22
	Shanmugam	0.340	0.094	0.045	0.032	8.9	12.18
	West						
	60/40	0.359	0.092	0.040	0.026	8.8	12.95
	70/30	0.384	0.088	0.033	0.020	9.3	13.68
	80/20	0.422	0.081	0.024	0.012	11.0	14.07
	90/10	0.485	0.064	0.011	0.004	13.0	12.87
	L O N G S T R E S S	Finite Element	40.96	8.51	-0.14	-8.25	
Cusens		27.50	7.33	4.39	3.47		
/Pama		24.58	7.37	5.34	4.61		
Shanmugam							
West		31.09	7.09	3.31	2.27		
60/40		32.51	6.92	2.91	1.87		
70/30		34.43	6.63	2.40	1.39		
80/20		37.22	6.05	1.74	0.84		
90/10		41.83	4.70	0.85	0.28		

60/40 - represents 60% of torsional inertia apportioned to the longitudinal grillage beams and 40% to the transverse grillage beams.

TABLE 4.2. - Comparison of web deflection (cm) and longitudinal flange stress (N/mm²) for various grillage idealizations. Asymmetrical loading condition. Three-cell structure.

No. of Cells	Grillage beam	second moment of area (cm ⁴)	Eff. shear area (cm ²)	distribution of torsional inertia(*10E3cm ⁴)							Torsional Inertia Cross-Section (cm ⁴)
				30/70	40/60	50/50	60/40	70/30	80/20	90/10	
T W O	Long. Outer	2232900.	180.	2592.	3456.	4320.	5184.	6048.	6912.	7776.	25920000.
	Long. Inner	4128300.	180.								
	Tran. Outer	1687500.	180.	2016.	1728.	1440.	1152.	864.	576.	288.	
	Tran. Inner	2700000.	0.01								
T H R E E	Long. Outer	2232900.	180.			5207.	6249.	7290.	8331.	9373.	41657000.
	Long. Inner	4128300.	180.								
	Tran. Outer	1687500.	180.			2314.	1851.	1388.	926.	463.	
	Tran. Inner	2700000.	0.01								
F O U R	Long. Outer	2232900.	180.			5760.	6912.	8064.	9216.	10368.	57600000.
	Long. Inner	4128300.	180.								
	Tran. Outer	1687500.	180.			3200.	2560.	1920.	1280.	640.	
	Tran. Inner	2700000.	0.01								

30/70 - 30% torsional inertia of cross-section allocated to longitudinal grillage beams
70% torsional inertia of cross-section allocated to transverse grillage beams

TABLE 4.3. - Two, Three and Four Cell structures.
Stiffness parameters for grillage idealization

Loading Details		Tran/long distrib Torsion Inertia	Web deflection		Long. Stress			
			Web 1	Web 2	Web 1	Web 2		
M I D S P A N	W E B	F.E.	0.432	0.207	35.78	13.86		
		30/70	0.426	0.219	36.27	17.57		
		40/60	0.433	0.211	36.86	16.92		
		50/50	0.442	0.202	37.59	16.11		
		60/40	0.453	0.190	38.55	15.04		
		70/30	0.470	0.172	39.88	13.57		
	O N E	80/20	0.494	0.145	41.85	11.38		
		90/10	0.537	0.099	45.16	7.72		
		W E B	F.E.	0.207	0.543	12.44	39.13	
			30/70	0.219	0.519	17.15	38.76	
			40/60	0.211	0.527	16.52	39.46	
			50/50	0.202	0.537	15.72	40.34	
60/40	0.190		0.551	14.68	41.50			
70/30	0.172		0.570	13.25	43.09			
T W O	80/20	0.145	0.599	11.12	45.45			
	90/10	0.099	0.648	7.54	49.41			
	U N I F O R M	W E B	F.E.	0.515	0.261	23.70	17.24	
			30/70	0.508	0.278	24.94	15.90	
			40/60	0.516	0.269	25.43	15.37	
			50/50	0.527	0.258	26.06	14.69	
60/40			0.541	0.242	26.90	13.78		
70/30			0.562	0.220	28.09	12.50		
O N E		80/20	0.593	0.186	29.90	10.55		
		90/10	0.648	0.127	32.99	7.20		
		L I N E	W E B	F.E.	0.262	0.630	16.35	25.00
				30/70	0.278	0.602	15.92	25.64
				40/60	0.269	0.612	15.39	26.22
				50/50	0.258	0.624	14.71	26.95
60/40	0.242			0.641	13.80	27.93		
70/30	0.220			0.666	12.52	29.32		
T W O	80/20		0.186	0.702	10.56	31.43		
	90/10		0.127	0.766	7.22	35.05		

TABLE 4.4. - Variation of web deflection (cm) and longitudinal flange stress (N/mm²) with distribution of torsional inertia Two-cell structure.

Loading Details		Tran/long distrib Torsion Inertia	Web deflection		Long. Stress	
			Web 1	Web 2	Web 1	Web 2
M I D S P A N	W E B	F.E.	0.389	0.119	32.70	8.38
		50/50	0.365	0.142	31.55	11.40
		60/40	0.380	0.135	32.78	10.72
		70/30	0.400	0.123	34.49	9.77
		80/20	0.433	0.106	37.10	8.32
		90/10	0.491	0.074	41.65	5.80
P O I N T	W E B	F.E.	0.237	0.641	13.90	44.12
		50/50	0.285	0.602	22.26	45.43
		60/40	0.269	0.610	20.93	46.17
		70/30	0.247	0.622	19.08	47.20
		80/20	0.212	0.641	16.25	48.76
		90/10	0.149	0.675	11.33	51.49
U N I F O R M	W E B	F.E.	0.461	0.150	20.24	10.62
		50/50	0.429	0.182	20.48	10.36
		60/40	0.447	0.172	21.53	9.79
		70/30	0.474	0.158	23.05	8.97
		80/20	0.515	0.135	25.41	7.69
		90/10	0.589	0.095	29.66	5.40
L I N E	W E B	F.E.	0.302	0.753	19.00	32.32
		50/50	0.363	0.707	20.75	31.64
		60/40	0.344	0.717	19.61	32.25
		70/30	0.315	0.733	17.97	33.14
		80/20	0.271	0.757	15.41	34.52
		90/10	0.190	0.800	10.32	37.00

TABLE 4.5. - Variation of web deflection (cm) and longitudinal flange stress (N/mm²) with distribution of torsional inertia Three-cell structure.

Loading Details		Tran/long distrib Torsion Inertia	Web deflection			Long. Stress		
			Web 1	Web 2	Web 3	Web 1	Web 2	Web 3
M I D S P A N	W E B 1	F.E.	0.382	0.091	0.042	32.64	6.76	3.73
		50/50	0.323	0.120	0.091	28.12	9.75	7.10
		60/40	0.338	0.116	0.083	29.43	9.35	6.44
		70/30	0.360	0.109	0.072	31.29	8.77	5.56
		80/20	0.395	0.099	0.056	34.13	7.83	4.27
		90/10	0.459	0.076	0.030	39.20	6.00	2.31
P O I N T	W E B 3	F.E.	0.042	0.122	0.490	2.18	7.44	35.56
		50/50	0.091	0.122	0.412	6.93	9.97	30.14
		60/40	0.083	0.118	0.429	6.29	9.59	31.62
		70/30	0.072	0.112	0.453	5.42	9.03	33.69
		80/20	0.056	0.102	0.491	4.17	8.13	36.89
		90/10	0.030	0.080	0.562	2.26	6.31	42.65
U N I F O R M	W E B 1	F.E.	0.450	0.116	0.054	20.03	8.60	5.05
		50/50	0.375	0.152	0.117	17.38	8.72	6.62
		60/40	0.395	0.147	0.106	18.50	8.41	6.04
		70/30	0.422	0.139	0.092	20.10	7.95	5.23
		80/20	0.466	0.126	0.071	22.65	7.17	4.04
		90/10	0.548	0.098	0.039	27.34	5.56	2.19
L I N E	W E B 3	F.E.	0.054	0.154	0.561	3.36	9.14	20.75
		50/50	0.117	0.155	0.466	6.63	8.90	17.89
		60/40	0.106	0.151	0.487	6.04	8.61	19.10
		70/30	0.092	0.143	0.517	5.23	8.17	20.84
		80/20	0.071	0.130	0.566	4.05	7.42	23.62
		90/10	0.039	0.103	0.656	2.20	5.83	29.25

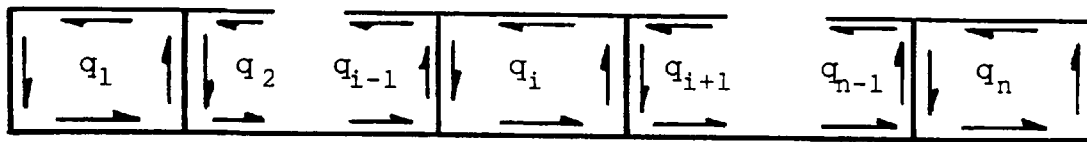
TABLE 4.6. - Variation of web deflection (cm) and longitudinal flange stress (N/mm²) with distribution of torsional inertia Four-cell structure.

No. of Cells	Load on Web		Web deflection			Long. Stress		
			Web 1	Web 2	Web 3	Web 1	Web 2	Web 3
T W O	1	F.E.	0.432	0.207		35.78	13.86	
		Gr.	0.431	0.213		36.71	17.07	
		%	-0.2	+2.9		+2.6	+23.1	
	2	F.E.	0.207	0.543		12.44	39.13	
		Gr.	0.213	0.525		16.68	39.29	
		%	+2.9	-3.3		+34.1	+0.4	
T H R E E	1	F.E.	0.389	0.119		32.70	8.38	
		Gr.	0.374	0.138		32.32	10.98	
		%	-3.8	+15.6		-1.2	+31.0	
	2	F.E.	0.237	0.641		13.90	44.12	
		Gr.	0.275	0.606		21.43	45.89	
		%	+16.0	-5.4		+54.2	+4.0	
F O U R	1	F.E.	0.382	0.091	0.042	32.64	6.76	3.73
		Gr.	0.378	0.104	0.064	32.54	8.36	4.98
		%	-1.0	+14.3	+52.4	-0.3	+23.8	+33.5
	3	F.E.	0.042	0.122	0.490	2.18	7.44	35.56
		Gr.	0.064	0.107	0.472	4.86	8.64	35.10
		%	+52.4	-12.3	-3.7	+123	+16.2	-1.3

TABLE 4.7. - Web deflection (cm) and longitudinal flange stress (N/mm²).
Finite Element and Grillage analyses.
Midspan Point Load.
Two, Three and Four cell structures.

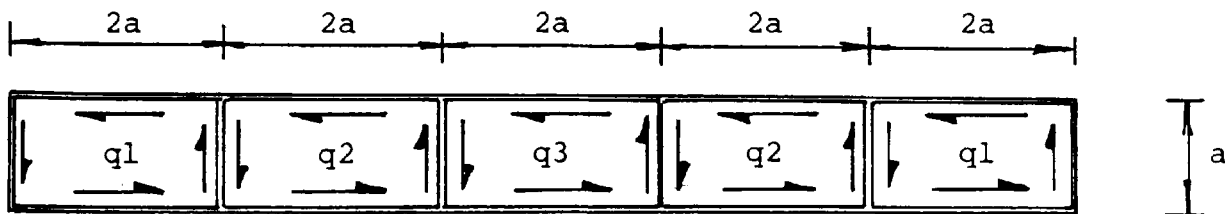
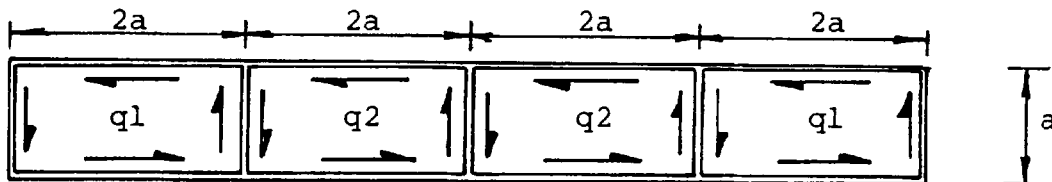
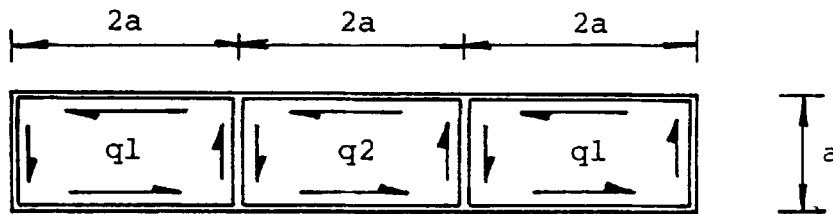
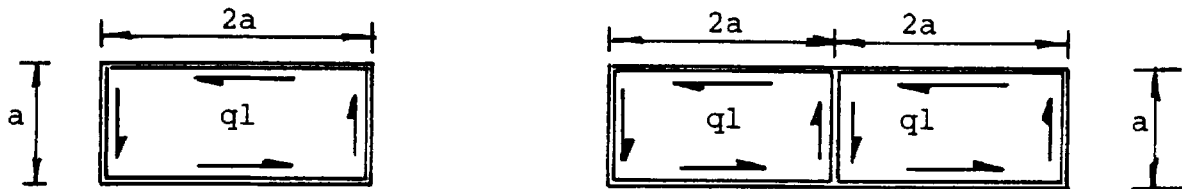
No. of Cells	Load on Web		Web deflection			Long. stress		
			Web 1	Web 2	Web 3	Web 1	Web 2	Web 3
T W O	1	F.E.	0.515	0.261		23.70	17.24	
		Gr.	0.514	0.271		25.71	15.79	
		⊗	-0.2	+3.9		+8.5	-8.4	
	2	F.E.	0.262	0.630		16.35	25.00	
		Gr.	0.271	0.610		15.79	26.52	
		⊗	+3.5	-3.3		-3.4	+6.1	
T H R E E	1	F.E.	0.461	0.150		20.24	10.62	
		Gr.	0.440	0.176		21.44	10.20	
		⊗	-4.6	+17.3		+5.9	-3.9	
	2	F.E.	0.302	0.753		19.00	32.32	
		Gr.	0.351	0.713		20.40	32.56	
		⊗	+16.3	-5.3		+7.4	+0.7	
F O U R	1	F.E.	0.450	0.116	0.054	20.03	8.60	5.05
		Gr.	0.444	0.132	0.081	21.56	7.75	4.78
		⊗	-1.3	+14.2	+50.9	+7.6	-9.9	-5.4
	3	F.E.	0.054	0.154	0.561	3.36	9.14	20.75
		Gr.	0.081	0.137	0.541	4.78	7.99	22.44
		⊗	+50.9	-11.0	-3.5	+42.2	-12.5	+8.1

TABLE 4.8. - Web deflection (cm) and longitudinal flange stress (N/mm²).
Finite Element and Grillage analyses.
Uniform Line Load.
Two, Three and Four cell structures.



typical cell i

(a) shear flow in n-cell structure.



flange thickness = web thickness = t

(b) Cross-section details of one to five-cell structures.

FIGURE 4.1 - DETAILS OF MULTI-CELL CROSS-SECTIONS USED FOR COMPARISON OF TORSIONAL INERTIA.

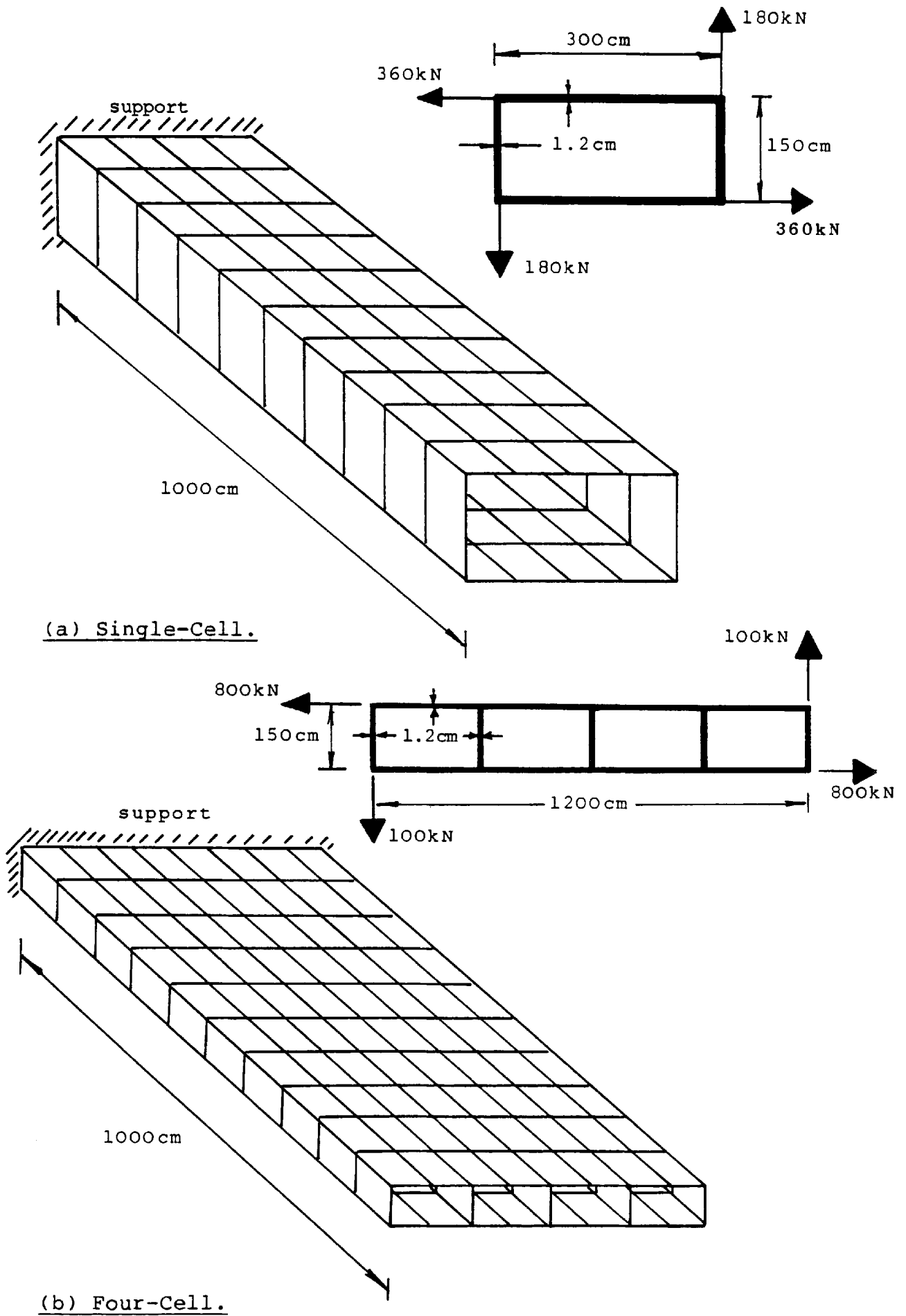
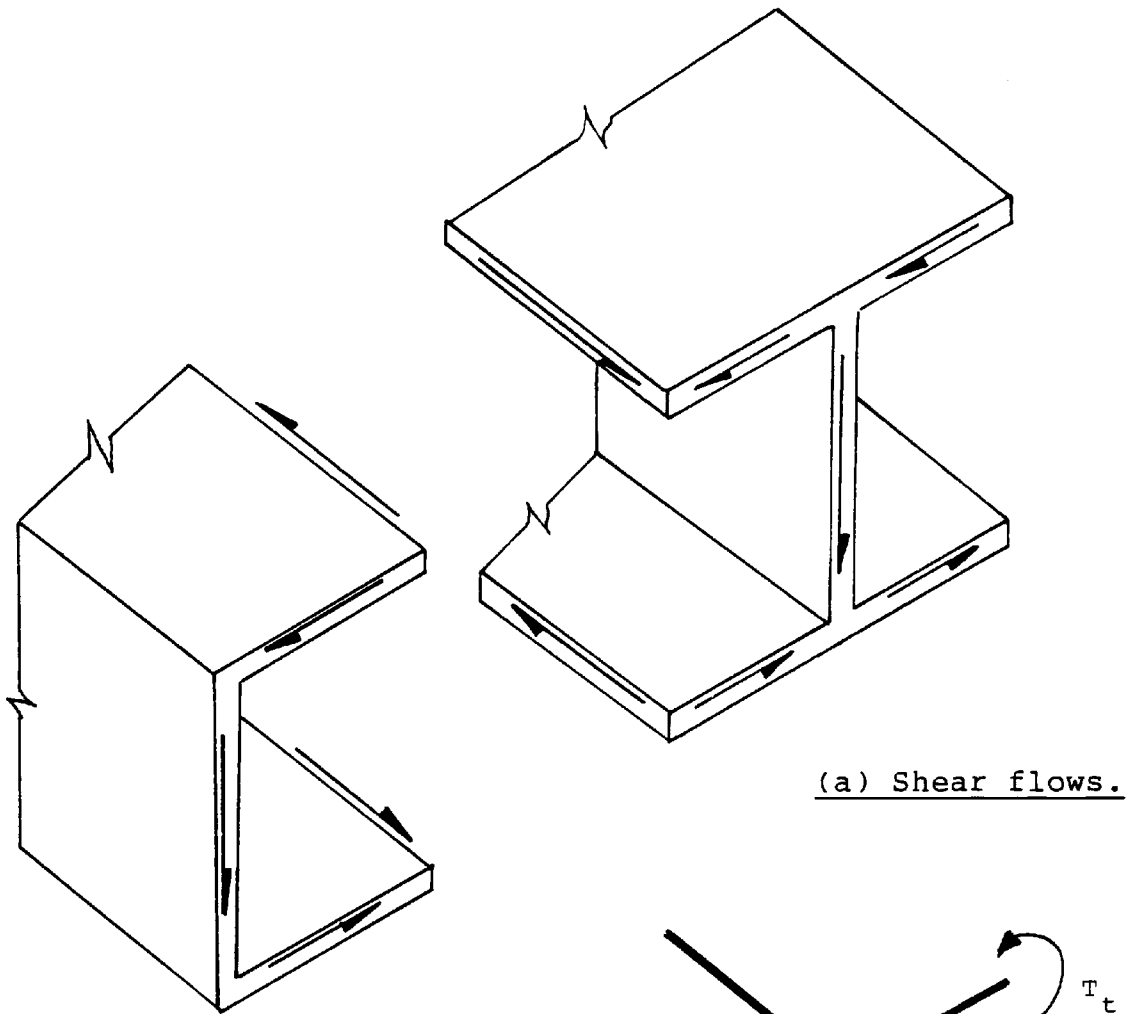
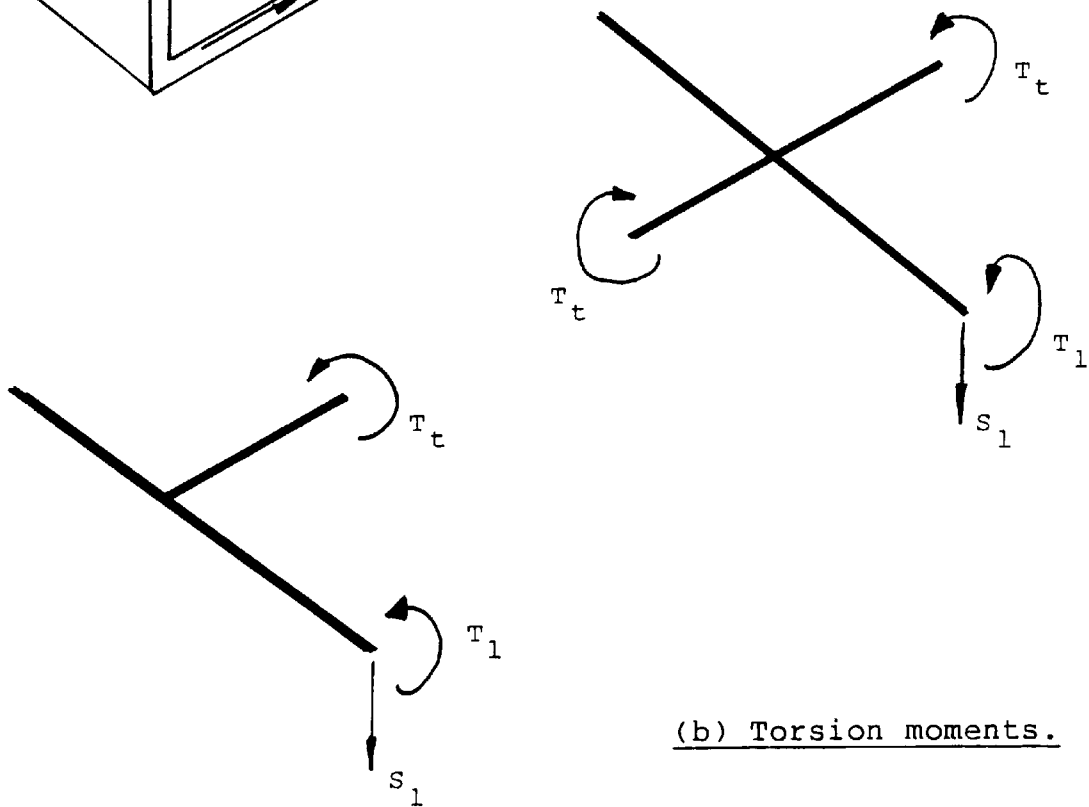


FIGURE 4.2 - DETAILS OF SINGLE AND FOUR CELL STRUCTURE USED IN TORSION STUDY.

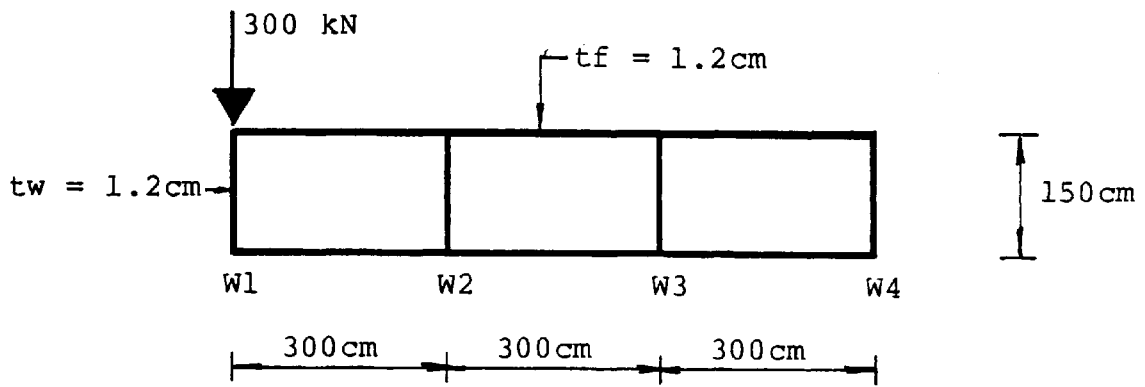


(a) Shear flows.

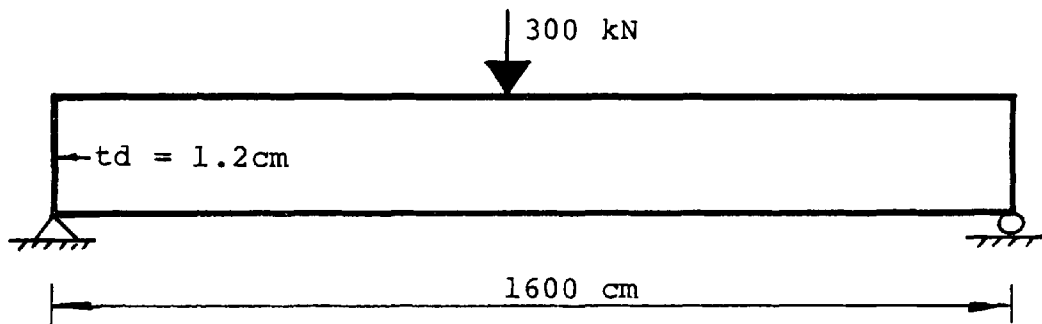


(b) Torsion moments.

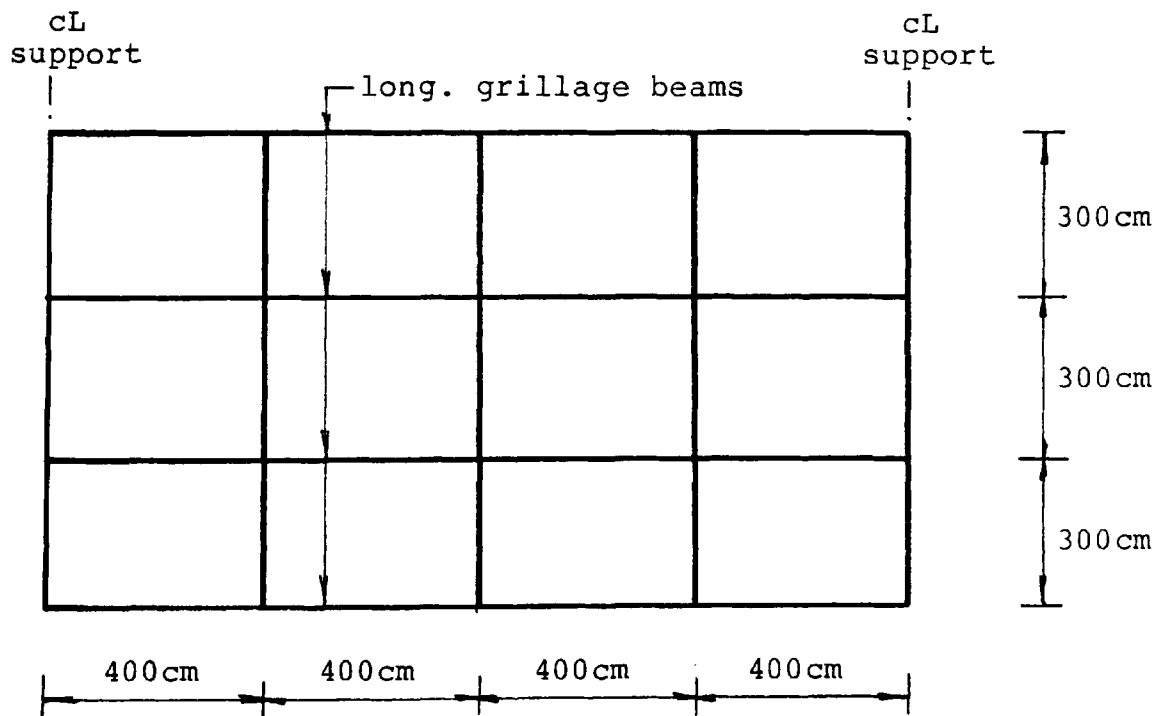
FIGURE 4.3 - SHEAR FLOWS IN MULTI-CELL STRUCTURE AND EQUIVALENT TORSION MOMENTS IN GRILLAGE.



(a) Cross-section.



(b) Longitudinal section.



(c) Grillage beam layout.

FIGURE 4.4 - THREE CELL STRUCTURE SUBJECTED TO TORSIONAL LOADING.

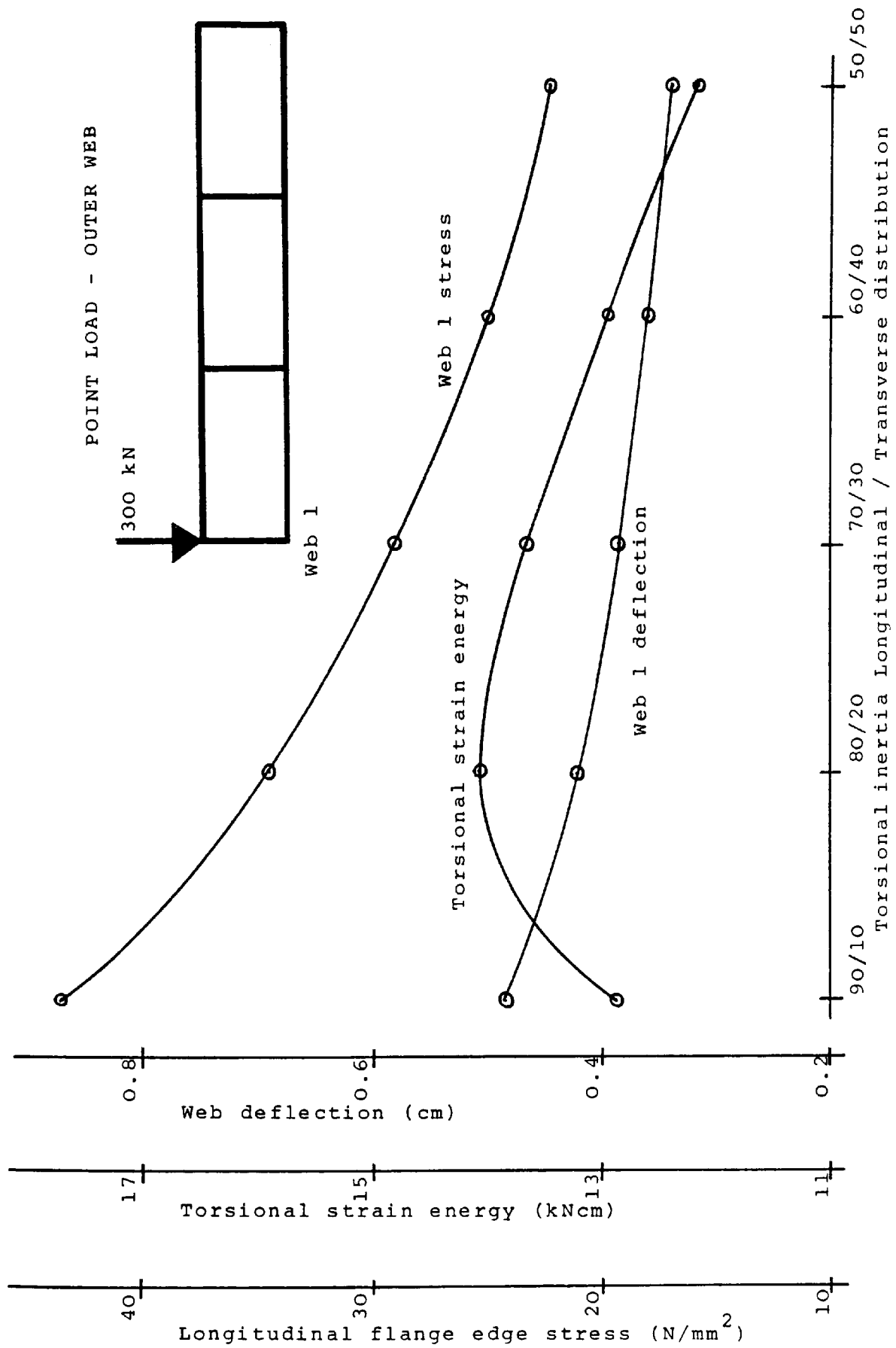
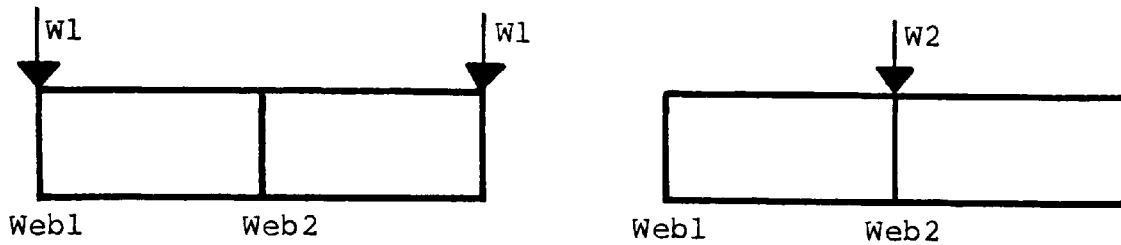
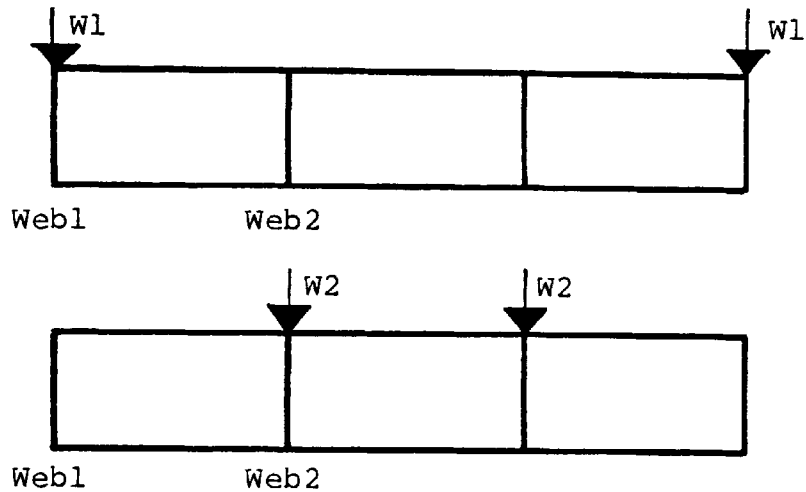


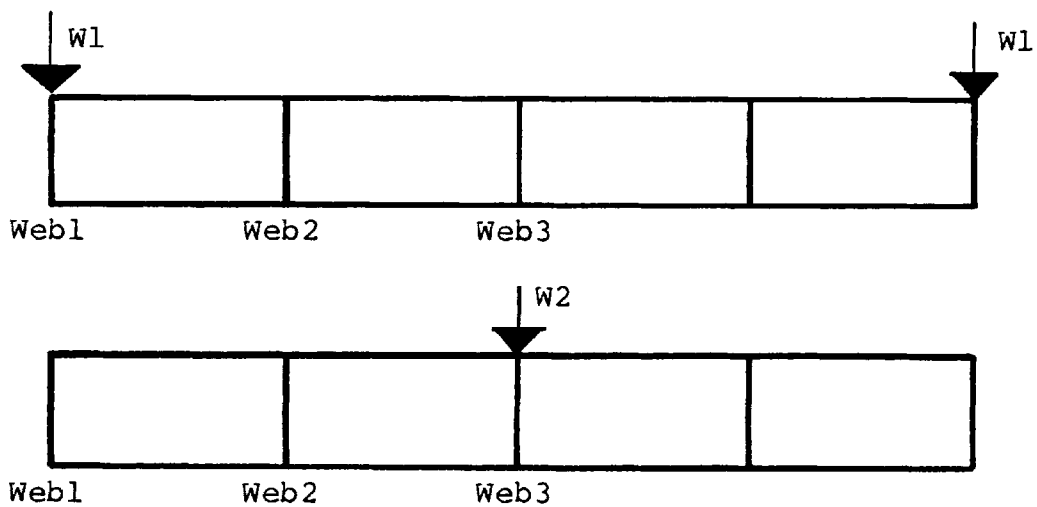
FIGURE 4.5 - VARIATION OF WEB DEFLECTION, LONGITUDINAL FLANGE EDGE STRESS AND TORSIONAL STRAIN ENERGY WITH PERCENTAGE ALLOCATION OF TORSIONAL INERTIA



(a) Two-cell structure.



(b) Three-cell structure.

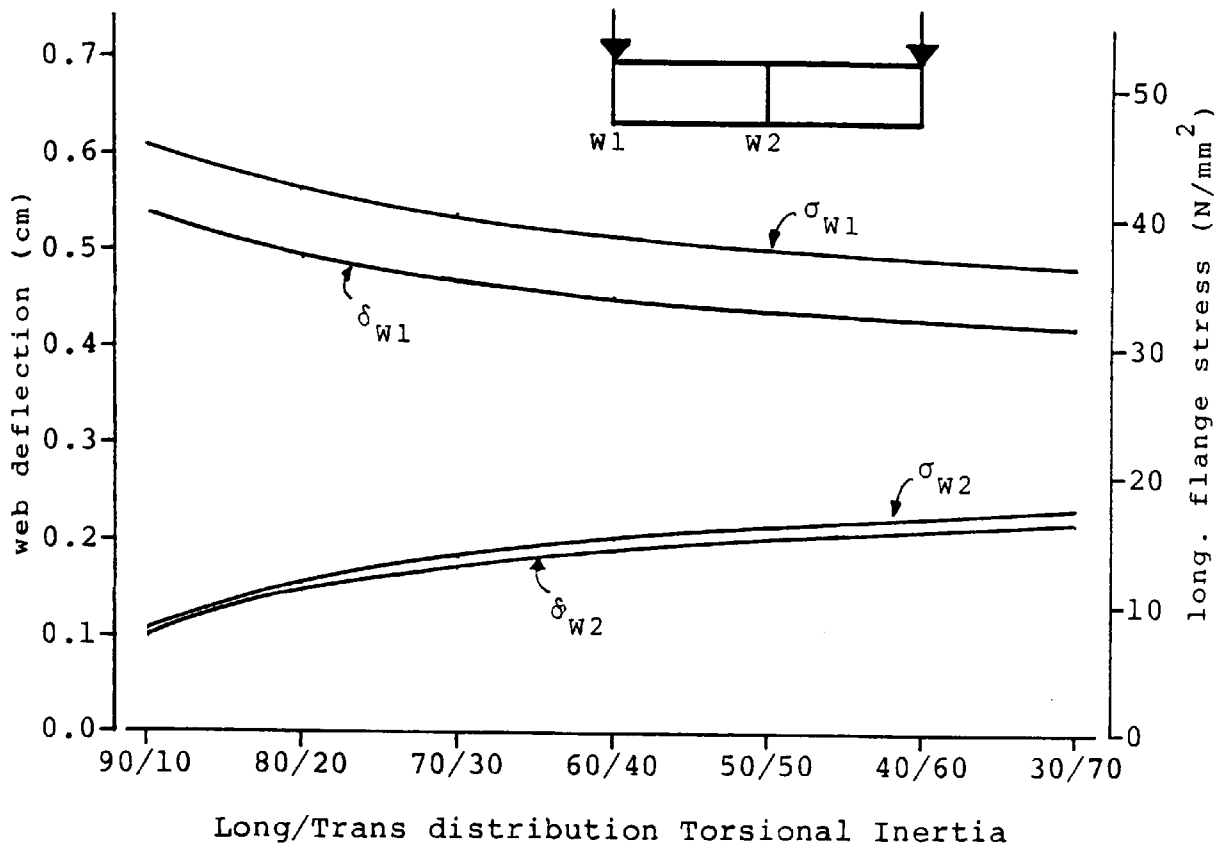


(c) Four-cell structure.

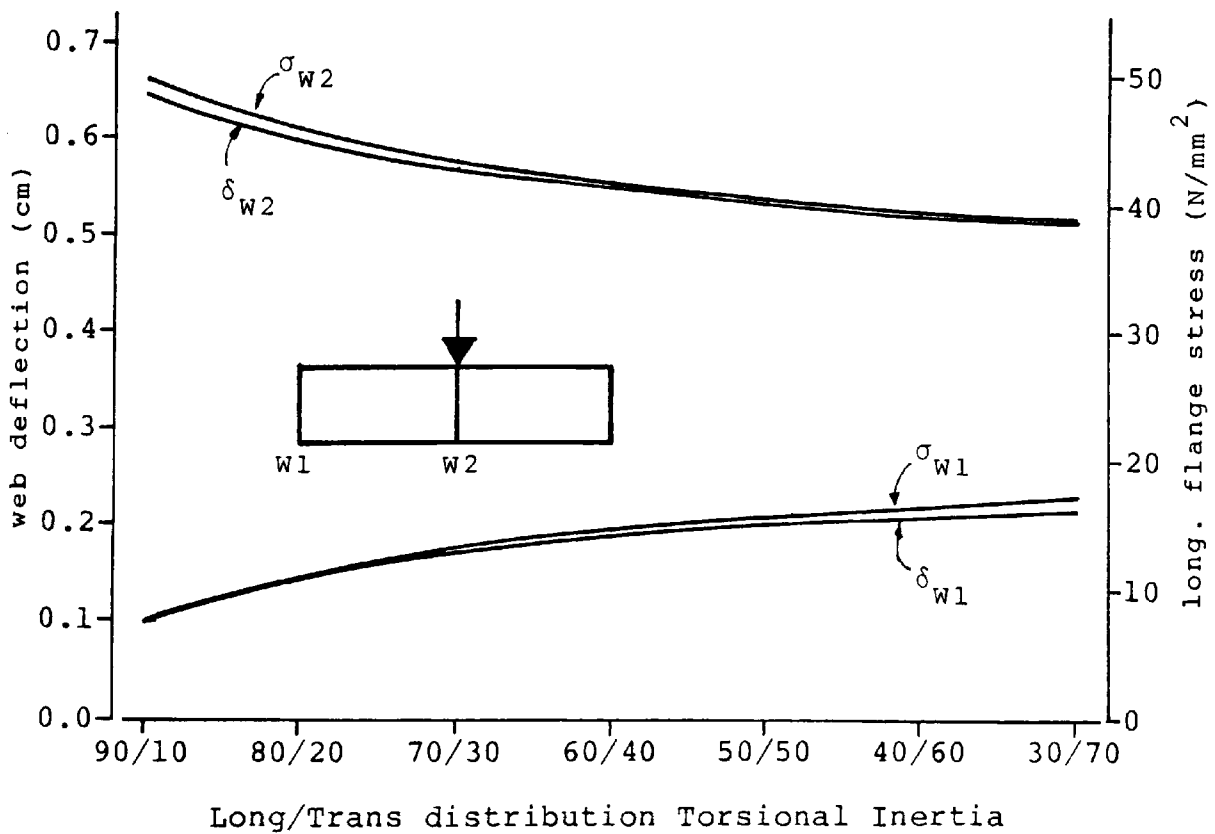
LOAD	W1 (kN)	W2 (kN)
Midspan point	300	600
Uniform line	600	1200

(d) Load details.

FIGURE 4.6 - DETAILS OF 2, 3 and 4-CELL STRUCTURES USED IN STUDY OF TORSIONAL INERTIA DISTRIBUTION.

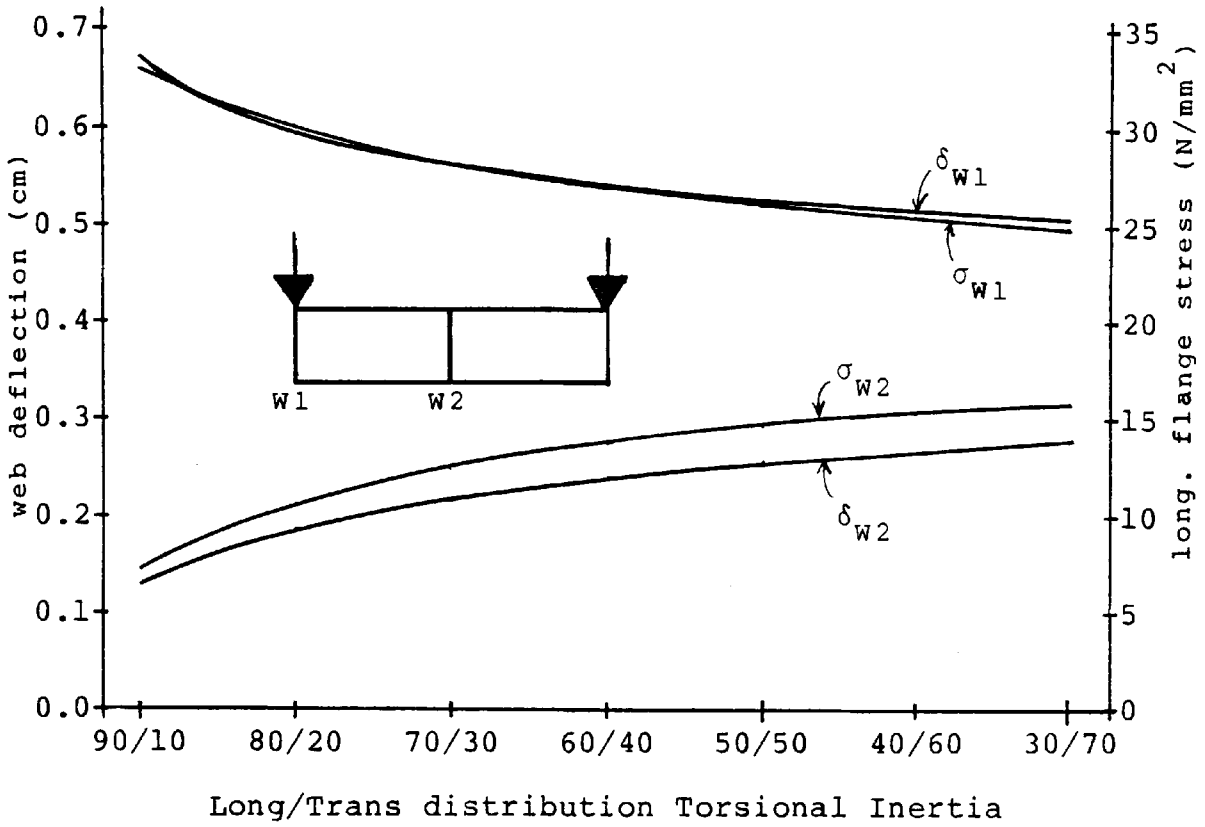


(a) Outer Web loaded.

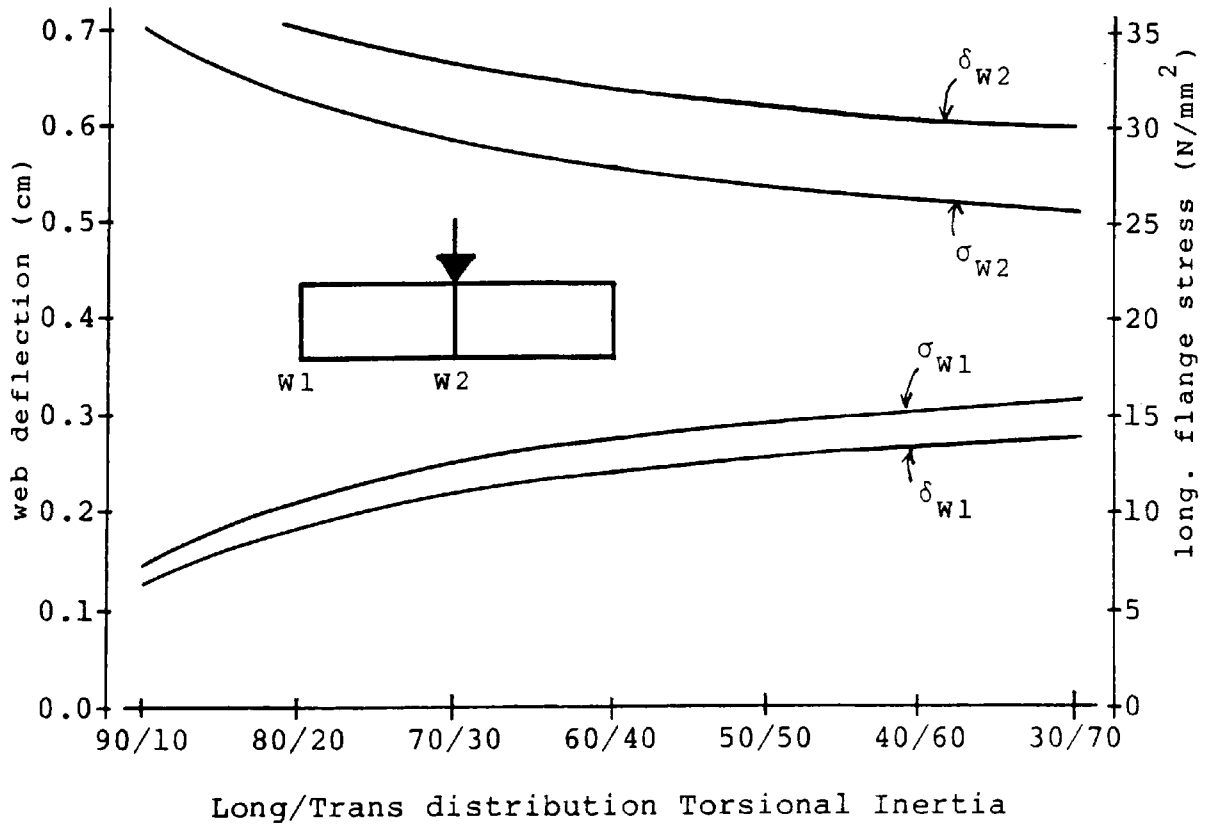


(b) Inner web loaded.

FIGURE 4.7 - VARIATION OF WEB DEFLECTION AND LONGITUDINAL FLANGE EDGE STRESS WITH TORSIONAL INERTIA DISTRIBUTION - TWO-CELL - MIDSPAN POINT LOAD.

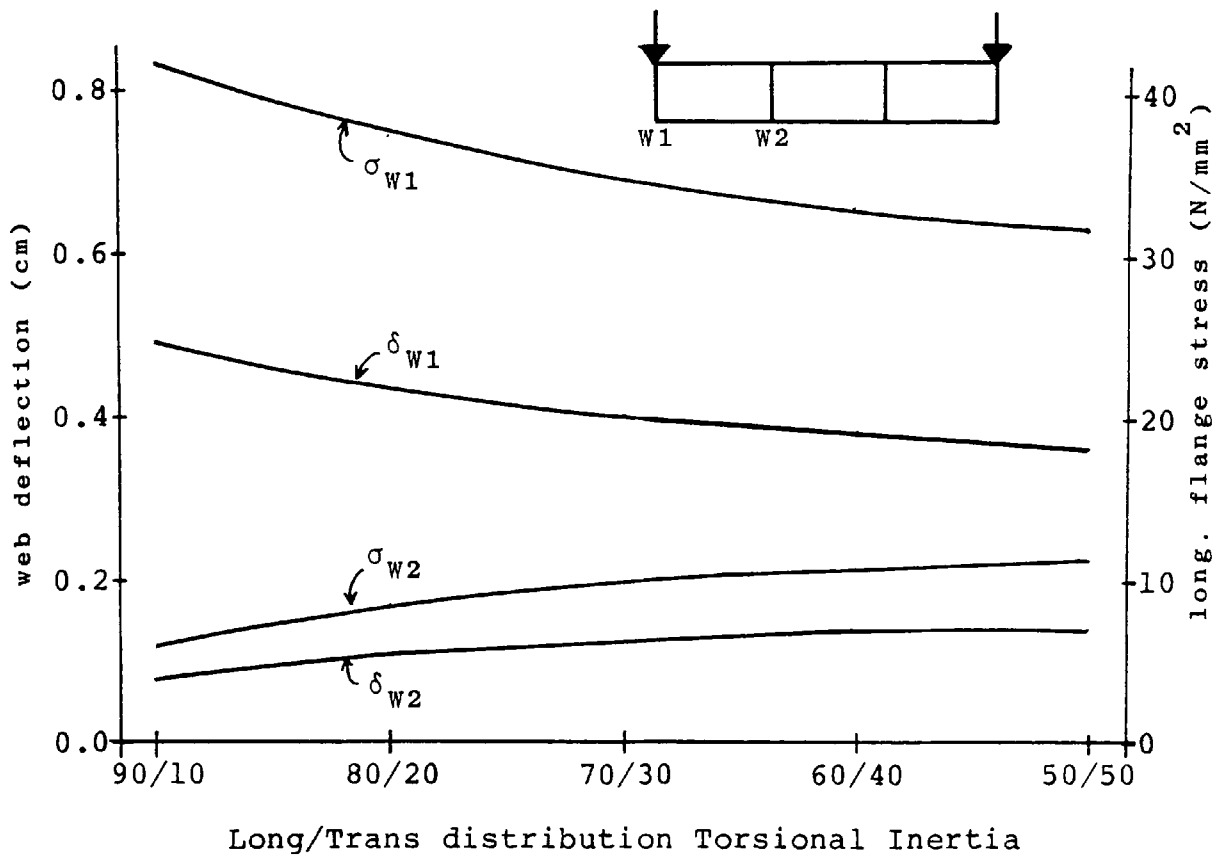


(a) Outer Web loaded.



(b) Inner web loaded.

FIGURE 4.8 - VARIATION OF WEB DEFLECTION AND LONGITUDINAL FLANGE EDGE STRESS WITH TORSIONAL INERTIA DISTRIBUTION - TWO-CELL - UNIFORM LINE LOAD.

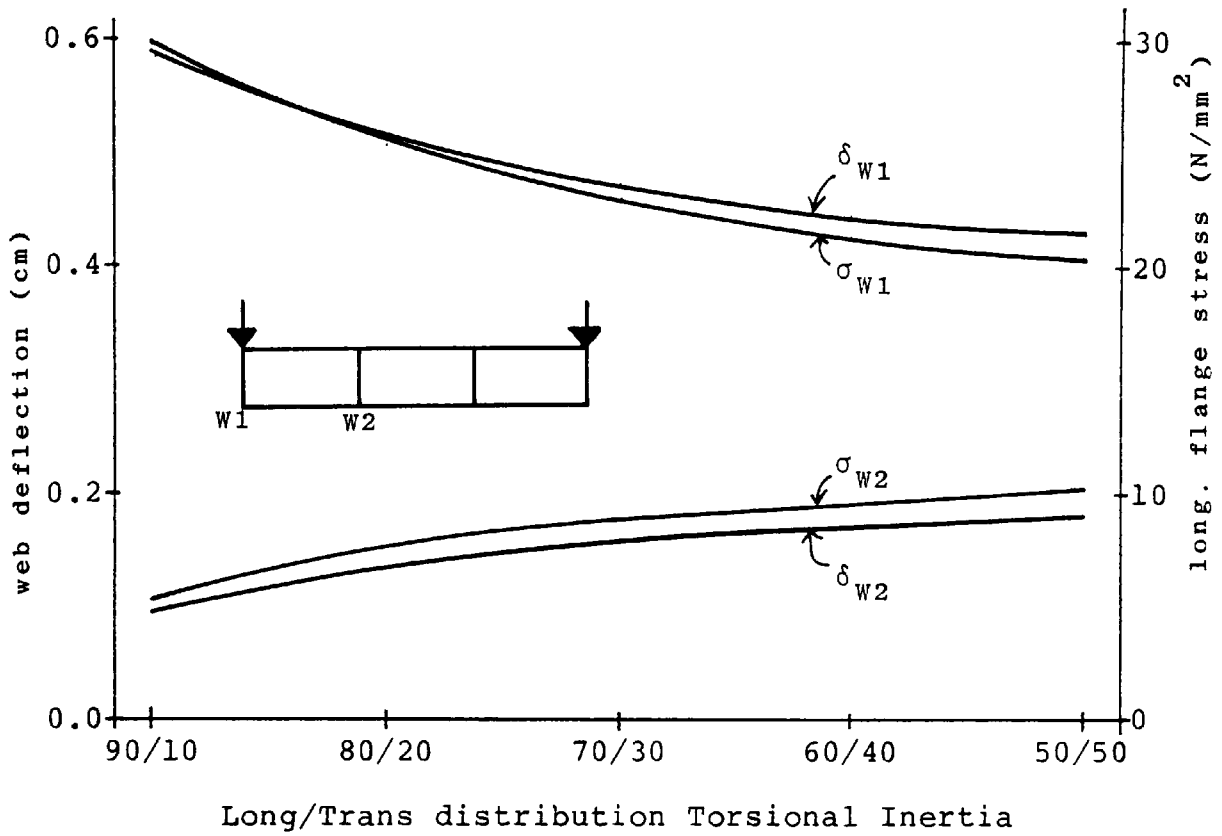


(a) Outer Web loaded.

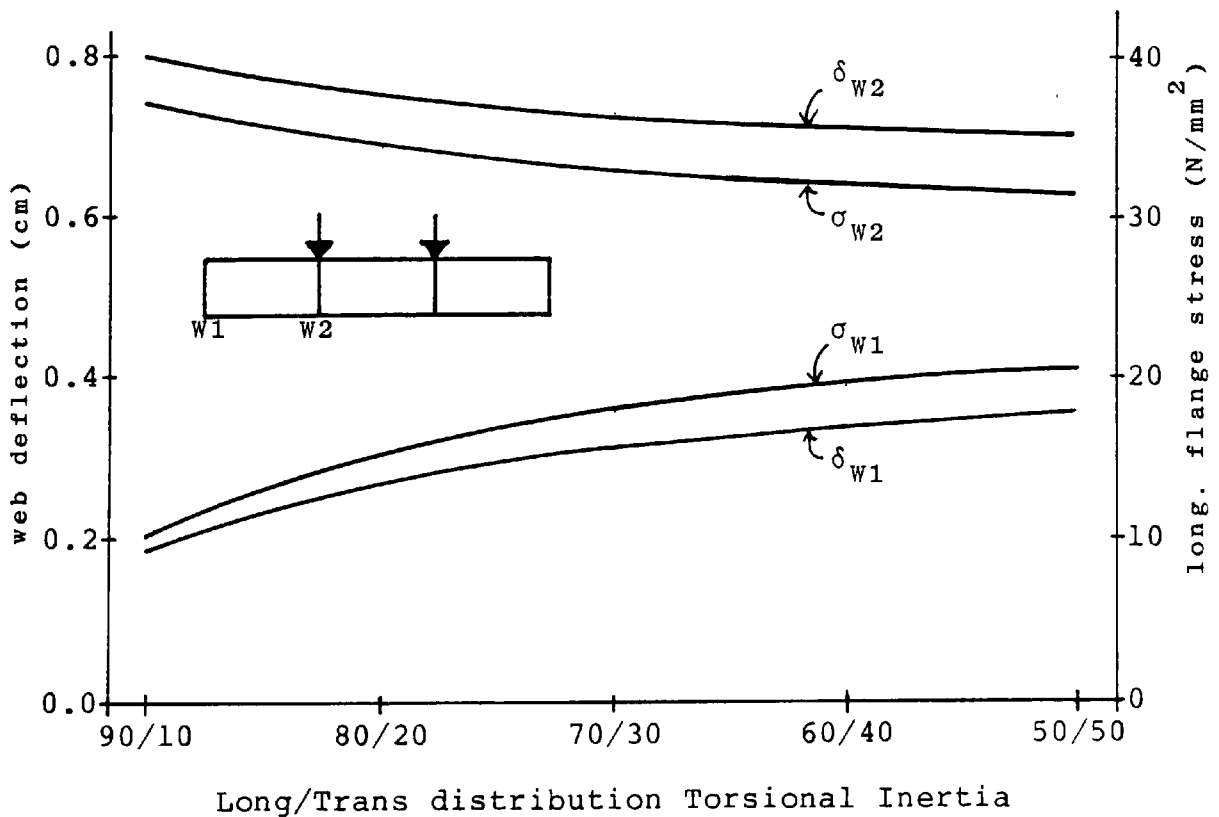


(b) Inner web loaded.

FIGURE 4.9 - VARIATION OF WEB DEFLECTION AND LONGITUDINAL FLANGE EDGE STRESS WITH TORSIONAL INERTIA DISTRIBUTION - THREE-CELL - MIDSPAN POINT LOAD.

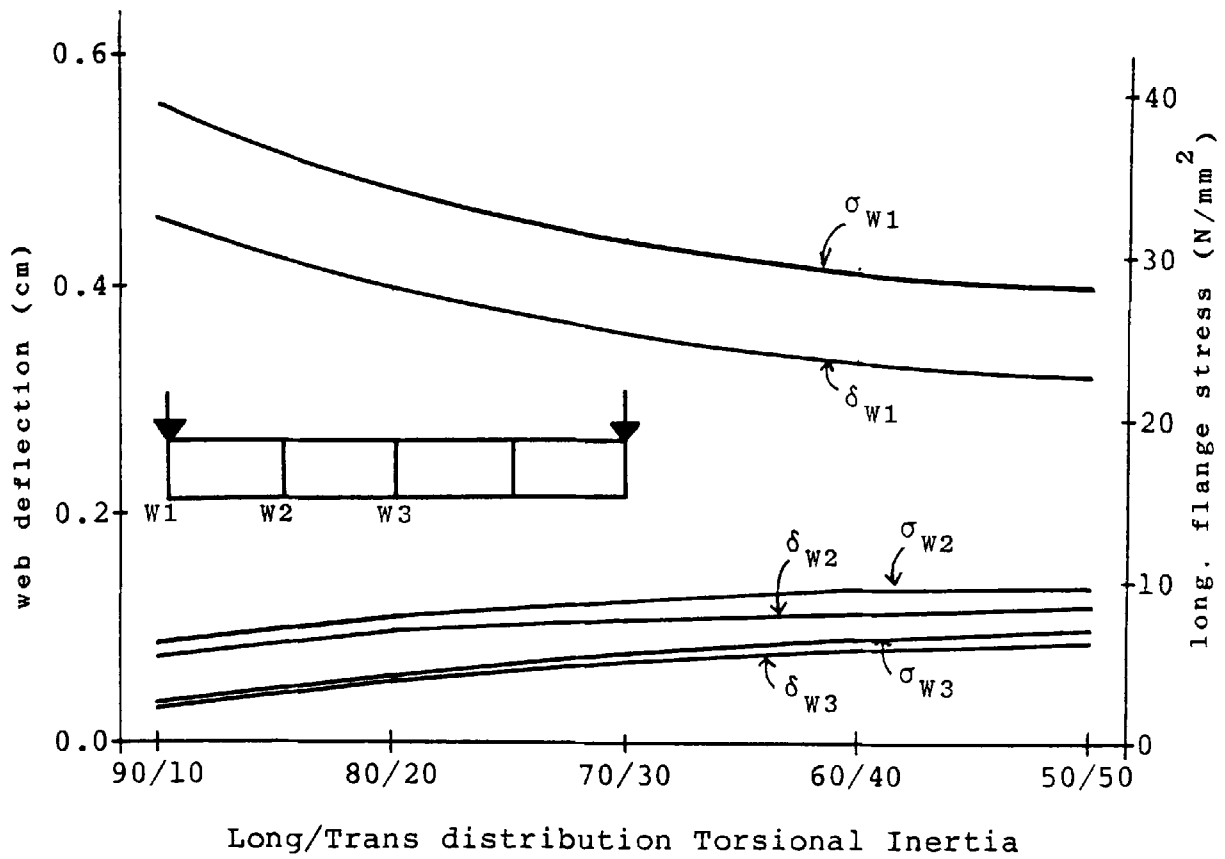


(a) Outer Web loaded.

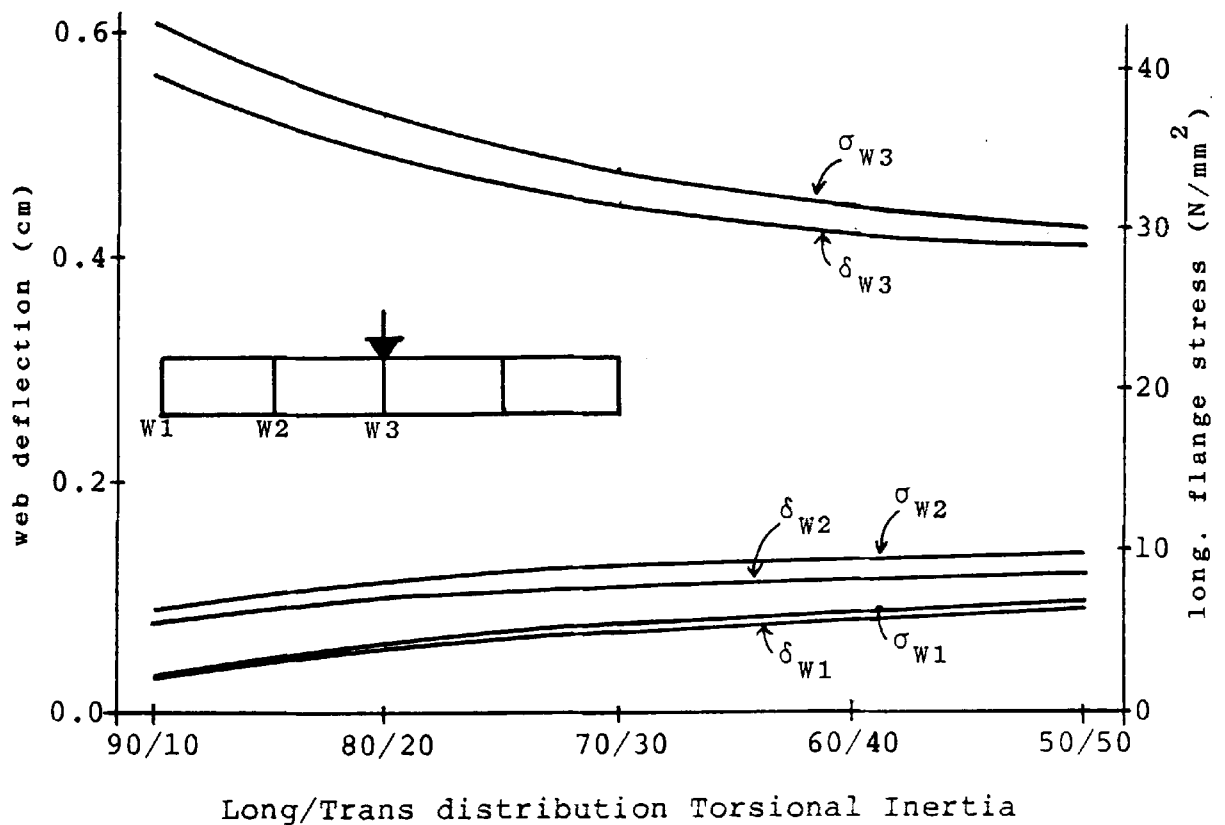


(b) Inner web loaded.

FIGURE 4.10 - VARIATION OF WEB DEFLECTION AND LONGITUDINAL FLANGE EDGE STRESS WITH TORSIONAL INERTIA DISTRIBUTION - THREE-CELL - UNIFORM LINE LOAD.

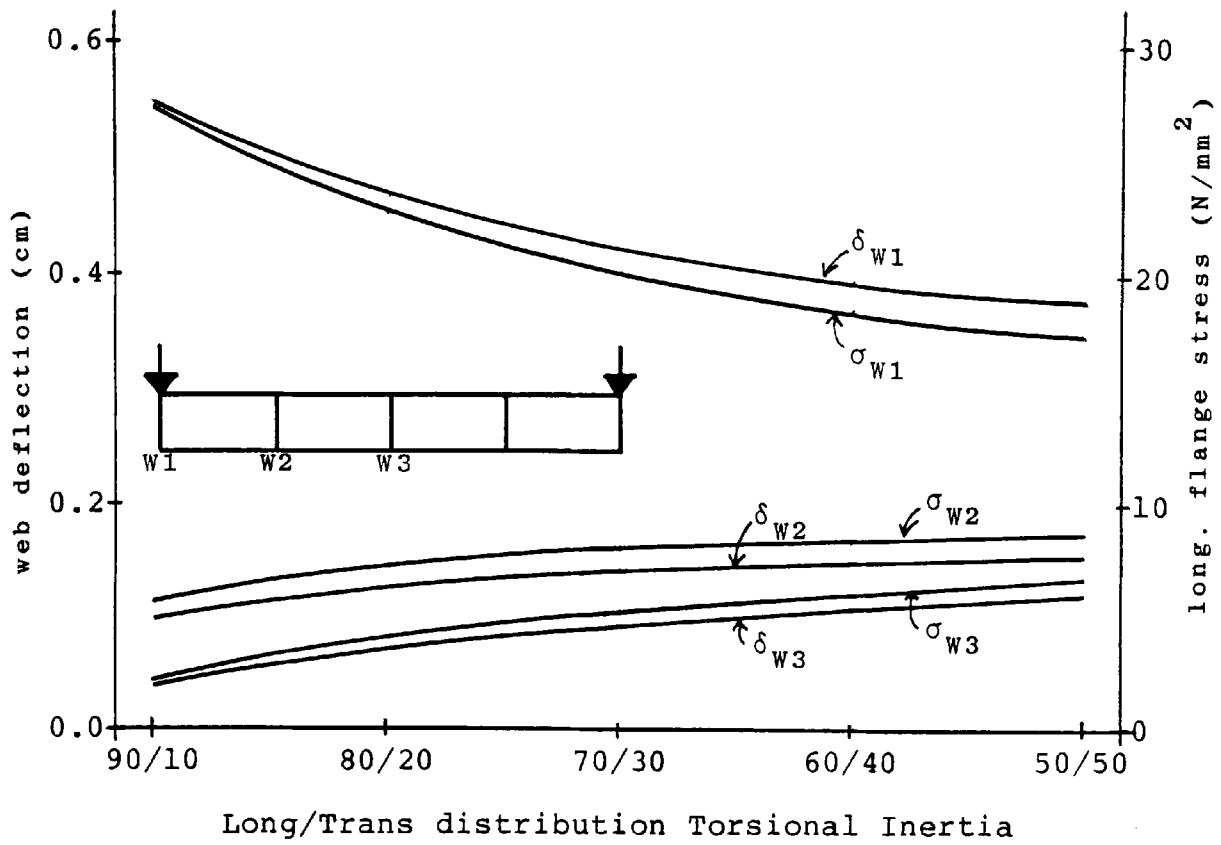


(a) Outer Web loaded.

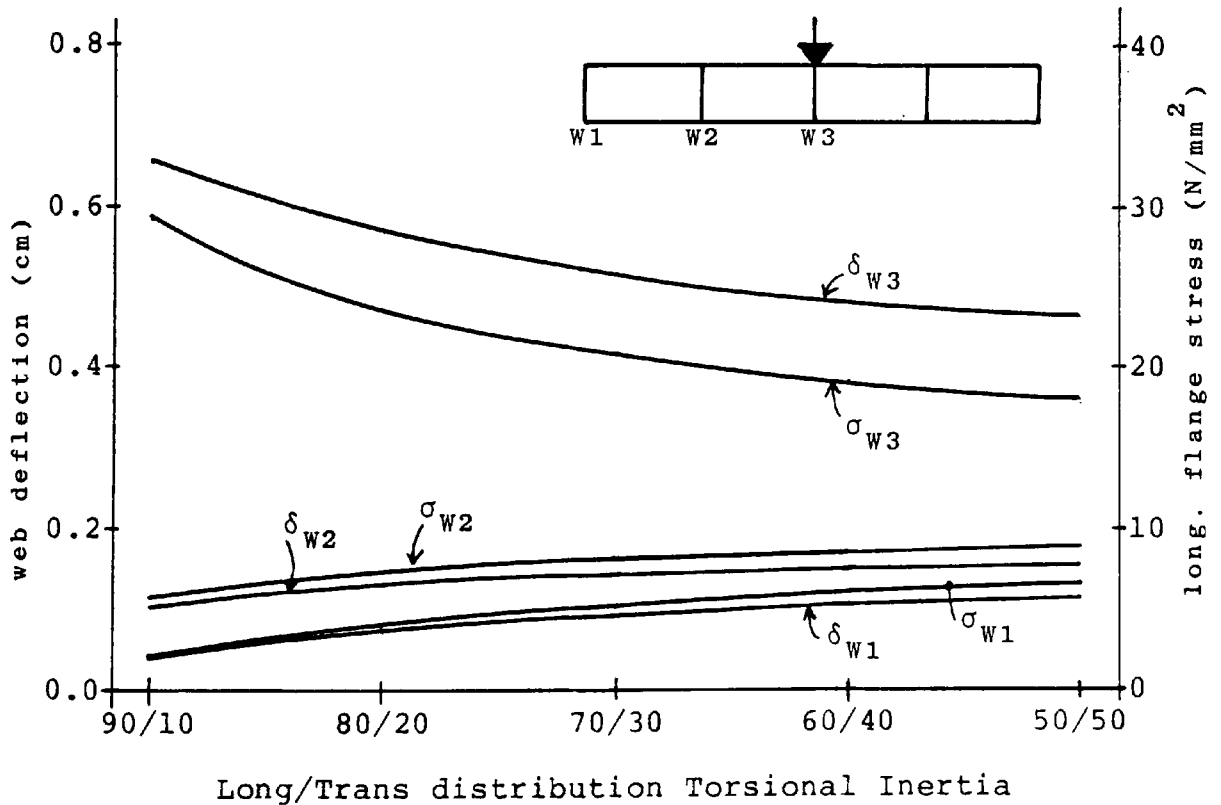


(b) Inner web loaded.

FIGURE 4.11 - VARIATION OF WEB DEFLECTION AND LONGITUDINAL FLANGE EDGE STRESS WITH TORSIONAL INERTIA DISTRIBUTION - FOUR-CELL - MIDSPAN POINT LOAD.



(a) Outer Web loaded.



(b) Inner web loaded.

FIGURE 4.12 - VARIATION OF WEB DEFLECTION AND LONGITUDINAL FLANGE EDGE STRESS WITH TORSIONAL INERTIA DISTRIBUTION - FOUR-CELL - UNIFORM LINE LOAD.

CHAPTER FIVE

GRILLAGE ANALYSIS OF STRAIGHT MULTI-CELL STRUCTURES

5.1. INTRODUCTION.

In the two previous chapters the grillage idealization of multi-cell structures was considered. It was shown that multi-cell structures resist applied loads by a combination of longitudinal bending, transverse bending, torsion and distortion. The determination of the appropriate stiffness parameters necessary to model these effects was studied in detail and recommendations made for their correct apportioning to the grillage beams.

In this chapter recommendations will be established for the appropriate geometrical idealization necessary to produce results of acceptable accuracy. The geometrical idealization determines the number of longitudinal and transverse grillage beams required to establish a grillage mesh that will accurately model the behaviour of the multi-cell structure.

In the longitudinal direction a grillage beam is used to represent each longitudinal web of the multi-cell cross-section, hence the number of longitudinal grillage beams is fixed by the number of cells in the cross-section. In the transverse direction, where no in-span diaphragms are present, any number of grillage beams may be used; the minimum number of beams recommended is five. The relationship between the number of transverse grillage

beams used and accuracy of solution achieved will be investigated for various loading conditions and cross-section details.

The chapter will be concluded with a study of the grillage analysis of straight multi-cell structures. A number of typical structures will be analysed where the recommendations of geometrical and sectional idealization will be incorporated in the grillage analysis. Comparisons will be made with results obtained from an analysis using the finite element program, QUEST.

5.2. EFFECT OF NUMBER OF TRANSVERSE GRILLAGE BEAMS ON ACCURACY OF ANALYSIS.

5.2.1. GENERAL.

To establish recommendations that incorporate variations in both loading and cross-section, two separate studies will be considered. In the first a four cell structure subjected to midspan point loading will be considered, whilst in the second a three cell structure subjected to uniform line loading will be considered. In both studies the number of transverse grillage beams will be varied from five to thirteen, and four different positions of the loading on the cross-section will be considered. Loads will be positioned so as to provide the most severe tests of solution accuracy.

5.2.2. FOUR CELL STRUCTURE - MIDSPAN POINT LOADING.

The four cell structure used in this investigation is shown in figure 5.1 together with the four loading conditions considered. The grillage layout consisted of five longitudinal grillage beams, whilst in the transverse direction the number of grillage beams was varied from five to thirteen.

The structure details were

overall breadth of structure	= 1200cm
span of structure	= 1600cm
depth of structure	= 150cm
web thickness	= 1.2cm
flange thickness	= 1.2cm
diaphragm thickness	= 1.2cm

The stiffness parameters of the grillage beams are presented in Table 5.1 for all five grillage layouts investigated.

The four loading conditions considered were

- (i) 300kN over outer webs, 600kN over inner webs
- (ii) 300kN over outer webs only
- (iii) 600kN over central web only
- (iv) 300kN over one outer web only

The results for midspan and quarterspan web deflection and flange edge stress are presented in Tables 5.2 and 5.3 respectively for all five grillage analyses and the comparative finite element study. The following conclusions were reached on consideration of these results.

1. The deflection values, presented in Table 5.2, were in close agreement for all five grillage meshes in all four loading cases. The 5 x 5 and 5 x 13 grillage meshes agreed to within 99% of each other at the loaded web positions.
2. The results for flange stress, presented in Table 5.3, were not so consistent as those for deflection. In load case one where all webs were loaded the predicted stresses were consistent for all five grillage meshes.
3. When both outer webs were loaded the midspan flange stress at the loaded web showed a variation from 34.01N/mm² to 32.20N/mm² for the 5 x 5 and 5 x 13 grillage meshes respectively. These values correspond to an overestimation of 4.2% for the 5 x 5 grillage and an underestimation of 1.3% for the 5 x 13 grillage when compared to the finite element value.
4. In load case three when the central web is loaded the results followed the same pattern as those for load case two, the actual flange stress values being 36.83N/mm² (+3.6%) and 34.70N/mm² (-2.4%) for the 5 x 5 and 5 x 13 grillage meshes respectively.
5. Load case four represents a torsional loading condition with a single load applied over one outer web. The 5 x 5 mesh flange stress value of 33.41N/mm² at the loaded web represented an underestimation of 3.1% of the finite element value of 34.49N/mm². The 5 x 13 mesh value of 31.67N/mm² represented an underestimation of 8.2%.

6. Earlier work in chapter three showed that overestimations of the order of 10% were predicted by the grillage method for midspan point loading cases. This was a direct result of using the effective breadth ratios from BS 5400 for the determination of the second moment of area of the longitudinal grillage beams. Consequently, it was considered that the 5 x 5 grillage mesh produced results for both web deflection and flange edge stress in all four loading cases which were consistent with those earlier results, and hence should form the basis for all subsequent analyses for midspan point loading conditions.

5.2.3. THREE CELL STRUCTURE - UNIFORM LINE LOADING.

The three cell structure used in this investigation is shown in figure 5.2, together with the four cases of uniform line loading considered. The grillage mesh arrangement consisted of four longitudinal beams and from five to thirteen transverse grillage beams. The structure details were the same as those for the four cell structure considered in section 5.2.2., except that the overall breadth of the structure was reduced from 1200cm to 900cm. The appropriate stiffness parameters are presented in Table 5.1 for all five grillage mesh arrangements.

The four loading conditions considered were

- (i) 600kN over outer webs, 1200kN over inner webs
- (ii) 600kN over both outer webs only
- (iii) 1200kN over both inner webs only
- (iv) 1200kN over one inner web only

The uniform line load along the web of the structure was represented in the grillage analysis in the normal manner by determining the equivalent nodal forces acting at the joints of the grillage structure. These are the equivalent fixed end shear forces of $W/2$ and the fixed end bending moments of $WL/12$. JUST (1981) considered that when the effects of shear deformation in the beams are taken into account the equivalent nodal forces must be modified. He considered that the fixed end shear force is unchanged, but the fixed end bending moment be calculated using the following equation

$$M = \frac{WL}{12} \left[1 - \frac{3}{4 + \frac{A_s * L^2}{6 * IY(1+v)}} \right] \quad \text{---- 5.1}$$

where W = total uniform load on member

L = length of member

A_s = effective shear area of member

IY = second moment of area of member

ν = poisson's ratio

JUST considered that with shearing deformation neglected the moment-rotation relationship may be expressed as

$$M(ns) = \frac{4 * E * IY}{L} \theta \quad \text{---- 5.2}$$

whilst when shear deformation is considered the relationship between moment and rotation becomes

$$M(s) = \frac{4 * E * IY * (N2)}{L} \theta \quad \text{---- 5.3}$$

These relationships are obtained from the element

stiffness matrices expressed in equations 3.3 and 3.4 of chapter three. For compatibility of rotation, θ , then

$$M(s) = M(ns) * N2 \quad \text{---- 5.4}$$

$$\text{where } N2 = (1 + 0.5N)/(1 + 2N)$$

$$N = \frac{6 * E * I_y}{G * A_s * L^2}$$

$$M(s) = \text{fixed end moment (shear considered)}$$

$$M(ns) = \text{fixed end moment (shear ignored)}$$

$$= WL/12$$

It can be easily proven that equations 5.1 and 5.4 are the same.

Using the principle of virtual work it was shown that the fixed end moments are in fact equal to $WL/12$ for uniform line loading on a fixed ended beam when shear deformation is considered. This fact was also confirmed in a finite element study using the program QUEST. The related calculations are presented in Appendix F. Consequently it was considered that the equivalent nodal forces used in the grillage program, SHEARGRID2, should be $W/2$ and $WL/12$ for the fixed end shear force and bending moment respectively.

The results for midspan and quarterspan web deflection and flange edge stress are presented in Tables 5.4 and 5.5 respectively for all five grillage analyses and the comparative finite element study. Consideration of these results produced the following conclusions.

1. The deflection values presented in Table 5.4 were in close agreement for all five grillage analyses in all

- four loading cases. The 4 x 5 and 4 x 13 grillage mesh values agreed to within 98% at the loaded web position.
2. The results for flange stress, presented in Table 5.5, were not so consistent as those for deflection. In load case one where all webs were loaded the stresses were consistent for all five grillage meshes.
 3. In load case two, when both outer webs were loaded the midspan flange stress at the loaded web showed a variation from 22.20N/mm² to 20.86N/mm² for the 4 x 5 and 4 x 13 meshes respectively. These values correspond to an overestimation of 9.7% and 3.1% when compared to the finite element value of 20.24N/mm².
 4. In load case three, when both inner webs were loaded, the midspan flange stress at the loaded web showed a variation from 32.64N/mm² (an overestimation of 1.0%) to 31.86 N/mm² (an underestimation of 1.4%) for the 4 x 5 and 4 x 13 grillage meshes respectively.
 5. In load case four which represents an asymmetrical load over one inner web the results followed the same pattern as those for load case three, the actual flange stress values being 23.93N/mm² (an overestimation of 0.7%) and 22.52N/mm² (an underestimation of 5.2%) for the 4 x 5 and 4 x 13 meshes respectively.
 6. It was concluded that the 4 x 9 grillage mesh produced the most consistent set of results for both web deflection and flange edge stress in all four loading cases. Hence it is recommended that when analysing

structures subjected to uniform line loading then nine transverse grillage beams should be used in the grillage idealization. This represents a difference from the midspan point load case where the recommendation was to use five transverse grillage beams. There will be more transverse distribution of loading in the uniform line load case, which will require the use of a greater number of transverse grillage beams to achieve results of comparable accuracy.

5.3. ANALYSIS OF STRAIGHT MULTI-CELL STRUCTURES.

5.3.1. INTRODUCTION.

In this section a number of examples will be considered where the recommendations presented in chapters three and four and the earlier part of this chapter will form the basis of idealization and analysis. This earlier work had revealed that the accuracy of the solution achieved by the grillage method was dependent on the following criteria :-

1. The number of cells in the structure.
2. The type and position of loading.
3. The influence of shear lag in the flange plates represented by the b/L ratio

where $2b$ = breadth of flange plates between webs

and L = span of structure

4. The distribution of torsional inertia between the transverse and longitudinal grillage beams, represented by the B/L ratio
where B = overall width of structure
5. The contribution of shear deflection to the overall deflection of the structure, represented by the ratio of flange thickness to web thickness.

Six examples were considered to illustrate the ability of the grillage method to analyse multi-cell structures where the loading, geometrical and sectional details were chosen to incorporate variations in these five important criteria. In the three examples which considered midspan point loading five transverse grillage beams were used in the grillage representation. In the other three examples, which considered uniform line loading over the full length of the webs, nine transverse grillage beams were used. In each case the results from the grillage analysis were compared with a solution achieved using the finite element program, QUEST. Details of the meshes used in the finite element analyses are shown in figure 5.3.

5.3.2. THREE CELL STRUCTURE - MIDSPAN POINT LOADING.

In this first example the calculation of the sectional properties of the grillage beams and the determination of the flange stresses will be presented. The structure details were

overall width, B	=	600cm
overall depth, D	=	100cm

$$\begin{aligned}
\text{overall span, } L &= 1200\text{cm} \\
\text{web thickness, } t_w &= 1.0\text{cm} \\
\text{flange thickness, } t_f &= 2.0\text{cm} \\
\text{diaphragm thickness, } t_d &= 2.0\text{cm}
\end{aligned}$$

hence

$$\begin{aligned}
b/L &= 0.0833 \\
B/L &= 0.5 \\
t_f/t_w &= 2
\end{aligned}$$

The three loading conditions considered were

- (i) 800kN at both outer webs and 1600kN at both inner webs
- (ii) 800kN at both outer webs
- (iii) 1600kN at both inner webs

5.3.2.1. CALCULATION OF SECTION PROPERTIES.

From Table 4, Part 3, BS 5400, effective breadth ratio for deflection calculations, $\psi = 0.95$

SECOND MOMENT OF AREA.

Longitudinal grillage beams.

$$\begin{aligned}
\text{Outer beam} &= I(\text{web}) + I(\text{flange}) \\
&= \frac{1 * 100^3}{12} + 2 * 0.95 * 100 * 2 * 50 * 50 \\
&= \underline{1\ 033\ 333\ \text{cm}^4} \\
\text{Inner beam} &= \frac{1 * 100^3}{12} + 2 * 0.95 * 200 * 2 * 50 * 50 \\
&= \underline{1\ 983\ 333\ \text{cm}^4}
\end{aligned}$$

Transverse grillage beams.

$$\begin{aligned}
\text{Inner beam (Eqn 3.11)} &= 2 * 1200/4 * 2 * 50 * 50 \\
&= \underline{1\ 500\ 000\ \text{cm}^4}
\end{aligned}$$

$$\begin{aligned}
\text{Outer beam} &= I(\text{dia}) + I(\text{flange}) \\
&= \frac{2 * 100^3}{12} + \frac{1 * 500 * 000}{2} \\
&= \underline{916\ 667\ \text{cm}^4}
\end{aligned}$$

EFFECTIVE SHEAR AREA.

Longitudinal grillage beams.

$$\begin{aligned}
A_s &= \text{cross sectional area of web} \\
&= \underline{100\ \text{cm}^2}
\end{aligned}$$

Transverse grillage beams.

$$\begin{aligned}
\text{Outer beam} &= \text{cross sectional area of diaphragm} \\
&= \underline{200\ \text{cm}^2}
\end{aligned}$$

Inner beam (Eqn 3.16)

$$\begin{aligned}
&= \frac{2^3 + 2^3}{200^2} \left[\frac{1^3 * 200}{1^3 * 200 + (2^3 + 2^3) * 100} \right] * 2.6 \\
&= 0.444 * 10E-4\ \text{cm}^2/\text{cm of flange} \\
&= \underline{0.007\ \text{cm}^2\ \text{per grillage beam}}
\end{aligned}$$

TORSIONAL INERTIA.

Torsional Inertia of cross-section (Eqn 4.7)

$$\begin{aligned}
&= \frac{2 * 600^2 * 100^2}{\left[\frac{600}{2} + \frac{100}{1} \right]} \\
&= \underline{18\ 000\ 000\ \text{cm}^4}
\end{aligned}$$

Longitudinal grillage beams.

$$\begin{aligned}
J(\text{long}) &= \frac{0.5 * 18\ 000\ 000}{4} \\
&= \underline{2\ 250\ 000\ \text{cm}^4}
\end{aligned}$$

Transverse grillage beams.

$$\begin{aligned}
J(\text{tran}) &= \frac{(1 - 0.5) * 18\ 000\ 000}{5} \\
&= \underline{1\ 800\ 000\ \text{cm}^4}
\end{aligned}$$

5.3.2.2. INTERPRETATION OF RESULTS.

The longitudinal flange stress values are predicted from the longitudinal grillage beam bending moment values using the simple beam theory relationship between bending stress and bending moment. The grillage analysis of load case two produced the following values of bending moment in the longitudinal grillage beams.

At quarterspan.

Outer web (joint 5)

77863 kNcm (member 4)

31811 kNcm (member 11) average = 54837 kNcm

Inner web (joint 6)

42136 kNcm (member 6)

88189 kNcm (member 13) average = 65162 kNcm

At Midspan.

Outer Web (joint 9) = 151760 kNcm (members 11 and 18)

Inner Web (joint 10) = 88240 kNcm (members 13 and 20)

From Table 13, Part 3, BS 5400, effective breadth ratios for stress calculations are

midspan, $\psi = 0.710$

quarterspan, $\psi = 1.000$

SECOND MOMENT OF AREA (STRESS CALCULATIONS).

Midspan.

$$\begin{aligned} \text{Outer beam} &= \frac{1 * 100^3}{12} + 2 * 0.710 * 100 * 2 * 50 * 50 \\ &= \underline{793\ 333\ \text{cm}^4} \end{aligned}$$

$$\begin{aligned} \text{Inner beam} &= \frac{1 * 100^3}{12} + 2 * 0.710 * 200 * 2 * 50 * 50 \\ &= \underline{1\ 503\ 333\ \text{cm}^4} \end{aligned}$$

Quarterspan.

$$\begin{aligned} \text{Outer beam} &= \frac{1 * 100^3}{12} + 2 * 1.000 * 100 * 2 * 50 * 50 \\ &= \underline{1\ 083\ 333\ \text{cm}^4} \end{aligned}$$

$$\begin{aligned} \text{Inner beam} &= \frac{1 * 100^3}{12} + 2 * 1.000 * 200 * 2 * 50 * 50 \\ &= \underline{2\ 083\ 333\ \text{cm}^4} \end{aligned}$$

hence longitudinal flange stresses are

Midspace.

$$\text{Outer web} = \frac{151760 * 50 * 10}{793333} = 95.65\ \text{N/mm}^2$$

$$\text{Inner web} = \frac{88240 * 50 * 10}{1503333} = 29.35\ \text{N/mm}^2$$

Quarterspan.

$$\text{Outer web} = \frac{54837 * 50 * 10}{1083333} = 25.31\ \text{N/mm}^2$$

$$\text{Inner web} = \frac{65162 * 50 * 10}{2083333} = 15.64\ \text{N/mm}^2$$

These results together with those for deflections and stresses for all three loading cases are presented in Table 5.6 and are compared with the finite element results. The results are also presented in graphical form in figure 5.4.

5.3.2.3. DISCUSSION OF RESULTS.

1. The web deflection values were accurately predicted by the grillage method in all three load cases at both web

positions for the midspan and quarterspan cross-sections, the grillage results showing a maximum overestimation of 4.0% and a maximum underestimation of 2.2% when compared to the finite element values. Considerable deformation of the cross-section occurred in load cases two and three which was accurately modelled by the grillage method.

2. The values for flange edge stress were less accurate than those for deflection. Considering the critical stress values at the loaded web positions then, at midspan the predicted stress was consistently overestimated, this overestimation being 10.5%, 1.3% and 3.6% for load cases one, two and three respectively. At the quarterspan position there was closer agreement between the grillage and finite element results apart from in load case two. The distribution of flange stress across the cross-section plotted in figure 5.4 shows the shear lag effect at midspan. At the quarterspan position, where the effective breadth ratio is unity, the variation of stress is practically linear.

3. The idealization used in the grillage analysis only allows the determination of stresses at the web/flange intersections. The intensity of stress at any position between the webs may be determined using the following equation from Appendix A, Part 3, BS 5400

$$\sigma_1 = \sigma_{\max} [X^4 + k(1 - X^4)] \quad \text{---- 5.5}$$

where

σ_1 = longitudinal stress at any point in the flange a distance x from the centre-line of the web

σ_{max} = maximum stress at the web/flange intersection

$X = (b-x)/b$

$2b$ = width of flange plates

$k = 0.25 * (5 \Psi - 1)$

Ψ = effective breadth ratio

Equation 5.5 assumes that σ_{max} has the same value at both web locations, i.e. only longitudinal bending action is present in the flange plate. In a multi-cell structure it is unlikely that both web stresses are equal because of the torsional and distortional behaviour of the structure. The variation in stress across the flange plate due to these actions is linear and hence the longitudinal bending stress can be isolated from the actual stress values. The stress at any position in the flange can be calculated using equation 5.5 together with a linear variation to cater for the torsional and distortional behaviour.

Consider a cell of a multi-cell structure, shown in Figure 5.5., where the flange stresses at the web positions are σ_l and σ_r . The stress distribution may be represented by the two components as shown, and the stress at any position between the webs may be determined using the equation

$$\sigma_l = \frac{(\sigma_l + \sigma_r)}{2} \left[X^4 + k (1 - X^4) \right] + \frac{(\sigma_l - \sigma_r) x}{2b} \quad \text{--- 5.6}$$

Using this equation the intermediate values of flange stress were calculated for load cases one and two at the midspan cross-section and are presented in Figure 5.5.

The correlation between calculated stress values based on the grillage method and the finite element stresses was shown to be extremely close for load case one. The mid-flange stress values were 99.46 N/mm² and 97.47 N/mm², an overestimation by the grillage method of 2.0%. In load case two, where the flange edge stress values were 95.65 N/mm² and 29.35 N/mm², the mid-flange stress values were 39.85 N/mm² and 36.71 N/mm², an overestimation of 8.6%.

Equation 5.6 was used to calculate the mid-flange stress values for all six examples considered. These stresses are shown plotted in Figures 5.4, and 5.6 to 5.14 inclusive for comparison with the finite element values.

5.3.3. THREE CELL STRUCTURE - UNIFORM LINE LOADING.

In this example all parameters were unchanged from the previous example, except the span which was increased to 1500cm, resulting in the following ratios

$$b/L = 0.0667$$

$$B/L = 0.4$$

$$t_f/t_w = 2$$

$$\Psi_{defl} = 0.972$$

$$\Psi_{str} = 0.972 \text{ (at quarterspan)}$$

$$\Psi_{str} = 0.975 \text{ (at midspan)}$$

The three loading cases considered were

- (i) 600kN along outer webs, 1200kN along inner webs
- (ii) 600kN along outer webs
- (iii) 1200kN along inner webs

The results of the grillage and finite element analyses are presented in Table 5.7 and figure 5.6. Consideration of these results produced the following conclusions.

1. The web deflection values were accurately predicted by the grillage method at both the midspan and quarterspan positions. The grillage values varied from a maximum overestimation of 4.7% to a maximum underestimation of 1.0%.
2. In load cases one and three the flange stresses at both the midspan and quarterspan positions were accurately predicted, revealing a maximum underestimation of 4.1% and a maximum overestimation of 5.4%.
3. In load case two the grillage method overestimated the midspan stress at the loaded web by 14.4% and underestimated the stress at the unloaded web by 8.9%. There was closer agreement at the quarterspan cross-section between the grillage and finite element values.
4. Overall the grillage method tended to overestimate the maximum flange stresses developed at the loaded web position, hence producing an upper bound solution. The maximum overestimation was 14.4% in load case two.

5.3.4. FOUR CELL STRUCTURE - MIDSPAN POINT LOADING.

The structure details were

overall width, B	=	960cm
overall depth, D	=	150cm
overall span, L	=	1600cm
web thickness, t_w	=	1.5cm
flange thickness, t_f	=	3.0cm
diaphragm thickness, t_d	=	3.0cm

hence

b/L	=	0.075
B/L	=	0.6
t_f/t_w	=	2
Ψ defl	=	0.953
Ψ str	=	0.735 (at midspan)
Ψ str	=	1.000 (at quarterspan)

The four loading conditions considered were

- (i) 750kN over webs 1, 1500kN over webs 2 and web 3
- (ii) 750kN over webs 1
- (iii) 1500kN over webs 2
- (iv) 1500kN over web 3

The results of the grillage and finite element analyses are presented in Table 5.8 and Figures 5.7 and 5.8., consideration of which produced the following conclusions.

1. The web deflection values for load case one were accurately predicted at both the midspan and quarterspan positions. The values varied from a maximum

underestimation of 2.0% to a maximum overestimation of 5.2%.

2. In load cases two, three and four the deflections of the loaded webs were accurately predicted. The deflection was consistently overestimated by the grillage method, the maximum overestimation being 2.4%. At the unloaded web positions the correlation between the grillage and finite element values in percentage terms was not so good, the maximum difference being 21.1%. However, the web deflection profile predicted by the grillage method closely follows the deflected shape of the cross-section calculated by the finite element method as illustrated in Figures 5.7 and 5.8.
3. In load case one the flange stress was consistently overestimated (5.9% to 14.5%) at the midspan cross-section. At the quarterspan cross-section the stresses varied from an underestimation of 2.7% to an overestimation of 4.8%.
4. In the other three load cases the flange stress at the loaded web positions was consistently overestimated. At the midspan cross-section the maximum overestimation was 8.2%, whilst at the quarterspan cross-section the maximum overestimation was 16.9%. The flange stress values at the unloaded web positions were not so accurately predicted in percentage terms, but the relative magnitude of the stress intensity agrees with the finite element values as shown in the plots of stress distribution in Figures 5.7 and 5.8.

5.3.5. FOUR CELL STRUCTURE - UNIFORM LINE LOADING.

In this example all parameters were unchanged from the previous example, except the span which was increased to 1920cm, resulting in the following ratios

$$b/L = 0.0625$$

$$B/L = 0.5$$

$$t_f/t_w = 2$$

$$\Psi_{defl} = 0.968$$

$$\Psi_{str} = 0.968 \text{ (at quarterspan)}$$

$$\Psi_{str} = 0.972 \text{ (at midspan)}$$

The four loading conditions considered were

- (i) 1200kN along webs 1, 2400kN along webs 2 and web 3
- (ii) 1200kN along webs 1
- (iii) 2400kN along webs 2
- (iv) 2400kN along web 3

The results of the grillage and finite element analyses are presented in Table 5.9 and Figures 5.9 and 5.10., consideration of which produced the following conclusions.

1. The web deflection values for load case one were accurately predicted at both the midspan and quarterspan positions. The values varied from a maximum underestimation of 1.6% to a maximum overestimation of 4.4%.
2. In load cases two, three and four the deflections of the loaded webs were accurately predicted. The grillage

method tended to overestimate the deflection value, the maximum overestimation being 3.1%. In load case three the deflection was underestimated by 0.7% at the quarterspan cross-section. At the unloaded web positions the maximum difference between the grillage and finite element values was 12.9%, showing an improvement over the previous example.

3. In load case one the flange stress was accurately predicted, the maximum underestimation was 1.3%, and the maximum overestimation 5.9%.
4. In load cases two, three and four the flange stress at the loaded web position was consistently overestimated (1.8% to 16.5%) for both the midspan and quarterspan cross-sections. The flange stress values at the unloaded web positions showed greater percentage variations (-9.9% to +17.4%), but it should be noted that the greatest percentage variations occurred when the magnitude of the flange stress is low.

5.3.6. FIVE CELL STRUCTURE - MIDSPAN POINT LOADING.

The structure details were

overall width, B	= 900cm
overall depth, D	= 150cm
overall span, L	= 1350cm
web thickness, t_w	= 1.2cm
flange thickness, t_f	= 3.0cm
diaphragm thickness, t_d	= 3.0cm

hence

$$\begin{aligned}b/L &= 0.0667 \\B/L &= 0.667 \\t_f/t_w &= 2.5 \\\Psi_{\text{defl}} &= 0.963 \\\Psi_{\text{str}} &= 0.757 \text{ (at midspan)} \\\Psi_{\text{str}} &= 1.000 \text{ (at quarterspan)}\end{aligned}$$

The four loading cases considered were

- (i) 750kN over webs 1, 1500kN over webs 2 and 3
- (ii) 750kN over webs 1
- (iii) 1500kN over webs 2
- (iv) 1500kN over webs 3

The results of the grillage and finite element analyses are presented in Table 5.10 and Figures 5.11 and 5.12., which may be summarized as follows.

1. The results for both web deflection and flange stress followed a similar pattern to those for the four cell midspan point loading example (Section 5.3.4.).
2. The web deflection values for load case one were accurately predicted at both the midspan and quarterspan positions. The values varied from a maximum underestimation of 1.9% to a maximum overestimation of 5.7%.
3. In load cases two, three and four the deflections of the loaded webs were accurately predicted. The values varied from a maximum underestimation of 0.7% to a maximum overestimation of 5.2%. The deflection values

at the unloaded web positions showed greater percentage variations (-13.8% to + 24.3%), but as in previous examples the greatest percentage variation occurred when the magnitude of the web deflection is low.

4. In load case one at the midspan cross-section the flange stress was consistently overestimated (5.7% to 15.9%). At the quarterspan cross-section the stresses varied from an underestimation of 2.8% to an overestimation of 5.8%.
5. In load cases two, three and four the flange stress at the loaded web positions were consistently overestimated. At the midspan cross-section the maximum overestimation was 12.5%, whilst at the quarterspan cross-section the maximum overestimation was 20.7%. At the unloaded web positions the numerical difference between the grillage and finite element analyses was consistent with that at the loaded webs.

5.3.7. FIVE CELL STRUCTURE - UNIFORM LINE LOAD.

The structure details were

overall width, B	= 900cm
overall depth, D	= 150cm
overall span, L	= 1500cm
web thickness, t_w	= 1.2cm
flange thickness, t_f	= 2.0cm
diaphragm thickness, t_d	= 2.0cm

hence

$$b/L = 0.06$$

$$B/L = 0.6$$

$$t_f/t_w = 1.67$$

$$\Psi_{\text{defl}} = 0.970$$

$$\Psi_{\text{str}} = 0.970 \text{ (at quarterspan)}$$

$$\Psi_{\text{str}} = 0.974 \text{ (at midspan)}$$

The four loading conditions considered were

- (i) 960kN along webs 1, 1920kN along webs 2 and 3
- (ii) 960kN along webs 1
- (iii) 1920kN along webs 2
- (iv) 1920kN along webs 3

The results of the grillage and finite element analyses are presented in Table 5.11 and Figures 5.13 and 5.14., which may be summarized as follows.

1. The results for both web deflection and flange stress followed a similar pattern to those for the four cell uniform line loading example (Section 5.3.5.).
2. The web deflection values for load case one were again accurately predicted at both the midspan and quarterspan positions. The values varied from a maximum underestimation of 2.0% to a maximum overestimation of 5.6%.
3. In load cases two, three and four the deflections of the loaded webs were accurately predicted. The values varied from a maximum underestimation of 4.2% to a maximum overestimation of 1.7%. The deflection values

at the unloaded web positions showed greater percentage variations (-5.1% to + 22.8%), but as in previous examples the greatest percentage variation occurred when the magnitude of the web deflection is low.

4. In load case one the predicted flange stress varied from an underestimation of 1.4% to an overestimation of 7.8%.
5. In the other three load cases the midspan flange stress values at the loaded web position were consistently overestimated within the range 5.8% to 15.6%. At the quarterspan cross-section the flange stress was predicted to a greater accuracy, varying from an underestimation of 1.6% to an overestimation of 5.6%. At the unloaded web positions the flange stress values were generally as accurate as the loaded web values with only one exception where the discrepancy was 28.5%.

5.4. CONCLUSIONS.

1. The results presented in this chapter have clearly demonstrated that the proposed grillage method can predict the overall behaviour of multi-cell structures to an acceptable degree of accuracy.
2. The convergence study in Section 5.2 revealed that the number of transverse grillage beams required in the grillage idealization should be five for midspan point loading cases and nine for uniform line loading cases. This permits the analysis to be accomplished using a low-cost micro-computer.
3. The six examples considered were chosen to cover a variation in the critical parameters affecting the accuracy of the grillage solution. The limits of these parameters were

b/L from 0.06 to 0.0833

B/L from 0.4 to 0.667

t_f/t_w from 1.67 to 2.5

It was considered that these variations were representative of the values that would be expected to occur in practice.

4. The web deflection values at the loaded webs were accurately predicted by the grillage method, the maximum underestimation and overestimation being -4.2% and +5.7% respectively. The deflection values at

unloaded webs were not so accurately predicted in percentage terms, but the deformation of the cross-section was closely modelled by the grillage method.

5. In the three examples which considered midspan point loading, the grillage method predicted the flange stress at the loaded web positions reasonably accurately, the tendency being to overestimate the stress. The maximum percentage overestimations were 15.9% and 20.7% at the midspan and quarterspan cross-sections respectively. It was considered that this degree of accuracy for multi-cell structures was consistent with the accuracy achieved from an exact solution of single cell structures using the effective breadth ratios and simple beam theory (chapter three).
6. The flange stress results for the uniform line loading cases were generally more accurate than the midspan point loading cases. This is consistent with the results from the single cell study of chapter three.
7. The grillage method calculates the flange stress at the web locations only. The variation of longitudinal flange stress across the full width of the flange plate can be determined using equation 5.6. This equation is based on the recommendations of Appendix A, Part 3, BS 5400.

8. The major advantage of the grillage method over the finite element method is its simplicity of analysis. All the grillage analyses considered in this chapter could be accomplished using a low-cost micro-computer. The solution time for the five cell structure would be of the order of fifteen minutes on such a machine. All the grillage and finite element analyses were in fact carried out on a Dec20/60 mainframe computer. Using the five cell structure as an example the execution times for the grillage and finite element programs were 3 cpu seconds and 468 cpu seconds respectively. It should also be considered that in the finite element analysis only one quarter of the structure was considered, whilst the full structure was considered in the grillage analysis. In addition to the huge saving in execution time and cost, the data preparation is far easier and faster for the grillage program.

The combination of reasonable accuracy, low cost and simplicity of use renders the grillage method a valuable design aid in the initial stages of design where a number of analyses may be required before the final proportions of the structure are achieved.

Dir- ect- ion	Stiffness Parameter	Location	No. Transverse Grillage Beams				
			5	7	9	11	13
T R A N S V E R S E	Second Moment of Area (*10E3cm4)	Outer	3037	2138	1687	1417	1237
		Inner	5400	3600	2700	2160	1800
	Eff. Shear Area (cm2)	Outer			180.		
		Inner	.020	.013	.010	.008	.007
	Torsion Inertia (*10E3cm4)	4 Cell	2880	2057	1600	1309	1108
		3 Cell	3645	2604	2025	1657	1402
L O N G I T U D I N A L	Second Moment of Area (cm4)	Outer	2 232 900				
		Inner	4 128 300				
	Eff. Shear Area (cm2)		180.				
	Torsion Inertia (cm4)	4 Cell	8 640 000				
3 Cell		5 858 000					

TABLE 5.1. - Stiffness parameters of grillage beams
Three and Four Cell Structures
Convergence study of transverse grillage beams

Load Case	Span posn	Web No.	Finite Element	Grillage Mesh				
				5x5	5x7	5x9	5x11	5x13
O N E	1/2	1	0.606	0.649	0.649	0.649	0.649	0.649
		2	0.757	0.747	0.747	0.747	0.747	
		3	0.775	0.750	0.750	0.750	0.750	
	1/4	1	0.400	0.431		0.431		0.431
		2	0.486	0.483		0.482		0.482
		3	0.498	0.485		0.485		0.485
T W O	1/2	1	0.382	0.379	0.376	0.375	0.375	0.375
		2	0.091	0.102	0.104	0.105	0.105	
		3	0.042	0.066	0.065	0.065	0.064	
	1/4	1	0.240	0.238		0.237		0.238
		2	0.065	0.073		0.074		0.074
		3	0.030	0.047		0.046		0.045
T H R E E	1/2	1	0.042	0.067	0.065	0.065	0.064	0.064
		2	0.122	0.105	0.107	0.108	0.108	
		3	0.490	0.474	0.470	0.470	0.470	
	1/4	1	0.030	0.047		0.046		0.045
		2	0.085	0.075		0.076		0.076
		3	0.297	0.288		0.286		0.286
F O U R	1/2	1	0.416	0.371	0.368	0.368	0.368	0.368
		3	0.021	0.033	0.032	0.032	0.032	
		5	-0.035	0.008	0.008	0.007	0.007	
	1/4	1	0.265	0.232		0.232		0.233
		3	0.015	0.024		0.023		0.023
		5	-0.025	0.006		0.005		0.005

-ve sign indicates upward deflection

TABLE 5.2. - Web deflection(cm) at midspan and quarterspan
Four Cell Structure - Midspan Point Loading
Convergence study of transverse grillage beams

Load Case	Span posn	Web No.	Finite Element	Grillage Mesh				
				5x5	5x7	5x9	5x11	5x13
O N E	1/2	1	45.45	53.61	53.69	53.73	53.74	53.76
		2	52.59	57.14	57.10	57.08	57.08	57.07
		3	53.75	57.38	57.36	57.36	57.36	57.36
	1/4	1	18.09	19.86		19.87		19.87
		2	20.43	20.18		20.18		20.18
		3	21.25	20.29		20.30		20.30
T W O	1/2	1	32.64	34.01	32.96	32.54	32.33	32.20
		2	6.76	7.65	8.16	8.36	8.47	8.53
		3	3.73	4.78	4.93	4.98	5.00	5.00
	1/4	1	8.24	9.09		8.98		9.02
		2	4.55	4.03		4.10		4.10
		3	2.78	2.67		2.64		2.60
T H R E E	1/2	1	2.18	4.67	4.81	4.86	4.88	4.89
		2	7.44	7.88	8.42	8.64	8.76	8.82
		3	35.56	36.83	35.59	35.10	34.85	34.70
	1/4	1	1.91	2.68		2.65		2.61
		2	4.81	4.14		4.22		4.22
		3	8.47	9.34		9.21		9.25
F O U R	1/2	1	34.49	33.41	32.39	31.98	31.78	31.67
		3	1.87	2.39	2.46	2.49	2.50	2.50
		5	-1.84	0.33	0.57	0.55	0.54	0.54
	1/4	1	9.90	8.73		8.67		8.73
		3	1.39	1.33		1.32		1.30
		5	-1.66	0.19		0.31		0.29

-ve sign indicates tension in top flange

TABLE 5.3. - Flange Stress (N/mm²) at midspan and quarterspan
Four Cell Structure - Midspan Point Loading
Convergence study of transverse grillage beams

Load Case	Span posn	Web No.	Finite Element	Grillage Mesh				
				5x5	5x7	5x9	5x11	5x13
O N E	1/2	1	0.763	0.791	0.792	0.792	0.792	0.792
		2	0.904	0.889	0.889	0.889	0.889	
	1/4	1	0.552	0.567		0.567		0.567
		2	0.654	0.640		0.640		0.640
T W O	1/2	1	0.461	0.446	0.441	0.440	0.440	0.440
		2	0.150	0.173	0.175	0.176	0.176	0.176
	1/4	1	0.341	0.319		0.316		0.316
		2	0.106	0.124		0.126		0.125
T H R E E	1/2	1	0.302	0.346	0.351	0.352	0.352	0.352
		2	0.753	0.716	0.714	0.713	0.713	0.713
	1/4	1	0.211	0.248		0.251		0.251
		2	0.549	0.516		0.514		0.514
F O U R	1/2	1	0.318	0.237	0.243	0.245	0.246	0.247
		2	0.610	0.557	0.552	0.551	0.551	0.551
		3	0.143	0.160	0.162	0.162	0.162	0.162
		4	-0.016	0.109	0.107	0.106	0.105	0.105
	1/4	1	0.222	0.170		0.175		0.176
		2	0.448	0.401		0.398		0.399
		3	0.101	0.115		0.116		0.115
		4	-0.011	0.078		0.076		0.075

-ve sign indicates upward deflection

TABLE 5.4. - Web deflection(cm) at midspan and quarterspan
Three Cell Structure - Uniform Line Loading
Convergence study of transverse grillage beams

Load Case	Span posn	Web No.	Finite Element	Grillage Mesh				
				5x5	5x7	5x9	5x11	5x13
O N E	1/2	1	39.24	41.09	41.15	41.18	41.19	41.20
		2	42.94	42.07	42.04	42.02	42.02	42.01
	1/4	1	30.05	31.35		31.39		31.39
		2	32.39	32.09		32.07		32.07
T W O	1/2	1	20.24	22.20	21.40	21.10	20.95	20.86
		2	10.62	9.43	9.86	10.03	10.11	10.15
	1/4	1	17.59	16.53		16.06		16.04
		2	7.13	7.41		7.66		7.68
T H R E E	1/2	1	19.00	18.88	19.75	20.08	20.25	20.34
		2	32.32	32.64	32.18	32.00	31.91	31.86
	1/4	1	12.46	14.82		15.33		15.36
		2	25.26	24.68		24.41		24.40
F O U R	1/2	1	19.92	13.02	13.76	14.05	14.20	14.29
		2	23.76	23.93	23.08	22.76	22.60	22.52
		3	8.56	8.71	9.09	9.23	9.30	9.34
		4	-0.92	5.86	5.99	6.03	6.04	6.05
	1/4	1	13.30	10.09		10.67		10.77
		2	19.22	17.85		17.36		17.33
		3	6.04	6.83		7.05		7.06
		4	-0.84	4.73		4.66		4.59

-ve sign indicates tension in top flange

TABLE 5.5. - Flange stress (N/mm²) at midspan and quarterspan
Three Cell Structure - Uniform Line Loading
Convergence study of transverse grillage beams

			MIDSPAN		QUARTERSPAN	
			Web 1	Web 2	Web 1	Web 2
L o a d A l l W e b s	S t r e s s	Gr	153.62	158.40	56.65	56.94
		FE	139.00	150.55	54.51	57.61
		%	+10.5	+ 5.2	+ 3.9	- 1.2
	D e f l n	Gr	1.651	1.964	1.080	1.238
		FE	1.609	1.990	1.047	1.248
		%	+ 2.6	- 1.3	+ 3.2	- 0.8
L o a d W e b 1	S t r e s s	Gr	95.65	29.35	25.31	15.64
		FE	94.46	25.96	21.69	17.35
		%	+ 1.3	+13.0	+16.7	- 9.9
	D e f l n	Gr	0.988	0.332	0.608	0.236
		FE	0.967	0.321	0.593	0.228
		%	+ 2.2	+ 3.4	+ 2.5	+ 3.5
L o a d W e b 2	S t r e s s	Gr	57.97	129.05	31.34	41.30
		FE	44.54	124.59	32.82	40.26
		%	+30.1	+ 3.6	- 4.5	+ 2.6
	D e f l n	Gr	0.663	1.632	0.472	1.002
		FE	0.642	1.669	0.454	1.020
		%	+ 3.3	- 2.2	+ 4.0	- 1.8

TABLE 5.6. - Longitudinal flange stress (N/mm²) and deflection (cm)
Grillage (Gr) and Finite Element (FE) analyses
Three Cell Structure - Midspan Point Loading

			MIDSPAN		QUARTERSPAN	
			Web 1	Web 2	Web 1	Web 2
L o a d A l l W e b s	S t r e s s	Gr	54.59	54.98	41.34	41.65
		FE	52.75	55.29	39.34	41.35
		%	+ 3.5	- 0.6	+ 5.1	+ 0.7
	D e f l n	Gr	1.370	1.518	0.981	1.092
		FE	1.327	1.515	0.954	1.093
		%	+ 3.2	+ 0.2	+ 2.8	- 0.1
L o a d W e b 1	S t r e s s	Gr	24.88	14.85	18.91	11.21
		FE	21.75	16.30	18.07	11.38
		%	+14.4	- 8.9	+ 4.6	- 1.5
	D e f l n	Gr	0.690	0.340	0.496	0.243
		FE	0.659	0.334	0.484	0.235
		%	+ 4.7	+ 1.8	+ 2.5	+ 3.4
L o a d W e b 2	S t r e s s	Gr	29.71	40.13	22.43	30.44
		FE	31.00	38.99	21.27	29.97
		%	- 4.1	+ 2.9	+ 5.4	+ 1.6
	D e f l n	Gr	0.680	1.178	0.485	0.849
		FE	0.668	1.181	0.470	0.858
		%	+ 1.8	- 0.3	+ 3.2	- 1.0

TABLE 5.7. - Longitudinal flange stress (N/mm²) and deflection (cm)
Grillage (Gr) and Finite Element (FE) analyses
Three Cell Structure - Uniform Line Loading

			MIDSPAN			QUARTERSPAN		
			Web 1	Web 2	Web 3	Web 1	Web 2	Web 3
Load All Webs	Stress	Gr	67.63	70.03	70.18	25.95	26.10	26.17
		FE	59.05	65.14	66.28	24.75	26.19	26.91
		%	+14.5	+ 7.5	+ 5.9	+ 4.8	- 0.3	- 2.7
	Defln	Gr	0.894	1.070	1.072	0.585	0.673	0.674
		FE	0.854	1.074	1.093	0.556	0.673	0.688
		%	+ 4.7	- 0.4	- 1.9	+ 5.2	0.0	- 2.0
Load Web 1	Stress	Gr	39.00	10.62	7.77	9.90	5.76	4.49
		FE	37.30	9.77	6.72	8.47	6.32	4.86
		%	+ 4.6	+ 8.7	+15.6	+16.9	- 8.9	- 7.6
	Defln	Gr	0.494	0.146	0.109	0.300	0.103	0.078
		FE	0.483	0.140	0.090	0.293	0.099	0.065
		%	+ 2.3	+ 4.3	+21.1	+ 2.4	+ 4.0	+20.0
Load Web 2	Stress	Gr	20.97	48.63	21.55	11.55	14.51	11.66
		FE	16.54	44.95	21.45	12.07	13.35	13.36
		%	+26.8	+ 8.2	+ 0.5	- 4.3	+ 8.7	-12.7
	Defln	Gr	0.291	0.776	0.296	0.207	0.465	0.210
		FE	0.281	0.763	0.342	0.198	0.455	0.239
		%	+ 3.6	+ 1.7	-13.4	+ 4.5	+ 2.2	-12.1
Load Web 3	Stress	Gr	7.66	10.78	40.86	4.50	5.83	10.02
		FE	5.21	10.42	38.11	4.21	6.52	8.69
		%	+47.0	+ 3.5	+ 7.2	+ 6.9	-10.6	+15.3
	Defln	Gr	0.109	0.148	0.667	0.078	0.105	0.386
		FE	0.090	0.171	0.661	0.065	0.119	0.384
		%	+21.1	-13.4	+ 0.9	+20.0	-11.8	+ 0.5

TABLE 5.8. - Longitudinal flange stress (N/mm²) and deflection (cm)
Grillage (Gr) and Finite Element (FE) analyses
Four Cell Structure - Midspan Point Loading

			MIDSPAN			QUARTERSPAN		
			Web 1	Web 2	Web 3	Web 1	Web 2	Web 3
Load All Webs	Stress	Gr	51.17	51.61	51.72	38.37	38.71	38.79
		FE	48.40	51.43	52.39	36.23	38.39	39.15
		%	+ 5.7	+ 0.3	- 1.3	+ 5.9	+ 0.8	- 0.9
	Defln	Gr	1.406	1.575	1.577	1.008	1.133	1.136
		FE	1.347	1.572	1.600	0.969	1.134	1.154
		%	+ 4.4	+ 0.2	- 1.4	+ 4.0	0.0	- 1.6
Load Web 1	Stress	Gr	20.02	11.12	8.90	15.09	8.28	6.71
		FE	17.19	11.79	9.87	14.82	8.35	6.50
		%	+16.5	- 5.7	- 9.9	+ 1.8	- 0.8	+ 3.2
	Defln	Gr	0.635	0.275	0.221	0.458	0.196	0.158
		FE	0.616	0.263	0.200	0.455	0.185	0.140
		%	+ 3.1	+ 4.6	+10.5	+ 0.7	+ 6.0	+12.9
Load Web 2	Stress	Gr	22.25	29.25	22.47	16.57	22.06	16.73
		FE	22.20	27.63	24.52	15.69	21.27	17.93
		%	+ 0.2	+ 5.9	- 8.3	+ 5.6	+ 3.7	- 6.7
	Defln	Gr	0.550	1.022	0.556	0.392	0.739	0.397
		FE	0.529	1.006	0.606	0.373	0.734	0.429
		%	+ 4.0	+ 1.6	- 8.2	+ 5.1	+ 0.7	- 7.5
Load Web 3	Stress	Gr	8.90	11.24	20.35	6.71	8.37	15.35
		FE	9.01	12.01	18.00	5.72	8.77	14.72
		%	- 1.2	- 6.4	+13.1	+17.4	- 4.6	+ 4.3
	Defln	Gr	0.221	0.278	0.800	0.158	0.198	0.581
		FE	0.202	0.303	0.794	0.141	0.215	0.585
		%	+ 9.4	- 8.2	+ 0.8	+12.1	- 7.9	- 0.7

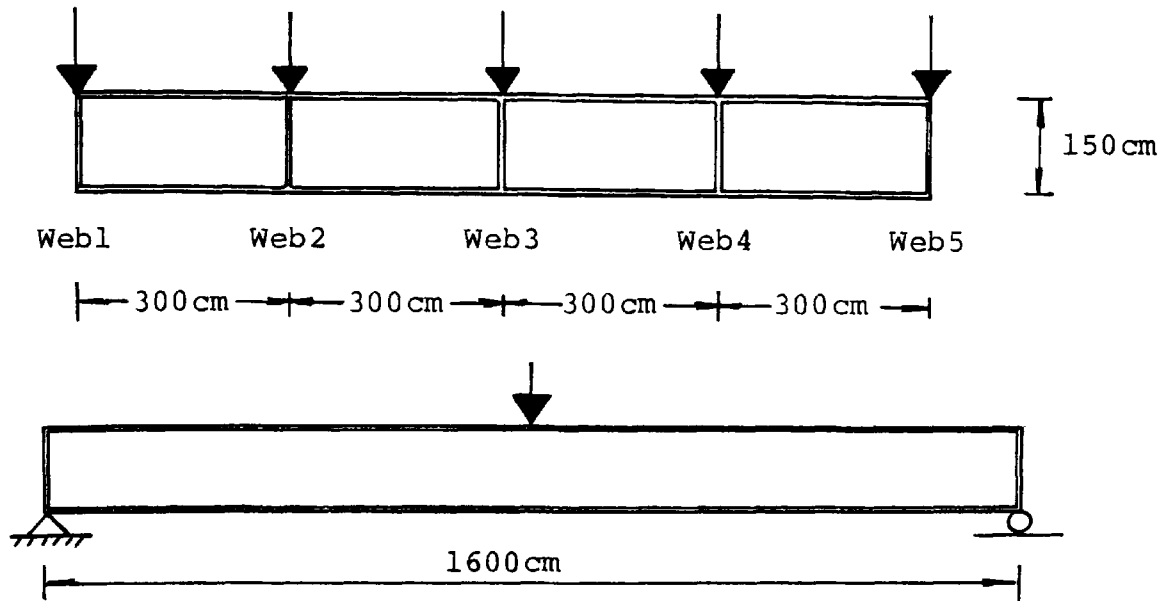
TABLE 5.9. - Longitudinal flange stress (N/mm²) and deflection (cm)
Grillage (Gr) and Finite Element (FE) analyses
Four Cell Structure - Uniform Line Loading

			MIDSPAN			QUARTERSPAN		
			Web 1	Web 2	Web 3	Web 1	Web 2	Web 3
Load All Webs	Stress	Gr	73.70	76.35	76.57	29.11	29.29	29.40
		FE	63.56	70.57	72.45	27.52	29.10	30.25
		%	+15.9	+ 8.2	+ 5.7	+ 5.8	+ 0.7	- 2.8
	Defln	Gr	0.752	0.935	0.937	0.484	0.577	0.579
		FE	0.713	0.931	0.955	0.458	0.574	0.590
		%	+ 5.5	+ 0.4	- 1.9	+ 5.7	+ 0.5	- 1.9
Load Web 1	Stress	Gr	40.99	10.36	6.20	10.25	5.70	3.71
		FE	37.86	10.12	5.72	8.49	6.26	4.12
		%	+ 8.3	+ 2.4	+ 8.4	+20.7	- 8.9	-10.0
	Defln	Gr	0.420	0.103	0.064	0.248	0.073	0.046
		FE	0.403	0.103	0.052	0.240	0.072	0.037
		%	+ 4.2	0.0	+23.0	+ 3.3	+ 1.4	+24.3
Load Web 2	Stress	Gr	20.46	49.19	16.80	11.42	14.07	9.52
		FE	17.22	43.71	17.56	12.10	12.23	11.04
		%	+18.8	+12.5	- 4.3	- 5.6	+15.0	-13.8
	Defln	Gr	0.205	0.663	0.169	0.145	0.384	0.120
		FE	0.206	0.632	0.196	0.144	0.365	0.137
		%	- 0.5	+ 4.9	-13.8	+ 0.7	+ 5.2	-12.4
Load Web 3	Stress	Gr	12.25	16.80	53.57	7.44	9.52	16.17
		FE	8.48	16.74	49.17	6.93	10.61	15.09
		%	+44.5	+ 0.4	+ 8.9	+ 7.4	-10.3	+ 7.2
	Defln	Gr	0.127	0.169	0.704	0.091	0.120	0.413
		FE	0.104	0.196	0.707	0.074	0.137	0.416
		%	+22.1	-13.8	- 0.4	+23.0	-12.4	- 0.7

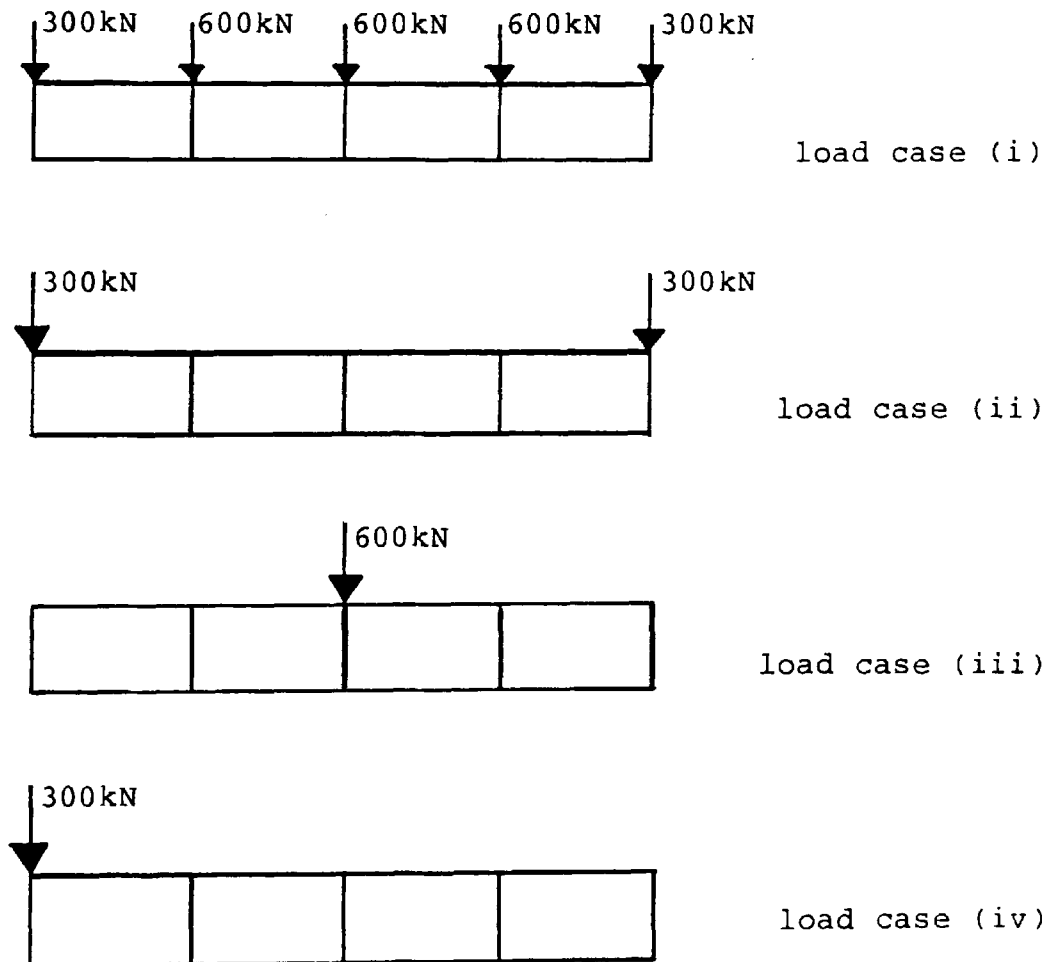
TABLE 5.10. - Longitudinal flange stress (N/mm²) and deflection (cm)
Grillage (Gr) and Finite Element (FE) analyses
Five Cell Structure - Midspan Point Loading

			MIDSPAN			QUARTERSPAN		
			Web 1	Web 2	Web 3	Web 1	Web 2	Web 3
L o a d A l l W e b s	S t r e s s	Gr	61.53	62.37	62.66	46.14	46.78	46.99
		FE	57.08	61.63	63.58	42.82	45.94	47.35
		%	+ 7.8	+ 1.2	- 1.4	+ 7.8	+ 1.8	- 0.8
	D e f l n	Gr	1.040	1.176	1.180	0.746	0.846	0.850
		FE	0.985	1.170	1.201	0.710	0.845	0.867
		%	+ 5.6	+ 0.5	- 1.7	+ 5.0	+ 0.1	- 2.0
L o a d W e b 1	S t r e s s	Gr	22.41	11.66	7.89	16.88	8.66	5.97
		FE	19.38	12.33	8.67	17.13	8.82	5.64
		%	+15.6	- 5.4	- 9.0	- 1.6	- 1.8	+ 5.8
	D e f l n	Gr	0.449	0.176	0.120	0.324	0.125	0.086
		FE	0.450	0.166	0.100	0.335	0.117	0.070
		%	- 0.2	+ 6.0	+20.0	- 3.3	+ 6.9	+22.8
L o a d W e b 2	S t r e s s	Gr	23.33	30.85	19.86	17.32	23.28	14.84
		FE	22.78	28.20	21.91	16.40	22.05	15.62
		%	+ 2.4	+ 9.4	- 9.4	+ 5.6	+ 5.6	- 5.0
	D e f l n	Gr	0.351	0.700	0.300	0.250	0.507	0.214
		FE	0.333	0.688	0.315	0.235	0.505	0.223
		%	+ 5.4	+ 1.7	- 4.8	+ 6.4	+ 0.4	- 4.0
L o a d W e b 3	S t r e s s	Gr	15.79	19.86	34.91	11.94	14.84	26.18
		FE	14.92	21.10	33.00	9.29	15.07	26.09
		%	+ 5.8	- 5.9	+ 5.8	+28.5	- 1.5	+ 0.3
	D e f l n	Gr	0.240	0.300	0.760	0.172	0.214	0.550
		FE	0.202	0.316	0.786	0.140	0.223	0.574
		%	+18.8	- 5.1	- 3.3	+22.8	- 4.0	- 4.2

TABLE 5.11. - Longitudinal flange stress (N/mm²) and deflection (cm)
Grillage (Gr) and Finite Element (FE) analyses
Five Cell Structure - Uniform Line Loading

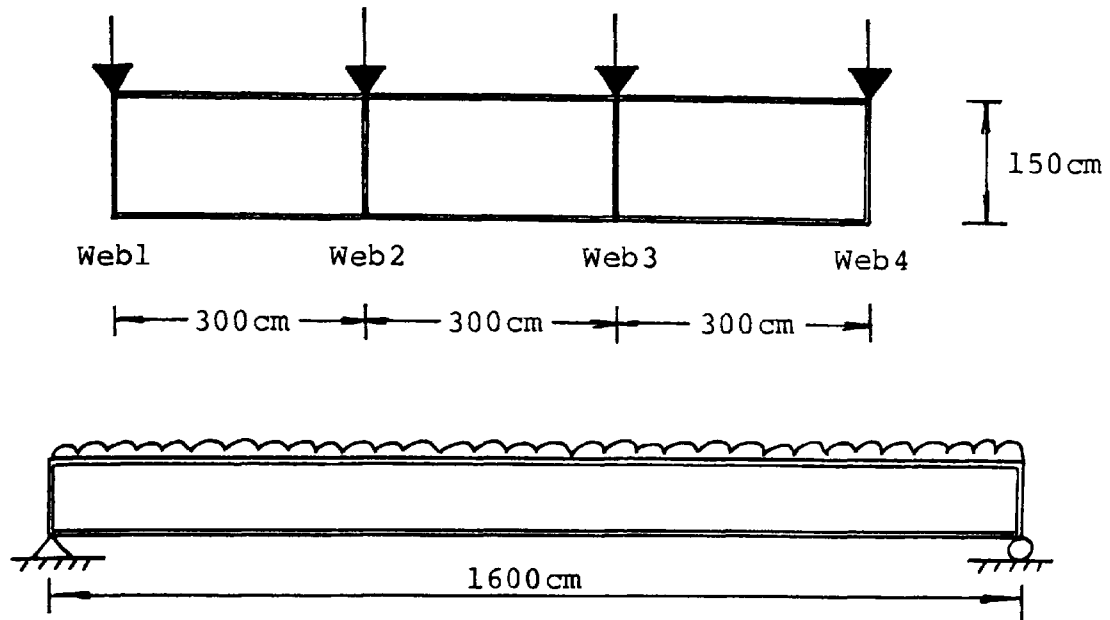


(a) Structure details.

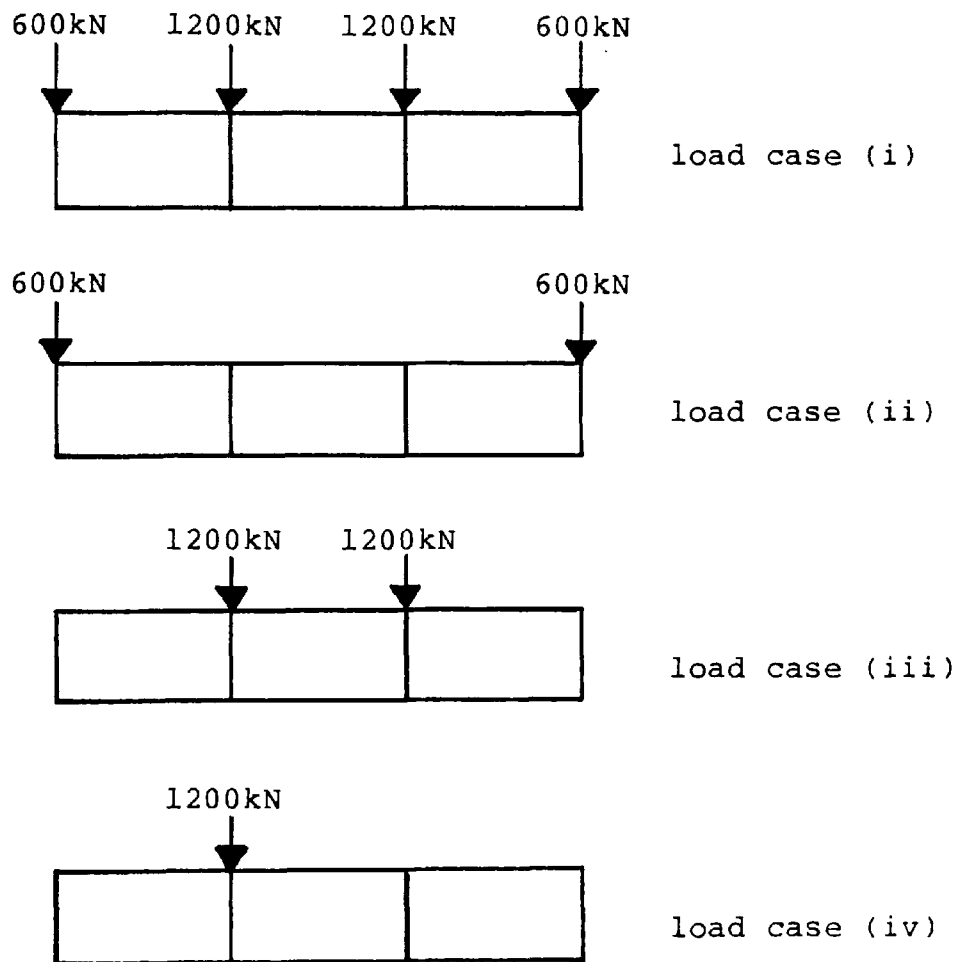


(b) Load details.

FIGURE 5.1 - TRANSVERSE GRILLAGE BEAM CONVERGENCE STUDY
FOUR-CELL STRUCTURE - MIDSPAN POINT LOADING.

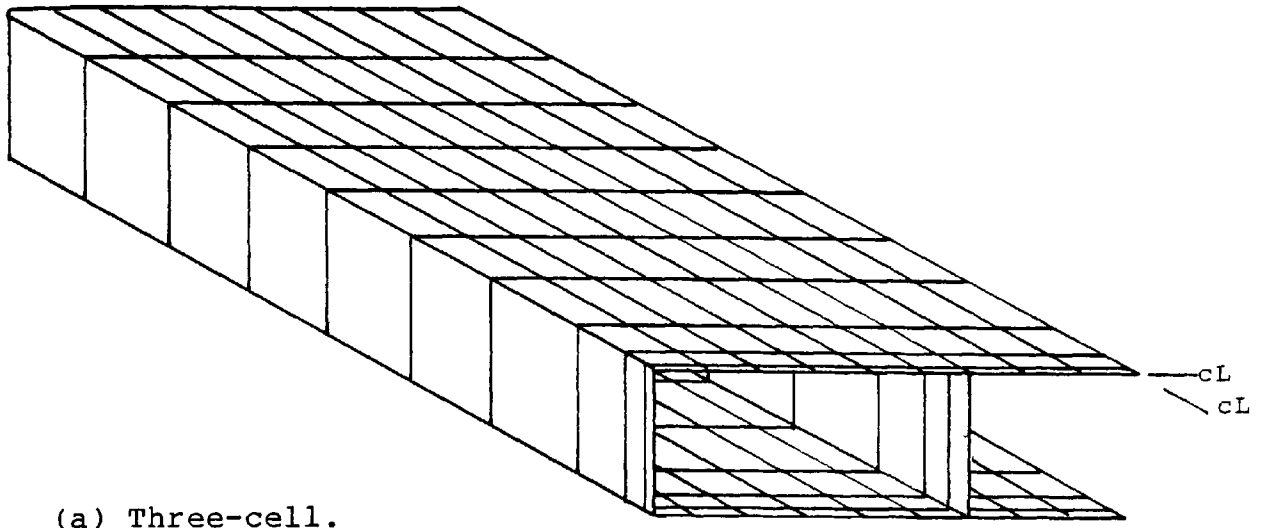


(a) Structure details.

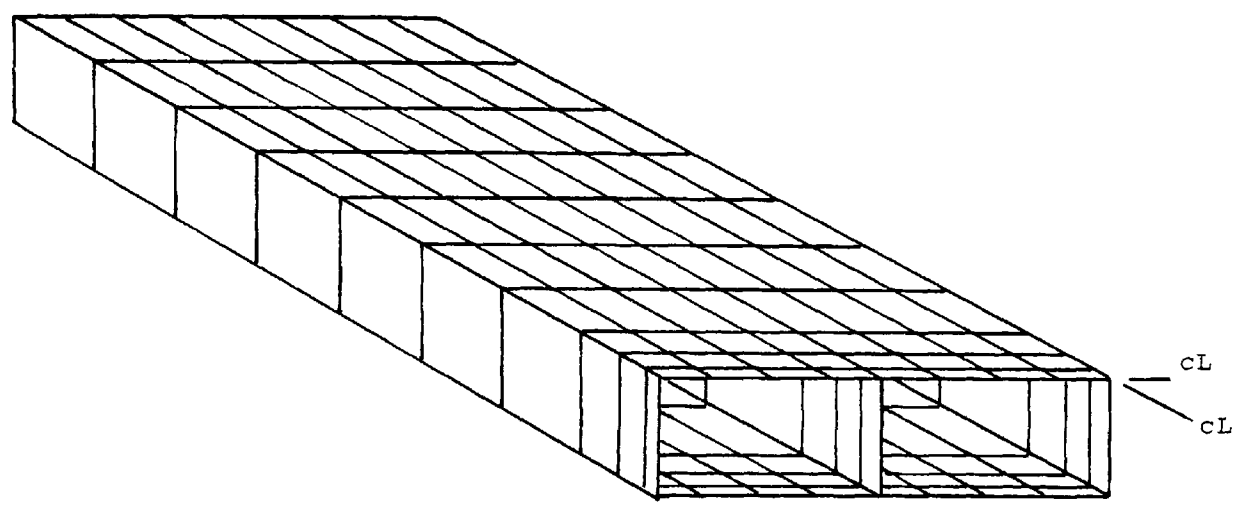


(b) Load details.

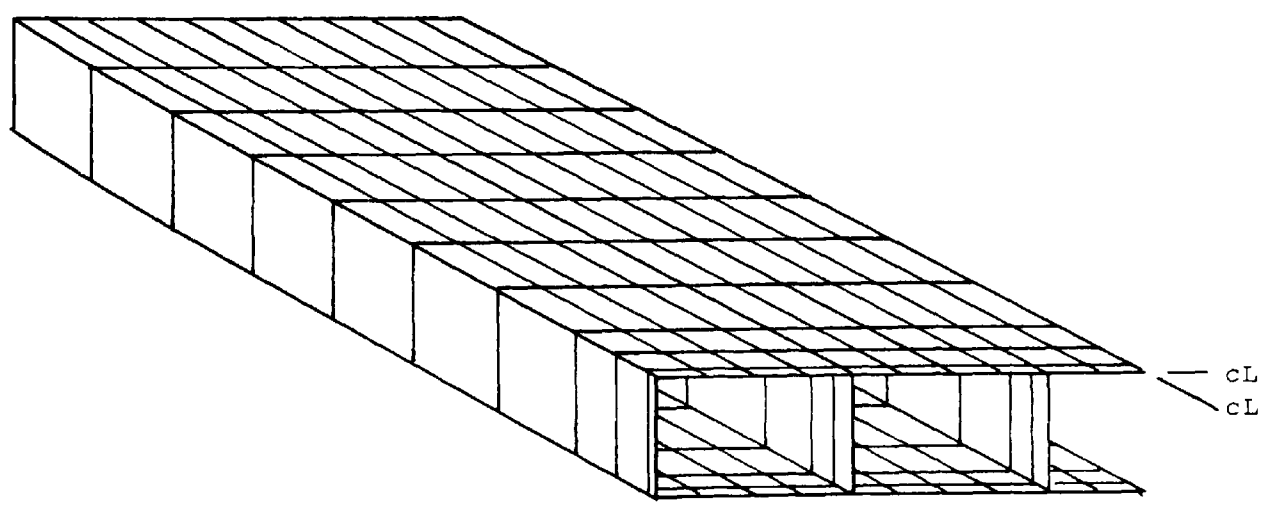
FIGURE 5.2 - TRANSVERSE GRILLAGE BEAM CONVERGENCE STUDY
THREE-CELL STRUCTURE - UNIFORM LINE LOADING.



(a) Three-cell.

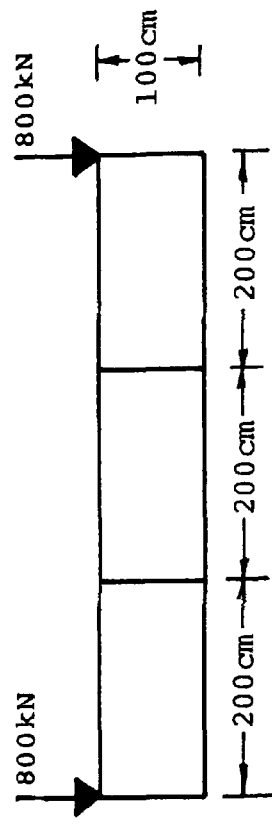


(b) Four-cell.

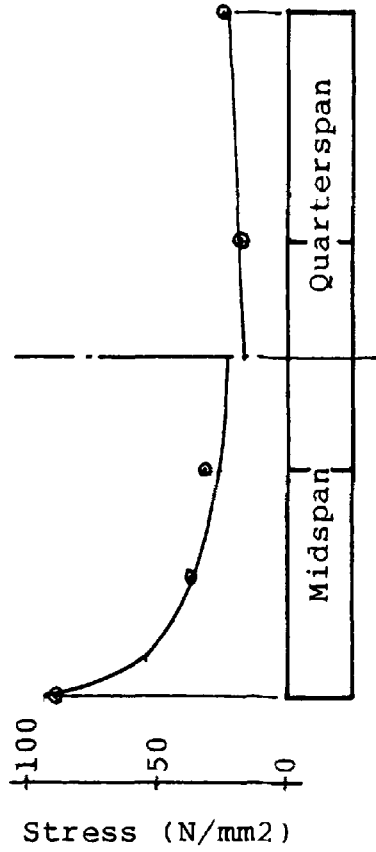


(c) Five-cell.

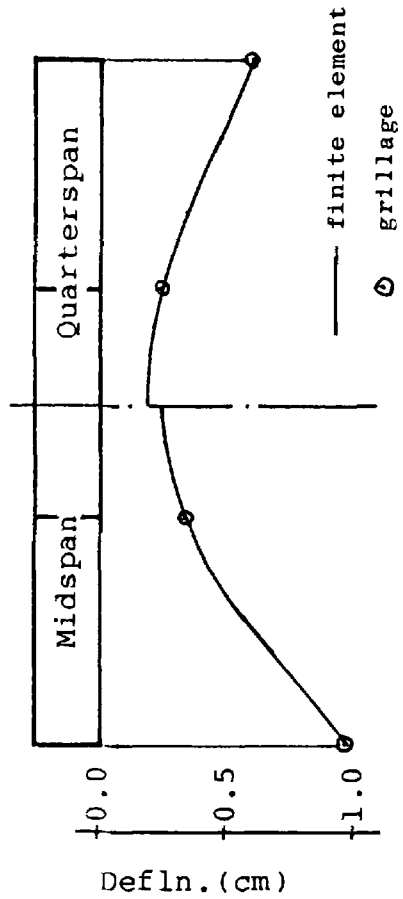
FIGURE 5.3 - FINITE ELEMENT IDEALIZATION
MULTI-CELL STRUCTURE ANALYSIS.



(a) Structure and load details.

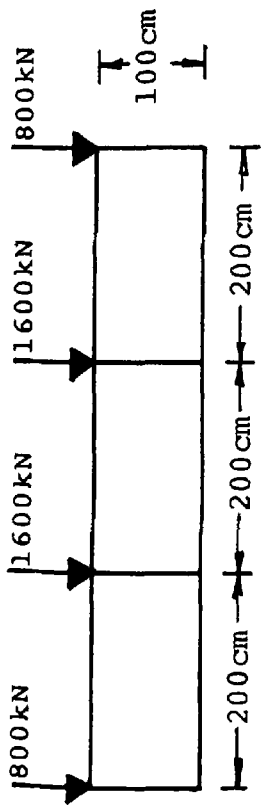


(b) Longitudinal flange stress.

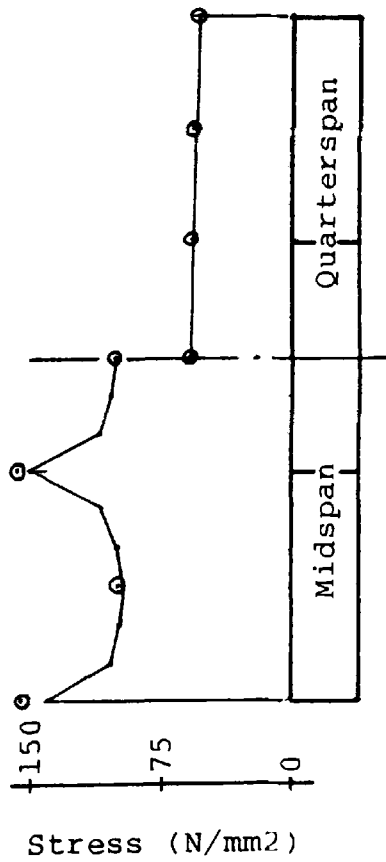


(c) Deflection.

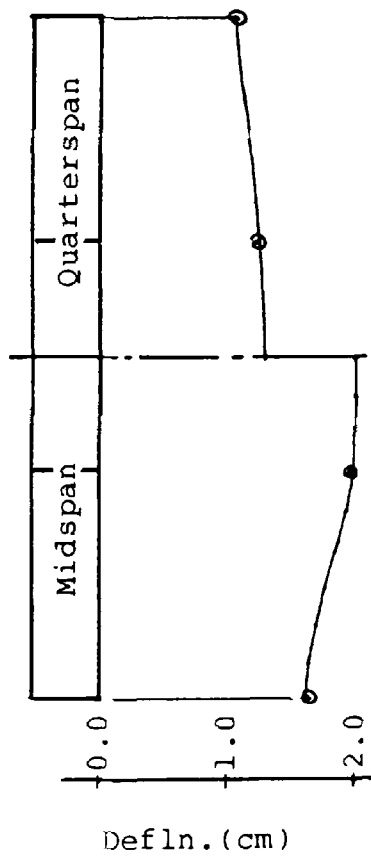
LOAD OVER OUTER WEBS.



(a) Structure and load details.



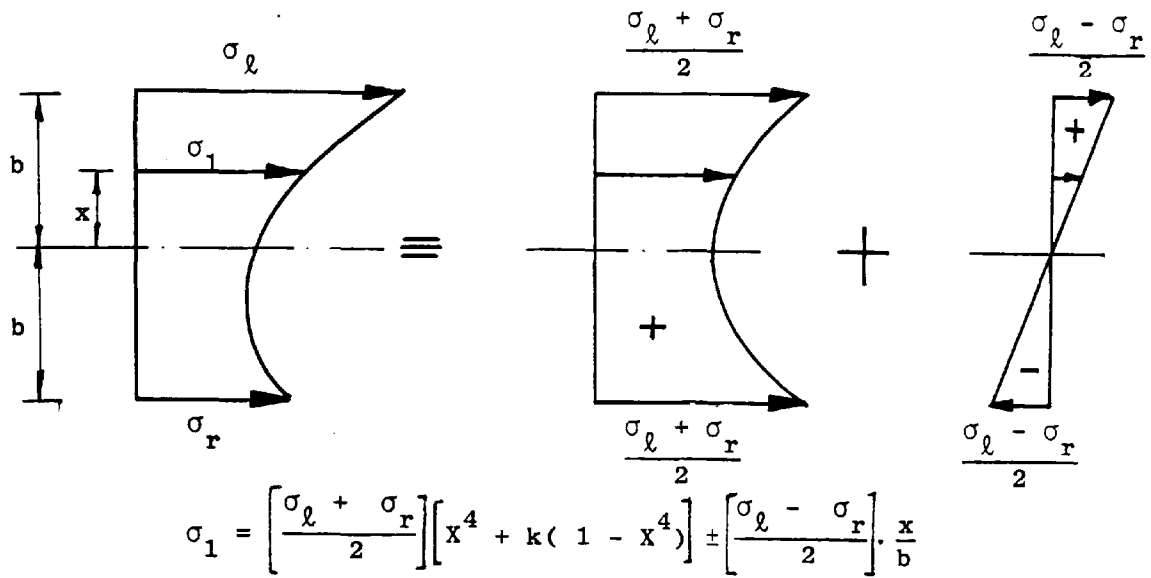
(b) Longitudinal flange stress.



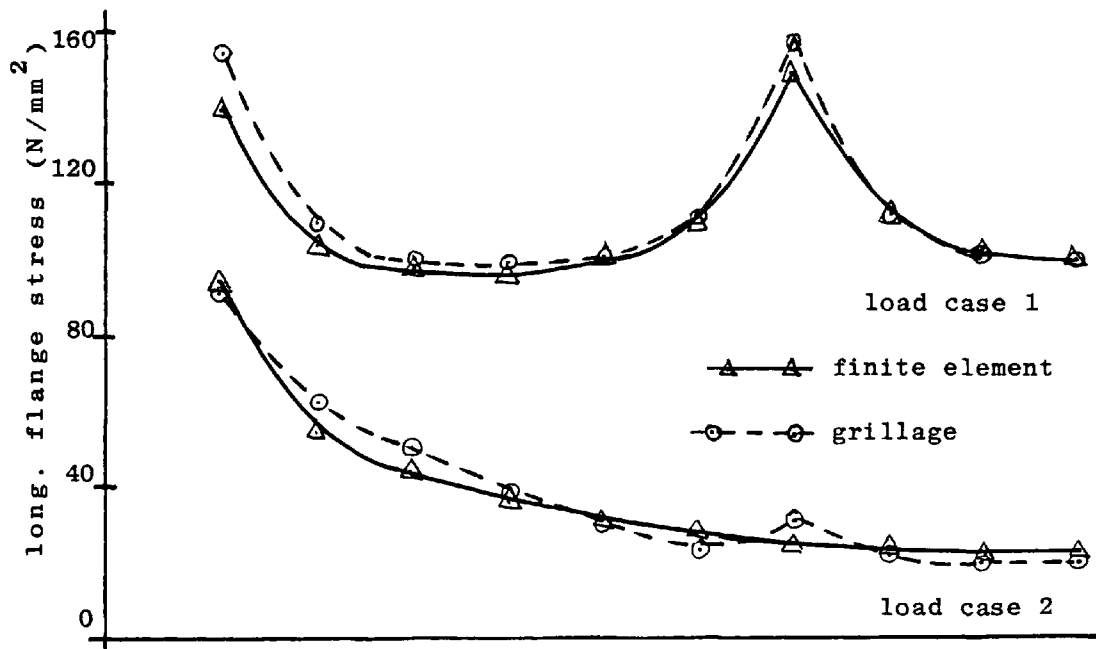
(c) Deflection.

LOAD OVER ALL WEBS.

FIGURE 5.4 - THREE CELL STRUCTURE - MIDSPAN POINT LOADING.



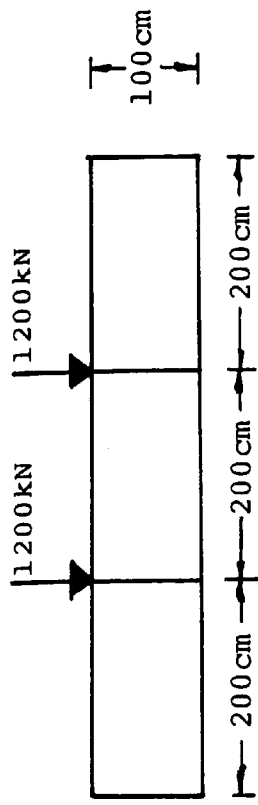
(a) Components of flange stress.



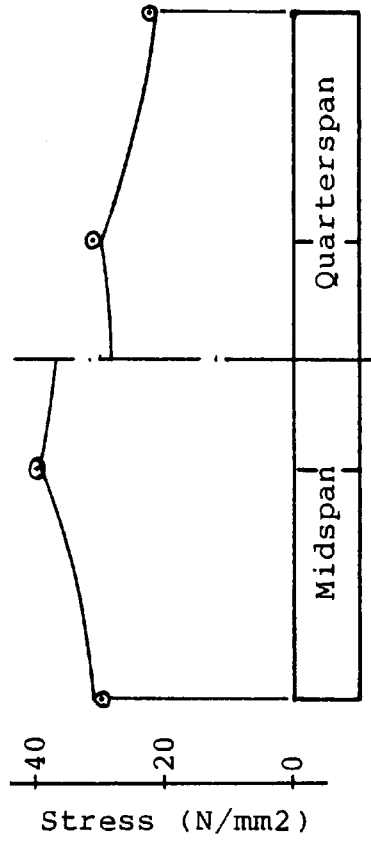
Load Case 1			Load Case 2		
Gr	FE	%	Gr	FE	%
153.62	139.00	+10.5	95.65	94.46	+4.3
109.04	103.82	+5.0	66.42	54.50	+21.9
99.35	98.50	+0.9	51.17	44.12	+16.0
99.46	97.47	+2.0	39.85	36.71	+8.6
100.95	101.56	-0.6	29.07	31.83	-8.7
112.22	109.88	+2.1	22.22	28.38	-21.7
158.40	150.55	+5.2	29.35	25.96	+13.0
112.32	111.12	+1.1	20.81	24.31	-14.4
101.68	104.09	-2.3	18.84	23.36	-19.3
100.98	101.41	-0.4	18.71	23.05	-18.8

(b) Longitudinal flange stress variation.

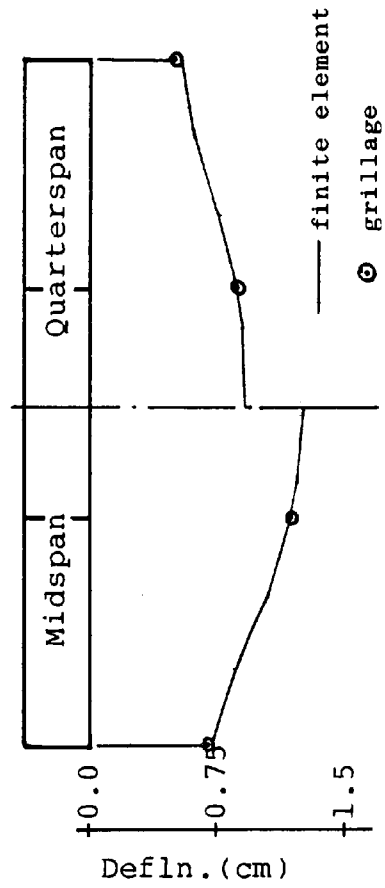
FIGURE 5.5 - VARIATION OF LONGITUDINAL FLANGE STRESS EQN. 5.6 AND GRILLAGE WEB VALUES COMPARED TO FINITE ELEMENT RESULTS.



(a) Structure and load details.

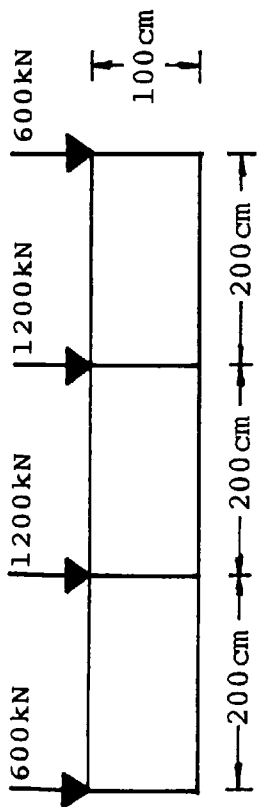


(b) Longitudinal flange stress.

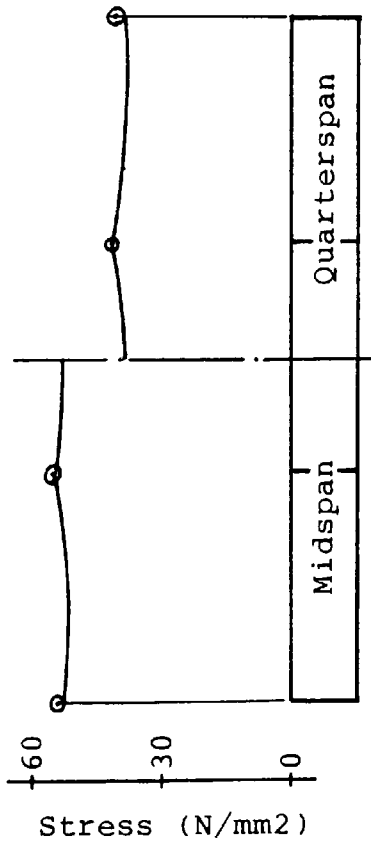


(c) Deflection.

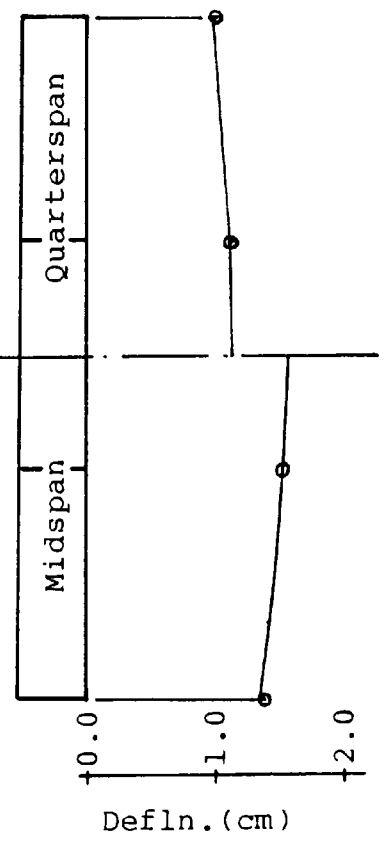
LOAD OVER INNER WEBS.



(a) Structure and load details.



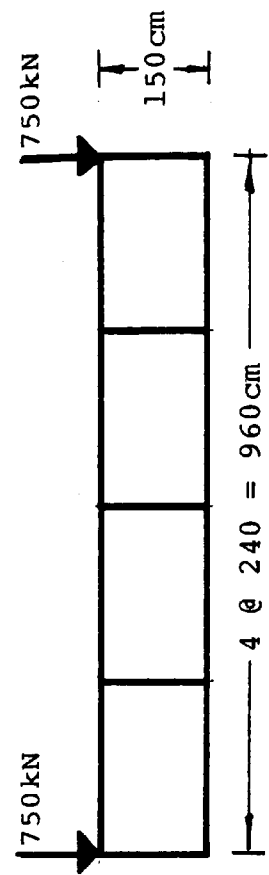
(b) Longitudinal flange stress.



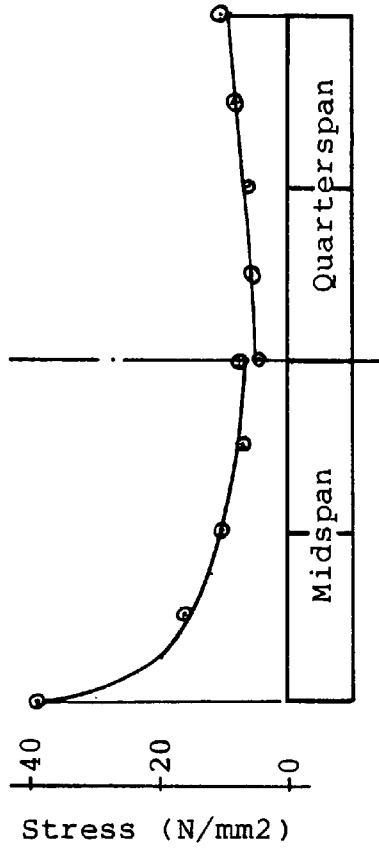
(c) Deflection.

LOAD OVER ALL WEBS.

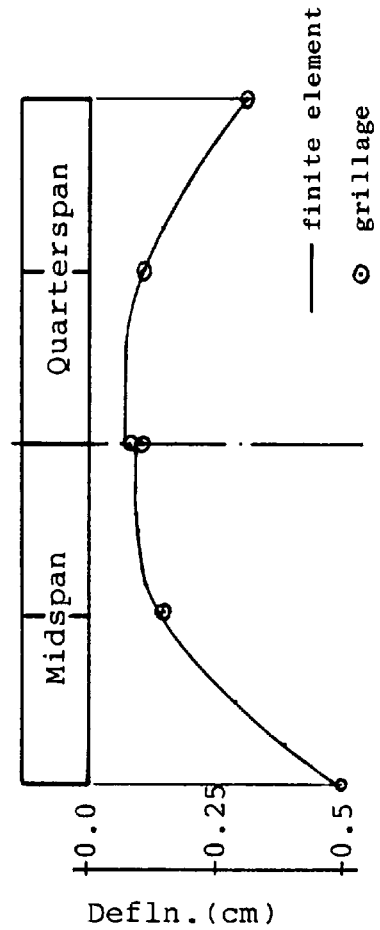
FIGURE 5.6 - THREE CELL STRUCTURE - UNIFORM LINE LOADING.



(a) Structure and load details.

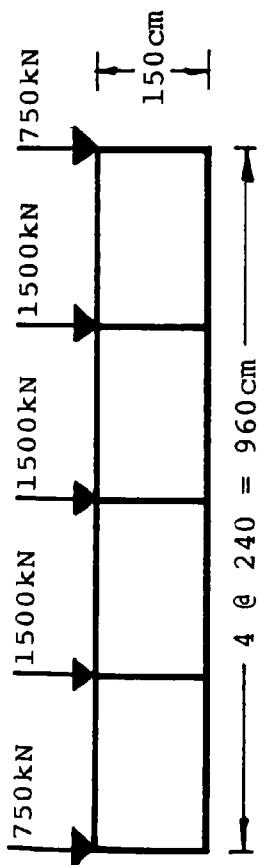


(b) Longitudinal flange stress.

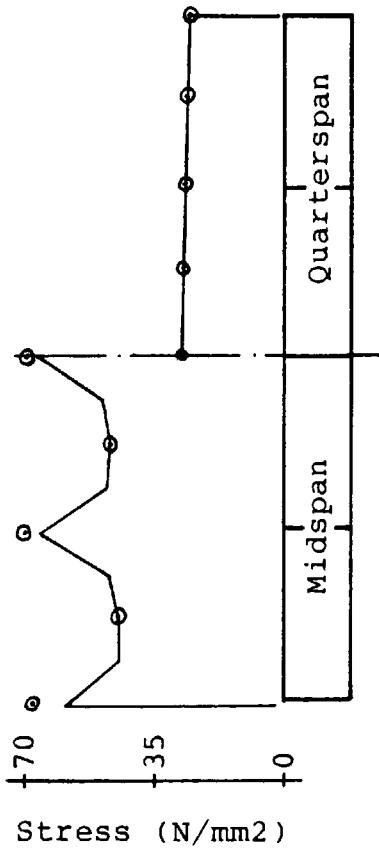


(c) Deflection.

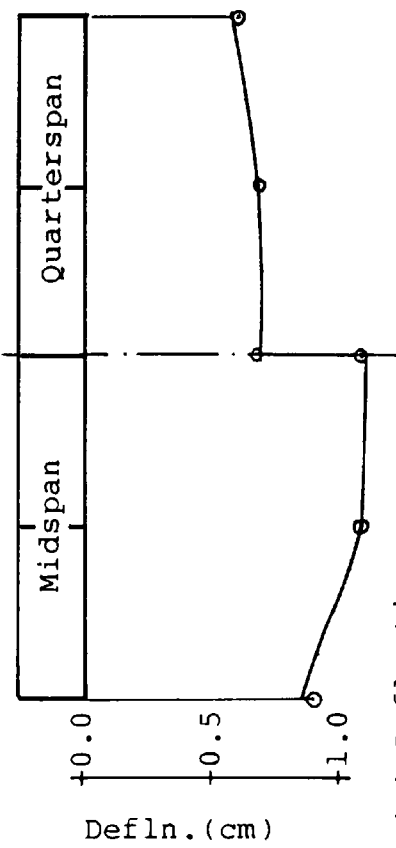
LOAD OVER WEB 1.



(a) Structure and load details.



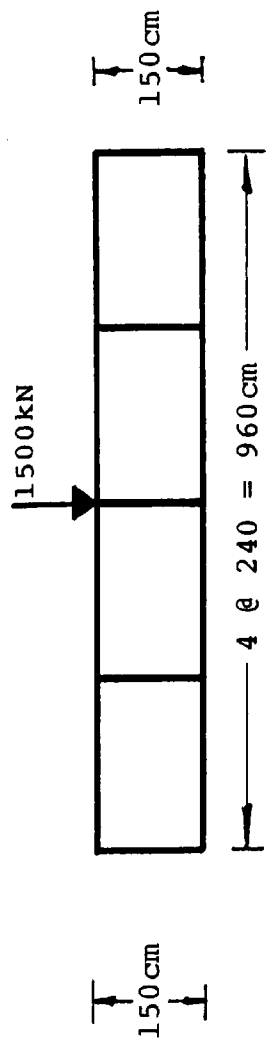
(b) Longitudinal flange stress.



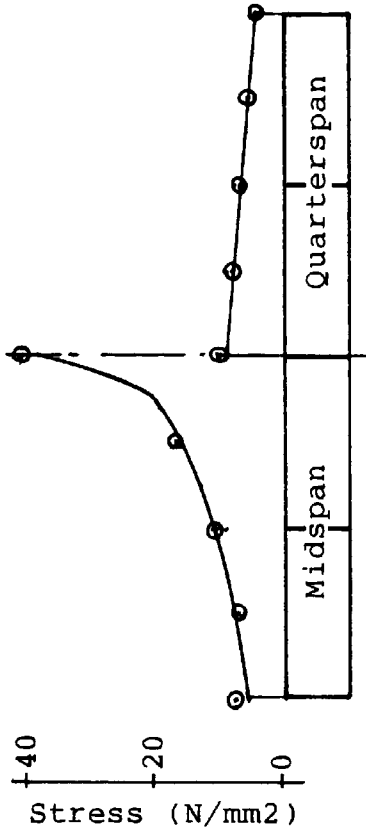
(c) Deflection.

LOAD OVER ALL WEBS.

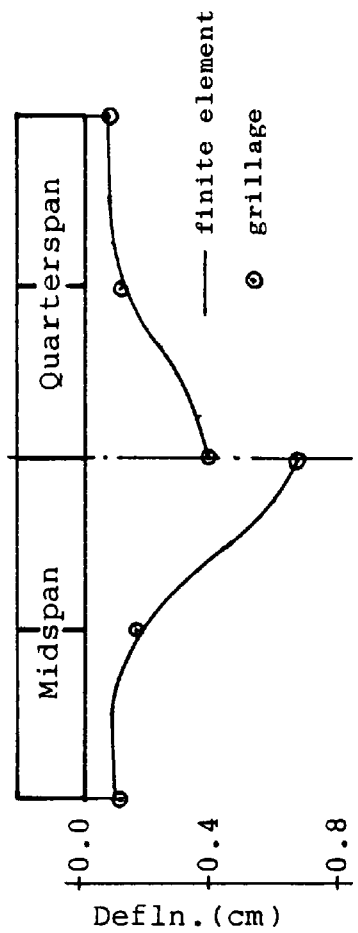
FIGURE 5.7 - FOUR CELL STRUCTURE - MIDSPAN POINT LOADING (a).



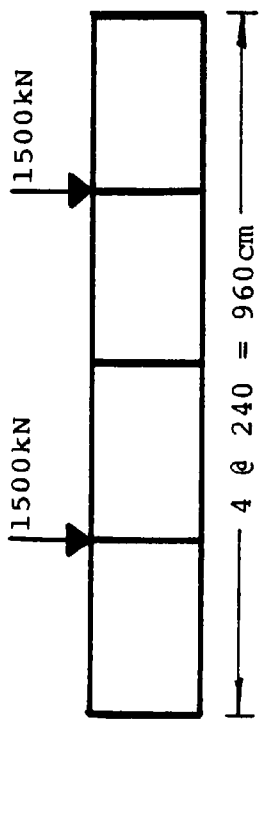
(a) Structure and load details.



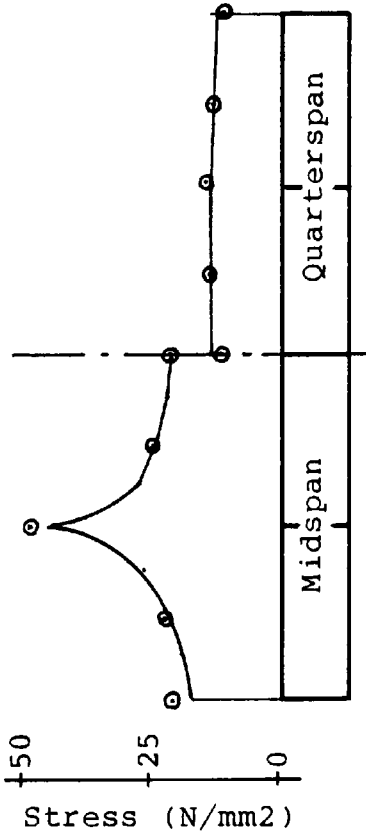
(b) Longitudinal flange stress.



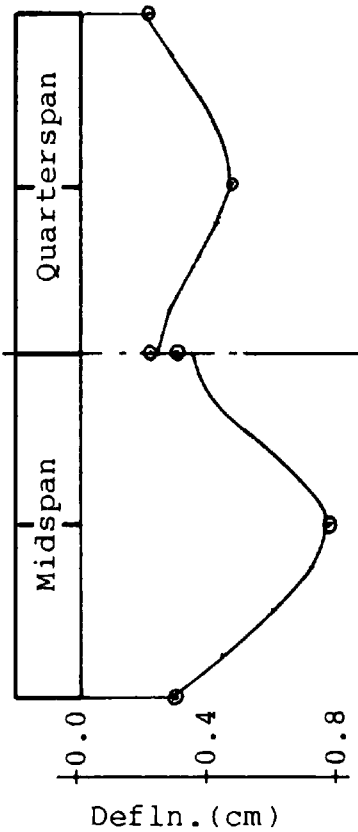
(c) Deflection.



(a) Structure and load details.



(b) Longitudinal flange stress.

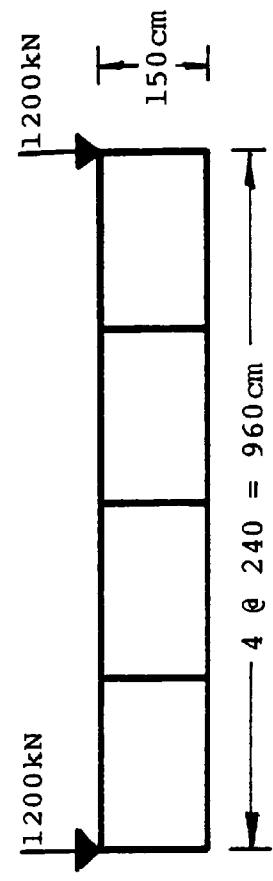


(c) Deflection.

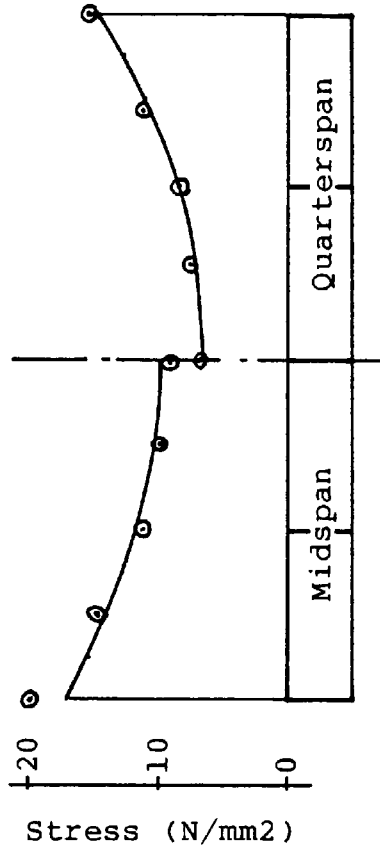
FIGURE 5.8 - FOUR CELL STRUCTURE - MIDSPAN POINT LOADING (b).

LOAD OVER WEB 3.

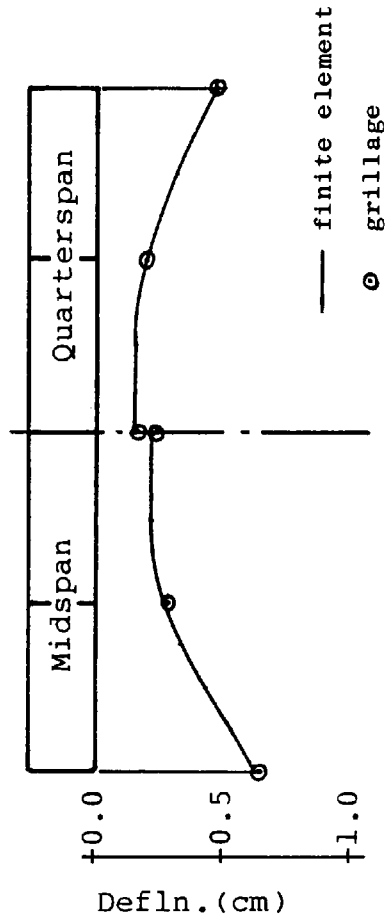
LOAD OVER WEB 2.



(a) Structure and load details.

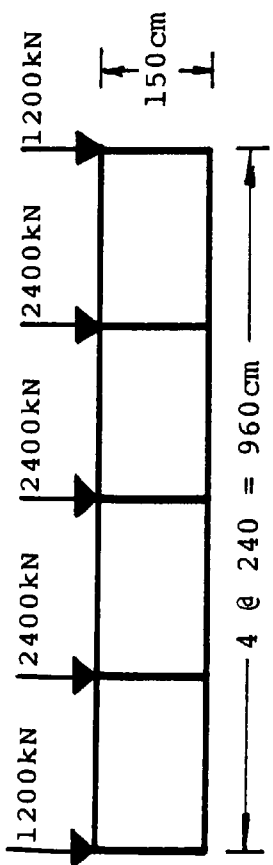


(b) Longitudinal flange stress.

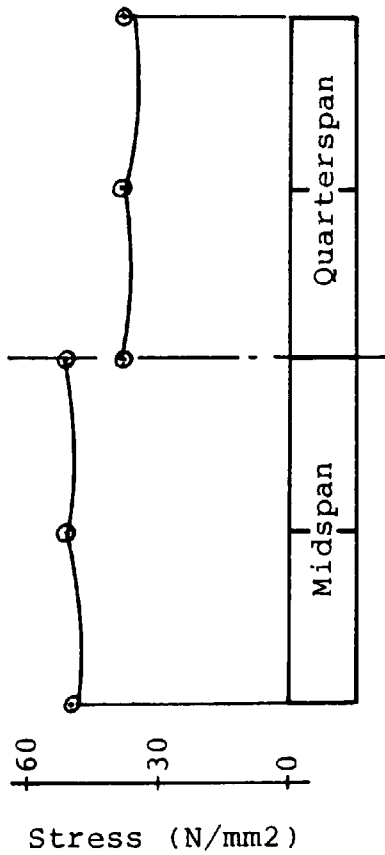


(c) Deflection.

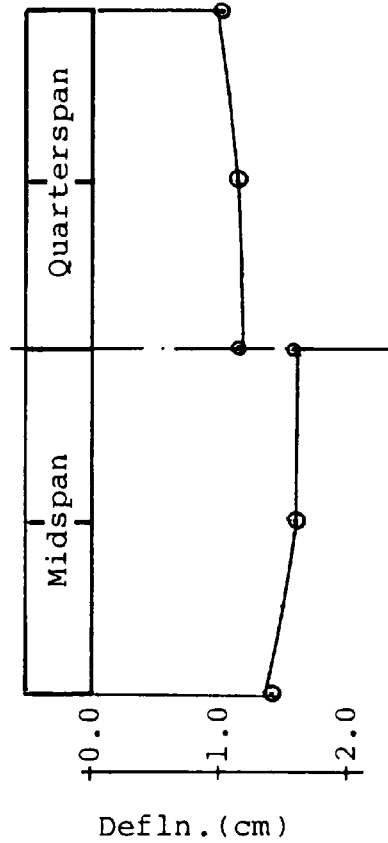
LOAD OVER WEB 1.



(a) Structure and load details.



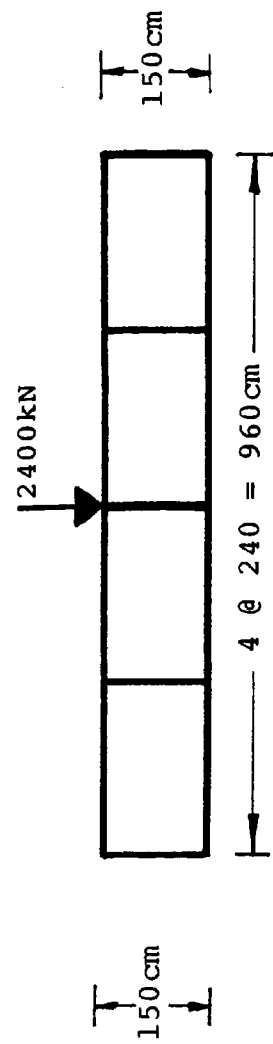
(b) Longitudinal flange stress.



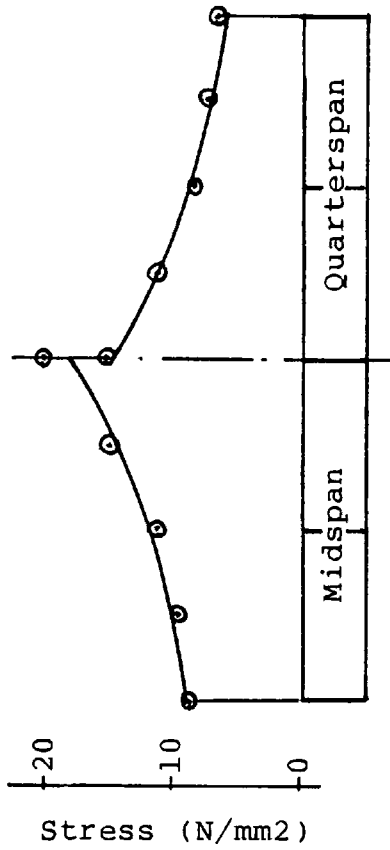
(c) Deflection.

LOAD OVER ALL WEBS.

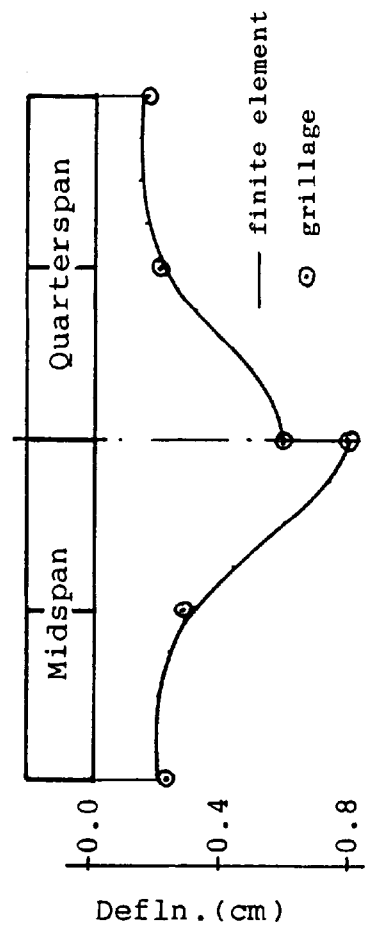
FIGURE 5.9 - FOUR CELL STRUCTURE - UNIFORM LINE LOADING (a).



(a) Structure and load details.

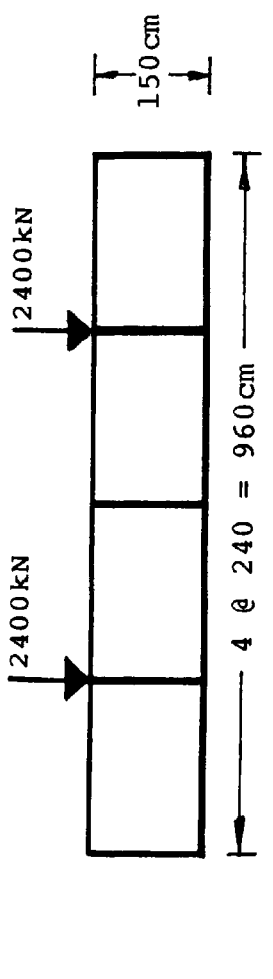


(b) Longitudinal flange stress.

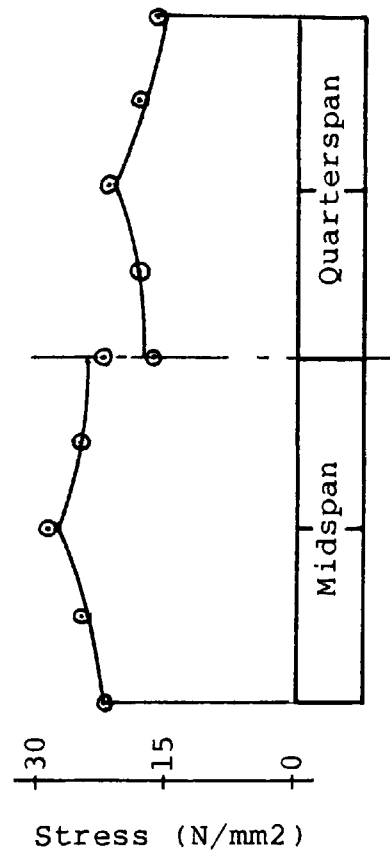


(c) Deflection.

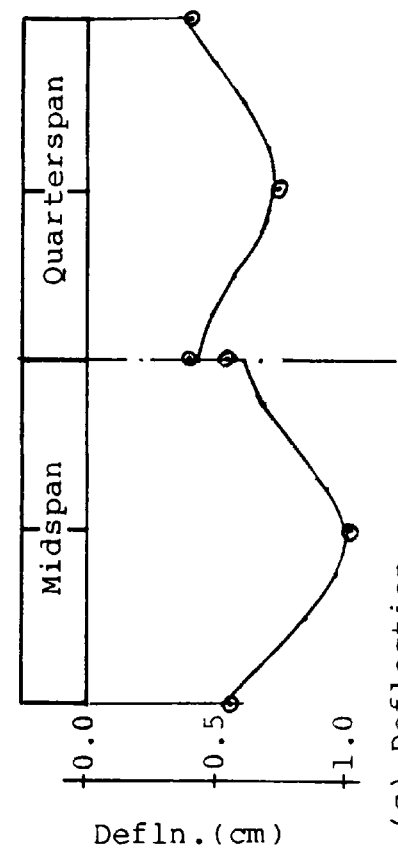
LOAD OVER WEB 3.



(a) Structure and load details.



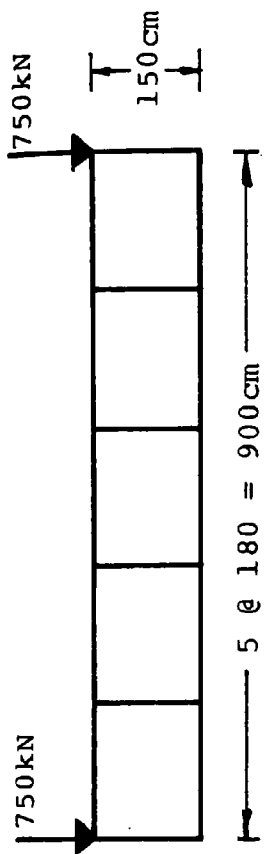
(b) Longitudinal flange stress.



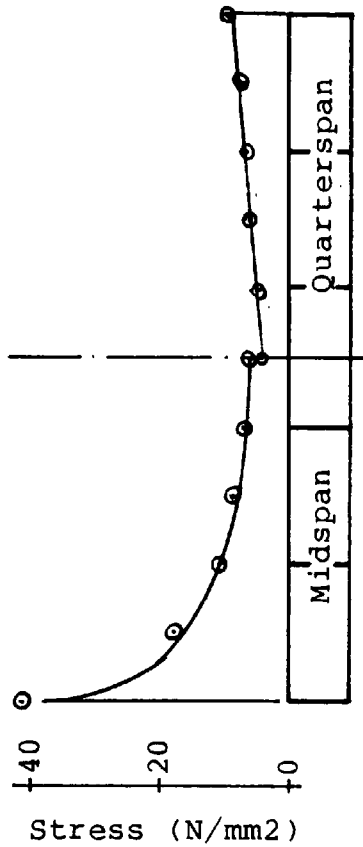
(c) Deflection.

LOAD OVER WEB 2.

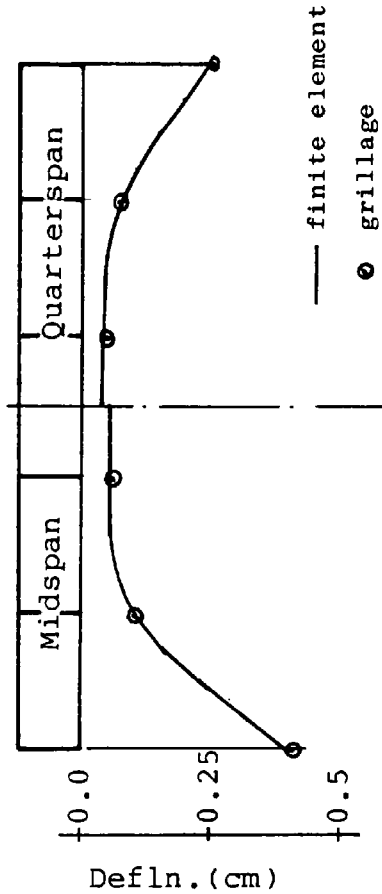
FIGURE 5.10 - FOUR CELL STRUCTURE - UNIFORM LINE LOADING (b).



(a) Structure and load details.

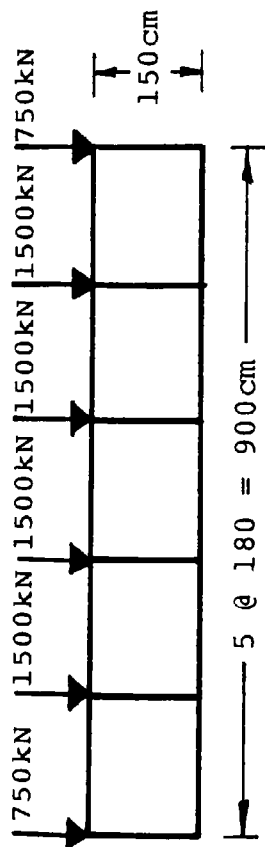


(b) Longitudinal flange stress.

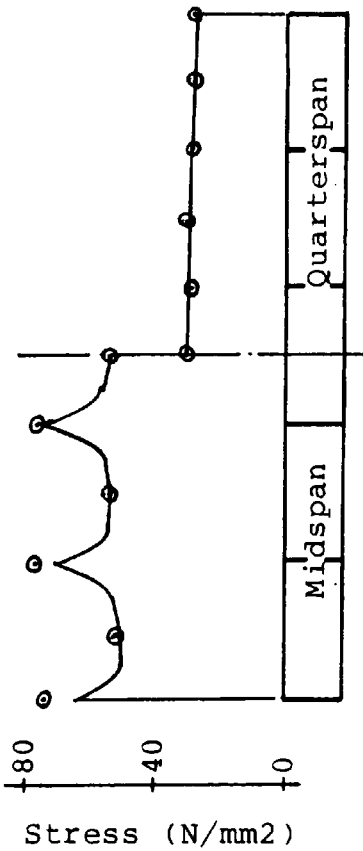


(c) Deflection.

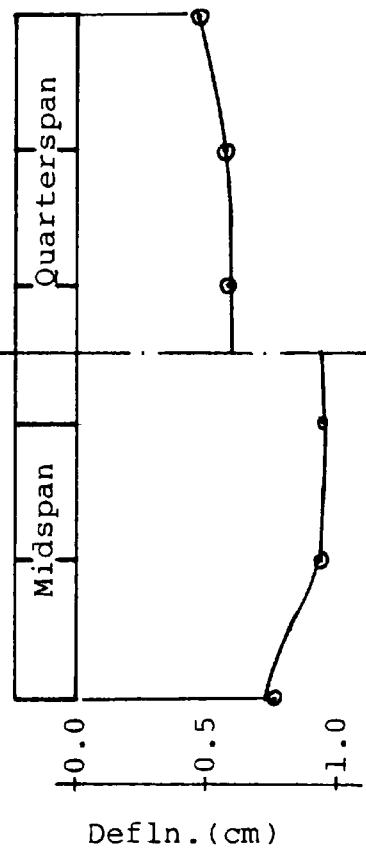
LOAD OVER WEB 1.



(a) Structure and load details.



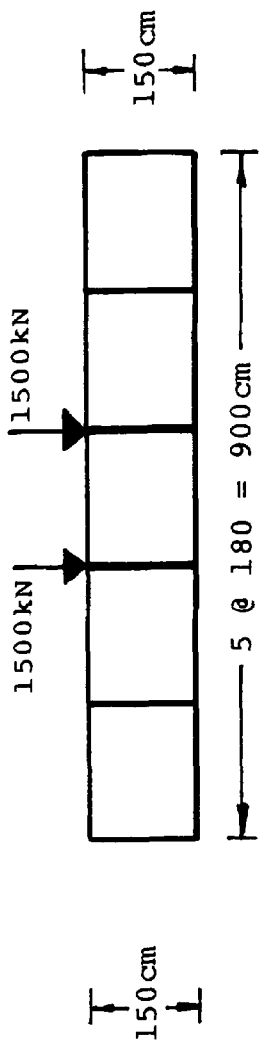
(b) Longitudinal flange stress.



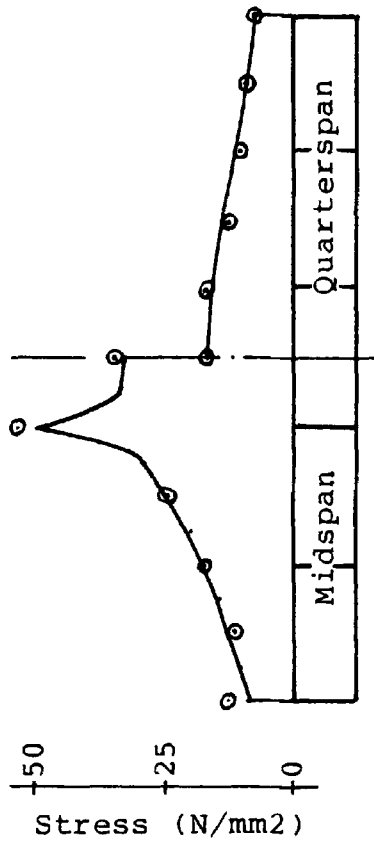
(c) Deflection.

LOAD OVER ALL WEBS.

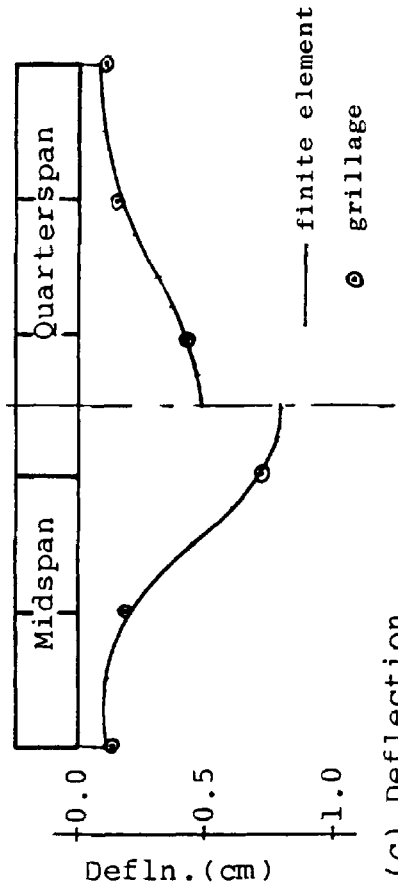
FIGURE 5.11 - FIVE CELL STRUCTURE - MIDSPAN POINT LOADING (a).



(a) Structure and load details.

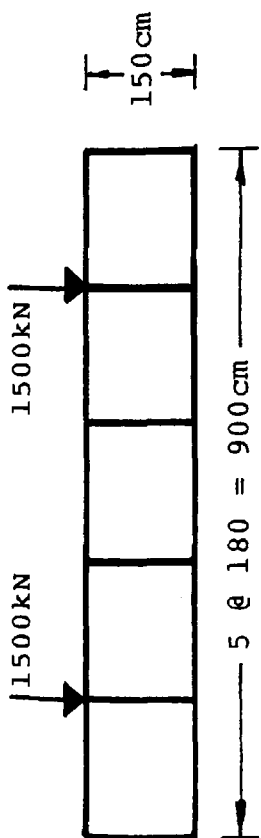


(b) Longitudinal flange stress.

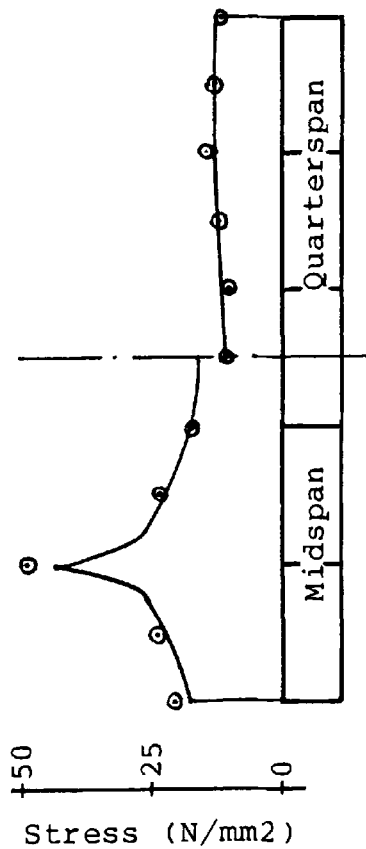


(c) Deflection.

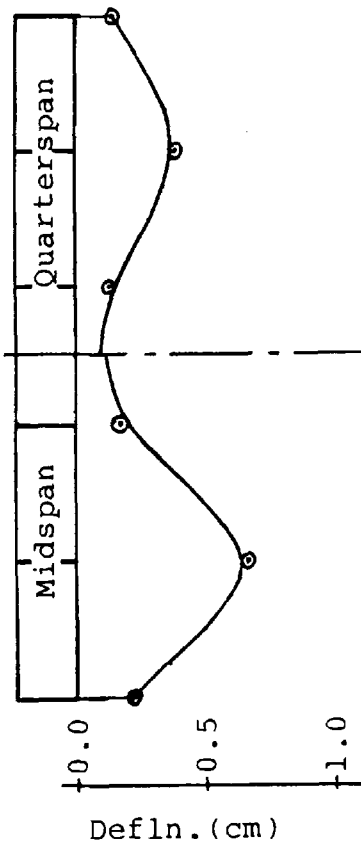
LOAD OVER WEB 3.



(a) Structure and load details.



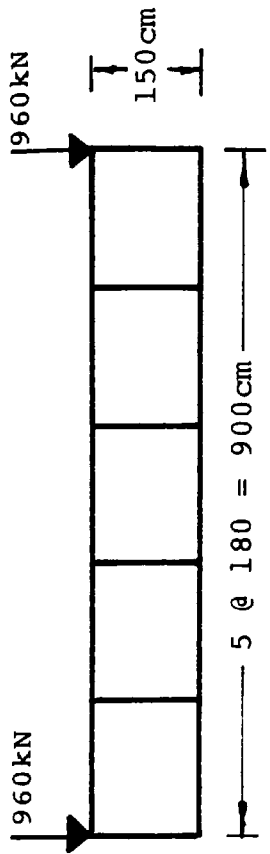
(b) Longitudinal flange stress.



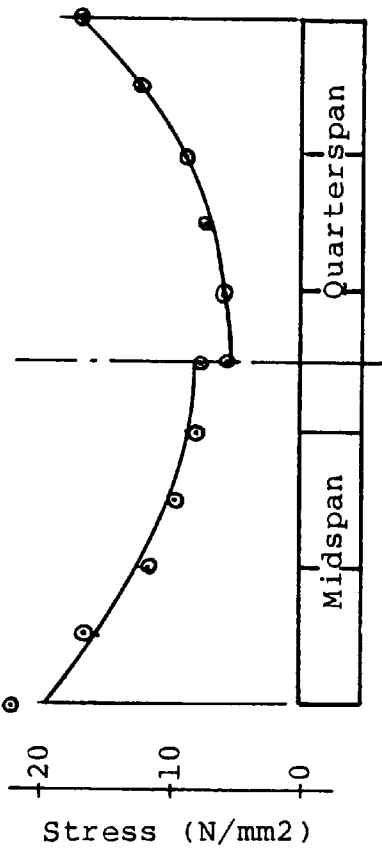
(c) Deflection.

LOAD OVER WEB 2.

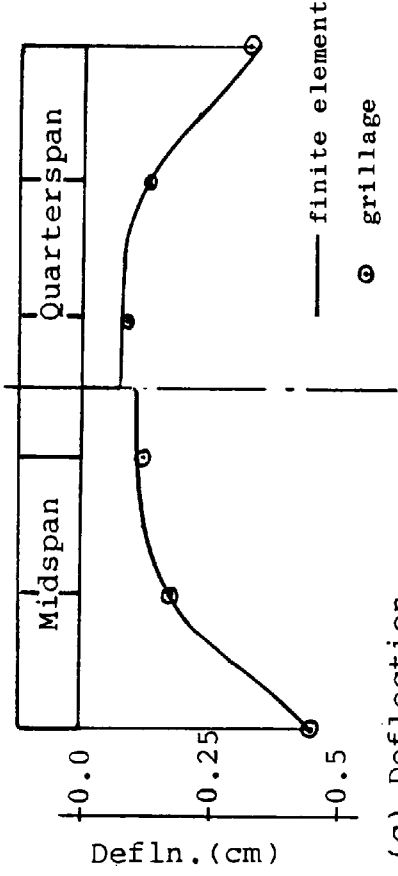
FIGURE 5.12 - FIVE CELL STRUCTURE - MIDSPAN POINT LOADING (b).



(a) Structure and load details.

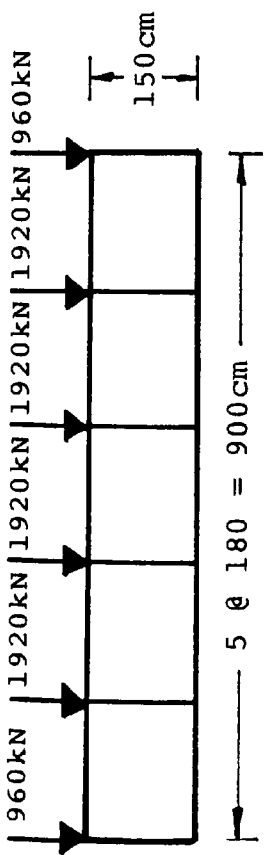


(b) Longitudinal flange stress.

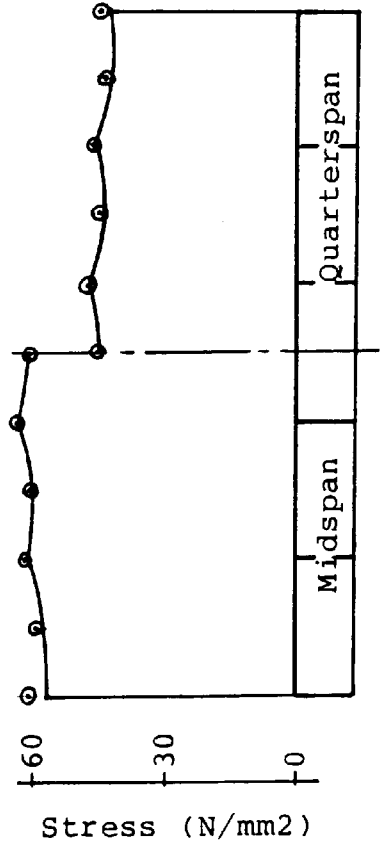


(c) Deflection.

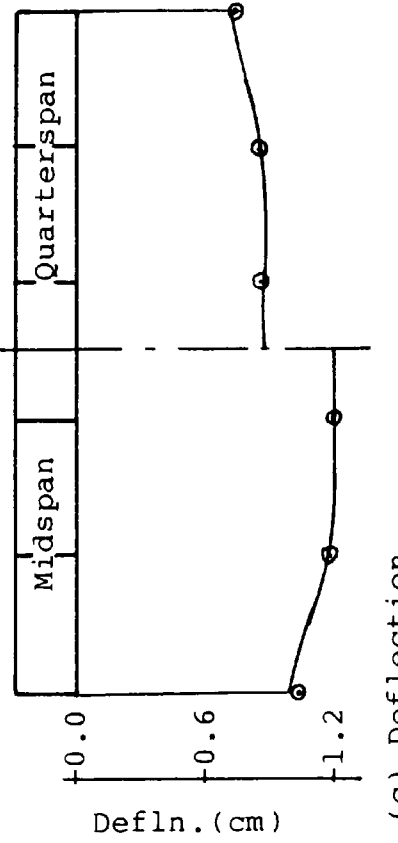
LOAD OVER WEB 1.



(a) Structure and load details.



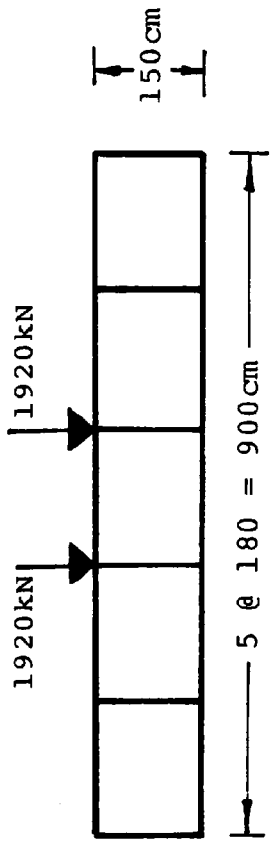
(b) Longitudinal flange stress.



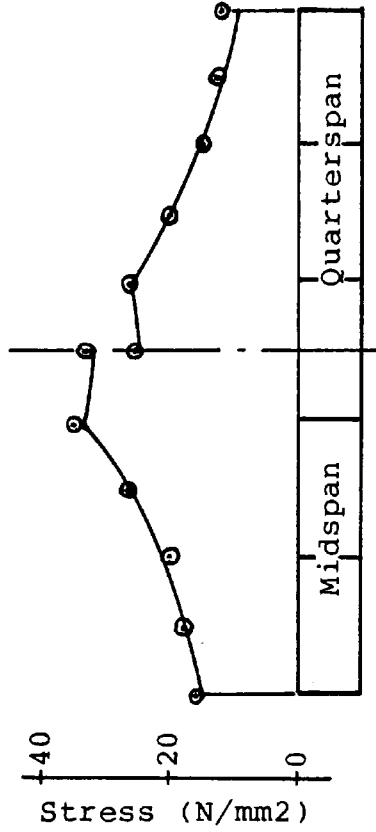
(c) Deflection.

LOAD OVER ALL WEBS.

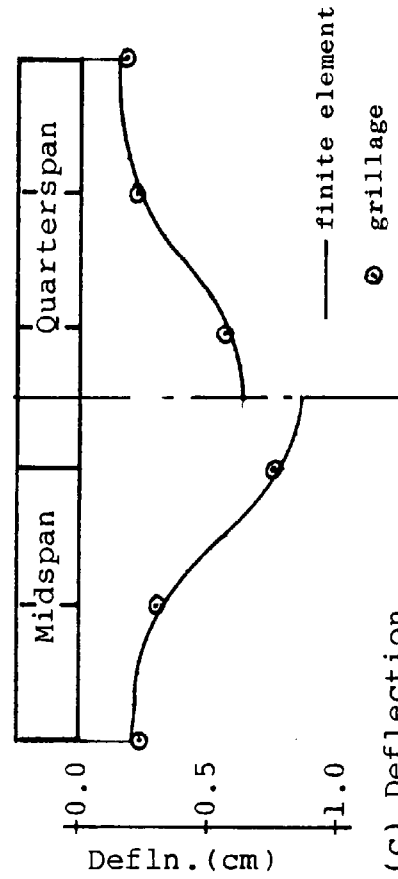
FIGURE 5.13 - FIVE-CELL STRUCTURE - UNIFORM LINE LOAD (a).



(a) Structure and load details.

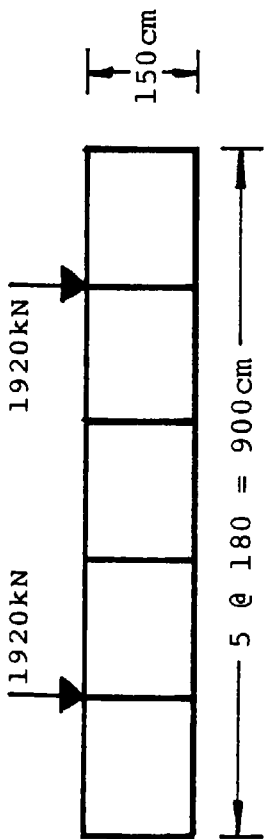


(b) Longitudinal flange stress.

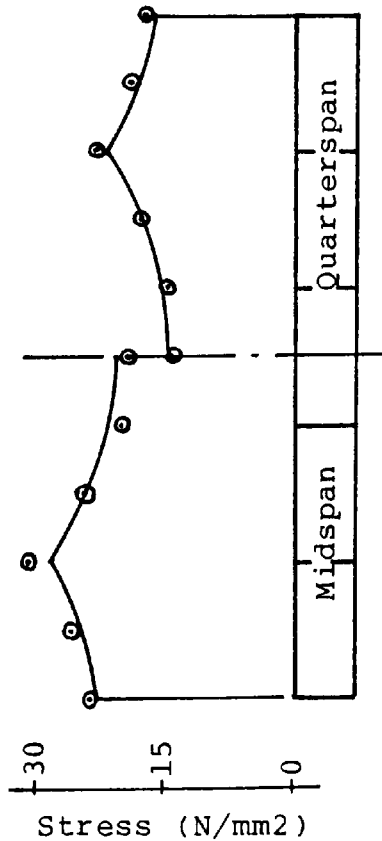


(c) Deflection.

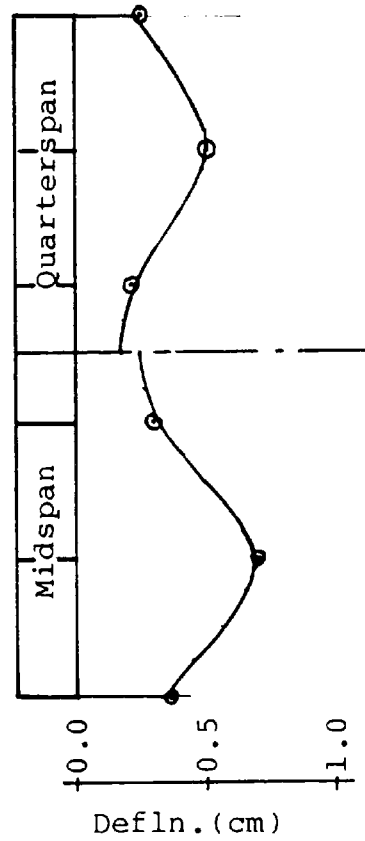
LOAD OVER WEB 3.



(a) Structure and load details.



(b) Longitudinal flange stress.



(c) Deflection.

LOAD OVER WEB 2.

FIGURE 5.14 - FIVE-CELL STRUCTURE - UNIFORM LINE LOAD (b).

CHAPTER SIX

FINITE ELEMENT ANALYSIS OF SKEW SINGLE CELL STRUCTURES

6.1. INTRODUCTION.

It has been shown in the three previous chapters that the grillage method can be used for the analysis of straight, or non-skewed, multi-cell structures. In the grillage idealization of the structure, the effective breadth concept is used in the calculation of the second moment of area of the longitudinal grillage beams. The effective breadth ratios, which are specified in Part 3, BS 5400, were determined from a comprehensive study of the shear lag phenomenon in box girders by MOFFATT and DOWLING (1975). In their study straight, symmetrically loaded box girders were analysed using the finite element method. Under these conditions the predominant structural action was longitudinal bending enabling the shear lag effect to be isolated.

When the structure is supported on skew supports, there is a considerable change in the behaviour of the structure. The development of considerable torsion within the structure results in a substantial change in the longitudinal stress distribution across the flange plates.

In this chapter it is proposed that the effect of skew on the distribution of longitudinal stress across the width of the flange plates be investigated. It will also be necessary to represent the effect of shear lag in such

plates by making use of the existing "effective breadth" concept. This will be achieved by separating the torsional stress and bending stress components in skew flange plates, thus allowing the effective breadth ratio to be determined from Part 3, BS 5400 for any combination of flange breadth, $2b$, span of structure, L and angle of skew, θ .

The effect of intermediate diaphragms on the shear lag effect in skew single cell structures will also be investigated in this chapter. Earlier work by MOFFATT and DOWLING (1972) and ROCKEY, EVANS and NAVARATNE (1976) showed that the shear lag effect in straight box girders remains virtually unaffected by the presence of intermediate diaphragms.

6.2. ASYMMETRICALLY LOADED STRAIGHT SINGLE CELL STRUCTURE.

Symmetrically loaded, skewed single cell structures produce considerable torsional effects which result in an asymmetrical distribution of longitudinal stress across the width of the flange plates. It was considered that an initial study of an asymmetrically loaded straight single cell structure would assist in the understanding of the distribution of longitudinal stress in skewed structures.

Consequently, the structure shown in figure 6.1(a), subjected to a single midspan point load over one web, was analysed using the finite element program, QUEST. The structure details were overall width, $2b = 300\text{cm}$; overall depth, $D = 150\text{cm}$; overall span, $L = 1600\text{cm}$; web,

flange and end diaphragm thickness = 1.2cm. The structure was analysed for four separate loading conditions, namely the asymmetrical condition and the three components of bending, pure torsion and distortion.

Figure 6.1(b) shows the method whereby the asymmetrical loading condition (i) may be represented by the two separate components of loading, one causing longitudinal bending (ii) and the other causing torsion (iii). The torsional loading component can be further sub-divided into a pure torsional component (iv) and a distortional component (v). The results for longitudinal flange stress and flange deflection are presented in Tables 6.1 and 6.2 respectively. The distribution of longitudinal flange stress is shown in figure 6.2 for both the midspan and quarterspan cross-sections.

These results show that although the pure torsional component will normally result in negligible longitudinal stresses and rotation of the cross-section, the distortional component will always tend to cause considerable deformation of the cross-section. This leads to distortional stresses in the transverse direction and warping stresses in the longitudinal direction. The magnitude of these distortional stresses is considerably in excess of the longitudinal stresses developed by the bending action, being 45.06 N/mm² and 24.10 N/mm² respectively at the midspan cross-section.

The results also show that the stress distribution for the asymmetrical loading condition may be

separated into the bending stress component and the torsional stress component. The bending stress component can be determined using simple beam theory with the appropriate allowance being made for the shear lag effect. The distortional component is linear, as shown in figure 6.2(b), although the midspan stress distribution does show a slight deviation near the web positions. This is most probably due to the influence of the concentrated point load at these positions on the finite element analysis.

The effective breadth ratio can be determined from the bending stress distribution (ii) using the equation

$$\psi = \frac{b_e}{b} = \frac{\int_0^b \sigma_x dy}{\sigma_{\max} b} \quad \text{---- 6.1}$$

as presented in figure 3.6. The integration of the flange stress, σ_x , may be accomplished using Simpson's Rule giving

$$\psi_{\frac{1}{2}} = \frac{24.10 + 4*(18.63 + 16.34) + 2*17.15 + 16.10}{12 * 24.10} = 0.741$$

and

$$\psi_{\frac{1}{4}} = \frac{9.50 + 4*(9.51 + 9.53) + 2*9.54 + 9.52}{12 * 9.50} = 1.002$$

The values for effective breadth ratio specified in Part 3, BS 5400 are 0.686 and 1.000 respectively

The effective breadth ratio may also be determined from the asymmetrical loading condition (i)

because the known linear variation in longitudinal stress due to torsion can be eliminated from the overall stress values as follows using the equation

$$= \frac{\int_0^{2b} \sigma_x dy}{\sigma_{av} b} \quad \text{----} \quad 6.2$$

where σ_{av} = average of both extreme flange stress values

Again using Simpson's Rule for the integration, the effective breadth ratios are

$$\psi_{\frac{1}{2}} = \frac{69.20 + 4 * \sigma_2 + 2 * \sigma_3 - 21.00}{24 * \left[\frac{69.20 - 21.00}{2} \right]} = 0.741$$

where $\sigma_2 = 48.45 + 25.79 + 6.89 - 11.20$

and $\sigma_3 = 36.43 + 16.10 - 2.13$

and

$$\psi_{\frac{3}{4}} = \frac{30.70 + 4 * \sigma_4 + 2 * \sigma_5 - 11.69}{24 * \left[\frac{30.70 - 11.69}{2} \right]} = 1.002$$

where $\sigma_4 = 25.21 + 14.78 + 4.28 - 6.19$

and $\sigma_5 = 20.03 + 9.52 - 0.96$

This latter method will form the basis whereby the effective breadth ratios for skewed structures will be determined.

Alternative methods exist for the analysis of asymmetrically loaded straight single-cell structures. The pure torsional effect can be analysed by determining the torsional shear flow in the thin-walled section, as described in chapter four. Various methods exist for the analysis of the distortional effect. WRIGHT et al (1968)

proposed a solution using the beam on elastic foundation analogy. RICHMOND (1966) proposed an approximate method of solution where the actual loading is represented by an equivalent sinusoidal loading arrangement.

6.3. SYMMETRICALLY LOADED SKEW SINGLE CELL STRUCTURE.

6.3.1. INTRODUCTION.

A single cell structure will be analysed using the finite element program, QUEST, for angles of skew ranging from 0 to 45 degrees. The structure considered is shown in figure 6.3(a), the relevant details being

overall width, $2b$	= 300cm
overall depth, D	= 150cm
overall skew span, L	= 1600cm
flange thickness, t_f	= 1.2cm
web thickness, t_w	= 1.2cm
diaphragm thickness, t_d	= 1.2cm
angle of skew, θ (degrees)	= 0, 10, 20, 30, 40 and 45

The full structure has to be modelled in the finite element analysis since the boundary conditions along the line of symmetry at the midspan cross-section are not known. The finite element mesh used in the study is shown in figure 6.3(b). Each flange plate was represented using 160 elements, 8 across the width and 20 along the span. The web plates and end diaphragms were represented using a single element in the depth of the structure. A convergence study was undertaken to confirm the suitability of this representation, details are presented in Appendix C.

Two separate loading conditions were considered

- (i) midspan point loads of 300kN over both webs
- (ii) uniform line loads of 900kN along both webs

6.3.2. LONGITUDINAL FLANGE STRESS.

The distribution of longitudinal stress across the full width of the top flange is shown in figures 6.4 and 6.5, and is presented in Tables 6.3 and 6.4. The values are presented for the midspan and quarterspan cross-section for both loading conditions. At the midspan cross-section the stresses are symmetrical about the centre-line of the flange. The fact that skew symmetry exists results in no torsional action occurring at this cross-section.

At the quarterspan cross-section no symmetry exists and the longitudinal stresses show that torsional action is present when the structure is skewed. This torsional action increases in magnitude with increasing angle of skew. The distribution of stress from torsional action is linear, and when combined with the constant stress distribution due to bending action for the midspan point load condition, produces the linear variation in the overall stress distribution shown in figure 6.4. In the case of the uniform line load the shear lag effect at the quarterspan cross-section results in a non-linear variation of stress due to longitudinal bending action, which when combined with the linear stress distribution from torsional action, produces the non-linear distribution shown in figure 6.5.

The variation of longitudinal stress along the edge of the top flange from point A to point B (see figure 6.3(a)) is shown plotted in figure 6.6 for both loading cases. In the midspan point loading case the maximum edge flange stress occurs under the point load at the midspan cross-section for all angles of skew. The intensity of this stress varies from 48.20 N/mm² to 46.13 N/mm² when the angle of skew is increased from 0 to 45 degrees. This small reduction in stress (about 4%) was attributed to the behaviour of the structure under this form of loading, which tends to span over the constant skew span distance of 16 metres.

In the uniform line load case the position of maximum longitudinal stress moved from midspan towards the acute corner support when the angle of skew was increased. This fact is reflected in the 45 degree skew structure where the quarterspan stress intensity of 48.61 N/mm² was marginally higher than the midspan stress intensity of 48.00 N/mm². In this case the structure tends to span in the direction normal to the support in the acute corner, thus reducing the maximum stress intensity.

In both loading cases hogging moments are developed in the obtuse corners of the structure resulting in the development of tension stresses in the top flange at these locations. Higher tension stresses at the obtuse corners were observed in the uniform line load case.

The variation of flange edge stress with angle of skew is shown in figure 6.7 for both loading cases. The

difference in the quarterspan cross-section stress values represent the torsional stress developed at this section. This torsional stress increases with increasing angle of skew, and is shown to be greater for the uniform line load case.

6.3.3. VERTICAL DEFLECTION OF FLANGE AND WEB.

The vertical deflection profiles of the top flange are shown in figures 6.8 and 6.9 for the midspan point load and the uniform line load cases respectively. These profiles show that at the midspan cross-section the deflection is symmetrical about the centre-line of the flange confirming that no torsional action occurs at this cross-section. At the quarterspan cross-section the deflection profile indicates torsional behaviour in the skew cases. These profiles confirm that torsional effects are higher for the uniform line load case and increases with increasing angle of skew.

The deflection profile of the web is shown in figure 6.10 for both loading cases for varying angles of skew. These profiles indicate that the maximum web deflection reduces with increasing angle of skew, that is as the square span distance reduces. The position of maximum deflection also moves towards the acute corner as the skew angle increases, this movement being more pronounced in the line load case, which is consistent with the higher torsional stresses developed in this load case.

6.3.4. EFFECTIVE BREADTH RATIO. - FINITE ELEMENT STUDY.

6.3.4.1. MIDSPAN CROSS-SECTION.

At the midspan cross-section the effective breadth ratio for skew structures can be determined using the principle derived for straight structures. In the skew structure the effective and actual flange dimensions, b_e and b , are measured normal to the web. Using the flange stress values presented in Tables 6.3 and 6.4 and equation 6.1, the effective breadth ratios were calculated and are also shown in Tables 6.3 and 6.4.

The variation of effective breadth ratio with angle of skew is shown plotted in figure 6.11 for both the midspan point and uniform line load cases. Both these curves exhibit a non-linear variation where the effective breadth ratio reduces with increasing angle of skew.

6.3.4.2. QUARTERSPAN CROSS-SECTION.

At the quarterspan cross-section, where torsional action occurs, the torsion and bending stress components have to be separated from the actual stress distribution before the effective breadth ratio can be determined. This separation can easily be achieved because of the linear nature of the torsion stress. The following two examples illustrate this process.

(i) Midspan point loading, 30 degree angle of skew.

position across fl.	longitudinal actual stress	flange stress = bending	(N/mm ²) + torsion
1	20.75	15.195	5.555
2	19.14	15.13	4.01
3	17.73	15.10	2.63
4	16.37	15.07	1.30
5	15.06	15.06	0
6	13.77	15.07	-1.30
7	12.47	15.10	-2.63
8	11.12	15.13	-4.01
9	9.64	15.195	-5.555

(ii) Uniform line loading, 45 degree angle of skew.

position across fl.	longitudinal actual stress	flange stress = bending	(N/mm ²) + torsion
1	48.61	34.065	14.545
2	38.11	28.10	10.01
3	31.02	24.515	6.505
4	25.44	22.29	3.15
5	21.46	21.46	0
6	19.14	22.29	-3.15
7	18.01	24.515	-6.505
8	18.09	28.10	-10.01
9	19.52	34.065	-14.545

The stress distributions for both these examples are shown plotted in figure 6.12. The bending stress distribution was calculated by averaging the two stress values at equal distances on either side of the centre-line of the flange. Subtraction of this bending stress component

from the actual stress distribution produces the torsion stress component. In both examples the torsion stress produced, and shown plotted in figure 6.12(iii), exhibited linear characteristics.

The effective breadth ratio at the quarterspan cross-section may be determined from the bending stress component in the normal manner using equation 6.1. It may also be calculated from the actual stress distribution using equation 6.2, the actual values for all angles of skew and both load cases are presented in Tables 6.3 and 6.4.

The variation of effective breadth ratio at the quarterspan cross-section with angle of skew is also shown plotted in figure 6.11 for both load cases. Again both these curves exhibit a non-linear variation where the effective breadth ratio reduces with increasing angle of skew.

6.3.5. EFFECTIVE BREADTH RATIO. - PART 3: BS 5400.

The effective breadth ratios specified in Part 3 of BS 5400 may be used to determine the equivalent flange breadth in straight structures. The effective breadth ratio is calculated for a specific value of b/L where

b = half distance between centres of webs

L = span of beam between centres of supports

When the structure is skewed through an angle, θ , then the half distance between centres of webs measured

across the skew section becomes $b/\cos\theta$, and the square span of the beam between centres of supports becomes $L\cos\theta$. Consequently, in skew structures it may be considered that the ratio of

$$\frac{(b/\cos\theta)}{L \cos\theta} = \frac{b}{L (\cos\theta)^2}$$

should be used for the determination of the effective breadth ratio.

Using this criterion the effective breadth ratios at the midspan and quarterspan cross-sections for both loading cases were calculated for all angles of skew from 0 to 45 degrees. These calculated values closely agreed with the predicted finite element values at the quarterspan cross-section for both loading cases and the midspan cross-section for the uniform line load case.

At the midspan cross-section for the midspan point load case there was less agreement between the BS 5400 predicted values and the finite element values. It was observed in Section 6.3.2. that in the midspan point load case, the edge flange stress showed no significant change with increasing angle of skew. Consequently it was considered that for this particular case the ratio of $b / L(\cos\theta)^{3/2}$ should be used for the determination of the effective breadth ratio.

The variation of effective breadth ratio with angle of skew is shown plotted in figure 6.11 The values are also presented in Table 6.5 and compared with the

values predicted by the finite element study. The two sets of values show close agreement, particularly at the midspan cross-section for both load cases. In the midspan point load case the value determined from BS 5400 tended to be lower than the finite element value, the percentage difference varying from 8% to 5.3% as the skew angle is increased from 0 to 45 degrees. At the quarterspan cross-section the BS 5400 values tended to be higher than the finite element values, the maximum difference being 5.5% when the skew angle was 45 degrees.

It was concluded that the use of the $b / L(\cos\theta)^2$ or the $b / L(\cos\theta)^{3/2}$ ratio and the appropriate Table from BS 5400 predicted the effective breadth ratio for skew flanges to an acceptable degree of accuracy for the particular ratio of span to breadth considered.

6.4. INFLUENCE OF SPAN / BREADTH RATIO.

The previous section was concerned with the analysis of a single cell structure where the ratio of skew span/overall breadth was 16/3 or 5.33. It was concluded that the effective breadth ratio of the skew flange plate was dependent on either the $b/L(\cos\theta)^2$ or $b/L(\cos\theta)^{3/2}$ ratio. In this section the validity of the proposal will be investigated for structures of various skew span/ overall breadth ratios. Further finite element studies were undertaken on skew single cell structures where the span of the structure was varied. The same cross-section detail as that used in the previous section

was used throughout the study. The range of spans considered and the corresponding span/breadth ratios were

<u>span</u>	<u>span/breadth</u>
9.6m	3.2
12.0m	4.0
19.2m	6.4
24.0m	8.0
30.0m	10.0

The structures were analysed for skew angles from 0 to 45 degrees and the two standard loading cases were considered. The results for the effective breadth ratio at the midspan cross-section for the midspan point load case are presented in Table 6.6. These results show that the BS 5400 predicted values based on the $b/L(\cos\theta)^{3/2}$ ratio are consistently higher than the values calculated from the finite element analysis. The variation of effective breadth ratio with angle of skew is shown plotted in figure 6.13 and shows the excellent agreement between the two sets of values.

The results at the midspan cross-section for the uniform line load case are presented in Table 6.7 and are shown plotted in figure 6.14. The two sets of values agree to an accuracy of 99% for all span values and all angles of skew.

The results at the quarterspan cross-section for the midspan point load case are presented in Table 6.8. The accuracy of these results diminishes with reducing skew span and increasing angle of skew. For the 45 degree skew

angle, the percentage difference increases from 4.0% to 16.4% when the skew span is reduced from 16m to 9.6m. The quarterspan cross-section results for the uniform line load case, presented in Table 6.9, follow a similar pattern, the percentage difference being 13.4% for the 9.6m skew span structure.

6.4.1. EFFECT OF END DIAPHRAGM THICKNESS.

The distribution of stress, and hence the effective breadth ratio, is influenced by the proximity of the support to the quarterspan cross-section. This was reflected in the accuracy of the results for effective breadth ratio at the quarterspan cross-section. It was considered that the stress distribution across the breadth of the flange plate was dependent on the rigidity of the end diaphragm within a region governed by Saint Venant's principle. For the flange width of 300cm then the quarterspan distances of 240cm and 300cm for the 9.6m and 12m span structures were considered to lie within this region.

The effect of the end diaphragm thickness on the stress distribution in the flange plates was considered for three conditions of skew span and angle of skew.

6.4.1.1. SKEW SPAN 9.6M. - SKEW ANGLE 0 DEGREES.

The end diaphragm thickness was increased from 1.2 to 7.2cm in increments of 1.2cm, and the results for flange edge stress and effective breadth ratio are presented in

Table 6.10. The variation of flange edge stress and effective breadth ratio at the quarterspan cross-section with end diaphragm thickness is shown plotted in figure 6.15 for both midspan point and uniform line loading.

These results reveal that the end diaphragm thickness has no influence on the flange stress distribution at the midspan cross-section. At the quarterspan cross-section the flange edge stress reduces and the effective breadth ratio increases with increasing end diaphragm thickness. This occurs because the in-plane shear stiffness of the flange plates is dependent on the lateral stiffness of the end diaphragm. Convergence of both flange stress and effective breadth ratio was observed for both loading cases.

6.4.1.2. SKEW SPAN 9.6M. - SKEW ANGLE 40 DEGREES.

The end diaphragm thickness was increased from 0.6cm to 7.2cm, and the results for flange edge stress and effective breadth ratio are presented in Table 6.10 and figure 6.16.

At the midspan cross-section both the flange edge stress and effective breadth ratio show minor variations with increasing end diaphragm thickness. The results show that a variation of 1% to 4% occurs when the diaphragm thickness is increased from 2.4cm to 7.2cm.

At the quarterspan cross-section the flange edge stress reduces and the effective breadth ratio increases

with increasing end diaphragm thickness in a similar manner to the 0 degree skew condition. Again, convergence of both flange stress and effective breadth ratio was observed for both loading cases.

6.4.1.3. SKEW SPAN 24M. - SKEW ANGLE 40 DEGREES.

In this study the end diaphragm thickness was increased from 1.2cm to 8.4cm in increments of 2.4cm, and only uniform line loading was considered. The following values of flange edge stress and effective breadth ratio were observed.

diaphragm thickness	flange edge stress (N/mm ²)			eff. breadth ratio	
	1/2sp	1/4sp(A)	1/4sp(O)	1/2span	1/4span
1.2cm	45.87	38.24	24.25	0.937	0.909
3.6cm	45.24	37.47	23.66	0.936	0.909
6.0cm	45.03	37.09	23.55	0.936	0.909
8.4cm	44.89	36.69	23.63	0.937	0.911

These results reveal no significant change in flange edge stress or effective breadth ratio at either the midspan or quarterspan cross-section. In this case the quarterspan section is 6 metres from the support, and hence lies outside the region governed by Saint Venant's principle.

6.4.1.4. SKEW SPAN 9.6M. - END DIAPHRAGM THICKNESS 7.2CM.

The investigation of the effect of end diaphragm thickness on flange edge stress and effective breadth ratio was concluded with a study of the 9.6 metres span

structure, with an end diaphragm thickness of 7.2cm for skew angles of 0, 10, 20, 30, 40 and 45 degrees. The results for effective breadth ratio at the quarterspan cross-section are included in Tables 6.8 and 6.9 for both midspan point and uniform line loading.

These results reveal a significant improvement in accuracy when compared to those for an end diaphragm thickness of 1.2cm. In the 45 degree skew case the percentage difference between the finite element and the BS 5400 values reduced from 16.4% to 2.4% when the end diaphragm thickness was increased from 1.2cm to 7.2cm for the midspan point load case.

In practice, where end diaphragms of suitable rigidity are provided, the effective breadth ratio determined from BS 5400 for skew structures should agree to within an accuracy of at least 90% of the value predicted by the finite element study.

6.5. INFLUENCE OF INTERMEDIATE DIAPHRAGMS.

It was shown in the earlier part of this chapter that skewed single cell box structures develop significant torsional action when subjected to symmetrical vertical loading systems. This results in the development of significant longitudinal normal stresses which are caused by torsional effects accompanied by deformation of the cross-section of the structure. These effects can be reduced by the introduction of intermediate diaphragms.

The influence of intermediate diaphragms at both the midspan and quarterspan cross-sections on the behaviour of a single cell structure will be considered for skew angles up to 40 degrees. The significance of diaphragm thickness will also be considered.

6.5.1. END AND MIDSPAN DIAPHRAGMS.

The structure used in this study was identical to the structure defined in Section 6.3.1 apart from the introduction of an intermediate diaphragm at the midspan cross-section. The diaphragm thickness was 1.2cm and was modelled in the finite element study in exactly the same manner as the end diaphragms. Angles of skew between 0 and 40 degrees in increments of 10 degrees, and the same two loading cases were considered.

The results for longitudinal flange stress and effective breadth ratio are presented in Tables 6.11 and 6.12 for the midspan point and uniform line load cases respectively. Comparison of these results with those for the study where no intermediate diaphragms were present (Tables 6.3 and 6.4) revealed the following.

At the quarterspan cross-section the results for longitudinal flange stress and hence the effective breadth ratio are identical for both studies.

At the midspan cross-section the longitudinal flange stresses show a marginal deviation between both sets of results, the maximum deviation being 6% at the flange /

web intersection. This difference was attributable to the accuracy of the finite element solution at the junction of the flange, web and diaphragm plates. Closer agreement was observed at the mid-flange position and with increasing angle of skew. Since the effective breadth ratio was determined from the longitudinal flange stress distribution they showed similar differences between the two studies.

The agreement between the flange stress distribution at the 15/32 span cross-section for both studies confirms that the difference in flange stress values at the midspan cross-section is due to the accuracy of the finite element program and not the influence of the intermediate diaphragm.

The web deflection values, presented in Table 6.17, for the midspan and quarterspan cross-sections are identical for both studies for all angles of skew in both loading cases.

For the two conditions of symmetrical loading considered, a line of skew symmetry occurs at the midspan cross-section resulting in no deformation of the cross-section occurring at this position. Hence, the introduction of a diaphragm at this location does not affect the behaviour of the structure.

In straight structures it is assumed that diaphragms are rigid in their own plane and absolutely flexible in a direction perpendicular to that plane. This results in no significant change in the longitudinal flange

stress distribution in straight boxes where intermediate diaphragms are present. The limited results presented here for skewed structures suggests that the diaphragms may also be assumed absolutely flexible in a direction parallel to the webs, at least for skew angles up to 40 degrees.

6.5.2. END, MIDSPAN AND QUARTERSPAN DIAPHRAGMS.

In this study two additional diaphragms, of 1.2cm thickness, were located at the quarterspan cross-sections of the structure considered in Section 6.5.1. The same two loading conditions and angles of skew up to 40 degrees were considered.

6.5.2.1. VERTICAL DEFLECTION OF FLANGE AND WEB.

The web deflection values presented in Table 6.17 show the influence of the intermediate diaphragms at the quarterspan cross-section on the deflected shape of the structure.

The midspan deflection is unchanged in the straight structure but as the angle of skew increases the deflection reduces, this reduction being 9.2% and 10.3% for the midspan point and uniform line load cases respectively at a skew angle of 40 degrees.

The vertical deflection profiles of the top flange at the quarterspan cross-section are shown plotted in figures 6.17 and 6.18. These profiles indicate the linear nature of the deflected shape of the cross-section

confirming that diaphragms of this thickness have sufficient rigidity to prevent deformation of the cross-section. These profiles also show that the deflection is a maximum at the obtuse corner edge, whereas in the structure with no intermediate diaphragms the maximum deflection occurred at the opposite acute corner edge (figures 6.8 and 6.9).

The web deflection profile from support to support is shown plotted in figure 6.19 for both loading cases. The position of maximum deflection remains close to midspan in the midspan point load case as the angle of skew is increased. In the uniform line load case the position of maximum deflection moves towards the obtuse corner support as the angle of skew is increased. In both cases the maximum deflection reduces with increasing angle of skew.

These results show that there is a significant change in the behaviour of a skewed structure when intermediate diaphragms are introduced to prevent cross-sectional deformation taking place, the most significant change being the reduction in maximum deflection.

6.5.2.2. LONGITUDINAL FLANGE STRESS.

The longitudinal flange stress values are presented in Tables 6.13 and 6.14 for the midspan point and uniform line load cases respectively. These results reveal a significant change from the two previous sets of results. This change is attributable to the removal of the

distortional effects at the quarterspan cross-section.

Consideration of the distribution of stress at the quarterspan cross-section and comparison with the results for the structure with no intermediate diaphragms (Tables 6.3 and 6.4) reveals the following.

In the straight structure there is a marginal change in the stress values, this being attributable to variations in the accuracy of the finite element program at diaphragm locations. The maximum deviation of 3% occurs at the web/flange/diaphragm intersection, with negligible differences occurring at the mid-flange position. This variation in the intensities of stress results in a change in the effective breadth ratio from 1.002 to 0.980 and 0.931 to 0.912 for the midspan point and uniform line load cases respectively.

In the skew cases the mid-flange stress intensity is consistent for both studies. The edge stress intensity was a maximum at the acute corner edge in the earlier study, whilst in this study the maximum occurs at the obtuse corner edge. This change is attributable to the diaphragm preventing distortion of the cross-section and hence the development of the longitudinal stresses associated with this action.

Considering the 40 degree skew, midspan point loading case the longitudinal flange stress can be separated as follows.

(i) No intermediate diaphragms.

position across fl.	longitudinal actual stress	flange stress = bending	(N/mm ²) + torsion
1	20.51	12.62	7.89
2	18.00	12.36	5.64
3	15.97	12.215	3.755
4	14.03	12.165	1.865
5	12.14	12.14	0
6	10.30	12.165	-1.865
7	8.46	12.215	-3.755
8	6.72	12.36	-5.64
9	4.73	12.62	-7.89

(ii) Quarterspan and midspan diaphragms.

position across fl.	longitudinal actual stress	flange stress = bending	(N/mm ²) + torsion
1	6.95	12.88	-5.93
2	8.94	12.495	-3.555
3	10.12	12.295	-2.175
4	11.14	12.165	-1.025
5	12.11	12.11	0
6	13.19	12.165	1.025
7	14.47	12.295	2.175
8	16.05	12.495	3.555
9	18.31	12.88	5.93

These stress components are shown plotted in figure 6.20. The bending stress components are in very close agreement giving effective breadth ratios of 0.971 and 0.959. The torsional stress components both exhibit linear characteristics. In the first case the torsion

component is made up of a pure torsion and distortional component, whilst in the second case predominantly pure torsion is present. The difference in the two torsional components gives the distortional stress which is eliminated by the introduction of the quarterspan diaphragms.

Consideration of the effective breadth ratios at the quarterspan cross-section for both load cases and all angles of skew indicate close agreement between the two structures, with and without diaphragms at the quarterspan cross-section. The difference, a maximum of 2%, can be attributed to the accuracy of the stress intensity at the web / flange / diaphragm intersection from the finite element solution.

It can be concluded that the introduction of diaphragms at the quarterspan cross-section has no effect on the effective breadth ratio at the quarterspan cross-section, which show close correlation with the BS 5400 predicted values as indicated in figure 6.21.

The influence of quarterspan diaphragms on the longitudinal flange stress distribution at the midspan cross-section will be considered with reference to the results from the studies with midspan diaphragms and midspan and quarterspan diaphragms (Tables 6.11, 6.12, 6.13 and 6.14).

For the straight structure the longitudinal stress distribution across the flange was unchanged for

both loading cases. The effective breadth ratios were also unchanged, being 0.704 (or 0.705) and 0.888 for the midspan point and uniform line load cases respectively.

There was no significant change in the flange stress at the mid-flange position for all angles of skew. However, the flange edge stress value was reduced by the introduction of the quarterspan diaphragms. This reduction in edge flange stress was greater for increasing angles of skew. The reduction in edge flange stress results in an increase in the effective breadth ratio at this cross-section. The variation in effective breadth ratio with angle of skew is shown plotted in figure 6.21.

The effective breadth ratio for the midspan point load case remained virtually constant at 0.7 for all angles of skew up to 40 degrees. In the uniform line load case the effective breadth ratio increased with increasing angle of skew, this tendency being the reverse of that experienced in all previous investigations.

Similar calculations at the 3/8-span cross-section showed that the effective breadth ratio remained virtually unchanged for all angles of skew in both load cases.

The variation of longitudinal flange edge stress along the top flange from support to support is shown plotted in figure 6.22 for both load cases and angles of skew of 0, 20 and 40 degrees. These profiles show the considerable local effect of the diaphragms at the

quarterspan cross-section on the longitudinal flange edge stress.

6.5.3. END AND QUARTERSPAN DIAPHRAGMS.

In this study the redundant midspan diaphragm was removed leaving end and quarterspan diaphragms only. Midspan point and uniform line load cases with angles of skew of 0, 20 and 40 degrees were considered. The exclusion of the midspan diaphragm permits a further consideration of the longitudinal flange edge stress distribution at the midspan cross-section. The stresses and effective breadth ratios are presented in Tables 6.15 and 6.16.

The quarterspan values are virtually unchanged from those for the structure with midspan and quarterspan diaphragms for all three angles of skew. This was expected because of the redundant nature of the midspan diaphragm for the two symmetrical load cases considered.

At the midspan cross-section the effective breadth ratios showed closer agreement to the BS 5400 predicted values than the ratios calculated for the structure with midspan and quarterspan diaphragms. The variation in effective breadth ratio with angle of skew is shown plotted in figure 6.21. In the midspan point load case the ratio tends to reduce with increasing angle of skew, whilst in the uniform line load case the ratio tends to increase with increasing angle of skew. In the 40 degree skew case the difference between the calculated and BS 5400 predicted values were 13.5% and 15.7% for the midspan point

and uniform line load cases respectively.

These, and earlier, observations question the validity of the proposed method for the determination of the effective breadth ratio from the Tables in Part 3 of BS 5400. It is considered that further investigation on the effect of intermediate diaphragms on the effective breadth ratio in skewed structures are necessary before conclusive design rules can be quantified.

On the basis of the limited investigation carried out it is considered that the rules developed for the determination of effective breadth ratios for single cell skew structures with no intermediate diaphragms, may be used where intermediate diaphragms are present. Use of these rules will tend to underestimate the effective breadth ratio and hence overestimate the longitudinal flange edge stress. Overestimations of the order of 15% should be expected on the basis of this limited investigation.

6.5.4. EFFECT OF QUARTERSPAN DIAPHRAGM THICKNESS.

To conclude this investigation into the influence of intermediate diaphragms on the behaviour of skew single cell structures, the effect of diaphragm thickness was considered. The structure used in this study was identical to the structure defined in Section 6.3.1 apart from the presence of intermediate diaphragms at the quarterspan cross-sections. The intermediate diaphragm thickness was varied from 0.0cm (i.e. no diaphragm present) to 3.6cm.

The two load cases of midspan point and uniform line load , with angles of skew of 0 and 40 degrees were considered.

The longitudinal flange stress, effective breadth ratio and deflection values for the straight structure are presented in Table 6.18. These results confirm that the introduction of intermediate diaphragms has no significant effect on the behaviour of the structure when symmetrically loaded.

The only small variation is in the longitudinal flange edge stress at the quarterspan cross-section which increases with increasing diaphragm thickness. This increase in stress results in a corresponding reduction in the effective breadth ratio at this cross-section. The midspan longitudinal flange stresses and the web deflections at both cross-sections were unchanged.

The longitudinal flange stress, effective breadth ratio and web deflection values for the 40 degree skew structure are presented in Table 6.19 and figures 6.23 and 6.24.

The longitudinal flange stress at the midspan cross-section was reduced with the introduction of the quarterspan diaphragms. No significant change in the stress value was observed in both load cases when the diaphragm thickness was increased above 1.2cm.

At the quarterspan cross-section the obtuse edge flange stress increased and the acute edge flange stress reduced when the quarterspan diaphragms of increasing

thickness were introduced. The introduction of the diaphragms prevents the deformation of the cross-section resulting in a reduction in the distortional stress component at this cross-section. In the midspan point load case the longitudinal flange edge stress showed no significant change for diaphragm thicknesses in excess of 1.2cm. Previous studies have shown that the presence of the diaphragm at the cross-section will cause some variation in the stress intensity predicted by the finite element program.

The uniform line load case followed a similar pattern to the midspan point load case, but there is no apparent diaphragm thickness at which the longitudinal flange edge stress attains a consistent value.

The longitudinal flange stress value at the mid-flange position of both the midspan and quarterspan cross-sections remained unchanged for all values of diaphragm thickness in both load cases.

The effective breadth ratio at the midspan cross-section increases with increasing diaphragm thickness in both load cases. The effective breadth ratio remained virtually unchanged for diaphragm thicknesses in excess of 1.2cm. At the quarterspan cross-section the effective breadth ratio showed no significant change when the diaphragm was introduced and its thickness increased.

The web deflection values at both cross-sections in both load cases remained virtually unchanged for diaphragm

thicknesses in excess of 1.2cm. The web deflection at midspan and the quarterspan acute corner edge reduced, and at the quarterspan obtuse corner edge increased when the diaphragm thickness was increased.

6.6. CONCLUSIONS.

1. The study on an asymmetrically loaded straight structure showed how the longitudinal bending stress component could be isolated from the overall longitudinal stress distribution by the removal of the linear longitudinal torsion stress component. The effective breadth ratio can be determined from the asymmetrical longitudinal stress distribution using equation 6.2, and it was shown to be unchanged from the value determined from a symmetrical loading condition which develops longitudinal bending action only.
2. The study on symmetrically loaded skewed structures showed that equation 6.2 could also be used to determine the effective breadth ratio for flanges of skewed structures. It was shown that the effective breadth ratio is dependent on the angle of skew, the ratio reducing for increasing angle of skew.
3. To extend the use of the effective breadth ratios specified in Part 3 of BS 5400 to the analysis of skewed structures, it is proposed that the angle of skew, θ , be incorporated in the b/L ratio as follows.

The effective breadth ratio at the midspan cross-section for the midspan point load condition should be determined from Table 13 using the

$$\frac{b}{L (\cos\theta)^{3/2}} \quad \text{ratio}$$

The effective breadth ratio at the midspan cross-section for the uniform line load condition and at the quarterspan cross-section for both load conditions should be determined from Table 4 or 13 using the

$$\frac{b}{L (\cos\theta)^2} \quad \text{ratio}$$

Use of these ratios provides effective breadth ratios for skewed structures to a comparable accuracy to those for straight structures using the standard b/L ratio.

4. The use of intermediate diaphragms in skewed structures reduces the deformation of the cross-section, resulting in a reduction in the maximum web deflection and flange stress values. The limited investigation on the effects of intermediate diaphragms on the values of effective breadth ratio for skewed structures does not produce any conclusive results. However, in the absence of the necessary further work, it is proposed that the rules specified in 3 above be used. The grillage method will overestimate the flange stress, with possible discrepancies of the order of 20 to 30% at skew angles of 40 degrees. This occurs because the effective

breadth ratio in the flange of a single-cell structure containing intermediate diaphragms was shown to be greater than that for a structure with no intermediate diaphragms.

5. The limited work on intermediate diaphragms suggests that the diaphragm will have sufficient rigidity to prevent distortion of the cross-section in skewed structures when plates of similar thickness to the web and flange plates are used. The presence of a diaphragm at the midspan cross-section did not alter the distribution of longitudinal flange stress at this cross-section. Hence, it can also be considered that the diaphragms are absolutely flexible in a direction parallel to the web for skew angles up to 40 degrees.

Sect -ion	Posit -ion	Longitudinal flange stress (N/mm ²)				
		Load Case				
		(ii)	(iv)	(v)	(ii,iv,v)	(i)
M I D S P A N	1	24.10	0.04	45.06	69.20	69.20
	2	18.63	0.02	29.80	48.45	48.45
	3	17.15	0.02	19.26	36.43	36.43
	4	16.34	0.01	9.44	25.79	25.79
	5	16.10	0.00	0.00	16.10	16.10
	6	16.34	-0.01	-9.44	6.89	6.89
	7	17.15	-0.02	-19.26	-2.13	-2.13
	8	18.63	-0.02	-29.80	-11.19	-11.20
	9	24.10	-0.04	-45.06	-21.00	-21.00
Q U A R T E R S P A N	1	9.50	0.03	21.17	30.70	30.70
	2	9.51	0.01	15.69	25.21	25.21
	3	9.54	0.02	10.47	20.03	20.03
	4	9.53	0.01	5.24	14.78	14.78
	5	9.52	0.00	0.00	9.52	9.52
	6	9.53	-0.01	-5.24	4.28	4.28
	7	9.54	-0.02	-10.47	-0.95	-0.96
	8	9.51	-0.01	-15.69	-6.19	-6.19
	9	9.50	-0.03	-21.17	-11.70	-11.69

-ve sign indicates tension in top flange

Table 6.1. - Longitudinal flange stress (N/mm²).
Bending, torsional and distortional
components of asymmetrical loading.
Straight single cell structure.

Sect -ion	Posit -ion	Flange deflection (cm)				
		Load Case				
		(ii)	(iv)	(v)	(ii,iv,v)	(i)
M I D S P A N	1	0.316	0.023	0.594	0.933	0.933
	2	0.313	0.014	0.576	0.903	0.903
	3	0.311	0.008	0.445	0.764	0.765
	4	0.310	0.004	0.241	0.555	0.555
	5	0.310	0.000	0.000	0.310	0.310
	6	0.310	-0.004	-0.241	0.065	0.065
	7	0.311	-0.008	-0.445	-0.142	-0.142
	8	0.313	-0.014	-0.576	-0.277	-0.277
	9	0.316	-0.023	-0.594	-0.301	-0.301
Q U A R T E R S P A N	1	0.208	0.013	0.403	0.624	0.624
	2	0.208	0.008	0.391	0.607	0.607
	3	0.207	0.005	0.303	0.515	0.515
	4	0.207	0.002	0.164	0.373	0.373
	5	0.206	0.000	0.000	0.206	0.206
	6	0.207	-0.002	-0.164	0.041	0.040
	7	0.207	-0.005	-0.303	-0.101	-0.101
	8	0.208	-0.008	-0.391	-0.191	-0.192
	9	0.208	-0.013	-0.403	-0.208	-0.208

-ve sign indicates upwards deflection of flange

Table 6.2. - Vertical deflection of flange (cm).
Bending, torsional and distortional
components of asymmetrical loading.
Straight single cell structure.

Sect-ion	Posit-ion	Angle of skew (degrees)					
		0	10	20	30	40	45
M I D S P A N	1	48.20	48.04	47.61	47.01	46.38	46.13
	2	37.26	36.91	35.87	34.22	32.04	30.79
	3	34.31	33.85	32.49	30.22	27.03	25.08
	4	32.68	32.19	30.71	28.21	24.58	22.27
	5	32.20	31.70	30.17	27.58	23.82	21.43
	ψ	0.741	0.735	0.716	0.682	0.630	0.596
15 -- 32 S P A N	1	40.78	41.12	41.08	40.76	40.46	
	3	33.72	33.63	32.63	30.77	28.13	
	5	31.94	31.42	29.86	27.25	23.52	
	7	33.72	32.90	31.19	28.60	25.14	
	9	40.78	40.07	39.12	38.16	37.45	
	ψ	0.849	0.842	0.821	0.783	0.722	
Q U A R T E R S P A N	1	19.00	20.27	20.78	20.75	20.51	20.38
	2	19.02	19.83	19.83	19.14	18.00	17.29
	3	19.07	19.43	18.95	17.73	15.97	14.94
	4	19.05	19.00	18.08	16.37	14.03	12.68
	5	19.05	18.59	17.24	15.06	12.14	10.44
	6	19.05	18.20	16.42	13.77	10.30	8.28
	7	19.07	17.80	15.59	12.47	8.46	6.18
	8	19.02	17.32	14.68	11.12	6.72	4.33
	9	19.00	16.85	13.72	9.64	4.73	2.23
ψ	1.002	1.002	1.000	0.994	0.973	0.944	

Table 6.3. - Longitudinal flange stress (N/mm²).
 Skew single cell structure.
 Midspan point load.
 End diaphragms only.

Sect-ion	Posit-ion	Angle of skew (degrees)					
		0	10	20	30	40	45
M I D S P A N	1	59.36	58.63	56.53	53.35	49.66	48.00
	2	57.37	56.53	54.08	50.20	45.21	42.49
	3	56.12	55.21	52.52	48.18	42.35	38.95
	4	55.36	54.42	51.59	46.98	40.66	36.90
	5	55.11	54.15	51.28	46.58	40.13	36.26
	ψ	0.951	0.948	0.937	0.914	0.869	0.833
15 -- 32 S P A N	1	59.03	58.64	56.91	54.17	51.13	
	3	55.77	55.04	52.54	48.42	42.88	
	5	54.77	53.82	50.96	46.28	39.83	
	7	55.77	54.70	51.85	47.33	41.30	
	9	59.03	57.97	55.51	51.95	47.83	
	ψ	0.951	0.947	0.936	0.913	0.867	
Q U A R T E R S P A N	1	44.77	46.64	47.42	47.62	48.08	48.61
	2	42.62	43.70	43.30	41.72	39.43	38.11
	3	41.36	41.66	40.27	37.40	33.38	31.02
	4	40.46	40.10	37.90	34.02	28.64	25.44
	5	40.15	39.19	36.33	31.66	25.28	21.46
	6	40.46	38.93	35.51	30.26	23.26	19.14
	7	41.36	39.26	35.32	29.62	22.23	18.01
	8	42.62	39.92	35.55	29.59	22.18	18.09
	9	44.77	41.51	36.74	30.60	23.33	19.52
	ψ	0.931	0.925	0.908	0.871	0.802	0.749

Table 6.4. - Longitudinal flange stress (N/mm²).
Skew single cell structure.
Uniform line load.
End diaphragms only.

Load Case	Sect-ion		Angle of skew (degrees)						
			0	10	20	30	40	45	
M I D S P A N	1 / 2	F.E.	0.741	0.735	0.716	0.682	0.630	0.596	
		BS5400	0.686	0.681	0.665	0.641	0.598	0.566	
		%	+8.0	+8.0	+7.7	+6.5	+5.0	+5.3	
	P O I N T	1 / 4	F.E.	1.002	1.002	1.000	0.994	0.973	0.944
			BS5400	1.000	1.000	0.999	0.995	0.988	0.982
			%	+0.2	+0.2	+0.1	-0.1	-1.5	-4.0
U N I F O R M	1 / 2	F.E.	0.951	0.948	0.937	0.914	0.869	0.833	
		BS5400	0.954	0.952	0.941	0.915	0.866	0.828	
		%	-0.3	-0.4	-0.4	-0.1	+0.3	+0.6	
	L I N E	1 / 4	F.E.	0.931	0.925	0.908	0.871	0.802	0.749
			BS5400	0.936	0.933	0.920	0.890	0.834	0.790
			%	-0.5	-0.9	-1.3	-2.2	-4.0	-5.5

Table 6.5. - Effective breadth ratios.
Skew single cell structure - span 16 metres.
Midspan point and uniform line loading.

Skew span		Angle of skew (degrees)					
		0	10	20	30	40	45
9.6	F.E.	0.609	0.603	0.583	0.546	0.488	0.450
	BS5400	0.569	0.562	0.541	0.501	0.454	0.421
	%	+7.1	+7.3	+7.7	+9.0	+7.6	+6.9
12	F.E.	0.671	0.664	0.644	0.608	0.552	0.515
	BS5400	0.625	0.620	0.603	0.571	0.514	0.479
	%	+7.4	+7.1	+6.8	+6.5	+7.3	+7.6
16	F.E.	0.741	0.735	0.716	0.682	0.630	0.596
	BS5400	0.686	0.681	0.665	0.641	0.598	0.566
	%	+7.4	+8.0	+7.7	+6.5	+5.0	+5.3
19.2	F.E.	0.781	0.775	0.757	0.725	0.677	0.645
	BS5400	0.727	0.722	0.707	0.678	0.640	0.613
	%	+7.4	+7.3	+7.1	+6.9	+5.7	+5.1
24	F.E.	0.824	0.819	0.804	0.775	0.732	0.702
	BS5400	0.768	0.764	0.752	0.728	0.688	0.661
	%	+7.4	+7.2	+7.0	+6.4	+6.4	+6.2
30	F.E.	0.861	0.857	0.844	0.818	0.779	0.754
	BS5400	0.800	0.797	0.787	0.769	0.736	0.711
	%	+7.6	+7.5	+7.2	+6.4	+5.8	+6.0

Table 6.6. - Effective breadth ratios.
Midspan cross-section - midspan point loading
Skew single cell structure.

Skew span		Angle of skew (degrees)					
		0	10	20	30	40	45
9.6	F.E.	0.873	0.865	0.840	0.790	0.702	0.637
	BS5400	0.871	0.858	0.842	0.798	0.711	0.640
	%	+0.2	+0.8	-0.3	-0.9	-1.2	-0.5
12	F.E.	0.916	0.911	0.893	0.857	0.789	0.737
	BS5400	0.915	0.909	0.891	0.857	0.790	0.735
	%	+0.1	+0.2	+0.2	0.0	-0.1	+0.3
16	F.E.	0.951	0.948	0.937	0.914	0.869	0.833
	BS5400	0.954	0.952	0.941	0.915	0.866	0.828
	%	-0.3	-0.4	-0.4	-0.1	+0.3	+0.6
19.2	F.E.	0.966	0.964	0.955	0.938	0.905	0.878
	BS5400	0.963	0.962	0.957	0.944	0.904	0.871
	%	+0.3	+0.2	-0.2	-0.6	+0.1	+0.7
24	F.E.	0.978	0.976	0.972	0.960	0.938	0.919
	BS5400	0.973	0.971	0.968	0.960	0.941	0.915
	%	+0.5	+0.5	+0.4	0.0	-0.3	+0.4
30	F.E.	0.986	0.985	0.981	0.974	0.959	0.947
	BS5400	0.980	0.979	0.976	0.970	0.959	0.950
	%	+0.6	+0.6	+0.5	+0.4	0.0	-0.3

Table 6.7. - Effective breadth ratios.
Midspan cross-section - uniform line loading
Skew single cell structure.

Skew span		Angle of skew (degrees)					
		0	10	20	30	40	45
9.6 td=1.2	F.E.	0.939	0.931	0.906	0.850	0.737	0.651
	BS5400	0.989	0.987	0.985	0.965	0.861	0.779
	⊗	-5.1	-5.7	-8.0	-11.9	-14.4	-16.4
9.6 td=7.2	F.E.	0.978	0.974	0.966	0.936	0.851	0.760
	BS5400	0.989	0.987	0.985	0.965	0.861	0.779
	⊗	-1.1	-0.9	-1.9	-3.1	-1.2	-2.4
12	F.E.	0.986	0.982	0.970	0.941	0.869	0.799
	BS5400	0.995	0.994	0.992	0.987	0.956	0.890
	⊗	-0.9	-1.2	-2.2	-4.7	-9.1	-10.2
16	F.E.	1.002	1.002	1.000	0.994	0.973	0.944
	BS5400	1.000	1.000	0.999	0.995	0.988	0.982
	⊗	+0.2	+0.2	+0.1	-0.1	-1.5	-4.0
19.2	F.E.	1.002	1.002	1.002	1.002	0.996	0.987
	BS5400	1.000	1.000	1.000	0.999	0.993	0.989
	⊗	+0.2	+0.2	+0.2	+0.3	+0.3	-0.2
24	F.E.	1.001	1.002	1.002	1.003	1.004	1.004
	BS5400	1.000	1.000	1.000	1.000	0.999	0.995
	⊗	+0.1	+0.2	+0.2	+0.3	+0.5	+0.9
30	F.E.	1.000	1.000	1.000	1.000	1.001	1.003
	BS5400	1.000	1.000	1.000	1.000	1.000	1.000
	⊗	0.0	0.0	0.0	0.0	+0.1	+0.3

Table 6.8. - Effective breadth ratios.
 Quarterspan cross-section.
 Midspan point loading.
 Skew single cell structure.

Skew span		Angle of skew (degrees)					
		0	10	20	30	40	45
9.6 td=1.2	F.E.	0.779	0.768	0.737	0.671	0.575	0.512
	BS5400	0.840	0.832	0.807	0.763	0.664	0.591
	⊗	-7.3	-7.7	-8.7	-12.1	-13.4	-13.4
9.6 td=7.2	F.E.	0.815	0.805	0.778	0.727	0.629	0.559
	BS5400	0.840	0.832	0.807	0.763	0.664	0.591
	⊗	-3.0	-3.3	-3.6	-4.7	-5.3	-5.4
12	F.E.	0.864	0.856	0.828	0.774	0.683	0.619
	BS5400	0.890	0.884	0.864	0.823	0.749	0.690
	⊗	-2.9	-3.1	-4.1	-6.0	-8.8	-10.3
16	F.E.	0.931	0.925	0.908	0.871	0.802	0.749
	BS5400	0.936	0.933	0.920	0.890	0.834	0.790
	⊗	-0.5	-0.9	-1.3	-2.1	-3.9	-5.2
19.2	F.E.	0.954	0.950	0.938	0.911	0.859	0.817
	BS5400	0.952	0.949	0.942	0.923	0.877	0.840
	⊗	+0.2	+0.1	-0.4	-1.3	-2.1	-2.7
24	F.E.	0.971	0.969	0.962	0.945	0.911	0.880
	BS5400	0.968	0.966	0.959	0.947	0.920	0.890
	⊗	+0.3	+0.3	+0.3	-0.2	-0.9	-1.1
30	F.E.	0.980	0.979	0.974	0.964	0.942	0.924
	BS5400	0.980	0.978	0.973	0.963	0.945	0.930
	⊗	0.0	+0.1	+0.1	+0.1	-0.3	-0.6

Table 6.9. - Effective breadth ratios.
Quarterspan cross-section.
Uniform line loading.
Skew single cell structure.

Load Case	Diaph thick (cm.)	flange edge stress (N/mm ²)		eff. breadth ratio	
		1/2span	1/4span	1/2span	1/4span
P O I N T	1.2	56.14	20.09	0.609	0.939
	2.4	56.14	19.79	0.609	0.955
	3.6	56.15	19.63	0.609	0.965
	4.8	56.15	19.52	0.609	0.971
	6.0	56.15	19.45	0.609	0.975
	7.2	56.16	19.39	0.609	0.978
U N I F O R M	1.2	63.34	51.46	0.873	0.779
	2.4	63.36	50.67	0.873	0.794
	3.6	63.37	50.22	0.872	0.802
	4.8	63.38	49.94	0.872	0.808
	6.0	63.38	49.74	0.872	0.812
	7.2	63.39	49.59	0.872	0.815

(a) 0 degree skew case.

Load Case	Diaph thick (cm.)	flange edge stress (N/mm ²)			eff. breadth ratio	
		1/2	1/4(A)	1/4(O)	1/2	1/4
P O I N T	0.6	59.07	31.89	6.26	0.495	0.709
	1.2	58.18	29.42	5.31	0.488	0.737
	2.4	57.37	26.94	4.45	0.483	0.779
	3.6	56.97	25.65	4.03	0.481	0.805
	4.2	56.84	25.20	3.89	0.480	0.815
	5.4	56.63	24.51	3.70	0.479	0.831
	6.0	56.55	24.23	3.63	0.479	0.838
U N I F O R M	7.2	56.41	23.73	3.53	0.478	0.851
	0.6	63.68	77.50	29.31	0.708	0.562
	1.2	61.85	72.17	27.36	0.702	0.575
	2.4	60.16	66.66	25.53	0.698	0.594
	3.6	59.30	63.76	24.61	0.697	0.607
	4.2	59.00	62.74	24.31	0.696	0.612
	5.4	58.56	61.17	23.89	0.696	0.620
6.0	58.39	60.53	23.74	0.696	0.623	
7.2	58.10	59.41	23.53	0.696	0.629	

1/4(A) - 1/4span acute corner
1/4(O) - 1/4span obtuse corner

(b) 40 degree skew case.

Table 6.10. - Variation of flange edge stress (N/mm²) and effective breadth ratio with end diaphragm thickness.
Span = 9.6 metres.

Sect-ion	Posit-ion	Angle of skew (degrees)				
		0	10	20	30	40
M I D S P A N	1	50.69	50.35	49.27	47.47	45.36
	2	36.90	36.62	35.75	34.22	31.94
	3	34.18	33.80	32.56	30.27	26.84
	4	32.46	32.02	30.64	28.18	24.50
	5	32.04	31.59	30.16	27.58	23.72
	ψ	0.704	0.702	0.694	0.676	0.640
15 -- 32 S P A N	1	40.80	41.05	40.98	40.71	40.62
	3	33.60	33.46	32.49	30.76	28.18
	5	31.84	31.35	29.83	27.24	23.46
	7	33.60	32.85	31.18	28.57	25.00
	9	40.80	40.22	39.33	38.21	37.07
	ψ	0.848	0.842	0.821	0.783	0.722
Q U A R T E R S P A N	1	19.00	20.26	20.77	20.75	20.53
	2	19.02	19.82	19.82	19.14	18.02
	3	19.07	19.43	18.94	17.73	15.99
	4	19.06	19.01	18.07	16.37	14.04
	5	19.06	18.60	17.24	15.06	12.14
	6	19.06	18.21	16.43	13.78	10.31
	7	19.07	17.80	15.59	12.47	8.48
	8	19.02	17.31	14.67	11.12	6.77
	9	19.00	16.84	13.70	9.63	4.81
	ψ	1.002	1.002	1.000	0.994	0.973

Table 6.11. - Longitudinal flange stress (N/mm²).
Skew single cell structure.
Midspan point load.
End and midspan diaphragms.

Sect-ion	Posit-ion	Angle of skew (degrees)				
		0	10	20	30	40
M I D S P A N	1	63.48	62.56	59.75	55.20	49.66
	2	56.79	56.05	53.83	50.17	45.18
	3	55.80	55.02	52.61	48.39	42.34
	4	54.90	54.05	51.44	46.99	40.67
	5	54.71	53.85	51.21	46.65	40.13
	ψ	0.888	0.888	0.889	0.887	0.869
15 -- 32 S P A N	1	59.10	58.53	56.71	53.98	51.12
	3	55.60	54.74	52.23	48.25	42.87
	5	54.59	53.67	50.90	46.30	39.84
	7	55.60	54.69	51.96	47.46	41.30
	9	59.10	58.28	56.01	52.38	47.80
	ψ	0.950	0.946	0.935	0.913	0.867
Q U A R T E R S P A N	1	44.75	46.63	47.40	47.60	48.08
	2	42.61	43.68	43.28	41.70	39.42
	3	41.36	41.66	40.26	37.38	33.38
	4	40.48	40.11	37.90	34.01	28.64
	5	40.18	39.21	36.34	31.66	25.28
	6	40.48	38.95	35.52	30.27	23.27
	7	41.36	39.26	35.32	29.61	22.24
	8	42.61	39.90	35.52	29.55	22.19
	9	44.75	41.47	36.68	30.53	23.34
	ψ	0.931	0.925	0.908	0.871	0.802

Table 6.12. - Longitudinal flange stress (N/mm²).
Skew single cell structure.
Uniform line load.
End and midspan diaphragms.

Sect-ion	Posit-ion	Angle of skew (degrees)				
		0	10	20	30	40
M I D S P A N	1	50.68	50.08	47.86	44.76	39.89
	2	36.90	36.47	35.48	32.70	28.89
	3	34.19	33.74	32.09	29.67	25.70
	4	32.47	32.01	30.62	28.11	24.45
	5	32.05	31.59	30.16	27.66	23.99
	ψ	0.705	0.704	0.708	0.698	0.687
15 -- 32 S P A N	1	40.78	40.25	38.74	36.11	32.27
	3	33.59	33.14	31.69	29.22	25.55
	5	31.86	31.35	29.89	27.34	23.68
	7	33.59	33.02	31.41	28.74	24.95
	9	40.78	40.45	39.24	37.09	33.77
	ψ	0.849	0.846	0.836	0.821	0.797
Q U A R T E R S P A N	1	19.58	17.14	13.97	10.42	6.95
	2	19.24	17.68	15.30	12.28	8.94
	3	19.16	18.05	16.07	13.34	10.12
	4	19.09	18.33	16.68	14.22	11.14
	5	19.07	18.61	17.25	15.05	12.11
	6	19.09	18.94	17.88	15.94	13.19
	7	19.16	19.36	18.64	17.00	14.47
	8	19.24	19.90	19.61	18.33	16.05
	9	19.58	21.10	21.54	20.79	18.81
	ψ	0.980	0.980	0.979	0.975	0.959

Table 6.13. - Longitudinal flange stress (N/mm²).
Skew single cell structure.
Midspan point load.
End, quarterspan and midspan diaphragms.

Sect-ion	Posit-ion	Angle of skew (degrees)				
		0	10	20	30	40
M I D S P A N	1	63.47	62.13	57.98	50.87	40.89
	2	56.78	55.82	52.85	47.76	40.31
	3	55.80	54.92	52.19	47.44	40.52
	4	54.91	54.04	51.36	46.88	40.59
	5	54.72	53.86	51.22	46.78	40.59
	ψ	0.888	0.892	0.906	0.936	0.991
15 -- 32 S P A N	1	59.06	57.25	53.14	46.65	37.73
	3	55.59	54.24	50.95	45.80	38.66
	5	54.62	53.71	50.97	46.45	40.20
	7	55.59	54.95	52.31	47.73	41.25
	9	59.06	58.63	55.87	50.60	42.53
	ψ	0.951	0.952	0.957	0.969	0.999
Q U A R T E R S P A N	1	46.01	42.01	36.85	31.21	26.07
	2	43.11	40.43	36.22	30.80	24.74
	3	41.55	39.52	35.73	30.39	23.89
	4	40.50	39.02	35.67	30.57	23.95
	5	40.16	39.20	36.33	31.62	25.21
	6	40.50	40.09	37.81	33.71	27.88
	7	41.55	41.77	40.18	36.84	31.83
	8	43.11	44.12	43.44	41.06	36.99
	9	46.01	48.49	49.28	48.31	45.62
	ψ	0.912	0.908	0.893	0.861	0.799

Table 6.14. - Longitudinal flange stress (N/mm²).
Skew single cell structure.
Uniform line load.
End, quarterspan and midspan diaphragms.

Sect -ion	Posit -ion	Angle of skew (degrees)				
		0	10	20	30	40
M I D S P A N	1	48.20		46.45		40.46
	2	37.25		35.26		28.95
	3	34.31		32.24		25.76
	4	32.68		30.67		24.42
	5	32.21		30.18		23.98
	ψ	0.741		0.726		0.679
Q U A R T E R S P A N	1	19.59		14.00		6.96
	2	19.25		15.33		8.93
	3	19.16		16.08		10.11
	4	19.08		16.68		11.13
	5	19.06		17.25		12.11
	6	19.08		17.87		13.18
	7	19.16		18.63		14.47
	8	19.25		19.61		16.04
	9	19.59		21.55		18.77
	ψ	0.980		0.978		0.959

Table 6.15. - Longitudinal flange stress (N/mm²).
 Skew single cell structure.
 Midspan point load.
 End and quarterspan diaphragms.

Sect -ion	Posit -ion	Angle of skew (degrees)				
		0	10	20	30	40
M I D S P A N	1	59.35		54.73		40.26
	2	57.36		53.14		40.29
	3	56.12		52.16		40.34
	4	55.37		51.56		40.41
	5	55.12		51.34		40.40
	ψ	0.951		0.958		1.002
Q U A R T E R S P A N	1	46.03		37.04		26.16
	2	43.12		36.38		24.78
	3	41.54		35.84		23.93
	4	40.48		35.74		23.97
	5	40.13		36.37		25.21
	6	40.48		37.83		27.86
	7	41.54		40.22		31.82
	8	43.12		43.49		36.96
	9	46.03		49.36		45.55
	ψ	0.912		0.892		0.799

Table 6.16. - Longitudinal flange stress (N/mm²).
Skew single cell structure.
Uniform line load.
End and quarterspan diaphragms.

load Case	Sect-ion	Diaph posn	Angle of skew (degrees)				
			0	10	20	30	40
M I D S P A N P O I N T	M	E	1.152	1.137	1.094	1.028	0.949
		EM	1.150	1.136	1.093	1.028	0.949
		EMQ	1.149	1.130	1.074	0.983	0.861
	Q(A)	E	0.832	0.833	0.814	0.779	0.735
		EM	0.832	0.832	0.813	0.779	0.735
		EMQ	0.830	0.807	0.757	0.685	0.593
	Q(O)	E	0.832	0.810	0.765	0.702	0.626
		EM	0.832	0.809	0.764	0.701	0.626
		EMQ	0.830	0.828	0.800	0.747	0.672
U N I F O R M L I N E	M	E	0.632	0.625	0.604	0.573	0.536
		EM	0.632	0.625	0.604	0.573	0.536
		EMQ	0.631	0.621	0.592	0.545	0.481
	Q(A)	E	0.417	0.419	0.410	0.393	0.372
		EM	0.416	0.418	0.410	0.393	0.372
		EMQ	0.416	0.402	0.375	0.335	0.284
	Q(O)	E	0.417	0.404	0.379	0.345	0.305
		EM	0.416	0.403	0.379	0.345	0.305
		EMQ	0.416	0.416	0.401	0.374	0.334

E - End diaphragms only
 EM - End and midspan diaphragms
 EMQ - End, midspan and quarterspan diaphragms
 M - Midspan
 Q(A) - Quarterspan acute corner
 Q(O) - Quarterspan obtuse corner

Table 6.17. - Influence of intermediate diaphragms on web deflection values at midspan and quarterspan cross-section. Midspan point and uniform line loading. Skew single cell structure.

load Case	Sect-ion		Diaphragm thickness (cm)				
			0	1.2	2.4	3.6	
M I D S P A N	1 / 2	f1	48.20	48.20	48.19	48.19	
		f5	32.20	32.21	32.21	32.22	
		Ψ	0.741	0.741	0.741	0.741	
		d1	0.632	0.631	0.631	0.631	
	P O I N T	1 / 4	f1	19.00	19.59	19.95	20.20
			f5	19.05	19.06	19.07	19.09
			Ψ	1.002	0.980	0.967	0.958
			d1	0.417	0.416	0.416	0.416
U N I F O R M L I N E	1 / 2	f1	59.36	59.35	59.34	59.34	
		f5	55.11	55.12	55.13	55.14	
		Ψ	0.951	0.951	0.952	0.952	
		d1	1.152	1.150	1.149	1.148	
	1 / 4	f1	44.77	46.03	46.81	47.35	
		f5	40.15	40.13	40.14	40.16	
		Ψ	0.931	0.912	0.901	0.894	
		d1	0.832	0.831	0.830	0.830	

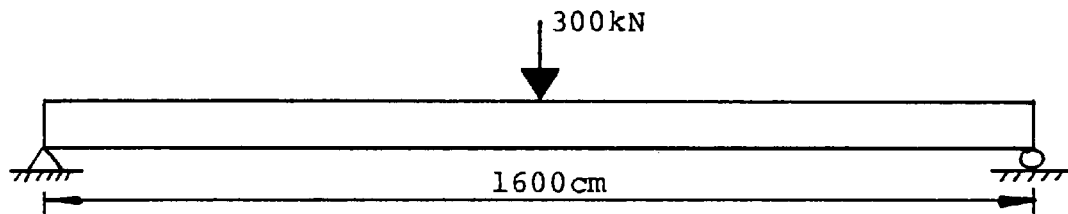
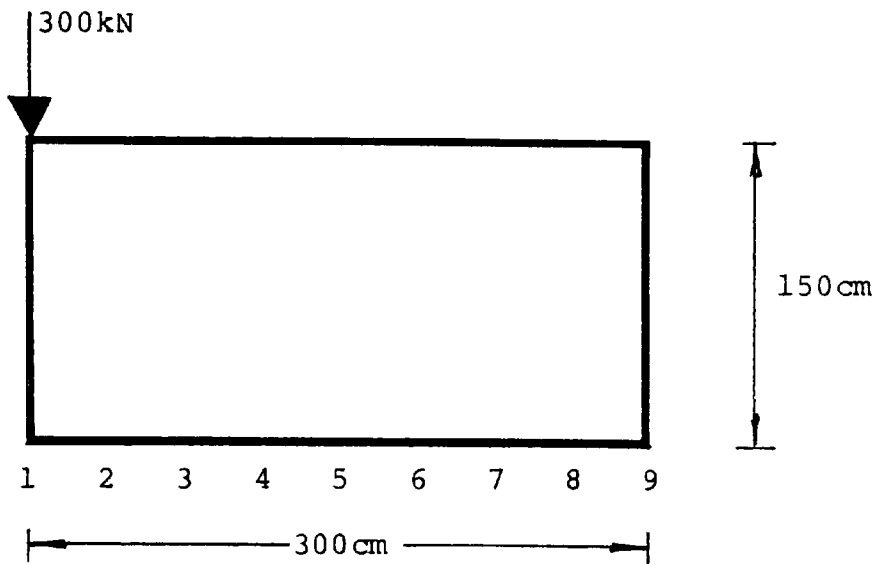
- f1 - longitudinal flange edge stress (N/mm²)
f5 - longitudinal mid-flange stress (N/mm²)
 Ψ - effective breadth ratio
d1 - web deflection (cm)

Table 6.18. - Influence of quarterspan diaphragm thickness on long. flange stress, effective breadth ratio and web deflection. Midspan point and uniform line loading. Straight single cell structure.

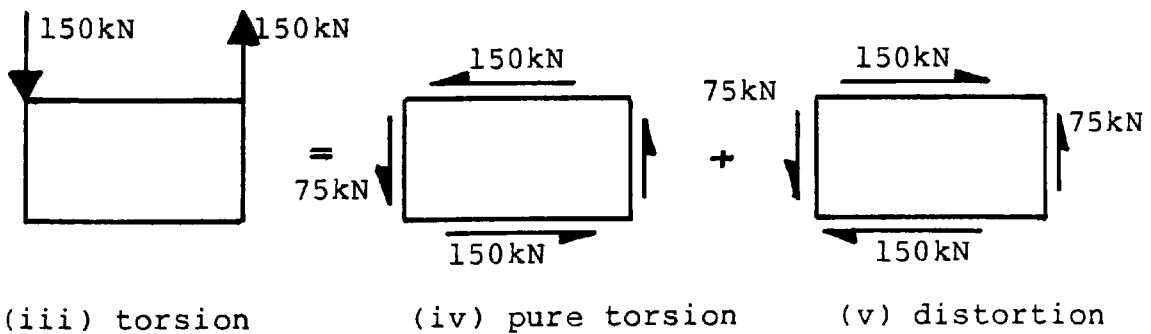
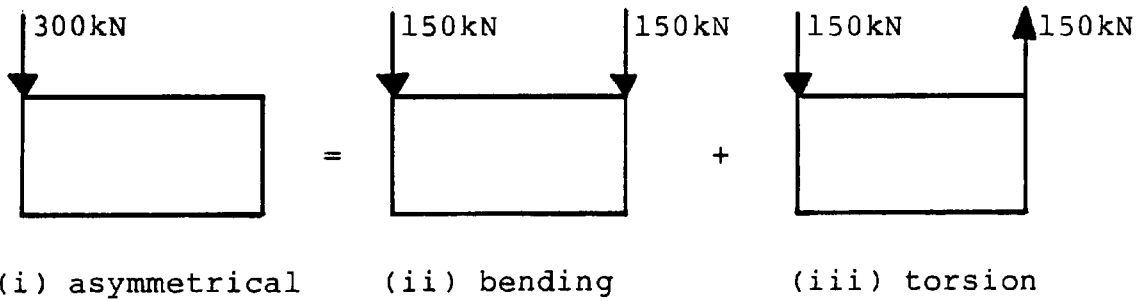
load case	Sect-ion		Diaphragm thickness (cm)						
			0.0	0.15	0.3	0.6	1.2	2.4	3.6
M I D S P A N P O I N T	1 / 2	f1	46.38	42.22	41.40	40.84	40.46	40.18	40.04
		f5	23.82	23.93	23.95	23.97	23.98	23.98	23.98
		ψ	0.630	0.663	0.670	0.675	0.679	0.681	0.683
		d1	0.536	0.496	0.489	0.484	0.480	0.478	0.477
	1 / 4	f1	20.51	11.03	9.16	7.85	6.96	6.34	6.07
		f5	12.14	12.07	12.07	12.08	12.11	12.17	12.22
		f9	4.73	14.20	16.13	17.60	18.77	19.83	20.44
		ψ	0.973	0.970	0.969	0.965	0.959	0.951	0.945
		d1	0.372	0.308	0.296	0.288	0.283	0.280	0.279
		d9	0.305	0.326	0.330	0.332	0.334	0.334	0.335
U N I F O R M L I N E	1 / 2	f1	49.66	43.05	41.74	40.85	40.26	39.85	39.65
		f5	40.13	40.31	40.35	40.38	40.40	40.41	40.42
		ψ	0.869	0.956	0.977	0.992	1.002	1.010	1.013
		d1	0.949	0.886	0.874	0.866	0.860	0.857	0.855
	1 / 4	f1	48.08	32.82	29.79	27.65	26.16	25.09	24.59
		f5	25.28	25.17	25.16	25.17	25.21	25.28	25.34
		f9	23.33	38.43	41.49	43.78	45.55	47.10	47.97
		ψ	0.802	0.802	0.802	0.801	0.799	0.797	0.795
		d1	0.735	0.632	0.613	0.600	0.592	0.587	0.585
		d9	0.626	0.658	0.665	0.669	0.670	0.672	0.672

f1,f9 - longitudinal flange edge stress (N/mm²)
f5 - longitudinal mid-flange stress (N/mm²)
ψ - effective breadth ratio
d1,d9 - web deflection (cm)

Table 6.19. - Influence of quarterspan diaphragm thickness on longitudinal flange stress, effective breadth ratio and web deflection. Midspan point and uniform line loading. 40 degree skew single cell structure.

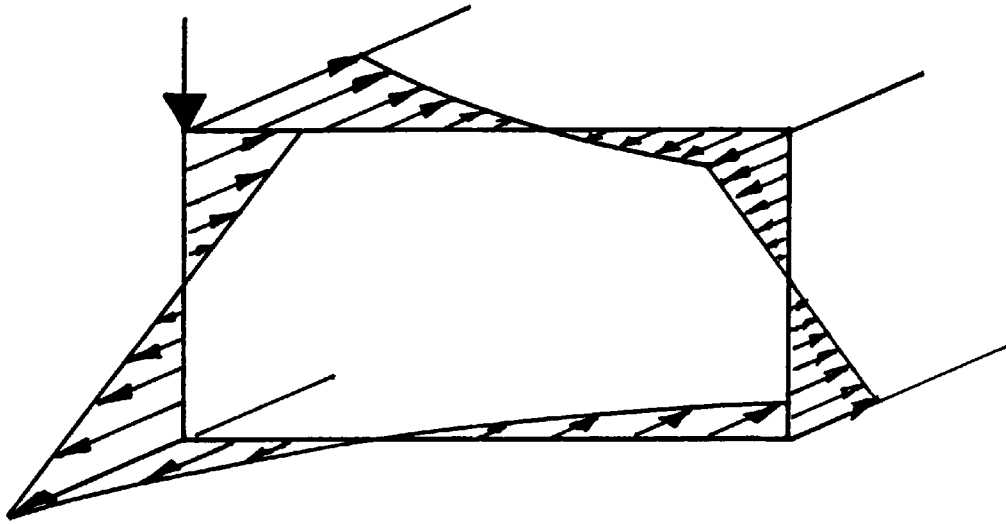


(a) Structure and loading details.

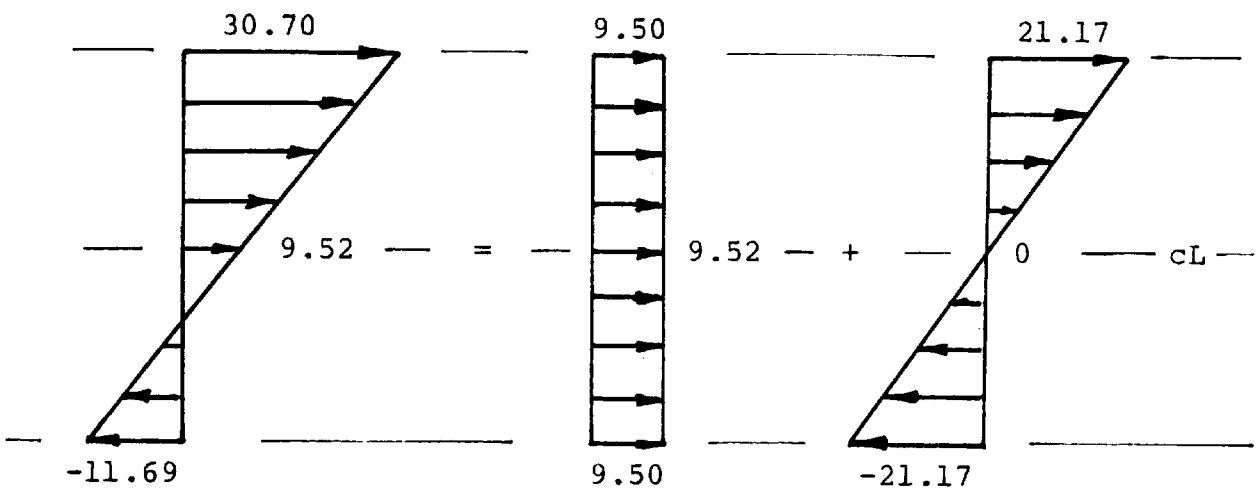


(b) Bending, torsional and distortional components.

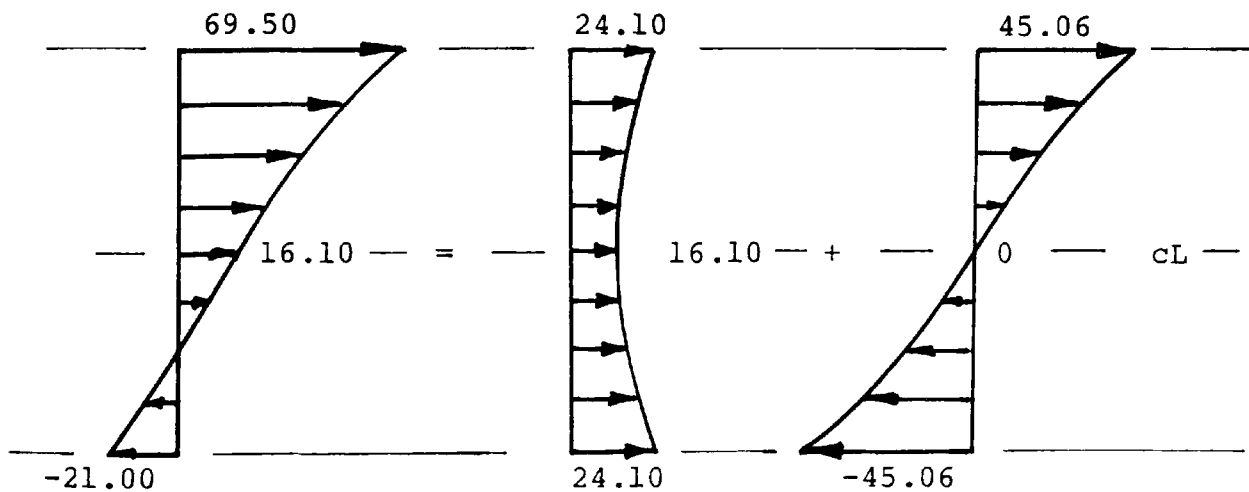
FIGURE 6.1 - ASYMMETRICAL LOADING DETAILS
STRAIGHT SINGLE CELL STRUCTURE.



(a) Distribution of longitudinal flange stress at midspan.

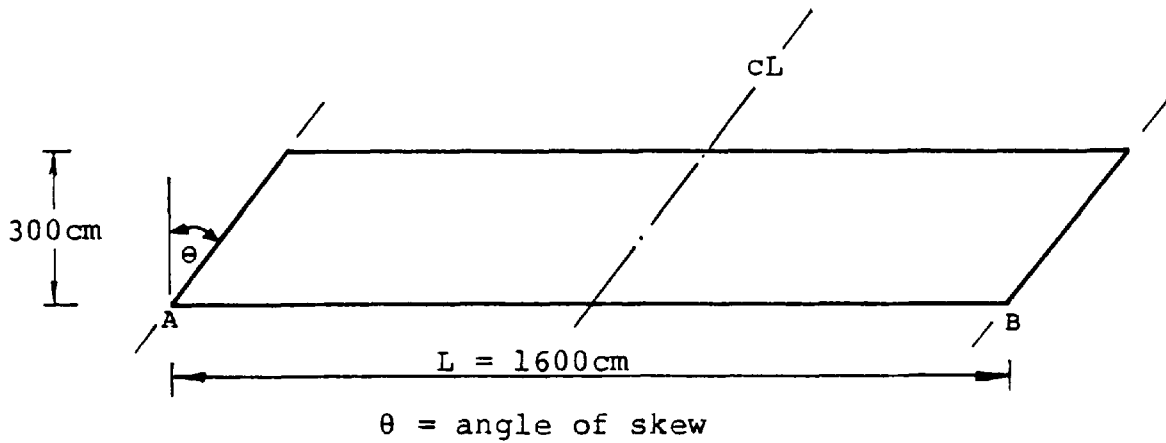


(b) Quarterspan.

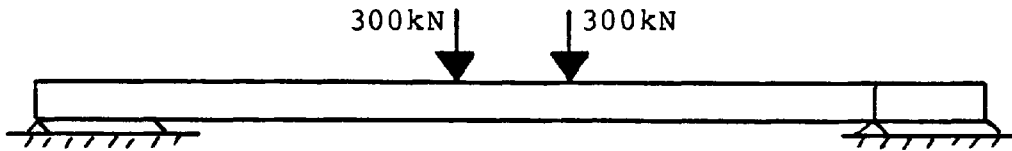


(c) Midspan.

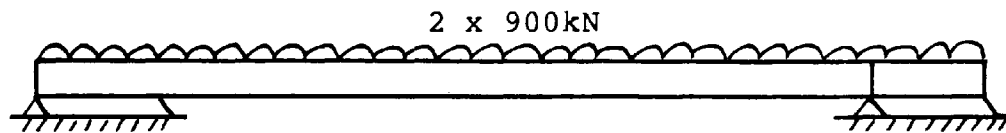
FIGURE 6.2 - LONGITUDINAL FLANGE STRESS DISTRIBUTION
ASYMMETRICAL LOADING, SINGLE CELL STRUCTURE.



Plan view.

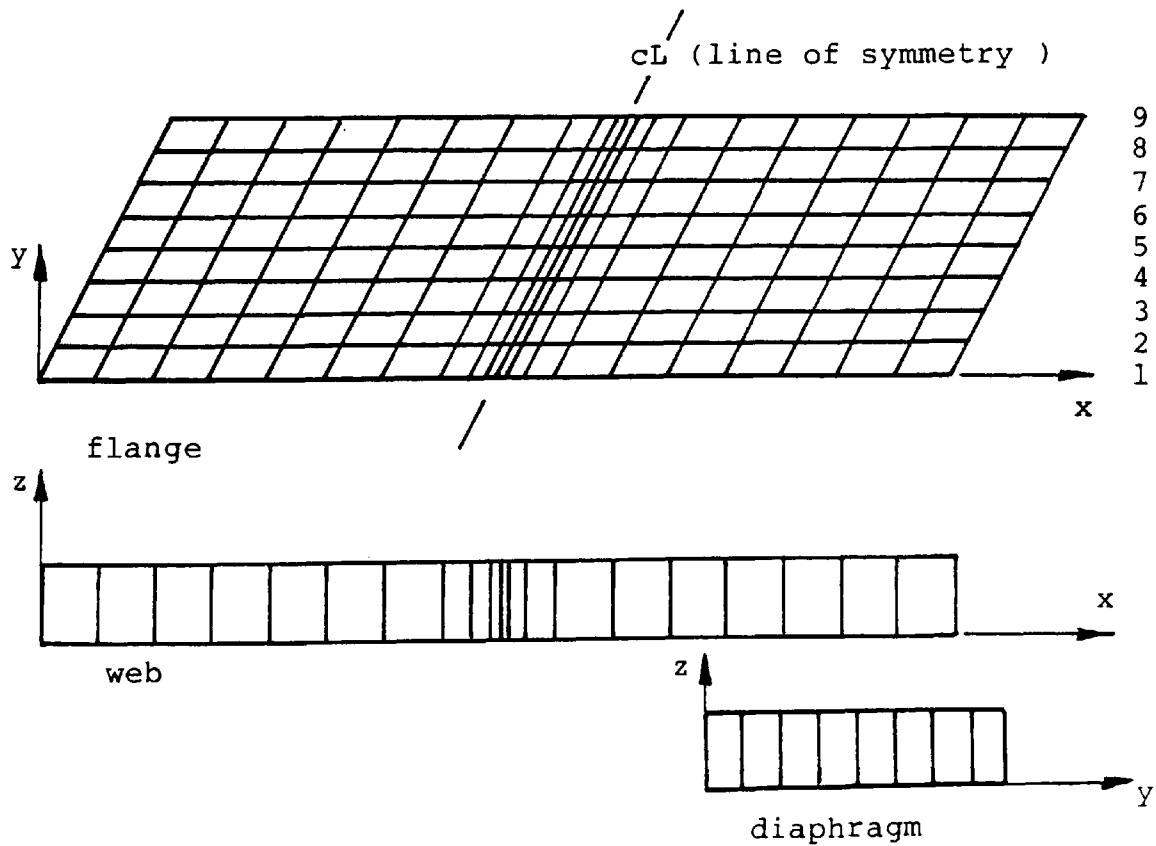


Midspan point load.



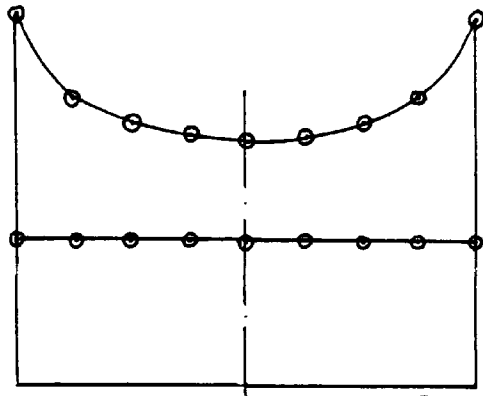
Uniform line load.

(a) Structure and loading details.

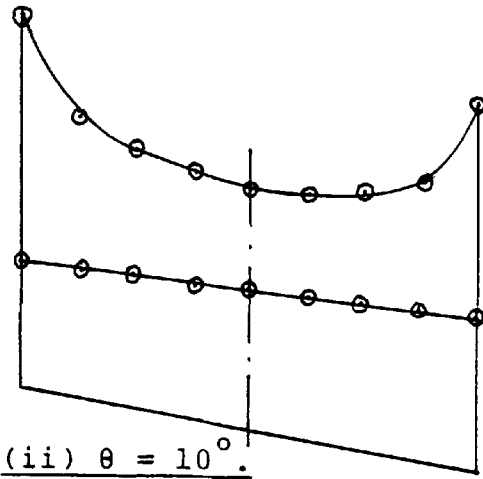


(b) Finite element mesh.

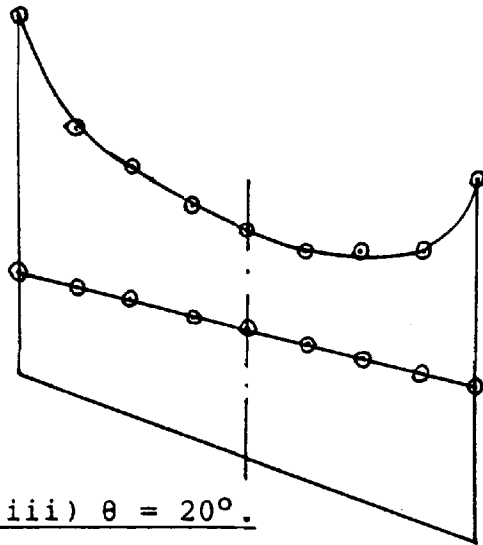
FIGURE 6.3 - DETAILS OF SKEW SINGLE CELL STRUCTURE.



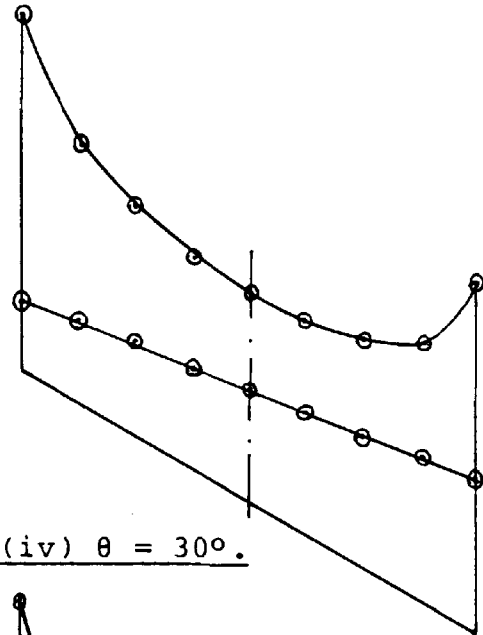
(i) skew angle, $\theta = 0^\circ$.



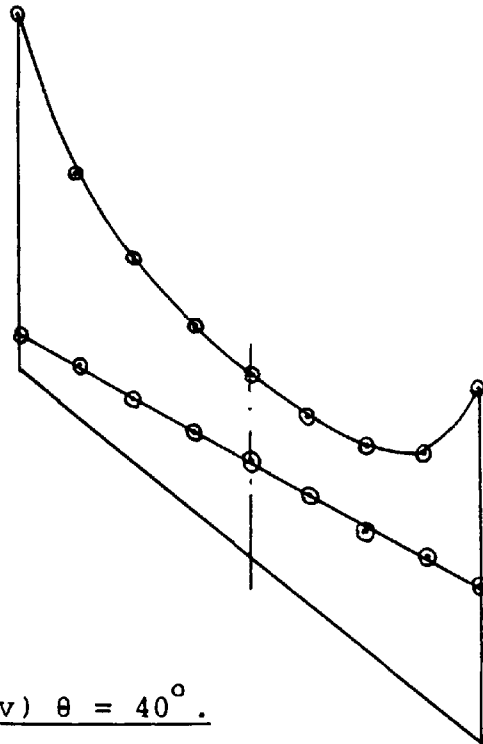
(ii) $\theta = 10^\circ$.



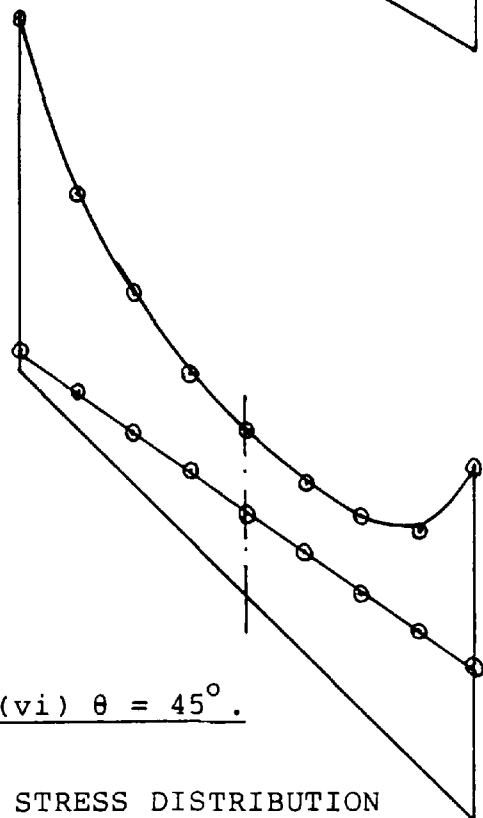
(iii) $\theta = 20^\circ$.



(iv) $\theta = 30^\circ$.

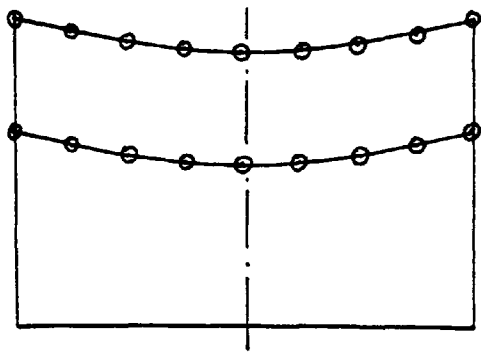


(v) $\theta = 40^\circ$.

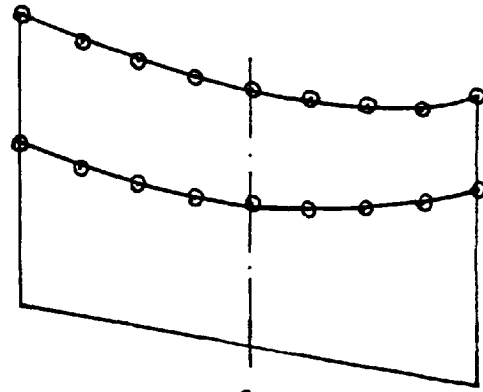


(vi) $\theta = 45^\circ$.

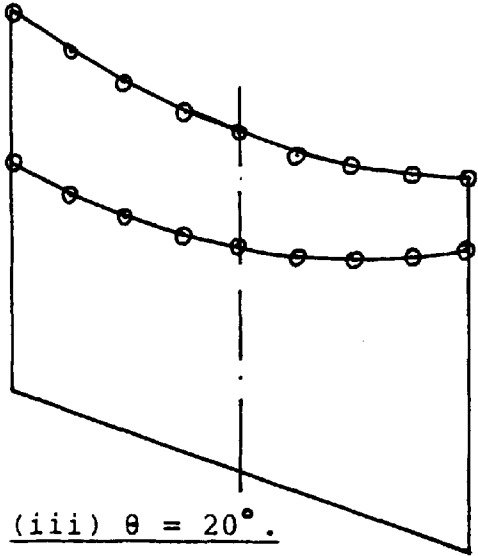
FIGURE 6.4 - LONGITUDINAL FLANGE STRESS DISTRIBUTION
MIDSPAN AND QUARTERSPAN CROSS-SECTIONS
MIDSPAN POINT LOAD, SKEW SINGLE CELL STRUCTURE.



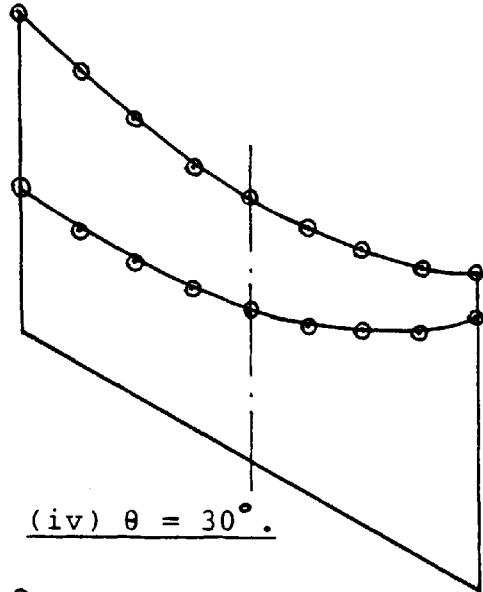
(i) skew angle, $\theta = 0^\circ$.



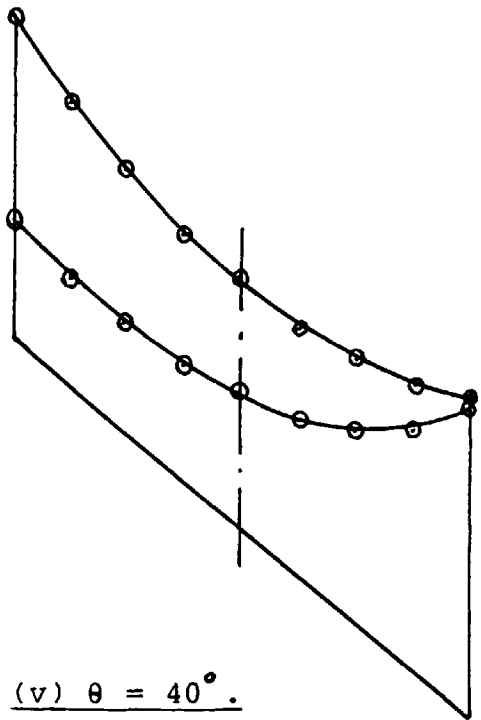
(ii) $\theta = 10^\circ$.



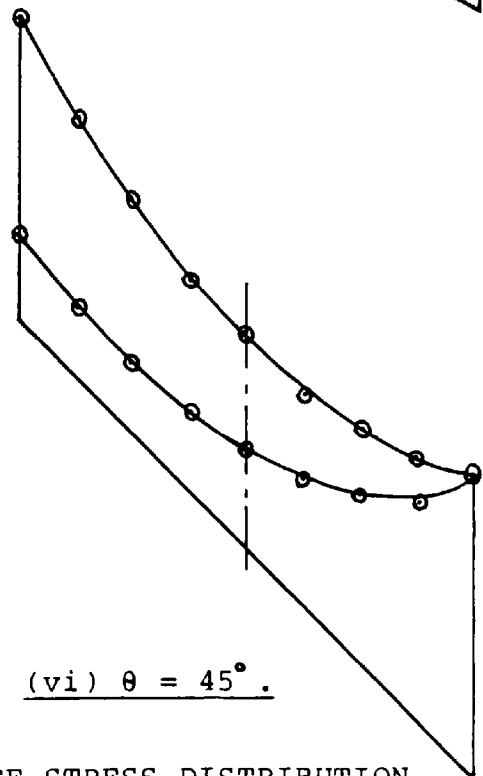
(iii) $\theta = 20^\circ$.



(iv) $\theta = 30^\circ$.

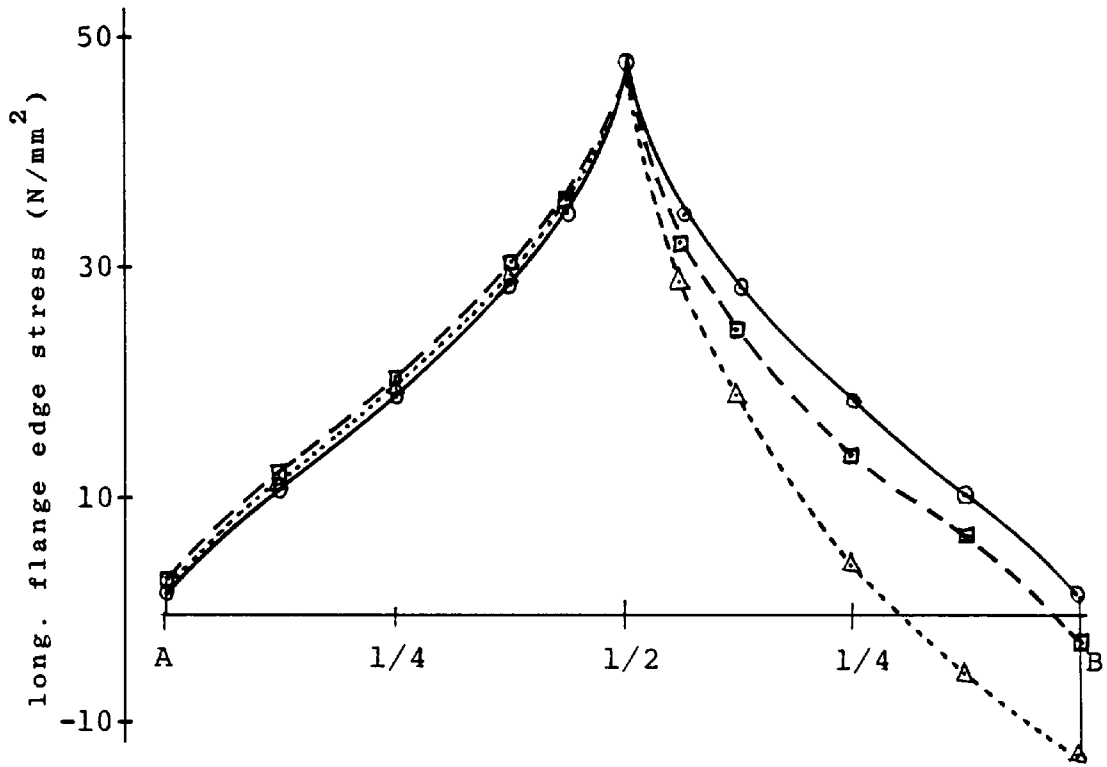


(v) $\theta = 40^\circ$.

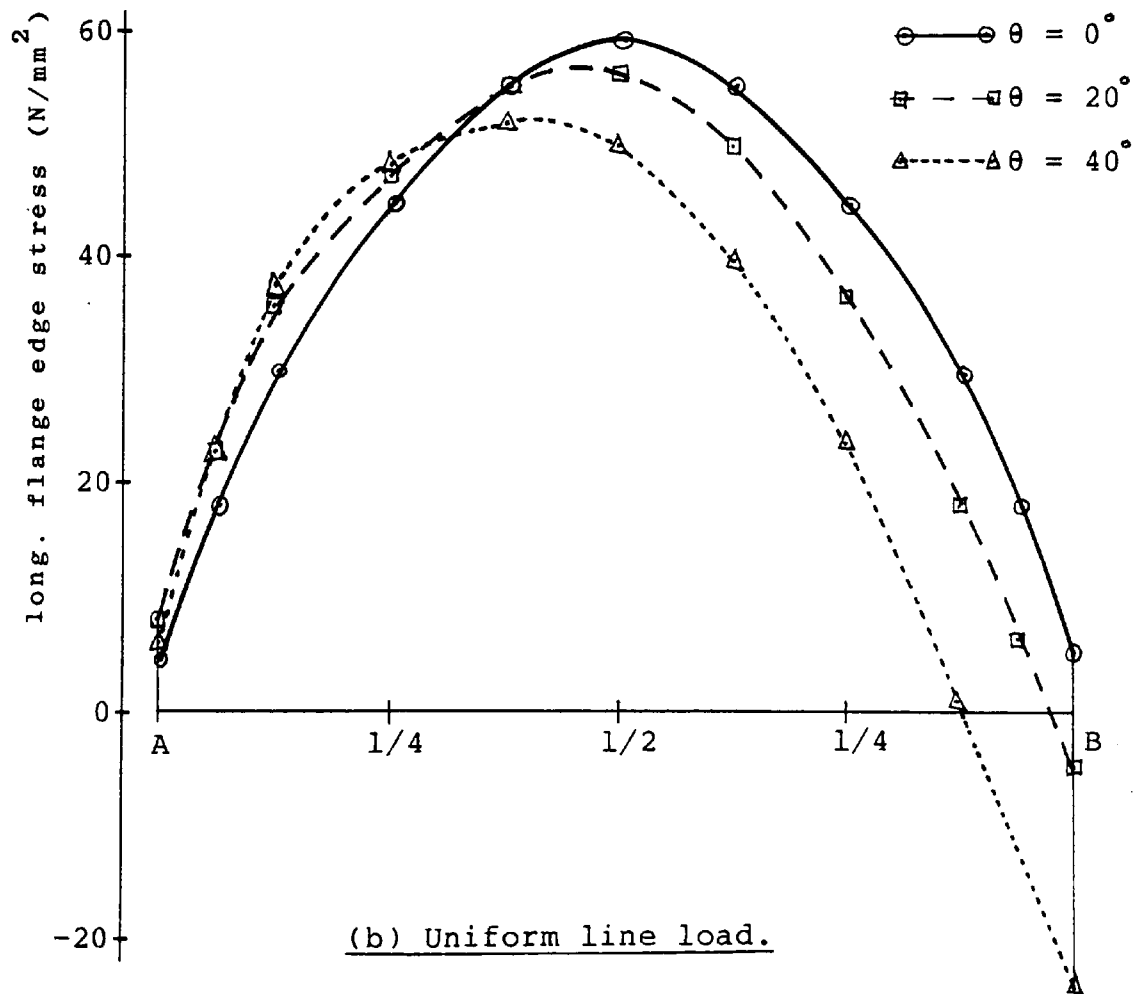


(vi) $\theta = 45^\circ$.

FIGURE 6.5 - LONGITUDINAL FLANGE STRESS DISTRIBUTION
MIDSPAN AND QUARTERSPAN CROSS-SECTIONS
UNIFORM LINE LOAD, SKEW SINGLE CELL STRUCTURE.

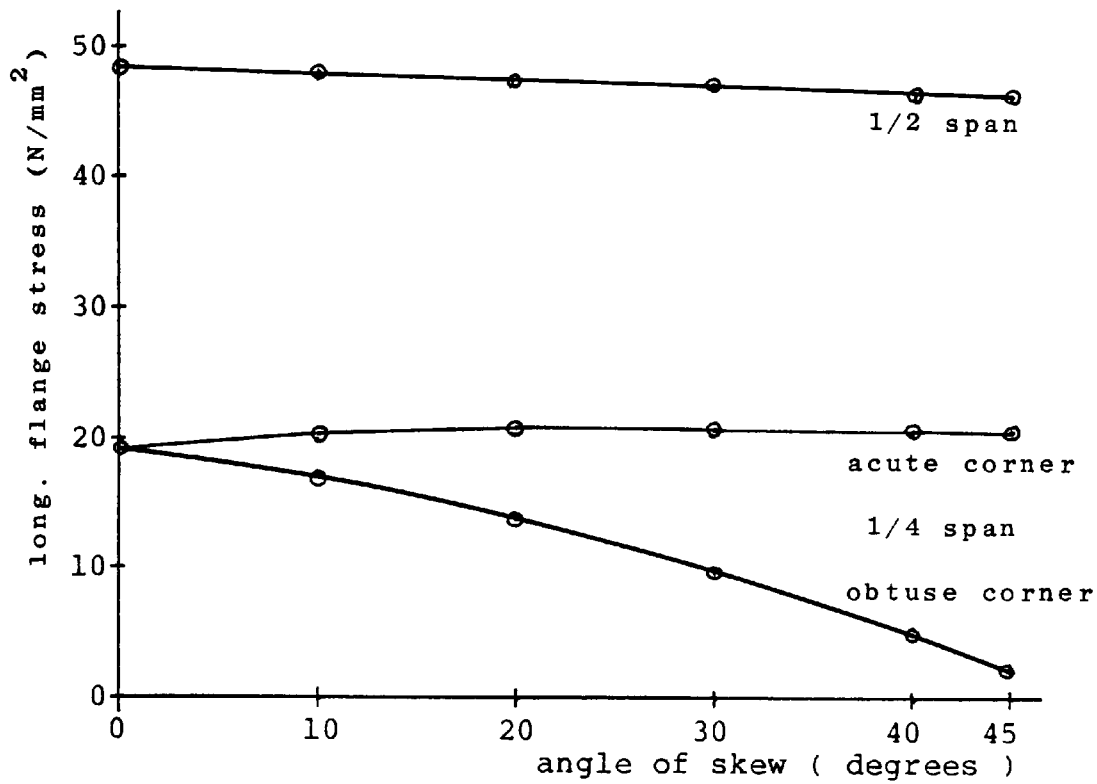


(a) Midspan point load.

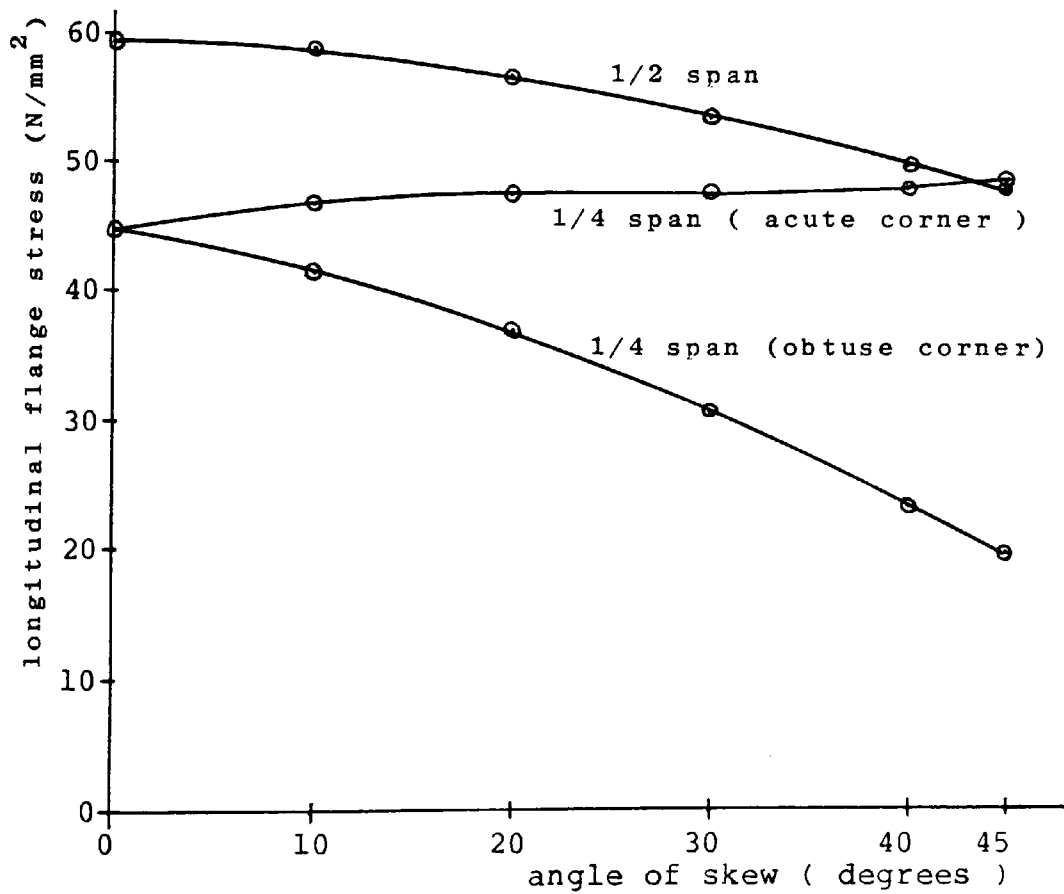


(b) Uniform line load.

FIGURE 6.6 - LONGITUDINAL FLANGE STRESS VARIATION ALONG EDGE OF TOP FLANGE.

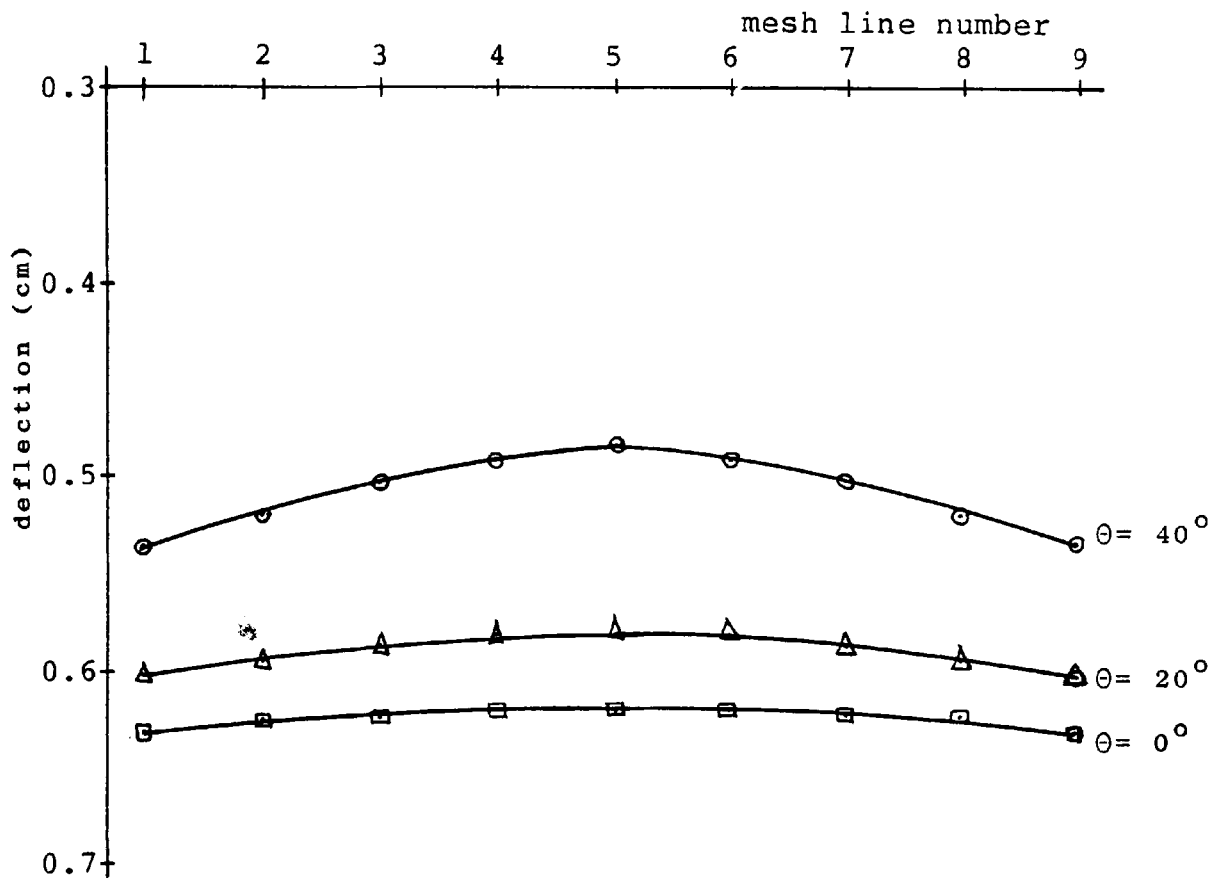


(a) Midspan point load.

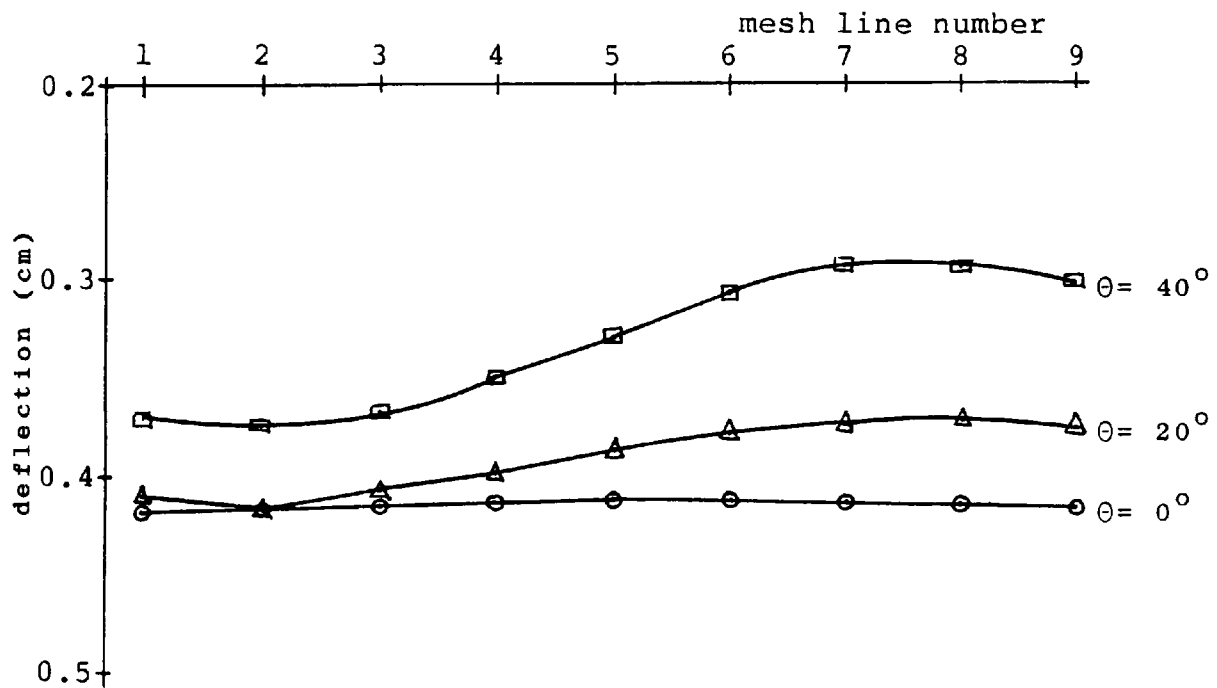


(b) Uniform line load.

FIGURE 6.7 - VARIATION OF LONGITUDINAL FLANGE EDGE STRESS WITH ANGLE OF SKEW.

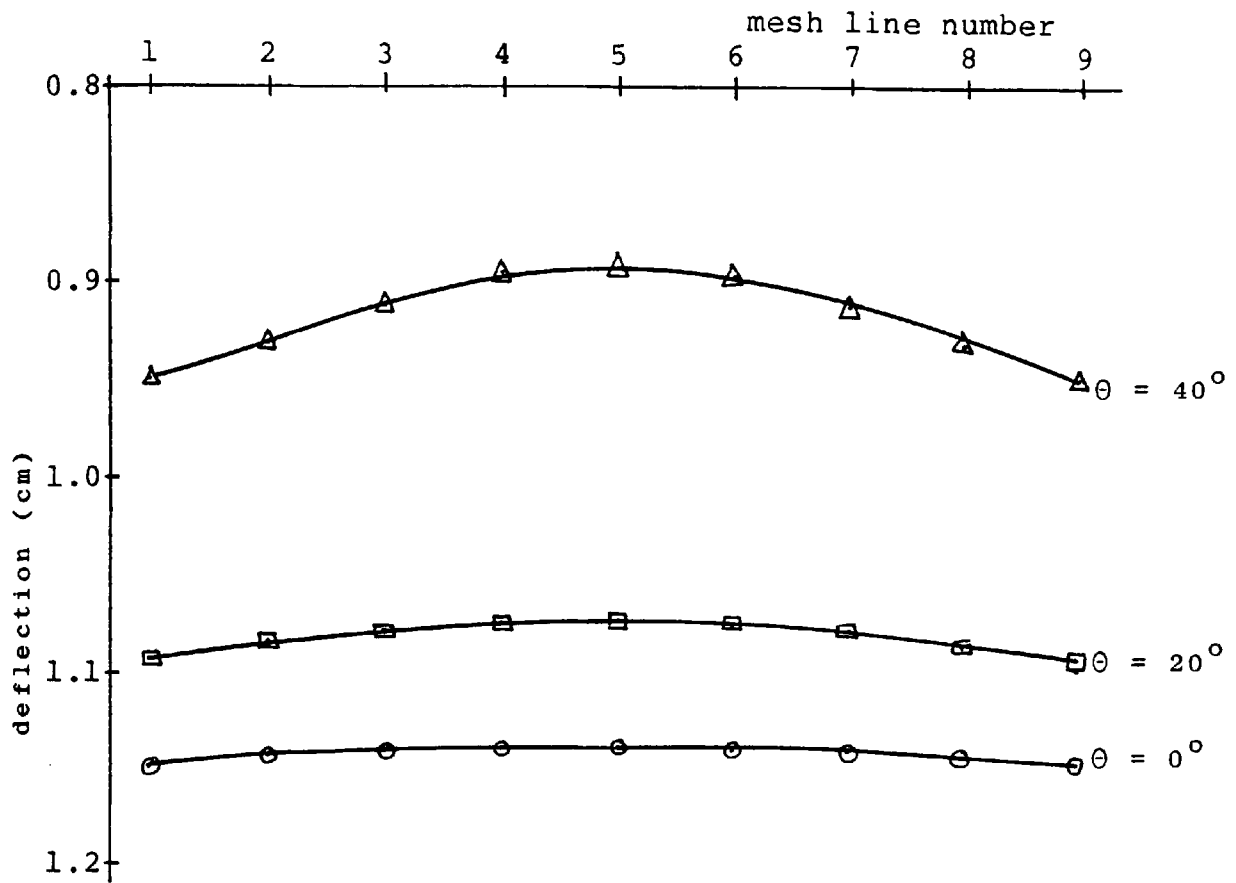


(a) Midspan.

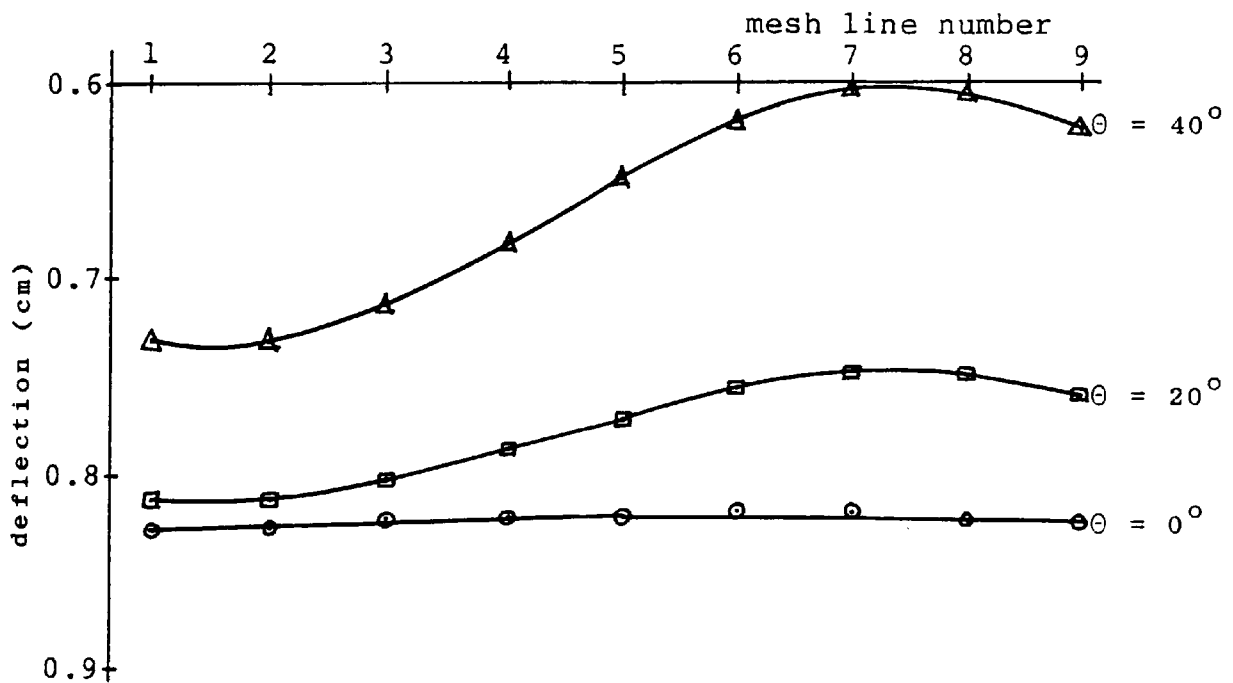


(b) Quarterspan.

FIGURE 6.8 - VERTICAL DEFLECTION PROFILE OF TOP FLANGE MIDSPAN AND QUARTERSPAN CROSS-SECTIONS MIDSPAN POINT LOAD.

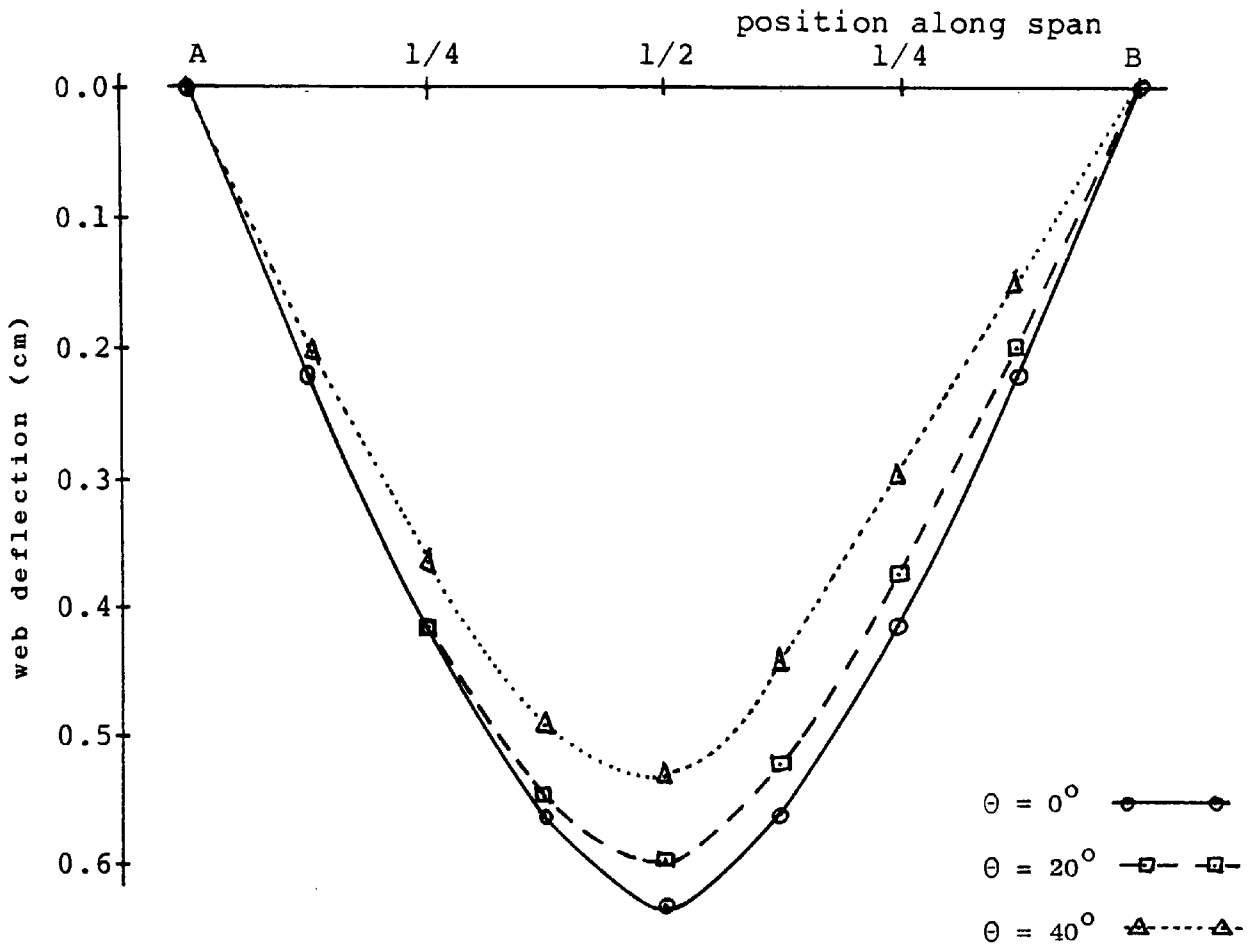


(a) Midspan.

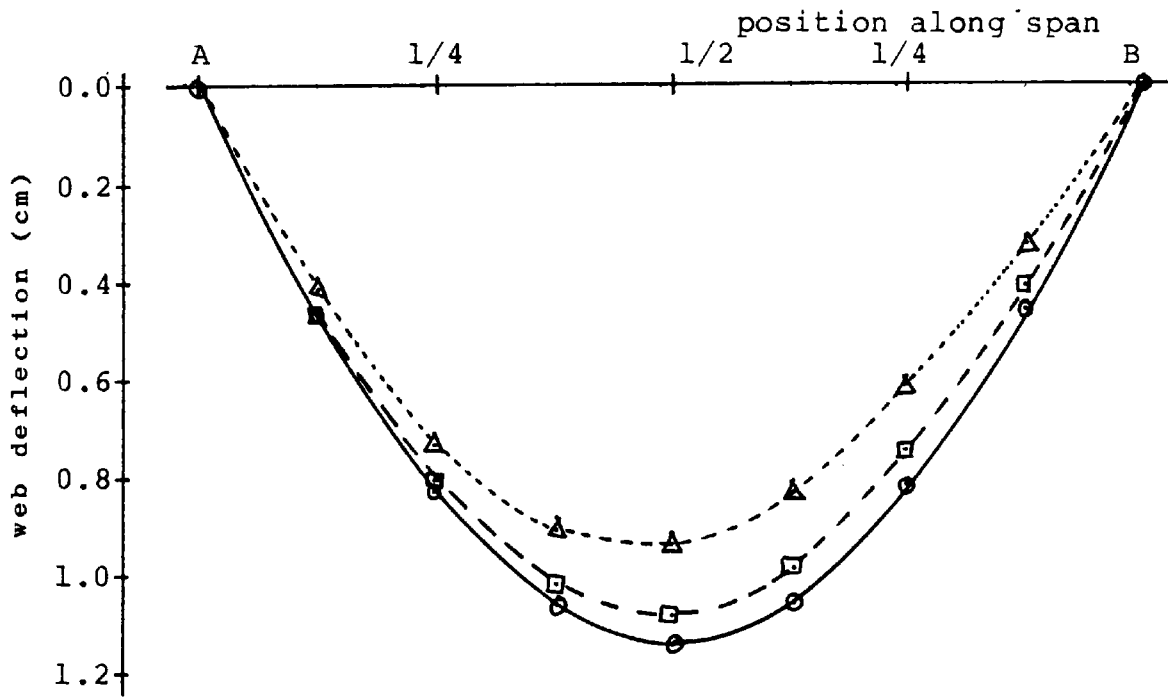


(b) Quarterspan.

FIGURE 6.9 - VERTICAL DEFLECTION PROFILE OF TOP FLANGE MIDSPAN AND QUARTERSPAN CROSS-SECTIONS UNIFORM LINE LOAD.

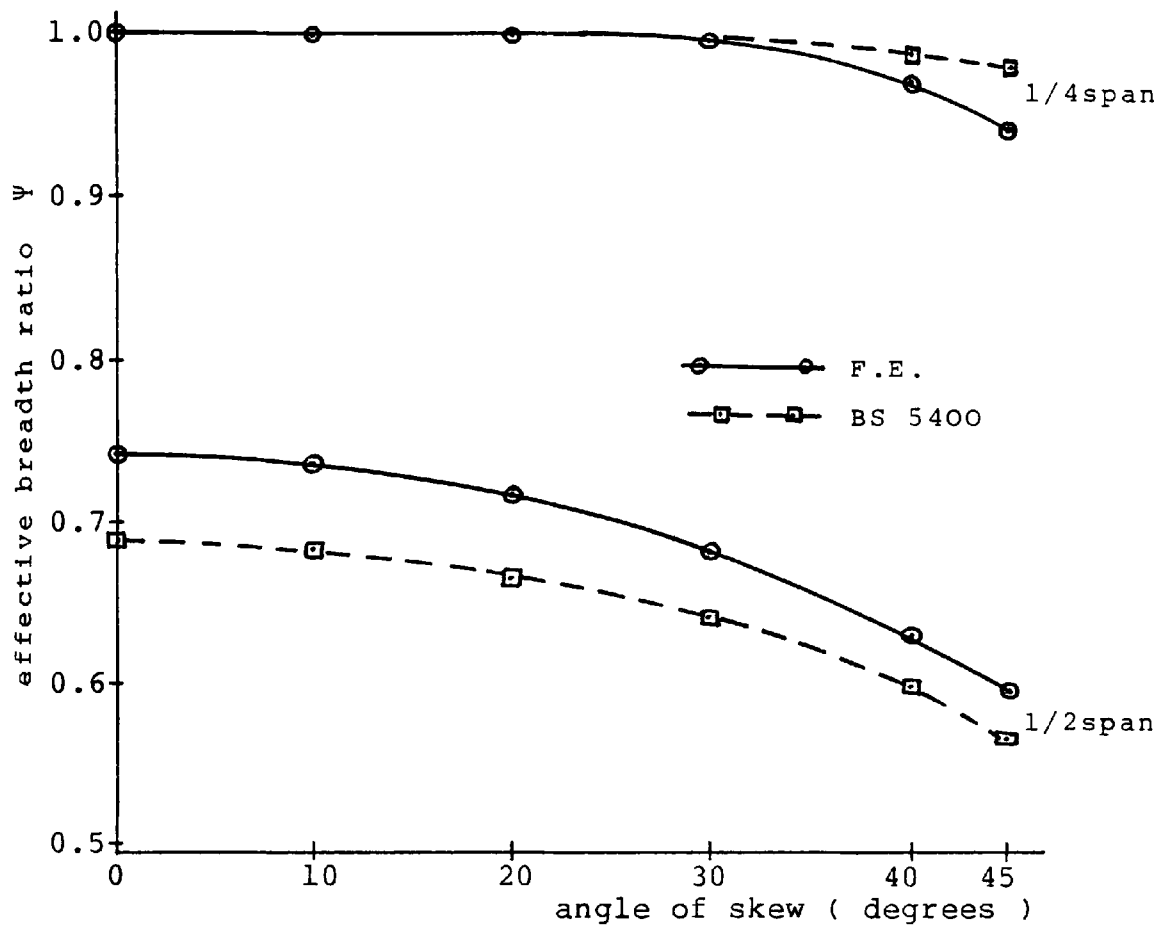


(a) Midspan point load.

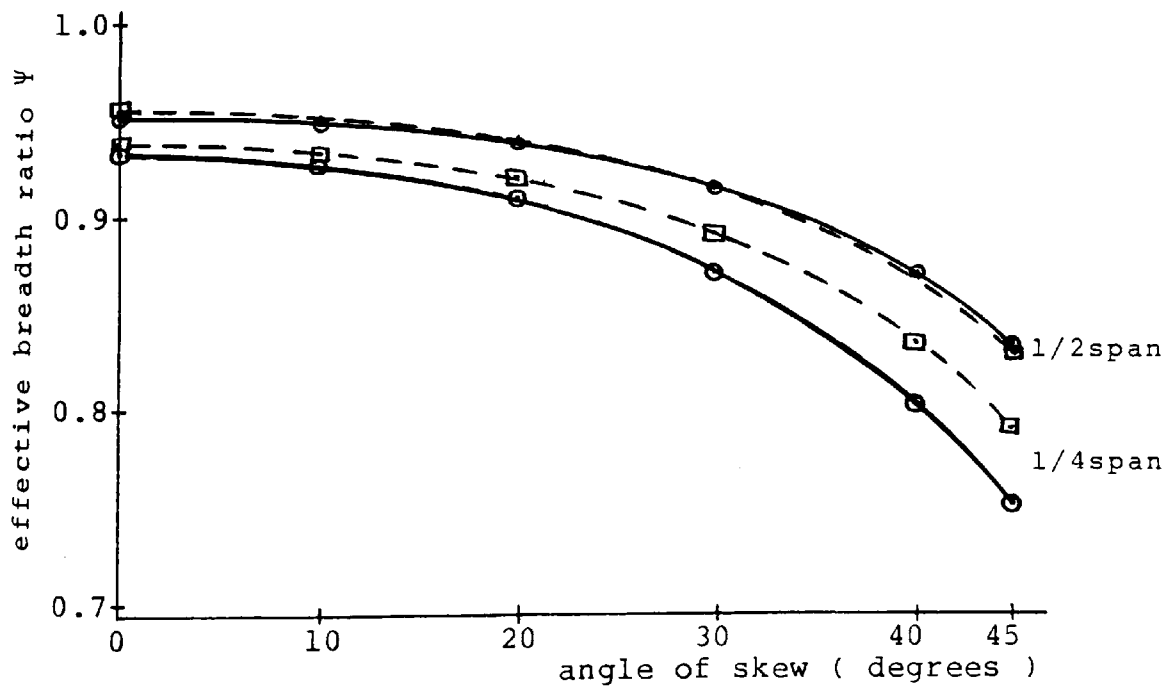


(b) Uniform line load.

FIGURE 6.10 - WEB DEFLECTION VARIATION ALONG SPAN
MIDSPAN POINT AND UNIFORM LINE LOADING.

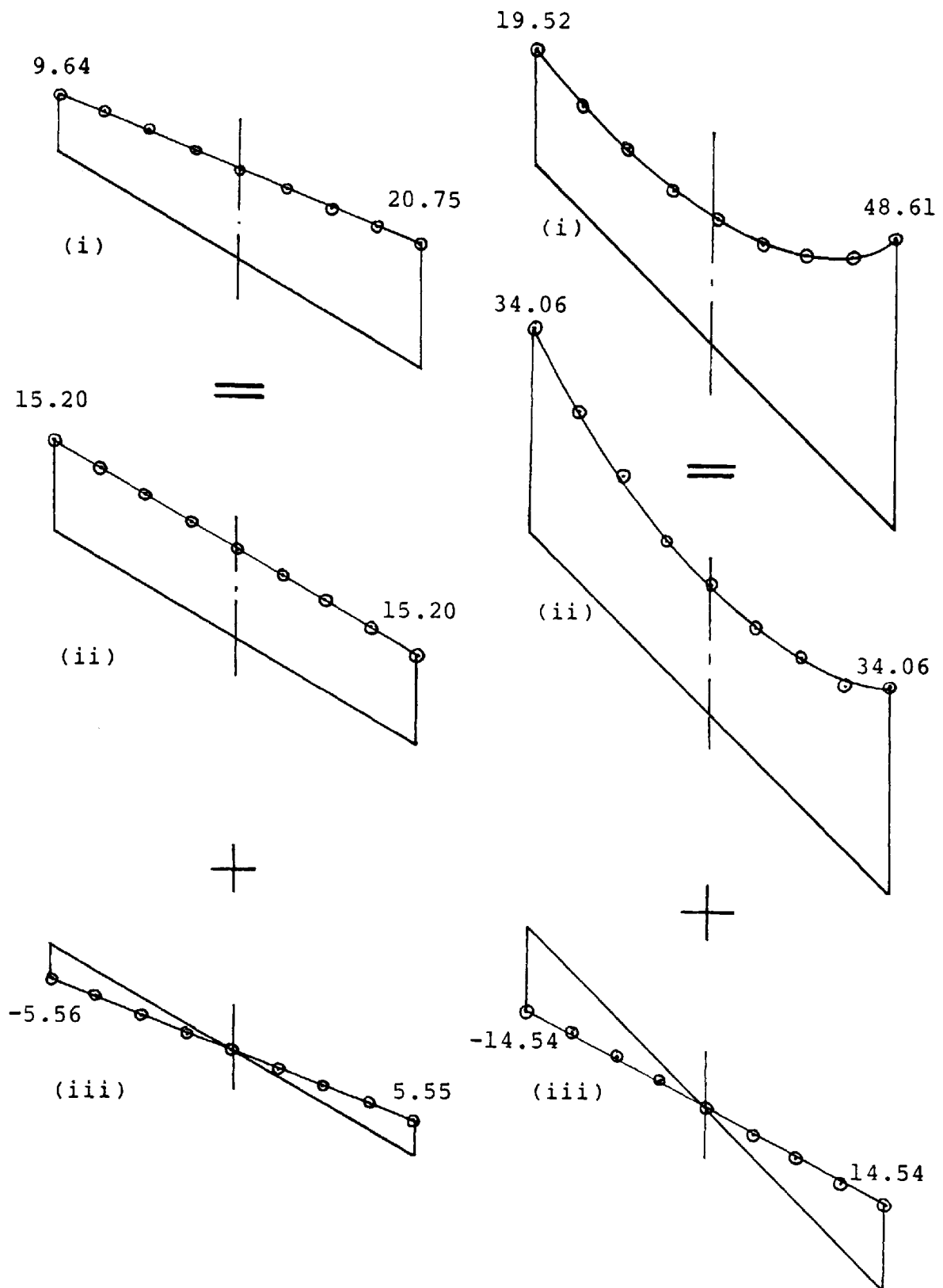


(a) Midspan point load.



(b) Uniform line load.

FIGURE 6.11 - VARIATION OF EFFECTIVE BREADTH RATIO, Ψ WITH ANGLE OF SKEW.



(a) Midspan point load.

(b) Uniform line load.

FIGURE 6.12 - LONGITUDINAL FLANGE STRESS DISTRIBUTION AT QUARTERSPAN CROSS-SECTION
 (i) ACTUAL, (ii) BENDING COMPONENT,
 (iii) TORSIONAL AND DISTORTIONAL COMPONENT.

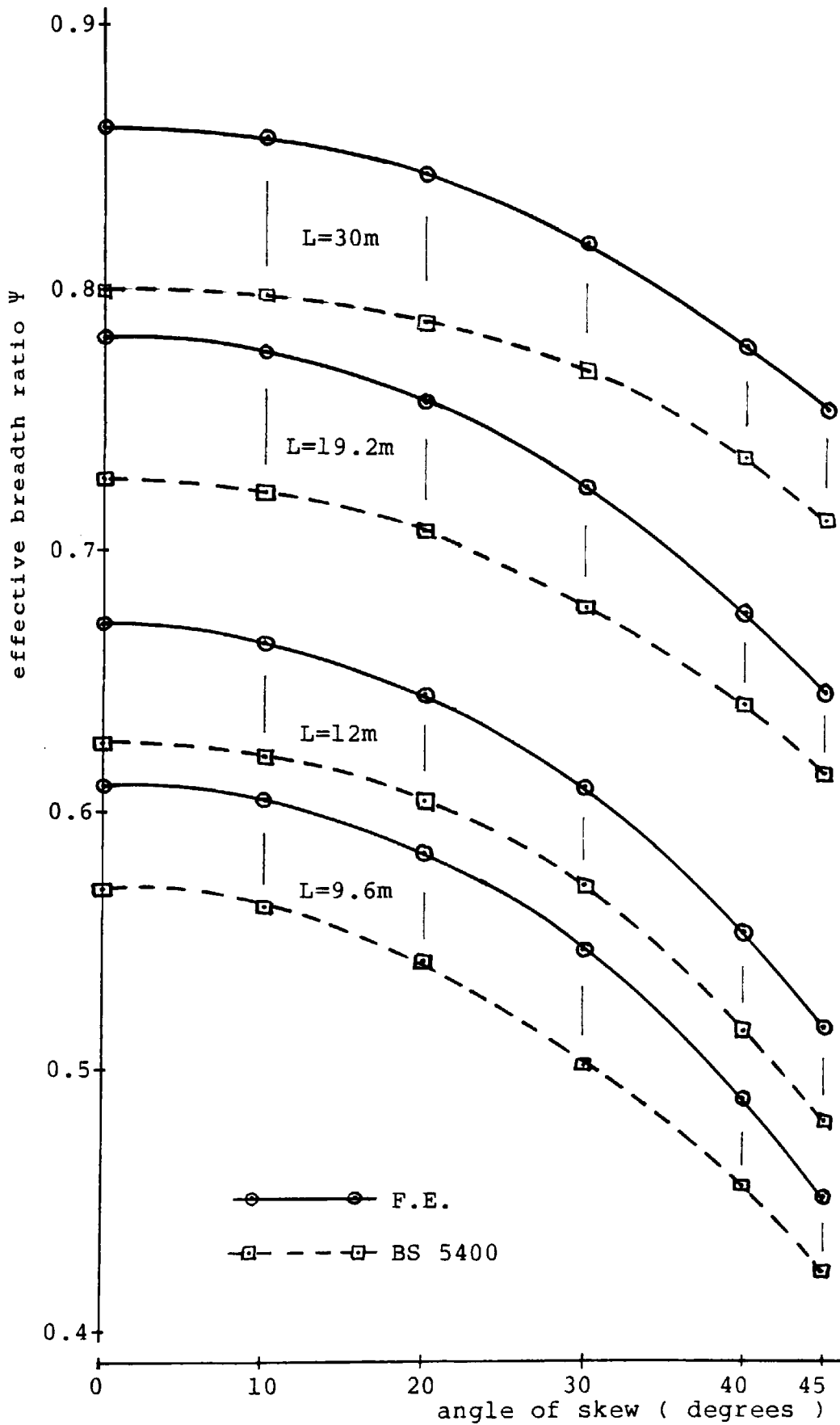


FIGURE 6.13 - VARIATION OF EFFECTIVE BREADTH RATIO WITH ANGLE OF SKEW - SINGLE CELL STRUCTURE MIDSPAN CROSS-SECTION - MIDSPAN POINT LOADING.

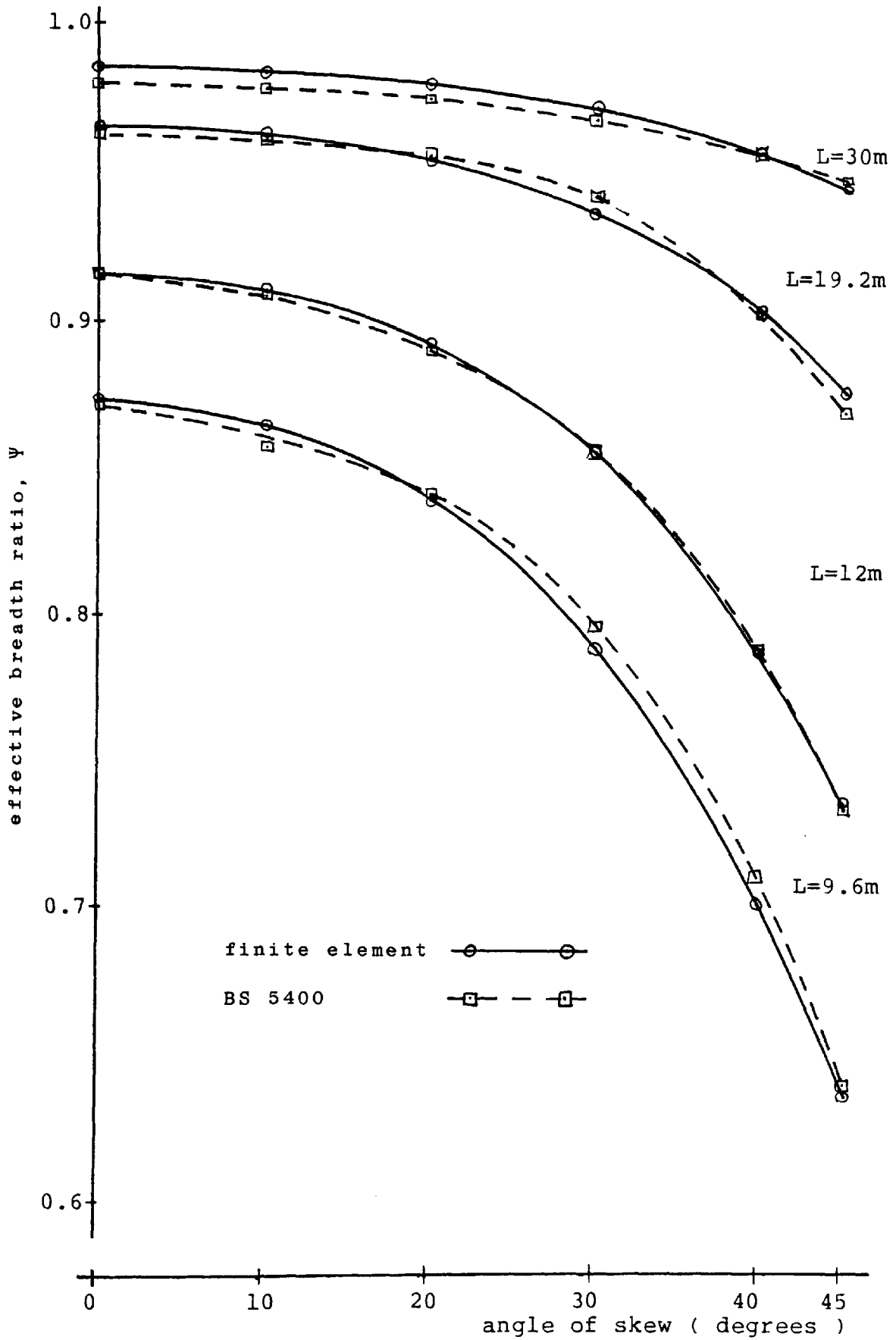
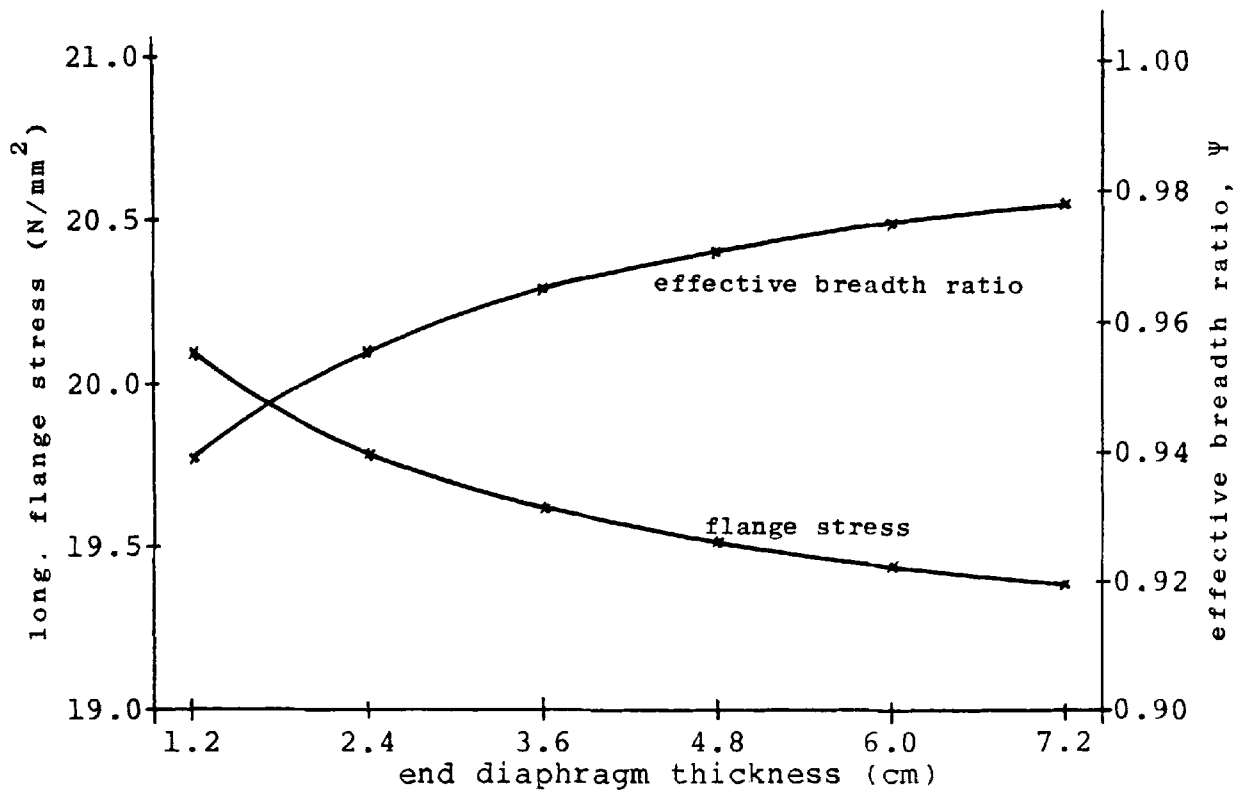
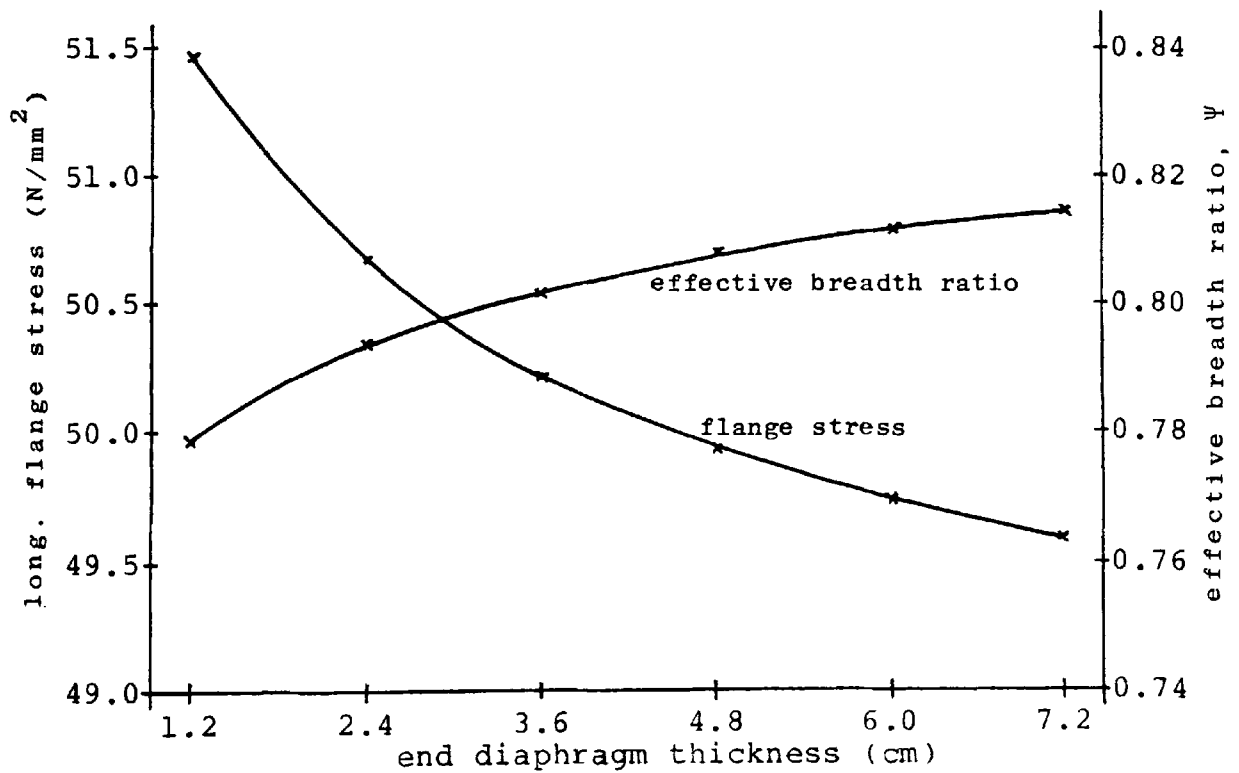


FIGURE 6.14 - VARIATION OF EFFECTIVE BREADTH RATIO WITH ANGLE OF SKEW - SINGLE CELL STRUCTURE MIDSPAN CROSS-SECTION - UNIFORM LINE LOADING.

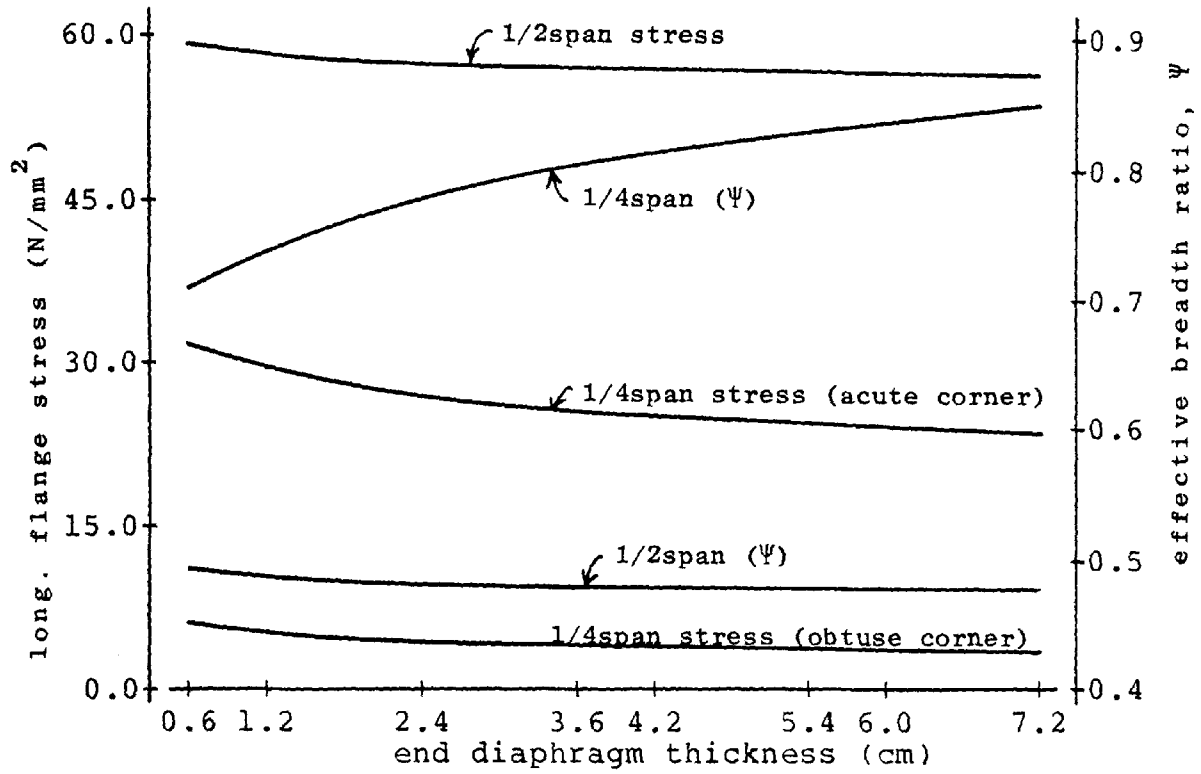


(a) Midspan point load.

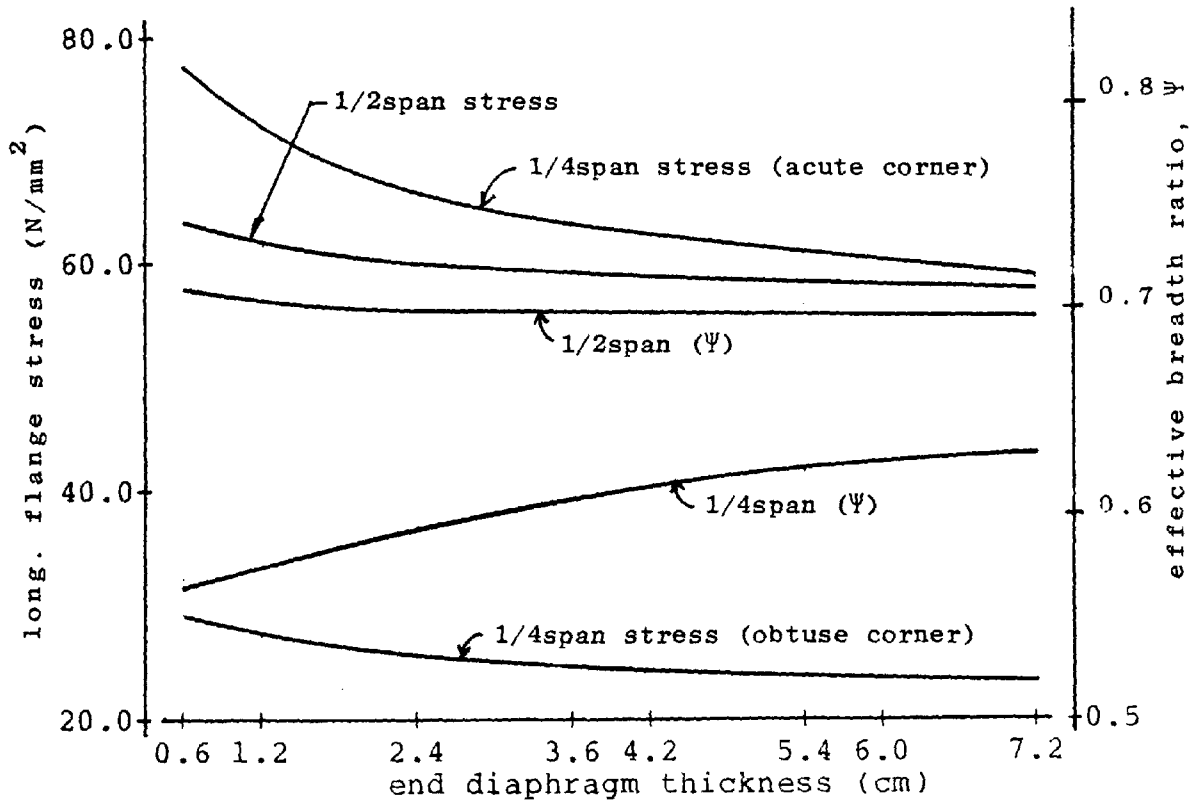


(b) Uniform line load.

FIGURE 6.15 - VARIATION OF FLANGE EDGE STRESS AND EFFECTIVE BREADTH RATIO AT QUARTERSPAN CROSS-SECTION WITH END DIAPHRAGM THICKNESS. 9.6M SPAN, SKEW ANGLE - 0 DEGREES.

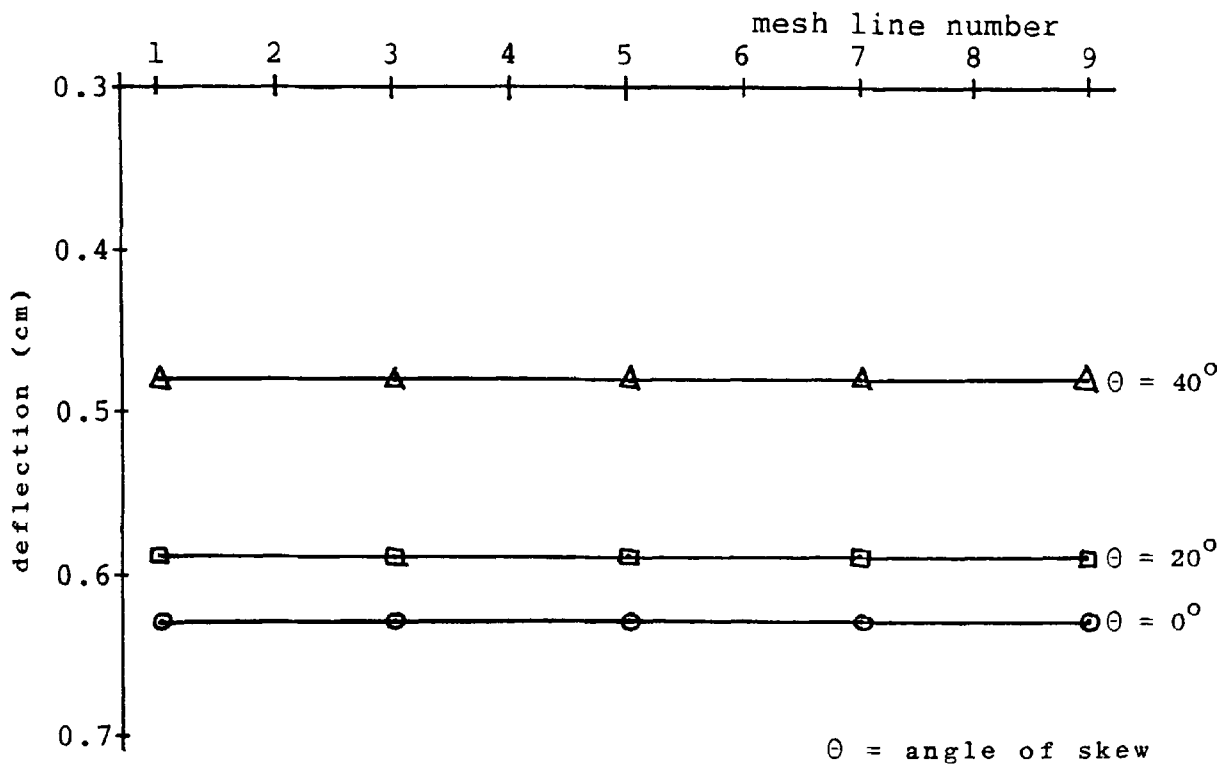


(a) Midspan point load.

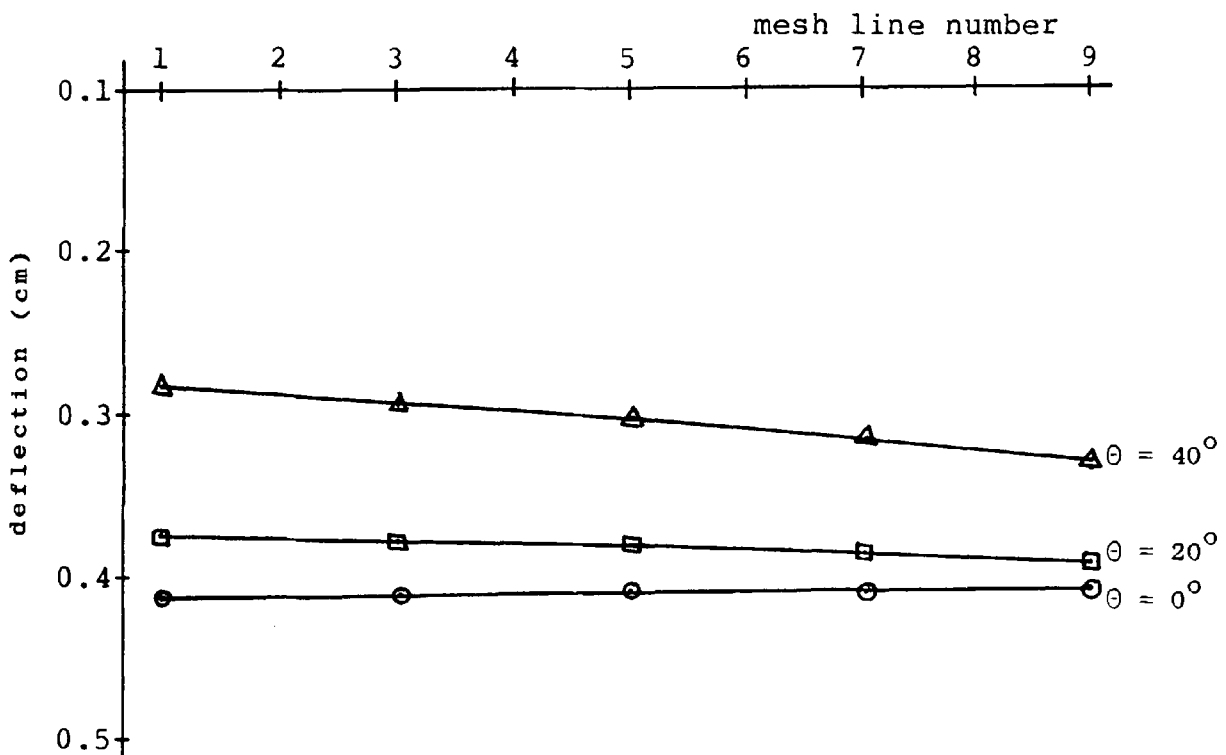


(b) Uniform line load.

FIGURE 6.16 - VARIATION OF FLANGE EDGE STRESS AND EFFECTIVE BREADTH RATIO WITH END DIAPHRAGM THICKNESS. 9.6M SPAN, SKEW ANGLE - 40 DEGREES.

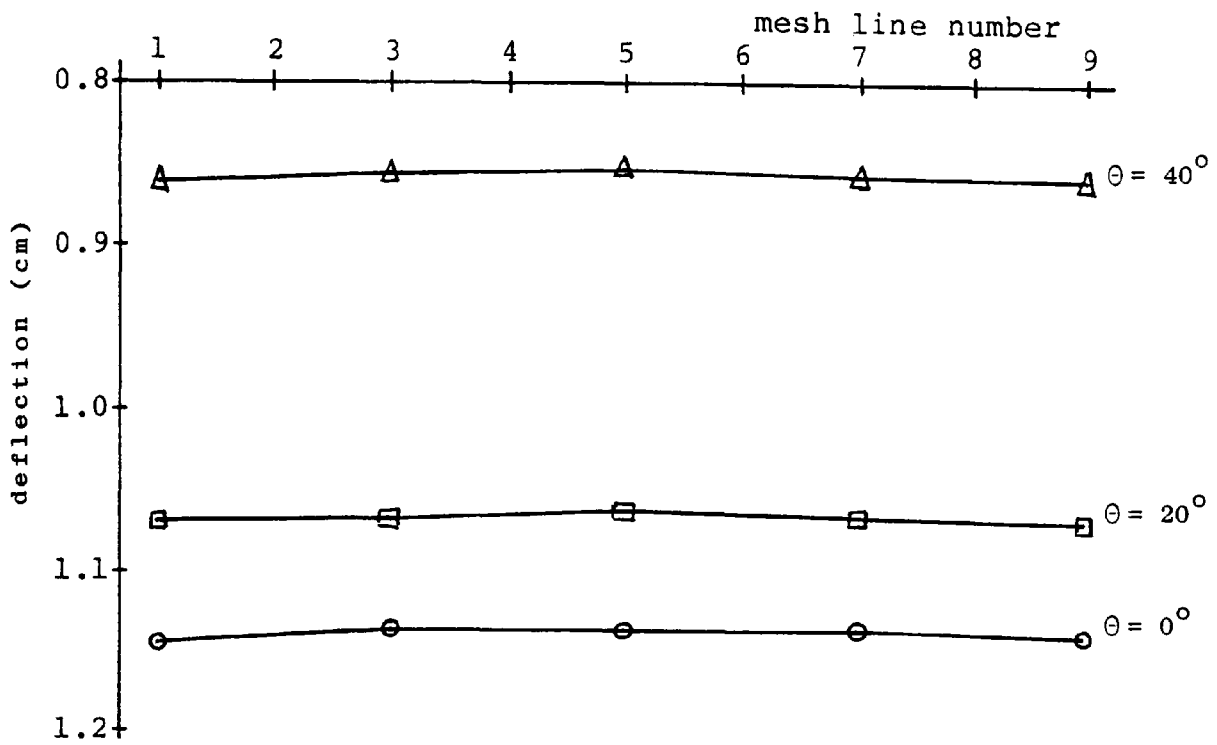


(a) Midspan.



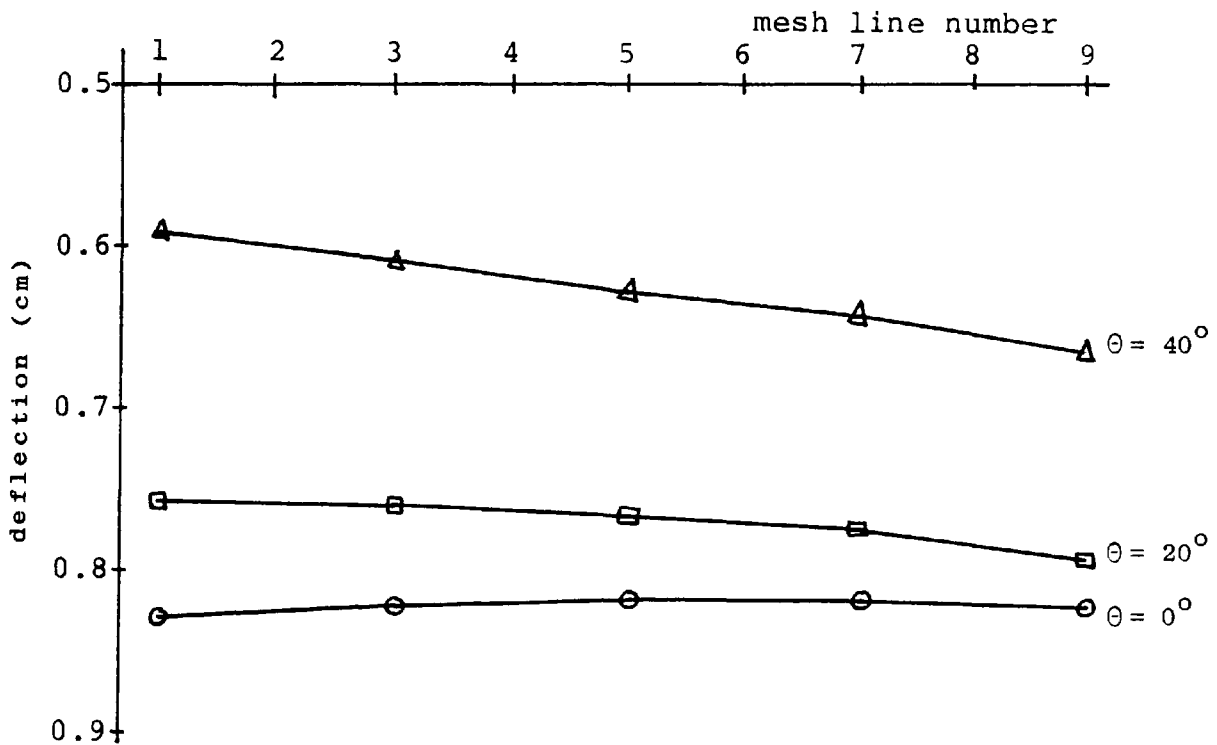
(b) Quarterspan.

FIGURE 6.17 - VERTICAL DEFLECTION PROFILE OF TOP FLANGE
MIDSPAN AND QUARTERSPAN CROSS-SECTIONS
MIDSPAN POINT LOADING.
END, QUARTERSPAN AND MIDSPAN DIAPHRAGMS.



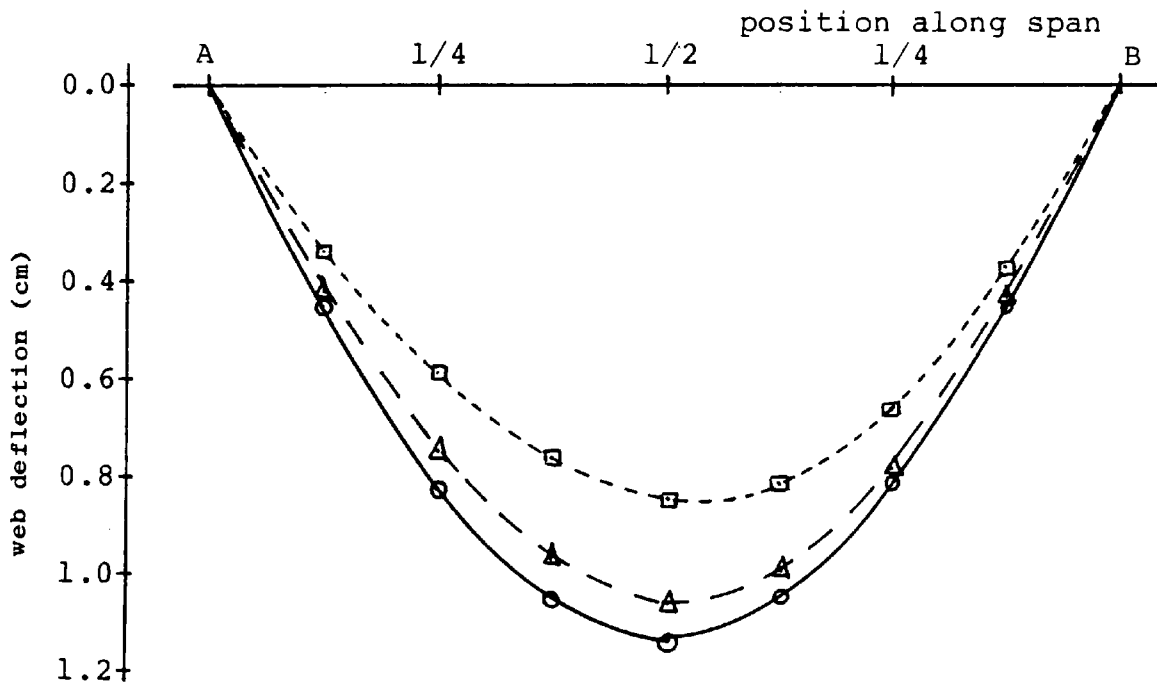
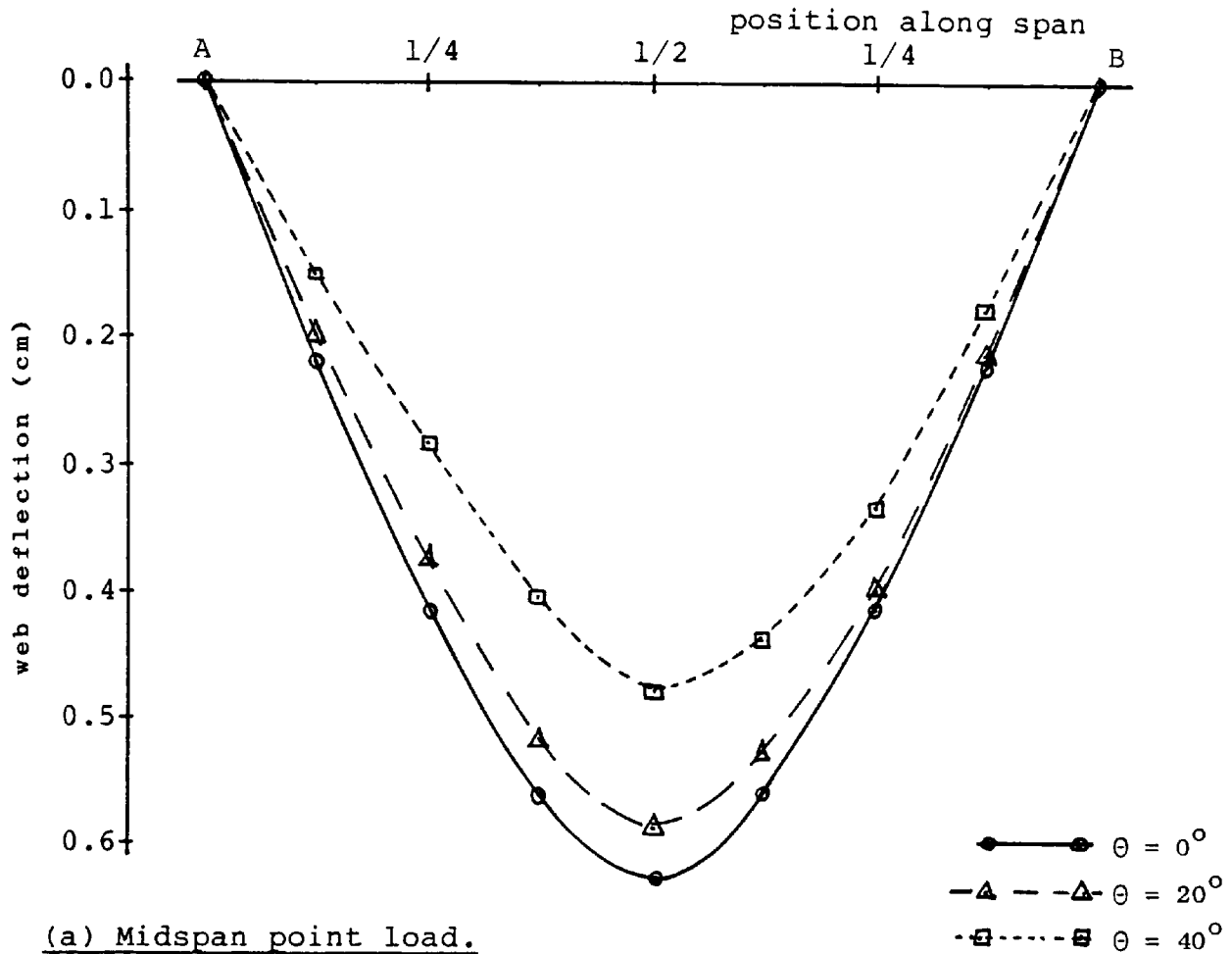
(a) Midspan.

θ = angle of skew



(b) Quarterspan.

FIGURE 6.18 - VERTICAL DEFLECTION PROFILE OF TOP FLANGE
MIDSPAN AND QUARTERSPAN CROSS-SECTIONS
UNIFORM LINE LOADING.
END, QUARTERSPAN AND MIDSPAN DIAPHRAGMS.



(b) Uniform line load.

FIGURE 6.19 - WEB DEFLECTION VARIATION ALONG SPAN
 MIDSPAN POINT AND UNIFORM LINE LOADING.
 END, QUARTERSPAN AND MIDSPAN DIAPHRAGMS.

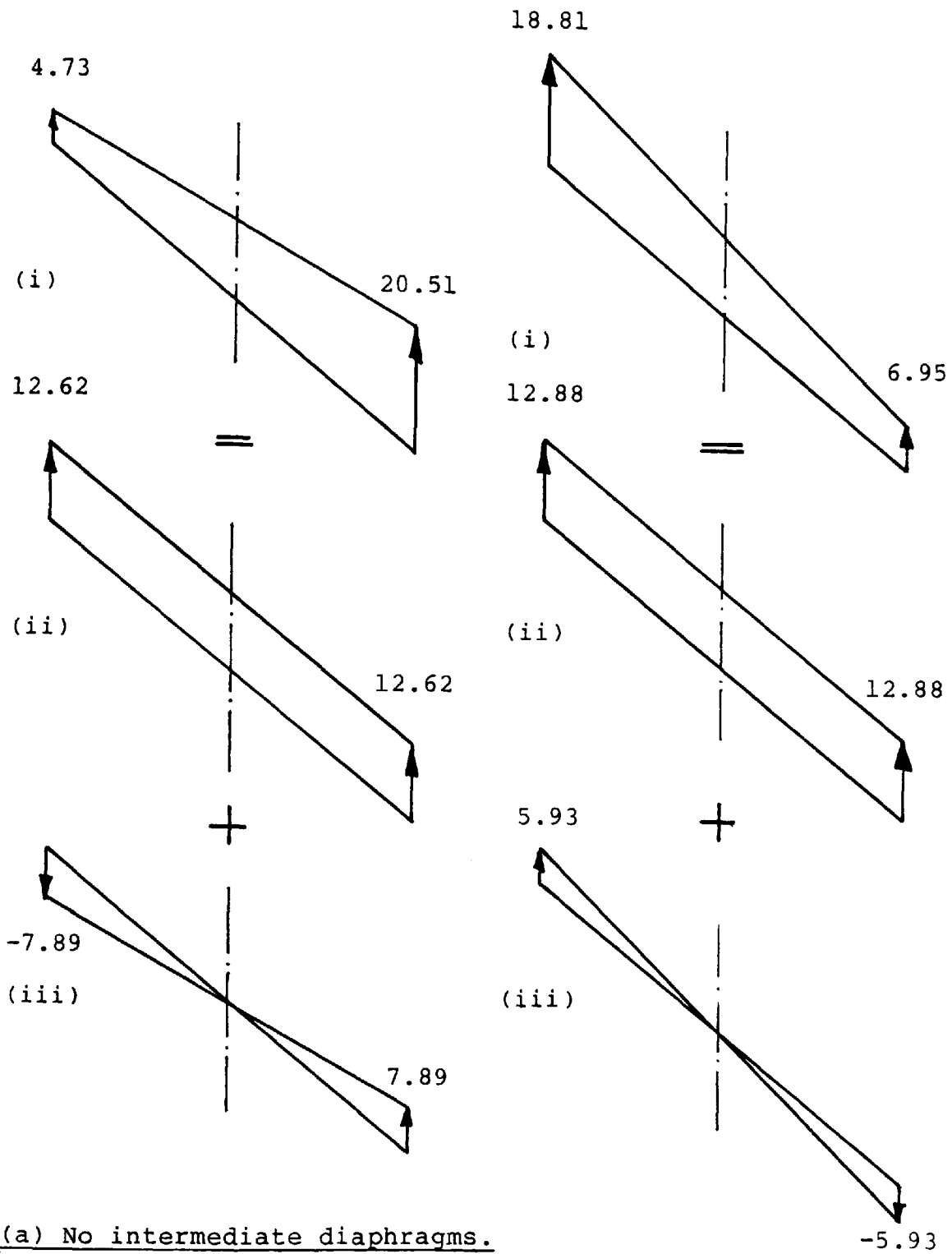
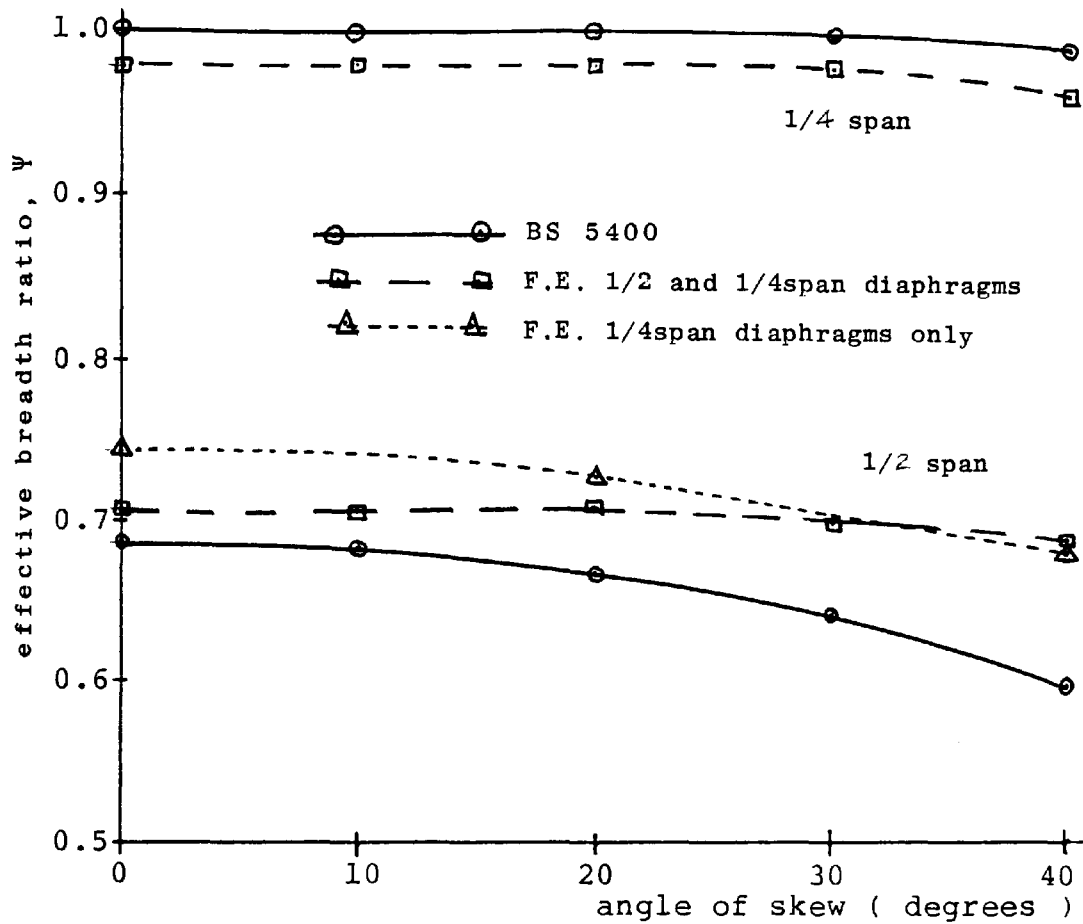
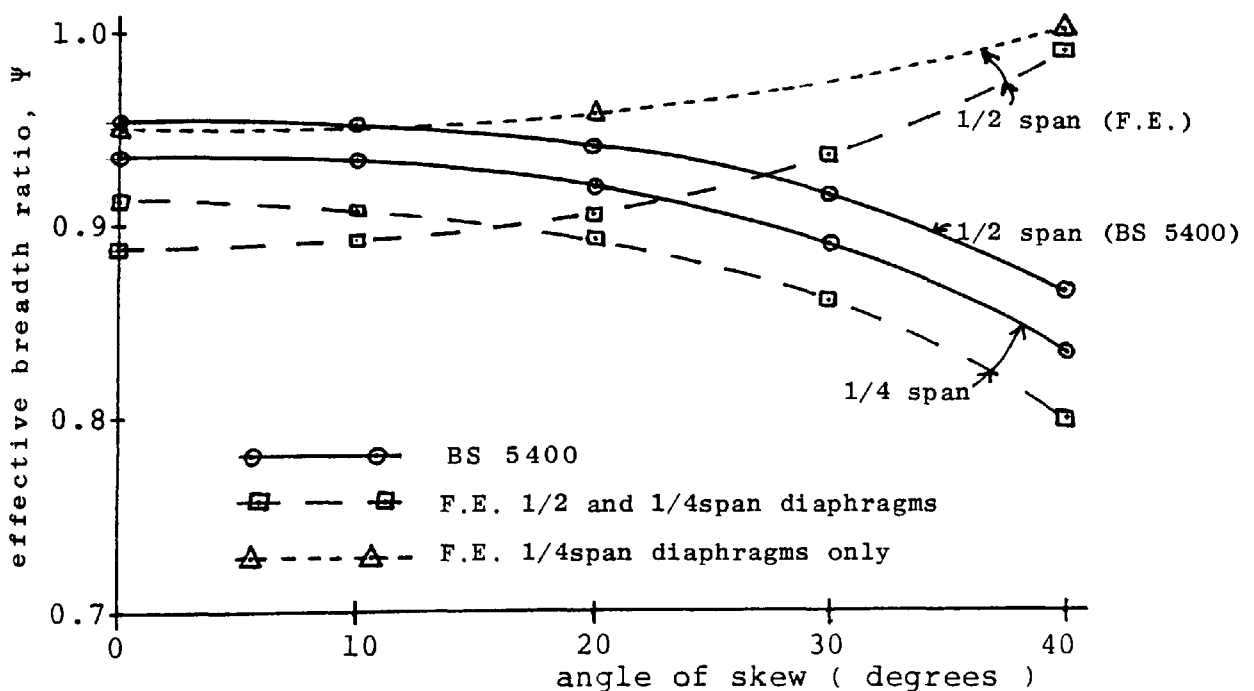


FIGURE 6.20 - LONGITUDINAL FLANGE STRESS DISTRIBUTION AT QUARTERSPAN CROSS-SECTION. MIDSPAN POINT LOADING, 40 DEGREE SKEW. (i) ACTUAL, (ii) BENDING COMPONENT (iii) TORSIONAL COMPONENT.

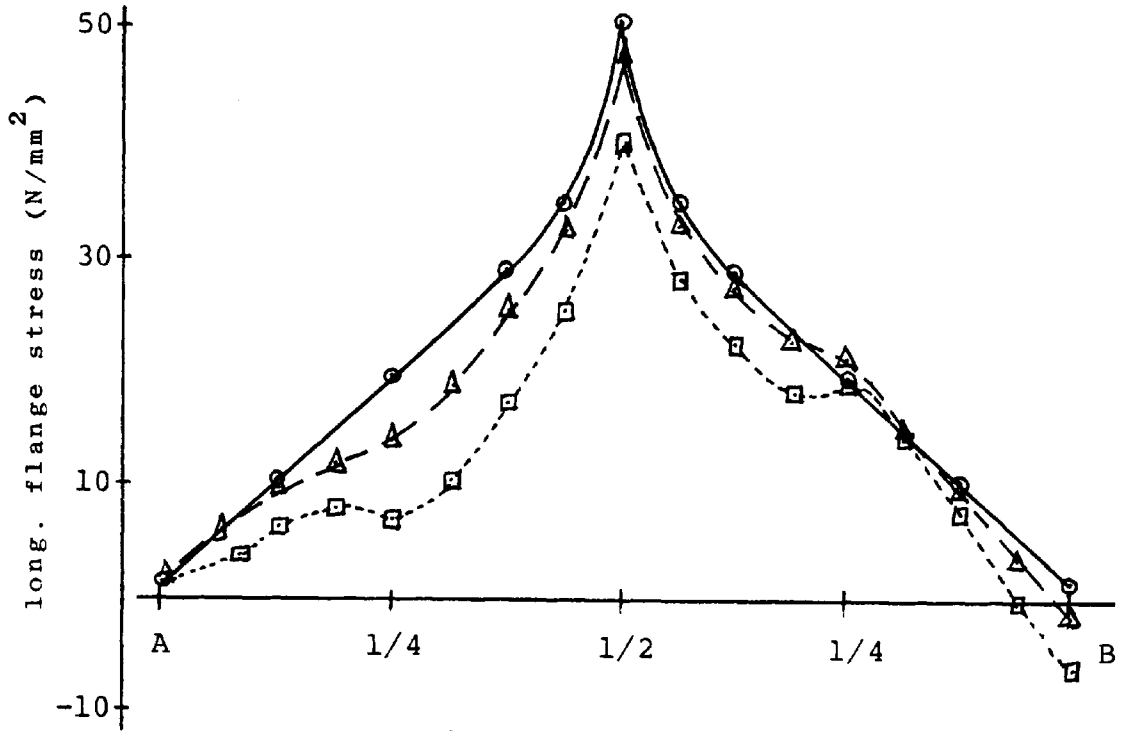


(a) Midspan point load.

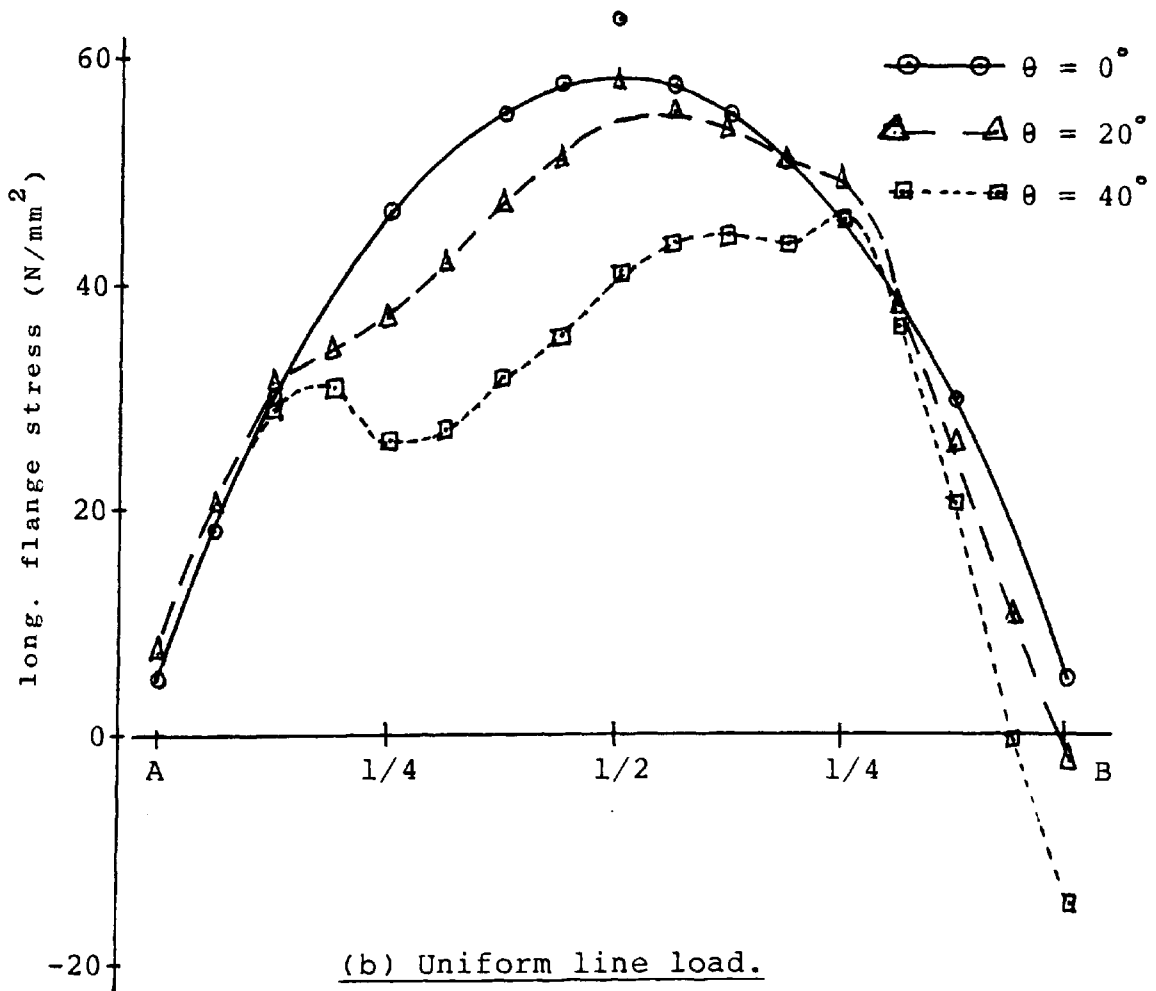


(b) Uniform line load.

FIGURE 6.21 - VARIATION OF EFFECTIVE BREADTH RATIO WITH ANGLE OF SKEW. END, QUARTERSPAN AND MIDSPAN DIAPHRAGMS. END AND QUARTERSPAN DIAPHRAGMS.



(a) Midspan point load.



(b) Uniform line load.

FIGURE 6.22 - LONGITUDINAL FLANGE STRESS VARIATION ALONG EDGE OF TOP FLANGE. END, QUARTERSPAN AND MIDSPAN DIAPHRAGMS.

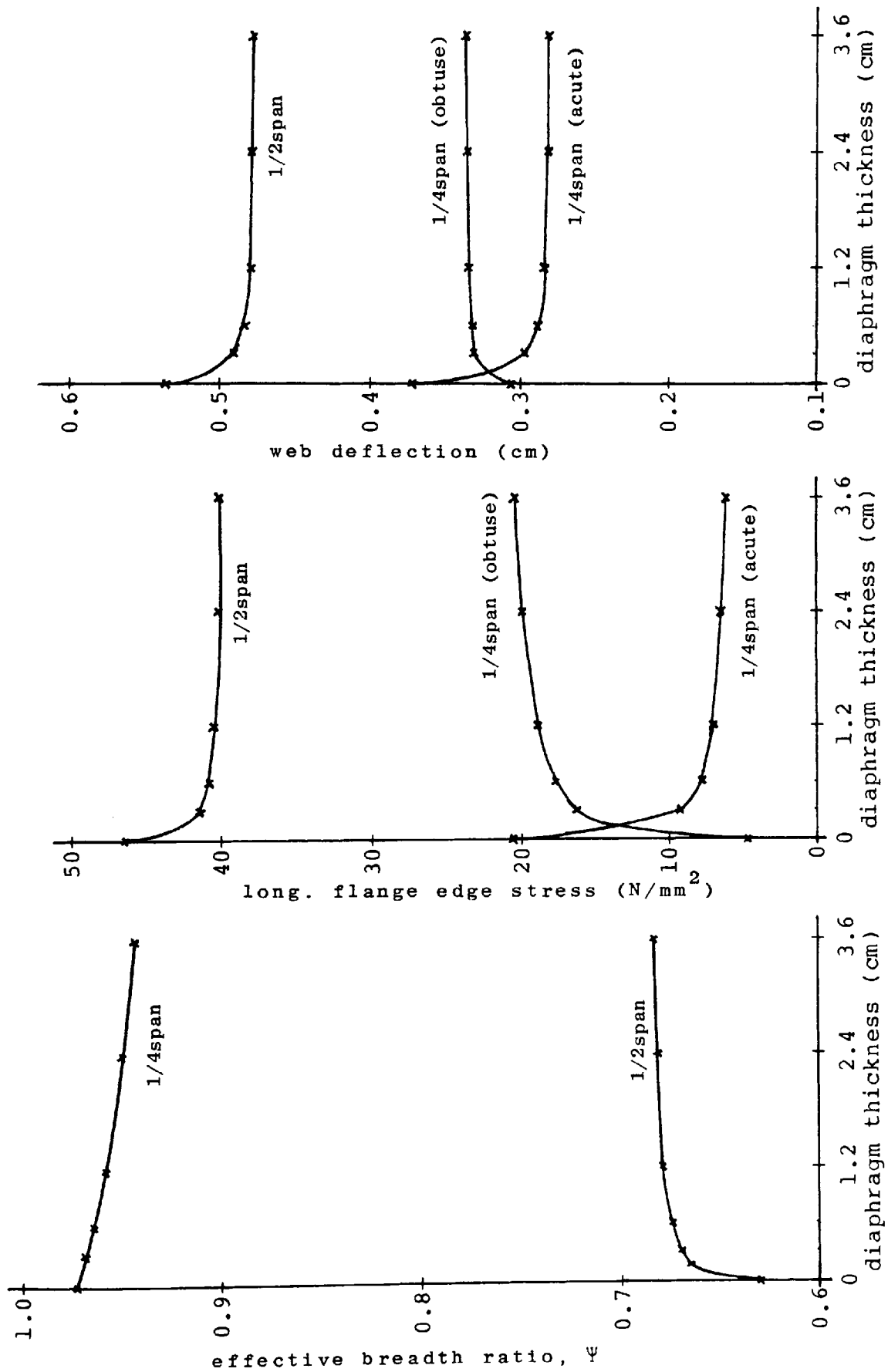


FIGURE 6.23 - VARIATION OF EFFECTIVE BREADTH RATIO, LONG. FLANGE STRESS AND WEB DEFLECTION WITH QUARTERSPAN DIAPHRAGM THICKNESS. 40 DEGREE SKEW, MIDSPAN POINT LOADING.

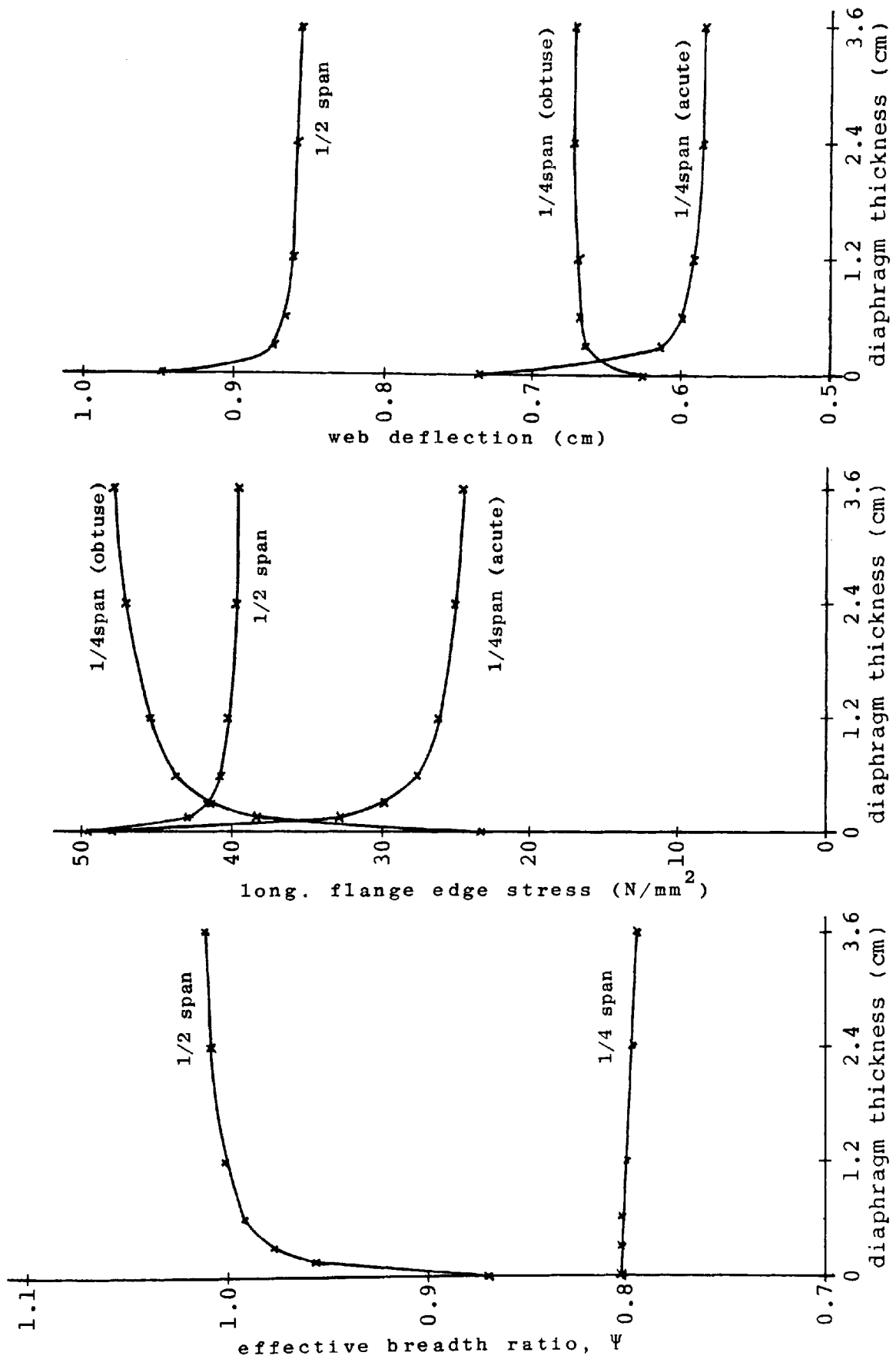


FIGURE 6.24 - VARIATION OF EFFECTIVE BREADTH RATIO, LONG. FLANGE STRESS AND WEB DEFLECTION WITH QUARTERSPAN DIAPHRAGM THICKNESS. 40 DEGREE SKEW, UNIFORM LINE LOADING.

CHAPTER SEVEN

GRILLAGE ANALYSIS OF SKEW MULTI-CELL STRUCTURES

7.1. INTRODUCTION.

This chapter will consider the grillage analysis of skew multi-cell structures. The recommendations for the analysis of straight multi-cell structures developed in chapter five and the conclusions reached from the finite element analysis of skew single cell structures in chapter six will form the basis for analysis.

It is well established that skew has a considerable effect on a structure's behaviour, which in the case of torsionally stiff multi-cell structures will result in the development of significant stresses and deflections associated with torsional action. The torsional idealization of multi-cell structures using the grillage method was considered in chapter four. This study revealed the limitations of the grillage method when high torsional effects were developed in straight structures under the action of asymmetrical loading.

The significance of these limitations on the ability of the grillage method to predict the web deflection and longitudinal flange stress values in skew structures to an acceptable degree of accuracy will be investigated in this chapter.

The grillage method has been used for a number of years in design offices for the analysis of skew

structures. It is a popular method of analysis and its application to the analysis of slab and pseudo-slab bridge decks has been extensively researched. WEST (1973) proposed that skew structures may be analysed with a grillage having either a skew or orthogonal mesh arrangement as shown in figure 7.1. In both mesh layouts the longitudinal grillage beams are parallel to the free edge, whilst the transverse grillage beams are either parallel to the skew support (skew mesh) or perpendicular to the longitudinal beams (orthogonal mesh).

The skew mesh represents the simplest geometrical layout, which permits the use of automatic mesh generation at the input stage. However, the method of apportioning the appropriate stiffness parameters to the longitudinal and transverse members is questionable, especially in the case where the overall torsional stiffness of the structure has to be apportioned to the longitudinal and transverse grillage beams.

In the study conducted by the HECB (1981) on the analysis of skew slab structures, it was concluded that skew grillages do not behave like skew plates and that the difference in behaviour is very pronounced for skew angles in excess of 15 degrees. This study revealed that the skew grillage predicted the longitudinal (or spanwise) bending moment reasonably accurately (17% difference at a skew angle of 60 degrees when compared to a finite element solution). However, the transverse bending moment and twisting moment exhibited substantial discrepancies.

In the skew grillage case the slab transverse bending moment and twisting moment are derived from the bending moment values in the transverse grillage beams and the torsion moment values from both the longitudinal and transverse grillage beams. The method whereby the grillage beam bending and torsion moments are averaged and resolved into the appropriate orthogonal directions does not adequately represent the different underlying structural behaviour between the two structures.

CLARK (1970) showed that in skew slab decks the grillage members should be placed parallel to the designed lines of strength, which are usually orthogonal. He concluded that the appropriate arrangement of steel reinforcement was dependent on the aspect ratio and degree of skew of the deck.

In the case of multi-cell structures the presence of longitudinal webs ensures that the predominant bending action is parallel to the free edge. Longitudinal grillage beams will be used to model these longitudinal webs in the usual manner. Transverse modelling will be considered using both skew and orthogonal mesh arrangements, and recommendations presented for the accuracy of both longitudinal flange stress and web deflection values at both the midspan and quarterspan cross-sections. The longitudinal flange stress values may be obtained from the bending moment values in the longitudinal grillage beams in the usual manner.

7.2. FINITE ELEMENT ANALYSIS OF THREE CELL STRUCTURE.

In the analysis of straight multi-cell structures the accuracy of the grillage method was compared to results obtained from a finite element study using the program QUEST. This procedure will again be followed in this chapter for the analysis of skew multi-cell structures. However, the complete structure has to be analysed in the skew case, which will limit the fineness of the mesh used to model the structures.

In order to assess the validity of the finite element results a convergence study was undertaken on the three-cell structure shown in figure 7.2. The appropriate details being

skew span , L	=	1600cm.
overall width, B	=	900cm.
overall depth, D	=	150cm.
skew angle, θ	=	40 degrees.
flange thickness, t_f	=	1.2cm.
web thickness, t_w	=	1.2cm.
end diaphragm thickness, t_d	=	1.2cm.

The structure was subjected to midspan point loads over all four webs, the load intensities being 300 kN and 600 kN over the outer and inner webs respectively.

Three analyses were considered using the following mesh details

number of elements along span	=	20
number of elements in depth	=	1
number of elements across width	=	2, 3, and 4 per cell

The mesh used in the third analysis is shown in figure 7.3. The total number of nodal points of 546 exceeded the maximum of 450 permitted in the standard program, and consequently the program had to be amended before the solution could be achieved. The results for longitudinal flange edge stress and web deflection at the quarterspan and midspan cross-sections are presented in Table 7.1.

Consideration of these results indicates that

1. The web deflection values at both cross-sections reveal close agreement in all three analyses, the maximum variation being less than 5%.
2. The longitudinal flange edge stress at the quarterspan cross-section also reveal close agreement. In this case the maximum variation was less than 6%.
3. At the midspan cross-section the longitudinal flange edge stress variation was about 9% for the three analyses. This variation is consistent with previous observations at this position, the stress intensity being influenced by the concentrated load applied at this location.
4. The distribution of longitudinal flange stress is shown plotted in figure 7.4 for both the midspan and quarterspan cross-sections. The stress distribution at quarterspan is approximately linear, which is consistent with the effective breadth ratio of unity at this cross-section.

The distribution at the midspan cross-section shows the presence of the shear lag effect at this location. The effective breadth ratio for the central box section was shown to be 0.658, which compares favourably with the values of 0.630 from the single cell study and 0.598 from Table 13, Part 3 of BS 5400.

The results from this study show that the program QUEST is capable of predicting the longitudinal flange stress and web deflection values to an acceptable degree of accuracy when the finite element mesh is defined within the limits set by the maximum number of nodal points of 450. All subsequent finite element analyses in this chapter will be carried out within these limits, with the exception of the results presented in Sections 7.3.1 and 7.3.2.

7.3. GRILLAGE ANALYSIS OF THREE-CELL STRUCTURE.

This section will consider the grillage analysis of the three-cell structure analysed in the previous section and defined in figure 7.2. The analysis will be accomplished using both a skew mesh and an orthogonal mesh arrangement.

7.3.1. SKEW MESH IDEALIZATION.

In the skew mesh idealization four longitudinal grillage beams were used, each one representing a longitudinal web of the multi-cell structure in the usual manner. In the transverse direction the internal grillage beams are used to represent the top and bottom flange

plates, and any number may be used. Three mesh arrangements were considered where transverse idealization was accomplished using 5, 9 and 13 grillage beams, thus allowing the relationship between number of transverse beams and accuracy of solution to be established.

The arrangement of the 4x13 grillage mesh is shown in figure 7.5, and solution was achieved using the program GRIDS developed by the author. This program automatically generates the mesh from the basic definition of the structure in terms of the span, overall width, skew angle, number of cells, and the number of longitudinal and transverse grillage beams.

7.3.1.1. CALCULATION OF SECTION PROPERTIES FOR 4x13 MESH.

The sectional idealization will be established using the recommendations developed for straight multi-cell structures in chapters three and four.

It was established in Section 6.3.5. that the effective breadth ratio for deflection calculations be determined from Table 4, Part 3 of BS 5400 on the basis of the $b/L(\cos\theta)^2$ ratio, i.e. $150/1600(\cos 40)^2 = 0.16$

$$\text{giving } \psi = 0.834$$

SECOND MOMENT OF AREA.

Longitudinal grillage beams.

$$\begin{aligned} \text{Outer beam} &= I(\text{web}) + I(\text{flange}) \\ &= \frac{1.2 * 150^3}{12} + 2 * 0.834 * 150 * 1.2 * 75^2 \end{aligned}$$

$$= \underline{2\,026\,350\text{ cm}^4}$$

$$\text{Inner beam} = \underline{3\,715\,200\text{ cm}^4}$$

Transverse grillage beams.

In the transverse direction equation 3.11 is used where the width of the flange plate represented by the grillage beams is related to the square span direction. Each internal grillage beam is assumed to represent

$$\frac{1600 * \cos 40}{12} = 102\text{cm of flange}$$

$$\text{Inner beam} = 2 * 102 * 1.2 * 75 * 75$$

$$= \underline{1\,377\,000\text{ cm}^4}$$

$$\text{Outer beam} = I(\text{diaph}) + I(\text{flange})$$

$$= 337\,500 + 688\,500$$

$$= \underline{1\,023\,000\text{ cm}^4}$$

EFFECTIVE SHEAR AREA.

Longitudinal grillage beams.

$$A_s = \text{c.s.a. of web}$$

$$= \underline{180\text{ cm}^2}$$

Transverse grillage beams.

Outer beam.

$$A_s = \text{c.s.a. of diaphragm} = 180\text{ cm}^2$$

Inner beam.

Equation 3.16 is used with an adjustment for the skew length of the grillage beam.

$$A_s = \frac{1.2^3 + 1.2^3}{300^2 (\cos 40)} \left[\frac{1.2^3 * 300}{1.2^3 * 300 + (1.2^3 + 1.2^3) * 150} \right] * 2.6$$

$$= 0.0000653\text{ cm}^2 / \text{cm of flange}$$

$$= 0.0067\text{ cm}^2 \text{ per grillage beam}$$

TORSIONAL INERTIA.

Torsional Inertia of cross-section (Eqn 4.7)

$$= 41\ 657\ 143\ \text{cm}^4$$

Considering that the ratio of overall breadth to square span is used to determine the percentage allocation of torsional inertia to the longitudinal grillage beams

$$\frac{\text{overall breadth}}{\text{square span}} = \frac{900}{1600\cos 40} = 0.734$$

Longitudinal grillage beams.

$$\begin{aligned} J(\text{long}) &= \frac{0.734 * 41\ 657\ 143}{4} \\ &= \underline{7\ 647\ 000\ \text{cm}^4} \end{aligned}$$

Transverse grillage beams.

$$\begin{aligned} J(\text{tran}) &= \frac{(1 - 0.734) * 41\ 657\ 143}{13} \\ &= \underline{852\ 370\ \text{cm}^4} \end{aligned}$$

7.3.1.2. INTERPRETATION OF RESULTS.

The grillage analysis of the 4x13 skew mesh produced the following values of bending moment in the longitudinal grillage beams at nodes 13 and 26 (figure 7.5).

Node 13.

member 18 - 41544 kNcm
member 25 - 42236 kNcm
average - 41890 kNcm

Node 26.

member 41 - 201083 kNcm
member 48 - 201083 kNcm

The effective breadth ratios for stress calculations are determined from Table 13, Part 3 of BS 5400 as follows

At midspan.

$$\frac{b}{L(\cos\theta)^{3/2}} = \frac{150}{1600(\cos 40)^{3/2}} = 0.14$$

hence $\Psi = 0.598$ and $I(\text{inner}) = 2\,759\,400 \text{ cm}^4$

At quarterspan.

$$\frac{b}{L(\cos\theta)^2} = \frac{150}{1600(\cos 40)^2} = 0.16$$

hence $\Psi = 0.988$ and $I(\text{outer}) = 2\,338\,200 \text{ cm}^4$

The longitudinal flange edge stresses are

At midspan (node 26).

$$\text{Web 2} = \frac{201083 * 75 * 10}{2\,759\,400} = 54.65 \text{ N/mm}^2$$

At quarterspan (node 13).

$$\text{Web 1} = \frac{41890 * 75 * 10}{2\,338\,200} = 13.44 \text{ N/mm}^2$$

The longitudinal flange edge stress and web deflection values are presented in Table 7.2 for all three grillage analyses.

The results indicate that the use of the "modified shear area" method to model transverse deformation of the cross-section produces symmetrical values for both deflection and stress at the quarterspan cross-section. Although the loading is symmetrical and skew symmetry exists in the geometry of the structure, no such symmetry exists at this cross-section.

The use of the low effective shear area in the transverse grillage beams tends to reduce the transverse distribution of loading throughout the structure. This

results in the longitudinal grillage beams acting as individual beams spanning along the skew span, and thus producing this symmetrical behaviour.

There was no significant variation in either the web deflection or longitudinal flange edge stress values for the three grillage mesh arrangements, which supports the view that the structure tends to span in the direction of the longitudinal grillage beams. The grillage method was unable to predict the deflection or stress intensities to an acceptable accuracy. At the midspan cross-section the web deflection was overestimated by 18.8%, whilst the longitudinal stress was overestimated by 32.2%.

The analysis using the three skew mesh arrangements was repeated with the effective shear area of the transverse grillage beams set to zero, i.e. modelling of cross-section deformation was removed from the grillage idealization. The results of these analyses are also presented in Table 7.2.

These results were more accurate than the previous set of results for the following reasons.

1. The deflection and stress values at the quarterspan cross-section were not symmetrical, indicating that the grillage model was tending to behave as expected.
2. The accuracy of the grillage solution improved with the use of more grillage beams in the transverse direction. The results for the 4x9 mesh were a little less

accurate than the 4x13 mesh, indicating that acceptable results can be achieved using a fairly coarse mesh arrangement.

3. The web deflection values at the midspan cross-section revealed an overestimation of +5.0% and an underestimation of -0.7% when compared to the finite element values. At the quarterspan cross-section the results were less accurate, the overestimation and underestimation being +24.4% and -7.6% respectively. This is attributable to the inability of the grillage method to model the transverse distortion that takes place at the quarterspan cross-section in the skew structure.
4. The longitudinal flange edge stress values at the midspan cross-section were overestimated by +6.1% and +6.9% when compared to the finite element values. However, the stresses at the quarterspan cross-section were seriously over and under estimated, the greatest disagreement occurring at the outer web positions consistent with the poor distortional modelling of the grillage method.

The two series of grillage analyses considered with a skew mesh arrangement were undertaken using the ratio of overall breadth to square span to allocate the torsional inertia of the cross-section to the longitudinal grillage beams. In order to assess the validity of this decision an investigation was carried^{out} using the 4x13 skew mesh where the distribution of torsional inertia between

the longitudinal and transverse grillage beams was varied.

Four ratios were considered namely 50/50, 60/40, 70/30 and 80/20. The results for web deflection and longitudinal flange edge stress are presented in Table 7.3. These results confirm the validity of the use of the overall breadth to square span ratio (0.734) to allocate the torsional inertia of the cross-section to the longitudinal grillage beams.

7.3.2. ORTHOGONAL MESH IDEALIZATION.

In the orthogonal mesh idealization four longitudinal beams will again be used to represent the longitudinal webs of the multi-cell structure. The number and position of orthogonal transverse beams will be dependent on the geometry of the structure. The orthogonal mesh used to analyse the 40 degree skew, three-cell structure is shown in figure 7.6.

The number and variable centres of the transverse beams results from the necessity for joints to be positioned at the quarterspan and midspan cross-sections in each longitudinal beam in order that deflection and member forces may be obtained at these locations for comparison. This results in a mesh arrangement which cannot be easily generated automatically. The grillage analysis was undertaken using the general stiffness program STRESS.

7.3.2.1. CALCULATION OF SECTION PROPERTIES.

The sectional idealization will be established using the recommendations for straight multi-cell structures in chapters three and four. No deviations from these recommendations will be necessary to allow for the skew nature of the structure, other than the need to distribute the section properties to the transverse grillage beams in accordance with the varying width of flange modelled by each beam.

SECOND MOMENT OF AREA.

Longitudinal grillage beams.

Outer beam = 2 232 900 cm⁴

Inner beam = 4 128 300 cm⁴

Transverse grillage beams.

Outer beam (diaphragm) = 337 500 cm⁴

Inner beam = 1 350 000 cm⁴ per metre of flange.

EFFECTIVE SHEAR AREA.

Longitudinal grillage beams.

As = 180 cm²

Transverse grillage beams.

Outer beam (diaphragm) = 180 cm²

Inner beam = 0.005 cm² per metre of flange.

TORSIONAL INERTIA.

In the case of the orthogonal mesh the ratio of overall breadth/ skew span = $900/1600 = 0.5625$ is used to allocate the torsional inertia of the cross-section to the longitudinal grillage beams.

Then Torsional Inertia of longitudinal beams

$$= \frac{0.5625 * 41\ 657\ 143}{4} = 5\ 858\ 035\ \text{cm}^4$$

and Torsional Inertia in transverse direction

$$= \frac{(1 - 0.5625) * 41\ 657\ 143}{16}$$
$$= 1\ 139\ 062\ \text{cm}^4\ \text{per metre of flange.}$$

7.3.2.2. INTERPRETATION OF RESULTS.

The longitudinal flange edge stress values at the midspan and quarterspan cross-sections are determined in the usual manner, where the effective breadth ratios for stress calculations are based on the b/L ratio. Preliminary investigations had shown it unnecessary to make any adjustment to this ratio for the effect of skew when using an orthogonal mesh. The values of web deflection and longitudinal flange edge stress are presented in Table 7.4.

The results were an improvement on the earlier skew mesh results for the following reasons.

1. The web deflection values at the quarterspan cross-section were considerably improved, the percentage difference between the orthogonal mesh

grillage and the finite element analyses being within the range -4.4% to +6.8%.

2. At the midspan cross-section there was very close agreement in the web deflection values, the percentage difference being within the range -1.8% to +2.7%. The orthogonal mesh grillage was marginally more accurate than the skew grillage results when compared to the finite element values.
3. At the midspan cross-section, the intensity of longitudinal flange edge stress at the inner web position was 43.82 N/mm². This value was exactly the same as that for the 4x13 skew mesh grillage analysis, and represents a 6.0% overestimation of the finite element value of 41.32 N/mm². At the outer web position the orthogonal mesh grillage slightly underestimated the stress, the value of 41.70N/mm² being 0.9% less than the finite element value of 42.08N/mm².
4. The longitudinal flange edge stress values at the quarterspan cross-section were less accurate, the percentage difference being within the range -9.9% to +58.9%. These results, although still disappointing, represent a significant improvement over the skew mesh grillage analysis.

7.3.3. DISCUSSION OF RESULTS FROM GRILLAGE ANALYSIS.

The results from the initial grillage analysis of the 40 degree skew, three cell structure, using both a skew and orthogonal mesh arrangement, were generally encouraging.

Both analyses accurately predicted the web deflection values at the midspan cross-section. At the quarterspan cross-section the results were less accurate and this reduction in accuracy can be attributed to the poor modelling characteristics of the grillage method with respect to cross-sectional distortion.

The variation of deflection along the inner and outer webs are plotted in figure 7.7, for the finite element and both grillage analyses. These profiles indicate that the greatest discrepancy occurs in the outer web in the obtuse corner region, this being the region where the twisting or torsional effects are expected to be greatest.

The variation of longitudinal flange edge stress at both the inner and outer webs are plotted in figure 7.8 for all three analyses. The profiles also indicate that the greatest discrepancy occurs at the outer web in the obtuse corner region. The grillage method was unable to predict the significant hogging moments developed in this region. The orthogonal grillage results are more consistent for all positions along the span for the outer web; the web where the greatest variation was observed.

The distribution of longitudinal flange stress

across the midspan and quarterspan skew sections are shown plotted in figure 7.4. for all three analyses. The intermediate flange stress values were calculated using equation 5.6. for both grillage analyses. The distribution of stress across the quarterspan cross-section confirms the greater accuracy of the orthogonal mesh grillage analysis, and also the poor distortional modelling of the skew mesh grillage analysis.

This initial study confirmed that both methods of analysis produced encouraging results for the determination of web deflections and longitudinal flange stresses. On the one hand, the orthogonal mesh analysis produced results of greater accuracy, whereas the skew mesh analysis was far easier and faster to execute.

The accuracy of both methods for the analysis of skew multi-cell structures subjected to a variety of load conditions will be considered in the next section.

7.3.4. CONSIDERATION OF LOADING.

In the earlier section the grillage method using orthogonal and skew mesh idealizations successfully analysed the 40 degree skew, three cell structure subjected to midspan point loading over all webs. Additional loading conditions were then considered, where the results from both grillage analyses were compared with those from a finite element analysis. The limitation of problem size only allowed the use of three elements across the width of each cell in the finite element idealization.

7.3.4.1. MIDSPAN POINT LOAD.

Two additional midspan point load cases were considered, namely

- (i) 300 kN over both outer webs.
- (ii) 600 kN over both inner webs.

The structure details were unchanged and both grillage mesh idealizations were considered.

The results from all three analyses are presented in Table 7.5 for both loading cases together with the initial load condition where all four webs were loaded.

The skew mesh idealization produced unacceptable results for both web deflection and longitudinal flange edge stress in both load cases considered. In this analysis the effective shear area of the transverse grillage beams was taken as zero, as indicated in Section 7.3.1.2., resulting in a grillage that was unable to model the cross-sectional distortion of the structure under these two loading conditions.

Further analysis where the appropriate effective shear area was re-introduced improved the results for web deflection, but the values for flange stress were still unacceptable.

It was concluded from this investigation that the use of a skew mesh using the idealization methods proposed was inappropriate except in the case where all webs are loaded, thereby producing relatively uniform web deflections over the full width of the cross-section.

The orthogonal mesh results were more accurate than those from the skew mesh analysis and warrant detailed discussion.

It was concluded in chapter five that for straight multi-cell structures the grillage method was able to predict the web deflection and longitudinal flange stress values at loaded web positions to an acceptable degree of accuracy for initial design purposes, and also was able to model the cross-sectional deformation of the structure. This will be the criterion whereby the method will be assessed for skew structures.

Consideration of the orthogonal mesh grillage results produced the following conclusions.

LONGITUDINAL FLANGE EDGE STRESS.

The distributions of longitudinal flange stress at both the midspan and quarterspan cross-sections are plotted in figures 7.9 and 7.10 for both outer web and inner web loading.

1. When both inner webs were loaded, the longitudinal flange edge stress at the loaded web was 37.28 N/mm² for the midspan cross-section. This represents an overestimation of 3.3% of the finite element value of 36.10 N/mm². The midspan longitudinal flange stress at the outer webs when these webs were loaded was underestimated by 18%, the grillage and finite element values being 28.37 N/mm² and 34.60 N/mm² respectively.

2. At the quarterspan cross-section the predicted values of stress were less accurate than at the midspan cross-section. Again the inner web load case results were more accurate than the outer web load case. Percentage errors of 109% were observed in the latter case, but the stress intensities were very low, only 3.22 N/mm² and 6.73 N/mm² from the finite element and grillage method respectively, and would not influence the girder design.
3. The longitudinal flange stress distributions plotted in figures 7.9 and 7.10 highlight the rapid variation of stress across the cross-section. It was considered that the grillage method predicted the distribution of stress reasonably successfully when one considers the severity of the imposed load conditions.
4. A possible explanation for the variation in accuracy between both load cases is that outer web loading produces hogging moments in the transverse direction, whilst inner web loading produces sagging moments in the transverse direction. Earlier investigations had shown that the grillage method was unable to predict with accuracy the hogging moments developed in the obtuse corner regions of the skew structure. Hence loading conditions which reduce the hogging effects of the skew geometry are more accurately analysed by the grillage method than those which enhance these hogging effects.

WEB DEFLECTION.

The deflection profiles at the midspan and quarterspan cross-sections are shown plotted in figure 7.11. These profiles indicate the severe cross-sectional distortion developed by the load cases considered.

5. The web deflections were consistently underestimated at the loaded web position and overestimated at the unloaded web position.
6. In the Inner web load case the loaded web deflections were accurately predicted by the grillage method, the underestimation being within the region of -2.0% and -4.3% at both the midspan and quarterspan cross-sections. Greater discrepancies in the region of -12.8% and -27.2% were observed at the loaded web position for the Outer web load case.
7. It was considered that the grillage method was able to predict to a satisfactory degree of accuracy for initial design purposes the cross-sectional distortion of the structure under the severe loading and skew conditions considered in this investigation.

7.3.4.2. UNIFORM LINE LOAD.

Three uniform line load cases were considered, namely

- (i) 600 kN over both outer webs, and
1200 kN over both inner webs.
- (ii) 600 kN over both outer webs.
- (iii) 1200 kN over both inner webs.

The structure details were unchanged. The results from the orthogonal mesh grillage and the finite element analyses are presented in Table 7.6. The distribution of longitudinal flange stress for load cases two and three are plotted in figures 7.12 and 7.13. The corresponding deflection profiles at the midspan and quarterspan cross-sections are plotted in figure 7.14.

These results may be summarized as follows

1. The longitudinal flange stresses and web deflections were accurately predicted by the grillage method for load case one, the percentage difference between the grillage and finite element method being less than 10% for all but one of the presented values. The longitudinal flange stress at the quarterspan cross-section in the obtuse corner web showed an overestimation of +28.2%.
2. In load case three, the longitudinal flange stress and web deflections were accurately predicted at the loaded web positions. Again the percentage difference between the two methods of analysis was less than 10% in all cases.
3. In load case two, the results were less accurate. The midspan cross-section values of longitudinal flange stress and web deflection were underestimated by the grillage method. The percentage differences were -24.7% and -20.9% respectively.

4. The results for all three load cases were consistent with those for the midspan point loading. The web deflection values were underestimated at loaded web positions and overestimated at unloaded web positions. The deflection profiles plotted in figure 7.14 confirm the severity of the loading conditions considered and the ability of the grillage method to model the deformation of the cross-section reasonably accurately, especially when the loading tended to produce transverse sagging moments.

5. The longitudinal flange stress distribution shown plotted in figures 7.12 and 7.13 show that the grillage method was able to predict the stress intensity at the inner web positions accurately, but was less accurate at the outer web positions.

7.4. ANALYSIS OF FOUR CELL STRUCTURE.

The analysis of the three cell structure in Section 7.3 had shown that the orthogonal mesh grillage idealization was the most appropriate for the analysis of skew multi-cell structures. The geometry of the mesh used in the analysis, and detailed in figure 7.6, was governed by the necessity to have joints at positions where bending moment and deflection values were required for comparison purposes. This resulted in the use of eighteen transverse grillage beams, and a structure consisting of 66 joints and 114 members.

The significance of orthogonal mesh fineness on the accuracy of the solution achieved will be investigated in this section. In order that the mesh geometry was made as simple as possible, the following four cell structure was considered.

overall width, B	=	800 cm
overall depth, D	=	150 cm
overall skew span, L	=	1600 cm
web thickness, t_w	=	1.0 cm
flange thickness, t_f	=	1.0 cm
diaphragm thickness, t_d	=	1.0 cm
angle of skew, θ	=	45 degrees

The structure was subjected to midspan point loading of intensity 200 kN over both outer webs and 400 kN over the three inner webs. The structure was analysed using both the orthogonal mesh grillage and the finite element method.

In the finite element method the limitation of problem size only allowed the use of two elements per cell in the transverse direction. This idealization should be considered the absolute minimum permissible and previous studies indicate that the midspan longitudinal flange stress values will be underestimated.

The two orthogonal meshes used in the grillage analysis are shown in figures 7.15 and 7.16 and will be referred to as the coarse and fine mesh respectively. Both meshes consist of five longitudinal grillage beams, and transverse grillage beams at either 200cm or 100cm centres.

Both mesh arrangements allow the determination of bending moments and web deflections at the quarterspan and midspan cross-sections.

The stiffness parameters used in the grillage analysis of both structures are given in Table 7.7. The results for longitudinal flange stress and web deflection are presented in Table 7.8, which may be summarized as follows.

1. The results from both grillage analyses revealed only a small percentage difference for both mesh configurations, the fine mesh results being marginally more accurate than the coarse mesh results for all values presented. The coarse mesh consists of eight equal divisions of the skew span dimension, and is comparable to the recommendation that nine transverse beams be used for the analysis of straight multi-cell structures subjected to uniform line loading.
2. The web deflection values at both the quarterspan and midspan cross-sections are consistently overestimated, the maximum overestimation being 13.7% at the quarterspan cross-section in the coarse mesh idealization. It is probable that the grillage results would show a closer agreement to finite element results from an analysis using a finer mesh, which contained more than two elements across the width of each cell.

3. At the midspan cross-section the longitudinal flange stress values were consistently overestimated, the maximum overestimation being 17.6% at the centre web in the coarse mesh idealization. Again these results could be improved if comparisons were made to results from a more accurate finite element analysis. If that were the case, it is probable that the grillage analysis marginally underestimates the intensity of stress at the outer web position.
4. At the quarterspan cross-section the longitudinal flange stress values were not so accurately predicted, the grillage method consistently overestimating the stress intensities across the width of the structure. This result is consistent with all previous analyses ^h were the distortional behaviour of the cross-section is not accurately modelled.
5. The overall results are encouraging and reinforce the belief that, using a reasonably coarse orthogonal mesh, the grillage method is able to analyse the behaviour of skew structures under certain load conditions.

7.5. EFFECT OF SKEW ANGLE ON ACCURACY OF ANALYSIS.

The influence of the angle of skew on the accuracy of the orthogonal mesh grillage analysis will be considered in this section. In order that comparisons could be made with the analysis of straight multi-cell structures, the three cell structure defined in Section 5.3.2 was used.

The structure details were

overall width, B	=	600 cm
overall depth, D	=	100 cm
overall skew span, L	=	1200 cm
web thickness, t_w	=	1.0 cm
flange thickness, t_f	=	2.0 cm
diaphragm thickness, t_d	=	2.0 cm

Three different angles of skew were considered, namely 18, 26 and 45 degrees. The angles were chosen to simplify the mesh geometry, and the mesh details are shown in figures 7.17, 7.18 and 7.19. The appropriate stiffness parameters for the longitudinal and transverse beams are presented in Table 7.9.

The spacing of the transverse grillage beams was kept constant at 100 cm in all three mesh geometries. This resulted in no joints being provided on the inner webs at the quarterspan and midspan cross-sections for the 18 degree skew structure, as shown in figure 7.17. Consequently, the bending moment and web deflection values at these locations were obtained by linear interpolation between the adjacent joints.

The structures were subjected to three midspan point load cases.

- (i) 600 kN over both outer webs and
1200 kN over both inner webs.
- (ii) 600 kN over both outer webs.
- (iii) 1200 kN over both inner webs

The 26 degree skew structure was subjected to an additional three uniform line load cases.

- (i) 1200 kN along both outer webs and
2400 kN along both inner webs.
- (ii) 1200 kN along both outer webs.
- (iii) 2400 kN along both inner webs.

The finite element idealization was again restricted by the limitation of problem size to the use of three elements across the width of each cell. The results for longitudinal flange stress and web deflection are presented in Tables 7.10, 7.11, 7.12 and 7.13 for both the grillage and finite element analyses. These results follow a similar pattern to the results from earlier studies and will not be discussed individually.

7.5.1. DISCUSSION OF RESULTS FOR MIDSPAN POINT LOADING.

The correlation between the grillage and finite element analyses for angles of skew from 0 to 45 degrees are presented in percentage terms in Table 7.14 for all three midspan point loading cases, and may be summarized as follows.

Load Case One.

1. The deflection of all webs was accurately predicted by the grillage method at both cross-sections over the full range of skew angles from 0 to 45 degrees. The percentage difference was within the range of -4.4% to + 11.2%.

2. The midspan longitudinal flange stresses were generally overestimated by the grillage method for all angles of skew considered, the maximum overestimation being +12.0%. At the quarterspan cross-section the results were less accurate, with the accuracy tending to diminish with increasing angle of skew. The transverse distortion of the cross-section tended to increase with increasing angle of skew thus producing this reduction in accuracy.

Load Case Two.

3. These results were the least accurate. The midspan web deflection of the loaded outer web tended to be underestimated. The underestimation increased with increasing angle of skew, being -19.0% at a skew angle of 45 degrees. The quarterspan results were also disappointing, where the discrepancy again increased with increasing angle of skew. However, the deflection of the outer web in the obtuse corner region was accurately predicted up to skew angles of 26 degrees.
4. The results for longitudinal flange stress were similar to those for deflection, with the midspan stress intensity being underestimated by -19.9% at a skew angle of 45 degrees.

Load Case Three.

5. The deflection of the inner loaded webs at both cross-sections were accurately predicted for all skew

angles. The maximum underestimation was -6.0%, whilst the maximum overestimation was +4.5%.

6. At the midspan cross-section, the maximum longitudinal flange stress developed in the loaded webs was accurately predicted for all angles of skew, the maximum underestimation and overestimation being -4.1% and +6.7% respectively. The quarterspan results were less accurate, although those for web three were consistently estimated with a maximum difference of only 2.6% of the finite element values.

7.5.2. UNIFORM LINE LOADING.

The results for the analysis of the 26 degree structure are presented in Table 7.12. for all three load cases, and may be summarized as follows.

Load Case One.

1. The web deflection values at both cross-sections were accurately predicted, the maximum overestimation being +7.6%. The grillage method tended to overestimate the deflection.
2. The longitudinal flange stresses at the midspan cross-section showed a maximum difference of only 3.1% of the finite element values. At the quarterspan cross-section the stress values were less accurate, but still within acceptable limits, the outer web, obtuse corner value being the least accurate, where the grillage method overestimated the stress by 24.8%.

Load Case Two.

3. Once again this was the least accurate loading condition considered, the results being very similar to those for the midspan point load case (Table 7.11).

Load Case Three.

4. The grillage results for web deflection and longitudinal flange stress at the loaded inner web positions were in close agreement with the finite element results. The maximum underestimation and overestimation were -1.9% and +4.7% respectively.
5. Generally the results for the uniform line load cases were more accurate than the midspan point load cases. This was consistent with the conclusions reached from the study of straight multi-cell structures reported in chapter five.

7.6. CONCLUSIONS.

1. The results presented in this chapter have demonstrated that the grillage method can predict the overall behaviour of multi-cell structures up to skew angles of 45 degrees to a degree of accuracy acceptable for initial design purposes.
2. The orthogonal mesh idealization will produce more accurate results than a skew mesh idealization, but requires far more time and effort in the preparation of input data.

3. On the basis of the limited investigation on skew mesh idealization, it is proposed that its use be limited to the analysis of skew structures subjected to loading that is reasonably uniform over the full width of the structure. This will result in limited transverse bending of the cross-section. Under this loading condition it is anticipated that the maximum longitudinal flange stress and web deflection values, which are developed at the midspan cross-section, will be accurately predicted. The grillage method will then tend to overestimate the values, with probable discrepancies of the order of 10% to 15%. A satisfactory skew mesh geometry can be achieved using nine transverse grillage beams.
4. The orthogonal mesh grillage will accurately predict the maximum midspan values of longitudinal flange stress and web deflection for skew angles up to 45 degrees under load conditions which tend to develop sagging moments in the transverse direction. These maximum effects will occur at a loaded web. The grillage method will tend to overestimate the stress intensity, the overestimation will be less than 15% of the finite element value. The results for web deflection will be more accurate, and should agree to within 90% to 95% of the finite element value.
5. The orthogonal mesh grillage cannot accurately predict the behaviour of skew structures when the loading develops substantial transverse hogging effects, i.e.

loading over outer webs only. The accuracy of analysis is directly proportional to the angle of skew. At a skew angle of 45 degrees, the grillage method will underestimate by 20% the longitudinal flange stress and web deflection. However, at a skew angle of 20 degrees, this underestimation will be reduced to less than 10%. Hence at low skew angles the grillage method will still provide a reasonable estimate of the midspan longitudinal flange stress and web deflection at the loaded web positions.

6. The quarterspan values of longitudinal flange stress and web deflection predicted by the grillage method generally do not compare very well with the finite element values in percentage terms. The correlation tends to diminish with increasing angle of skew. This is attributable to the poor idealization with respect to transverse distortion of the cross-section.

However, it is considered that the grillage method models the behaviour of the structure with respect to stress and deflection reasonably closely, providing the designer with an understanding of the response of the structure to a variety of loading conditions at an early stage of the design process at minimal cost.

7. The presence of skew increases the complexity of analysis in structures of all forms. The lack of any line of symmetry dictates that the complete structure has to be analysed, whatever method is adopted. The limitation of problem size, imposed by the finite

element program QUEST, produced results of questionable accuracy. In order to produce satisfactory results the program had to be modified, an option not readily available in normal design office practice.

The finite element mesh used in Section 7.2, where 546 nodes were defined, produced a structure with 3,250 degrees of freedom and the solution time was 1,335 cpu seconds of a DEC 20/60 computer. The grillage method on the other hand used a standard program. There were 66 joints in the orthogonal mesh, resulting in only 186 degrees of freedom and a solution time of only 13 cpu seconds, i.e. only one hundredth of the finite element solution time.

The complexity of analysis of skew structures reinforces the belief that the grillage method is a valuable design aid, which can produce results of acceptable accuracy for a range of loading conditions, in the early stages of design.

	Sect-ion	Web No.	No. transverse elements per cell		
			2	3	4
f l a n g e s t r e s s	1 / 4	1	10.95	11.04	11.43
		2	11.61	11.27	11.24
		3	10.93	10.82	10.71
		4	11.13	10.78	10.55
	1 / 2	1/4	38.61	40.93	42.08
		2/3	37.91	40.07	41.32
w e b d e f l e c t i o n	1 / 4	1	0.301	0.312	0.316
		2	0.336	0.339	0.340
		3	0.333	0.337	0.338
		4	0.297	0.304	0.307
	1 / 2	1/4	0.477	0.490	0.496
		2/3	0.551	0.558	0.560

Table 7.1. - Variation of longitudinal flange stress (N/mm²) and web deflection (cm) with number of elements across width of cell. Finite element study - 40 degree skew, 3-cell structure.

		Span posn	Web No	Finite Element	Grillage mesh		
					4x5	4x9	4x13
With Modified As	Defln	1/4	1	0.316	0.347	0.352	0.355
			2	0.340	0.409	0.414	0.417
			3	0.338	0.409	0.414	0.417
			4	0.307	0.347	0.352	0.355
	Stress	1/4	1	11.43	13.03	13.26	13.44
			2	11.24	13.77	14.06	14.25
			3	10.71	13.77	14.06	14.25
			4	10.55	13.03	13.26	13.44
Stress	1/2	1	42.08	49.15	49.69	50.01	
		2	41.32	54.03	54.38	54.65	
		1	0.316	0.305	0.294	0.292	
		2	0.340	0.347	0.339	0.337	
Without Modified As	Defln	1/4	3	0.338	0.369	0.360	0.359
			4	0.307	0.395	0.385	0.382
			1	0.496	0.541	0.525	0.521
			2	0.560	0.568	0.558	0.556
	Stress	1/4	1	11.43	6.12	6.68	6.83
			2	11.24	11.10	10.59	10.53
			3	10.71	13.94	13.30	13.19
			4	10.55	20.95	18.72	18.30
Stress	1/2	1	42.08	48.14	45.70	44.97	
		2	41.32	45.64	44.19	43.82	

Table 7.2 - Variation of longitudinal flange stress (N/mm²) and web deflection (cm) with number of transverse grillage beams. Skew grillage analysis - 40 degree skew, 3-cell structure.

	Span posn	Web No	Finite Element	Distribution Torsional Inertia			
				50/50	60/40	70/30	80/20
D e f l e c t i o n	1/4	1	0.316	0.332	0.314	0.297	0.283
		2	0.340	0.369	0.354	0.341	0.330
		3	0.338	0.386	0.373	0.362	0.352
		4	0.307	0.405	0.395	0.385	0.377
	1/2	1	0.496	0.566	0.545	0.527	0.511
		2	0.560	0.597	0.578	0.561	0.547
S t r e s s	1/4	1	11.43	9.65	8.36	7.20	6.15
		2	11.24	12.34	11.49	10.76	10.13
		3	10.71	14.56	13.92	13.36	12.88
		4	10.55	18.89	18.60	18.36	18.18
	1/2	1	42.08	48.33	46.75	45.39	44.21
		2	41.32	47.05	45.51	44.22	43.13

Distribution of torsional inertia
60/40 - 60% apportioned to longitudinal beams
40% to transverse beams

Table 7.3 - Variation of longitudinal flange stress (N/mm²) and web deflection (cm) with distribution of torsional inertia.
4x13 skew grillage analysis - 40 degree skew,
3-cell structure.

	Sect-ion	Web No.	Finite Element	Orthogonal Grillage	%	
f l a n g e s t r e s s	1 / 4	1	11.43	10.29	-9.9	
		2	11.24	13.06	+16.2	
		3	10.71	13.16	+22.9	
		4	10.55	16.79	+58.9	
	1 / 2	1/4	42.08	41.70	-0.9	
		2/3	41.32	43.82	+6.0	
	w e b d e f l e c t i o n	1 / 4	1	0.316	0.302	-4.4
			2	0.340	0.358	+5.3
3			0.338	0.360	+6.5	
4			0.307	0.328	+6.8	
1 / 2		1/4	0.496	0.487	-1.8	
		2/3	0.560	0.575	+2.7	

Table 7.4. - Longitudinal flange edge stress (N/mm²) and web deflection (cm). Orthogonal mesh grillage analysis 40 degree skew 3-cell structure.

			MIDSPAN		QUARTERSPAN			
			Web 1	Web 2	Web 1	Web 2	Web 3	Web 4
L o a d A l l W e b s	S t r e s s	FE	40.93	40.06	11.04	11.27	10.82	10.77
		Go %	41.70 +1.9	43.82 +9.4	10.29 -6.8	13.06 +15.9	13.16 +21.6	16.79 +55.9
		Gs %	44.97 +9.9	43.77 +9.3	6.84 -38.0	10.53 -6.6	13.19 +21.9	18.30 +69.9
	D e f l n	FE	0.491	0.558	0.312	0.339	0.336	0.304
		Go %	0.487 -0.8	0.575 +3.0	0.302 -3.2	0.358 +5.6	0.360 +7.1	0.328 +7.9
		Gs %	0.521 +6.1	0.556 -0.3	0.292 -6.4	0.337 -0.6	0.358 +6.5	0.382 +25.7
L o a d O u t e r W e b s	S t r e s s	FE	34.60	3.96	15.36	4.57	-0.95	3.22
		Go %	28.37 -18.0	6.54	7.79 -49.3	4.52	1.88	6.73 +109
		Gs %	19.35 -44.1	11.38	3.27 -78.7	4.13	3.90	4.78 +48.4
	D e f l n	FE	0.409	0.041	0.283	0.038	0.013	0.227
		Go %	0.326 -20.3	0.080	0.206 -27.2	0.063	0.050	0.198 -12.8
		Gs %	0.198 -51.6	0.162	0.112 -60.4	0.107	0.108	0.130 -42.7
L o a d I n n e r W e b s	S t r e s s	FE	6.33	36.10	-4.32	6.70	11.77	7.55
		Go %	13.33	37.28 +3.3	2.50	8.54 +19.0	11.28 -4.2	10.06
		Gs %	25.62	32.39 -10.3	3.57	6.40 -4.5	9.29 -21.1	13.52
	D e f l n	FE	0.082	0.517	0.029	0.301	0.323	0.077
		Go %	0.161	0.495 -4.3	0.096	0.295 -2.0	0.310 -4.0	0.130
		Gs %	0.323	0.394 -23.8	0.180	0.230 -23.6	0.250 -22.6	0.252

Table 7.5. Longitudinal flange stress (N/mm²) and deflection (cm) Orthogonal (Go) and Skew (Gs) Grillage and Finite Element (FE) analysis. 40 degree skew, Three Cell Structure. Midspan Point Loading

			MIDSPAN		QUARTERSPAN			
			Web 1	Web 2	Web 1	Web 2	Web 3	Web 4
L o a d A l l W e b s	S t r e s s	FE	30.55	29.10	20.31	20.09	19.42	19.87
		Go	30.37	30.47	18.61	21.73	21.34	25.47
		%	-0.6	+4.7	-8.3	+8.2	+9.9	+28.2
	D e f l n	FE	0.573	0.639	0.415	0.459	0.456	0.402
		Go	0.582	0.671	0.403	0.479	0.479	0.428
		%	+1.6	+5.0	-2.9	+4.3	+5.0	+6.5
L o a d O u t e r W e b s	S t r e s s	FE	23.28	4.76	27.03	5.23	-0.91	10.09
		Go	17.52	6.13	14.41	5.81	2.84	12.70
		%	-24.7		-46.7			+25.9
	D e f l n	FE	0.478	0.049	0.387	0.045	0.017	0.308
		Go	0.378	0.102	0.278	0.079	0.064	0.266
		%	-20.9		-28.2			-13.6
L o a d I n n e r W e b s	S t r e s s	FE	7.27	24.34	-6.72	14.86	20.33	9.78
		Go	12.85	24.34	4.20	15.92	18.50	12.77
		%		0.0		+7.1	-9.0	
	D e f l n	FE	0.095	0.590	0.028	0.414	0.439	0.094
		Go	0.204	0.569	0.125	0.400	0.415	0.162
		%		-3.6		-3.4	-5.5	

Table 7.6. Longitudinal flange stress (N/mm²) and deflection (cm). Orthogonal (Go) Grillage and Finite Element (FE) analysis. 40 degree skew, Three Cell Structure. Uniform Line Loading.

Dir- ect- ion	Stiffness Parameter	Beam Location	Orthogonal Mesh	
			Coarse	Fine
T R A N S V E R S E	Second Moment of Area (cm ⁴)	Outer	281 250	281 250
		Inner	2 250 000	1 125 000
	Eff. Shear Area (cm ²)	Outer	150.	150.
Inner		0.0104	0.0052	
	Torsion Inertia (cm ⁴)	Both	1 894 737	891 641
L O N G I T U D I N A L	Second Moment of Area (defl) (cm ⁴)	Outer	1 369 687	1 369 687
		Inner	2 458 125	2 458 125
	Eff. Shear Area (cm ²)	Both	150.	150.
	Torsion Inertia (cm ⁴)	Both	3 031 579	3 031 579
	Second Moment of Area (stress) (cm ⁴)	1/2span Outer	1 144 690	1 144 690
1/2span Inner		2 008 125	2 008 125	
1/4span Outer		1 406 250	1 406 250	
1/4span Inner		2 531 250	2 531 250	

Table 7.7. Stiffness parameters of grillage beams.
Orthogonal mesh grillage analysis.
45 degree skew, four cell structure.

	Span posn		Web Number				
			1	2	3	4	5
W e b D e f l e c t i o n	1 / 4	F.E.	0.282	0.319	0.313	0.314	0.299
		Gr1.	0.292	0.351	0.354	0.357	0.331
		%	+3.5	+10.0	+13.1	+13.7	+10.7
		Gr2.	0.290	0.347	0.349	0.350	0.327
		%	+2.8	+8.8	+11.5	+11.5	+9.4
	1 / 2	F.E.	0.462	0.518	0.513		
		Gr1.	0.478	0.561	0.561		
		%	+3.5	+8.3	+9.4		
		Gr2.	0.475	0.554	0.553		
		%	+2.8	+6.9	+7.8		
L o n g f l a n g e s t r e s s	1 / 4	F.E.	5.81	11.65	11.02	10.61	13.71
		Gr1.	9.38	13.23	14.05	14.67	18.43
		%	+61.4	+13.6	+27.5	+38.3	+34.4
		Gr2.	9.22	13.13	13.68	14.02	18.15
		%	+58.8	+12.7	+24.1	+32.2	+32.4
	1 / 2	F.E.	38.21	37.32	36.66		
		Gr1.	39.67	43.36	43.11		
		%	+3.8	+16.2	+17.6		
		Gr2.	39.21	42.60	42.25		
		%	+2.6	+14.2	+15.2		

Table 7.8. Web deflection (cm) and longitudinal flange edge stress (N/mm²). Coarse (Gr1.) and Fine (Gr2.) Orthogonal mesh Grillage analysis. 45 degree skew, four cell structure.

Dir- ect- ion	Stiffness Parameter	Beam Location	Angle of Skew		
			18	26	45
T R A N S V E R S E	Second Moment of Area (cm ⁴)	Outer	1166666	1166666	1166666
		Inner	1000000	1000000	1000000
	Eff. Shear Area (cm ²)	Outer	200.	200.	200.
Inner		0.0116	0.0116	0.0116	
	Torsion Inertia (cm ⁴)	Both	692308	750000	692308
L O N G I T U D I N A L	Second Moment of Area (defl) (cm ⁴)	Outer	1030333	1030333	1030333
		Inner	1977333	1977333	1977333
	Eff. Shear Area (cm ²)	Both	100.	100.	100.
	Torsion Inertia (cm ⁴)	Both	2250000	2250000	2250000
	Second Moment of Area (stress) (cm ⁴)	1/2span Outer	796333	796333	796333
		1/2span Inner	1509333	1509333	1509333
		1/4span Outer	1083333	1083333	1083333
1/4span Inner		2083333	2083333	2083333	

Table 7.9. Stiffness parameters of grillage beams.
Orthogonal mesh grillage analysis.
Three cell structure.
18, 26 and 45 degree skew.

			MIDSPAN		QUARTERSPAN			
			Web 1	Web 2	Web 1	Web 2	Web 3	Web 4
L o a d A l l W e b s	S t r e s s	FE	98.43	102.69	39.22	39.27	38.06	33.94
		Go	109.16	104.65	35.72	39.32	40.40	43.31
		%	+10.9	+1.9	-8.9	+0.1	+6.1	+27.6
	D e f l e c t i o n	FE	1.145	1.407	0.745	0.875	0.872	0.725
		Go	1.179	1.369	0.754	0.878	0.882	0.782
		%	+3.2	-2.7	+1.2	+0.3	+1.1	+7.9
L o a d O u t e r W e b s	S t r e s s	FE	67.71	17.60	23.53	13.99	8.51	8.07
		Go	63.56	23.06	16.70	12.26	10.61	16.58
		%	-6.1	+31.0	-29.0	-12.4	+24.6	+105
	D e f l e c t i o n	FE	0.725	0.210	0.471	0.158	0.137	0.412
		Go	0.691	0.244	0.424	0.176	0.169	0.422
		%	-4.7	+16.2	-10.0	+11.4	+23.3	+2.4
L o a d I n n e r W e b s	S t r e s s	FE	30.72	85.09	15.69	25.28	29.55	25.87
		Go	45.60	81.59	19.02	27.06	29.79	26.73
		%	+48.4	-4.1	+21.2	+7.0	+0.8	+3.3
	D e f l e c t i o n	FE	0.420	1.197	0.274	0.717	0.735	0.313
		Go	0.488	1.125	0.330	0.702	0.713	0.360
		%	+16.2	-6.0	+20.4	-2.1	-3.0	+15.0

Table 7.10. Longitudinal flange stress (N/mm²) and deflection (cm). Orthogonal (Go) Grillage and Finite Element (FE) analysis. 18 degree skew, Three Cell Structure. Midspan Point Loading.

			MIDSPAN		QUARTERSPAN			
			Web 1	Web 2	Web 1	Web 2	Web 3	Web 4
Load All e w e b s	S t r e s s	FE	97.00	97.34	34.82	34.94	33.29	29.46
		Go	103.84	107.64	31.27	36.05	37.50	41.92
		%	+7.0	+10.6	-10.2	+3.2	+12.6	+42.3
	D e f l n	FE	1.090	1.325	0.702	0.814	0.810	0.679
		Go	1.120	1.356	0.704	0.842	0.847	0.744
		%	+2.8	+2.3	+0.3	+3.4	+4.6	+9.6
L o a d O u t e r W e b s	S t r e s s	FE	69.20	15.68	26.05	13.46	5.44	5.13
		Go	62.04	21.10	15.98	11.70	9.11	15.53
		%	-10.3	+34.6	-38.7	-13.1	+67.5	+203
	D e f l n	FE	0.732	0.179	0.484	0.139	0.109	0.403
		Go	0.674	0.223	0.412	0.163	0.152	0.408
		%	-7.9	+24.6	-14.9	+17.3	+39.4	+1.2
L o a d I n n e r W e b s	S t r e s s	FE	27.80	81.66	8.77	21.48	27.85	24.33
		Go	41.80	86.54	15.29	24.35	28.39	26.39
		%	+50.4	+6.0	+74.3	+13.4	+1.9	+8.5
	D e f l n	FE	0.358	1.146	0.218	0.675	0.701	0.276
		Go	0.446	1.133	0.292	0.679	0.695	0.336
		%	+24.6	-1.1	+33.9	+0.6	-0.9	+21.7

Table 7.11. Longitudinal flange stress (N/mm²) and deflection (cm). Orthogonal (Go) Grillage and Finite Element (FE) analysis. 26 degree skew, Three Cell Structure. Midspan Point Loading.

			MIDSPAN		QUARTERSPAN			
			Web 1	Web 2	Web 1	Web 2	Web 3	Web 4
Load All Webs	Stress	FE	76.42	76.96	56.29	56.33	54.41	51.10
		Go	78.10	79.38	52.56	58.10	59.55	63.78
		%	+2.2	+3.1	-6.6	+3.1	+9.4	+24.8
	Defln	FE	1.287	1.525	0.935	1.104	1.098	0.911
		Go	1.339	1.578	0.940	1.135	1.139	0.980
		%	+4.0	+3.5	+0.5	+2.8	+3.7	+7.6
Load Outer Webs	Stress	FE	42.09	19.30	46.93	16.08	7.76	20.81
		Go	38.87	19.52	29.52	15.95	13.17	28.58
		%	-7.6	+1.2	-37.1	-0.8	+69.7	+37.3
	Defln	FE	0.842	0.224	0.668	0.170	0.137	0.564
		Go	0.772	0.284	0.559	0.208	0.196	0.553
		%	-8.3	+26.8	-16.3	+22.3	+43.1	-1.9
Load Inner Webs	Stress	FE	34.33	57.66	9.36	40.25	46.65	30.29
		Go	39.23	59.86	23.04	42.15	46.38	35.20
		%	+14.3	+3.8	+146	+4.7	-0.6	+16.2
	Defln	FE	0.445	1.301	0.267	0.934	0.961	0.347
		Go	0.567	1.294	0.381	0.927	0.943	0.427
		%	+27.4	-0.5	+42.7	-0.7	-1.9	+23.1

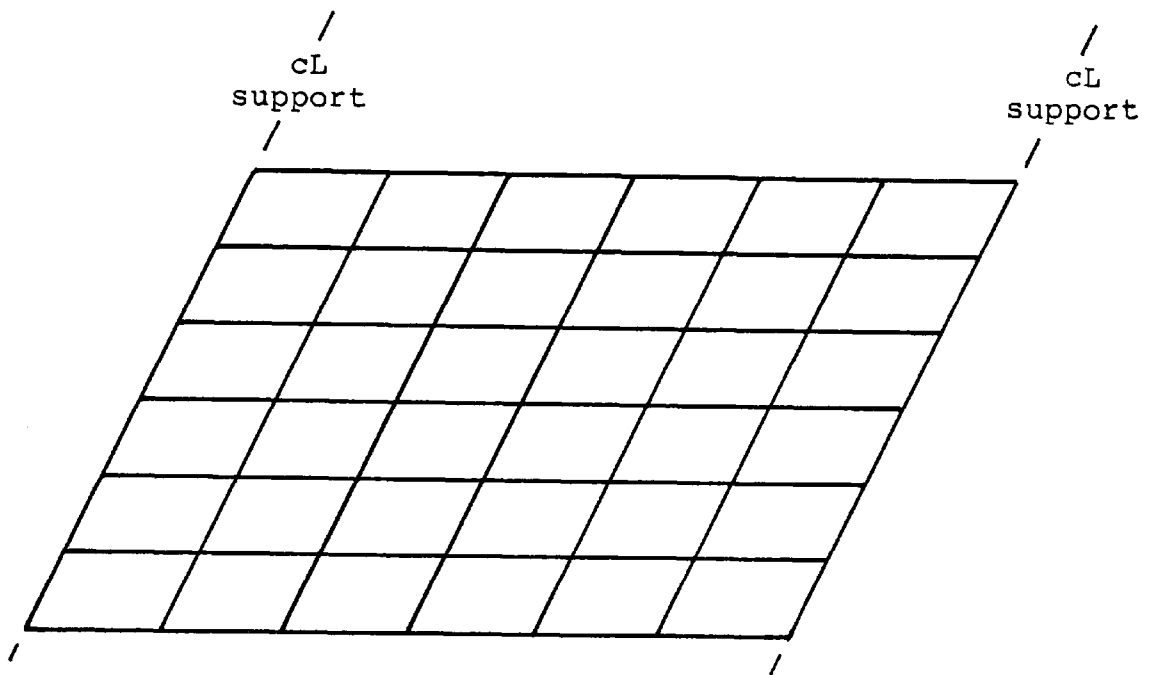
Table 7.12. Longitudinal flange stress (N/mm²) and deflection (cm). Orthogonal (Go) Grillage and Finite Element (FE) analysis. 26 degree skew, Three Cell Structure. Uniform Line Loading.

			MIDSPAN		QUARTERSPAN			
			Web 1	Web 2	Web 1	Web 2	Web 3	Web 4
Load All Webs	Stress	FE	86.80	77.85	18.83	20.79	18.90	23.52
		Go	83.37	87.24	18.70	25.75	25.96	33.36
		%	-3.9	+12.0	-0.7	+23.9	+37.3	+41.8
	Defln	FE	0.919	1.060	0.564	0.623	0.614	0.562
		Go	0.896	1.132	0.539	0.683	0.683	0.593
		%	-2.5	+6.8	-4.4	+9.6	+11.2	+5.5
Load Outer Webs	Stress	FE	72.70	7.86	32.43	10.37	-3.36	5.04
		Go	58.24	12.55	14.19	9.42	3.38	12.37
		%	-19.9		-56.2			+145
	Defln	FE	0.774	0.072	0.526	0.072	0.019	0.416
		Go	0.627	0.135	0.381	0.107	0.083	0.372
		%	-19.0		-27.6			-10.6
Load Inner Webs	Stress	FE	14.10	69.99	-13.60	10.42	22.26	18.48
		Go	25.13	74.69	4.51	16.33	22.58	20.99
		%		+6.7		+56.7	+1.4	
	Defln	FE	0.145	0.988	0.038	0.551	0.595	0.146
		Go	0.269	0.997	0.158	0.576	0.600	0.221
		%		+0.9		+4.5	+0.8	

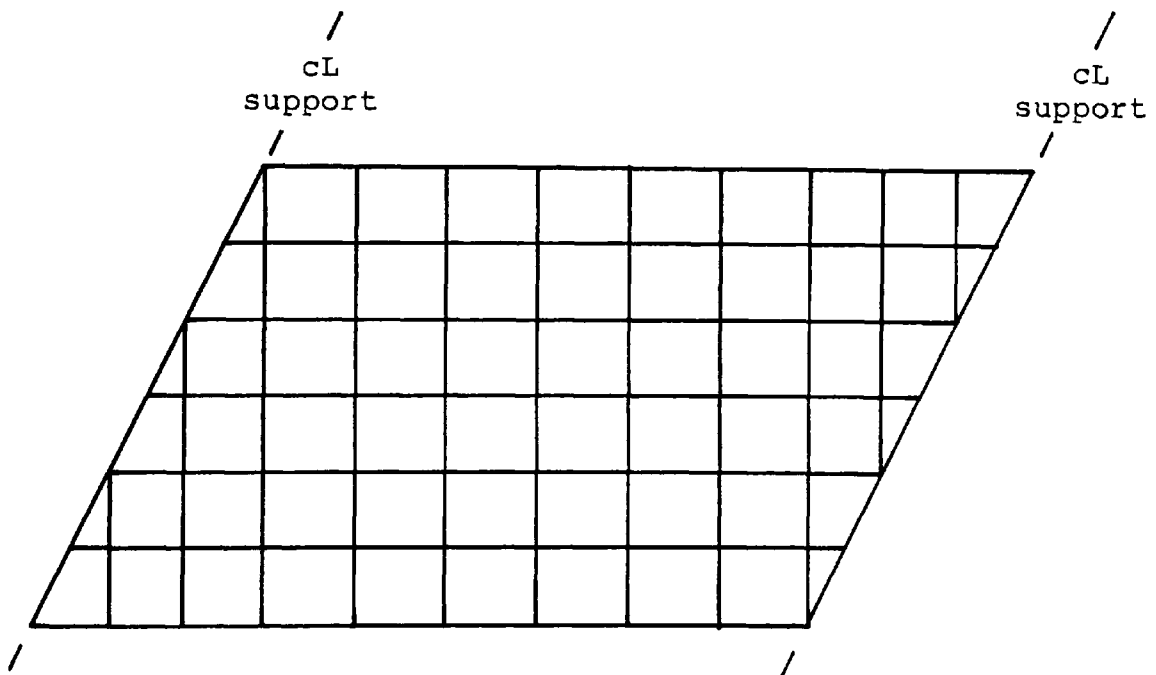
Table 7.13. Longitudinal flange stress (N/mm²) and deflection (cm).
Orthogonal (Go) Grillage and Finite Element (FE) analysis.
45 degree skew, Three Cell Structure.
Midspan Point Loading.

		Skew Angle	MIDSPAN		QUARTERSPAN				
			Web 1	Web 2	Web 1	Web 2	Web 3	Web 4	
L o a d A l l W e b s	S t r e s s	0	+10.5	+5.2	+3.9	-1.2	-1.2	+3.9	
		18	+10.9	+1.9	-8.9	+0.1	+6.1	+27.6	
		26	+7.0	+10.6	-10.2	+3.2	+12.6	+42.3	
		45	-3.9	+12.0	-0.7	+23.9	+37.3	+41.8	
	D e f l n	0	+2.6	-1.3	+3.2	-0.8	-0.8	+3.2	
		18	+3.2	-2.7	+1.2	+0.3	+1.1	+7.9	
		26	+2.8	+2.3	+0.3	+3.4	+4.6	+9.6	
		45	-2.5	+6.8	-4.4	+9.6	+11.2	+5.5	
L o a d O u t e r W e b s	S t r e s s	0	+1.3		+16.7			+16.7	
		18	-6.1		-29.0			+105	
		26	-10.3		-38.7			+203	
		45	-19.9		-56.2			+145	
	D e f l n	0	+2.2		+2.5			+2.5	
		18	-4.7		-10.0			+2.4	
		26	-7.9		-14.9			+1.2	
		45	-19.0		-27.6			-10.6	
L o a d I n n e r W e b s	S t r e s s	0		+3.6		+2.6	+2.6		
		18		-4.1		+7.0	+0.8		
		26		+6.0		+13.4	+1.9		
		45		+6.7		+56.7	+1.4		
	D e f l n	0			-2.2		-1.8	-1.8	
		18			-6.0		-2.1	-3.0	
		26			-1.1		+0.6	-0.9	
		45			+0.9		+4.5	+0.8	

Table 7.14. Longitudinal flange stress and web deflection. Percentage difference between grillage and finite element analysis for skew angles of 0, 18, 26 and 45 degrees. Midspan point loading, three cell structure.

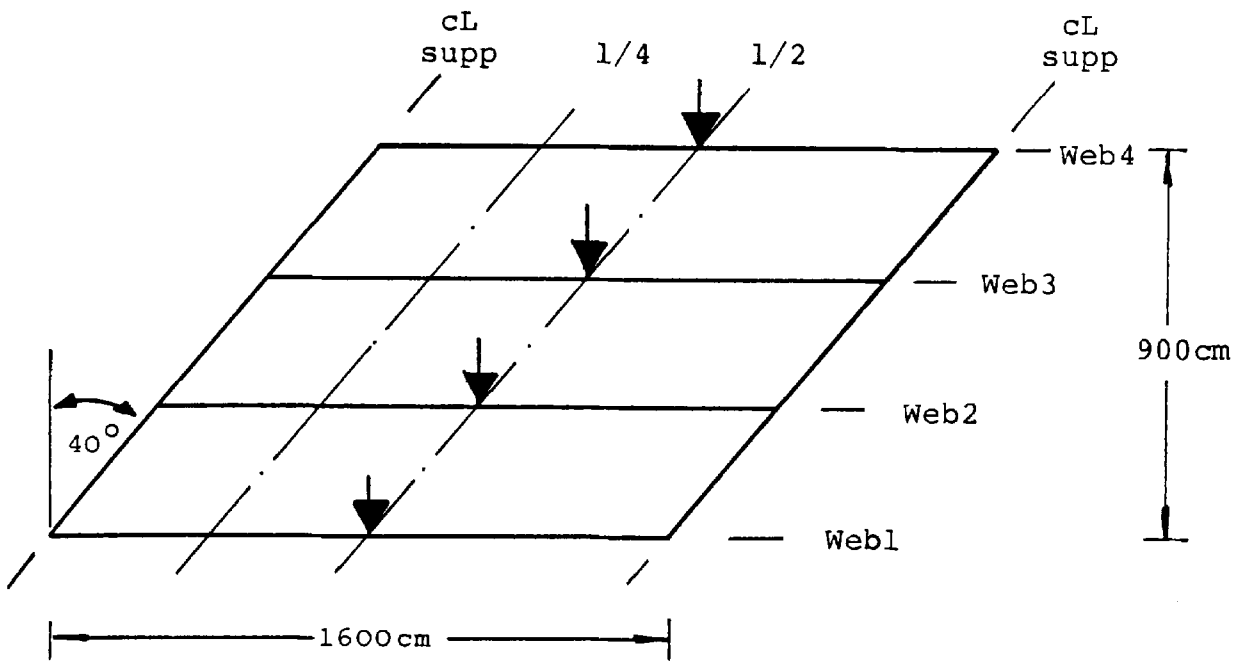


(a) Skew mesh.

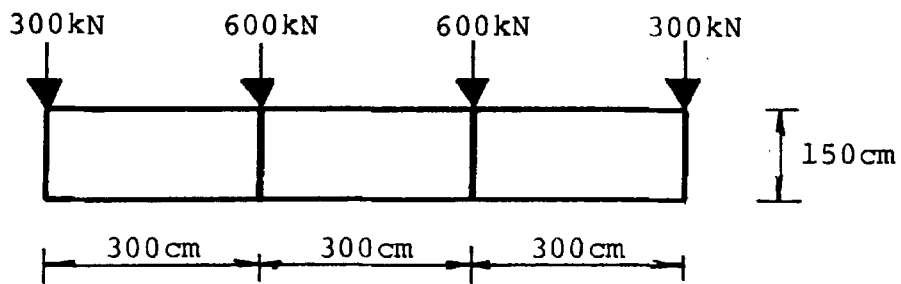


(b) Orthogonal mesh.

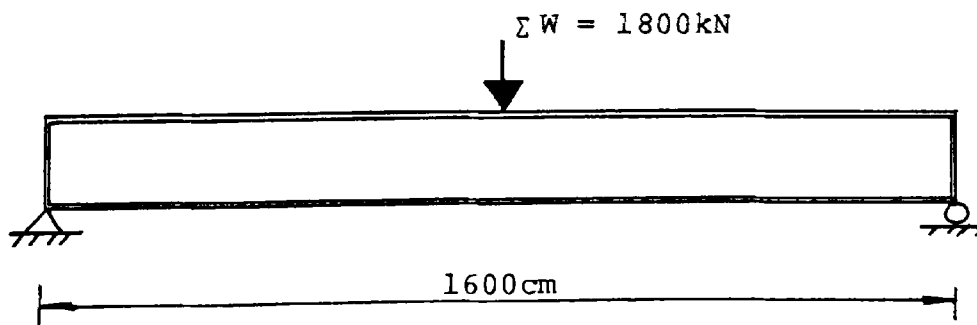
FIGURE 7.1 - EXAMPLES OF SKEW AND ORTHOGONAL GRILLAGE MESH GEOMETRIES.



(a) Plan.



(b) Cross-section and load details.



(c) Longitudinal section.

FIGURE 7.2 - FINITE ELEMENT CONVERGENCE STUDY
40 DEGREE SKEW, THREE-CELL STRUCTURE.

x, y, z - global axes for structure

x', y', z' - local axes for flange plates

number of nodes = 546

number of members = 584

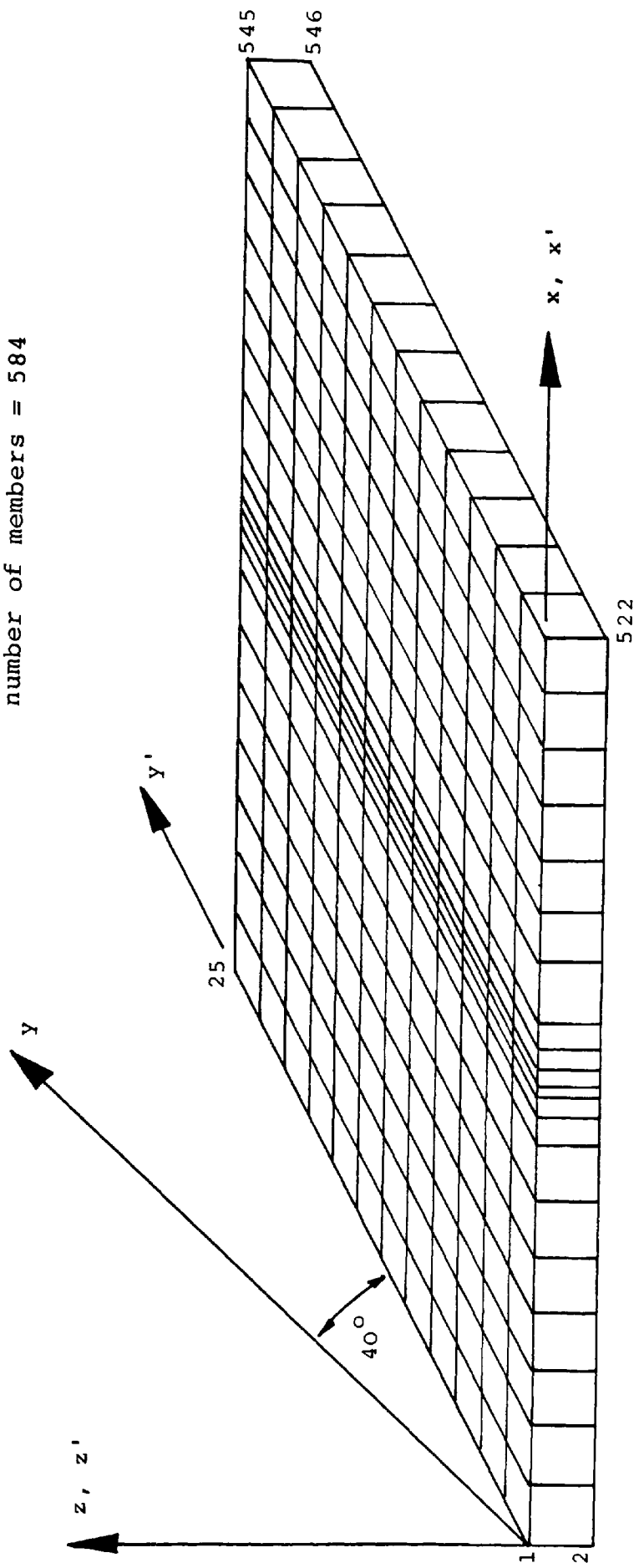


FIGURE 7.3 - DETAILS OF FINITE ELEMENT MESH
40 DEGREE SKEW, THREE-CELL STRUCTURE.

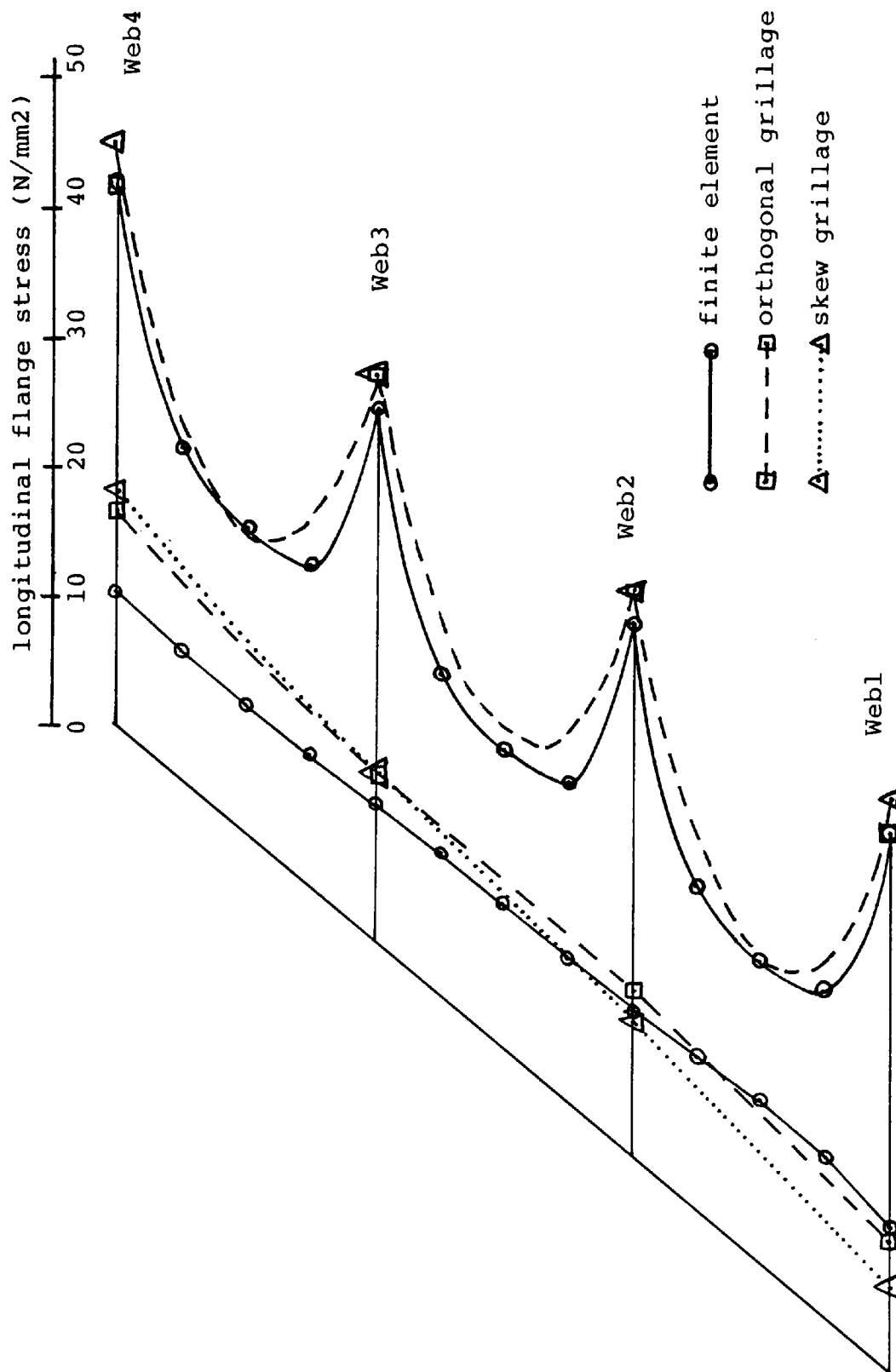


FIGURE 7.4 - LONGITUDINAL FLANGE STRESS DISTRIBUTION AT MIDSPAN AND QUARTERSPAN CROSS-SECTIONS 40 DEGREE SKEW, THREE-CELL STRUCTURE.

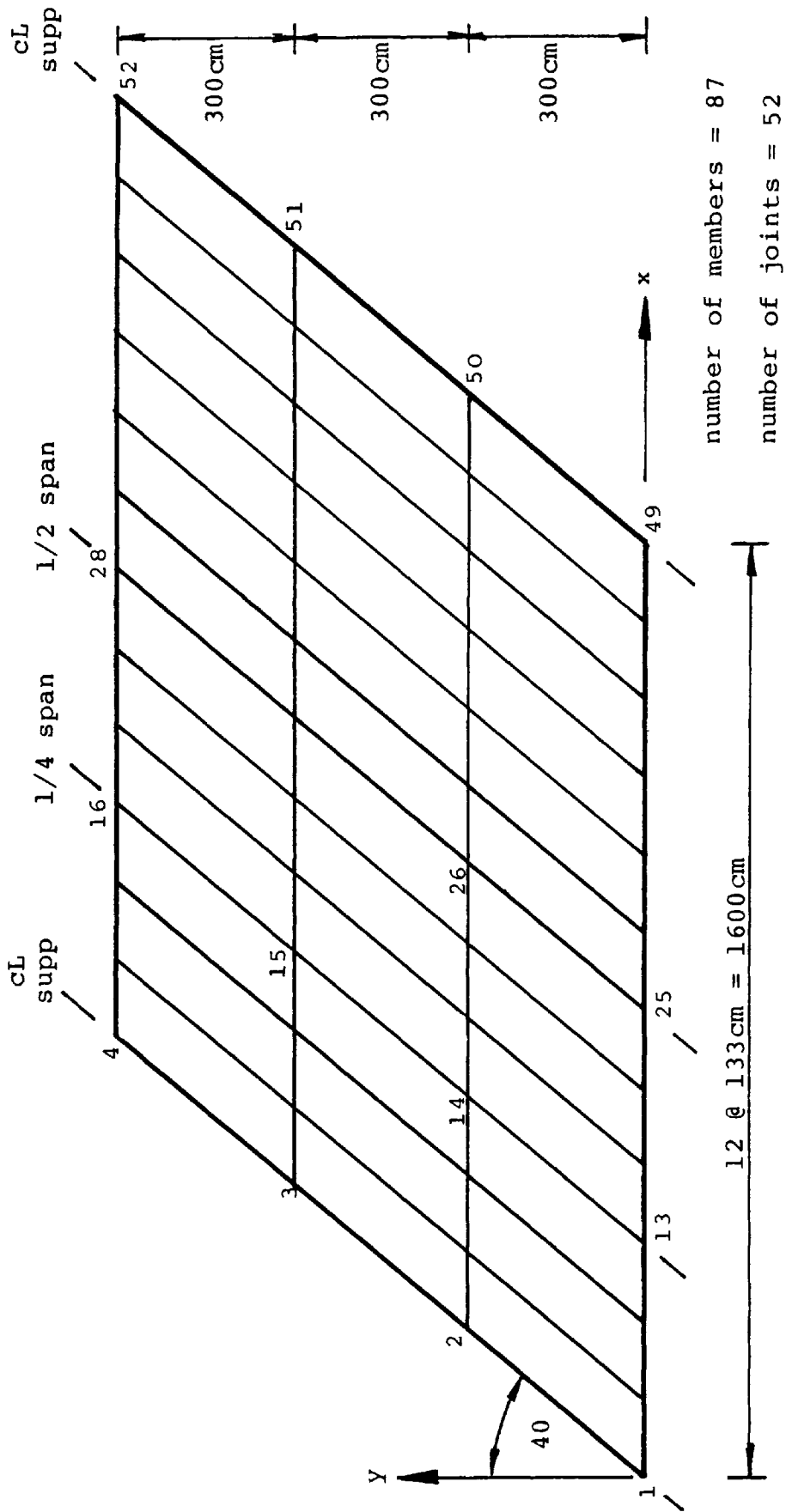


FIGURE 7.5 - DETAILS OF 4 x 13 SKEW GRILLAGE MESH
 40 DEGREE SKEW, THREE-CELL STRUCTURE.

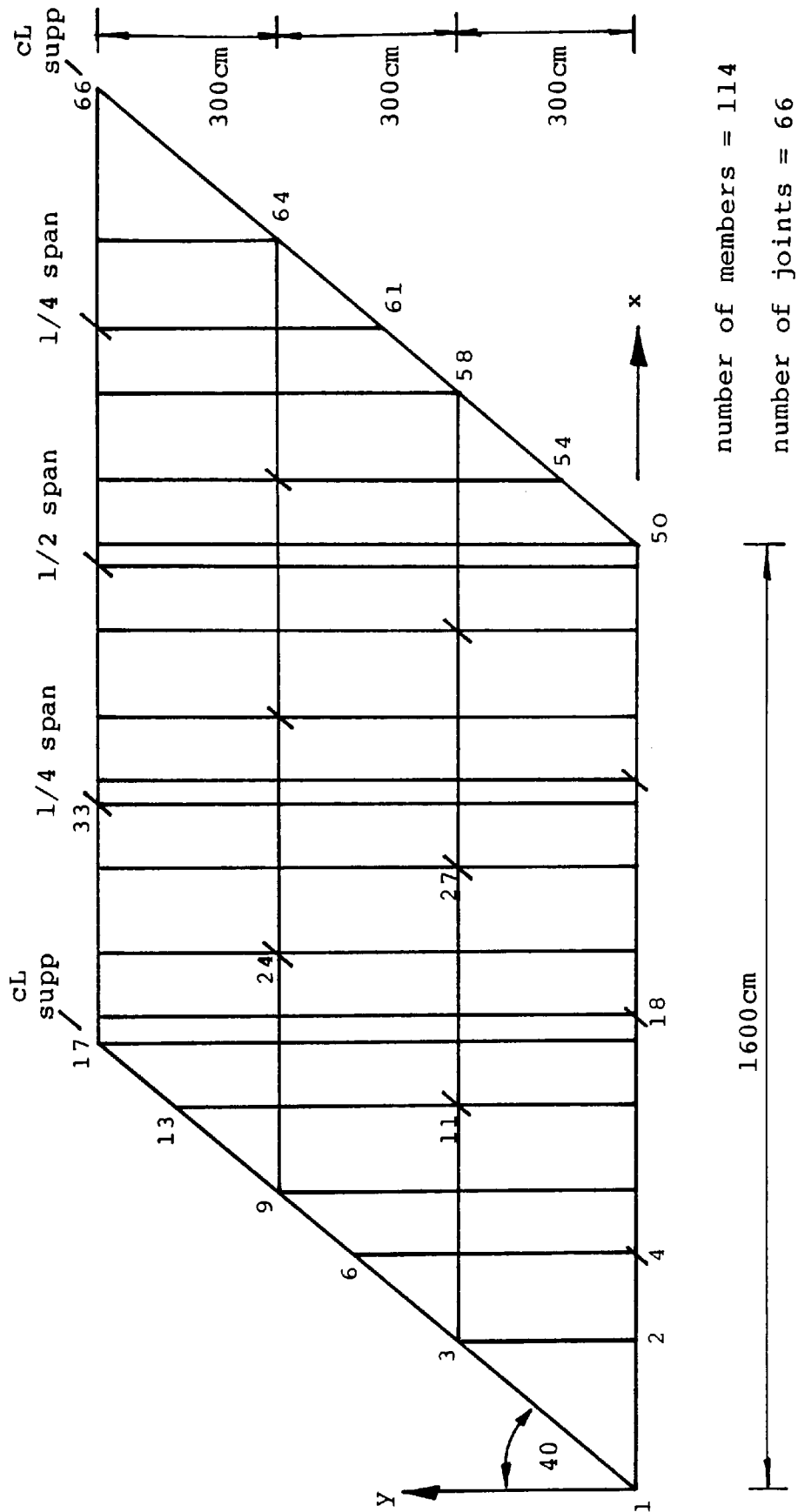
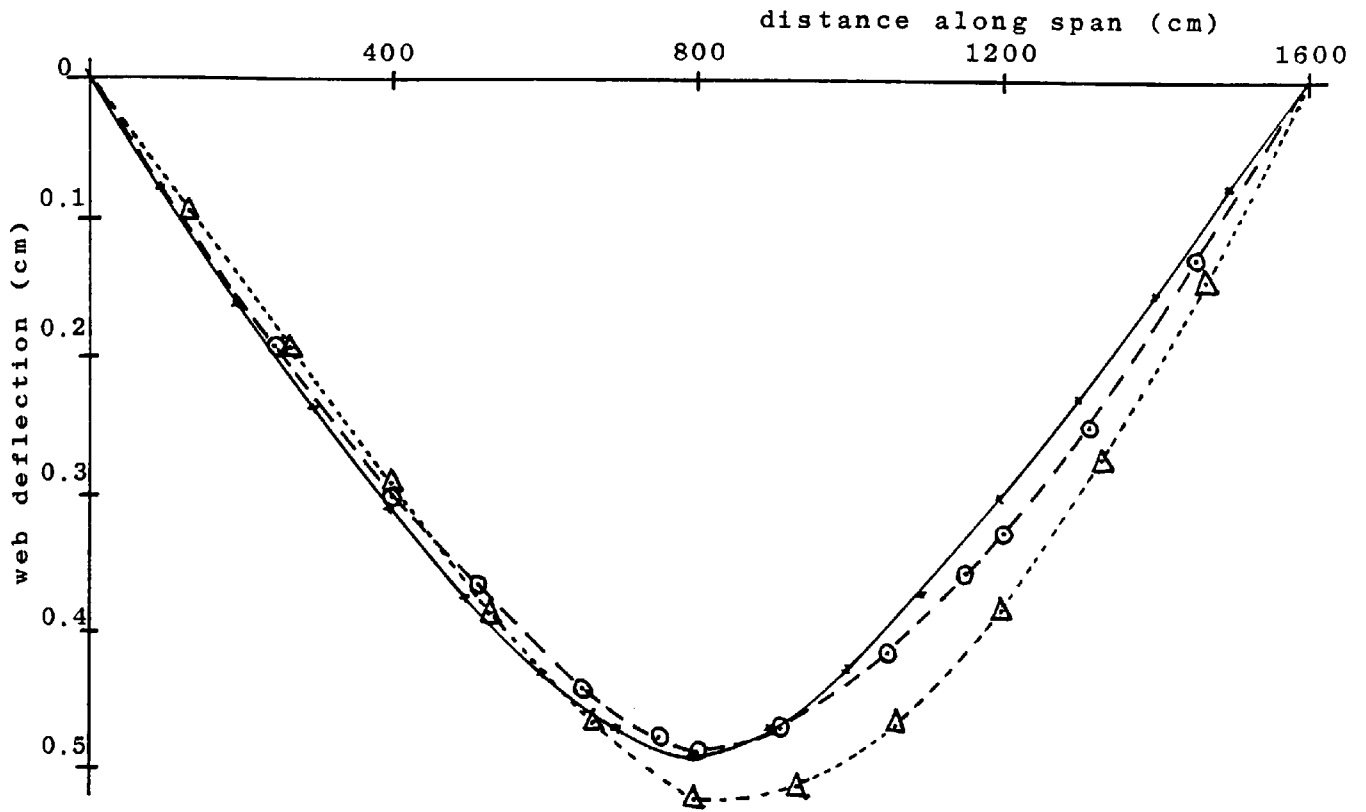
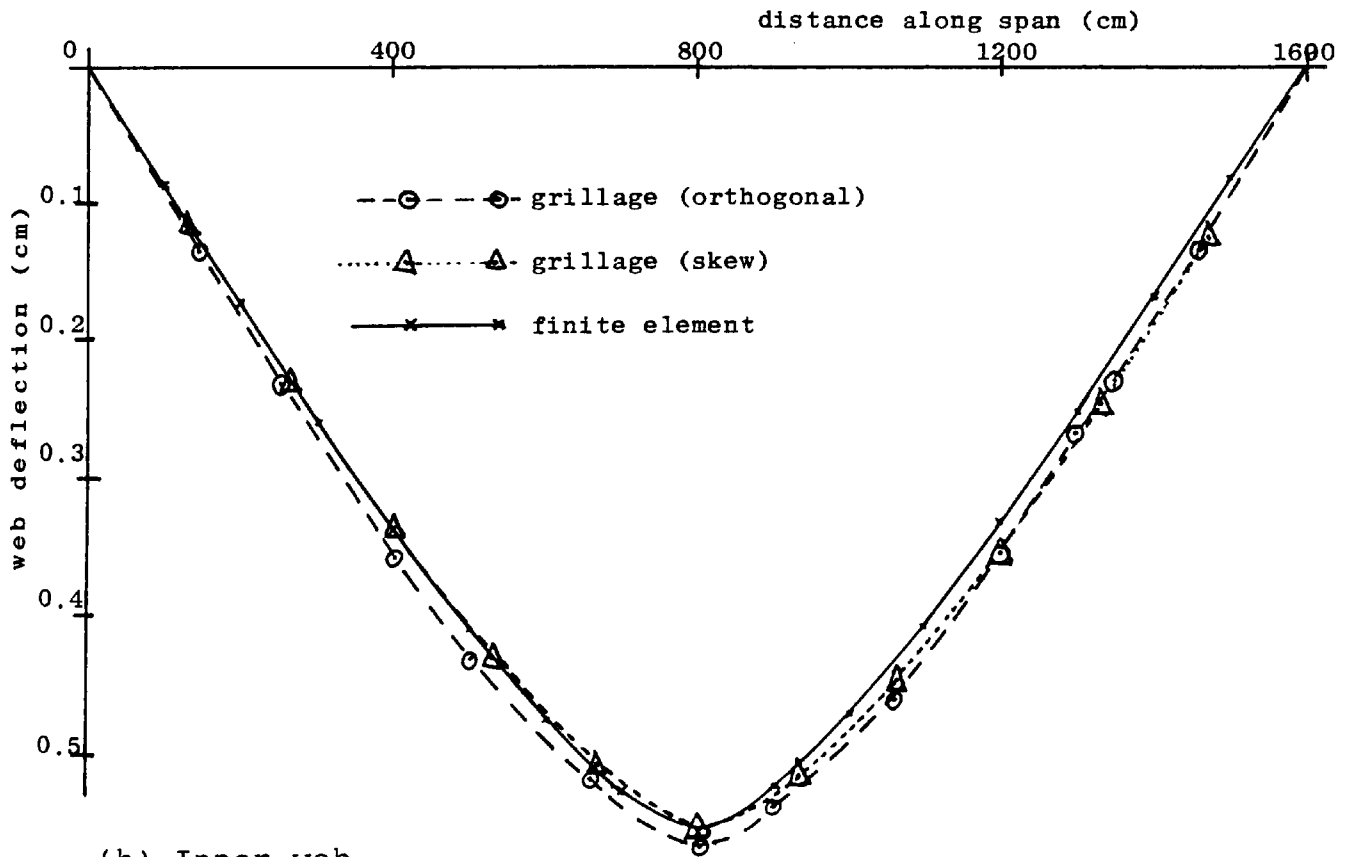


FIGURE 7.6 - DETAILS OF ORTHOGONAL GRILLAGE MESH
40 DEGREE SKEW, THREE-CELL STRUCTURE.

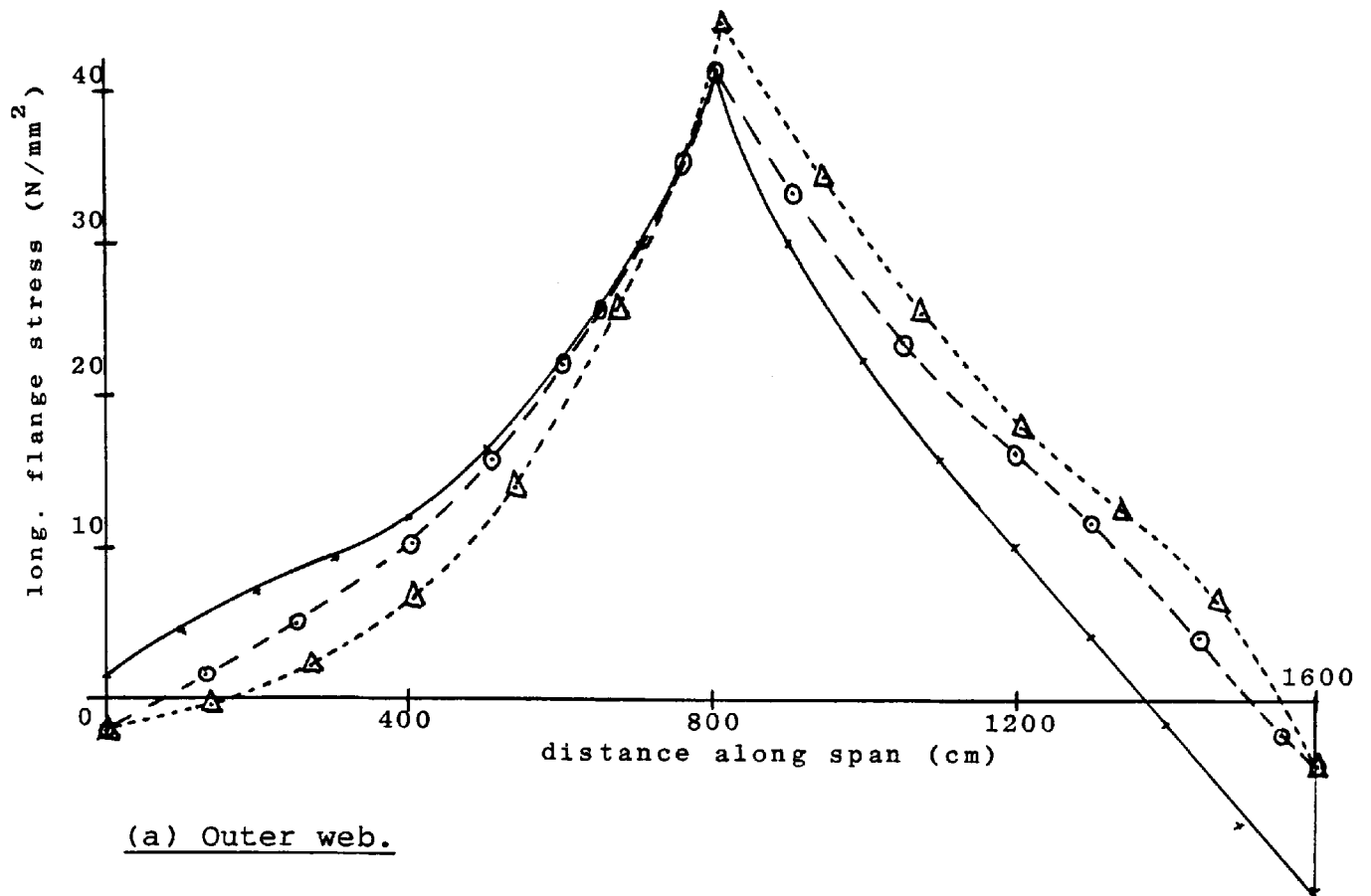


(a) Outer web.

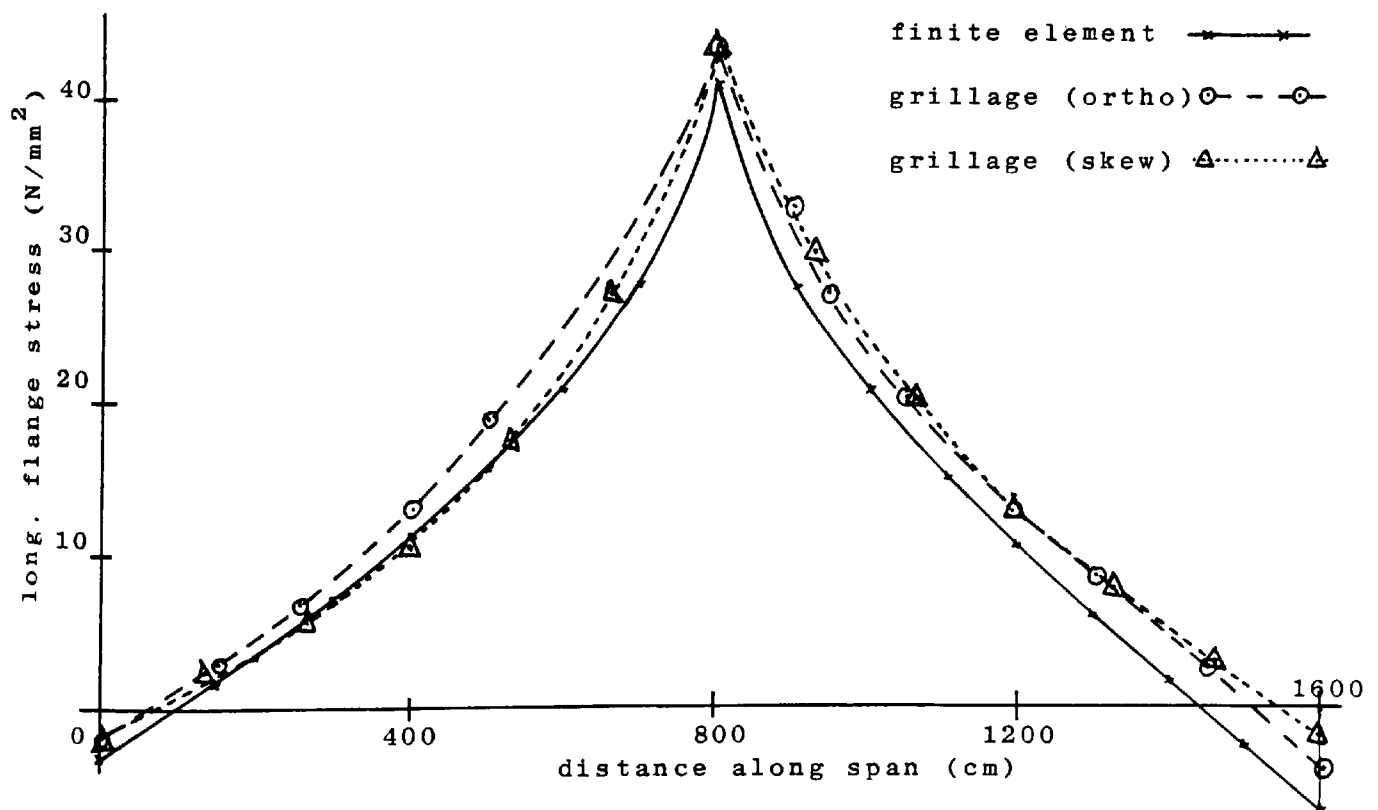


(b) Inner web.

FIGURE 7.7 - DISTRIBUTION OF WEB DEFLECTION ALONG WEBS
40 DEGREE SKEW, THREE-CELL STRUCTURE.



(a) Outer web.



(b) Inner web.

FIGURE 7.8 - DISTRIBUTION OF LONGITUDINAL FLANGE EDGE STRESS ALONG OUTER AND INNER WEBS 40 DEGREE SKEW, THREE-CELL STRUCTURE.

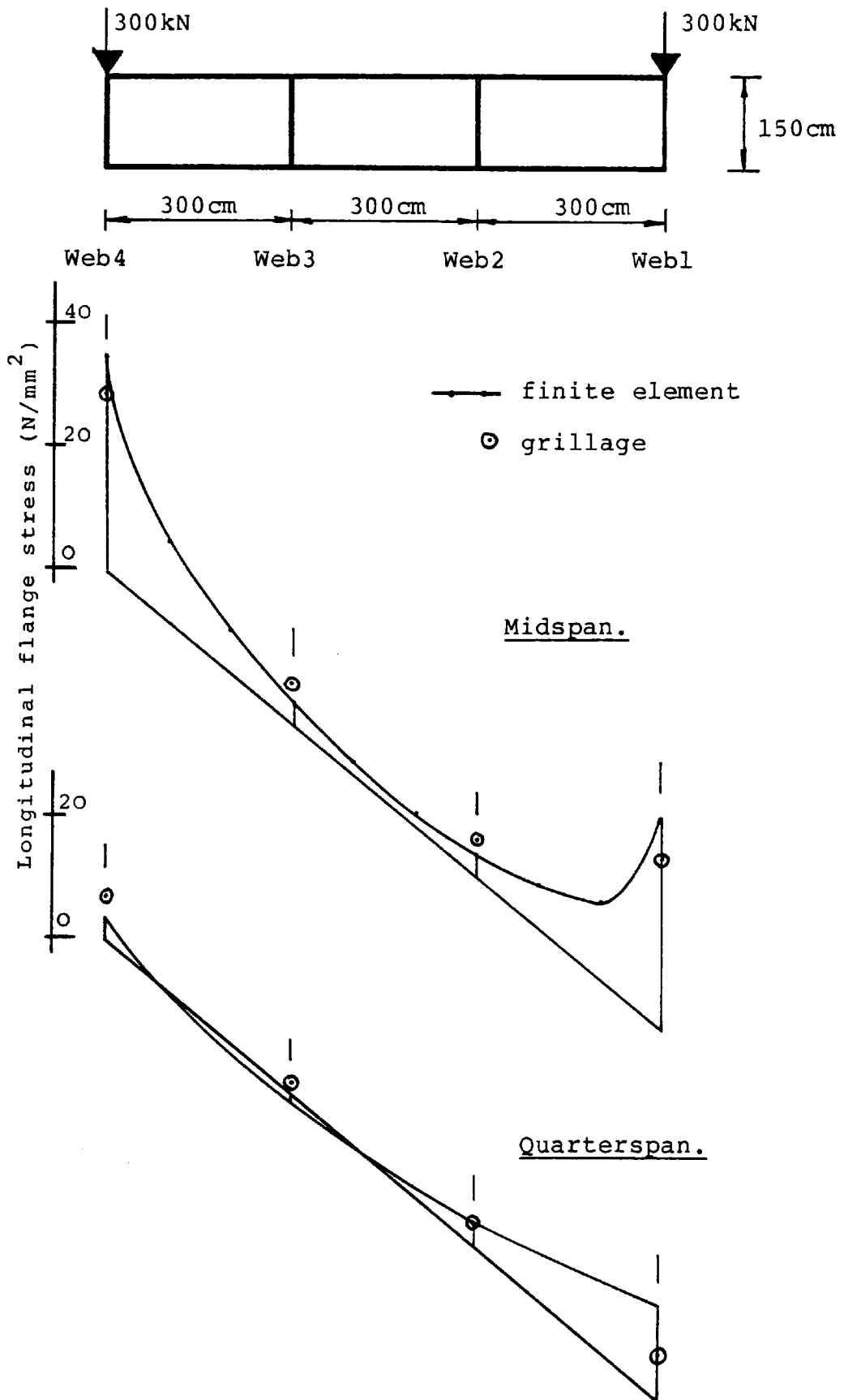


FIGURE 7.9 - LONGITUDINAL FLANGE STRESS DISTRIBUTION AT MIDSPAN AND QUARTERSPAN CROSS-SECTIONS 40 DEGREE SKEW, THREE-CELL STRUCTURE MIDSPAN POINT LOADING OVER OUTER WEBS.

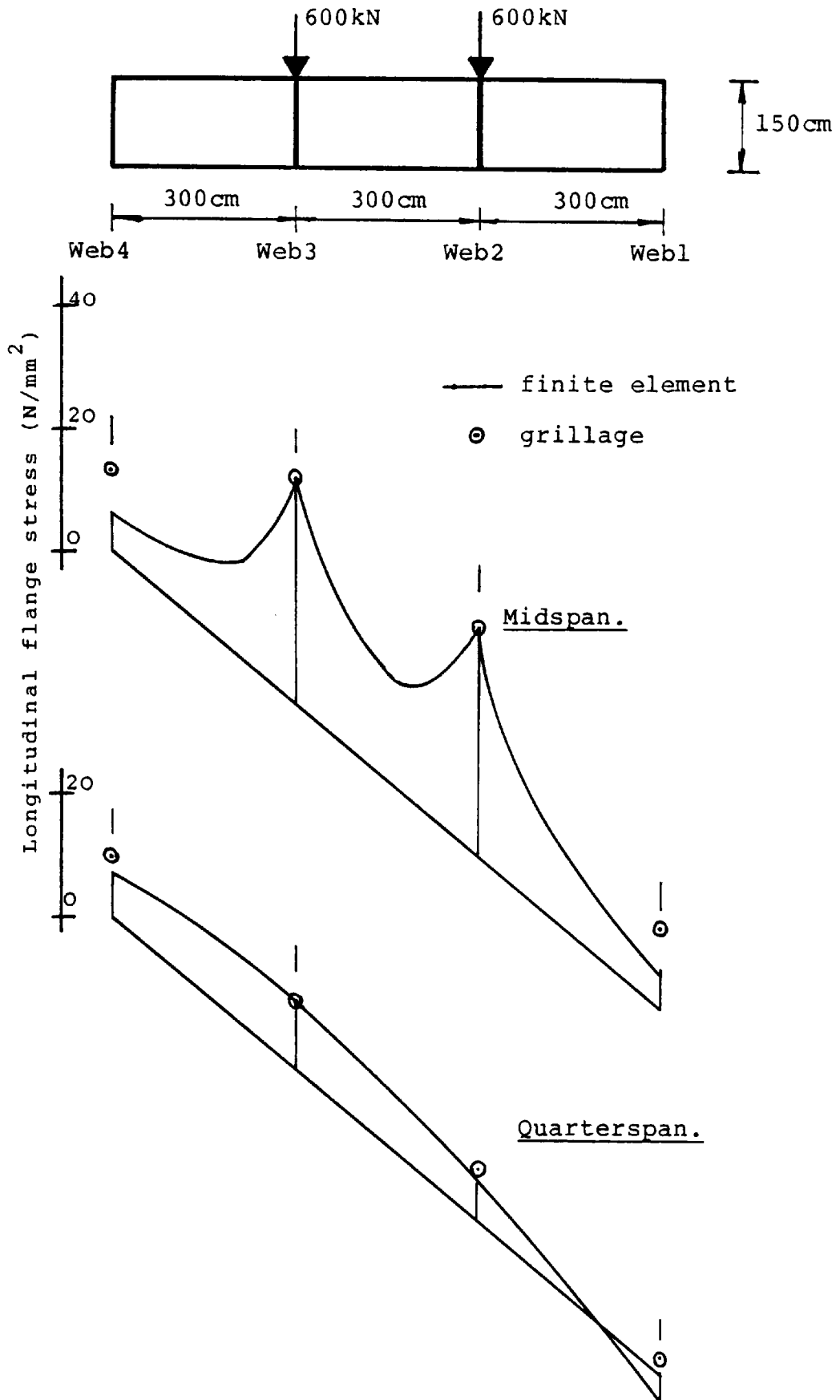


FIGURE 7.10 - LONGITUDINAL FLANGE STRESS DISTRIBUTION AT MIDSPAN AND QUARTERSPAN CROSS-SECTIONS 40 DEGREE SKEW, THREE-CELL STRUCTURE MIDSPAN POINT LOADING OVER INNER WEBS.

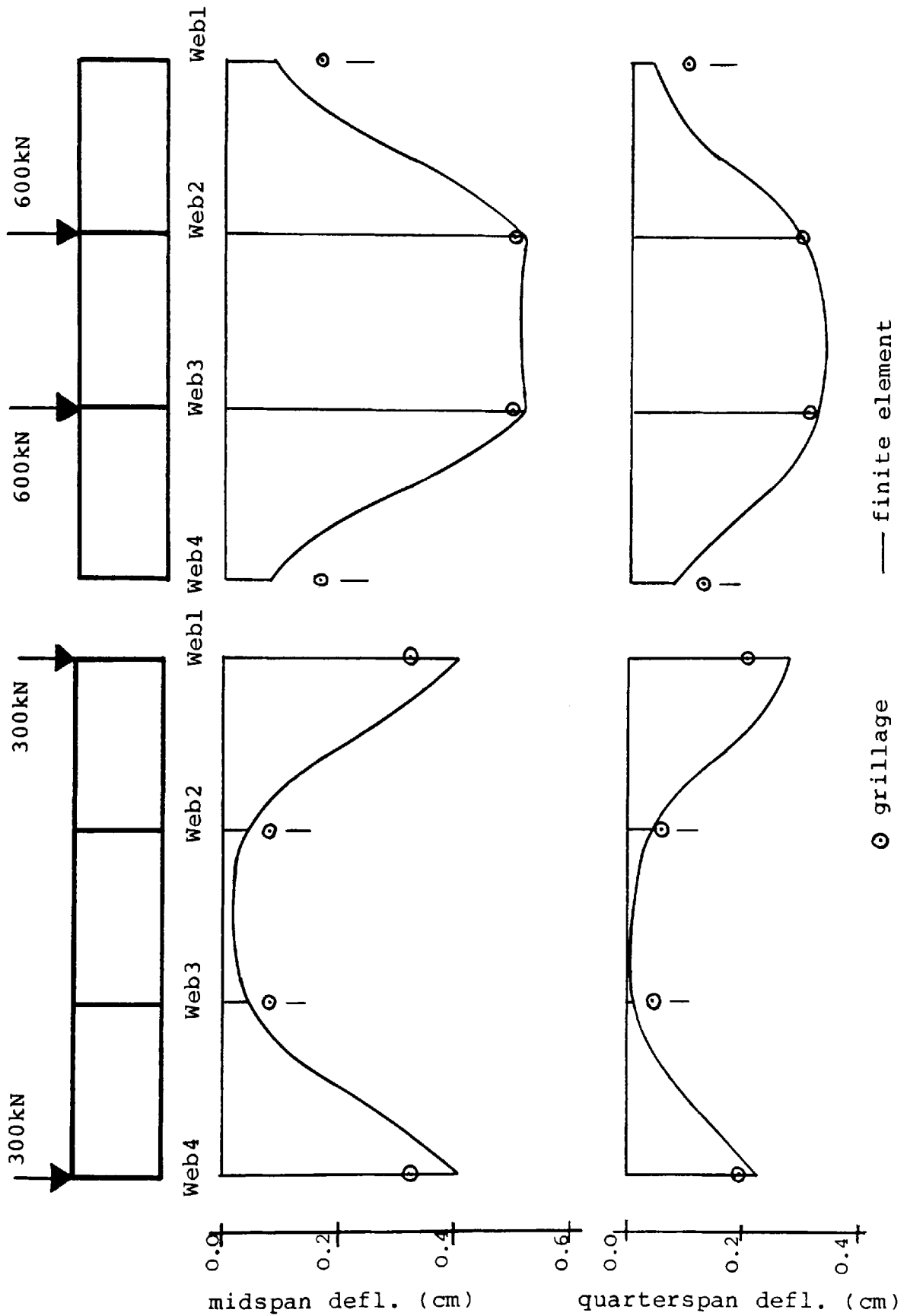


FIGURE 7.11 - DEFLECTION PROFILES AT MIDSPAN AND QUARTERSPAN CROSS-SECTIONS 40 DEGREE SKEW, THREE-CELL STRUCTURE MIDSPAN POINT LOADING.

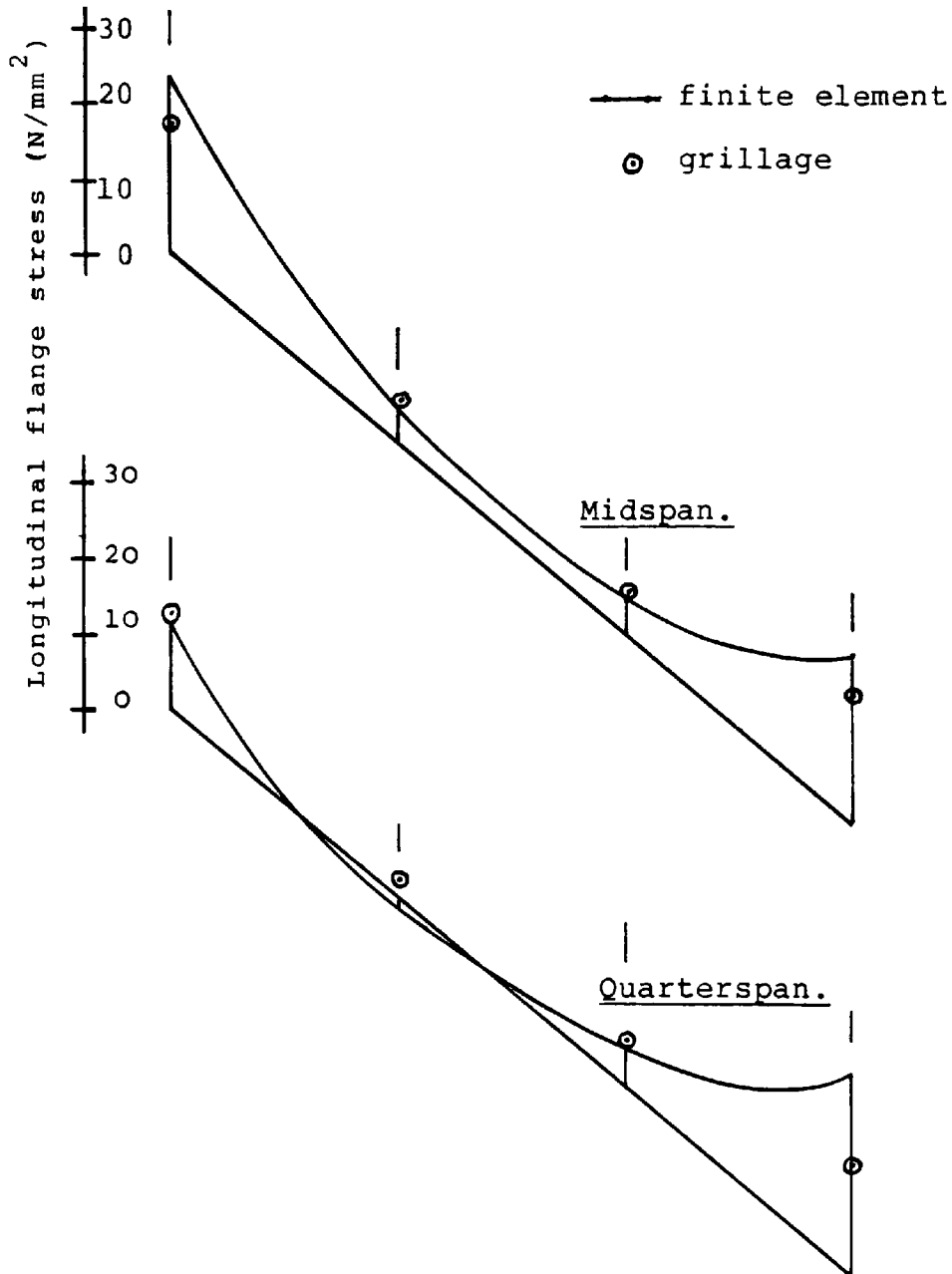
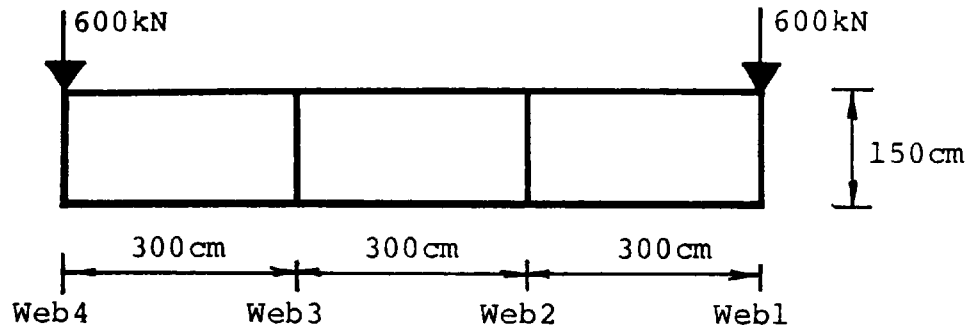


FIGURE 7.12 - LONGITUDINAL FLANGE STRESS DISTRIBUTION AT MIDSPAN AND QUARTERSPAN CROSS-SECTIONS 40 DEGREE SKEW, THREE-CELL STRUCTURE UNIFORM LINE LOADING OVER OUTER WEBS.

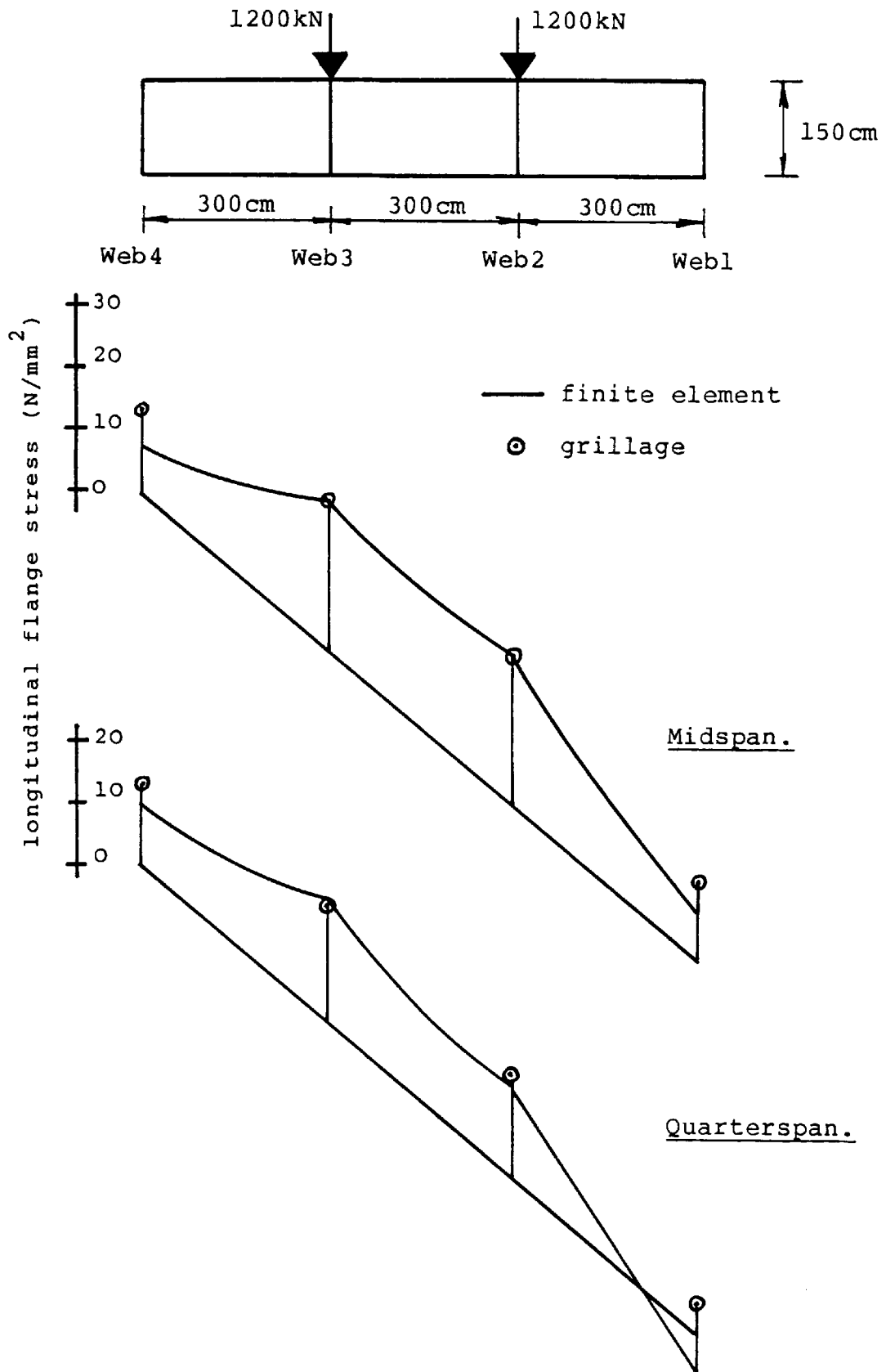


FIGURE 7.13 - LONGITUDINAL FLANGE STRESS DISTRIBUTION AT MIDSPAN AND QUARTERSPAN CROSS-SECTIONS 40 DEGREE SKEW, THREE-CELL STRUCTURE UNIFORM LINE LOADING OVER INNER WEBS.

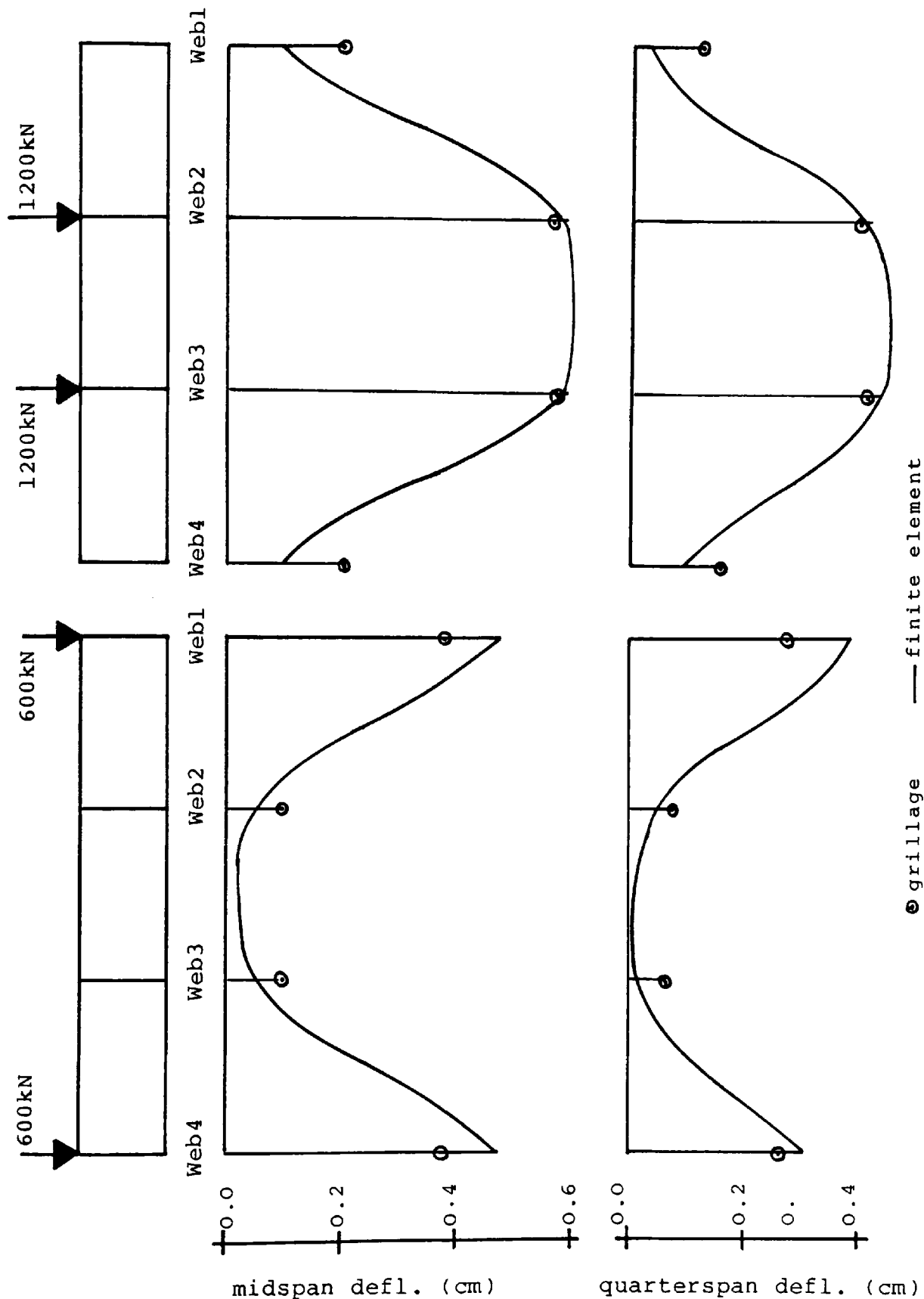


FIGURE 7.14 - DEFLECTION PROFILES AT MIDSPAN AND QUARTERSPAN CROSS-SECTIONS 40 DEGREE SKEW, THREE-CELL STRUCTURE UNIFORM LINE LOADING.

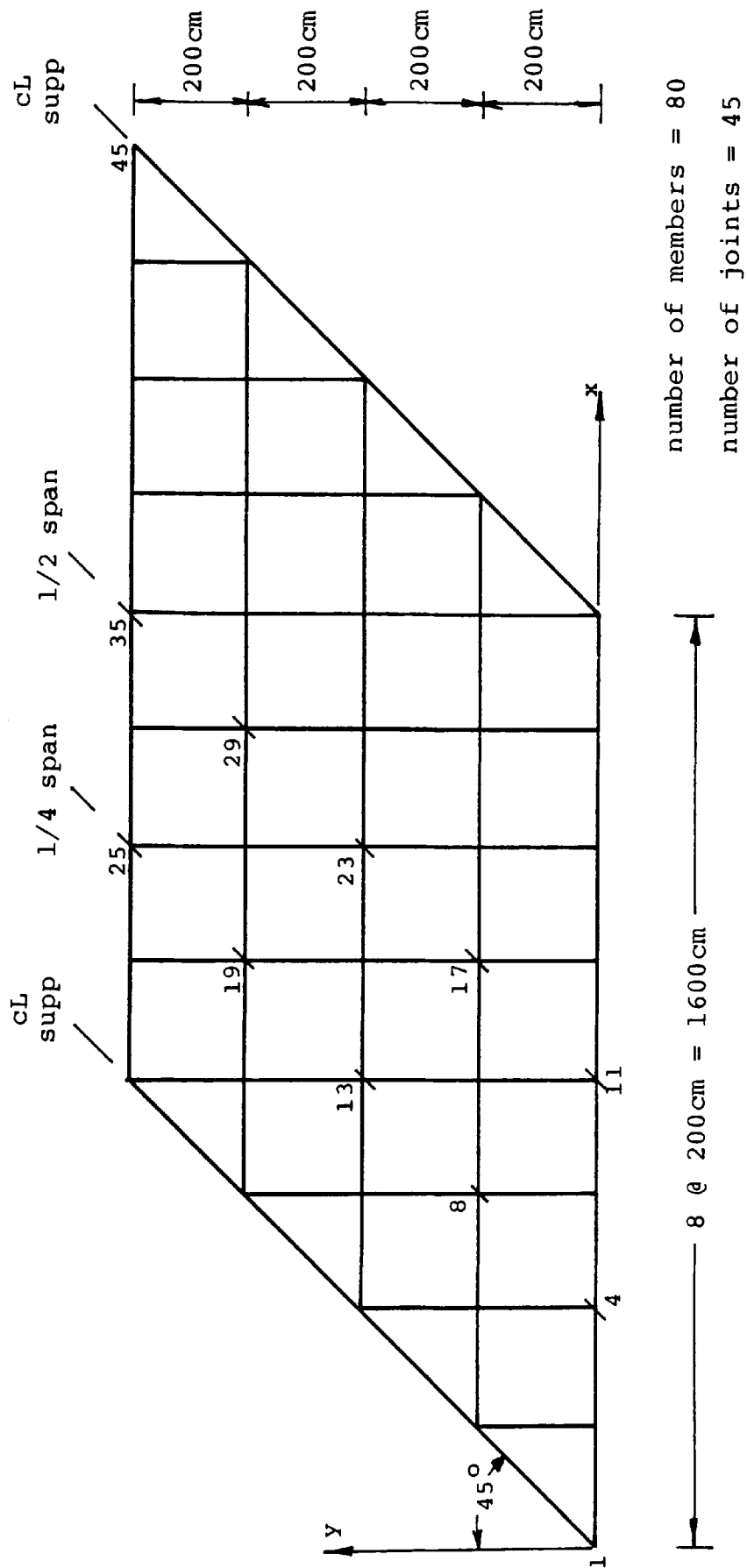


FIGURE 7.15 - COURSE ORTHOGONAL GRILLAGE MESH
45 DEGREE SKEW, FOUR-CELL STRUCTURE.

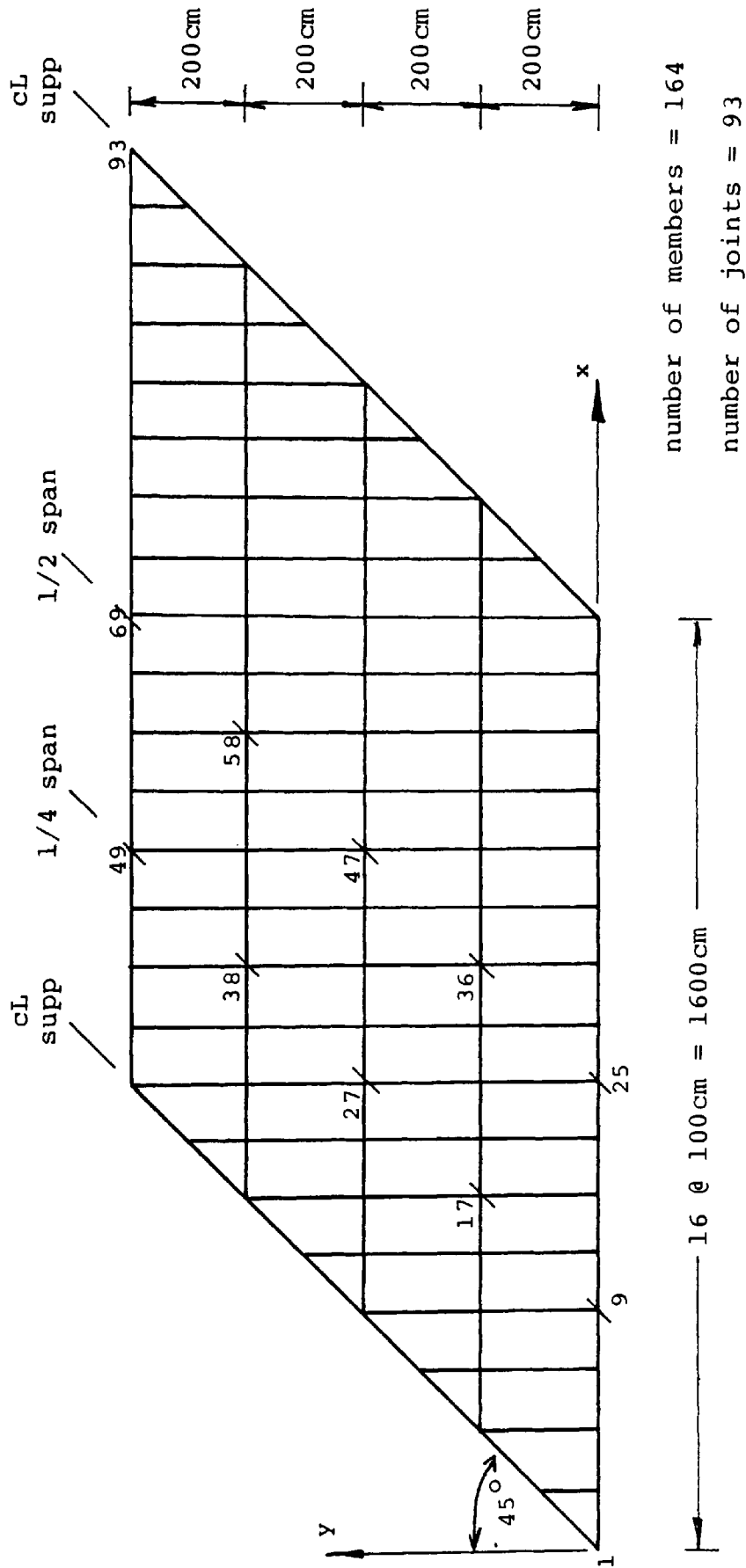


FIGURE 7.16 - FINE ORTHOGONAL GRILLAGE MESH
45 DEGREE SKEW, FOUR-CELL STRUCTURE.

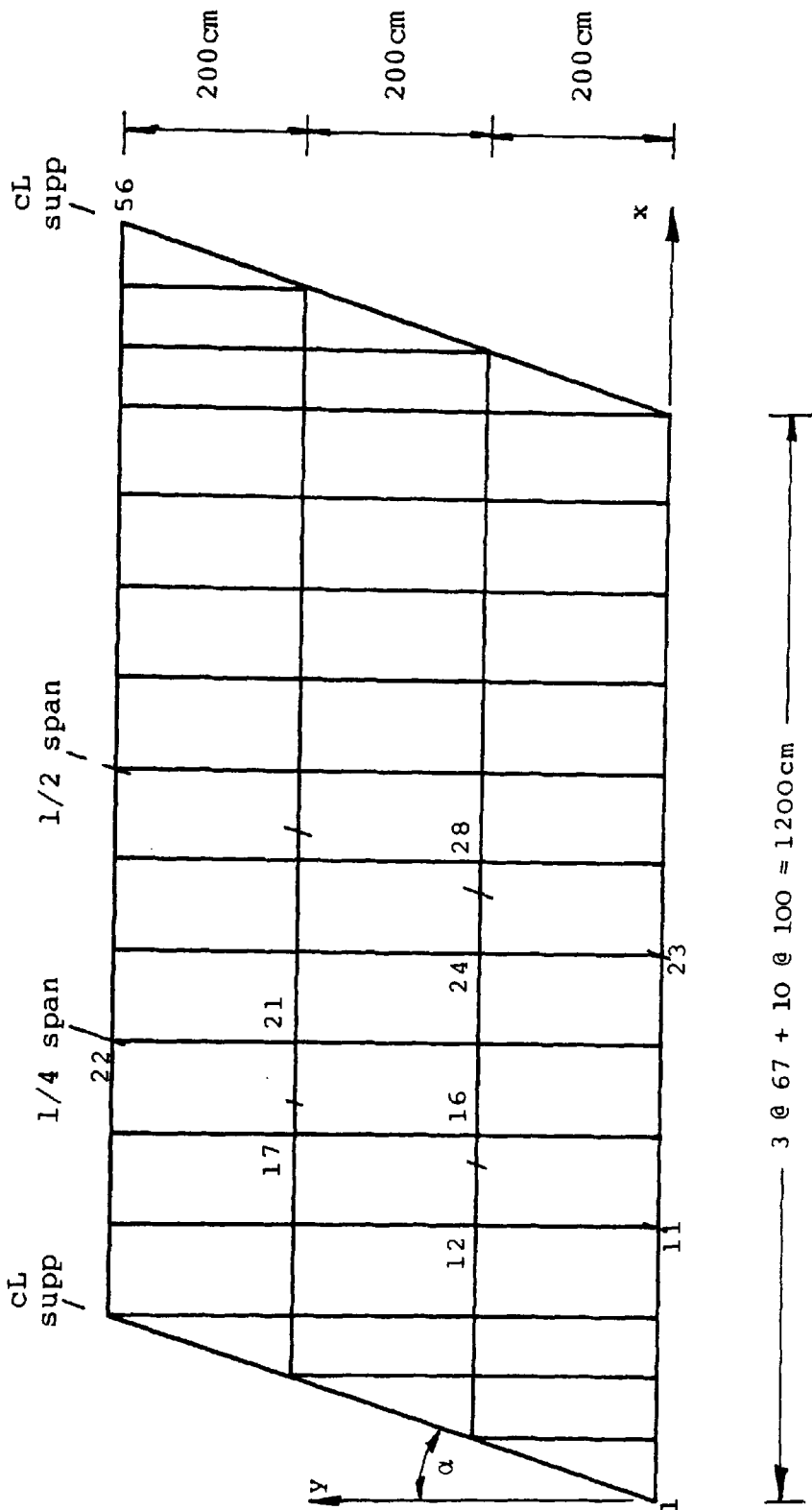


FIGURE 7.17 - DETAILS OF ORTHOGONAL GRILLAGE MESH
18 DEGREE SKEW, THREE-CELL STRUCTURE.

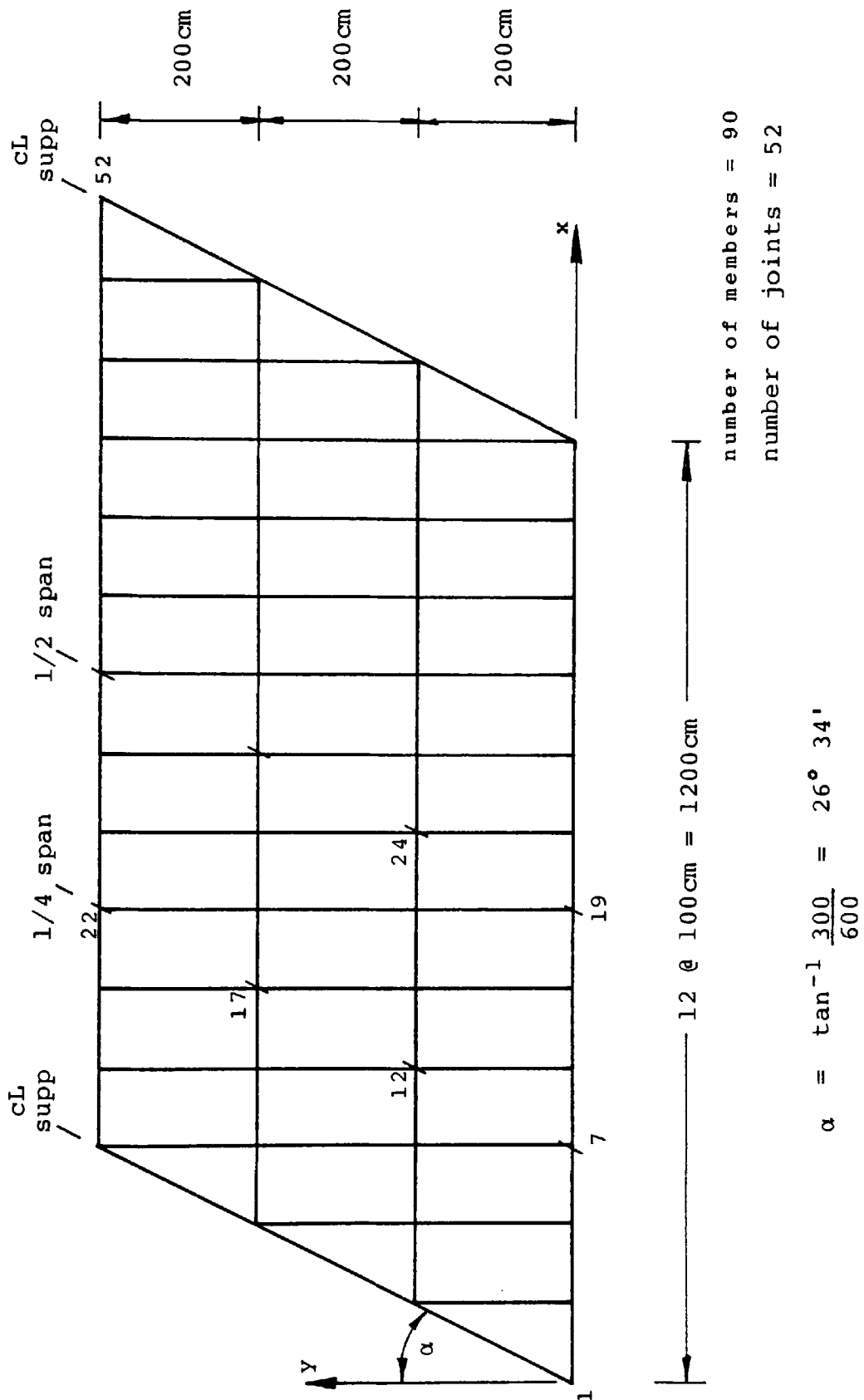


FIGURE 7.18 - DETAILS OF ORTHOGONAL GRILLAGE MESH
26 DEGREE SKEW, THREE-CELL STRUCTURE.

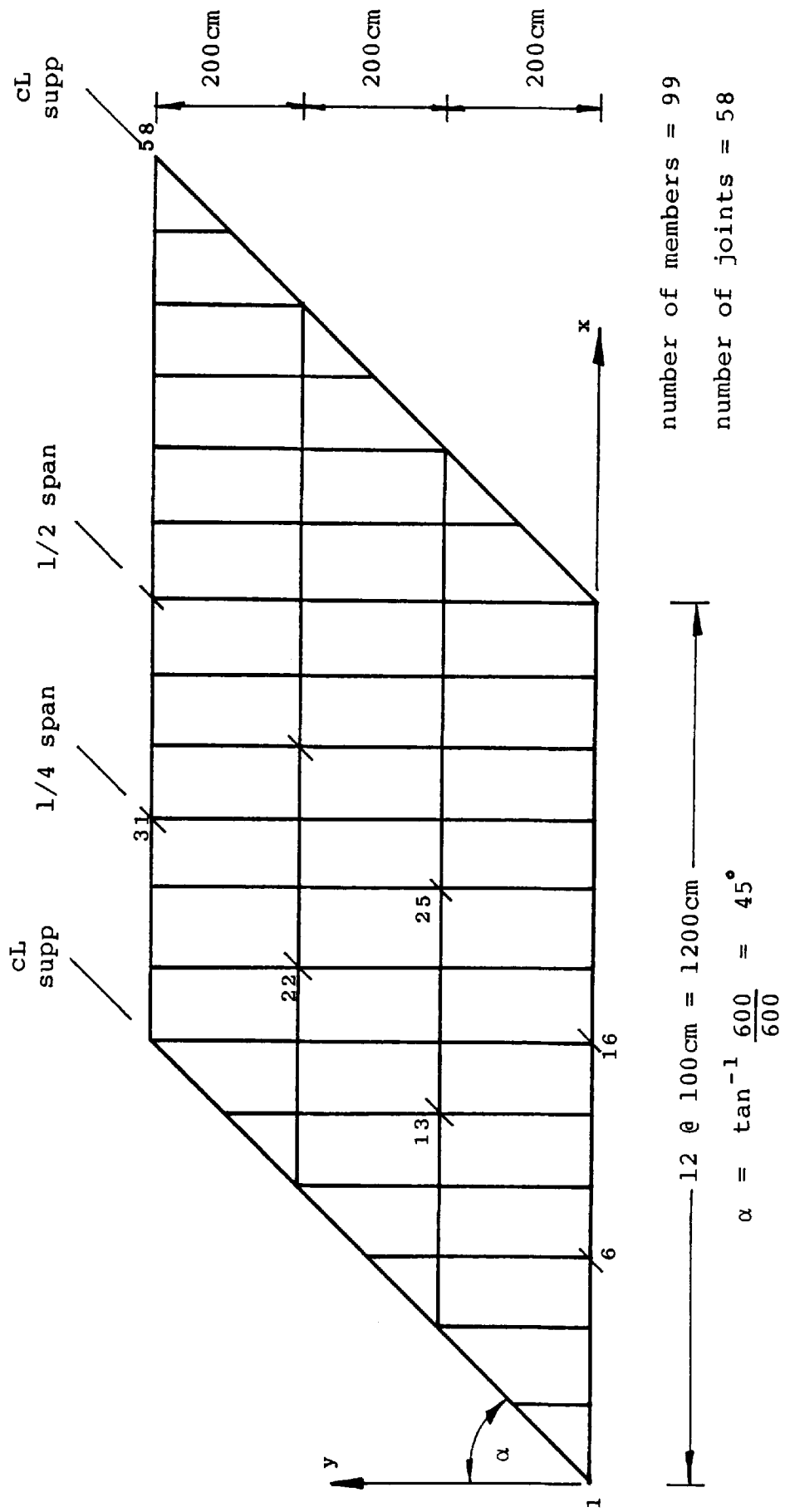


FIGURE 7.19 - DETAILS OF ORTHOGONAL GRILLAGE MESH
45 DEGREE SKEW, THREE-CELL STRUCTURE.

CHAPTER EIGHT

CONCLUSIONS AND RECOMMENDATIONS FOR FURTHER WORK

8.1. CONCLUSIONS.

The conclusions reached from each stage of the investigation have been discussed in detail at the end of each chapter. A summary of these observations will now be presented.

As a result of the work carried out it can be concluded that the grillage method is capable of modelling the overall behaviour of multi-cell structures. The following conclusions were reached with respect to geometrical and sectional idealization.

1. The effective shear area of the longitudinal grillage beams may be taken as equal to the cross-sectional area of the web when the ratio of depth of section to effective breadth of flange is not less than 2.
2. The effective breadth ratios specified in Part 3 of BS 5400 may be used to determine the second moment of area of the longitudinal grillage beams to an acceptable degree of accuracy.
3. The grillage method was capable of modelling transverse cell distortion. Either by using an equivalent beam or an equivalent frame such that the deformation of the equivalent element is

comparable to that of a Vierendeel frame of the same proportions as the cross-section of the multi-cell structure.

4. The overall torsional behaviour of a multi-cell structure may be represented by the torsional inertia of the transverse cross-section. The torsional inertia is calculated on the basis of the equivalent single cell represented by the flanges and outer webs only. The ratio of overall breadth to span of structure is used to determine the percentage allocation of this torsional inertia to the longitudinal grillage beams. The remainder is allocated to the transverse grillage beams. The torsional inertia in each direction is shared equally to all beams.

5. In the analysis of straight multi-cell structures results of acceptable accuracy were achieved using five transverse grillage beams for midspan point loading cases, whilst the use of nine transverse grillage beams is recommended for uniform line loading. In the case of skew structures the use of nine transverse grillage beams will produce results to an acceptable degree of accuracy. However, it is anticipated that more than nine grillage beams will be necessary to produce a suitable mesh arrangement.

The following conclusions were reached with respect to the accuracy of the grillage method as a result of the study of straight multi-cell structures presented in chapter 5.

6. The web deflection values at the loaded webs was accurately predicted. The maximum underestimation being -4.2% and the maximum overestimation being +5.7%. The deflection values at unloaded webs were not so accurately predicted, but the overall deformation of the cross-section was closely modelled.
7. The longitudinal flange stress at the loaded web positions was predicted to an acceptable degree of accuracy. In all the examples considered the grillage method tended to overestimate the stress, the maximum overestimation being +15.9% at the critical midspan cross-section. The results for uniform line loading were generally more accurate than the midspan point loading cases.

The finite element study of skew single cell structures in chapter 6 produced the following conclusions.

8. The effective breadth ratios specified in Part 3 of BS 5400 may be used to determine the effective breadth of flange plates in skew structures.

The effective breadth ratio at the midspan cross-section for midspan point load conditions should be determined from Table 13 using the

$$\frac{b}{L (\cos\theta)^{3/2}} \quad \text{ratio}$$

The effective breadth ratio at the midspan cross-section for the uniform line load condition and at the quarterspan cross-section for both load conditions should be determined from Table 4 or 13 using the

$$\frac{b}{L (\cos\theta)^2} \quad \text{ratio}$$

Use of these ratios provide effective breadth values for skewed structures to a comparable accuracy to those for straight structures using the standard b/L ratio.

9. The use of intermediate diaphragms in skewed structures reduces the deformation of the cross-section, resulting in a reduction in the maximum web deflection and longitudinal flange stress values. It can also be assumed that the diaphragms are absolutely flexible in a direction parallel to the web for skew angles up to 40 degrees.

The study of skew multi-cell structures reported in chapter 7 demonstrated that the grillage method can predict the overall behaviour for angles of skew up to 45 degrees to an acceptable degree of accuracy. The conclusions can be summarized as follows.

10. The orthogonal mesh grillage will produce more accurate results than a skew mesh idealization.

11. When the loading develops sagging moments in the transverse direction the results for web deflection and longitudinal flange stress at the midspan cross-section are comparable to those for straight structures. The results when the loading causes transverse hogging effects were less accurate, the degree of accuracy reducing with increasing angle of skew.

The overall conclusion reached from the investigation may be summarized as follows.

12. The finite element analysis of skew multi-cell structures may require up to 100 times more cpu time than the grillage method. This represents a substantial cost to the designer. The grillage solution is also easily obtained using a low cost micro-computer system.

These facts reinforce the belief that the grillage method developed in this thesis represents a valuable initial design aid for the analysis of straight and skew multi-cell structures. The method has been proven to produce results of acceptable accuracy under a variety of definable loading conditions.

8.2. RECOMMENDATIONS FOR FURTHER WORK.

The proposals for further work have been established on the basis that the simplicity of the grillage method of analysis be retained.

1. There is need to reconsider the method adopted for modelling cell distortion. The method as it stands cannot accurately model the effect of asymmetrical loading in straight multi-cell structures or loading on skew structures which develop transverse hogging effects. This may require an alternative to the Vierendeel frame approach considered in this thesis for the development of the transverse grillage beam sectional properties.
2. In the development of an orthogonal mesh for the analysis of skew multi-cell structures, joints have to be inserted at positions along the longitudinal webs where member forces or web deflections are required. This can result in a mesh layout with an excessive number of variably spaced transverse grillage beams. The use of the linear parametric element described by DELPAK and PESHKAM (1984) for the longitudinal grillage beams would result in a mesh layout with regularly spaced transverse grillage beams. This would assist in the development of the grillage mesh using automatic mesh generation facilities within the program. This beam element provides displacements and member

forces at any specified interval along its length, thus assisting in the determination of the maximum effects which may occur at any position when a skew structure is subjected to uniformly distributed loading. The use of this element would not substantially increase the number of degrees of freedom required for solution and hence would have little effect on computer storage requirements, etc..

3. The program in its present form can analyse continuous straight and skew structures and a study could be undertaken to consider the accuracy of the method for structures of this nature. In addition, the application to the analysis of structures of variable cross-section can readily be accomplished with the inclusion in the program of the stiffness matrix for an element of variable section.
4. The effect of diaphragms in skew single cell structures was considered in chapter 6 and tentative recommendations were given with respect to the expected accuracy of the effective breadth ratios when diaphragms are present. The application of the grillage method to the analysis of multi-cell structures with intermediate diaphragms needs to be considered, in order that conclusive recommendations may be presented for structures which incorporate intermediate diaphragms.

REFERENCES

AL-NAJJAR, K.M.A. (1984), "The Analysis of Multi-Cellular Structures ", M.Sc. Thesis (CNA), The Polytechnic of Wales.

BS 5400, Part 3 (1982), " Code of practice for design of steel bridges ", British Standards Institution, London.

CHEUNG, Y.K. (1968), "The finite strip method in the analysis of elastic plates with two opposite simply supported ends ", Proc. I.C.E. Dec 1968, Vol 40.

CLARK, L.A. (1970), "The provision of reinforcement in simply supported skew bridge slabs in accordance with elastic moment fields ", Cement and Concrete Assoc. Technical Report No. 42.450

CLOUGH, R.W. (1960), "The finite element in plane stress analysis ", Proc. 2nd A.S.C.E. Conf. on Electronic Computation, Pittsburgh.

COMARTIN, C.D. and SCORDELIS, A.C. (1972), " Analysis and design of skew box girder bridges ", SESM 72-14, University of California, Berkeley.

Committee of Inquiry into the basis for design and method of erection of steel box girder bridges, INTERIM DESIGN AND WORKMANSHIP RULES, D.o.E. London, 1973.

CRISFIELD, M.A. (1971), " Finite Element methods for the analysis of multi-cellular structures ", Proc. I.C.E., March 1971, Vol 48.

CUSENS, A.R. (1974), " Load Distribution in Concrete Bridge Decks ", CIRIA Report Number 53.

CUSENS, A.R. and PAMA R.P. (1975), " Bridge Deck Analysis " John Wiley and Sons.

DE FRIES-SKENE, A. and SCORDELIS, A.C. (1964), " Direct Stiffness solution for folded plates ", Proc. A.S.C.E., ST 4.

DELPACK, R and PESKHAM, V. (1984), " Use of linear parametric element in analysing space structures ", Proc. Third Inter. Conference on Space Structures, Univ. of Surrey, Sept 1984.

EVANS, H.R. and SHANMUGAM, N.E. (1979), " An approximate grillage approach to the analysis of cellular structures ", Proc. I.C.E., March 1979, Vol. 67

GERE, J.M. and WEAVER, W. (1965), " Analysis of framed structures ", Van Nostrand.

GOLDBERG, J.E. and LEVE, H.L. (1957), "Theory of prismatic folded plate structures ", I.A.B.S.E., Zurich, No. 87.

HAMBLY, E.C. (1976), " Bridge Deck Behaviour ", Chapman and Hall, London.

HIGHWAY ENGINEERING COMPUTER BRANCH, D.o.E., London,
HECB/BI/5, " Design charts for orthotropic right bridge
decks ", September 1973.

HIGHWAY ENGINEERING COMPUTER BRANCH, D.o.E., London,
HECB/BI/7, " User guide for slab and pseudo-slab bridge
decks ", Chapters 3 and 4, October 1981.

JUST, D.J. (1978), " Deep plane frameworks with stiffened
joints ", Structural Engineer, Vol 56B, No. 4 (Dec).

JUST, D.J. (1981), " Behaviour of skewed beam and slab
bridge decks ", Journal A.S.C.E., No. 107, ST 2.

KOLLBRUNNER, C.F. and BASLER, K. (1969), " Torsion in
Structures ", translated from the German edition by E.C.
Glauser, Springer-Verlag, Berlin.

KRISTEK, V, (1979), " Theory of box girders ",
John Wiley and Sons.

KRISTEK, V. (1983), " Folded plates with deformable end
cross-sections ", Proc. I.C.E., Sept 1983, Vol. 75.

MAISEL, B.I., ROWE, R.E. and SWANN, R.A., (1973),
" Concrete box girder bridges ", Structural Engineer,
Vol. 51, No. 10 (Oct).

Discussion on above, (1974), Structural Engineer,
Vol 52, No. 7 (July).

McHENRY, D. (1943), " A lattice analogy for the solution of stress problems ", Proc. I.C.E., Dec 1943, Vol 21.

MEGSON, T.H.G. (1974), " Linear analysis of thin walled elastic structures ", Surrey University Press.

MEGSON, T.H.G. (1980), " Strength of materials for Civil Engineers ", Nelson.

MOFFATT, K.R. and DOWLING, P.J. (1972), " Parametric study on the shear lag phenomenon in steel box girder bridges ", Engineering Structures Laboratory, Civil Eng. Dept., Imperial College, London, CESLIC Report BG 17.

MOFFATT, K.R. and DOWLING, P.J. (1975), " Shear lag in box girder bridges ", Structural Engineer, Vol 53, No.10 (Oct).

MORICE, P.B. and LITTLE, G. (1956), " Right Bridge decks subjected to Abnormal loads ", Cement and Concrete Assoc.

RICHMOND, B, (1966), " Twisting of thin-walled box girders ", Proc. I.C.E., April 1966, Vol 33.

ROCKEY, K.C., BANNISTER, J.L. and EVANS, H.R. (1971), " Developments in Bridge Design and Construction ", Crosby Lockwood, London.

ROCKEY, K.C. and EVANS, H.R. (1972), " The Nodal Section Method - Basic theory and validation ", Report No. NS/C/9, University College, Cardiff.

ROCKEY, K.C. and EVANS, H.R. (1975), " The Nodal Section Method for the analysis of box girders ",
I.A.B.S.E., Zurich

ROCKEY, K.C., EVANS, H.R. and NAVARATNE, L.G. (1976),
" A Theoretical investigation of box girders containing intermediate diaphragms ", Report No. NS/DIA/1,
University College, Cardiff.

SAWKO, F. (1968), " Recent developments in the analysis of steel bridges using electronic computers ", B.C.S.A. Conference on Steel Bridges, London.

SAWKO, F. and COPE, R.J. (1969), " Analysis of multi-cell bridges without transverse diaphragms - a finite element approach ", Structural Engineer, Vol 47, No.11 (Nov).

SCORDELIS, A.C. (1966), " Analysis of simply supported box girder bridges ", Report SESM 66-17, Univ. of California, Berkeley.

SHANMUGAM, N.E. (1978), " The design of Multi-Cell Structures ", Ph.D. Thesis, University College, Cardiff.

SMYTH, W.J.R. and SRINIVASAN, S. (1973), " The analysis of Gateshead Highway ", Structural Engineer, Vol. 51, No. 2.

TAHERIAN, A.R. and EVANS, H.R. (1977), " The bar simulation method for the calculation of shear lag in multi-cell and continuous box girders ", Proc. I.C.E., Dec 1977, Vol 63.

TURNER, M.J., CLOUGH, R.W., MARTIN, H.C. and TOPP, L.J. (1956), " Stiffness and deflection analysis of complex structures ", Journal Aero. Sc., Vol 23.

WEST, R. (1973), " Recommendations on the use of grillage analysis for Slab and Pseudo-slab bridge decks ", Cement and Concrete Association / CIRIA.

WITTRICK, W.H. (1963), " Torsion of a multi-webbed rectangular tube ", Aircraft Eng., No. 25

WRIGHT, R.N., ABDEL-SAMAD, S.R. and ROBINSON, A.R. (1968), " BEF for analysis of box girders ", Journal A.S.C.E. No. 94, ST 7.

ZEINKIEWICZ, O.C. (1977), " The finite element method ", McGraw Hill.

COMPUTER PROGRAMS.

BOXGDR, " Analysis of box-girders using the nodal section method ", Highway Engineering Computer Branch, D.o.E., Report HECB/B/18.

GRIDS, " Program for the analysis of shear deformable grillages ", Dept. of Civil Engineering, The Polytechnic of Wales, (1981).

MUPDI, " Analysis of multi-cell box girders with rigid diaphragms and elastic supports ", Highway Engineering Computer Branch, D.o.E., Report HECB/B/11, (1976).

QUEST, " Program for the analysis of box girder bridges ", Highway Engineering Computer Branch, D.o.E. Report HECB/B/14, (1975).

SHEARGRID2, " Grillage analysis of multi-cell structures", Dept. of Civil Engineering, The Polytechnic of Wales, (1980).

STRESS, " Structural Engineering System Solver ", Massachusetts Institute of Technology, (1964).

AUTHOR'S PUBLICATION.

PUGH, D.K., DELPAK, R. and EVANS, H.R. (1983), " The use of micro-computers in the elastic analysis of multi-cell structures ", Third Inter. Conf. on Engineering Software, Imperial College, London, April 1983.

APPENDIX A.

DEVELOPMENT OF SHEAR DEFORMABLE
GRILLAGE ELEMENT STIFFNESS MATRIX.

Neglecting the action of torsion, the beam element member forces can be defined as shown in figure A.1(a). The beam is subjected to a positive vertical deflection and rotation at end 1 given by d_{z1} and θ_{y1} respectively as shown in figure A.1(b).

At a section X-X, a distance x from end 1

$$\text{Bending moment, } M = -M_{y1} + P_{z1} * x$$

$$\text{Shear force, } Q = -P_{z1}$$

The relationship between end member forces and displacements can be determined using the principle of virtual work as follows

The action of a unit virtual vertical force at end 1, figure A.1(c), produces

$$\text{virtual bending moment at X-X, } m = 1 * x$$

$$\text{and virtual shear force at X-X, } q = -1$$

The principle of virtual work gives

$$\begin{aligned} 1 * d_{z1} &= \int_0^L \frac{m * M}{EI} dx + \int_0^L \frac{q * Q}{GAs} dx \\ d_{z1} &= \frac{1}{EI} \int_0^L x(-M_{y1} + P_{z1} * x) dx + \frac{1}{GAs} \int_0^L P_{z1} dx \\ &= \frac{P_{z1} * L^3}{3EI} + \frac{P_{z1} * L}{GAs} - \frac{M_{y1} * L^2}{2EI} \end{aligned}$$

substituting $n = \frac{6EI}{GA_s L^2}$ gives

$$dz_1 = \frac{Pz_1 * L^3 (1 + n)}{3EI} - \frac{Myl * L^2}{2EI} \quad \text{----- Eqn A.1}$$

The action of a unit virtual moment at end 1, figure A.1(d) produces

virtual bending moment at X-X, $m = -1$

and virtual shear force at X-X, $q = 0$

The principle of virtual work gives

$$\begin{aligned} 1 * \theta_{y1} &= \int_0^L \frac{m * M}{EI} dx + \int_0^L \frac{q * Q}{GA_s} dx \\ \theta_{y1} &= \frac{1}{EI} \int_0^L (Myl - Pz_1 * x) dx + 0 \\ &= \frac{-Pz_1 * L^2}{2EI} + \frac{Myl * L}{EI} \quad \text{----- Eqn A.2} \end{aligned}$$

Equations A.1 and A.2 can be expressed in matrix form as

$$\begin{Bmatrix} dz_1 \\ \theta_{y1} \end{Bmatrix} = \begin{bmatrix} \frac{L^3(1+n)}{3EI} & \frac{-L^2}{2EI} \\ \frac{-L^2}{2EI} & \frac{L}{EI} \end{bmatrix} \begin{Bmatrix} Pz_1 \\ My_1 \end{Bmatrix} \quad \text{----- Eqn A.3}$$

The inverse of which gives

$$\begin{Bmatrix} Pz1 \\ My1 \end{Bmatrix} = \begin{bmatrix} \frac{12EI}{L^3} \cdot \frac{1}{1+2n} & \frac{6EI}{L^2} \cdot \frac{1}{1+2n} \\ \frac{6EI}{L^2} \cdot \frac{1}{1+2n} & \frac{4EI}{L} \cdot \frac{1+n/2}{1+2n} \end{bmatrix} \begin{Bmatrix} dz1 \\ \theta y1 \end{Bmatrix} \quad \text{----- Eqn A.4}$$

Equilibrium of beam element gives

$$Pz2 = -Pz1$$

$$\text{and } My2 = -My1 + Pz1 * L$$

which gives

$$\begin{Bmatrix} Pz2 \\ My2 \end{Bmatrix} = \begin{bmatrix} \frac{-12EI}{L^3} \cdot \frac{1}{1+2n} & \frac{-6EI}{L^2} \cdot \frac{1}{1+2n} \\ \frac{6EI}{L^2} \cdot \frac{1}{1+2n} & \frac{2EI}{L} \cdot \frac{1-n}{1+2n} \end{bmatrix} \begin{Bmatrix} dz1 \\ \theta y1 \end{Bmatrix} \quad \text{----- Eqn A.5}$$

Similarly the beam element can be subjected to displacements at end 2, resulting in the following overall stiffness matrix

$$\begin{Bmatrix} Pz1 \\ My1 \\ Pz2 \\ My2 \end{Bmatrix} = \begin{bmatrix} \frac{12EI}{L^3} \frac{1}{1+2n} & \frac{6EI}{L^2} \frac{1}{1+2n} & -\frac{12EI}{L^3} \frac{1}{1+2n} & \frac{6EI}{L^2} \frac{1}{1+2n} \\ & \frac{4EI}{L} \frac{1+n/2}{1+2n} & -\frac{6EI}{L^2} \frac{1}{1+2n} & \frac{2EI}{L} \frac{1-n}{1+2n} \\ \text{symmetrical} & & \frac{12EI}{L^3} \frac{1}{1+2n} & -\frac{6EI}{L^2} \frac{1}{1+2n} \\ & & & \frac{4EI}{L} \frac{1+n/2}{1+2n} \end{bmatrix} \begin{Bmatrix} dz1 \\ \theta y1 \\ dz2 \\ \theta y2 \end{Bmatrix}$$

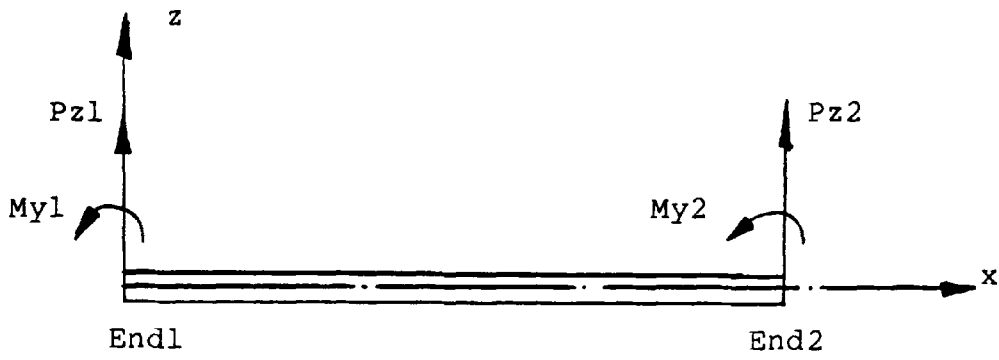
The relationship between torsional moment and rotation is not affected by displacements dz and θy and can be expressed as

$$\begin{Bmatrix} Mx1 \\ Mx2 \end{Bmatrix} = \begin{bmatrix} \frac{GJ}{L} & -\frac{GJ}{L} \\ -\frac{GJ}{L} & \frac{GJ}{L} \end{bmatrix} \begin{Bmatrix} \theta x1 \\ \theta x2 \end{Bmatrix} \quad \text{----- Eqn A.7}$$

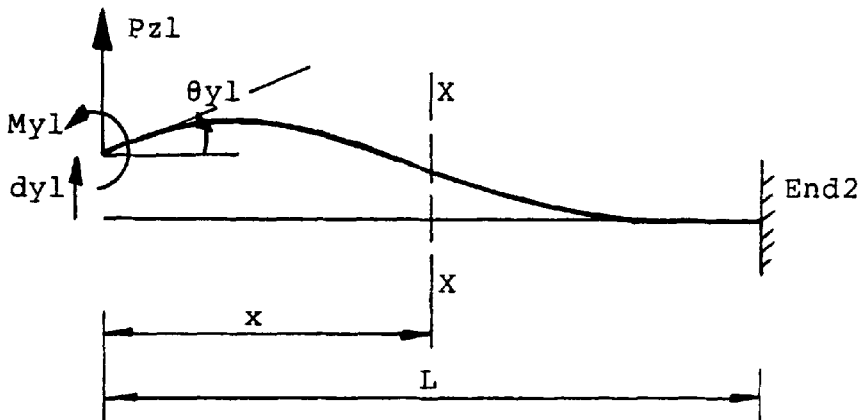
resulting in the following element stiffness matrix

$$\begin{bmatrix} Pz1 \\ Mx1 \\ My1 \\ Pz2 \\ Mx2 \\ My2 \end{bmatrix} = \begin{bmatrix} \frac{12EI}{L^3} \cdot \frac{1}{1+2n} & 0 & \frac{6EI}{L^2} \cdot \frac{1}{1+2n} & -\frac{12EI}{L^3} \cdot \frac{1}{1+2n} & 0 & \frac{6EI}{L^2} \cdot \frac{1}{1+2n} \\ 0 & \frac{GJ}{L} & 0 & 0 & -\frac{GJ}{L} & 0 \\ \frac{4EI}{L} \cdot \frac{1+n/2}{1+2n} & 0 & -\frac{6EI}{L^2} \cdot \frac{1}{1+2n} & \frac{12EI}{L^3} \cdot \frac{1}{1+2n} & 0 & \frac{2EI}{L} \cdot \frac{1-n}{1+2n} \\ 0 & 0 & \frac{6EI}{L^2} \cdot \frac{1}{1+2n} & -\frac{12EI}{L^3} \cdot \frac{1}{1+2n} & 0 & -\frac{6EI}{L^2} \cdot \frac{1}{1+2n} \\ 0 & \frac{GJ}{L} & 0 & 0 & \frac{GJ}{L} & 0 \\ \frac{4EI}{L} \cdot \frac{1+n/2}{1+2n} & 0 & 0 & 0 & 0 & \frac{4EI}{L} \cdot \frac{1+n/2}{1+2n} \end{bmatrix} \begin{bmatrix} dz1 \\ \theta x1 \\ \theta y1 \\ dz2 \\ \theta x2 \\ \theta y2 \end{bmatrix}$$

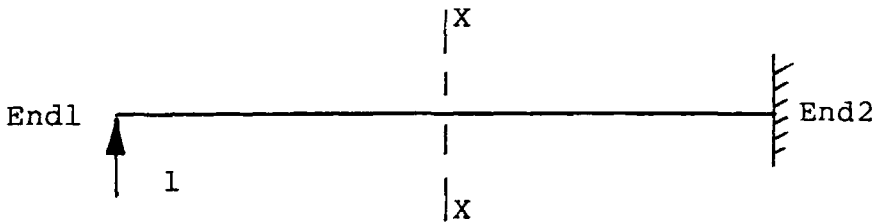
symmetrical



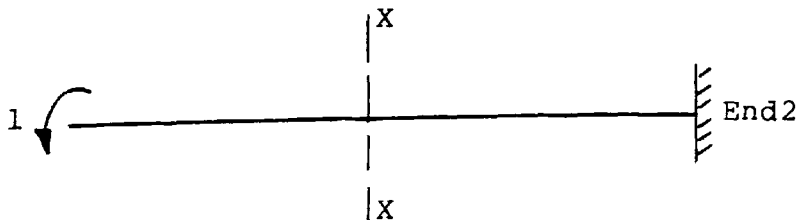
(a) beam element member forces.



(b) end one displacements.



(c) unit virtual vertical force.



(d) unit virtual moment.

FIGURE A.1 - Shear deformable grillage beam element.

APPENDIX B.

DERIVATION OF DEFLECTION FORMULAE FOR
SHEAR-DEFORMABLE SIMPLY SUPPORTED BEAM

The principle of virtual work is used for the determination of the deflection formulae, integration of the equations being carried out graphically. The loading diagrams and corresponding bending moment and shear force diagrams are shown in figures B.1 and B.2.

The principle of virtual work gives

$$l \cdot d = \int_0^L \frac{m M dx}{EIY} + \int_0^L \frac{q Q dx}{GAs} \quad \text{---- eqn B.1.}$$

where l = unit virtual force

d = beam deflection at position of unit virtual force

m = bending moment in beam due to unit virtual force

M = bending moment in beam due to applied loads

IY = second moment of area of beam cross-section

q = shear force in beam due to unit virtual force

Q = shear force in beam due to applied loads

As = effective shear area of beam cross-section

When graphical integration is used, equation B.1 may be expressed as

$$1.d = \sum \frac{m(o) A(m)}{EIY} + \sum \frac{q(o) A(q)}{GAs} \text{ ---- eqn B.2.}$$

where A(m) = area of B.M. diagram due to applied loads

m(o) = ordinate of virtual unit load B.M. diagram
at centroid of A(m) diagram

A(q) = area of S.F. diagram due to applied loads

q(o) = ordinate of virtual unit load S.F. diagram
at centroid of A(q) diagram

Using equation B.2. the following deflection formulae were derived

1. MIDSPAN POINT LOAD.

(a) Midspan Deflection.

$$d = \frac{2}{EIY} \left[\frac{WL}{4} \cdot \frac{L}{4} \cdot \frac{L}{6} \right] + \frac{2}{GAs} \left[\frac{W}{2} \cdot \frac{L}{2} \cdot \frac{1}{2} \right]$$

$$= \frac{WL^3}{48 EIY} + \frac{WL}{4 GAs} \text{ ---- eqn B.3.}$$

(b) Quarterspan Deflection.

$$d = \frac{1}{EIY} \left[\frac{WL \cdot L \cdot L}{8 \cdot 8 \cdot 8} + \frac{WL \cdot L \cdot L}{8 \cdot 8 \cdot 6} + \frac{WL \cdot L \cdot 7L}{4 \cdot 8 \cdot 48} + \frac{WL \cdot L \cdot L}{4 \cdot 4 \cdot 12} \right]$$

$$+ \frac{1}{GAs} \left[\frac{-W \cdot L \cdot -3}{2 \cdot 4 \cdot 4} + \frac{-W \cdot L \cdot 1}{2 \cdot 4 \cdot 4} + \frac{W \cdot L \cdot 1}{2 \cdot 2 \cdot 4} \right]$$

$$= \frac{11 WL^3}{768 EIY} + \frac{WL}{8 GAs} \text{ ---- eqn B.4.}$$

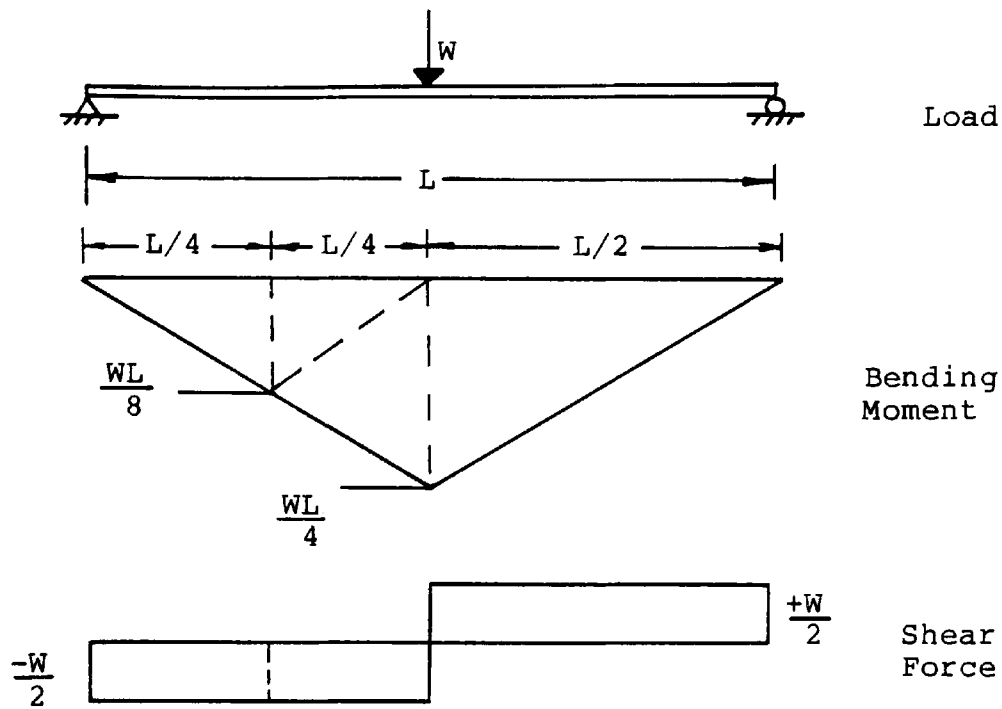
2. UNIFORM LINE LOAD.

(a) Midspan Deflection.

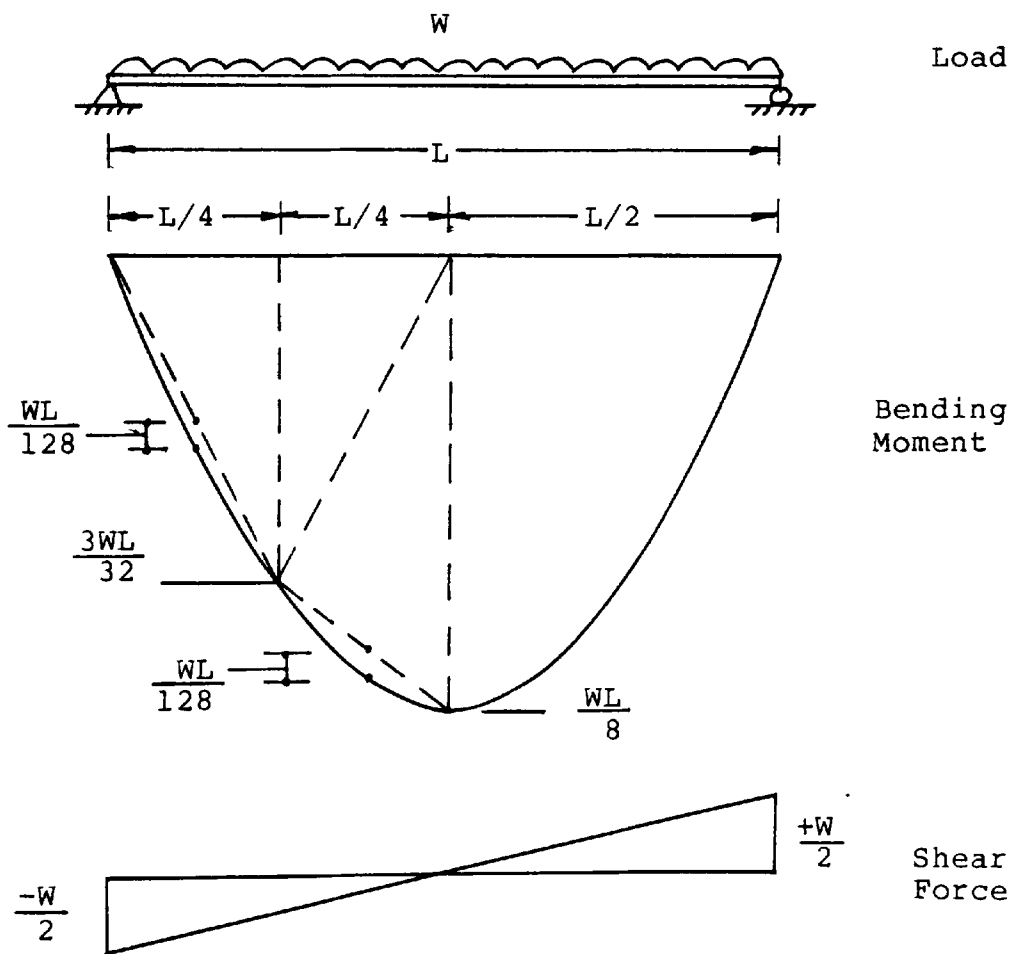
$$\begin{aligned}
 d &= \frac{2}{EIY} \left[\frac{2}{3} \cdot \frac{WL}{8} \cdot \frac{L}{2} \cdot \frac{5L}{32} \right] + \frac{2}{GAs} \left[\frac{W}{2} \cdot \frac{L}{4} \cdot \frac{1}{2} \right] \\
 &= \frac{5 W L^3}{384 EIY} + \frac{W L}{8 GAs} \quad \text{----- eqn B.5.}
 \end{aligned}$$

(b) Quarterspan Deflection.

$$\begin{aligned}
 d &= \frac{1}{EIY} \left[\frac{3WL}{32} \cdot \frac{L}{8} \cdot \frac{L}{8} + \frac{2}{3} \cdot \frac{WL}{128} \cdot \frac{L}{4} \cdot \frac{3L}{32} + \frac{3WL}{32} \cdot \frac{L}{8} \cdot \frac{L}{6} \right. \\
 &\quad \left. + \frac{WL}{8} \cdot \frac{L}{8} \cdot \frac{7L}{48} + \frac{2}{3} \cdot \frac{WL}{128} \cdot \frac{L}{4} \cdot \frac{5L}{32} + \frac{2}{3} \cdot \frac{WL}{8} \cdot \frac{L}{2} \cdot \frac{5L}{64} \right] \\
 &\quad + \frac{1}{GAs} \left[\frac{-3W}{8} \cdot \frac{L}{4} \cdot \frac{-3}{4} + \frac{-W}{4} \cdot \frac{L}{8} \cdot \frac{1}{4} + \frac{W}{2} \cdot \frac{L}{4} \cdot \frac{1}{4} \right] \\
 &= \frac{19 W L^3}{2048 EIY} + \frac{3 W L}{32 GAs} \quad \text{----- eqn B.6.}
 \end{aligned}$$



(a) Midspan Point Load.



(b) Uniform line load.

FIGURE B.1 - Load, bending moment and shear force diagrams. Midspan point and uniform line loads.

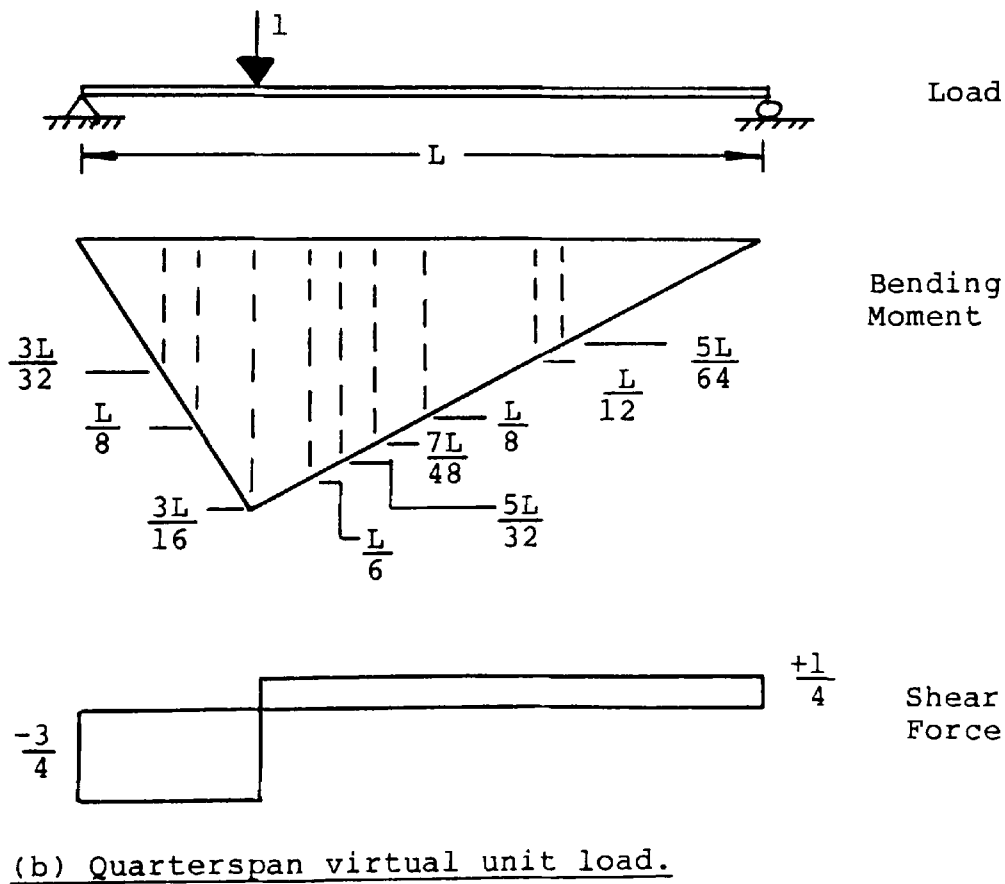
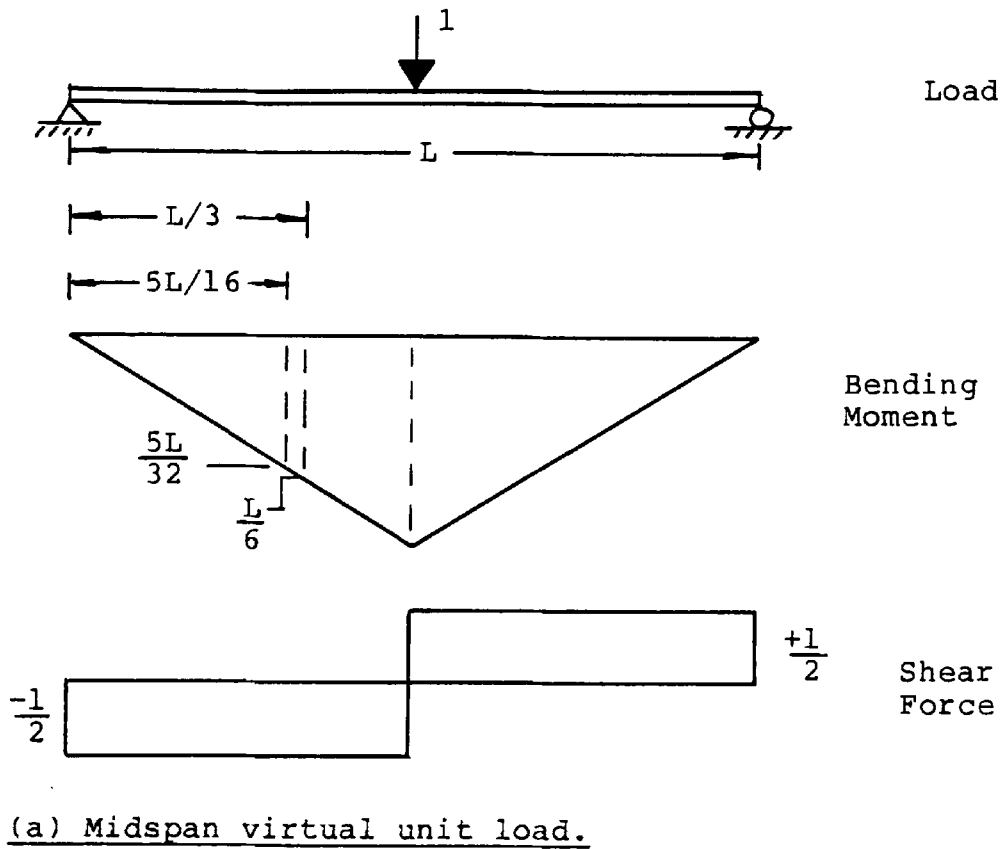


FIGURE B.2 - Load, bending moment and shear force diagrams. Midspan and quarterspan virtual unit loads.

APPENDIX C.

CONVERGENCE STUDY OF THE FINITE ELEMENT PROGRAM - QUEST

The finite element analysis employed in this thesis is based on the computer program - QUEST issued by the Highway Engineering Computer Branch of the Department of the Environment. The program utilizes a thin shell quadrilateral finite element and is of established accuracy. A study of the convergence characteristics of the method in the analysis of steel, single and multi-cell, straight and skewed structures will be considered in this Appendix.

1. STRAIGHT SINGLE CELL STUDY.

(i) One element in the depth of the web plate.

In this study a single cell straight box was subjected to midspan point loading over both webs, and the significance of mesh grading in both the longitudinal and transverse directions of the flange was considered.

Initially, the number of elements across the width of the flange was kept constant, 8 elements were used, whilst the number of elements along the span was varied from 12 to 24 in increments of 4. The values of longitudinal flange stress and web deflection are presented in Table C.1.(a). Secondly, the number of elements along the span was kept constant at 20, whilst the number of elements across the width was varied. 4, 6 and 8 elements

were used, and the results for longitudinal flange stress and web deflection are presented in Table C.1.(b).

In both cases the mesh was graded either side of the midspan section, as illustrated in the typical finite element mesh shown in figure 3.10.(a). It can be seen from the Tables that the values of longitudinal flange stress and web deflection converge as the mesh size in both directions decreases. As a result of this study it was concluded that a finite element mesh comprising 20 elements along the span and 8 elements across the width, together with 1 element in the depth of the structure produced results of acceptable accuracy.

(ii) Variation of number of elements in the web depth.

Although the QUEST user manual states that only one element is necessary to model the web over the depth of the structure, it was considered that the significance of shear deflection warranted an investigation of the effect of the number of elements in the depth of the web on the accuracy of the finite element solution.

Consequently, a study was undertaken where one quarter of the structure was analysed (use being taken of two-way symmetry) where the mesh grading was as follows

20 elements along the span direction

8 elements across the width of the flange

1 to 8 elements in the depth of the web

The structure was subjected to both midspan point and uniform line loading conditions, and the results for

longitudinal flange stress and web deflection are presented in Table C.2. The variation of longitudinal flange edge stress at the midspan cross-section with the number of elements in the depth of the web is presented in figure C.1.(a).

The stresses for midspan point loading reveal a discontinuity in the variation when 2 elements were used to represent the web, but when the number of elements was consequently increased, the stress was seen to converge. The stress intensity of 48.20 N/mm² (for the single element mesh) represents a 5% underestimation of the stress intensity of 50.71 N/mm² (when 8 elements were used). This confirms that only one element in the depth of the web is required to model the behaviour of the web.

The variation of longitudinal flange edge stress along the structure is plotted in figure C.1.(b) for the single and two element representation in the midspan point load case. These profiles reveal the discontinuity to be localised in the vicinity of the concentrated load and the effect of this discontinuity can be reduced if the load is applied more evenly over the depth of the section. No such discontinuity exists for the stress due to uniform line loading or in the results for web deflection in either loading cases considered.

2. STRAIGHT MULTI-CELL STRUCTURE STUDY.

In this study a three cell structure was considered and subjected to midspan point loading over all

webs. The number of elements used in the finite element model was as follows

20 elements along the span

1 element in the depth of the structure

2, 3, 4 and 6 elements across the width of each cell

The results for longitudinal flange stress and web deflection are presented in Table C.3. and are seen to converge. As a result of this study it was considered that the maximum possible number of elements permitted by the capacity of the program should be used to represent the width of each cell of the structure.

3. SKEW SINGLE CELL STUDY.

To assess the significance of skew on the accuracy of solution achieved, a 40 degree skew single cell structure subjected to midspan point loading was considered. The effect of mesh grading in both the longitudinal and transverse directions was considered.

Details of the mesh configurations used and the results for longitudinal flange stress and web deflection are presented in Table C.4. The results show that both the stress and deflection values converge with increasing fineness of mesh.

As a result of this study it was concluded that a finite element mesh, comprising 20 elements along the span, 8 elements across the width and a single element in the depth of the structure, may be used for the analysis of skew single cell structures.

(a) 20 elements along span.

		No. elements across flange		
		4	6	8
1 / 2 S P A N	edge stress	47.28	47.95	48.20
	mid fl. str.	31.96	32.09	32.20
	web defln.	0.630	0.632	0.632
	ψ	0.745	0.743	0.741
1 / 4 S P A N	edge stress	19.00	19.00	19.00
	mid fl. str.	19.07	19.05	19.05
	web defln.	0.416	0.417	0.417
	ψ	1.002	1.002	1.002

(b) 8 elements across width of flange.

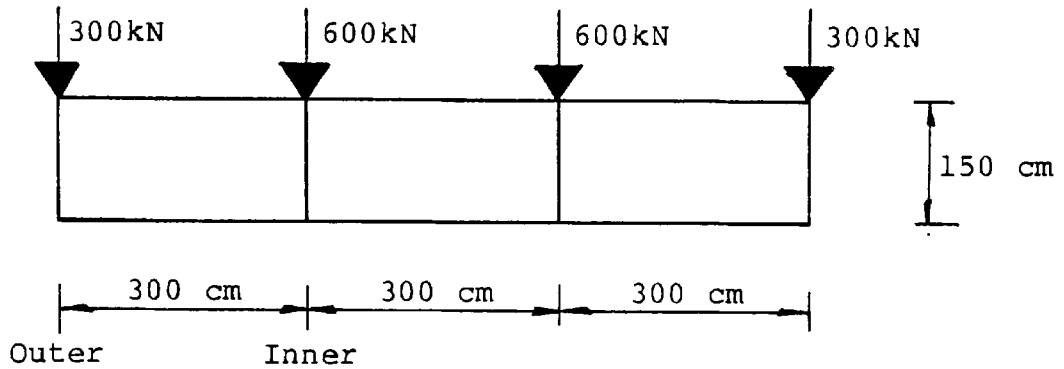
		No. elements along span			
		12	16	20	24
1 / 2 S P A N	edge stress	46.58	47.63	48.20	48.61
	mid fl. str.	32.21	32.21	32.20	32.20
	web defln.	0.626	0.630	0.632	0.633
	ψ	0.764	0.749	0.741	0.735
1 / 4 S P A N	edge stress	19.18	18.93	19.00	19.00
	mid fl. str.	18.77	18.99	19.05	19.05
	web defln.	0.412	0.415	0.417	0.418
	ψ	0.986	1.006	1.002	1.002

ψ - effective breadth ratio

TABLE C.1. - Convergence study on straight single cell structure - Midspan point loading.
Span - 16 metres, width - 3 metres,
depth - 1.5 metres, plate thickness - 1.2 cm.

	No. of elements in depth	Long. fl. edge str.		web deflection	
		1/2span	1/4span	1/2span	1/4span
M I D S P A N P O I N T	1	48.20	19.00	0.632	0.417
	2	45.77	18.98	0.634	0.417
	3	48.94	19.14	0.638	0.422
	4	49.54	19.14	0.638	0.422
	6	50.38	19.14	0.638	0.422
	8	50.71	19.08	0.634	0.419
U N I F O R M L I N E	1	59.36	44.77	1.152	0.832
	2	59.57	44.92	1.150	0.831
	3	59.51	45.26	1.162	0.844
	4	59.51	45.26	1.163	0.844
	6	59.50	45.26	1.163	0.845
	8	59.49	45.12	1.153	0.835

TABLE C.2. - Convergence study on straight single cell structure. Span - 16 metres, width - 3 metres, depth - 1.5 metres, plate thickness - 1.2 cm. Midspan point and Uniform line loading. 20 elements along span, 8 elements across width.



span = 16 metres

Details of cross-section and loading.

	Position		No. of elements per cell			
	span	web	2	3	4	6
S T R E S S	1	Outer	44.32	45.82	46.71	47.40
	/					
	2	Inner	49.80	51.60	52.64	53.55
D E F L N	1	Outer	0.615	0.622	0.625	0.626
	/					
	2	Inner	0.751	0.756	0.758	0.760
	1	Outer	0.407	0.411	0.412	0.414
	/					
	4	Inner	0.482	0.486	0.487	0.487

TABLE C.3. - Convergence study on straight three-cell structure - Midspan point loading. Variation of longitudinal flange stress (N/mm²) and web deflection (cm) with number of elements per cell.

(a) 20 elements along span.

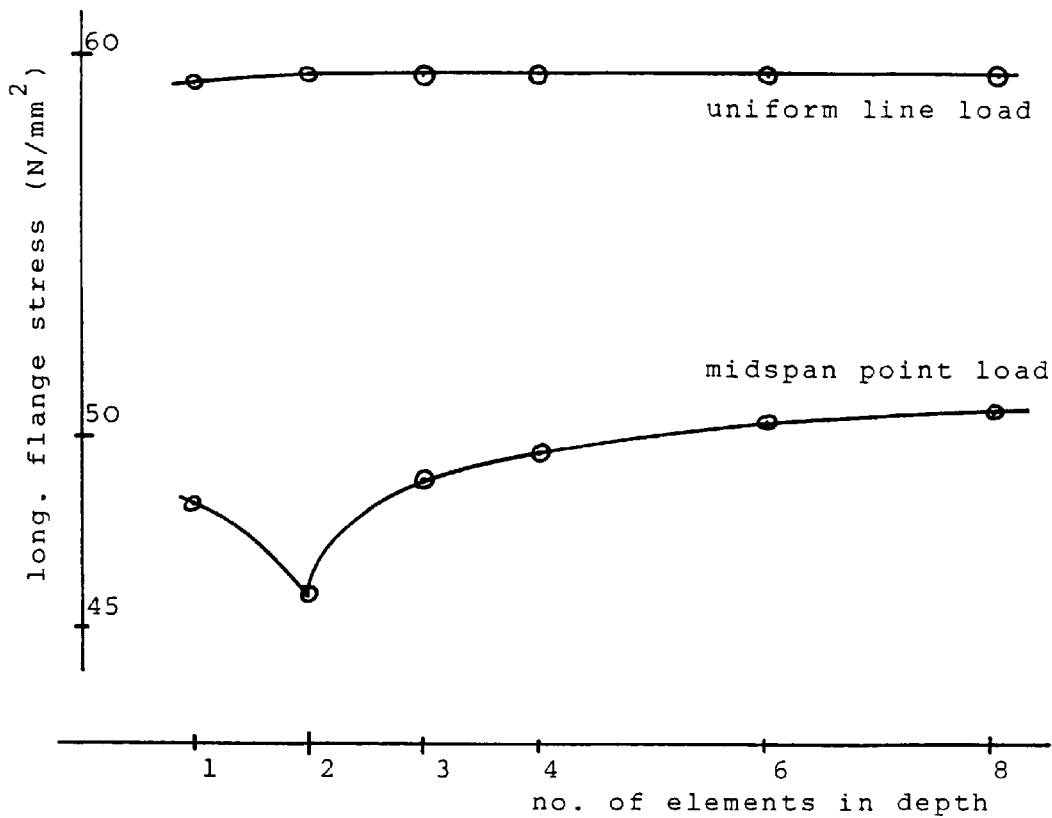
		No. elements across flange		
		4	6	8
1 / 2 S P A N	edge stress	44.98	45.95	46.38
	mid fl. str.	23.00	23.59	23.82
	web defln.	0.530	0.534	0.536
	Ψ	0.633	0.633	0.630
1 / 4 S P A N	edge 1 str.	20.45	20.57	20.51
	edge 2 str.	4.24	4.61	4.73
	mid fl. str.	12.14	12.16	12.14
	web 1 defln.	0.367	0.369	0.372
	web 2 defln.	0.303	0.305	0.305
	Ψ	0.988	0.974	0.973

(b) 8 elements across width of flange.

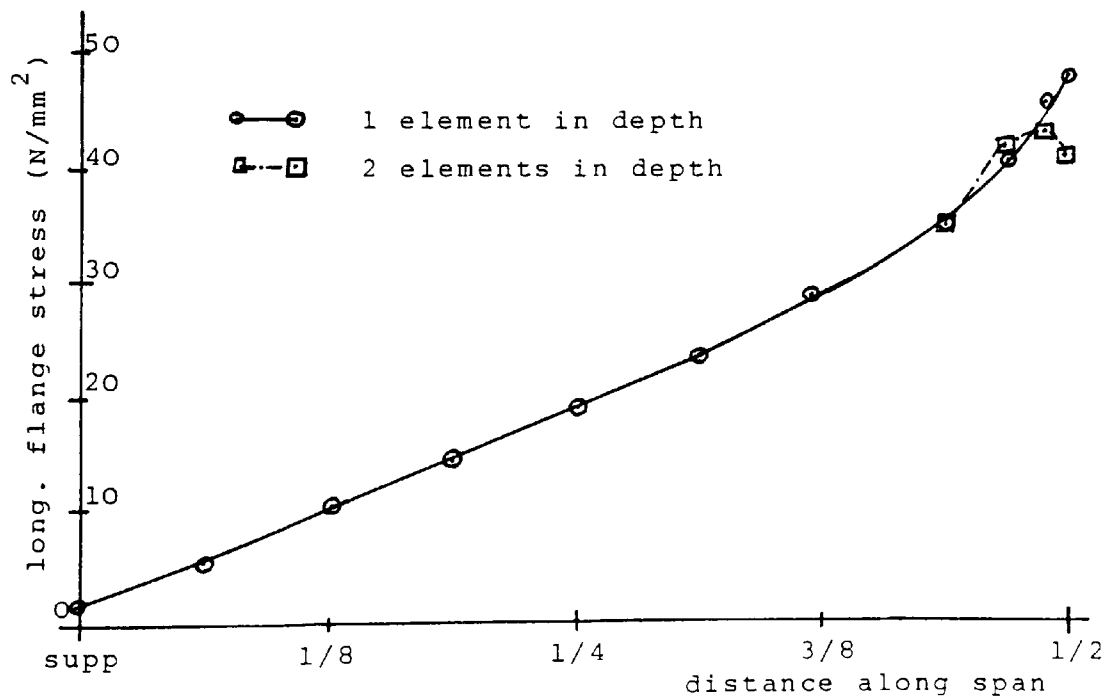
		No. elements along span			
		12	16	20	24
1 / 2 S P A N	edge stress	44.66	45.82	46.38	46.72
	mid fl. str.	23.77	23.82	23.82	23.85
	web defln.	0.520	0.530	0.536	0.538
	Ψ	0.648	0.636	0.630	0.627
1 / 4 S P A N	edge 1 str.	19.13	19.99	20.51	20.66
	edge 2 str.	6.64	5.23	4.73	4.55
	mid fl. str.	11.79	12.05	12.14	12.20
	web 1 defln.	0.354	0.365	0.372	0.373
	web 2 defln.	0.301	0.303	0.305	0.307
	Ψ	0.948	0.971	0.973	0.976

Ψ - effective breadth ratio

TABLE C.4. - Convergence study on 40 degree skew single cell structure - Midspan point loading.
Span - 16 metres, width - 3 metres,
depth - 1.5 metres, plate thickness - 1.2 cm.



(a) Variation of longitudinal flange edge stress with number of elements in depth of web.



(b) Distribution of longitudinal flange edge stress along structure - midspan point loading.

FIGURE C.1 - Finite Element Convergence Study of Straight single cell structure.

APPENDIX D.

DEVELOPMENT OF EQUIVALENT FRAME

ELEMENT STIFFNESS MATRIX

Consider the cantilever frame shown in figure D.1(a) where

I_w = second moment of area of vertical member

I_f = second moment of area of horizontal member

b = length of horizontal member

d = length of vertical member

Under the action of a positive vertical force P_2 and a positive moment M_2 applied at end 2, the displacements at end 2 will be d_2 and θ_2 as shown in figure D.1(b). The relationship between end forces and displacements can be determined using the slope deflection method by making use of the frame symmetry as shown in figure D.1(c).

The basic slope deflection equations are

$$M_{ab} = \frac{2 E I_f}{b} \theta_2 - \frac{6 E I_f}{b^2} d_2 \quad \text{---- eqn D.1}$$

$$M_{ba} = \frac{4 E I_f}{b} \theta_2 - \frac{6 E I_f}{b^2} d_2 \quad \text{---- eqn D.2}$$

$$M_{bc} = \frac{3 E I_w}{d/2} \theta_2 = \frac{6 E I_w}{d} \theta_2 \quad \text{---- eqn D.3}$$

Joint and sway equilibrium may be expressed as follows

$$0.5 M_2 = M_{ba} + M_{bc}$$

$$0.5 P_2 = -(M_{ab} + M_{ba}) / b$$

which give the following force / displacement relationship

$$\begin{Bmatrix} P_2 \\ M_2 \end{Bmatrix} = \begin{bmatrix} \frac{24 E I_f}{b^3} & \frac{-12 E I_f}{b^2} \\ \frac{-12 E I_f}{b^2} & \frac{8 E I_f}{b} + \frac{12 E I_w}{d} \end{bmatrix} \begin{Bmatrix} d_2 \\ \theta_2 \end{Bmatrix} \quad \text{----- eqn D.4}$$

the inverse of which is

$$\begin{Bmatrix} d_2 \\ \theta_2 \end{Bmatrix} = \begin{bmatrix} \frac{b^3 (2 I_f d + 3 I_w b)}{12 E I_f (I_f d + 6 I_w b)} & \frac{b^2 d}{4 E (I_f d + 6 I_w b)} \\ \frac{b^2 d}{4 E (I_f d + 6 I_w b)} & \frac{b d}{2 E (I_f d + 6 I_w b)} \end{bmatrix} \begin{Bmatrix} P_2 \\ M_2 \end{Bmatrix} \quad \text{---- D.5}$$

substitution of d_2 and θ_2 into equation D.1. gives

$$M_{ab} = \frac{-b(I_f d + 3 I_w b)}{2(I_f d + 6 I_w b)} * P_2 - \frac{I_f d}{2(I_f d + 6 I_w b)} * M_2$$

$$\text{now } P_1 = -P_2$$

$$\text{and } M_1 = 2 * M_{ab}$$

which gives the following force / displacement relationship

$$\begin{Bmatrix} P1 \\ M1 \end{Bmatrix} = \begin{bmatrix} \frac{-24 E I f}{b^3} & \frac{12 E I f}{b^2} \\ \frac{-12 E I f}{b^2} & \frac{4 E I f}{b} \end{bmatrix} \begin{Bmatrix} d2 \\ \theta2 \end{Bmatrix} \quad \text{----- eqn D.6}$$

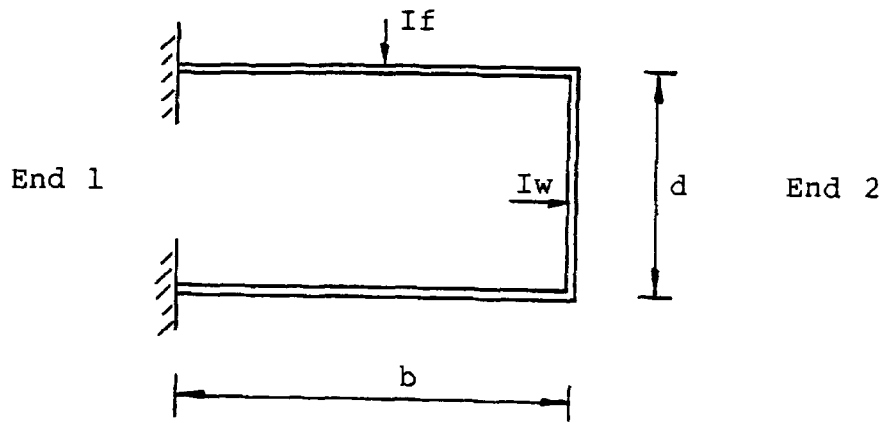
Similarly the frame element can be subjected to the displacements at end 1 resulting in the following overall stiffness matrix.

$$\begin{Bmatrix} P1 \\ M1 \\ P2 \\ M2 \end{Bmatrix} = \begin{bmatrix} \frac{24EIf}{b^3} & \frac{12EIf}{b^2} & \frac{-24EIf}{b^3} & \frac{12EIf}{b^2} \\ & \frac{8EIf}{b} + \frac{12EIw}{d} & \frac{-12EIf}{b^2} & \frac{4EIf}{b} \\ & & \frac{24EIf}{b^3} & \frac{-12EIf}{b^2} \\ \text{symmetrical} & & & \frac{8EIf}{b} + \frac{12EIw}{d} \end{bmatrix} \begin{Bmatrix} d1 \\ \theta1 \\ d2 \\ \theta2 \end{Bmatrix}$$

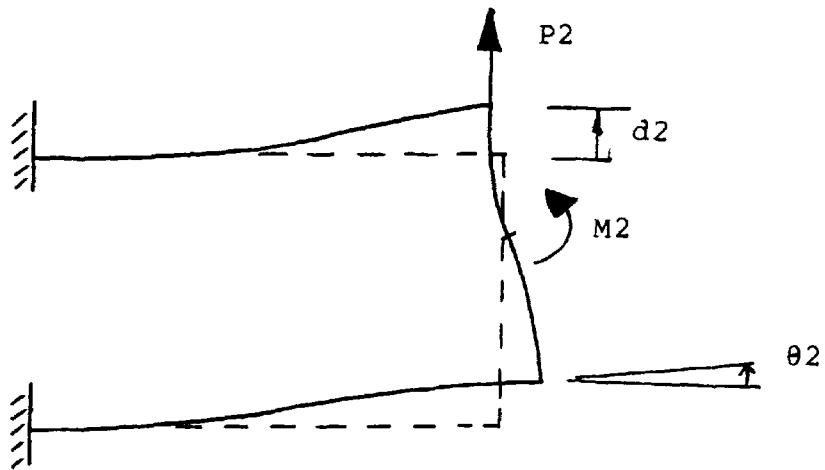
This equation D.7 caters for in-plane bending and shear effects. When the torsion moment / displacement relationship specified by equation A.7 is added to the equivalent frame element stiffness matrix the following overall element stiffness matrix is obtained.

$$\begin{Bmatrix} Pz1 \\ Mx1 \\ My1 \\ Pz2 \\ Mx2 \\ My2 \end{Bmatrix} = \begin{bmatrix} \frac{24EIf}{b^3} & 0 & \frac{12EIf}{b^2} & -\frac{24EIf}{b^3} & 0 & \frac{12EIf}{b^2} \\ 0 & \frac{GJ}{b} & 0 & 0 & -\frac{GJ}{b} & 0 \\ \frac{8EIf + 12EIw}{b} & \frac{12EIf + 12EIw}{d} & \frac{4EIf}{b} & -\frac{12EIf}{b^2} & 0 & \frac{4EIf}{b} \\ \frac{24EIf}{b^3} & 0 & \frac{24EIf}{b^3} & -\frac{12EIf}{b^2} & 0 & -\frac{12EIf}{b^2} \\ 0 & \frac{GJ}{b} & 0 & 0 & \frac{GJ}{b} & 0 \\ \frac{8EIf + 12EIw}{b} & \frac{12EIf + 12EIw}{d} & \frac{8EIf + 12EIw}{b} & 0 & 0 & \frac{8EIf + 12EIw}{d} \end{bmatrix} \begin{Bmatrix} dz1 \\ \theta x1 \\ \theta y1 \\ dz2 \\ \theta x2 \\ \theta y2 \end{Bmatrix}$$

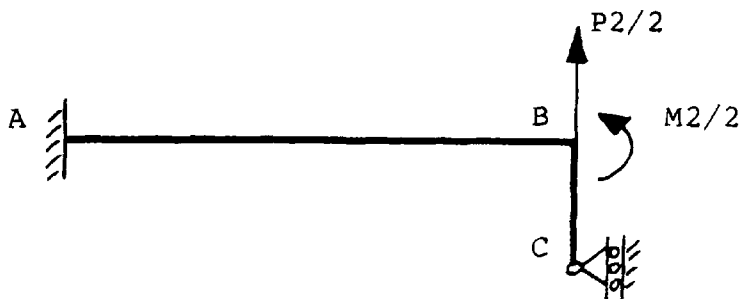
symmetrical



(a) Details of equivalent frame.



(b) Deflected shape due to P_2 and M_2 .



(c) Frame used in slope deflection analysis.

FIGURE D.1 - Equivalent frame element details.

APPENDIX E.

DERIVATION OF STRAIN ENERGY FORMULAE FOR GRILLAGE BEAM.

It can be shown, i.e. MEGSON (1980), that the total strain energy, U , in a grillage beam can be expressed as follows

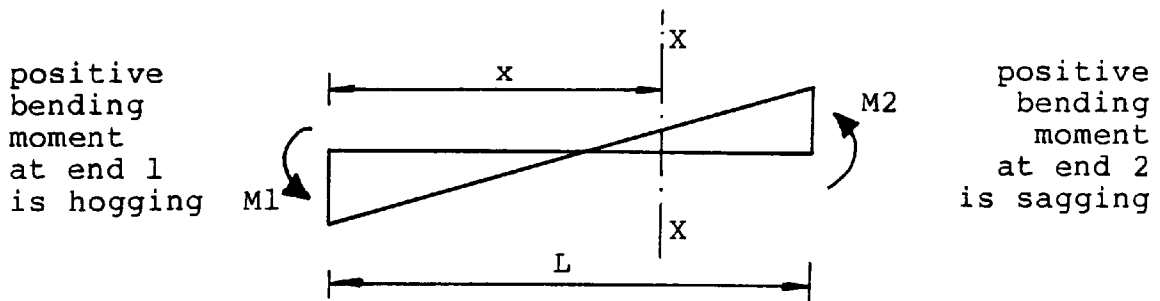
$$\begin{aligned}
 U &= U(\text{bending}) + U(\text{torsion}) + U(\text{shear}) \\
 &= \int_0^L \frac{Mx^2}{2EI} dx + \frac{T^2 L}{2GJ} + \frac{Q^2 L}{2GAs}
 \end{aligned}$$

where Mx = linearly varying bending moment in the beam

T = constant torsion moment in the beam

Q = constant shear force in the beam

The strain energy contribution from bending can be expressed in terms of the end moments as follows



The sagging bending moment at section $X-X$, a distance x from end 1, can be expressed as

$$Mx = -M_1 + [M_1 + M_2] * \frac{x}{L}$$

$$\text{hence } U(\text{bending}) = \frac{1}{2EI} \int_0^L \left(-M_1 + [M_1 + M_2] * \frac{x}{L} \right)^2 dx$$

which reduces to

$$U(\text{bending}) = \frac{L}{6EI} (M_1^2 - M_1 * M_2 + M_2^2)$$

A sub-routine was incorporated into the program SHEARGRID2 which calculated the strain energy contributions due to bending, torsion and shear in both the longitudinal and transverse directions.

The external work done by the applied loads was also calculated using the expression

$$\text{Ext. work done} = \frac{1}{2} W d$$

where W = intensity of applied load

and d = displacement of structure in direction of load

The external work done was shown to equal the total internal strain energy of the grillage structure.

The following examples illustrate the strain energy contributions for three of the structures considered.

1. 3-cell structure subjected to midspan point loading producing uniform midspan deflection across width of structure (figure 3.12).

Strain Energy in Shear.

Longitudinal grillage beams = 114.82

Transverse grillage beams = 0.00

Strain Energy in Torsion.

Longitudinal grillage beams = 0.00

Transverse grillage beams = 1.36

Strain Energy in Bending.

Longitudinal grillage beams = 509.72

Transverse grillage beams = 0.00

Total Strain Energy in Structure = 625.90

External Work Done by loads = 625.90

This example illustrates that under uniform loading the predominant structural actions are longitudinal bending and shear.

2. 3-cell structure as example 1 subjected to uniform line load over outer webs.

Strain Energy in Shear.

Longitudinal grillage beams = 30.90

Transverse grillage beams = 0.07

Strain Energy in Torsion.

Longitudinal grillage beams = 0.00

Transverse grillage beams = 26.37

Strain Energy in Bending.

Longitudinal grillage beams = 106.37

Transverse grillage beams = 0.00

Total Strain Energy in Structure = 163.72

External Work Done by loads = 163.72

3. 3-cell structure as example 1 subjected to uniform line load over inner webs.

Strain Energy in Shear.

Longitudinal grillage beams	=	123.68
Transverse grillage beams	=	0.14

Strain Energy in Torsion.

Longitudinal grillage beams	=	0.00
Transverse grillage beams	=	30.75

Strain Energy in Bending.

Longitudinal grillage beams	=	380.15
Transverse grillage beams	=	0.00

Total Strain Energy in Structure	=	534.72
----------------------------------	---	--------

External Work Done by loads	=	534.72
-----------------------------	---	--------

Examples 2 and 3 illustrate the contribution of torsion strain energy when the loading produces distortion of the cross-section of the structure. The percentage contribution being 5.8% when transverse sagging moments are developed, whilst the percentage contribution increases to 16.1% when transverse hogging moments are developed.

APPENDIX F.

ANALYSIS OF SHEAR-DEFORMABLE FIXED-ENDED BEAMS.

The support reactions for the fixed-ended beam shown in figure F.1(a) can be determined using the principle of virtual work as follows.

The bending moment and shear force at the section X-X, a distance x from end 1 as shown in figure F.1(b), can be expressed as follows

$$M(0) = -M_1 + P_1 x - 0.5w x^2$$

and $Q(0) = -P_1 + w x$

The structure is reduced to a statically determinate cantilever by removal of the restraints at end 1.

It is subjected to a virtual unit vertical force at end 1 which develop the following virtual bending moment and shear force at section X-X, figure F.1(c).

$$m(1) = 1 x$$

and $q(1) = -1$

and also a virtual unit moment at end 1, figure F.1(d), with the corresponding bending moment and shear force values of

$$m(2) = -1$$

and $q(2) = 0$

The principle of virtual work gives

$$1 \cdot dl = \int_0^L \frac{m(1) M(0) dx}{EI} + \int_0^L \frac{q(1) Q(0) dx}{GAs} \quad \text{---- eqn F.1}$$

$$1 \cdot \theta 1 = \int_0^L \frac{m(2) M(0) dx}{EI} + \int_0^L \frac{q(2) Q(0) dx}{GAs} \quad \text{---- eqn F.2}$$

now $dl = 0$ and $\theta 1 = 0$ for the fixed end condition,
hence equation F.1 becomes

$$0 = \frac{1}{EI} \int_0^L x(-M1 + P1 x - 0.5w x^2) dx + \frac{1}{GAs} \int_0^L -1(-P1 + w x) dx$$

which reduces to

$$0 = \frac{1}{EI} \left[\frac{-M1 L^2}{2} + \frac{P1 L^3}{3} - \frac{w L^4}{8} \right] + \frac{1}{GAs} \left[P1 L - \frac{w L^2}{2} \right]$$

$$\text{now } n = \frac{6 EI}{GAs L^2}$$

$$\text{or } \frac{1}{GAs} = \frac{n L^2}{6 EI} \quad \text{which gives}$$

$$0 = \frac{-M1 L^2}{2 EI} + \frac{P1 L^3(2+n)}{6 EI} - \frac{w L^4(3+2n)}{24 EI} \quad \text{---- eqn F.3}$$

similarly equation F.2 becomes

$$0 = \frac{1}{EI} \int_0^L -1(-M1 + P1 x - 0.5w x^2) dx$$

$$0 = \frac{M1 L}{EI} - \frac{P1 L^2}{2 EI} + \frac{w L^3}{6 EI} \quad \text{---- eqn F.4}$$

Solution of equations F.3 and F.4 produces the following solution

$$\underline{M_1 = \frac{w L^2}{12}} \quad \text{and} \quad \underline{P_1 = \frac{w L}{2}}$$

The midspan vertical deflection can be determined from figure F.1(e) where the bending moment and shear force at section X-X due to a virtual unit vertical force at midspan can be expressed as follows

$$m(x) = -1(x - 0.5L)$$

and $q(x) = 1$

The principle of virtual work gives

$$1 \cdot d_3 = \int_0^L \frac{m(x) M(x) dx}{EI} + \int_0^L \frac{q(x) Q(x) dx}{GAs}$$

which produces a midspan deflection of

$$\underline{\frac{w L^4}{384 EI} + \frac{w L^2}{8 GAs}} \quad \text{----- eqn F.7}$$

The fixed ended beam shown in figure F.2(a) was analysed using the finite element program QUEST using the mesh shown in figure F.2(b).

The horizontal reaction values at the support nodes were calculated as follows

<u>Support 1</u>		<u>Midspan</u>	
<u>Node No.</u>	<u>Force (kN)</u>	<u>Node No.</u>	<u>Force (kN)</u>
1	82.670	61	37.610
2	73.955	62	43.688
3	2.524	63	-1.426
4	-69.710	64	-46.540
5	-83.737	65	-39.036

Hence support 1 moment

$$= 75*(82.670 + 83.737) + 37.5*(73.955 + 69.710)$$

$$= 17868 \text{ kNcm.}$$

cf. theoretical fixed end moment value of 18000 kNcm

and midspan bending moment

$$= 75*(37.610 + 39.036) + 37.5*(43.688 + 46.540)$$

$$= 9132 \text{ kNcm.}$$

cf. theoretical midspan bending moment value of 9000 kNcm.

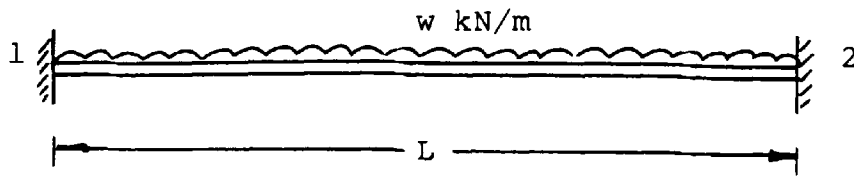
The finite element values of bending moment agreed closely to the theoretical values at both the support and midspan sections.

The midspan deflection values were predicted as follows

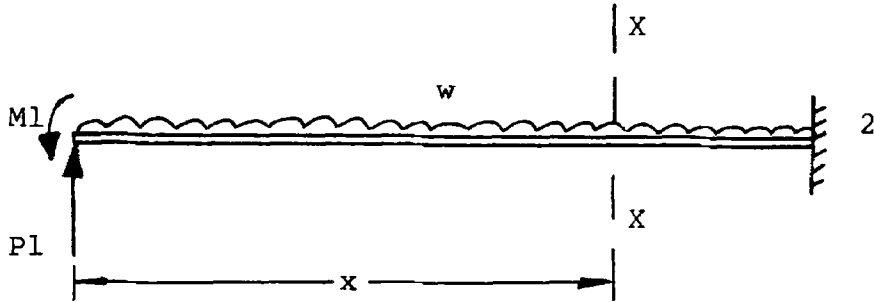
$$\text{from equation F.7} = 0.0866 \text{ cm.}$$

$$\text{from finite element analysis} = 0.0836 \text{ cm.}$$

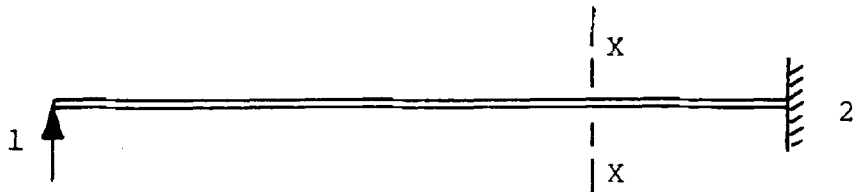
i.e. the finite element program underestimated the deflection by 3.4%.



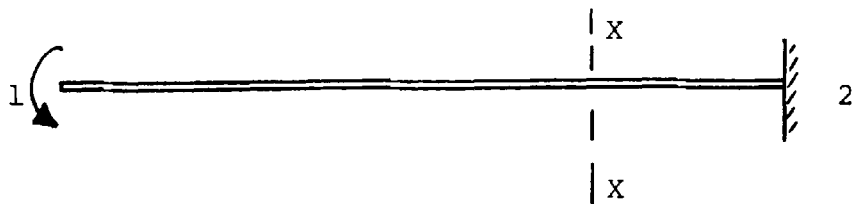
(a) Structure details.



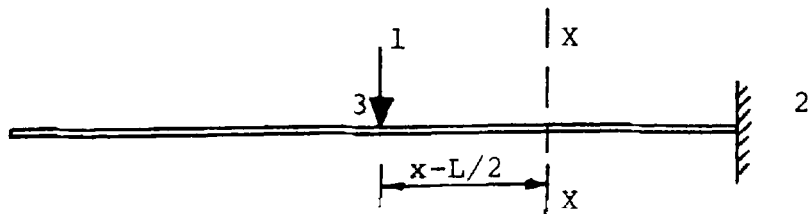
(b) Real forces (system 0).



(c) virtual unit vertical force at end 1 (system 1).

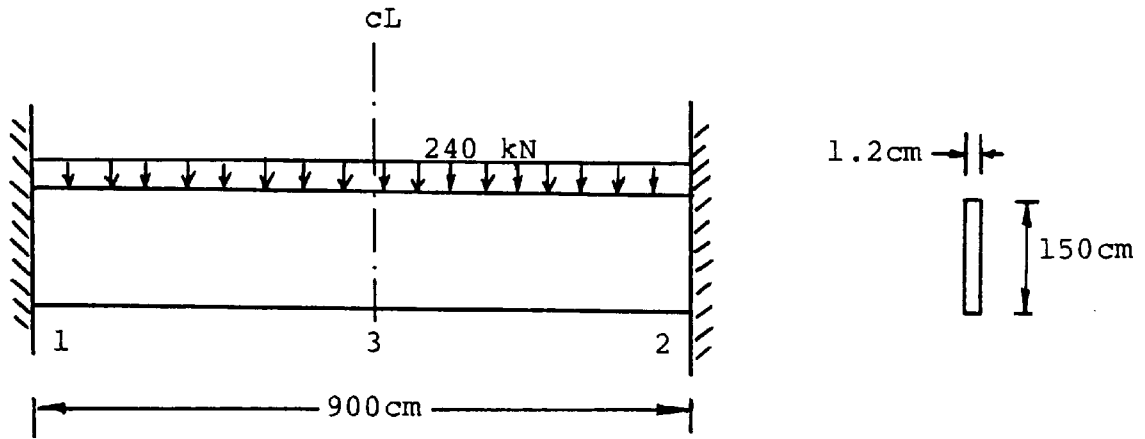


(d) virtual unit moment at end 1 (system 2).

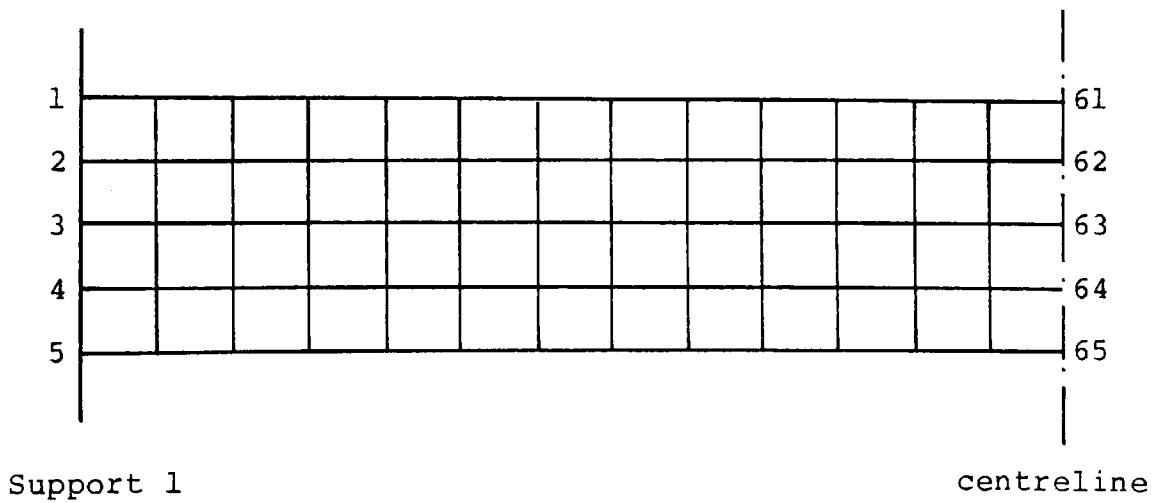


(e) virtual unit vertical force at midspan (system 3).

FIGURE F.1 - Virtual work analysis of fixed ended beam.



(a) Structure and loading detail.



(b) finite element mesh.

FIGURE F.2 - Finite element analysis of fixed ended beam subjected to uniformly distributed load.